

© 2012

Suhail Albhaisi

ALL RIGHTS RESERVED

**EFFECT OF SUBSTRUCTURE STIFFNESS ON THE PERFORMANCE OF
INTEGRAL ABUTMENT BRIDGES UNDER THERMAL LOADS**

By

SUHAIL ALBHAISI, P.E.

A Dissertation submitted to the

Graduate School-New Brunswick

Rutgers, The State University of New Jersey

in partial fulfillment of the requirements

for the degree of

Doctor of Philosophy

Graduate Program in Civil and Environmental Engineering

Written under the direction of

Hani H. Nassif, PhD., P.E.

and approved by

New Brunswick, New Jersey

May, 2012

ABSTRACT OF THE DISSERTATION

EFFECT OF SUBSTRUCTURE STIFFNESS ON THE PERFORMANCE OF INTEGRAL ABUTMENT BRIDGES UNDER THERMAL LOADS

by SUHAIL ALBHAISI, P.E.

Dissertation Director:

Hani Nassif, PhD., P.E.

This research investigates the effect of substructure stiffness on the performance of short and medium span length Integral Abutment Bridges (IABs) subjected to thermal load. Various parameters such as foundation soil stiffness, pile orientation, pile type, and abutment geometry on the performance of IABs, are considered.

Three-dimensional (3D) Finite Element (FE) models were developed using the FE software LUSAS to capture the behavior of IABs including the variations in displacement and rotation in the transverse direction for the various components of the superstructure as well as the substructure. Field measurements from a recently constructed two-span steel girder IAB were utilized to validate the 3D FE models. Using the validated model, a parametric study was carried out to study the effect of the above parameters on the performance of IABs under thermal loading using AASHTO-LRFD temperature ranges.

The study shows that among the investigated parameters, the foundation soil stiffness stands as the most important factor that affects the performance of IABs. In general, the bridge behavior is more sensitive to the foundation soil stiffness during

bridge contraction. The results from the study show considerable variations in displacement and rotation in the transverse direction for the various components of the superstructure and the substructure in relatively wide IABs. This research suggests that Prestressed Concrete Piles can be a viable alternative to steel H-Piles for short span bridges. It was also noticed that the stress level due to thermal loading in the various components of the bridge can be significantly reduced by enclosing the top part of the pile in an enclosure filled with crushed stone or loose sand. Moreover, the research suggests that the pile orientation has a minimum effect on the behavior of IABs. It also suggests that a slight increase in the abutment height can significantly reduce the displacement and rotation along the piles during bridge expansion. The research also suggests that 3D models are necessary to capture the behavior of IABs especially during bridge expansion. The research provides simple equations and charts to help bridge engineers calculate the displacement and rotation along the substructure.

DEDICATION

I dedicate my dissertation work to my beloved, hard working parents who sacrificed their lives to provide for me and my siblings and provided unconditional love and care. I love them so much for their inspiration, resilience and encouragement to always pursuit the highest level of education, and I would not have made it this far without them.

I also would like to dedicate this work to my loving wife Duna for her love, support, dedication and encouragement through the stress and demand of combining work, family and my academic pursuit to complete my PhD.

Finally, special gratitude to my brothers, sisters and their families for their loving support.

ACKNOWLEDGEMENTS

I want to express my deep appreciation and genuine gratitude to my advisor Dr. Hani Nassif for his guidance, support, and overall contribution to the work of this dissertation. It was a great fortune to have him as my advisor and mentor. I also appreciate his help and encouragement throughout the many years I have known him.

My sincere acknowledgement is expressed to Dr. Husam Najm, Dr. Kaan Ozbay, and Dr. Thomas Tsakalakos for being on my dissertation committee and for providing effective responses to my inquiries.

The details of the bridges in this research were provided by the New Jersey Department of Transportation (NJDOT). Also the 3D model was validated using the data from a study sponsored by NJDOT and that is gratefully acknowledged. The photos of the new Scotch Road bridge were provided by Arora and Associates, P.C. and that is gratefully acknowledged.

The financial support of Rutgers University and the help of Rutgers students Khalid Machich and Gregory Wisniewski are gratefully acknowledged. I also want to thank my colleagues at Rutgers University, Dr. Talat Abu-Amra, Dr. Nakin Suksawang, Dr. Joseph Davis, Dr. Raymond El-Koury, Dan Sue, and Anuoluwa Adediji for their friendship and support throughout the years.

My appreciation is extended to the departmental staff Gina Cullari and Linda Szary and to my former and current colleagues at Rutgers University for their friendship and support throughout the years.

I would like to thank Mr. Salah Khayyat who introduced me to the topic of Integral Abutment Bridges and Dr. Murat Dicleli who was the first to work with me on this topic. Finally, I would like also to thank my supervisor at Jacobs Engineering Mrs. Lynne Baumann for providing me with flexible working hours.

TABLE OF CONTENTS

ABSTRACT.....	ii
DEDICATION	iv
ACKNOWLEDGMENT	v
TABLE OF CONTENTS.....	vii
LIST OF TABLES.....	xii
LIST OF FIGURES	xiv
LIST OF SYMBOLS	xxx

Chapter	Page
1. INTRODUCTION	1
1.1 GENERAL	1
1.2 PROBLEM STATEMENT	6
1.3 RESEARCH OBJECTIVE	8
1.4 EXPECTED CONTRIBUTION	9
1.5 STRUCTURE OF THE DISSERTATION.....	9
2. LITERATURE REVIEW AND BACKGROUND	11
2.1 GENERAL.....	11
2.2 HISTORICAL BACKGROUND.....	12
2.3 ATTRIBUTES OF INTEGRAL ABUTMENT BRIDGES.....	16
2.4 LIMITATIONS OF INTEGRAL ABUTMENT BRIDGES	18
2.5 DESIGN CODES.....	20
2.5.1 AASHTO Code.....	20
2.5.2 International Codes	21
2.6 CURRENT PRACTICE.....	23
2.6.1 Limits on the Geometry of IABs	23
2.6.1.1 Limits on the Geometry of IABs in the United States	23
2.6.1.2 Limits on the Geometry of IABs in Other Countries.....	30

2.6.2 Superstructure	32
2.6.3 Foundations.....	36
2.6.3.1 Piles.....	36
2.6.3.2 Abutment-Pile Connection.....	40
2.6.3.3 Soil-Pile Interaction	41
2.6.4 Backfill.....	44
2.6.5 Construction Sequence.....	46
2.7 FOUNDATIONS FOR INTEGRAL ABUTMENT BRIDGES	48
2.7.1 Steel H-Piles.....	48
2.8 SOIL-STRUCTURE INTERACTION	50
2.8.1 Foundation-Soil Interaction	50
2.8.2 Abutment- Backfill Interaction	52
2.9 TEMPERATURE VARIATION IN INTEGRAL ABUTMENT BRIDGES.....	59
2.10 EFFECT OF SKEW IN INTEGRAL ABUTMENT BRIDGES	61
2.11 SEISMIC DESIGN OF INTEGRAL ABUTMENT BRIDGES.....	63
2.12 MATERIALS IN INTEGRAL ABUTMENT BRIDGES	63
2.13 MAJOR STUDIES.....	64
3. FOUNDATIONS FOR INTEGRAL ABUTMENT BRIDGES	68
3.1 GENERAL	68
3.2 STEEL H-PILES.....	69
3.2.1 Material Properties	71
3.2.2 Stability of Steel H-Piles.....	74
3.2.2.1 AISC Approach to Local Buckling in Steel Sections	75
3.2.2.2 Kato's (1989) Web-Flange Interaction Approach to Local Buckling in Steel H-Piles Sections	77
3.2.3 Moment-Curvature Relationships	79
3.2.4 Abutment-H-Pile Connection	82
3.3 PRESTRESSED CONCRETE PILES (PCPs).....	85
3.4 STEEL PIPE PILES.....	87

4. SOIL-STRUCTURE INTERACTION	89
4.1 GENERAL	89
4.2 PILE-FOUNDATION SOIL INTERACTION	92
4.3 MODELING OF SOIL-PILE INTERACTION FOR Laterally Loaded PILES	94
4.4 SOIL BEHAVIOR FOR Laterally Loaded PILES IN CLAY	96
4.4.1. Estimation of Ultimate Soil Resistance (p_u)	98
4.4.2. Estimation of Soil Modulus (E_s)	101
4.5 SOIL BEHAVIOR FOR Laterally Loaded PILES IN SAND	107
4.5.1 Estimation of Ultimate Soil Resistance	109
4.5.2 Procedure to Construct p - y Curves in Sand	110
4.6 ABUTMENT-SOIL INTERACTION	117
5. FINITE ELEMENT MODELING AND VALIDATION	120
5.1 GENERAL	120
5.2 3D FE MODELS	121
5.2.1 Modeling of Superstructure and Substructure	121
5.2.2 Modeling of Foundation Soil and Backfill soil	125
5.3 MODEL VALIDATION	125
5.3.1 Bridge Description	126
5.3.2 Bridge FE Model	132
5.3.3 Validation of Results	135
5.4 TWO-DIMENSIONAL 2D FE MODEL	139
6. PARAMETRIC STUDY SETUP	140
6.1 GENERAL	140
6.2 PARAMETERS IN THE STUDY	140
6.3 BRIDGES IN THE STUDY	142
6.4 SOIL MODELS	145
6.5 TERMINOLOGY IN THE STUDY	148

7. PARAMETRIC STUDY RESULTS	152
7.1 GENERAL.....	152
7.2 EFFECT OF SOIL STIFFNESS.....	154
7.2.1 Effect of Soil Stiffness on the Displacement and the Rotation of the Abutment and the Piles	154
7.2.2 Effect of Soil Stiffness on the Moment Along the Piles.....	168
7.2.3 Effect of Soil Stiffness on the Stresses in the Girders	176
7.2.4 Effect of Soil Stiffness on the Backfill Pressure on the Abutment.....	180
7.3 EFFECT OF PILE ENCLOSURE	184
7.3.1 Effect of Pile Enclosure on the Displacement and the Rotation of the Abutment and the Piles	184
7.3.2 Effect of Pile Enclosure on the Moment Along the Piles	193
7.3.3 Effect of Pile Enclosure on the Stresses in the Girders	196
7.3.4 Effect of Pile Enclosure on the Backfill Pressure on the Abutment.....	198
7.4 EFFECT OF PILE ORIENTATION	200
7.4.1 Effect of Pile Orientation on the Displacement and the Rotation of the Abutment and the Piles	200
7.4.2 Effect of Pile Orientation on the Moment along the Piles.....	209
7.4.3 Effect of Pile Orientation on the Stresses in the Girders	214
7.4.4 Effect of Pile Orientation on the Backfill Pressure on the Abutment.....	215
7.5 EFFECT OF ABUTMENT HEIGHT.....	216
7.5.1 Effect of Pile Orientation on the Displacement and the Rotation of the Abutment and the Piles	216
7.5.2 Effect of Pile Orientation on the Moment along the Piles.....	222
7.5.3 Effect of Pile Orientation on the Stresses in the Girders	224
7.5.4 Effect of Pile Orientation on the Backfill Pressure on the Abutment.....	225
7.6 EFFECT OF PILE TYPE (PRESTRESSED CONCRETE PILES VERSUS STEEL H-PILES)	226
7.6.1 Effect of Pile Type on the Displacement and the Rotation of the Abutment and the Piles	226

7.6.2 Effect of Pile Type on the Moment along the Piles	231
7.6.3 Effect of Pile Type on the Stresses in the Girders	233
7.6.4 Effect of Pile Type on the Backfill Pressure on the Abutment.....	234
 8. ANALYSIS OF INTEGRAL ABUTMENT BRIDGES	235
8.1 GENERAL.....	235
8.2 SUBSTRUCTURE DISPLACEMENT	236
8.3 SUBSTRUCTURE ROTATION	243
8.4 2D VERSUS 3D	249
8.5 PILE IDEALIZATION	265
8.6 BRIDGE’S DISPLACEMENT CAPACITY (ALBHAISI 2003)	272
8.6.1 H-Pile’s Displacement Capacity	272
8.6.2 Relative Displacement of Abutment at Pile’s Failure	277
 9. SUMMARY AND CONCLUSIONS	282
9.1 SUMMARY	282
9.2 CONCLUSIONS.....	283
9.2.1 Foundation Soil.....	283
9.2.2 Pile Enclosure	284
9.2.3 Pile Orientation	285
9.2.4 Abutment Height.....	285
9.2.5 H-Piles versus Prestressed Concrete Piles (PCPs).....	285
9.2.6 2D versus 3D.....	286
9.2.7 Additional Conclusions.....	286
9.3 RECOMMENDATIONS FOR FUTURE RESEARCH.....	287
 APPENDIX A: ADDITIONAL FIGURES	288
APPENDIX B: DISTRIBUTION OF STRESSES IN GIRDERS AND PILES	308
 REFERENCES	315
 CURRICULUM VITA	324

LIST OF TABLES

Table	Page
Table 2.1 History of Use of IABs in the United States (Parachos and Amle 2011)	13
Table 2.2 Number of In-Service IAB Designed and Built Since 1995 (Maruri and petro, 2005)	15
Table 2.3 Geometric Limits on IABs in the United States (Kunin and Alampalli 1999)	24
Table 2.4 Geometric Limits on IABs in the United States (Maruri and Petro, 2005).....	26
Table 2.5 Geometric Limits on IABs in the United States (Bakeer et al., 2005).....	27
Table 2.6 Length Limits of IABs Supported on H Piles (Dunker and Liu, 2007)	29
Table 2.7: Summary of Selected Criteria used by European Countries (White 2007)	31
Table 2.8 Specifications for Pre-drilling Pile Foundation Locations (Olson et al. 2009)	39
Table 2.9 Length of Fixity (L_e) for H-Piles with Strong Axix Orientation (Maine DOT 2003)	42
Table 2.10 Approximate Magnitude of Movement Required to Reach Minimum Active and Maximum Passive Earth Pressure Conditions (Clough And Duncan 1991).....	55
Table 2.11 Uniform Temperature Ranges (AASHTO-LRFD, 2010)	59
Table 2.12 Major Recent Studies on IABs.....	65
Table 3.1 Properties of H-Piles available in North America.....	72
Table 3.2 Mechanical properties steels in used in H-Piles.....	73
Table 3.3 Limiting Ratios for Steel Sections under Compression (AISC, 2005)	75
Table 3.4 Width-Thickness Ratios for H-P Sections (AISC, 2005, A572 Grade 50 Steel) .	76
Table 3.5 Slenderness Parameter s of HP Sections (Kato, 1989, A572 – Grade 50).....	78
Table 3.6 Summary of MCRs for H-Pile Sections (Weak Orientation, A572 grade 50)...	80
Table 3.7 Summary of MCRs for H-Pile Sections (Strong Orientation, A572 grade 50) .	81
Table 3.8 Minimum Required Pile Embedment Length inside the Abutment to Develop Fixity for $f'_c = 23$ MPa (3.3 ksi) and $f_y = 250$ MPa (36 ksi) (ODOT 2004).....	83
Table 3.9 Minimum Required Pile Embedment Length inside the Abutment to Develop Fixity for $f'_c = 27$ MPa (4 ksi) and $f_y = 345$ MPa (50 ksi)	84
Table 4.1 Properties of Clay Used in the Study (Reese and Van Impe 2001)	102
Table 4.2 Properties of Sand Used in the Study (*Reese and Van Impe 2001)	109

Table 5.1 Linear 3D Thick Beam Element (LUSAS, 2008)	122
Table 5.2 Nonlinear 3D Thick Beam Element (LUSAS, 2008).....	123
Table 5.3 3D Thick Shell Elements (LUSAS, 2008)	124
Table 5.4 Comparison between Field Data and FEM Model Results	139
Table 6.1 List of the Parameters Considered in The Study.....	141
Table 6.2 Steel Plate Girders Dimensions.....	144
Table 6.3 Spring Constants for Cohesive Soils.....	145
Table 6.4 Spring Constants for Cohesionless Soils.....	146
Table 6.5 Spring Constants for Backfill Soil	146
Table 8.1 2D versus 3D (Short Bridge – Contraction - Interior Location)	250
Table 8.2 2D versus 3D Results (Short Bridge - Contraction – Exterior Location)	252
Table 8.3 2D versus 3D Results (Short Bridge - Expansion – Interior Location)	254
Table 8.5 2D versus 3D (Long Bridge – Contraction - Interior Location)	258
Table 8.6 2D versus 3D Results (Long Bridge - Contraction – Exterior Location)	260
Table 8.8 2D versus 3D Results (Long Bridge - Expansion – Exterior Location)	264
Table 8.9 Initial Soil Stiffness, k_h	266
Table 8.10 The Effective Pile Length L_e for H-Piles Embedded in Soft Clay	268
Table 8.11 The Effective Pile Length L_e for H-Piles Embedded in Medium Clay	269
Table 8.12 The Effective Pile Length L_e for H-Piles Embedded in Stiff Clay	270
Table 8.12 The Effective Pile Length L_e for H-Piles Embedded in Very Stiff Clay	271

LIST OF FIGURES

Figure	Page
Figure 1.1 Typical Single - Span Jointed Bridge	2
Figure 1.2 Typical Single - Span Integral Bridge	4
Figure 2.1 Evolution of Integral Abutment Bridges in the United States (Paraschos and Amde 2011)	14
Figure 2.2 Maximum Bridge Length Limits in Feet (MnDot 2011).....	29
Figure 2.3 Current NYSDOT Integral Abutment Details for Steel Superstructure	33
Figure 2.4 Current NYSDOT Integral Abutment Details for Precast Prestressed Concrete Superstructure.....	34
Figure 2.5 Sleeves Surrounding H-Piles at a Construction Site in New Jersey.....	38
Figure 2.6 Bending of pile carrying vertical and horizontal loads at head (a) Partly embedded pile (b) Equivalent fixed base pile or column (Tomlinson and Woodward 2008)	41
Figure 2.7 Simplified Model for IABs (Najm et al. 2005)	42
Figure 2.8 Modeling of the Soil by Springs.....	43
Figure 2.9 Plot of Passive Pressure Coefficient K_p vs Relative Wall Displacement (Δ/H) (MassDOT 2009)	45
Figure 2.10 Typical Construction Stages for IABs (Harvey et al. 2006).....	46
Figure 2.11 Genral P-Y Curve for Laterally Loaded Piles	51
Figure 2.12 Characteristics Shapes of p-y Curves for Soft Clay in the Presence of Free Water under Cyclic Loading (Matlock 1970).....	52
Figure 2.13 Relationship between Wall Movement and Earth Pressure for Ideal Cases of Walls That Are “Wished” Into Place (Clough And Duncan 1991)	55
Figure 2.14 Relationship between Wall Movement and Earth Pressure For Backfill Compacted To Medium-Dense Condition (Clough And Duncan 1991)	56
Figure 2.15 Effect of Wall Movement on Wall Pressure (Navy 1971)	57
Figure 2.16 Young's modulus (E_s) of Backfill Soil for a Range of in-Situ Dry Densities (ρ_d), Mean Effective Stresses (p') and Average Shear Strain Levels (γ) (Lehane et al. 1999)..	58

Figure 2.17 Positive Vertical Temperature Gradient in Concrete and Steel Superstructures (AASHTO-LRFD, 2010)	60
Figure 2.18 Soil Pressure Load, P_p , and Soil Abutment Interface Friction, F_{af} . (Oesterle and Lotfi 2005)	61
Figure 3.1 H-Pile Orientation.....	69
Figure 3.2 Typical Stress -Strain Relationship for Steel.....	71
Figure 3.3 Simplified Stress -Strain Relationship for Steel	73
Figure 3.4 Typical Moment-Curvature Relationship	79
Figure 3.5 Free Body Diagram of Pile Embedded in Abutment (ODOT, 2004).....	83
Figure 3.6 Typical Precast-Prestressed Concrete Pile Details (Delaware DOT, 2005) .	86
Figure 3.7 Typical Section of a Steel Pipe Pile Filled with Concrete.....	87
Figure 3.8 Steel Pipe Pile Filled with Concrete Details (Courtesy of NJDOT).....	88
Figure 4.1 Abutment Detail in Jointed Bridges (Delaware DOT, 2005)	89
Figure 4.2 Abutment Detail in IABs, Ohio DOT.....	90
Figure 4.3 Three-Dimensional Soil Pile Interaction (Wang and Isenhower, 2010)	92
Figure 4.4 Nonlinear Load-Deflection Behavior of Soil-Structure System.....	93
Figure 4.5 Two-Dimensional Soil Pile Interaction (Reese and Van Impe 2001)	94
Figure 4.6 A typical P-Y Curve and Approximate Elsto-Plastic curve	95
Figure 4.7 p - y Curve for Soft Clay with Free Water (Matlock 1970)	96
Figure 4.8 p - y Curve for Stiff Clay with No Free Water (Welch and Reese 1972).....	97
Figure 4.9 Model of Soil at Ground Surface (Reese and Van Impe 2001).....	98
Figure 4.10 Ultimate Soil Resistances with Transition Depth in Clay	99
Figure 4.11 Backfill and Embankment Pressures Distribution on the Abutment and the Foundation Soil	100
Figure 4.12 Variation of Soil Modulus with Depth for Clay	101
Figure 4.13 p - y Curves for H-Piles in Soft Clay.....	103
Figure 4.14 p - y Curves for H-Piles in Medium Clay	103
Figure 4.15 p - y Curves for H-Piles in Stiff Clay	104
Figure 4.16 p - y Curves for H-Piles in Very Stiff Clay	104
Figure 4.17 p - y Curves for PPCP in Soft clay	105
Figure 4.18 p - y Curves for PPCP in Medium Clay.....	105

Figure 4.19 p - y Curves for PPCP in Stiff Clay	106
Figure 4.20 p - y Curves for PPCP in Very Stiff Clay	106
Figure 4.21 Characteristic Shape of a Set of p - y Curves for Static and Cyclic Loading in Sand (Reese and Van Impe 2001).....	107
Figure 4.22 Variation of Soil Modulus with Depth in Sand	108
Figure 4.23 Values of Coefficients A_c and A_s (Reese and Van Impe 2001)	112
Figure 4.24 Non-dimensional Coefficient B for soil resistance versus depth (Reese and Van Impe 2001).....	112
Figure 4.25 p - y Curves for PPCP356X356 in Loose Sand	114
Figure 4.26 p - y Curves for PPCP356X356 in Medium Sand	114
Figure 4.27 p - y Curves for PPCP356X356 in Dense Sand.....	115
Figure 4.28 p - y Curves for HP310X125 in Loose Sand	115
Figure 4.29 p - y Curves for HP310X125 in Medium Sand	116
Figure 4.30 p - y Curves for HP310X125 in Dense Sand.....	116
Figure 4.31 Relationship Between Wall Movement and Earth Pressure for w Wall (Clough And Duncan, 1991).....	118
Figure 5.1 A Typical 3D FE Model for the Single-Span Bridge	121
Figure 5.2 Aerial View Scotch Road Interchange (Photo Courtesy of NJDOT)	126
Figure 5.3a Scotch Road Bridge – Plan (Courtesy of NJDOT).....	127
Figure 5.3b Scotch Road Bridge – Elevation (Courtesy of NJDOT)	127
Figure 5.4 Scotch Road Bridge – Girders, Abutment and Piles (Courtesy of NJDOT)	128
Figure 5.5 Scotch Road Bridge – Interior Pier Elevation (Courtesy of NJDOT)	128
Figure 5.6 Scotch Road Bridge - Foundation Details (Courtesy of NJDOT)	129
Figure 5.7 H-Piles Enclosed by Aluminum Sleeves (Courtesy of NJDOT).....	130
Figure 5.8 Scotch Road Bridge – Construction Stages.....	131
Figure 5.9 Abutment- Girder Connection (Courtesy of ARORA and ASSOCIATES, P.C).....	131
Figure 5.10 Scotch Road Bridge LUSAS 3D FE Model- Isometric View	133
Figure 5.11 Underside of the Bridge Deck	133
Figure 5.12 Linear Spring Models for (a) Abutment and (b) Piles	134
Figure 5.13 Longitudinal Bridge Displacement at the Relief Slab (Hassiotis et al., 2006) ..	135
Figure 5.14 Temperature Variations at the Top of Girder 2 (Hassiotis et al., 2006)	136

Figure 5.15 Stresses at Top of Piles 3, 6, and 9 (Hassiotis et al., 2005)	136
Figure 5.16 Bridge Expansion (mm) in the Longitudinal Direction, $\Delta T=25^{\circ}\text{C}$	137
Figure 5.17 Bridge Contraction (mm) in the Longitudinal Direction, $\Delta T=-25^{\circ}\text{C}$	137
Figure 5.18 Pile Inside Face Top Stresses (N/m^2), $\Delta T=25^{\circ}\text{C}$ (a) Pile 3 (b) Pile 6	138
Figure 5.19 Pile Inside Face Top Stresses (N/m^2), $\Delta T=-25^{\circ}\text{C}$ (a) Pile 3 (b) Pile 6	138
Figure 5.20 A Typical 2D FE Model for the Single-Span Bridge	139
Figure 6.1 Cross Section of the Short Bridge	143
Figure 6.2 Cross Section of the Long Bridge	143
Figure 6.3 A Typical Plate Girder Cross Section	144
Figure 6.4 Spring Adjustment Factor Illustration- 10 mm Displacement in Soft Clay	147
Figure 6.5: Single-Span Bridge, General Deflection Shape - Expansion	149
Figure 6.6 Single-Span Bridge, General Deflection Shape - Contraction	149
Figure 6.7 Two-Span Bridge, General Deflection Shape - Contraction	150
Figure 6.8 Two-Span Bridge, General Deflection Shape - Expansion	150
Figure 6.9 Pile's General Deflection Shape and Moment Diagram	151
Figure 7.1 Displacement at Interior and Exterior Locations (38-m Bridge, Clay, 3m Abutment, HP310X125 weak orientation)	154
Figure 7.2 Displacement along the Abutment and the Interior Pile (38-m Bridge, Clay, 3m Abutment, HP310X125 Weak Orientation)	156
Figure 7.3 Rotation at Interior and Exterior Locations (38-m Bridge, Clay, 3m Abutment, HP310X125 Weak Orientation)	157
Figure 7.4 Rotation along the Abutment and the Interior Pile (38-m Bridge, Clay, 3m Abutment, HP310X125 Weak Orientation)	158
Figure 7.5 Displacement at Interior and Exterior Locations (38-m Bridge, Sand, 3m Abutment, HP310X125 Weak Orientation)	159
Figure 7.6 Displacement along the Abutment and the Interior Pile (38-m Bridge, Sand, 3m Abutment, HP310X125 Weak Orientation)	160
Figure 7.7 Rotation at Interior and Exterior Locations (38-m Bridge, Clay, 3m Abutment, HP310X125 Weak Orientation)	160
Figure 7.8 Rotation along the Abutment and the Interior Pile (38-m Bridge, Sand, 3m Abutment, HP310X125 Weak Orientation)	161

Figure 7.9 Displacement at Interior and Exterior Locations (90-m Bridge, Clay, 3m Abutment, HP360X152 Weak Orientation)	162
Figure 7.10 Displacement along the Abutment and the Interior Pile (90-m Bridge, Clay, 3m Abutment, HP360X152 Weak Orientation)	163
Figure 7.11 Rotation at Interior and Exterior Locations (90-m Bridge, Clay, 3m Abutment, HP360X152 Weak Orientation)	164
Figure 7.12 Rotation along the Abutment and the Interior Pile (90-m Bridge, Clay, 3m Abutment, HP360X152 Weak Orientation)	165
Figure 7.13 Displacement at Interior and Exterior Locations (90-m Bridge, Sand, 3m Abutment, HP360X152 Weak Orientation)	166
Figure 7.14 Displacement along the Abutment and the Interior Pile (90-m Bridge, Sand, 3m Abutment, HP360X152 Weak Orientation)	166
Figure 7.15 Rotation at Interior and Exterior Locations (90-m Bridge, Sand, 3m Abutment, HP360X152 Weak Orientation)	167
Figure 7.16 Rotation along the Abutment and the Interior Pile (90-m Bridge, Sand, 3m Abutment, HP360X1152 Weak Orientation)	167
Figure 7.17 Moment at the Top of the Pile (38-m Bridge, Clay, 3m Abutment, HP310X125 Weak Orientation)	168
Figure 7.18 Moment at the Top of the Pile (90-m Bridge, Sand, 3m Abutment, HP360X1152 Weak Orientation)	169
Figure 7.19 Moment Loads along the Interior Pile (38-m Bridge, Clay, 3m Abutment, HP310X125 Weak Orientation)	170
Figure 7.20 Moment along the Interior Pile (90-m Bridge, Clay, 3m Abutment, HP360X152 Weak Orientation)	171
Figure 7.21 Moment at the Top of the Pile (38-m Bridge, Sand, 3m Abutment, HP310X125 Weak Orientation)	172
Figure 7.22 Moment along the Interior Pile (38-m Bridge, Sand, 3m Abutment, HP310X125 Weak Orientation)	173
Figure 7.23 Moment at the Top of the Pile (90-m Bridge, Clay, 3m Abutment, HP360X152 Weak Orientation)	174

Figure 7.24 Moment along the Interior Pile (90-m Bridge, Sand, 3m Abutment, HP360X152 Weak Orientation)	175
Figure 7.25 Stresses in the Girders (38-m Bridge, Clay, 3m Abutment, HP310X125 Weak Orientation)	176
Figure 7.26 Stresses in the Girders (38-m Bridge, Sand, 3m Abutment, HP310X125 Weak Orientation)	177
Figure 7.27 Stresses in the Girders (90-m Bridge, Clay, 3m Abutment, HP360X152 Weak Orientation)	178
Figure 7.28 Stresses in the Girders (90-m Bridge, Sand, 3m Abutment, HP360X152 Weak Orientation)	179
Figure 7.29 Backfill Pressure on the Abutment (38-m Bridge, Clay, 3m Abutment, HP310X125 Weak Orientation)	180
Figure 7.30 Backfill Pressure on the Abutment (38-m Bridge, Sand, 3m Abutment, HP310X125 Weak Orientation)	181
Figure 7.31 Backfill Pressure on the Abutment (90-m Bridge, Clay, 3m Abutment, HP360X152 Weak Orientation)	182
Figure 7.32 Backfill Pressure on the Abutment (90-m Bridge, Sand, 3m Abutment, HP360X152 Weak Orientation)	183
Figure 7.33 Displacement (Contraction) at the Interior Location (38-m Bridge, Clay, 3m Abutment, HP310X125 Weak Orientation with Pile Enclosure) ...	184
Figure 7.34 Displacement (Contraction) along the Abutment and the Interior Pile (38-m Bridge, Clay, 3m Abutment, HP310X125 Weak Orientation with Pile Enclosure) ..	185
Figure 7.35 Displacement (Expansion) at the Interior Location (38-m Bridge, Clay, 3m Abutment, HP310X125 Weak Orientation with Pile Enclosure) ..	186
Figure 7.36 Displacement (Expansion) along the Abutment and the Interior Pile (38-m Bridge, Clay, 3m Abutment, HP310X125 Weak Orientation with Pile Enclosure) .	187
Figure 7.37 Displacement (Contraction) at the Interior Location (90-m Bridge, Clay, 3m Abutment, HP360X152 Weak Orientation with Pile Enclosure) ..	188
Figure 7.38 Displacement (Expansion) at the Interior Location (90-m Bridge, Clay, 3m Abutment, 360X152 Weak Orientation with Pile Enclosure)	188

Figure 7.39 Displacement (Contraction) along the Abutment and the Interior Pile (90-m Bridge, Clay, 3m Abutment, 360X152 Weak Orientation with Pile Enclosure)	189
Figure 7.40 Rotation (Contraction) at the Interior Location (38-m Bridge, Clay, 3m Abutment, HP310X125 Weak Orientation with Pile Enclosure) ..	190
Figure 7.41 Rotation (Contraction) along the Abutment and the Interior Pile (38-m Bridge, Clay, 3m Abutment, HP310X125 Weak Orientation with Pile Enclosure) .	191
Figure 7.42 Rotation (Contraction) at the Interior Location (90-m Bridge, Clay, 3m Abutment, HP360X152 Weak Orientation with Pile Enclosure)...	192
Figure 7.43 Rotation (Expansion) at the Interior Location (90-m Bridge, Clay, 3m Abutment, HP360X152 Weak Orientation with Pile Enclosure) ...	193
Figure 7.44 Moment at the Top of the Exterior Pile (38-m Bridge, Clay, 3m Abutment, HP310X125 Weak Orientation with Pile Enclosure) ..	194
Figure 7.45 Moment (Contraction) along the Exterior Pile (38-m Bridge, Clay, 3m Abutment, HP310X125 Weak Orientation with Pile Enclosure) ...	195
Figure 7.46 Moment at the Top of the Exterior Pile (90-m Bridge, Clay, 3m Abutment, HP360X152 Weak Orientation with Pile Enclosure) ..	195
Figure 7.47 Moment (Contraction) along the Exterior Pile (90-m Bridge, Clay, 3m Abutment, HP360X152 Weak Orientation with Pile Enclosure)..	196
Figure 7.48 Stresses in the Interior Girder (38-m Bridge, Clay, 3m Abutment, HP310X125 Weak Orientation with Pile Enclosure)...	197
Figure 7.49 Stresses in the Interior Girder (90-m Bridge, Clay, 3m Abutment, HP360X152 Weak Orientation with Pile Enclosure)...	197
Figure 7.50 Backfill Pressure on the Abutment (38-m Bridge, Clay, 3m Abutment, HP310X125 Weak Orientation with Pile Enclosure) ..	198
Figure 7.51 Backfill Pressure on the Abutment (90-m Bridge, Clay, 3m Abutment, HP360X152 Weak Orientation with Pile Enclosure) ..	199
Figure 7.52 Displacement (Expansion) at Interior and Exterior Locations (38-m Bridge, Clay, 3m Abutment, HP310X125 Strong and Weak Orientation).....	200
Figure 7.53 Displacement (Expansion) along the Abutment and the Interior Pile (38-m Bridge, Clay, 3m Abutment, HP310X125 Strong and Weak Orientation).....	201

Figure 7.54 Rotation (Expansion) at Interior and Exterior Locations (38-m Bridge, Clay, 3m Abutment, HP310X125 Strong and Weak Orientation).....	202
Figure 7.55 Rotation (Expansion) the Abutment and the Interior Pile (38-m Bridge, Clay, 3m Abutment, HP310X125 Strong and Weak Orientation).....	202
Figure 7.56 Displacement (Contraction) at Interior and Exterior Locations (38-m Bridge, Clay, 3m Abutment, HP310X125 Strong and Weak Orientation).....	203
Figure 7.57 Displacement (Contraction) along the Abutment and the Interior Pile (38-m Bridge, Clay, 3m Abutment, HP310X125 Strong and Weak Orientation).....	204
Figure 7.58 Rotation (Contraction) at Interior and Exterior Locations (38-m Bridge, Clay, 3m Abutment, HP310X125 Strong and Weak Orientation).....	204
Figure 7.59 Rotation (Contraction) along the Abutment and the Interior Pile (38-m Bridge, Clay, 3m Abutment, HP310X125 Strong and Weak Orientation).....	205
Figure 7.60 Displacement (Contraction) at Interior and Exterior Locations (38-m Bridge, Sand, 3m Abutment, HP310X125 Strong and Weak Orientation)	206
Figure 7.61 Rotation (Contraction) at Interior and Exterior Locations (38-m Bridge, Sand, 3m Abutment, HP310X125 Strong and Weak Orientation)	206
Figure 7.62 Displacement (Contraction) along the Abutment and the Pile at the Interior Location (38-m Bridge, Sand, 3m Abutment, HP310X125 Strong and Weak Orientation) .	207
Figure 7.63 Rotation (Contraction) along the Abutment and the Interior Pile (38-m Bridge, Sand, 3m Abutment, HP310X125 Strong and Weak Orientation)	207
Figure 7.64 Displacement (Contraction) along the Abutment and the Interior Pile (90-m Bridge, Clay, 3m Abutment, HP360X152 Strong and Weak Orientation).....	208
Figure 7.65 Rotation (Contraction) along the Abutment and the Interior Pile (90-m Bridge, Clay, 3m Abutment, HP360X152 Strong and Weak Orientation).....	208
Figure 7.66 Moment at the top of the Interior Pile (38-m Bridge, Clay, 3m Abutment, HP310X125 Weak and Strong Orientation).....	209
Figure 7.67 Moment (Expansion) along the Interior Pile (38-m Bridge, Clay, 3m Abutment, HP310X125 Weak and Strong Orientation).....	210
Figure 7.68 Moment (Contraction) along the Interior Pile (38-m Bridge, Clay, 3m Abutment, HP310X125 Weak and Strong Orientation).....	211

Figure 7.69 Moment (Expansion) along the Interior Pile (38-m Bridge, Sand, 3m Abutment, HP310X125 Weak and Strong Orientation)	212
Figure 7.70 Moment (Contraction) along the Interior Pile (38-m Bridge, Sand, 3m Abutment, HP310X125 Weak and Strong Orientation)	212
Figure 7.71 Moment (Expansion) along the Interior Pile (90-m Bridge, Clay, 3m Abutment, HP360X152 Weak and Strong Orientation)	213
Figure 7.72 Moment (Contraction) along the Interior Pile (90-m Bridge, Clay, 3m Abutment, HP360X152 Weak and Strong Orientation)	213
Figure 7.73 Stresses in the Interior Girder (38-m Bridge, Clay, 3m Abutment, HP310X125 Weak and Strong Orientation)	214
Figure 7.74 Stresses in the Interior Girder (90-m Bridge, Clay, 3m Abutment, HP360X152 Weak and Strong Orientation)	214
Figure 7.75 Backfill Pressure on the Abutment (38-m Bridge, Clay, 3m Abutment, HP310X125 Weak and Strong Orientation)	215
Figure 7.76 Backfill Pressure on the Abutment (90-m Bridge, Clay, 3m Abutment, HP360X152 Weak and Strong Orientation)	215
Figure 7.77 Displacement (Expansion) at Exterior Locations (38-m Bridge, Clay, Variable Abutment Height, HP310X125 Weak Orientation)	216
Figure 7.78 Displacement (Contraction) at the Exterior Location (38-m Bridge, Clay, Variable Abutment Height, HP310X125 Weak Orientation)	217
Figure 7.79 Rotation (Expansion) at the Exterior Location (38-m Bridge, Clay, Variable Abutment Height, HP310X125 Weak Orientation)	218
Figure 7.80 Rotation (Contraction) at the Exterior Location (38-m Bridge, Clay, Variable Abutment Height, HP310X125 Weak Orientation)	219
Figure 7.81 Displacement (Expansion) along the Abutment and the Interior Pile (38-m Bridge, Clay, Variable Abutment Height, HP310X125 Weak Orientation)	200
Figure 7.82 Rotation (Expansion) along the Abutment and the Interior Pile (38-m Bridge, Clay, Variable Abutment Height, HP310X125 Weak Orientation)	221
Figure 7.83 Moment at the Top of the Interior Pile (38-m Bridge, Clay, Variable Abutment Height, HP310X125 Weak Orientation)	222

Figure 7.84 Moment (Expansion) along the Interior Pile (38-m Bridge, Clay, Variable Abutment Height, HP310X125 Weak Orientation).....	223
Figure 7.85 Stresses in the Girders (38-m Bridge, Clay, Variable Abutment Height, HP310X125 Weak Orientation).....	224
Figure 7.86 Backfill Pressure on the Abutment (38-m Bridge, Clay, Variable Abutment Height, HP310X125 Weak Orientation).....	225
Figure 7.87 Displacement (Expansion) at Interior and Exterior Locations (38-m Bridge, Clay, 3m Abutment, PCP 356X356 versus HP310X125 Weak Orientation)	226
Figure 7.88 Displacement (Contraction) at Interior and Exterior Locations (38-m Bridge, Clay, 3m Abutment, PCP 356X356 versus HP310X125 Weak Orientation)	227
Figure 7.89 Rotation (Expansion) at Interior and Exterior Locations (38-m Bridge, Clay, 3m Abutment, PCP 356X356 versus HP310X125 Weak Orientation)..	228
Figure 7.90 Rotation (Contraction) at Interior and Exterior Locations (38-m Bridge, Clay, 3m Abutment, PCP 356X356 versus HP310X125 Weak Orientation)	228
Figure 7.91 Displacement (Contraction) along the Abutment and the Interior Pile (38-m Bridge, Clay, 3m Abutment, PCP 356X356 versus HP310X125 Weak Orientation)	229
Figure 7.92 Rotation (Contraction) along the Abutment and the Interior Pile (38-m Bridge, Clay, 3m Abutment, PCP 356X356 versus HP310X125 Weak Orientation)	230
Figure 7.93 Moment at the top of the Interior Pile (38-m Bridge, Clay, 3m Abutment, PCP 356X356 versus HP310X125 Weak Orientation)	231
Figure 7.94 Moment (Expansion) along the Interior Pile (38-m Bridge, Clay, 3m Abutment, PCP 356X356 versus HP310X125 Weak Orientation)	232
Figure 7.95 Moment (Contraction) along the Interior Pile	
(38-m Bridge, Clay, 3m Abutment, PCP 356X356 versus HP310X125 Weak Orientation)	232
Figure 7.96 Stresses in the Girders (38-m Bridge, Clay, 3m Abutment, PCP 356X356 versus HP310X125 Weak Orientation)	233
Figure 7.97 Backfill Pressure on the Abutment (38-m Bridge, Clay, 3m Abutment, PCP 356X356 versus HP310X125 Weak Orientation)	234
Figure 8.1 Deformed Shape of the Abutment and the Pile	236
Figure 8.2 Substructure Displacement Ratios (Weak, Contraction, Clay)	238
Figure 8.3 Substructure Displacement Ratios (Weak, Expansion, Clay)	239

Figure 8.4 Substructure Displacement Ratios (Weak, Contraction, Sand).....	240
Figure 8.5 Substructure Displacement Ratios (Weak, Expansion, Sand).....	240
Figure 8.6 Substructure Displacement Ratios (Strong, Contraction, Clay).....	241
Figure 8.7 Substructure Displacement Ratios (Strong, Expansion, Clay).....	241
Figure 8.8 Substructure Displacement Ratios (Strong, Contraction, Sand).....	242
Figure 8.9 Substructure Displacement Ratios (Strong, Expansion, Sand).....	242
Figure 8.10 Simplified Model for the Abutment Displacement	243
Figure 8.11 Substructure Rotation Ratios (Weak, Contraction, Clay).....	244
Figure 8.12 Substructure Rotation Ratios (Weak, Expansion, Clay).....	245
Figure 8.13 Substructure Rotation Ratios (Weak, Contraction, Sand)	245
Figure 8.14 Substructure Rotation Ratios (Weak, Expansion, Sand)	246
Figure 8.15 Substructure Rotation Ratios (Strong, Contraction, Clay)	246
Figure 8.16 Substructure Rotation Ratios (Strong, Expansion, Clay)	247
Figure 8.17 Substructure Rotation Ratios (Strong, Contraction, Sand).....	247
Figure 8.18 Substructure Rotation Ratios (Strong, Expansion, Sand).....	248
Figure 8.19 Displacement (Contraction) at Interior Location 2D Versus3D (38-m Bridge, Clay, 3m Abutment, HP310X125 Weak Orientation)	249
Figure 8.20 2D Versus 3D, Rotation (Contraction) at Interior Location (38-m Bridge, Clay, 3m Abutment, HP310X125 Weak Orientation)	250
Figure 8.21 Displacement (Contraction) at Exterior Location 2D Versus3D (38-m Bridge, Clay, 3m Abutment, HP310X125 Weak Orientation)	251
Figure 8.22 2D Versus 3D, Rotation (Contraction) at Exterior Location (38-m Bridge, Clay, 3m Abutment, HP310X125 Weak Orientation)	252
Figure 8.23 Displacement (Expansion) at Interior Location 2D Versus3D (38-m Bridge, Clay, 3m Abutment, HP310X125 Weak Orientation)	253
Figure 8.24 2D Versus 3D, Rotation (Expansion) at Interior Location (38-m Bridge, Clay, 3m Abutment, HP310X125 Weak Orientation)	254
Figure 8.25 Displacement (Expansion) at Exterior Location 2D Versus3D (38-m Bridge, Clay, 3m Abutment, HP310X125 Weak Orientation)	255
Figure 8.26 2D Versus 3D, Rotation (Expansion) at Exterior Location (38-m Bridge, Clay, 3m Abutment, HP310X125 Weak Orientation)	256

Figure 8.27 Displacement (Contraction) at Interior Location 2D Versus3D (90-m Bridge, Clay, 3m Abutment, HP360X152 Weak Orientation)	257
Figure 8.28 2D Versus 3D, Rotation (Contraction) at Interior Location (90-m Bridge, Clay, 3m Abutment, HP360X152 Weak Orientation)	258
Figure 8.29 Displacement (Contraction) at Exterior Location 2D Versus3D (90-m Bridge, Clay, 3m Abutment, HP360X152 Weak Orientation)	259
Figure 8.30 2D Versus 3D, Rotation (Contraction) at Exterior Location (90-m Bridge, Clay, 3m Abutment, HP360X152 Weak Orientation)	260
Figure 8.31 Displacement (Expansion) at Interior Location 2D Versus3D (90-m Bridge, Clay, 3m Abutment, HP360X152 Weak Orientation)	261
Figure 8.32 2D Versus3D, Rotation (Expansion) at Interior Location (90-m Bridge, Clay, 3m Abutment, HP360X152 Weak Orientation)	262
Figure 8.33 Displacement (Expansion) at Exterior Location 2D Versus3D (90-m Bridge, Clay, 3m Abutment, HP360X152 Weak Orientation)	263
Figure 8.34 2D Versus3D, Rotation (Expansion) at Exterior Location (90-m Bridge, Clay, 3m Abutment, HP360X152 Weak Orientation)	264
Figure 8.35 Pile Idealization as Equivalent Cantilever (Girton et al. 1989).....	265
Figure 8.36 Equivalent Cantilevers for Fixed-Head Piles Embedded in Uniform Soil (Girton et al. 1989).....	267
Figure 8.37 Pile's Displacement Components (Albhaisi 2003).....	272
Figure 8.38 Moment Distribution along the Idealized Pile (Albhaisi2003)	273
Figure 8.39 Simplified Model for the Abutment-Deck Rotation (Albhaisi, 2003).....	274
Figure 8.40 Simplified Model for the Abutment Displacement (Albhaisi 2003)	277
Figure 8.41 Equivalent shear length, l_{ev} (Albhaisi 2003).....	279
Figure A.1 Displacement at Interior and Exterior Locations (38-m Bridge, Clay, 3m Abutment, HP310X125 Strong Orientation)	288
Figure A.2 Displacement along the Abutment and the Interior Pile (38-m Bridge, Clay, 3m Abutment, HP310X125 Strong Orientation)	288
Figure A.3 Rotation at Interior and Exterior Locations (38-m Bridge, Clay, 3m Abutment, HP310X125 Strong Orientation)	289

Figure A.4 Rotation along the Abutment and the Interior Pile (38-m Bridge, Clay, 3m Abutment, HP310X125 Strong Orientation)	289
Figure A.5 Displacement at Interior and Exterior Locations (38-m Bridge, Sand, 3m Abutment, HP310X125 Strong Orientation)	290
Figure A.6 Displacement along the Abutment and the Interior Pile (38-m Bridge, Sand, 3m Abutment, HP310X125 Strong Orientation)	290
Figure A.7 Rotation at Interior and Exterior Locations (38-m Bridge, Sand, 3m Abutment, HP310X125 Strong Orientation)	291
Figure A.8 Rotation along the Abutment and the Interior Pile (38-m Bridge, Sand, 3m Abutment, HP310X125 Strong Orientation)	291
Figure A.9 Displacement at Interior and Exterior Locations (90-m Bridge, Clay, 3m Abutment, HP360X152 Strong Orientation)	292
Figure A.10 Displacement along the Abutment and the Interior Pile (90-m Bridge, Clay, 3m Abutment, HP360X152 Strong Orientation)	292
Figure A.11 Rotation at Interior and Exterior Locations (90-m Bridge, Clay, 3m Abutment, HP360X152 Strong Orientation)	293
Figure A.12 Rotation along the Abutment and the Interior Pile (90-m Bridge, Clay, 3m Abutment, HP360X152 Strong Orientation)	293
Figure A.13 Displacement at Interior and Exterior Locations (90-m Bridge, Sand, 3m Abutment, HP360X152 Strong Orientation)	294
Figure A.14 Displacement along the Abutment and the Interior Pile (90-m Bridge, Sand, 3m Abutment, HP360X152 Strong Orientation)	294
Figure A.15 Rotation at Interior and Exterior Locations (90-m Bridge, Sand, 3m Abutment, HP360X152 Strong Orientation)	295
Figure A.16 Rotation along the Abutment and the Interior pile (90-m Bridge, Sand, 3m Abutment, HP360X1152 Strong Orientation)	295
Figure A.17 Moment at the Top of the Pile (38-m Bridge, Clay, 3m Abutment, HP310X125 Strong Orientation)	296
Figure A.18 Moment at the top of the Pile (90-m Bridge, Clay, 3m Abutment, HP360X152 Strong Orientation)	296

Figure A.19 Moment Loads along the Interior Pile (38-m Bridge, Clay, 3m Abutment, HP310X125 Strong Orientation)	297
Figure A.20 Moment along the Interior Pile (90-m Bridge, Clay, 3m Abutment, HP360X152 Strong Orientation)	297
Figure A.21 Moment at the Top of the Pile (38-m Bridge, Sand, 3m Abutment, HP310X125 Strong Orientation)	298
Figure A.22 Moment along the Interior Pile (38-m Bridge, Sand, 3m Abutment, HP310X125 Strong Orientation)	298
Figure A.23 Moment at the Top of the Pile (90-m Bridge, Clay, 3m Abutment, HP360X152 Strong Orientation)	299
Figure A.24 Moment along the Interior Pile (90-m Bridge, Sand, 3m Abutment, HP360X152 Strong Orientation)	299
Figure A.25 Stresses in the Girders (38-m Bridge, Clay, 3m Abutment, HP310X125 Strong Orientation)	300
Figure A.26 Stresses in the Girders (38-m Bridge, Sand, 3m Abutment, HP310X125 Strong Orientation)	300
Figure A.27 Stresses in the Girders (90-m Bridge, Clay, 3m Abutment, HP360X152 Strong Orientation)	301
Figure A.28 Stresses in the Girders (90-m Bridge, Sand, 3m Abutment, HP360X152 Strong Orientation)	301
Figure A.29 Rotation (Expansion) at the Interior Location (90-m Bridge, Clay, 3m Abutment, 360X152 Weak Orientation with Pile Enclosure) .	302
Figure A.30 Displacement (Expansion) along the Abutment and the Interior Pile (90-m Bridge, Clay, 3m Abutment, HP310X125 Weak Orientation with Pile Enclosure)	302
Figure A.31 Rotation (Expansion) along the Abutment and the Interior Pile (90-m Bridge, Clay, 3m Abutment, HP310X125 Weak Orientation with Pile Enclosure)	303
Figure A.32 Moment (Expansion) along the Exterior Pile (90-m Bridge, Clay, 3m Abutment, HP310X125 Weak Orientation with Pile Enclosure)	303
Figure A.33 Moment at Top of Interior Pile (Contraction) 2D Versus 3D (38-m Bridge, Clay, 3m Abutment, HP310X125 Weak Orientation)	304

Figure A.34 Moment at Top of Exterior Pile (Contraction) 2D Versus 3D (38-m Bridge, Clay, 3m Abutment, HP310X125 Weak Orientation)	304
Figure A.35 Moment at Top of Interior Pile (Expansion) 2D Versus 3D (38-m Bridge, Clay, 3m Abutment, HP310X125 Weak Orientation)	305
Figure A.36 Moment at Top of Exterior Pile (Expansion) 2D Versus 3D (38-m Bridge, Clay, 3m Abutment, HP310X125 Weak Orientation)	305
Figure A.37 Moment at Top of Interior Pile (Contraction) 2D Versus 3D (90-m Bridge, Clay, 3m Abutment, 360X152 Weak Orientation with Pile Enclosure)	306
Figure A.38 Moment at Top of Exterior Pile (Contraction) 2D Versus 3D (90-m Bridge, Clay, 3m Abutment, HP310X125 Weak Orientation with Pile Enclosure).....	306
Figure A.39 Moment at Top of Interior Pile (Expansion) 2D Versus 3D (90-m Bridge, Clay, 3m Abutment, HP310X125 Weak Orientation with Pile Enclosure).....	307
Figure A.40 Moment at Top of Exterior Pile (Expansion) 2D Versus 3D (90-m Bridge, Clay, 3m Abutment, HP310X125 Weak Orientation with Pile Enclosure).....	307
Figure B.1 Stress Distribution in the Interior Girder (Contraction, Girder's End) (38-m Bridge, Very Stiff Clay, 3m Abutment, HP310X125 Weak Orientation)	308
Figure B.2 Stress Distribution in the Interior Girder (Contraction, Mid-Span) (38-m Bridge, Very Stiff Clay, 3m Abutment, HP310X125 Weak Orientation)	308
Figure B.3 Stress Distribution in the Interior Girder (Expansion, Girder's End) (38-m Bridge, Very Stiff Clay, 3m Abutment, HP310X125 Weak Orientation)	309
Figure B.4 Stress Distribution in the Interior Girder (Expansion, Mid-Span) (38-m Bridge, Very Stiff Clay, 3m Abutment, HP310X125 Weak Orientation)	309
Figure B.5 Stress Distribution in the Interior Girder (Contraction, Girder's End) (90-m Bridge, Medium Clay, 3m Abutment, HP360X152 Weak Orientation).....	310
Figure B.6 Stress Distribution in the Interior Girder (Contraction, 1/4-Span from End) (90-m Bridge, Medium Clay, 3m Abutment, HP360X152 Weak Orientation).....	310
Figure B.7 Stress Distribution in the Interior Girder (Contraction, At Pier) (90-m Bridge, Medium Clay, 3m Abutment, HP360X152 Weak Orientation).....	311
Figure B.8 Stress Distribution in the Interior Girder (Expansion, Girder's End) (90-m Bridge, Stiff Clay, 3m Abutment, HP360X152 Weak Orientation)	311

Figure B.9 Stress Distribution in the Interior Girder (Expansion, Mid-Span)	
(90-m Bridge, Stiff Clay, 3m Abutment, HP360X152 Weak Orientation)	312
Figure B.10 Stress Distribution in the Interior Girder (Expansion, At Pier)	
(90-m Bridge, Stiff Clay, 3m Abutment, HP360X152 Weak Orientation)	312
Figure B.11 Stress Distribution in the Piles (Contraction)	
(38-m Bridge, Soft Clay, 3m Abutment, HP310X125 Weak Orientation).....	313
Figure B.12 Stress Distribution in the Piles (Contraction)	
(38-m Bridge, Stiff Clay, 3m Abutment, HP310X125 Strong Orientation).....	313
Figure B.13 Stress Distribution in the Piles (Expansion)	
(90-m Bridge, Stiff Clay, 3m Abutment, HP360X152 Weak Orientation)	314
Figure B.14 Stress Distribution in the Piles (Expansion)	
(90-m Bridge, Stiff Clay, 3m Abutment, HP360X152 Strong Orientation).....	315

LIST OF SYMBOLS

A_s	=	non-dimensional coefficient
B_s	=	non-dimensional coefficient
b	=	width of pile
C_u	=	clay shear strength
dP	=	change in backfill pressure
E_s	=	soil modulus
E	=	structural steel modulus of elasticity
F_y	=	yield stress
F_{af}	=	abutment interface friction
h	=	clear height of the web plate between flanges
H	=	wall height
J	=	non-dimensional coefficient
K	=	coefficient of earth pressure
k	=	modulus of subgrade reaction
K_0	=	at-rest coefficient of earth pressure
K_a	=	active coefficient of earth pressure
K_p	=	passive coefficient of earth pressure
K_{spring}	=	spring constant
L	=	bridge length
M_Y	=	moment at yield
M_{sh}	=	moment at strain hardening
M_u	=	moment at ultimate
P	=	pile axial force
P_y	=	pile axial yield force
p	=	lateral soil resistance per unit length of pile
p_{unw}	=	ultimate soil resistance without wedge action
p_y	=	axial yield capacity of the section
p'	=	mean effective stresses

P_p	=	soil pressure load
(p)	=	pressure at any depth
Q_u	=	ultimate soil strength
s	=	normalized critical stress
t_f	=	flange width
t_w	=	web width
y	=	lateral deflection of the soil at the same location
y_y	=	deflection of soil at ultimate resistance
y_{50}	=	50% (one-half) of the deflection of soil at ultimate resistance
z_t	=	depth of the soil under wedge action
z	=	soil depth measured from the ground surface
U	=	global displacement in the x-direction
V	=	global displacement in the y-direction
W	=	global displacement in the z-direction
α	=	thermal expansion coefficient
α_f	=	slenderness parameters for the flange
α_w	=	slenderness parameters for the web
β	=	the angle of the wedge with the ground surface
γ	=	unit weight of soil
Δ	=	wall displacement
Δ_B	=	total displacement of the bridge
Δ_p	=	displacement of the pile
Δ_A	=	displacement of the top of the abutment relative to the top of the pile
Δ_{Bc}	=	total displacement of the bridge at contraction
Δ_{Be}	=	total displacement of the bridge at expansion
ΔL	=	top of abutment displacement
ΔT	=	change in temperature
ϵ	=	tensile Stress
ϵ_{sh}	=	strain in steel at strain hardening
ϵ_u	=	ultimate strain

ε_{cr}	=	critical strain at local buckling
ε_{50}	=	strain corresponding to one-half the maximum principle stress difference
θ_x	=	local or global rotation in the x-direction
θ_y	=	local or global rotation in the y-direction
θ_z	=	local or global rotation in the z-direction
θ_α	=	nodal rotation for thick shells
θ_β	=	nodal rotation for thick shells
λ_p	=	limiting width to thickness ratios for compact sections
λ_r	=	limiting width to thickness ratios for non-compact sections
ρ_d	=	in-situ dry densities
σ	=	tensile stress
σ_{cr}	=	critical stress at local buckling
σ_u	=	ultimate stress
σ_y	=	yield stress
ϕ_y	=	curvature at yield
ϕ_{sh}	=	curvature at strain hardening
ϕ_u	=	curvature at ultimate
\emptyset	=	angle of internal friction

CHAPTER 1

INTRODUCTION

1.1 GENERAL

Conventional (jointed) bridges have expansion joints and flexible bearings to allow for the expansion and contraction of the bridge superstructure due to daily and seasonal temperature variations. These bridges have at least one expansion joint and one set of bearings at each end of the bridge. A single span jointed bridge is shown in Figure 1.1. The size and details of the expansion joints and the bearings depend mainly on the bridge geometry, structural materials, and seasonal temperature changes at the bridge site. These expansion joints and bearings require special handling during construction because of the small construction tolerance allowed and they are expensive in terms of material, installation and maintenance costs. They require periodic inspection and maintenance and may need to be replaced several times throughout the bridge life. This is especially true for areas with considerable snow amounts where deicing chemicals are used throughout the cold season and where snowplows could repeatedly hit and damage the joints. Furthermore, expansion joints may allow water and deicing chemicals to penetrate through them and cause extensive deterioration to the bearings, superstructure and substructure components.

Leakage at the joint accounts for 70% of the deterioration at the end of the girders (Maruri and Petro, 2005). Consequently, expansion joints and bearings on bridges have provided considerable construction and maintenance challenge for most transportation agencies.

For the above reasons, many transportation agencies around the world consider the elimination of expansion joints and end bearings when possible and instead build jointless (Integral) bridges. The elimination of expansion joint will reduce the construction cost, maintenance cost, overcome many of the maintenance problems, and increase the stability and durability of the bridges. These economic and functional advantages are generally recognized by bridge engineers.

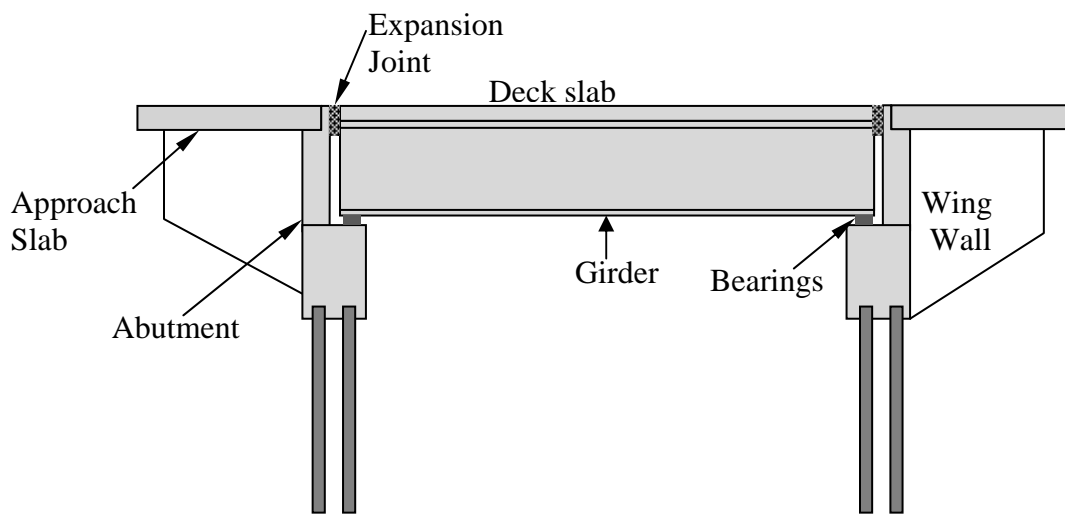


Figure 1.1 Typical Single - Span Jointed Bridge

Integral bridges are becoming popular in many parts of the world and are considered as a more economical alternative to conventional jointed bridges. More integral bridges are built every year in the United States and all over the world. In fact, according to Tennessee Department of Transportation (TDOT), 85% of the new bridges built in the State are integral bridges (Wasserman 2009).

In the United Kingdom, British Highways Agency Design Manual for Roads and Bridges recommends that all new bridges less than 60 meters (200 feet) in length and skews not

exceeding 30° shall be designed as integral bridges. A 2004 survey about integral bridges carried out by the Federal Highway Administration (FHWA) and West Virginia University (WVU) (Maruri and Petro, 2005) shows that there are approximately 13,000 integral bridges in service in the United States with 9,000 of those are fully integral abutment bridges with no joints. The survey also suggests that generally the number of integral abutment bridges has increased in the past decade. Northern States have more integral abutment bridges than southern States with most transportation agencies plan to replace jointed bridges with integral bridges when conditions permit.

An integral bridge is single-span or multiple-span bridge with a continuous superstructure built monotonically with the abutment. The abutment is usually short (stub) and supported by a single row of piles to provide a laterally flexible system to accommodate the expansion and contraction of the superstructure due to temperature variations. A sketch for a typical single-span Integral Abutment Bridge is shown in Figure 1.2.

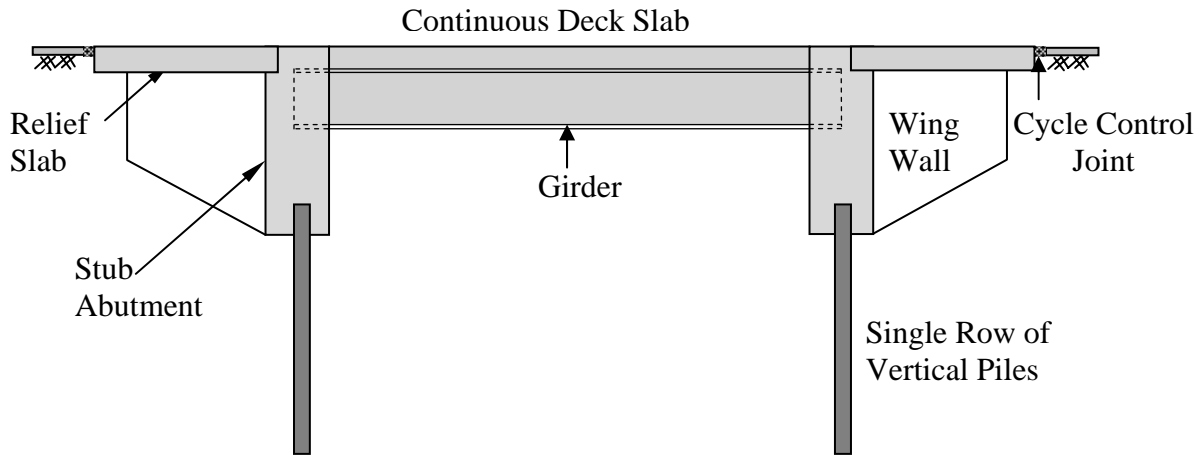


Figure 1.2 Typical Single - Span Integral Bridge

In a conventional jointed bridge, the bearings on top of the abutment will transfer mainly vertical loads from the superstructure to the abutment. These bearings usually have a small stiffness in the horizontal direction to allow for the movement of the superstructure due to temperature variations. Therefore, the abutment provides negligible constrain to the lateral movement or the rotation of the superstructure. As a result, only a small horizontal force is transferred from the superstructure to the abutment or vice versa. Bridge engineers consider that active earth load is the only lateral force that affects the abutment throughout the life of the bridge.

Unlike the case of conventional jointed bridges, the superstructure and the abutments of an integral bridge are built monolithically and will move together. When the temperature

increases, the superstructure will expand pushing the abutment towards the backfill soil and bring it to its passive status which may subject the abutments to large forces. In return, the substructure and backfill soil will exert restraining compression forces (secondary forces) in the superstructure. When the temperature drops, the superstructure will contract pulling the abutment away from backfill soil and active soil conditions will develop. The substructure will exert restraining tension forces on the superstructure. The magnitude of these compression and tension forces depends on the length and material of the superstructure, temperature changes and the lateral stiffness of the substructure and the backfill. These axial forces could reach significant levels and need to be considered in the design of the superstructure and the substructure (Burke, 2009). To minimize these force effects most of the transportation agencies limit the length and the skew angle of integral abutment bridges. Moreover, the height of the abutments in integral bridges are kept at minimum height and called stub abutments. In addition and to minimize the restraining effect of the foundation on the abutments and superstructure and to provide a relatively flexible support system, only a single row of vertical piles is used to support the abutment. These piles are usually steel H-Piles. In few recent cases, bridge engineers used prestressed concrete piles, concrete filled steel pipes, and drilled shafts to support the abutment. In the case of H-Piles, some bridge engineers choose to orient the piles to bend around the weak axis in order to further increase the flexibility of the foundation supporting the abutment.

1.2 PROBLEM STATEMENT

Neither AASHTO-LRFD bridge design specifications nor the Standard AASHTO bridge design specifications have provided design criteria for the design of integral abutment bridges. In the absence of unified design criteria for integral bridges, most States developed their own design criteria and geometric limits. These limits are mainly imposed on the maximum bridge length, skew angle, pile type, pile orientation and the type and compaction level of backfill material behind the abutment. For example the State of Oklahoma limits the total bridge length to 200-feet and the skew angle to zero while the neighboring State of Missouri limits their integral bridges to 600-feet with no limits on the skew angle. Tennessee, who owns the longest integral bridge in the nation with a total length of over 1,175 feet (358 m), limits the bridge movement at the abutment to two inches with no limits on the skew angle while California uses one inch to cap the movement and limits the skew angle to 30 degrees to minimize the thermal effects on their integral bridges. The limit on the skew angle used by Minnesota is inversely proportional to the length of the bridge with 45 degrees as the absolute maximum skew angle.

Bridge engineers try to reduce the stiffness of the substructure to accommodate the movement of the superstructure and to minimize the stresses in the superstructure during thermal expansion and contraction. They usually use a stub abutment supported by a single row of piles. A FHWA and WVU survey (Maruri and Petro, 2005) shows that 70% of the States use bearing type steel H-Piles to support integral bridges without consensus on the orientation of the piles with respect to the centerline of the bearings. 46% of the States orient the piles so that the pile's weak axis is parallel to centerline of the bearings while 33% use a strong axis orientation. The rest of the States either have no preference

or leave it to the designer to decide on the pile orientation. To further reduce the stiffness of the substructure, many States enclose the top part of the H-Piles by a sleeve and fill the sleeve with loose sand or crushed stones.

Some states (e.g. Iowa and Tennessee) consider, in addition to steel H-Piles, prestressed concrete piles to support the abutment. Although drilled shaft foundation are considered much stiffer than other deep foundation types and are not allowed to be used by many States in the foundation of integral bridges, Hawaii used drilled shaft to support integral abutment because of the severe corrosion conditions in the State that prohibits the use of steel H-Piles (Ooi et al. 2010).

Many States use the same backfill behind the abutment as for jointed bridge and most States require that the backfill be compacted. Some States require the use of polystyrene or other compressible or porous material behind the abutment in order to reduce the earth pressure on the bridge.

For some States these limits and criteria discussed above are the same for both steel and concrete bridge while other States use different limits for different bridge types. In general, these limits are based on the State experience with existing integral bridges and limited research. Many States provide design details and recommendations to be used by bridge engineers. These recommendations and details have continuously changed in the past decade. In general bridge engineers used different guidelines and different techniques to analyze and design integral bridges.

While the goal of the design criteria and limits discussed above is the same which is to limit the movement and stresses in integral bridges by limiting the length and skew of the bridge and by reducing the stiffness of the substructure, the large variation between the

limits and practice clearly indicates the need for more research to better understand the behavior IABs and to improve the performance of IABs.

1.3 RESEARCH OBJECTIVE

The objective of this research is to study effect of substructure stiffness on the performance of integral abutment bridges under thermal loads. To achieve this objective, the following steps will serve as a guide throughout the research:

- Perform an extensive literature review of the available information on the different factors that affect the behavior of integral bridges under lateral loads. These factors include but not limited to structural materials, geometry of integral bridges, current practice in the design of integral bridges, soil structure interaction and modeling of integral bridges for analysis.
- Analyze two integral bridges using finite element method (FEM). The FEM software LUSAS will be used for this purpose. The finite difference software LPILE will be utilized to adjust the soil parameters for the foundation. Both bridges will depict real life bridges constructed recently in the United States.
- Validate the accuracy of the FEM models. The models will be validated using the analytical and experimental data available in the literature.
- Perform a parametric study to investigate the effect of the substructure stiffness on the behavior of integral bridges.
- Summarize the results from the parametric study.

1.4 EXPECTED CONTRIBUTION

The following are the expected contribution of this research:

- Provide a better understanding of the effect of the substructure stiffness on the behavior of integral bridges.
- Provide recommendations to improve the performance of integral bridges.
- Provide simple equations and charts to help bridge engineers in the analysis and design of IABs.

1.5 STRUCTURE OF THE DISSERTATION

The dissertation is organized into nine chapters. After the introduction in chapter one, an extensive literature review is presented in chapter two. Among other subjects, the literature review provides a brief history of IABs in the United States and around the world. It also summarizes the recent developments and research activities in the field of IABs and the current practice in the design and construction of IABs. Chapter three presents a description of the different types of foundations used to support IABs with emphasis on steel H-Piles which are the most common piles used to support IABs in the United States.

The soil-structure interaction is presented in chapter four. In this chapter, detailed discussions on the behavior of piles under lateral loads in clay and in sand are presented followed by a discussion on the modeling of backfill soil. Chapter five introduces the 3D finite element models used throughout the study and the validation of the 3D models using field data available in the literature. The substructure parameters under investigation and the setup of the parametric study are presented in chapter six followed by the results of the parametric study in chapter seven which also includes discussions on the effects of the various parameters on the behavior of IABs.

Chapter eight presents a comparison of the results obtained from three-dimensional analysis to those obtained from simple two-dimensional analysis. It also introduces simple equations and charts to calculate the displacement and rotation along the substructure. Finally, the summary and conclusions of this research are presented in chapter nine. Appendix A contains additional figures showing additional results from the parametric study. The distribution of stresses in the girders and the piles is presented in Appendix B.

CHAPTER 2

LITERATURE REVIEW AND BACKGROUND

2.1 GENERAL

When compared to conventional jointed bridges, the design and construction of IABs is relatively new and it is fair to say that very few bridge engineers have experience with IABs. The same is true for the literature available on IABs. The literature available on IABs is fairly recent and most of the research on IABs was conducted in the last 15 years. As a first step in the research, an extensive literature review was conducted on the available literature in the field of IABs. The literature review will start by presenting a historical background on IABs and the attributes and limitations of these bridges. Then, the review will focus on the factors that affect the performance of integral bridges. Among these factors are foundation types and properties, soil structure interaction, the gravity and temperature loading on IABs, and the geometry of IABs. The literature review will also research the latest developments in the field of Integral Bridges and the current design practice in the United States and other regions around the world. Many in-service IABs were instrumented for research purposes. The results and recommendations from some of these research projects will be presented. The FEM analysis results in this study will also be verified by the data available in the literature review.

2.2 HISTORICAL BACKGROUND

The use of Integral bridges began thousands of years ago in the shape of masonry arches. Today there are many of similar arches survived for more than a hundred years (Hambly 1997). The construction of reinforced concrete arch bridges in North America began in the early decades of the 20th century (Burke 1993a, b). Colorado built the first integral bridge in the United States in 1920 followed by Massachusetts in 1930 (Paraschos and Amde 2011). The trend of building IABs and eliminating the deck joints at piers and abutments started after the moment distribution method was first developed in early 1930s (Cross 1932) allowing engineers to analyze statically indeterminate structures such as rigid frame bridges. Ohio and Kansas started building IABs in the 1930s followed by Oregon, Pennsylvania, North Dakota and Mississippi in the 1940s. By the mid-20th century, concrete rigid frame bridges became a standard type of construction for many departments of transportation (Burke, 1993b).

Washington and Tennessee had their first integral bridges in the 1960s and New York State began building integral bridges in the late 1970s (Alampali and Yannotti 1998). By 1980, 30 states were using integral abutment bridges as a standard form of construction. The State of New Jersey had its first integral bridge built in 1998 and has a very satisfying experience with IABs since. The history of use of IABs in the United States is summarized in Table 2.1.

Japan and South Korea had their first integral bridges built in the late 1990s and early 2000s respectively. The use of IABs in Australia is not as widespread as in the United States (Connal, 2004).

Table 2.1 History of Use of IABs in the United States (Paraschos and Amde 2011).

State	Year First Built IABs	State	Year First Built IABs
Alabama	Never	Montana	1970
Alaska	1975	Nebraska	1977
Arizona	1975	Nevada	1978
Arkansas	2001	New Hampshire	1992
California	1950	New Jersey	1988
Colorado	1920	New Mexico	1955
Connecticut	1995	New York	1980
Delaware	Never	North Carolina	2006
Florida	1989	North Dakota	1960
Georgia	1970	Ohio	1935
Hawaii	2001	Oklahoma	1980
Idaho	1970	Oregon	1940
Illinois	1978	Pennsylvania	1946
Indiana	1978	Rhode Island	2004
Iowa	1965	South California	2001
Kansas	1965	South Dakota	1948
Kentucky	1970	Tennessee	1965
Louisiana	Never	Texas	1994
Maine	1988	Utah	1984
Maryland	1990	Vermont	1981
Massachusetts	1930	Virginia	1982
Michigan	1991	Washington	1965
Minnesota	1960	West Virginia	1994
Mississippi	1945	Wisconsin	1960
Missouri	1969	Wyoming	1957

A 2009 survey conducted by University of Maryland (Paraschos and Amde 2011) shows that as of 2009, 41 out of 50 States currently use IABs. Figure 2.1 Depicted from the survey shows the evolution of IABs in the United States. The figure shows rapid increase in the use of IABs in the United States between 1930 and 1994. The survey indicates that Alabama, Delaware and Louisiana have never used IABs in their infrastructure. The survey also indicates that six States have decided to stop using IABs. Alaska, Arizona and Mississippi discontinued the use of IABs because they found serious problems in recently constructed bridges and Florida, Texas and Washington discontinued the construction of IABs because they think IABs do not offer any advantages over jointed bridges.

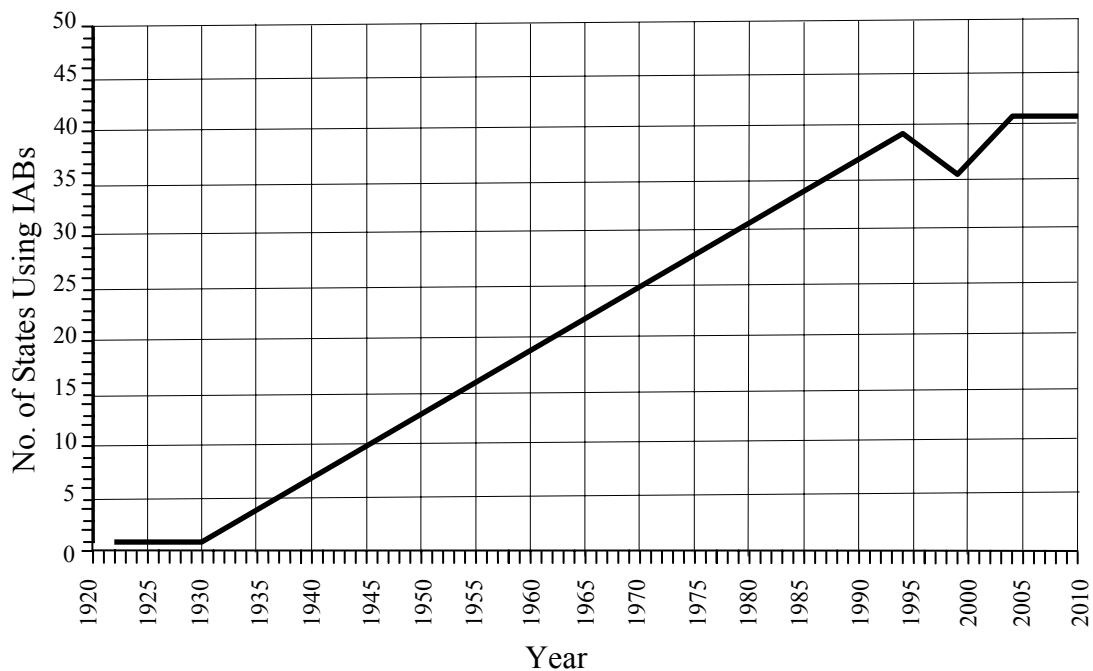


Figure 2.1 Evolution of IABs in the United States (Paraschos and Amde 2011)

The survey also indicates that 25 States reported no issue with performance of IABs and 12 States reported minor to moderate problems with their IABs. 4 States eliminated problems faced in IABs by adjusting their design and construction practice. The survey also shows that Missouri reported the highest number of IABs in their inventory with more than 4,000 IABs. Table 2.2 shows a breakdown of the number of integral bridges designed and built between 1995 and 2004 in the United States (Maruri and Petro, 2005).

Table 2.2 Number of In-Service IABs Designed and Built Since 1995 (Maruri and Petro 2005)

Bridge Type	DESIGNED since 1995	BUILT since 1995	IN SERVICE (TOTAL)
Integral Abutment	~ 7000	~ 8900	~ 13000
Full Integral	~ 5700	~ 6400	~ 9000
Semi Integral	~ 1600	~ 1600	~ 4000
Deck Extension	~ 1100	~ 1100	~ 3900

The number of IABs in the United States is increasing rapidly.

In the past few decades, engineers started to notice the benefits of integral bridges over jointed bridges in terms of their superior stability and serviceability and lower maintenance demand. Consequently, most bridge engineers focused their attention on the design and construction practice of integral bridges. Nowadays, most departments of transportation in the United States consider the integral bridge construction as a standard form of construction. 85% of the new bridges constructed in Tennessee are integral bridges. New Jersey Department of Transportation (NJDOT) requires bridge designers to consider integral abutment Type Bridge as the preferred choice for new bridges or bridge replacement. The following is a quote from New Jersey Department of Transportation (NJDOT 2009) design manual for bridges and structures “integral abutment jointless type bridge structures are single or multiple span continuous bridge structures that have their

superstructure cast integrally with their substructure. Due to the elimination of deck joints, construction and maintenance cost are lowered and fewer foundation piles are required. Also, research has indicated that this type of bridge structures will perform better than a conventional bridge structure in a seismic event. For these reasons, Designers should consider an Integral Abutment Jointless Bridge as the preferred choice when planning for a bridge replacement or new bridge design”.

In the United Kingdom, Bridge engineers use integral bridges routinely for short and medium bridges.

2.3 ATTRIBUTES OF INTEGRAL ABUTMENT BRIDGES

The primary attribute of integral bridges is their jointless construction. Open-deck joints permit contaminated deck drainage to penetrate joints and cause extensive below-deck deterioration (Burke 1993a). Also, the presence of expansion joints and expansion bearings increases the construction cost of jointed bridges. Not only the materials for expansion joints and expansion bearings are expensive, the small tolerance associated with them could also create construction problems. Integral bridges are more efficient in resisting longitudinal and lateral forces. Unlike the abutments in jointed bridges, abutments in integral bridges carry longitudinal and lateral loads and can help reduce the size of intermediate bents. Abutments in integral bridges can also carry vertical loads in both the up and down directions which lead to solving the uplift problem at the end spans and allow the bridge engineers to have more flexibility in determining the length of the end spans in continuous construction. These end spans will also experience a better and more reliable live load distribution than in jointed bridges because of the action of the integral abutment. Under seismic loads, Integral abutments provide a very reliable seating

for the superstructure and that could prevent the loss of bridge seating often seen after earthquakes. Furthermore, jointed bridges take more time to build and need much more maintenance than integral bridges. More recently, bridge engineers have recognized these economical and functional advantages as well as the improved durability of integral abutment bridges, in lieu of expansion joints and bearings (Thippeswamy and Gangaro, 1995).

Only a single row of uniformly spaced vertical piles constitutes the abutment foundation of integral abutment bridges. Typical abutment foundation of jointed bridges consists of at least two or more rows of both vertical and battered piles. It is a well-known fact that the material and installation cost of piles is very expensive. As integral abutment bridges possess less number of piles at abutments than that of jointed bridges, their economical advantage becomes more clear (Burke 1993a). Furthermore, the behavior of vertical piles is better understood than that of battered piles. Extensive research has been conducted to predict the behavior of laterally and axially loaded vertical piles (Abendroth and Greiman 1989; Anagnostopoulos and Georgiadis 1993; Amde et al. 1997). However, research on lateral behavior of battered piles is scarce. This also makes the design of integral abutment bridges more reliable as only vertical piles are used at the abutments. Researchers have found that the distribution of stress slab in IABs is more uniform than that in their jointed counterparts (Mourad and Tabsh 1999).

2.4 LIMITATIONS OF INTEGRAL ABUTMENT BRIDGES

Lengths of integral abutment bridges should be limited to minimize the detrimental effects of large longitudinal movements of the bridge on the performance of its structural components (Burke 1993a). Continuous steel bridges with integral abutments have performed successfully for years in the 91 meter (300 foot) range in North Dakota, South Dakota, and Tennessee and continuous concrete integral bridges, in the range of 152-183 meters (500-600 feet) long have been constructed in Kansas, California, Colorado, and Tennessee (Greimann et al. 1987). For years, bridge design engineers have depended on such crude data to determine the maximum length of integral bridges. In some cases, the decision on the maximum length of an integral abutment bridge has been based on non-technical criteria. In Tennessee, a structural engineer can measure his/her design ability by seeing how long a bridge he/she can design without inserting an expansion joint (Loveall 1985). The State of Tennessee is leading the way in constructing integral bridges with maximum bridge length exceeding double the maximum allowed in most of the other States. State Route 50 over Happy Hollow Creek in Tennessee is 358 meters in length. The effect of temperature on Integral bridges with lengths less than 90 meters is usually small and can be neglected (Yochia 1997). New York and New Jersey limit the maximum length of their integral bridges to 140 meters (450 feet) and recommends the use of steel H-Piles oriented to bend about their weak axis for integral bridges with lengths exceeding 47 meters (150 feet) (NYSODT 2008, NJDOT 2009). Washington State department of transportation has specified maximum lengths for integral bridges according to their types (Van Laund and Brecto 1999). They limit the lengths of their steel and concrete bridges to 91 meters and 107 meters respectively. The province of

Ontario in Canada limits the maximum length of its steel bridges to 100 meters and its concrete bridges to 125 meters (Husain and Bagnariol 1996).

Stresses in the steel H-Piles supporting the abutments could reach the yield strength for long bridges (Girton et al. 1989). Based on the capacity of steel H-Piles, Albhaisi (2003) suggests that for concrete bridges the maximum length range shall be between 180 - 230 meters in cold climates and 200 – 280 meters in moderate climates and for steel bridges, the range shall be between 100 - 110 meters in cold climates and 110 – 170 meters in moderate climates.

Other researchers suggest that IABs should not be used where skew is larger than 30° or where the horizontal curvature exceeds 5° as large axial compressive or tensile stresses may be imposed on the piles in such bridges (Burke 1993a). For integral bridges with a large angle of skew, diagonal deck slab cracks located at acute corners of the bridge are occasionally reported (Burke 1999).

The lateral movement of the piles may be restricted if the surrounding foundation soil has large stiffness. In such cases, predrilled oversize holes filled with loose sand or crushed stones are generally provided around the piles to facilitate their lateral movements (Abendroth and Greimann 1989; Husain and Bagnariol 1996).

2.5 DESIGN CODES

2.5.1 AASHTO Code

Neither AASHTO-LRFD bridge design specifications nor the standard AASHTO bridge design specifications have provided design criteria for the design of integral bridges. Both design documents including the recently published fifth edition of AASHTO-LRFD bridge design specification (AASHTO 2010) refer the designer to FHWA technical advisory T 5140.13 (FHWA 1980) for design and maximum length considerations and let the States have the final decision in design and construction based on local experience. In fact most of the advancements in the field of IABs happened in the last three decades after its technical advisory was published. So the advisory is outdated and does not provide the guidance needed for the design and construction of modern IABs.

AASHTO-LRFD bridge design specifications define integral abutments as “abutments that are rigidly attached to the superstructure and are supported on a spread or deep foundations capable of permitting necessary horizontal movements”. It does not allow the construction of integral abutments on spread footings founded or keyed into rock unless one end of the span is free to displace longitudinally.

The specification requires that integral abutments be designed to accommodate and/or resist creep, shrinkage and thermal deformation of the superstructure and that the superstructure movement calculations shall consider temperature, creep and long-term loss of prestress force. To avoid water intrusion behind the abutment, the specification requires that the approach slab be directly connected to the abutment and not to the wingwall and to provide drainage for any entrapped water. The specification also suggests the use of refined analysis methods for skewed bridges and/or curved steel

bridges with integral abutments. In the refined analysis the stiffness or the lateral restraint provided by integral abutments shall be considered.

The requirements provided above sum all the provisions related to the design of IABs in the current AASHTO-LRFD bridge design specifications. In the absence of unified design criteria for integral bridges, most States developed their own design criteria and geometric limits. The current practice in the design and construction of IABs will be discussed in detail in subsequent sections.

2.5.2 International Codes

Similar to the case in the United States, European codes have not provided a uniform design criteria for the design of integral bridges (White et al. 2010) and different design criteria are followed by different countries in Europe. For example, while Finland, England and Ireland have limits on skew angle, Germany and Sweden have no restrictions. The same is true in the Australian experience. The Australian Bridge Design Code does not provide particular guidance on the design of IABs (Connal 2004) and bridge engineers must refer to the general design requirements contained in the code and to local experience.

In a supplement to the Canadian Highway Bridge Design Code (CHBDC 2006), the British Columbia Ministry of Transportation (BCMOT 2007) requires the design of IABs to take into account for soil-structure interaction behind the abutments, specifically the lateral soil pressure build-up and settlements due thermal cycling. Similar to the AASHTO-LRFD, the supplement requires that Integral abutments shall not be constructed on spread footings founded on or keyed into rock and that the movement calculations shall consider temperature, creep, and long-term prestress shortening in determining potential movements at the abutment. Moreover, the supplement sets the

maximum skew angle for IABs to be 30° . The supplement also refers the bridge engineers to useful and acceptable design standards including the British Standard BA 42/96 (including Amendment No. 1 dated May 2003) which requires that all bridges less than 60 m (200 ft) and with a skew less than 30° be constructed as an Integral Abutment Bridge unless there are overriding reasons. The document adds “Experience in North America with jointless superstructures of limited backwall height using integral pile-supported end-diaphragms, or semi-integral abutment designs has demonstrated that superstructures of this type may be designed longer than the 60 meter limit in BA 42/96, provided that the effects described therein are properly accounted for”. The current practice in the design and construction of IABs in Europe, Australia and Canada will be discussed in detail in subsequent sections.

2.6 CURRENT PRACTICE

In the absence of unified design criteria for IABs in the United States and around the world most States within the United States, countries in Europe, Australia, Canada and other countries have developed their own design criteria and geometric limits on IABs to ensure the safety of their bridges. These limits are mainly imposed on the maximum bridge length, skew angle, pile type, pile orientation, backfill material type and degree of compaction and other structural and geotechnical properties of IABs. This section discusses the current practice in the design and construction of IABs in the United States and around the world.

2.6.1 Limits on the Geometry of IABs

2.6.1.1 Limits on the Geometry of IABs in the United States

To limit the stresses in various parts of IABs and to insure the safety of their bridges, most States enforce limits on the geometry of IABs. The main aim of these limits is to limit the total and differential lateral movement of the superstructure and subsequently limit the stresses in the superstructure and the substructure. In general, these limits are based on the State experience with existing IABs and the research performed by local universities.

Table 2.3 presents the limits enforced on the design of IABs by different Departments of Transportation on the geometric properties of different types of IABs (Kunin and Alampalli 2000). These properties include bridge length, skew angle, tolerance for pile location and the abutment height. Similar but more recent limits on IABs geometry are summarized in tables 2.4 and 2.5 (Maruri and Petro 2005 and Bakeer et al. 2005).

Table 2.3 Geometric Limits on IABs in the United States (Kunin and Alampalli 1999)

State or Province	Thermal Movement (cm)	Length (m)			Skew Angle (Degrees)	Tolerance For Pile Location (Cm)	Height (m)	
		Steel Girder	Precast-Concrete Girder	CIP Concrete Girder			Abutment	Stem
AK	—	—	61.0	—	30	7.6	—	—
AR	—	91.5	91.5	—	15	Per specs	No limit	No limit
CA	1.3	31.5	50.9	50.9	21	10.2	4.3	2.7
CO	10.2	91.5	183.0	152.5	No limit	15.2	No limit	No limit
GA	No limit	No limit	No limit	No limit	30	No specs	No limit	No limit
IL	No limit	83.9	114.4	114.4	30	Standard	No limit	No limit
IA	LBL*	Undetermined	152.5	152.5	30	7.6	0.9 to 1.5	Length dependent
KS	5.1	91.5	152.5	152.5	45	7.6	By Design	By design
KY	No limit	91.5	122.0	122.0	30	15.2	No limit	0.9 m min pile cap
ME	9.5	90.0	150.0	150.0	25	5.1	3.6	—
MD	2.5	—	18.3	—	30	15.2	3.1 to 4.6	3.1
MA	Not defined	99.1	99.1	99.1	30	7.6	Minimize	Minimize
MI	No limit	No limit	No limit	No limit	30	15.2		—
MN	No limit	61.0	61.0	61.0	20	No specs	0.1	1.0
NV	2.5	76.3	122.0	122.0	20 to 45		Design	Design
NH	3.8	45.8	24.4	—	10			—

Table 2.3 Continues

State or Province	Thermal Movement (cm)	Length (m)			Skew Angle (Degrees)	Tolerance For Pile Location (Cm)	Height (m)	
		Steel Girder	Precast-Concrete Girder	CIP Concrete Girder			Abutment	Stem
NY	LBL	140.0	140.0	140.0	30	2,5		0.3 to 0.6
ND	LBL	122.0	122.0	48.8	30	No specs	3.7	1.5 to 1.8
OK	————	91.5	122.0	————	No skew	15.2	3.1	1.8
OR	No limit	No limit	No limit	No limit	45	No specs	No limit	No limit
PA	5.1	91.5 to 122	122.0	Not Used	20		No limit	————
QC ^a	No limit	————	78.1	————	20° 15'	5.0		1.9
SD	LBL	106.8	213.5	213.5	30	15.2	0.3	————
TN	5.1	130.8	244.0	244.0	No limit	No specs	No limit	No limit
VT	LBL	24.4	————	————	15	Standard		No limit
VA	3.8	91.5/46.8 ^b	152.5/79.3 ^b		30	7.6	No limit	No limit
WA	No limit	Not used	106.8	61.0	30	15.2	No limit	3.7
WV	5.1	———— ^c	———— ^c	———— ^c	30	7.6		No limit
WY	5.0	100.0	130.0	100.0	45	2.0	No limit	No limit
Max	No limit	No limit	No limit	No limit	No limit	Per specs	No limit	No limit
Min	1.3	24.4	18.3	48.8	No skew	2.0	0.9	0.3

LBL=Limited By Length

^aQC = Quebec, ^bLesser value used with maximum skew, ^cMovement is limited, not length.

Table 2.4 Geometric Limits on IABs in the United States (Maruri and Petro, 2005)

PRESTRESSED CONCRETE GIRDERS	RANGE	STEEL GIRDERS	RANGE
MAXIMUM SPAN	(FT)	MAXIMUM SPAN	(FT)
Full integral	60-200	Full integral	65-300
Semi integral	90-200	Semi integral	65-200
Deck extensions	90-200	Deck extensions	80-200
Integral piers	120-200	Integral piers	100-300
TOTAL LENGTH	(FT)	TOTAL LENGTH	(FT)
Full integral	150-1175	Full integral	150-650
Semi integral	90-3280	Semi integral	90-500
Deck extensions	200-750	Deck extensions	200-450
Integral piers	300-400	Integral piers	150-1000
MAXIMUM SKEW	(Degrees)	MAXIMUM SKEW	(Degrees)
Full integral	15-70	Full integral	15-70
Semi integral	20-45	Semi integral	30-40
Deck extensions	20-45	Deck extensions	20-45
Integral piers	15-80	Integral piers	15-no limit
MAXIMUM CURVATURE	(Degrees)	MAXIMUM CURVATURE	(Degrees)
Full integral	0-10	Full integral	0-10
Semi integral	0-10	Semi integral	0-10
Deck extensions	0-10	Deck extensions	0-10
Integral piers	3-no limit	Integral piers	0-no limit

Table 2.5 Geometric Limits on IABs in the United States (Bakeer et al. 2005)

State	First Year Built	Length Limit feet (m)	Skew Angle (degrees)
Arkansas	1996	260 (79)	33
California	1950	1 inch (25mm) c	45
Georgia	1975	410/260 (125/79)	0/40
Hawaii	NA	250 (76)	NA
Illinois	1983	300 (92)	30
Indiana	NA	300 (92)	30
Idaho	NA	400 (122)	30
Iowa	1962	300 (92)	30
Kansas	1935	450 (137)	NA
Kentucky	1970	400 (122)	30
Louisiana	1989	1,000 (305)	0
Maine	1983	150 (46)	30
Michigan	1990	None	30
Missouri	NA	600 (183)	NA
Massachusetts	1930	300 (92)	30
North Dakota	1960	400 (122)	30
Nevada	1980	200 (61)	45
New York	1980	300 (92)	30
Ohio	NA	375 (114)	30
Oklahoma	1980	210 (64)	0
Pennsylvania	1946	600 (183)	20
Oregon	1940	200 (61)	25
South Dakota	1948	700 (214)	35
South Carolina	NA	500 (153)	30
Tennessee	1965	2 inch (25mm) movement	No Limits
Utah	NA	300 (92)	20
Virginia	1982	500 (153)	NA
Wyoming	1957	360 (110)	30
Washington	1965	450 (137)	40
Wisconsin	NA	300 (92)	30

New Jersey Department of Transportation (NJDOT) limits the maximum length of integral abutment bridges to 137 meters (450 feet) and limits the maximum skew angle to 30 degrees (NJDOT 2009). Skew angles greater than 30 degrees or Superstructure configurations that require the use of horizontally curved girder schemes also preclude the use of integral abutment jointless bridge in New Jersey.

Minnesota Department of Transportation (MnDOT) limits the maximum length of IABs with skew angle up to 20° to 91 meters (300 feet) and to 30 meters (100 feet) for IABs with skew of 45° (MnDOT 2011). MnDOT has a unique linear relationship to calculate the maximum length limits for IABs with skew angle between 20° and 45° . The maximum bridge length decreases linearly between skew angles 20° and 45° . That relationship is shown in Figure 2.2. Skew angles greater than 45 degrees preclude the use of integral abutment jointless bridge in Minnesota. MnDOT prefers straight horizontal alignment but it also allows slight horizontal curvature based on case-by-case.

Researchers in the United States have also studied the maximum length limits of IABs as presented in table 2.6. These limits were mainly calculated based on the capacity of the steel H-Piles supporting the abutment. The researches were based on field measurements and/or analytical tools. Some researchers have provided analytical tools to calculate the bridge length limits based on the capacity of the steel H-Piles supporting the abutment and shear and flexural capacity of the abutment (Albhaisi, 2003). In general, these limits are in agreement with each other but they exceed the limits set by the States.

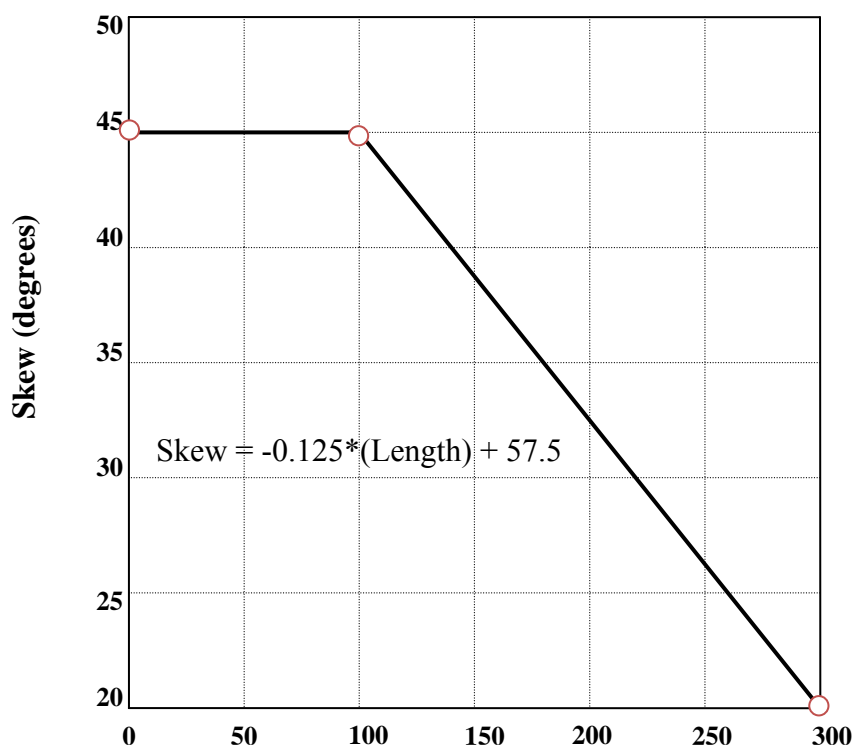


Figure 2.2 Maximum Bridge Length Limits in Feet (MnDot 2011)

Table 2.6 Length Limits on IABs Supported on H-Piles (Dunker and Liu 2007)

Climate	Bridge material	Skew (degree)	Yield (MPa)	Length (m)	Reference
Moderate (Tennessee)	Concrete	0	248	336	Burdette et al. (2002)
	Steel	0	248	224	
Moderate	Concrete	0	248	260	Dicleli and Albhaisi (2004)
	Steel	0	248	180	
Cold	Concrete	0	248	210	
	Steel	0	248	120	
Cold (Iowa)	Concrete	0	248	245	Abendroth and Greimann (2005)
	Concrete	40	248	178	
	Concrete	0	345	153	
	Concrete	40	345	91	

2.6.1.2 Limits on the Geometry of IABs in Other Countries.

Similar to the US experience, different countries in Europe and around the world have developed their own design criteria and limits on IABs with the same goal which is to insure the safety of their bridges and limit the stresses in the superstructure and the substructure. These limits are also based on the country experience with existing IABs and the research performed by local universities. According to a study sponsored by NYSDOT to compare the current practice in the design and construction of IABs in the United States and Europe (White 2007), most European countries, with the exception of Finland, do not enforce maximum bridge limits on IABs.

Finland was the only country to enforce total bridge limit of 70 meters (230 feet). Other countries limit their IABs lengths by enforcing the limits on pile stresses or other design criteria. Of those European countries that indicated a limit on the bridge skew angle, the maximum allowable reported skew angle is 30°. Only Sweden indicated a maximum roadway grade of 4% (White 2007). Table 2.7 presents the limits enforced on the geometry of IABs in Sweden, Germany, Ireland, Finland and England.

Table 2.7: Summary of Selected Criteria used by European Countries (White 2007)

Criteria	England	Finland	Ireland	Germany	Sweden
Use fully IABs?	Yes	Yes	Yes	Yes	Yes
Maximum Skew angle?	30 ⁰ +	30 ⁰	30 ⁰ +	None	None
Steel pile foundation used?	Yes	Yes	Yes	Rarely	Yes
Steel pipe pile filled with reinforced concrete used?	Rarely	Yes	Yes	Rarely	Yes
Reinforced concrete pile foundation used?	Yes	Rarely	Yes	Yes	Yes
PS piles used?	Rarely	No	Rarely	No	Yes
Spread footing used?	Yes	No	Yes	Yes	Yes
Use active soil pressure, full passive soil pressure, Or other requirement?	OR	DOSL	OR	Passive	DOSL
Approach slabs recommended?	No	Yes	No	Yes	Varies
Wingwalls permitted to be cast rigidly with abutment stem?	Yes	Yes	Yes	Yes	Yes
Use Semi IABs?	Yes	Yes	Yes	No	Yes
Maximum Skew angle?	30 ⁰ +	30 ⁰	30 ⁰ +	——	None
Steel pile foundation used?	Yes	Yes	Yes	——	Yes
Steel pipe pile filled with reinforced concrete used?	Rarely	Yes	Yes	——	Yes
Reinforced concrete pile foundation used?	Yes	Rarely	Yes	——	——
PS piles used?	Rarely	No	Rarely	——	Yes
Spread footing used?	Yes	Yes	Yes	——	Yes
Use active soil pressure, full passive soil pressure, or other requirement?	OR	DONL	OR	——	DOSL
Approach slabs recommended?	No	Yes	No	——	Varies
Wingwalls permitted to be cast rigidly with abutment stem?	Yes	Yes	Yes	——	Yes

DOSL=Depens on Span Length, OR=Other Requirements

2.6.2 Superstructure

In the United States, steel plate girders and precast prestressed concrete girders are the predominant types for superstructures in IABs. Most States have enough experience with both types of superstructure. In general, structural steel hot rolled beams, steel plate girders, precast prestressed concrete girders, prestressed box beams, spread precast prestressed box beams may be used for IABs. When using prestressed concrete superstructures, creep and long-term loss of prestress force are usually considered in the design. When asked about their experience with steel girders and prestressed-concrete girders, seventeen agencies in the United States had enough experience with both types of superstructure. Thirteen out of the seventeen agencies find no difference between both types, but four have observed some differences (Kunin and Alampalli 1999). Some States, including New York State, reported less cracking in decks supported by steel girders. Figure 2.3 and 2.4 show the current integral abutment details used by New York State Department of Transportation (NYSDOT 2008) for steel girders superstructure and prestressed concrete girders superstructure respectively. The details used by NJDOT are very similar. These piles are no longer connected to the superstructure as it was the case in the older details. Many States use different length limits for steel and concrete superstructures because of the different level of sensitivity to thermal variation. In general, concrete bridges could reach longer lengths because they are less sensitive to thermal changes.

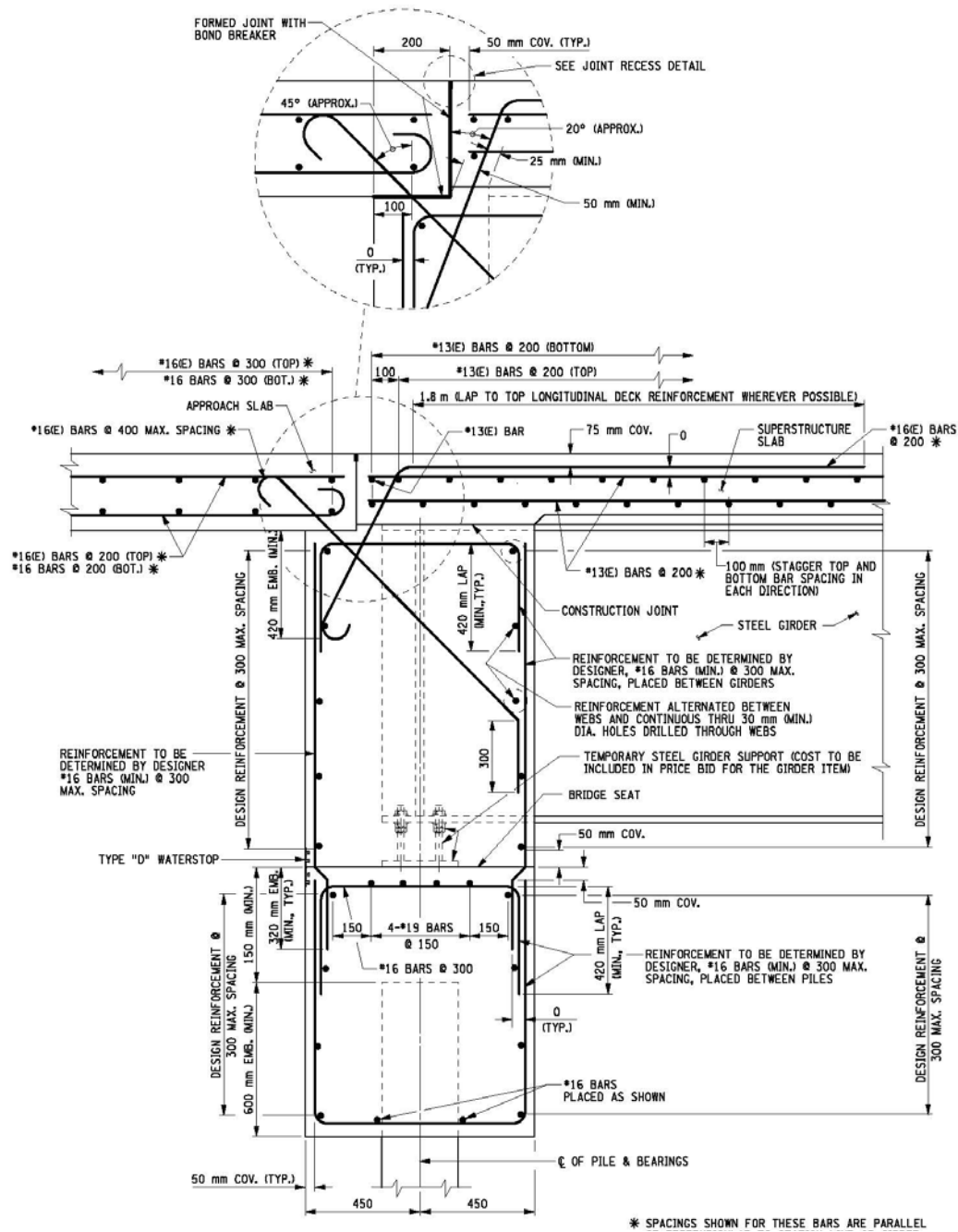


Figure 2.3 Current NYSDOT Integral Abutment Details for Steel Superstructure

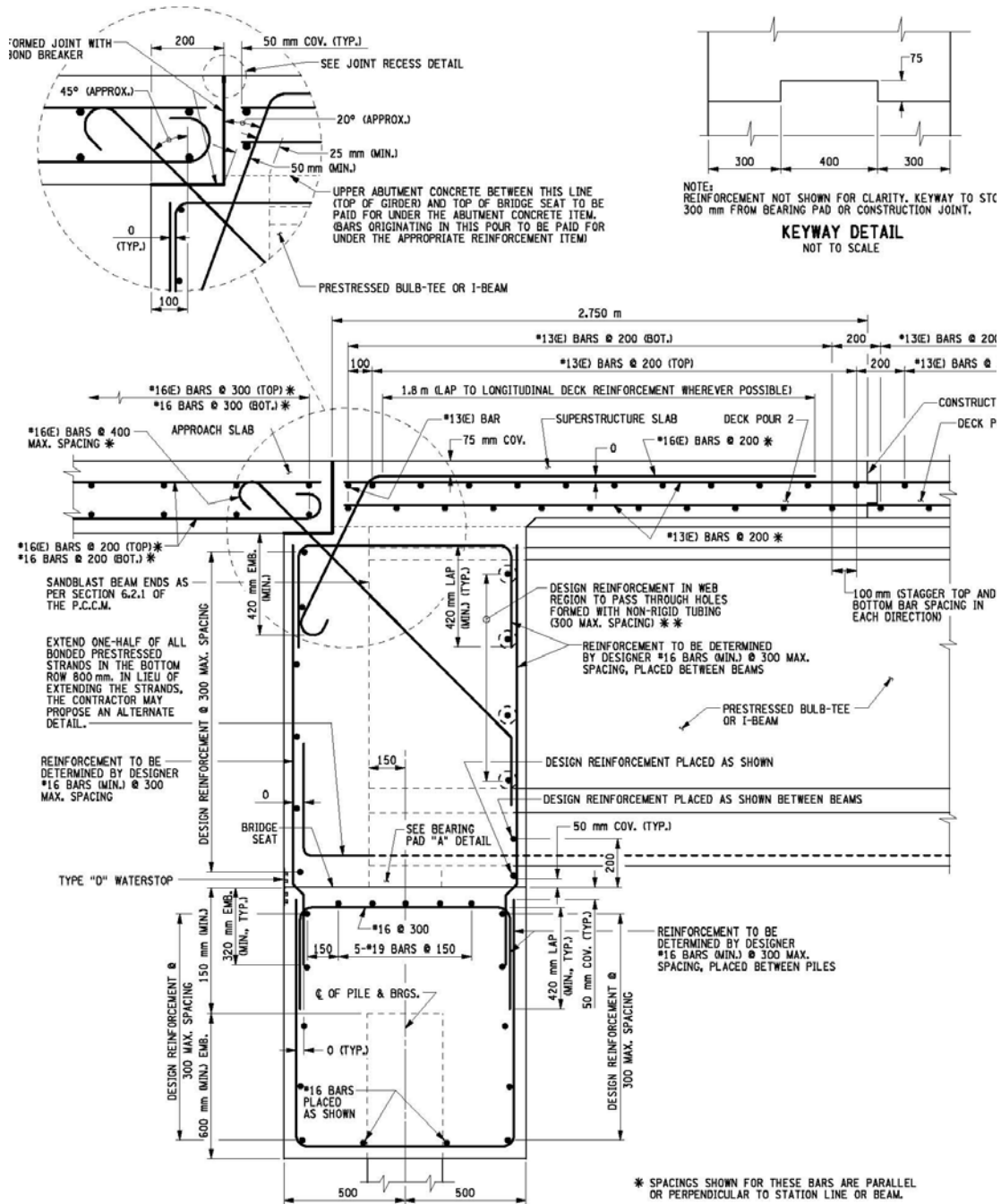


Figure 2.4 Current NYSDOT Integral Abutment Details for Precast Prestressed Concrete Superstructure

New Jersey and most States require the connection between the abutment and the superstructure to be assumed as a pin connection when analyzing the superstructure and to include a check for the effect of superstructure-abutment fixity (NJDOT 2009).

In Europe the beams are also analyzed for pin connection between the superstructure and the abutment to calculate the maximum positive moment in the span and for fixed condition between the superstructure and the abutment to determine the maximum end moments that may be induced in the abutment (Kunin and Alampalli 1999).

In Europe, the predominate beam used in IABs are precast prestressed concrete beams. Steel beams are also permitted with a minimum of one box or two I beams in the superstructure. Although allowed to be used by most transportation agencies in Europe, cast in place concrete beams are seldomly used except for short bridges (Kunin and Alampalli 1999).

2.6.3 Foundations

During expansion and contraction of the bridge, the superstructure will experience compression and tension forces due to the movement constraints provided by the abutment and the piles. The magnitude of these forces depends mainly on the bridge length, temperature change and the stiffness of the superstructure and the substructure.

The stress level in the superstructure is usually proportional to the stiffness of the substructure. For this reason, bridge engineers try to design a flexible foundation system to reduce the stresses in the superstructure and to accommodate the movement of the superstructure. To insure the flexibility of the substructure, AASHTO-LRFD does not allow the construction of integral abutments on spread footings founded or keyed into rock and therefore most IABs are supported by piles. To further reduce the stiffness of the substructure and subsequently allow the movement of the superstructure, IABs are usually supported by a single row of piles. In general, short piles are not allowed because they do not provide the flexibility required. In New Jersey (NJDOT 2009) piles with an effective depth less than 4.6 m (15 ft) are not allowed in IABs. Battered piles are not preferred in IABs because of their large lateral stiffness. When battered piles are used, the slope of the pile is usually less than 1/10.

2.6.3.1 Piles

Steel H-Piles are the most common type of foundations used to support IABs in the United States. Steel H-Piles provide the flexibility needed to reduce the stresses in the superstructure and the ductility needed to accommodate relatively large displacements at the top of the pile. They could be oriented to bend around the strong axis, the weak axis, or perpendicular to traffic regardless of the skew of the bridge. Steel H-Piles are not recommended in severe corrosion conditions. When the bearing capacity of steel H-Piles

is not enough, engineers use hybrid pile arrangement where the lower part of the steel H-Pile is embedded inside a larger Cast In Place (CIP) concrete piles or drilled shafts. Prestressed concrete piles are also used to support IABs. They are mainly used in the United States when steel H-Piles are not a viable option like in the case of very corrosive environments when the bearing capacity of H-Piles is not enough to support the bridge. Prestressed concrete piles are common in Iowa and Tennessee. Tennessee DOT uses prestressed concrete piles in the western part of the State. Other less common types of piles are also used to support integral abutment in the United States. These include Timber piles, sheet piles and spread footings (Dunker and Liu 2007). Although drilled shafts are considered relatively stiff and are usually not allowed in IABs, they have been used to support integral abutments in recent projects (Ooi et al. 2010). NJDOT allows Cast-in-place concrete piles, hollow steel pipe piles, prestressed concrete piles and steel H-Piles to be used for bridges with total lengths of 150 feet or less. Only steel H-Piles are allowed by NJDOT when the total length exceeds 150 feet.

Steel pipe piles filled with reinforced concrete with diameters up to 1.2 meters (4 feet) are the most common type of foundation piles used to support integral abutment in Europe. Using prestressed concrete piles to support IABs is also common in Europe. With the exception of England and Ireland, Steel piles are rarely used to support IABs (White 2007). Steel H-Piles, prestressed concrete piles and pipe piles will be discussed in greater details in chapter 3.

To further reduce the stiffness of the pile-soil system, many transportation agencies in the United States and Europe enclose the top part of the pile in sleeves filled usually with

loose sand or crushed stones. These sleeves will reduce the restraining action by the foundation soil on the pile. Figure 2.5 shows sleeves surrounding H-Piles in a construction site in New Jersey. The height of the enclosure depends usually on the length of the bridge and the surrounding foundation soil type and stiffness.



Figure 2.5 Sleeves Surrounding H-Piles at a Construction Site in New Jersey

Pr-bored holes for the piles are also used to facilitate the expansion of IABs. The hole depth and width varies between States. For example, California uses 1.5 m deep and 15.25 cm oversized holes and Iowa uses 2.4 m deep and 10.15 cm oversized holes (Kunin and Alampalli 1999). NJDOT requires that the pre-bored holes be at least 2.5 meters (8 feet) below the bottom of the planned finished ground elevations for IABs with lengths of 30 meters (100 feet) or more. It also requires the size of the hole to be twice the size of the pile. Similar requirements are imposed by NYSDOT. Table 2.8 summarizes the different requirements for pre-drilling by different Departments of Transportation (DOTs) in the United States.

Table 2.8 Specifications for Pre-drilling Pile Foundation Locations (Olson et al. 2009)

State	Comments
IA	Predrill to 8 feet for bridges over 130 feet long, and fill the hole with bentonite
IN	Predrill to 8 feet if foundation soil is hard
KS	Not reported
MA	Predrill to 8 feet and fill with loose granular material
ME	Predrill to 10 feet
MI	Predrill to 10 feet
MN	Predrill only in very compact soil to facilitate pile driving rather than to influence IAB behavior
MO	Predrill only in new fill to prevent downdrag on the piles
NE	Predrill to the engineer's recommendation
NJ	Predrill to 8 feet for bridges over 100 feet long
NY	Predrill to 8 feet and fill with loose granular material
OH	Not recommended
OR	Not recommended
SD	Predrill to 10 feet
TN	Not reported
VT	Predrill only in very compact soil
WI	Not reported
WV	Predrill to 15 feet, or predrill to bedrock if rock is between 10 and 15 feet below ground surface

2.6.3.2 Abutment-Pile Connection

In conventional jointed bridges, the lateral loads are usually resisted by using battered piles and the lateral load carrying capacity of vertical piles is ignored. Therefore; piles are embedded a minimum length inside the abutment to allow for the transfer of axial and shear forces from the abutment to the piles and moment connection between the pile and the abutment is not required. In the case of CIP concrete piles, the top of pile reinforcement is extended inside the abutment. The minimum embedment length of piles inside the abutment in jointed bridges is 300 mm (12 in) (NJDOT 2009, ODOT 2004).

In IABs, the Abutment-Pile connection, also referred to as top of pile connection, is usually detailed to provide fixity at the top of the pile. The minimum embedment length to insure fixity at top of the pile depends on several factors but the major factor is the size of the pile. Most States specify constant embedment length regardless of the size of the piles. NYSDOT uses pile embedment length of 600 mm for all piles as shown in Figures 2.3 and 2.4. NJDOT uses embedment lengths similar to what is used by NYSDOT. The embedment length shown in the figures is twice the length required in jointed bridges.

Recent researches (Albhaisi 2003) have shown that a pin connection between the pile and the abutment will reduce the stresses in the abutment by moving the location of the maximum moment along the pile from the top of the pile to a location well below the bottom of the abutment. That will also lead to larger limits on IABs lengths. The Embedment length and abutment-pile connection will be discussed in greater details in chapter 3.

2.6.3.3 Soil-Pile Interaction

To avoid the complexity of the soil pile interaction, many transportation agencies use the concept of equivalent cantilever length in the bridge analysis model. The concept of equivalent cantilever length (L_e) is shown in figure 2.6. In that concept, an equivalent length is calculated based on the geometric properties of the pile and the geotechnical properties of the surrounding soil and used in the analysis of the bridge.

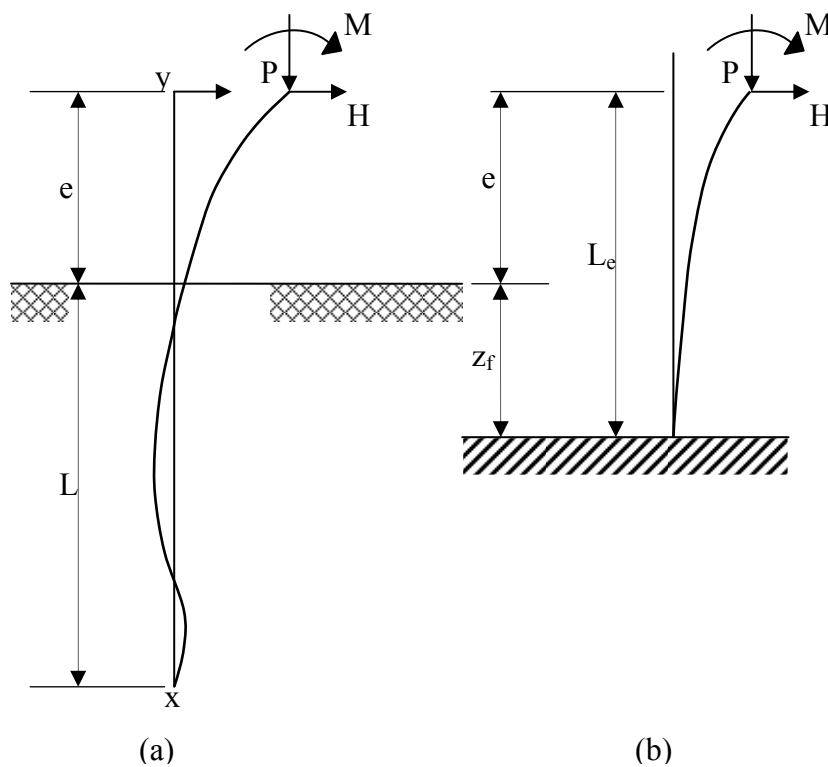


Figure 2.6 Bending of pile carrying vertical and horizontal loads at head (a) Partly embedded pile (b) Equivalent fixed base pile or column (Tomlinson and Woodward 2008)

The length of fixity or the equivalent cantilever length for steel H-Piles oriented to bend around the strong axis and embedded in different types of soil as suggested by Maine Department of Transportation are summarized in table 2.9.

Table 2.9 Length of Fixity (L_e) for H-Piles with strong axis orientation (Maine DOT 2003)

Pile Section	Sand m (ft)			Clay m (ft)		
	Loose	Medium	Dense	Soft	Medium	Stiff
HP 10X42	7.3 (24)	6.1 (20)	5.5 (18)	6.7 (22)	5.5 (18)	4.9 (16)
HP 10X57	7.9 (26)	6.7 (22)	5.8 (19)	7.3 (24)	6.1 (20)	5.5 (18)
HP 12X53	8.5 (28)	7.3 (24)	6.1 (20)	7.9 (26)	6.4 (21)	5.8 (19)
HP 12X63	9.1 (30)	7.6 (25)	6.4 (21)	8.2 (27)	6.7 (22)	5.8 (19)
HP 12X74	9.4 (31)	7.6 (25)	6.7 (22)	8.2 (27)	6.7 (22)	6.1 (20)
HP 13X60	9.4 (31)	7.6 (25)	6.4 (21)	8.2 (27)	6.7 (22)	5.8 (19)
HP 13X73	9.8 (32)	7.9 (26)	6.7 (22)	8.5 (28)	7.0 (23)	6.4 (21)
HP 13X87	9.8 (32)	7.9 (26)	7.0 (23)	8.8 (29)	7.6 (25)	6.4 (21)
HP 14X73	9.8 (32)	7.9 (26)	7.0 (23)	8.8 (29)	7.3 (24)	6.4 (21)
HP 14X89	10.1 (33)	8.2 (27)	7.3 (24)	9.4 (31)	7.6 (25)	6.7 (22)
HP 14X102	10.7 (35)	8.5 (28)	7.6 (25)	9.4 (31)	7.9 (26)	6.7 (22)
HP 14X117	11.0 (36)	8.8 (29)	7.6 (25)	9.8 (32)	7.9 (26)	7.3 (24)

Once the equivalent cantilever length is calculated it can be used in the bridge analysis as shown in figure 2.7.

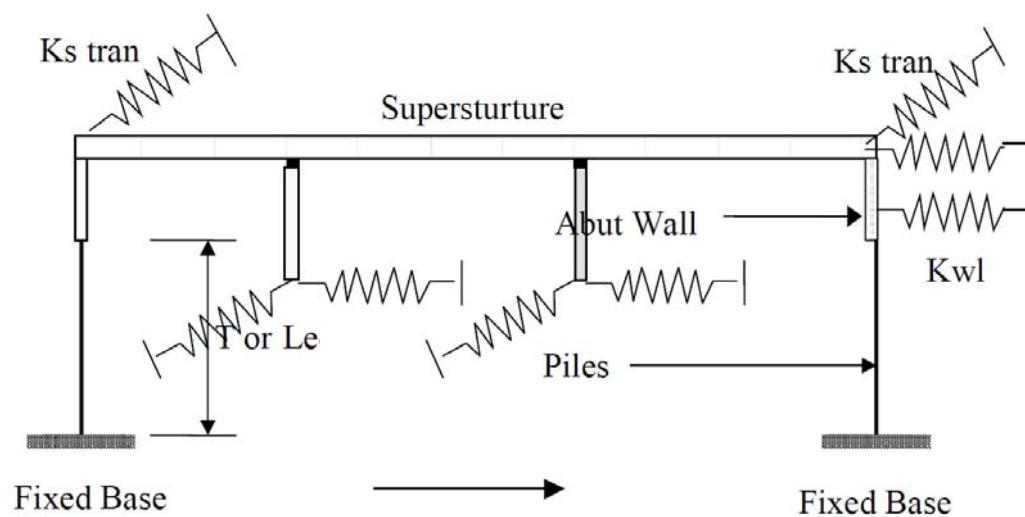


Figure 2.7 Simplified Model for IABs (Najm et al. 2005)

With the advancement in computer computations, large stiffness matrixes can be processed in a relatively small time and instead of the simplified model shown in figure 2.7, a more accurate mathematical model can be used in the analysis of IABs. In the more accurate models, the soil around the pile is modeled by springs as shown in figure 2.8.

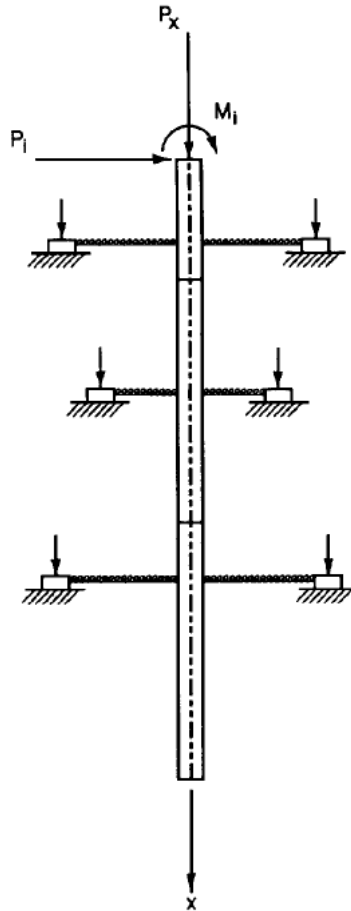


Figure 2.8 Modeling of the Soil by Springs (Reese and Van Impe 2001).

Soil linear properties are usually used in the analysis. For more detailed analysis nonlinear properties are used.

2.6.4 Backfill

The abutment generally experience active soil pressure during bridge contraction and passive soil pressure during bridge expansion. Most transportation agencies in the United States use compacted granular backfill behind the abutment (White 2007). This is especially true when sleeper slabs are used to prevent the settlement of the slab and avoid additional stresses. While the majority of States use granular compacted backfill behind integral abutments, some States use non-compacted backfill to reduce the pressure on the abutment during bridge expansion. New Hampshire stopped using non-compacted backfill after settlement of sleeper slabs (Kunin and Alampalli 1999). Other States use compressible material (i.e high-density foam) behind the abutment for the same reason.

Other types of back fill used in the United States include geotextile-reinforced backfill and flow fill with low-density foam (Kunin and Alampalli 1999).

Different States use different estimates of the passive pressure on the abutment during bridge expansion. According to Massachusetts Department of Transportation (MassDOT) bridge design manual (MassDOT 2009) the passive pressure coefficient K_p for compacted gravel borrow backfill is a function of the relative wall displacement (Wall displacement Δ /Wall Height H) and shall be calculated as follows:

$$K_p = 0.43 + 5.7 \left[e^{-190(\Delta/H)} \right] \quad (2.1)$$

The relationship above is illustrated in figure 2.9.

California and Alaska use much higher passive pressure than other States to account for higher pressures during seismic events. California and Alaska assume soil pressure of 53 MPa (7.7 KSF) and that is more than seven times the pressure assumed by North Dakota which uses 6.9 MPa (1 KSF).

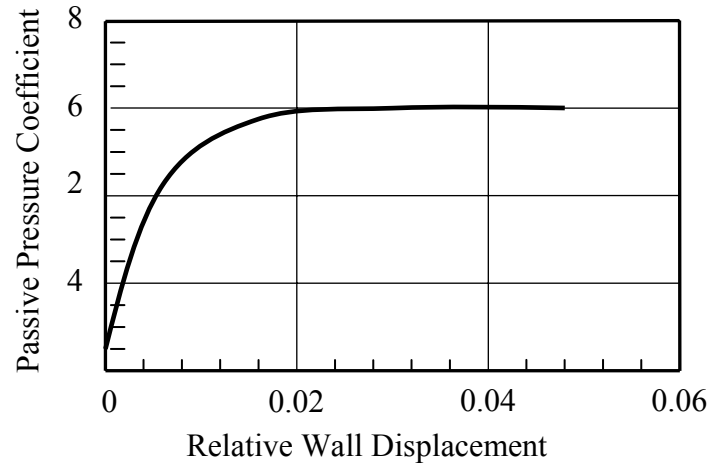


Figure 2.9 Plot of Passive Pressure Coefficient K_p vs Relative Wall Displacement (Δ/H) (MassDOT 2009)

The majority of European countries use well compacted gravel or sand without compressible materials behind the abutment and some countries require the backfill compaction to be done evenly behind the abutments (White 2007). European countries like the States have different methods in estimating the passive pressure behind the abutment. Germany uses full passive pressure regardless of the bridge movement and Sweeden uses passive pressure when the abutment movement exceeds 0.005 times the abutment stem height (White 2007). In Alberta, Canada, abutment movements between 60 mm and 80 mm are required before full passive pressure can be assumed in granular backfill (Alberta, 2008).

2.6.5 Construction Sequence

The sequence of construction of IABs has a significant effect on the stresses in the foundation (Stanford et al. 2006). To reduce the moment and rotation transferred from the superstructure to the foundation due to dead load of the superstructure, the connection between the superstructure and the substructure is made monolithic in the last stage of construction. Typically, most of the deck is poured first without the end areas. After the hardening of the deck, the end portion of the deck and the top part of the abutment (backwall) are poured together to form a rigid connection. A typical IAB construction stages for steel girder IABs are shown in Figure 2.10.

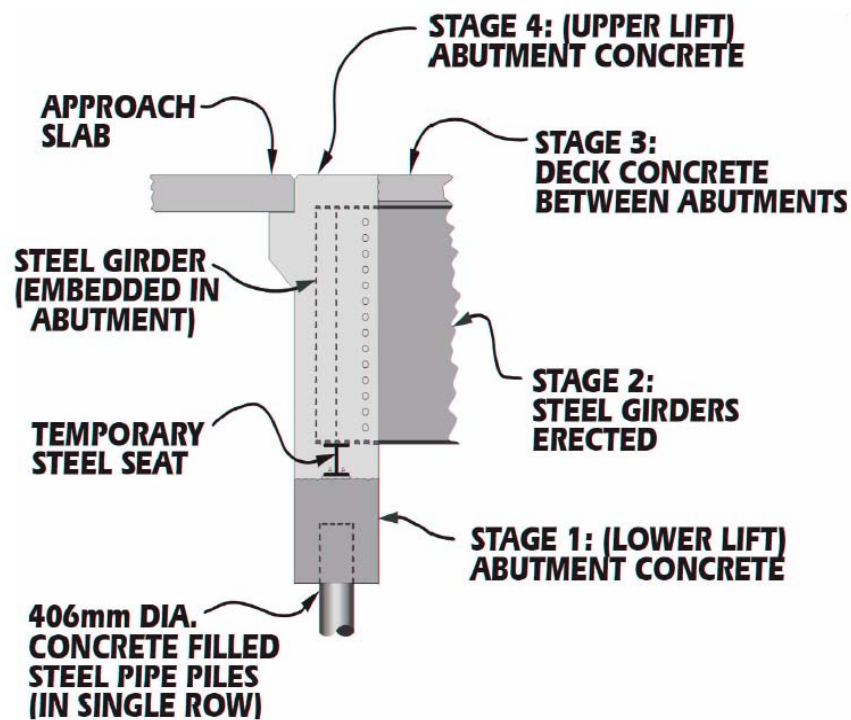


Figure 2.10 Typical Construction Stages for IABs (Harvey et al. 2006)

When the construction stages in the figure are followed, the foundation needs to be designed to resist all axial, shear and flexural force effect due to the superimposed dead

load, live load, earth pressure, temperature induced loads, shrinkage, creep and seismic loads and only the vertical dead load from the superstructure.

MassDOT (MassDOT 2009) requires Integral abutments to be constructed in two stages as follows:

Stage 1:

A pile cap supported on one row of vertical piles shall be constructed. The top of the pile cap shall reach the bottom of the erection pads under the girders. The top of the pile cap shall be smooth in the area directly under the girders and a strip of 2 inches wide around this area. Other areas shall be intentionally roughened (rake finished).

Stage 2:

After pouring the entire deck slab, except for the portions of the deck within 4 feet from the front face of the abutments, the abutment diaphragm encasing the ends of the bridge girders shall be poured. The end 4 feet of the deck shall be poured simultaneously with the abutment diaphragm. The concrete diaphragm and the end portion of the deck shall be poured when the surface temperature is between 35° F and 89° F. The expected air temperature during the six (6) hours following pouring this concrete should be within the same range. The abutment diaphragm shall have the same width as the pile cap constructed in Stage 1 and shall extend from the top of the pile cap to the top surface of the deck slab.

Similar construction stages are required and/or allowed by other transportation agencies (e.g. New Jersey DOT and Indiana DOT).

2.7 FOUNDATIONS FOR INTEGRAL ABUTMENT BRIDGES

2.7.1 Steel H-Piles

The behavior of steel H-Piles subjected to a lateral displacement at the pile head involves a combination of material instability (Plastic collapse) and geometric instability (local buckling of the flanges and web). To accommodate the large strains associated with plastic hinge rotations of the piles, the width-thickness ratios of the pile's web and flanges must be adequate to prevent their local buckling (Abendroth et al. 1989). The global instability or lateral torsional buckling of the piles is generally not of a concern due to the confining effect of the surrounding soil.

Many researchers have addressed the stability and the ductility capacity of various steel sections. Limited research has been conducted specifically on the ductility capacity and stability of steel H-Piles (Wold-Tinsae et al. 1988b; Abendroth and Greinman 1989; Kato 1989; Kuhlmann, 1989; Abendroth and Greimann, 1989; Amed et al. 1997). However, many other researchers have tried to address the problems associated with the stability and ductility of general steel sections used in buildings or bridges as beams or beam-columns (Lay and Galamaboss 1967; Lukey and Adams, 1969; Yura et al. 1978; Kemp 1986 and Kemp 1996).

Low-cycle fatigue may be a critical issue in the case of piles supporting the abutments of integral abutment bridges since such piles may be subjected to large inelastic cyclic deformations due to temperature variations. The literature review conducted on low-cycle fatigue behavior of steel members has revealed that the low-cycle fatigue behavior of reinforcing bars and prestressing tendons was investigated by some researches (Koh and Stephenson 1991; Mander et al. 1994). Shama et al. (2001) has extrapolated the low-cycle fatigue behavior of reinforcing bars to predict the low-cycle fatigue behavior of steel H-

Piles under cyclic lateral loading. The analytical predictions were compared to experimental results and a reasonably good agreement was found. A similar approach is used in this study to predict the low-cycle fatigue behavior of steel H-Piles under temperature-induced cyclic loading.

Low cycle fatigue damage of steel beams and connections has been addressed by some researchers (Popove, and Bertero, 1973; Ballio, et al. 1997). Daali and Korol (1995) presented low cycle fatigue damage models for steel beams using the results from experiments conducted on W-shapes. This model was initially employed in this research to predict the low-cycle behavior of steel H-Piles. Dowling (2006) presented extensive information on the fatigue of different metals. More recently, Zenner, Simburger, and Liu (2000) provided a mathematical model on the fatigue limit of ductile metals under complex multiaxial loading. A study by Huang et al. (2004) suggests that in most integral abutment bridges low-cycle fatigue of H-Piles need not to be considered. Vermont Agency of Transportation (VTrans, 2008) provides detailed recommendations for the analysis of piles in IABs.

2.8 SOIL-STRUCTURE INTERACTION

Understanding Soil-Structure interaction is very critical when designing IABs. That includes the interaction between the foundation and the surrounding soil (Foundation-Soil Interaction) and between the abutment and the backfill (Abutment-Backfill Interaction). The handling of soil-structure interaction in the analysis and design of IABs has always been problematic, usually requiring iterative analysis wherein the soil reactions are manually adjusted depending on the deformation level behind the abutment wall and adjacent to each supporting pile (Ting, 1998). It is known that the lateral earth pressure behind the abutments escalate to values considerably in excess of those at the time the structure entered service. However, the upper limits of the stress escalation are to be explored (England et al. 2000).

2.8.1 Foundation-Soil Interaction

Foundation-Soil interaction is one of the most important factors that affect the behavior of IABs under lateral movement. In general, the soil-structure interaction is not linear in nature and an analysis that incorporates the non-linear response of the soil to structure movement might be essential when studying the behavior of IABs. Extensive research has been conducted to theoretically predict the behavior of laterally loaded piles (Matlock 1970, Haliburton 1971, Reese et al. 1974, Wolde-Tinsae et al. 1988a, and Abendroth et al. 1990). The researchers suggested analytical models and analyses methods to simulate the interaction between a laterally loaded pile and the surrounding soil.

Generally, the soil-pile interaction for a particular point along the pile is defined by a nonlinear load (p)–deformation (y) curve or p - y curve, where p is the lateral soil resistance per unit length of pile and y is the lateral deflection of the soil at the same location. The computation of the lateral force-displacement response of a pile involves

the construction of a full set of p - y curves along the pile to model the force deformation response of the soil. A typical p - y curve is shown in Figure 2.11. In the Figure, the p - y relationship is nonlinear. For short and medium length IABs, the maximum pile deflection (soil deformation) is not expected to bring the soil behavior to the heavily nonlinear stage and the soil behavior can be approximated using linear behavior.

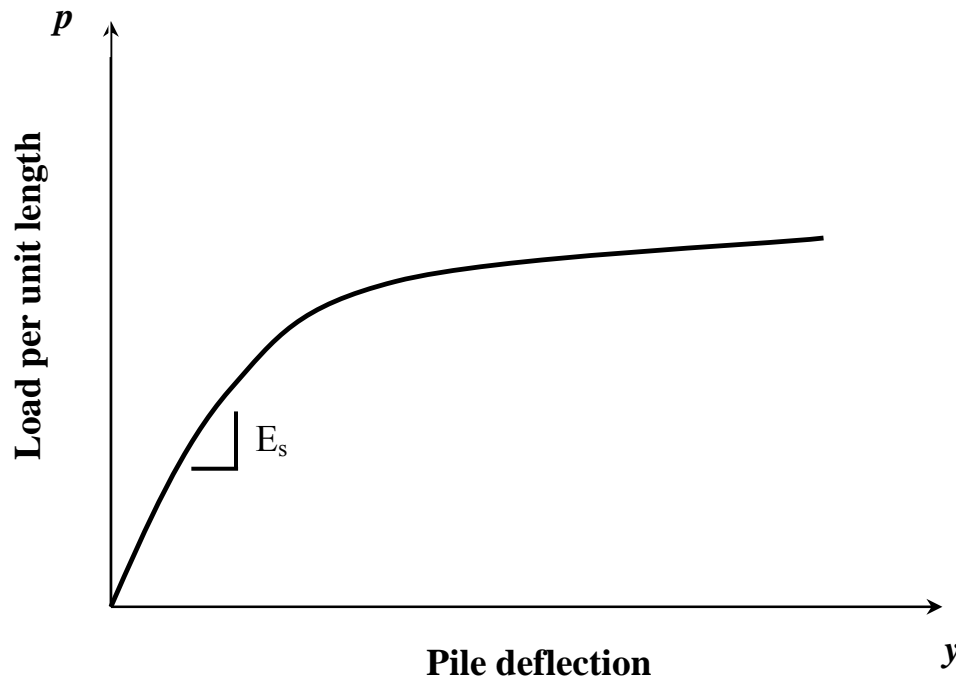


Figure 2.11 Genral P-Y Curve for Laterally Loaded Piles

The soil resistance to lateral load is expected to be reduced under significant cyclic lateral load. For a given soil, the loss of soil resistance is a function of the number of cycles (Reese and Van Impe 2001). At low magnitudes of deflection, the initial stiffness of the soil (E_s) is almost the same under static and cyclic loads. Cyclic loading has a significant effect on the lateral resistance of the soil when the deflection is large enough to bring the soil to the heavily nonlinear zone.

Figure 2.12 shows the characteristics shape of p-y curves for soft clay in the presence of free water under cyclic loading (Matlock 1970). Cyclic loading is not expected to have major impact in the design of IABs and it will be ignored in this research. The interaction between piles and the surrounding soil is discussed in greater details in chapter 4.

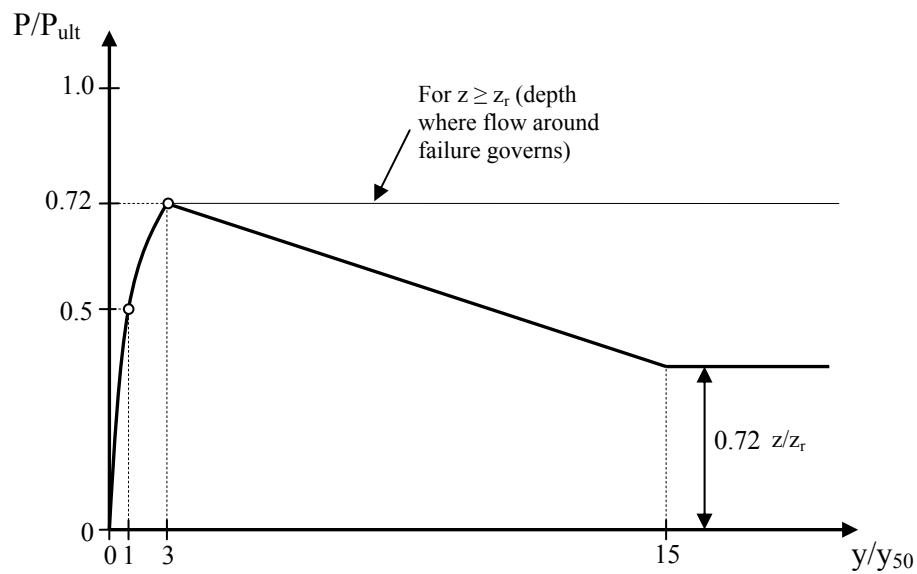


Figure 2.12 Characteristics Shape of p-y Curves for Soft Clay in the Presence of Free Water under Cyclic Loading (Matlock 1970)

2.8.2 Abutment- Backfill Interaction

Integral abutments experience variable earth pressure during the life time of the bridge.

The variation in earth pressure occurs mainly because of the contraction and expansion of the bridge. The horizontal or lateral pressure on the abutment at any point is directly proportional to the weight of the soil above that point. The ratio of the horizontal component of earth pressure to the vertical stress caused by the weight of the soil is

called the coefficient of earth pressure K . So the pressure (p) at any depth (z) along the abutment measured from the top of the backfill can be calculated as follows:

$$p = K\gamma z \quad (2.1)$$

The coefficient of earth pressure varies throughout the year based on the abutment movement.

Under initial conditions the abutment experiences negligible movement and the pressure behind the abutment can be calculated using at-rest coefficient of earth pressure K_0 . During negative thermal variation the pressure experienced by the abutment starts to decrease and with enough contraction in the bridges it reaches a constant value. At this stage the abutment experience minimum earth pressure and the pressure can be calculated using the active coefficient of earth pressure K_a . Active earth pressure is usually ignored in the design of IABs. This practice is conservative since the superstructure is mainly under tension forces during the contraction of the bridge.

During the hot season, the bridge expands and pushes the abutment towards the backfill. As the bridge expands, the pressure behind the abutment starts to increase rapidly and with enough expansion in the bridge, the pressure reaches full passive state. At this stage the pressure behind the abutment can be calculated using passive coefficient of earth pressure K_p . The magnitude of the passive earth pressure experienced by the abutment depends mainly on the magnitude of abutment expansion, the geotechnical properties of the soil and the geometric properties of the abutment.

Estimating the passive pressure behind the abutment during the expansion and contraction of the bridge presents a challenge for bridge engineers. It is obvious from the current practice discussion in section 2.6.5 that different methods are used to estimate the

passive pressure behind the abutment during bridge expansion. While most of transportation agencies consider the high passive pressure behind the abutment to have negative effect on the performance of IABs, others consider it beneficial. The different types and compaction level of backfill add to the challenge of estimating the pressure behind the abutment during the expansion and contraction of the bridge.

Many researchers have studied the behavior of backfill material under lateral loading to obtain analytical models simulating the interaction between the abutment and backfill soil. Clough and Duncan (1991) developed relationships to estimate the earth pressure during wall (abutment) movements. These relationships are based on experimental data and finite element analyses. In these relationships, the earth pressure is a function of the wall movement (Δ) / wall height (H). The relationships for loose and dense sand are shown in Figure 2.13. The figure shows large variation in pressure behind the abutment throughout the year. For the dense sand case the coefficient of earth pressure could increase from 0.17 in the full active case to 5.8 in the full passive case. This is more than 34 times increase in earth pressure behind the abutment. The figure also shows that the coefficient of earth pressure in the dense sand case is smaller than that for the loose sand in active and at-rest cases.

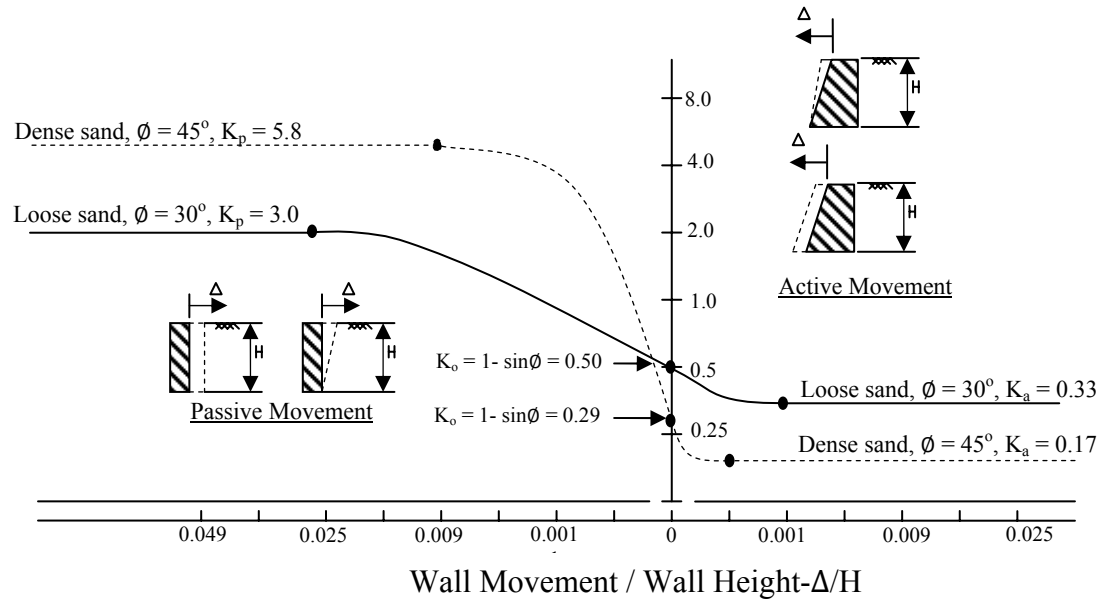


Fig 2.13 Relationship between Wall Movement and Earth Pressure for Ideal Cases of Walls That Are “Wished” Into Place (Clough And Duncan 1991).

The relative wall movement required to develop full active and full passive pressure states depends on the type of backfill. The approximate magnitude of movements required to reach minimum active and maximum passive earth pressure conditions based on finite element analysis are shown in table 2.10

Table 2.10 Approximate Magnitude of Movement Required to Reach Minimum Active and Maximum Passive Earth Pressure Conditions (Clough And Duncan 1991).

Type of Backfill	Value of Δ/H	
	Active	Passive
Dense sand	0.001	0.01
Medium-Dense sand	0.002	0.02
Loose sand	0.004	0.04
Compacted silt	0.002	0.02
Compacted lean clay	0.01	0.05
Compacted fat clay	0.01	0.05

As a rule of thumb, a relative wall movement of 0.004 and 0.04 are enough to produce maximum active and passive pressure respectively (Clough And Duncan 1991).

The relationships shown in figure 2.13 present ideal cases when walls are wished into place inside the sand and do not reflect the behavior of backfill. Figure 2.14 presents a more realistic relationship between wall movement and earth pressure coefficient for a backfill compacted to medium-dense condition movement. The relationship shown in the figure will be used in modeling backfill soil throughout this research and will be discussed in greater details in chapter 4.

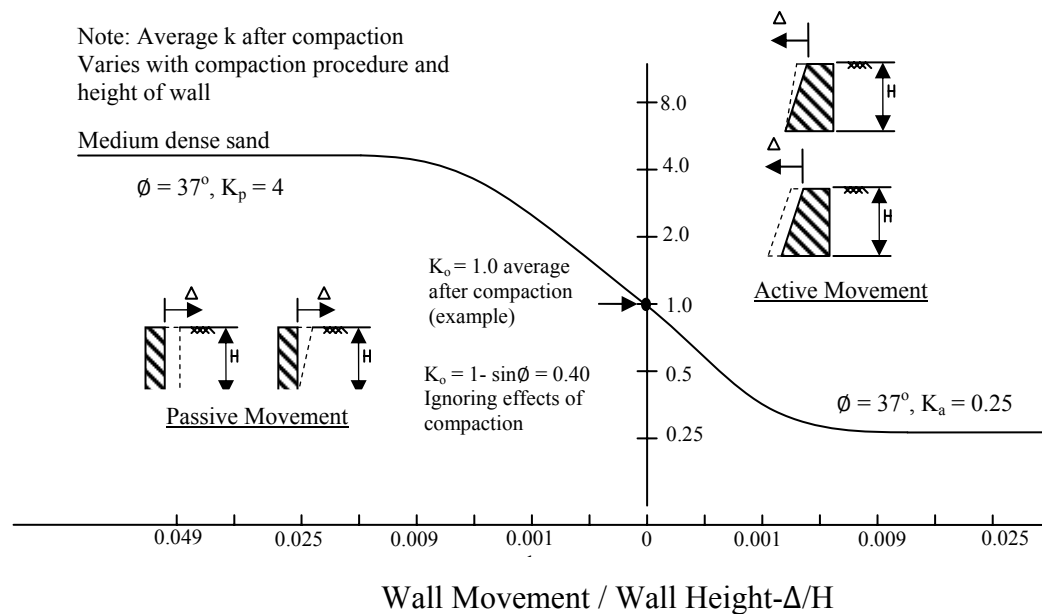


Fig 2.14 Relationship between Wall Movement and Earth Pressure For Backfill Compacted To Medium-Dense Condition (Clough And Duncan 1991).

Full scale wall tests performed by University of Massachusetts (UMASS) (Lutenegger and Thomson 1998) shows reasonable agreement between field test and the predicted values provide by the Navy design manual for foundation and structures NAVFAC_DM7_02 (Navy 1971) and National Cooperative Highway Research Program (NCHRP) report number 343. The values of the coefficient of passive pressure as function of the relative wall displacement (Wall displacement D /Wall Height H) as provide by the Navy are shown in figure 2.15.

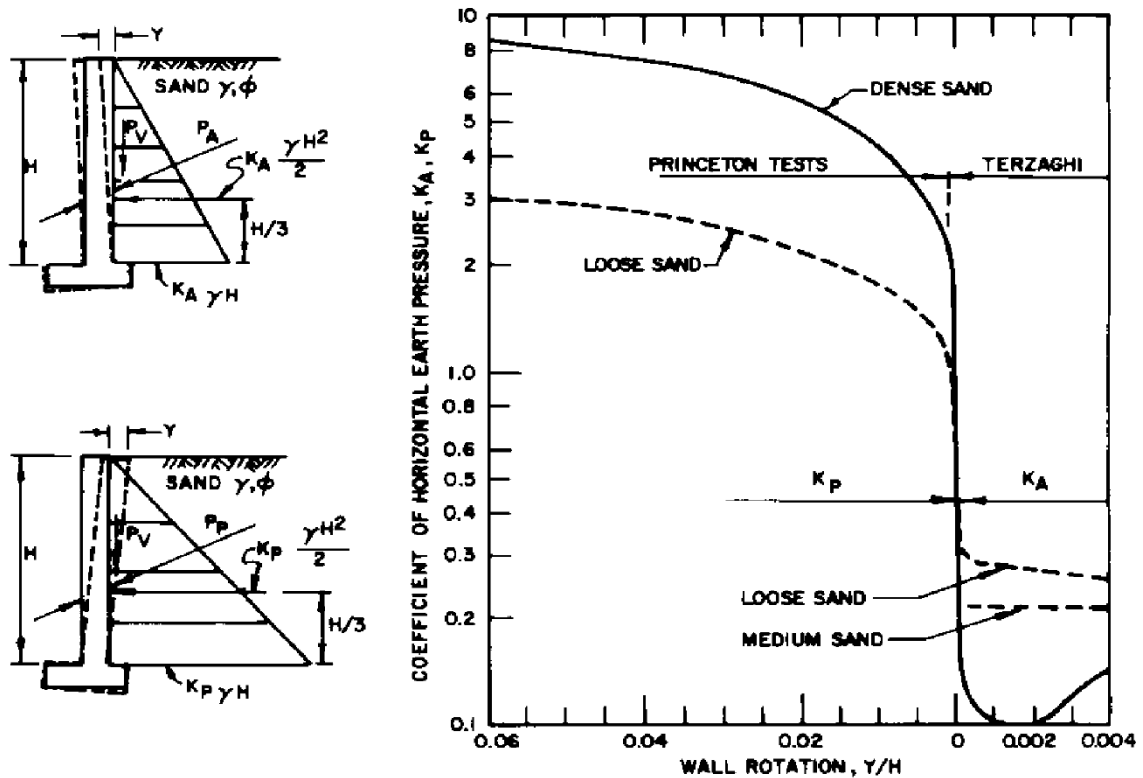


Fig 2.15 Effect of Wall Movement on Wall Pressure (Navy 1971).

Lehane, et al. (1999), presented a simplified analytical model to simulate the interaction between the abutment movement and backfill pressure for bridges with high abutments. The model uses an equivalent abutment height with a single translational spring to simulate the combined resistance offered by the actual abutment and the soil. Expressions for the equivalent abutment height and the spring stiffness are derived using data obtained from parametric computer studies which modeled the backfill soil as a linear elastic continuum of stiffness E_s as shown in figure 2.16.

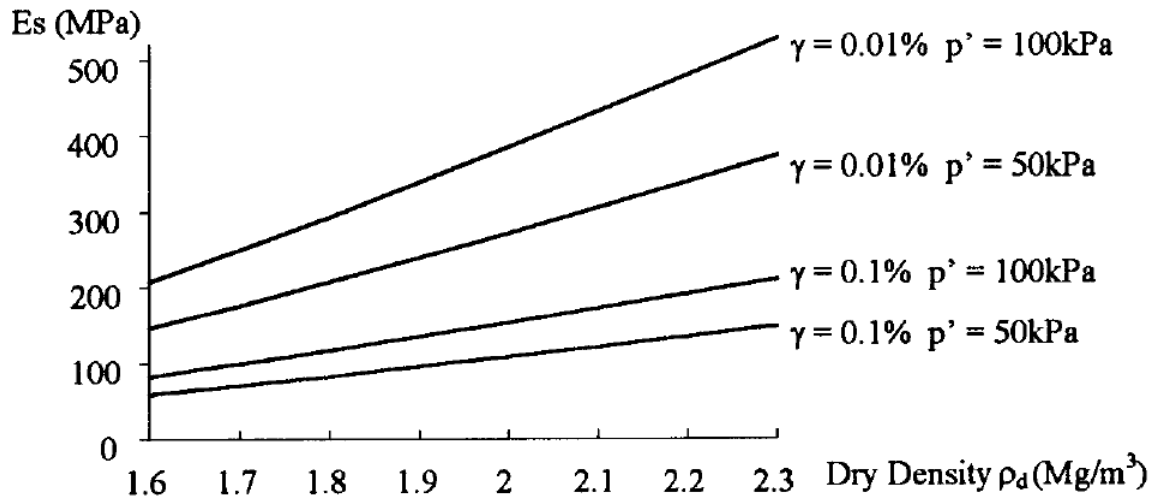


Fig 2.16 Young's Modulus (E_s) of Backfill Soil for a Range of In-Situ Dry Densities (ρ_d), Mean Effective Stresses (p') and Average Shear Strain Levels (γ) (Lehane et al. 1999)

In general, the use of un-compacted backfill is not recommended because it reduces the vertical support of the approach slab and results in greater stresses and moments in the approach slab (Olson et al. 2009)

2.9 TEMPERATURE VARIATION IN INTEGRAL ABUTMENT BRIDGES

The temperature ranges specified in the AASHTO-LRFD are usually used in the design of IABs and they will be used in this research. Two types of temperature variation are specified in the AASHTO-LRFD. Those are the uniform temperature (TU) and the temperature gradient (TG). AASHTO-LRFD specifies different uniform temperature ranges for both steel and concrete bridges in cold and moderate climates. Those temperature ranges are summarized in table 2.11. The difference between the base construction temperature and the lower and upper values shown in table 2.8 shall be used to calculate thermal deformation effect.

Table 2.11 Uniform Temperature Ranges (AASHTO-LRFD, 2010)

Climate	Steel	Concrete
Moderate	-18° to 50° C (0° to 120° F)	-12° to 27° C (10° to 80° F)
Cold	-35° to 50° C (-30° to 120° F)	-18° to 27° C (0° to 80° F)

Roeder (2003) suggests that higher temperature and consequently larger movements are required in the north central regions of the United States. Field measurements from a study on concrete IABs bridges in Minnesota showed that the deck temperature exceeded the 50° C (120°F) specified by AASHTO-LRFD (Huang et al. 2004). The Study suggests that the superstructure temperature range in AASHTO-LRFD should be increased to 130°F, for the design of concrete bridges in Minnesota.

Field measurements from other studies showed superstructure temperature ranges well inside the range suggested by AASHTO-LRFD (Hassiotis et al. 2006, Breña et al. 2007).

Vertical temperature change or temperature gradient for steel and concrete superstructures with concrete decks as recommended by AASHTO-LRFD is shown in figure 2.17.

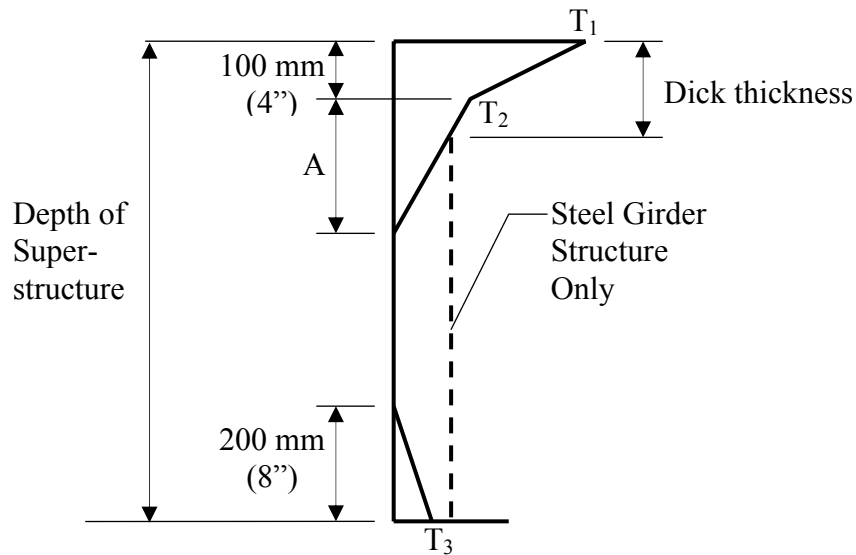


Figure 2.17 Positive Vertical Temperature Gradient in Concrete and Steel Superstructures (AASHTO-LRFD, 2010).

The dimension A in the figure varies based on the superstructure material and geometric properties. The temperatures T_1 and T_2 are specified for four different zones in the United States for positive and negative temperature variations. The temperatures T_1 shall be taken as -18°C (0°F) and can be raised to no more than -15°C (5°F) if supported by site specific data.

Temperature gradient is a major contributor to the total stresses in the superstructure and at the superstructure and abutment joint (Thippeswamy et al. 2002).

2.10 EFFECT OF SKEW IN INTEGRAL ABUTMENT BRIDGES

In general, skew has negative effects on the performance of IABs. For this reason, most States enforce a maximum value on the skew angle allowed in IABs. The value for the maximum skew angle ranges from zero to no limits with most States require maximum skew angle to be limited to 30° as can be seen in tables 2.3 through 2.5. Skew has a significant effect on the magnitude of stresses in the superstructure and substructure elements. It has also a significant effect on the magnitude and the distribution of pressure behind the abutment. Oesterle and Hamid (2005) suggest that during the expansion of IABs, the pressure on the abutment at one side of the bridge does not act in the same line of action as the pressure on the abutment at the other side as shown in figure 2.18.

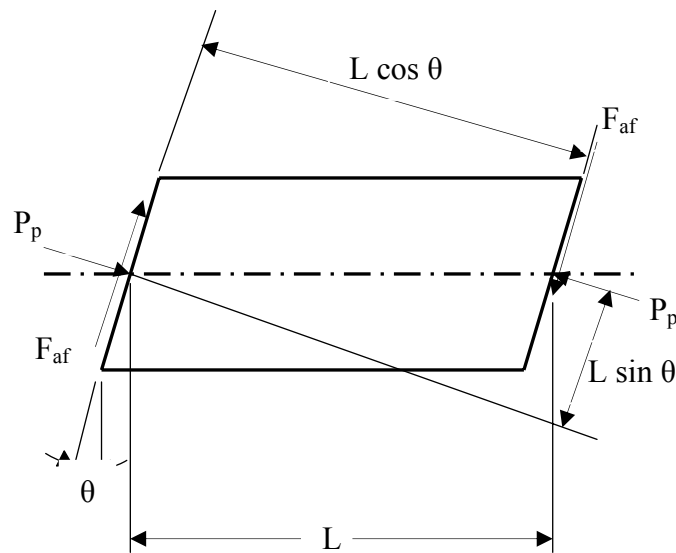


Figure 2.18 Soil Pressure Load, P_p , and Soil Abutment Interface Friction, F_{af} . (Oesterle and Hamid 2005)

The couple due to the difference in the line of action of the passive pressure on the abutment at each end of the bridge will be resisted by another couple from the friction forces between the backfill and the abutment at each end of the bridge. With large enough skew angle, the couple from the passive pressure will exceed friction couple causing the abutment to rotate. They suggest that a skew angle of 20° represents a reasonable upper limit for skewed integral bridges below for which special considerations for transverse forces or transverse movements are not needed. That angle was based on a conservative assumption for the friction angle between the backfill soil and the concrete in the abutment.

The effects of skew angle on the distribution of earth pressure behind the abutment can be significant even for relatively small skews. When a bridge with 20° skew angle in Maine was instrumented to measure the pressure behind the abutment for a bridge, researchers have found that when the greatest deck expansion occurs, the pressures at 3 meters (10 feet) from centerline on the obtuse side reach almost three times the value at the corresponding distance on the acute side (Sandford, and Elgaaly 1993). MnDOT limits the maximum length of IABs with skew angle up to 20° to 91 meters (300 feet) and to 30 meters (100 feet) for IABs with skew of 45° as can be seen in figure 2.2. In a study sponsored by MNDOT, horizontal rotation of the slab and significant biaxial bending of piles were observed in a skewed IAB with a 45° skew angle (Huang et al. 2004).

2.11 SEISMIC DESIGN OF INTEGRAL ABUTMENT BRIDGES

Research has indicated that an IAB will perform better than a conventional bridge structure in a seismic event (NJDOT 2009). IABs also eliminate the bridge seats. Inadequate bridge seats are the reason for most of the catastrophic bridge collapses due to seismic loads. The lateral stiffness of the abutment-pile support system is considered when analyzing IABs for seismic loads. Moreover, the lateral stiffness provided by the backfill soil is also considered in the analysis. Little literature is available about the design of IABs for seismic loads. Frosch et al. (2009) studied the earthquake resistance of IABs. The study does not recommend the use of pin details between the pile and the abutment and instead recommends the use of 2-foot minimum pile embedment length inside the abutment. The study also recommends a maximum total length of 300 meters (1000 feet) for IABs with special confinement reinforcement requirement for bridges longer than 150 meters (500 feet).

Itani and Pekcan (2011) suggest that the flexibility of the superstructure due to inadequate embedment in the abutment has a significant effect on the dynamic characteristics of the bridge. The engineers can also take advantage of the reduction in lateral stiffness provided by placing the top part of the pile in a sleeve (Khan, 2004).

2.12 MATERIALS IN INTEGRAL ABUTMENT BRIDGES

Structural steel and concrete are the main components of an integral bridge. The superstructure of modern integral bridges is usually composed of steel or prestressed concrete girders built monotonically with reinforced concrete stub abutments. Tennessee had a satisfying experience with concrete IABs built with High Performance Concrete (HPC) (Knickerbocker et al. 2003). Concrete and/or steel are also the main components

in the foundations for IABs. Timber piles also have been used to support IABs (Dunker and Liu, 2007). The inelastic (plastic) properties of the structural materials in integral bridge are of extreme importance due to the nature of loading on the bridge. Under normal loading conditions, the secondary forces in the superstructure could reach considerable levels. The strength of concrete used in bridges is increasing rapidly and it is common to specify concrete strength in excess of 55 MPa (8ksi) in precast prestressed concrete elements. Nowadays, the usual material specification for steel H-Piles is ASTM A572 Grade 50. Steel H-Piles are also available in ASTM grades A36 and A572 grade 42. Granular backfills are usually used behind the abutments in IABs. Other States use compressible materials and/or geofoam blocks behind the abutment instead of regular backfill to reduce backfill pressure on the abutment (Kunin and Alampalli 1999, Horvath 2000). Materials for IABs foundations will be discussed in greater details in chapters 3 and 4.

2.13 MAJOR STUDIES

Table 2.8 below summarizes the major studies that were carried out in the last 15 years to study the behavior of IABs.

Table 2.12 Major Recent Studies on IABs.

Reference	State	Research Topic	Bridge(s) In The Research	Type of Superstructure	Type of Foundation
Kim et al., 2011	Pennsylvania	Field Monitoring	- 4 Spans, 420' Long - 3 Spans, 172' Long - 1 Span, 114' Long - 1 Span, 62' Long	P.C Girders	Weak-Axis HP12x74 (HP 310X110)
Ooi et al., 2010	Hawaii	Field Behavior of an IAB Supported on Drilled Shafts	- 1 Span, 24.4 m Long	P.C Girders	NA
Huang et al. 2008	Minnesota	Parametric Study of Concrete IABs	- 3 Spans, 67 m Long	P.C Girders	Weak-Axis HP 10X42 (HP 200X63)
Davids et al., 2007	Maine	Field-Measured Response of an IAB with Short Steel H-Piles	- 1 Span, 30.92 m Long	P.C Girders	Weak-Axis HP14x89 (HP 360X132)
Breña et al. 2007	Massachusetts	Evaluation of Seasonal and Yearly Behavior of an IAB	- 3 Spans, 82.3 m Long	Steel Plate Girders	Weak-Axis HP 10X57 (HP 250X85)
Civjan et al., 2007	Massachusetts	IAB Behavior: Parametric Analysis	- 3 Spans, 82.3 m Long	Steel Plate Girders	Weak-Axis HP 10X57 (HP 250X85)
Abendroth et al., 2007	Iowa	An IAB with Precast Concrete Piles	- 1 Spans, 110' Long	P.C Girders	Precast, Prestressed Concrete Piles
Hassiotis et al., 2006	New Jersey	Field Testing	- 2 Spans, 298' Long	Steel Plate Girders	Weak-Axis HP14X102 (HP 360X152)

Table 2.12 Major Recent Studies on IABs. (Continues)

Reference	State	Research Topic	Bridge(s) In The Research	Type of Superstructure	Type of Foundation
Laman et al., 2006	Pennsylvania	Field Monitoring	- 4 Spans, 420' Long	P.C Girders	Weak-Axis HP12x74 (HP 310X110)
Abendroth et al., 2005	Iowa	Field Testing of IABs	- 3 Spans, 318' Long - 3 Spans, 201'4'' Long	P.C Girders	Weak-Axis HP 10X42 (HP 200X63)
Najm et al., 2005	New Jersey	Seismic Analysis of Retaining Walls, Buried Structures, Embankment, and IABs	- 3 Spans, 260' Long	P.C Girders	Precast Concrete Piles
Huang et al., 2004	Minnesota	Behavior of Concrete IABs	- 3 Spans, 216.6' Long	P.C Girders	Weak-Axis HP 12x53 (HP 310X79)
Burdette et al., 2004	Tennessee	Lateral Load Tests on Prestrissed Concrete Piles Supporting IABs	N.A	NA	Prestressed Concrete Piles, 14 in. (356 mm) Square
Albhaisi, 2003	Illinois	Maximum Length of IABs	N.A	P.C Girders and Steel Plate Girders	Weak and Strong Axis HP
Arsoy et al., 1999	Virginia	Field Results and a Finite Element Analysis	- 2 Spans, 30 to 98 m Long - 3 Spans, 56 m Long - 4 Spans, 55 m Long	P.C Girders	Weak-Axis HP10x42 (HP 250X63)

This page is intentionally left blank

CHAPTER 3

FOUNDATIONS FOR INTEGRAL ABUTMENT BRIDGES

3.1 GENERAL

After decades of building IABs in the United States and around the world, bridge engineers agree on the need for flexible foundation system to support IABs. For this reason they use a single row of piles to support the abutment. Steel H-Piles are the most common type of foundations used to support IABs in the United States. Steel H-Piles provide the flexibility needed to reduce the stresses in the superstructure and the ductility needed to accommodate relatively large displacements at the top of the pile. When the bearing capacity of steel H-Piles is not adequate or when noise and vibration are not desired, engineers use hybrid pile arrangement where the lower part of the steel H-Pile is embedded inside a larger concrete pile with a predrilled hole (drilled shaft). A 2005 survey (Maruri and Petro 2005) showed that 70% of the States use bearing type steel H-Piles to support IABs.

Some States (e.g. Iowa and Tennessee) consider, in addition to steel H-Piles, the use of Prestressed Concrete Piles (PCP) to support the abutment. Steel pipe piles filled with reinforced concrete are the most common type of foundations used to support IABs in Europe (White 2007). This type of piles is gaining popularity in the United States because of its superior bearing capacity. Although drilled shaft foundation are considered much stiffer than other deep foundation types and are not allowed to be used by many States in the foundation of integral bridges, Hawaii used drilled shafts to support integral abutment because of the severe corrosion conditions in the State that prohibits the use of steel H-Piles (Ooi et al. 2010).

Steel IABs bridges supported by Steel H-Piles will be the focus of this research and it will be discussed in greater details in the next section. This chapter will also include a brief description of the different types of foundations used in IABs.

3.2 STEEL H-PILES

Bridge engineers agree on the benefits of steel H-Piles in IABs but without an agreement on the orientation of the piles. Steel H-Piles could be oriented so the majority of bending (direction of traffic and thermal loading) occurs around the strong axis (Strong axis orientation) or around the weak axis (Weak axis orientation). Strong axis (X-X) orientation and weak axis orientation (Y-Y) are shown in figure 3.1.

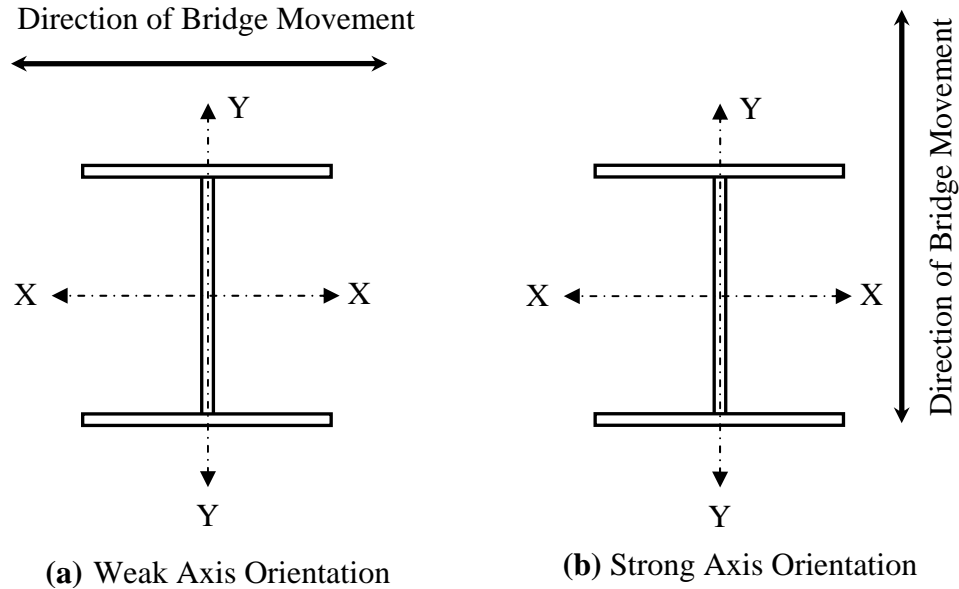


Fig. 3.1 H-Pile Orientation

A 2005 survey showed that 46% of the States orient the piles so that the pile's weak axis is parallel to the centerline of the bearings (weak axis orientation) while 33% use a strong axis orientation. The rest of the States either have no preference or leave it to the designer to decide on the pile orientation (Maruri and Petro 2005).

The section properties of all the steel H-Piles available in North America in both the strong axis orientation and weak axis orientation are presented in table 2.1. Two new sizes were added recently to the available H-Piles in North America. Those are size 410 mm (16 inch) and size 460 mm (18 in) with six sections added to size 410 mm and four sections added to size 460 mm. These sections were adopted in the 14th edition of the American Institute of Steel Construction Manual of Steel Construction (AISC 2011). One of the unique properties of steel H-Piles is their almost equal width and depth and therefore pile orientation has little effect on the lateral geotechnical capacity of the foundation soil.

Unlike the case in jointed bridges, battered (sloped) piles are not permitted in IABs and the relatively large lateral loads on the bridge are resisted by the lateral flexural rigidity of the pile-foundation system. Moreover many States orient steel H-Piles to bend around the weak axis. The combination of large lateral loads, lack of battered pile, and weak axis orientation will expose the pile to close to yield flexural stresses. This is especially true for piles oriented to bend around the weak axis where local yielding is common at the edges of the pile's flanges. From a structural point of view, weak axis orientation is not an economical choice because the full flexural capacity of the pile is not utilized. Still bridge engineers use weak axis orientation because it provides greater translational and rotational flexibility compared to strong axis orientation. As the length of the integral

abutment bridges becomes longer, the temperature-induced displacements and rotations in the steel H-Piles become larger as well. Consequently, the piles may experience deformations beyond their elastic limit especially for H-Piles with weak axis orientation. Results from research have demonstrated that stresses in the steel H-piles supporting the abutments in IABs could reach the yield strength of the pile material for long bridges

Material Properties

Nowadays, the standard material specification for steel H-Piles in the United States is ASTM A572 Grade 50. Steel H-piles are also available in ASTM A36 and A572 grade 42. A typical stress-strain relationship and a simplified stress-strain relationship for structural steel are shown in figures 3.2 and 3.3 respectively.

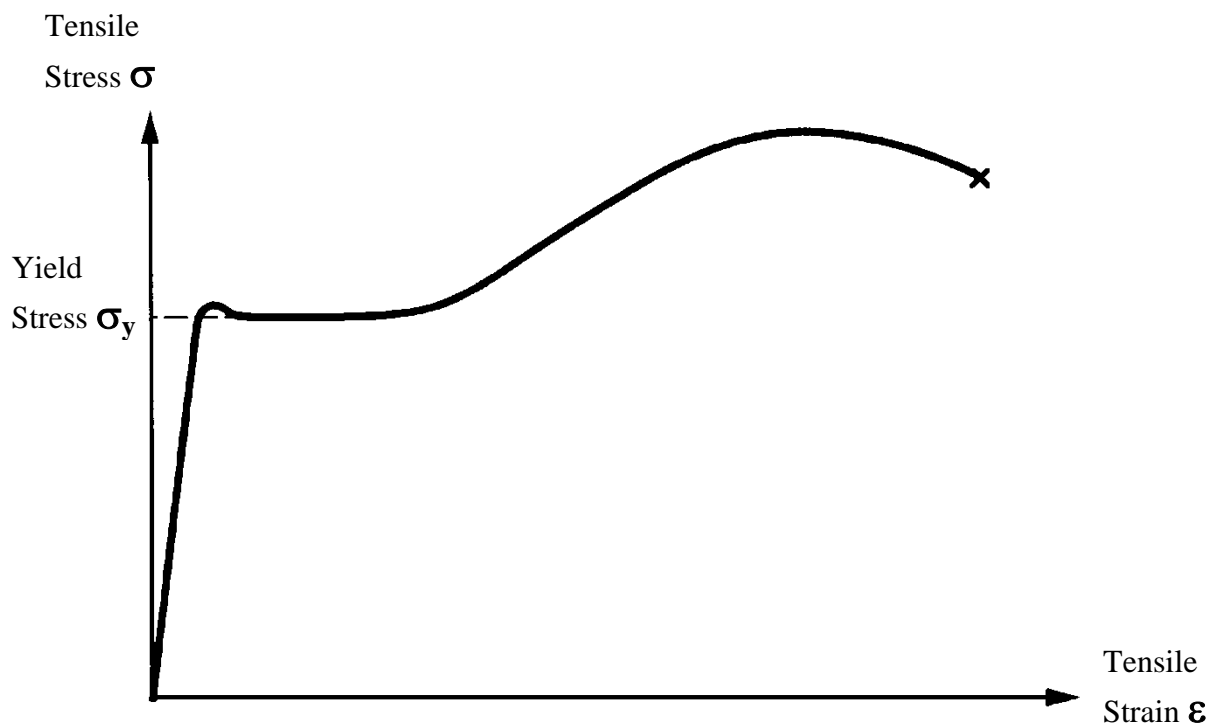


Fig. 3.2 Typical Stress -Strain Relationship for Steel

Table 3.1 Properties of H-Piles Available in North America (AISC 2005)

AISC LABEL	H	Weight	Area	Depth	BF	TW	TF	IX	ZX	SX	IY	ZY	SY	J
Metric (English)	(mm) (in)	(kg/m) (lb/ft)	(mm²) (in²)	(mm) (in)	(mm) (in)	(mm) (in)	(mm) (in)	(mm⁴) (in⁴)	(mm³) (in³)	(mm³) (in³)	(mm⁴) (in⁴)	(mm³) (in³)	(mm³) (in³)	(mm⁴) (in⁴)
HP360X174 (HP14X117)	360 (14)	174 (117)	22200 (34.4)	361 (14.2)	378 (14.9)	20.4 (0.805)	20.4 (0.805)	5.08E+08 (1220)	3.18E+06 (194)	2.82E+06 (172)	1.84E+08 (443)	1.50E+06 (91.4)	9.75E+05 (59.5)	3.34E+06 (8.02)
HP360X152 (HP14X102)	360 (14)	152 (102)	19400 (30.0)	356 (14.0)	376 (14.8)	17.9 (0.705)	17.9 (0.705)	4.37E+08 (1050)	2.77E+06 (169)	2.46E+06 (150)	1.58E+08 (380)	1.29E+06 (78.8)	8.42E+05 (51.4)	2.24E+06 (5.39)
HP360X132 (HP14X89)	360 (14)	132 (89.0)	16800 (26.1)	351 (13.8)	373 (14.7)	15.6 (0.615)	15.6 (0.615)	3.76E+08 (904)	2.39E+06 (146)	2.15E+06 (131)	1.36E+08 (326)	1.11E+06 (67.7)	7.26E+05 (44.3)	1.49E+06 (3.59)
HP360X108 (HP14X73)	360 (14)	108 (73)	13800 (21.4)	345 (13.6)	371 (14.6)	12.8 (0.505)	12.8 (0.505)	3.03E+08 (729)	1.93E+06 (118)	1.75E+06 (107)	1.09E+08 (261)	8.95E+05 (54.6)	5.87E+05 (35.8)	8.37E+05 (2.01)
HP310X125 (HP12X84)	310 (12)	125 (84.0)	15900 (24.6)	312 (12.3)	312 (12.3)	17.4 (0.685)	17.4 (0.685)	2.71E+08 (650)	1.97E+06 (120)	1.74E+06 (106)	8.87E+07 (213)	8.72E+05 (53.2)	5.67E+05 (34.6)	1.76E+06 (4.24)
HP310X110 (HP12X74)	310 (12)	110 (74)	14100 (21.8)	307 (12.1)	310 (12.2)	15.4 (0.605)	15.5 (0.610)	2.37E+08 (569)	1.72E+06 (105)	1.54E+06 (93.8)	7.74E+07 (186)	7.64E+05 (46.6)	4.98E+05 (30.4)	1.24E+06 (2.98)
HP310X93 (HP12X63)	310 (12)	93.0 (63.0)	11900 (18.4)	302 (11.9)	307 (12.1)	13.1 (0.515)	13.1 (0.515)	1.96E+08 (472)	1.45E+06 (88.3)	1.30E+06 (79.1)	6.37E+07 (153)	6.34E+05 (38.7)	4.15E+05 (25.3)	7.62E+05 (1.83)
HP310X79 (HP12X53)	310 (12)	79.0 (53)	10000 (15.5)	300 (11.8)	305 (12.0)	11.0 (0.435)	11.0 (0.435)	1.64E+08 (393)	1.21E+06 (74)	1.09E+06 (66.7)	5.29E+07 (127)	5.28E+05 (32.2)	3.46E+05 (21.1)	4.66E+05 (1.12)
HP250X85 (HP10X57)	250 (10)	85.0 (57.0)	10800 (16.8)	254 (10.0)	259 (10.2)	14.4 (0.565)	14.4 (0.565)	1.22E+08 (294)	1.09E+06 (66.5)	9.64E+05 (58.8)	4.20E+07 (101)	4.97E+05 (30.3)	3.23E+05 (19.7)	8.20E+05 (1.97)
HP250X62 (HP10X42)	250 (10)	62.0 (42)	8000 (12.4)	246 (9.7)	257 (10.1)	10.5 (0.415)	10.7 (0.420)	8.74E+07 (210)	7.91E+05 (48.3)	7.11E+05 (43.4)	2.98E+07 (71.7)	3.57E+05 (21.8)	2.33E+05 (14.2)	3.38E+05 (0.813)
HP200X53 (HP8X36)	200 (8)	53.0 (36.0)	6840 (10.6)	204 (8.02)	207 (8.16)	11.3 (0.445)	11.3 (0.445)	4.95E+07 (119)	5.51E+05 (33.6)	4.88E+05 (29.8)	1.68E+07 (40.3)	2.49E+05 (15.2)	1.62E+05 (9.88)	3.21E+05 (0.770)

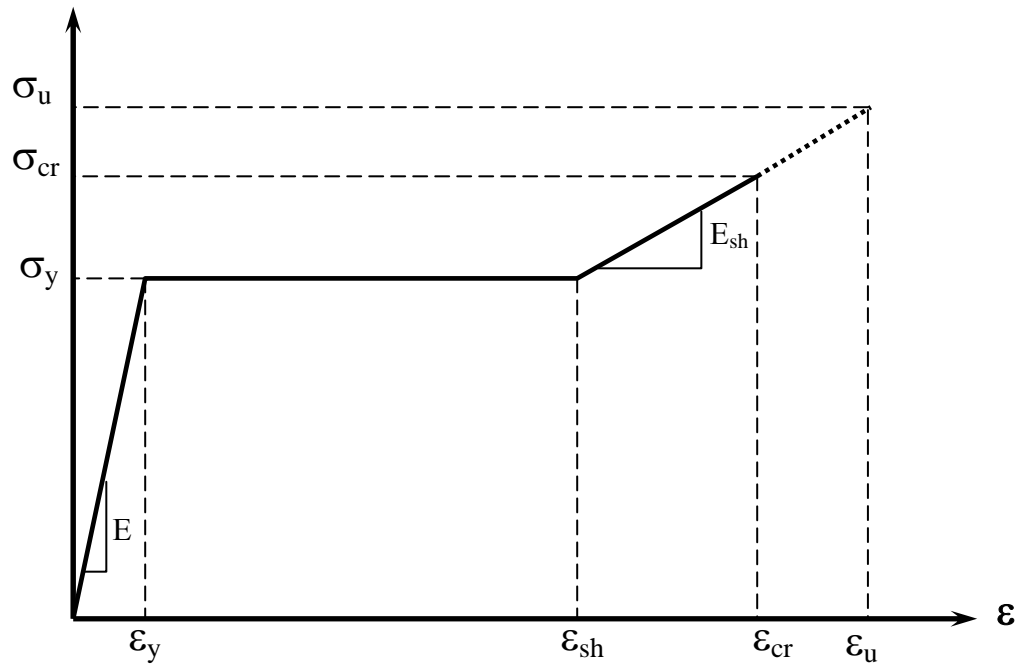


Fig. 3.3 Simplified Stress -Strain Relationship for Steel

In figure 3.3 ϵ_y is the strain in steel at yield, ϵ_{sh} is the strain in steel at strain hardening, ϵ_u is the ultimate strain, σ_y is the yielding stress, and σ_u is the ultimate stress. The terms, σ_{cr} and ϵ_{cr} in the figure above are the critical stress and strain at local buckling (Kato 1998). The material properties indicated on the stress-strain curve of figure 3.3 are tabulated in Table 3.2 for steel grades ASTM A36 and A572 grade 42 and 50.

Table 3.2 Mechanical Properties of Steels in Used in H-Piles (ASTM 2007, 2008, Galambos and Ravindra 1978)

ASTM Designation	E (MPa)	E _{sh} (MPa)	ϵ_y (m/m)	ϵ_{sh}/ϵ_y	ϵ_u/ϵ_y	σ_y (MPa)
ASTM A36	200000	4100	0.00125	10	70	250
ASTM A572grade 42	200000	2600	0.00145	8.7	86	290
ASTM A572 grade 50	200000	2600	0.00173	8.7	86	345

3.2.1 Stability of Steel H-Piles

The flexural capacity and displacement capacity of steel members are affected by their buckling instability. Instability in steel structural members includes local buckling of the plates forming the cross-section of the member as well as lateral torsional and global buckling of the steel member. Local buckling instability in steel H-Piles may occur in either the flange or web or both depending on the width to thickness ratios of the flange and web plates. Lateral torsional buckling, which occurs when steel members are subjected to bending about their strong axis, is critical for steel sections with relatively narrow flanges and is not critical in steel H-Piles that have wider flanges and almost equal width and depth. Furthermore, as the steel H-piles in integral abutment bridges are laterally supported by the surrounding soil, the lateral-torsional and global buckling instability need not be considered. Thus, the local buckling is usually the only instability type that considered when calculating the flexural capacity and the displacement capacity of steel H-Piles fully embedded in soil.

3.2.2.1 AISC Approach to Local Buckling in Steel Sections

The manual of steel construction (AISC, 2005) divides the steel sections into three categories based on their ability to reach a certain compressive stress level and deform without experiencing local buckling problems. These are compact sections, non-compact sections, and sections with slender plate elements (web and/or flange). Compact sections are capable of developing full plastic flexural capacity. Non-compact sections cannot develop full plastic capacity, but are capable of developing yield stress in compression elements. The third category covers steel sections with slender plate elements that experience local buckling before reaching the yield stress. The dividing lines between these three categories are defined by slenderness parameters λ_p and λ_r that define the limiting width to thickness ratios for compact and non-compact sections respectively. For compact sections, the width to thickness ratios for the web and flange are smaller than λ_p . For non-compact sections, they are larger than λ_p but smaller than λ_r and for slender sections, they are larger than λ_r . Table 3.3 displays the expressions for λ_p and λ_r for flexure in flanges and webs of hot rolled I-Shaped sections under compression.

Table 3.3 Limiting Ratios for Steel Sections under Compression (AISC, 2005)

Width-Thickness Ratio	Limiting Width-Thickness Ratios	
	λ_p (ASTM 572 Grade 50)	λ_r (ASTM 572 Grade 50)
b/t	$0.38 \sqrt{\frac{E}{F_y}}$	$1.0 \sqrt{\frac{E}{F_y}}$
h/t_w	$3.76 \sqrt{\frac{E}{F_y}}$	$5.7 \sqrt{\frac{E}{F_y}}$

b is half the flange width, h is the clear height of the web plate between flanges, t_f is the flange width, t_w is the web width, E is the structural steel modulus of elasticity, and F_y is the yield stress.

A summary of the width-thickness ratios for the flange and the web for all the H-Piles sections are presented in table 3.4. The table shows HP360X174, HP310X125, HP250X85, and HP200X53 are compact sections ($\lambda < \lambda_p$). The rest of the sections are not capable of developing full plastic flexural capacity but can develop strength above the yield flexural strength ($\lambda_p < \lambda < \lambda_r$).

Table 3.4 Width-Thickness Ratios for H-P Sections (AISC, 2005, A572 Grade 50 Steel)

Shape Metric (US)	Flange			Wed		
	λ	λ_p	λ_r	λ	λ_p	λ_r
HP360X174 (HP14X117)	8.8	9.2	24.1	14.0	90.6	137.3
HP360X152 (HP14X102)	9.9	9.2	24.1	16.0	90.6	137.3
HP360X132 (HP14X89)	11.2	9.2	24.1	18.3	90.6	137.3
HP360X108 (HP14X73)	13.5	9.2	24.1	22.3	90.6	137.3
HP310X125 (HP12X84)	9.0	9.2	24.1	13.9	90.6	137.3
HP310X110 (HP12X74)	9.9	9.2	24.1	15.7	90.6	137.3
HP310X93 (HP12X63)	11.6	9.2	24.1	18.4	90.6	137.3
HP310X79 (HP12X53)	13.6	9.2	24.1	21.8	90.6	137.3
HP250X85 (HP10X57)	8.8	9.2	24.1	13.3	90.6	137.3
HP250X62 (HP10X42)	11.5	9.2	24.1	18.1	90.6	137.3
HP200X53 (HP8X36)	9.0	9.2	24.1	12.9	90.6	137.3

3.2.2.2 Kato's (1989) Web-Flange Interaction Approach to Local Buckling in Steel H-Piles Sections

Kato (1998) has introduced a web-flange interaction approach to calculate the local buckling strength of steel H-Pile sections. The approach defined the local buckling strength of an H-Pile section considering the interaction between the web and flanges since the web restrains the buckling of the flanges and vice versa the flanges restrain the buckling of the web.

Using a total of 68 test data on stub-columns made of HP sections, Kato developed the following linear regression formula to relate the maximum stress, σ_u , that an HP section can undergo without local buckling, to the yield stress, σ_y , of the material.

$$\frac{1}{s} = 0.6003 + \frac{1.600}{\alpha_f} + \frac{0.1535}{\alpha_w} \quad (3.1)$$

Where s is the normalized critical stress $= \sigma_u/\sigma_y$ and, α_f and α_w are the slenderness parameters for the flange and web respectively. The slenderness parameters, α_f and α_w are defined as functions of the geometric and material properties of the HP-sections as follows;

$$\alpha_f = \frac{E}{\sigma_y} \left(\frac{t_f}{b_f/2} \right)^2 \quad (3.2)$$

$$\alpha_w = \frac{E}{\sigma_y} \left(\frac{t_w}{d_w} \right)^2 \quad (3.3)$$

A summary of the slenderness parameters for the flange and the web and the normalized critical stress for all the H-Piles sections are presented in table 3.5 (Albhaisi 2003). The table shows that the normalized critical stress s for HP360X174, HP310X125, HP250X85, and HP200X53 is greater than 1.1. Those are the same sections that were classified as compact sections in the AISC method.

Table 3.5 Slenderness Parameter s of HP Sections (Kato, 1989, A572 – Grade 50)

Shape Metric (US)	α_f	α_w	s
HP360X174 (HP14X117)	6.757	2.354	1.108
HP360X152 (HP14X102)	5.258	1.813	1.011
HP360X132 (HP14X89)	4.058	1.380	0.904
HP360X108 (HP14X73)	2.762	0.926	0.743
HP310X125 (HP12X84)	7.216	2.285	1.125
HP310X110 (HP12X74)	5.800	1.816	1.041
HP310X93 (HP12X63)	4.197	1.299	0.909
HP310X79 (HP12X53)	2.998	0.915	0.768
HP250X85 (HP10X57)	7.116	2.371	1.104
HP250X62 (HP10X42)	4.053	1.316	0.900
HP200X53 (HP8X36)	6.914	2.251	1.111

3.2.2 Moment-Curvature Relationships

Albhaisi (2003) developed the moment-curvature relationships (MCRs) for the HP sections that can develop yielding stress before local buckling. Those are the sections with normalized critical stress, s , equal or larger than 1. The MCRs were developed using spreadsheets for different levels of axial loads on the piles. The MCRs will be used to estimate the displacement capacity of the steel H-piles under cyclic loading. In the development of MCRs, the round corners at the intersection of web and flanges are assumed straight. This resulted in an error of less than 1 % in the geometric properties such as cross-section area and plastic modulus. MCRs were developed for both strong and weak axis bending. The axial load on the piles ranges from 0% to 60% of the axial yield capacity, P_y , of the section. Tables 3.6 and 3.7 summarize the results of the MCR calculations for the strong and weak axes bending for ASTM A572 grade 50 steel (Albhaisi 2003). The parameters used in the tables are depicted from the moment-curvature diagram shown in figure 3.4.

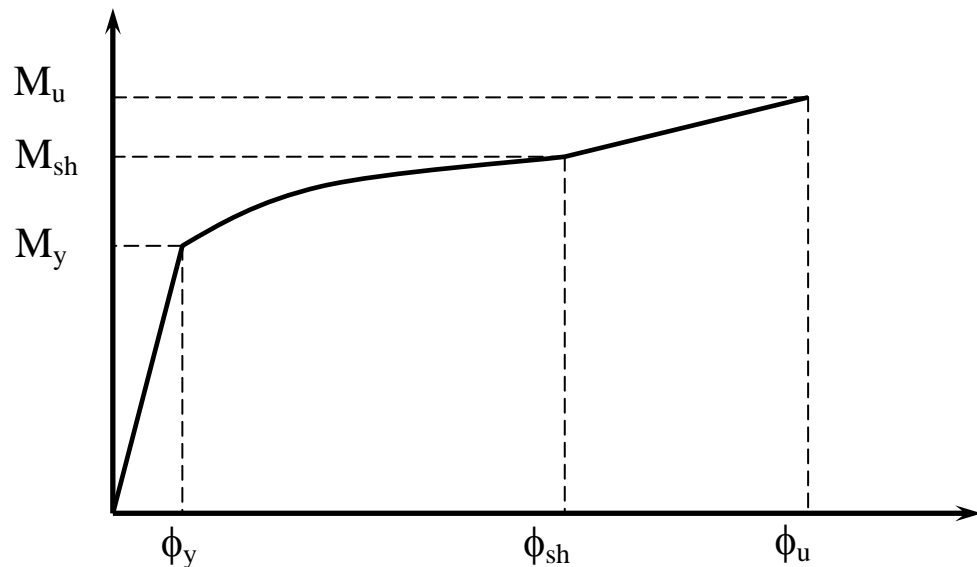


Fig 3.4 Typical Moment-Curvature Relationship

Table 3.6 Summary of MCRs for H-Pile Sections (Weak Orientation, A572 grade 50)

Section	P/P _y	ϕ_y	M _y (KN.m)	ϕ_{sh}	M _{sh} (KN.m)	ϕ_u	M _u (KN.m)
HP360X174	0.0	0.00901	335.1	0.08198	503.9	0.1600	533.9
	0.1	0.00811	301.6	0.07632	502.7	0.1505	528.3
	0.2	0.00721	268.1	0.07397	500.8	0.1474	525.0
	0.3	0.00631	234.6	0.07146	496.9	0.1470	519.6
	0.4	0.00541	201.1	0.06796	487.0	0.1350	507.4
	0.5	0.00451	167.5	0.06112	456.6	0.1204	477.1
	0.6	0.00361	134.0	0.05504	404.4	0.1085	429.4
HP360X152	0.0	0.00906	290.8	0.08304	436.9	0.0910	438.2
	0.1	0.00816	261.8	0.07672	435.7	0.0842	436.6
	0.2	0.00725	232.7	0.07437	434.2	0.0818	435.2
	0.3	0.00634	203.6	0.07193	431.1	0.0890	432.4
	0.4	0.00544	174.5	0.06849	423.1	0.0753	424.3
	0.5	0.00453	145.4	0.06149	396.7	0.0673	397.5
	0.6	0.00362	116.3	0.05537	351.4	0.0606	352.4
HP310X125	0.0	0.01092	194.7	0.09535	292.8	0.1992	312.0
	0.1	0.00983	175.3	0.09253	292.3	0.1959	310.4
	0.2	0.00874	155.8	0.08961	291.3	0.1853	303.7
	0.3	0.00765	136.3	0.08677	289.1	0.1901	305.0
	0.4	0.00655	116.8	0.08273	283.7	0.1776	298.4
	0.5	0.00546	97.4	0.07406	265.3	0.1527	273.5
	0.6	0.00437	77.9	0.06669	235.0	0.1383	244.3
HP310X110	0.0	0.01099	171.2	0.09595	257.1	0.1303	260.8
	0.1	0.00989	154.1	0.09313	256.7	0.1273	260.0
	0.2	0.00879	137.0	0.09033	255.8	0.1243	259.1
	0.3	0.00769	119.9	0.08769	254.3	0.1301	257.4
	0.4	0.00659	102.7	0.08346	249.6	0.1150	252.7
	0.5	0.00550	85.6	0.07536	235.5	0.1025	238.1
	0.6	0.00440	68.5	0.06766	209.2	0.0921	212.6
HP250X85	0.0	0.01311	111.9	0.11442	168.2	0.2382	179.1
	0.1	0.01180	100.7	0.11099	168.0	0.2342	178.2
	0.2	0.01048	89.5	0.10761	167.4	0.2295	177.0
	0.3	0.00917	78.3	0.10399	166.0	0.2273	175.1
	0.4	0.00786	67.2	0.09900	162.8	0.2113	171.1
	0.5	0.00655	56.0	0.08920	153.0	0.1885	161.1
	0.6	0.00524	44.8	0.08024	135.6	0.1697	145.4
HP200X63	0.0	0.01646	55.7	0.14371	83.7	0.2834	88.4
	0.1	0.01482	50.1	0.13944	83.5	0.2785	88.0
	0.2	0.01317	44.5	0.13521	83.2	0.2729	87.4
	0.3	0.01152	39.0	0.13072	82.6	0.2718	86.5
	0.4	0.00988	33.4	0.12455	81.0	0.2517	84.6
	0.5	0.00823	27.8	0.11225	76.2	0.2242	79.7
	0.6	0.00658	22.3	0.10092	67.6	0.2016	71.9

Table 3.7 Summary of MCRs for H-Pile Sections (Strong Orientation, A572 grade 50)

Section	P/P _y	ϕ_y	M _y (KN.m)	ϕ_{sh}	M _{sh} (KN.m)	ϕ_u	Mu (KN.m)
HP360X174	0.0	0.0095	961.17	0.0827	1083.90	0.1615	1176.3
	0.1	0.0086	865.1	0.0641	1062.9	0.1341	1131.9
	0.2	0.0076	768.9	0.0521	1001.0	0.1096	1081.2
	0.3	0.0067	672.8	0.0472	893.6	0.0914	998.6
	0.4	0.0057	576.7	0.0458	768.8	0.0875	878.6
	0.5	0.0048	480.6	0.0446	642.4	0.0859	752.5
	0.6	0.0038	384.5	0.0433	515.4	0.0845	624.6
HP360X152	0.0	0.0097	839.94	0.0839	941.09	0.0919	944.53
	0.1	0.0087	755.9	0.0648	922.8	0.0714	926.0
	0.2	0.0077	672.0	0.0527	868.9	0.0579	873.5
	0.3	0.0068	588.0	0.0477	775.2	0.0519	781.8
	0.4	0.0058	504.0	0.0463	666.6	0.0505	673.3
	0.5	0.0048	420.0	0.0451	557.0	0.0492	563.4
	0.6	0.0039	336.0	0.0438	446.8	0.0479	453.0
HP310X125	0.0	0.0110	589.02	0.0957	665.45	0.2006	731.43
	0.1	0.0099	530.1	0.0747	652.9	0.1679	703.8
	0.2	0.0088	471.2	0.0610	615.8	0.1391	671.8
	0.3	0.0077	412.3	0.0547	549.8	0.1159	622.9
	0.4	0.0066	353.4	0.0531	474.6	0.1087	552.7
	0.5	0.0055	294.5	0.0517	396.6	0.1067	475.3
	0.6	0.0044	235.6	0.0502	318.2	0.1051	396.3
HP310X110	0.0	0.0110	589.02	0.0957	665.45	0.2006	731.43
	0.1	0.0099	530.1	0.0747	652.9	0.1679	703.8
	0.2	0.0088	471.2	0.0610	615.8	0.1391	671.8
	0.3	0.0077	412.3	0.0547	551.4	0.1164	624.2
	0.4	0.0066	353.4	0.0531	474.6	0.1087	552.7
	0.5	0.0055	294.5	0.0517	396.6	0.1067	475.3
	0.6	0.0044	235.6	0.0502	318.2	0.1051	396.3
HP250X85	0.0	0.0135	329.03	0.1176	371.57	0.2455	408.16
	0.1	0.0122	296.1	0.0914	364.5	0.2051	392.6
	0.2	0.0108	263.2	0.0745	343.5	0.1695	374.8
	0.3	0.0095	230.3	0.0672	307.1	0.1414	347.8
	0.4	0.0081	197.4	0.0652	264.3	0.1331	307.6
	0.5	0.0068	164.5	0.0634	220.8	0.1306	264.4
	0.6	0.0054	131.6	0.0616	177.2	0.1286	220.5
HP200X63	0.0	0.0140	210.0	0.1214	237.43	0.2402	258.25
	0.1	0.0126	189.0	0.0970	233.3	0.2028	249.2
	0.2	0.0112	168.0	0.0805	221.3	0.1701	238.3
	0.3	0.0098	147.0	0.0700	200.7	0.1441	222.3
	0.4	0.0084	126.0	0.0676	173.0	0.1305	197.9
	0.5	0.0070	105.0	0.0657	144.6	0.1278	169.6
	0.6	0.0056	84.0	0.0637	116.1	0.1257	140.8

3.2.3 Abutment-H-Pile Connection

In jointed bridges, AASHTO LRFD requires the pile to be embedded or projected at least 300 mm (12 in) inside the pile cap after all damaged material has been removed (AASHTO, 2010). If the pile is attached to the cap by embedded bars or strands, the pile shall extend no less than 150 mm (6.0 in) into the cap. Similar requirements are used by most States. These embedment lengths are required to transfer forces between the pile and pile cap and are not expected to allow for the development of full flexural capacity of the pile at the connection. When large lateral loads on the abutments and/or the piers exist, they are usually resisted by battered piles. The slope of battered piles could be up to $1/3$.

In general, battered piles are not allowed to support abutments in IABs because of their large lateral stiffness and only a single row of piles is used to support the abutment and to resist lateral loads. To utilize the pile full lateral load carrying capacities, piles must be embedded in the abutment adequately to develop the full moment capacity of the pile. In the majority of IAB's, bridge engineers design the pile's top connection for fixed condition and a moment connection is assumed between the pile and the abutment in the analysis. To insure the required fixity, the minimum embedment length shall be calculated.

The minimum embedment length required to develop a moment connection for steel H-Piles inside the abutment is significantly higher than the 300 mm required in jointed bridges. Equations 3.4 and 3.5 are used by Oregon Department of Transportation (ODOT 2004) to calculate the minimum pile embedment length based on the free body diagram of the pile shown in Figure 3.5.

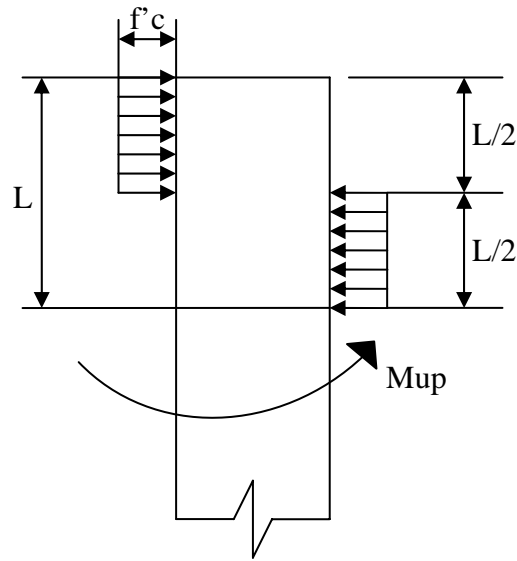


Figure 3.5 Free Body Diagram of Pile Embedded in Abutment (ODOT, 2004)

Where,

$$M_{up} = \phi f'cD \left(\frac{L}{2} \times \frac{3L}{4} - \frac{L}{2} \times \frac{L}{4} \right) \quad (3.4)$$

$$4M_{up} = \phi f'cDL^2 \Rightarrow L = \sqrt{\frac{4M_{up}}{\phi f'cD}} \quad (3.5)$$

Based on the above equation, ODOT recommends the minimum embedment length given in table 3.8 for different piles.

Table 3.8 Minimum Required Pile Embedment Length inside the Abutment to Develop Fixity for $f'c = 23 \text{ MPa}$ (3.3 ksi) and $f_y = 250 \text{ MPa}$ (36 ksi) (ODOT 2004)

Pile	Minimum Embedment Length
HP250X62 (10X42) HP310X79 (12X53)	500 mm (20")
HP310X110 (12X74) HP360X152 (14X89)	600 mm (24")
HP360X174 (14X117)	700 mm (27")

The values shown in the table are based on concrete strength of 23 MPa (3.3 ksi) and steel yield strength f_y of 250 MPa (36 ksi). The values given in the table are for strong axis orientation of the pile.

Using the same equations, the minimum embedment length can be calculated for the more grade of steel H-Piles ASTM A572 Grade 50. The values in table 3.9 are based on concrete strength of 27 MPa (4 ksi) and steel yield strength f_y of 345 MPa (50 ksi). The values given in the table are for strong axis orientation of the pile.

Table 3.9 Minimum Required Pile Embedment Length inside the Abutment to Develop Fixity for $f'_c = 27$ MPa (4 ksi) and $f_y = 345$ MPa (50 ksi)

Pile	Minimum Embedment Length	
	Strong Axis Orientation	Weak Axis Orientation
HP250X62 (10X42) HP310X79 (12X53)	550 mm (22")	380 mm (15")
HP310X110 (12X74) HP360X132 (14X89)	700 mm (28")	500 mm (20")
HP360X174 (14X117)	800 mm (32")	560 mm (22")

So for the largest H-Pile available in North America, the minimum embedment length required when the pile is oriented to bend around the weak axis is 560 mm. Laboratory testing showed that an embedment length of 600 mm (24 in) was enough to develop the full later load carrying capacity of HP360X132 (14X89) (Frosch et al. 2009). The testing also showed that embedment length of 380 mm (15 in) was not enough to develop the full later load carrying capacity of HP310X79 (12X53). The values in table 2.5 are in agreement with embedment length specified by different transportation agencies in the United States. Figures 2.3 and 2.4 show that the minimum embedment length used by NYSDOT is 600 mm. Similar minimum lengths are required by other States. MNDOT uses 760 mm (2'-6") embedment length for fixed head conditions (MNDOT 2004).

Unless noted otherwise, a moment connection is assumed between the pile and the abutment throughout this research.

3.3 PRESTRESSED CONCRETE PILES (PCPs)

PCPs are commonly used to support the abutment in IAB's in Europe (White 2007) but have not been widely used to support IABs in the United States because of concerns over pile flexibility and the potential for concrete cracking and prestressing strand corrosion (Abendroth et al. 2007). PCPs are allowed by some States (e.g. New Jersey, Iowa, and Tennessee) especially in harsh corrosive conditions where the use of H-Piles is prohibited. NJDOT allows the use of PCPs for bridges shorter than 150 feet (46 meters) without restriction on the size of the pile (NJDOT 2009).

For longer bridges, special considerations are needed to reduce the tensile stresses in the PCPs. One of these considerations is to provide more rotational freedom at the top of the pile to reduce the moment. Kamel et al. (1995) suggested the use of a joint consists of neoprene bearing pad with a Teflon layer. IOWA Department of Transportation used a different technique to reduce the moment at the top of the pile. The pile top of a 110-ft long bridge was wrapped with a double layer of carpet prior to placing the abutment concrete and the bridge was instrumented to measure the effectiveness of this technique (Abendroth et al. 2007). The results from the field data were inconclusive and the researchers could not decide on the effectiveness of the technique. A study sponsored by Tennessee Department of Transportation (TDOT) (Burdette et al. 2004) showed that PC 356X356 piles could take horizontal displacement in excess of 25 mm (1.0 inch) before failure. PCP 356mmX356mm (14 in X 14 in) is the most common pile used in IABs.

The effect of using PCP's on the performance of IABs will be studied in this research.

Typical Precast-Prestressed Concrete Pile details are shown in figure 3.6.

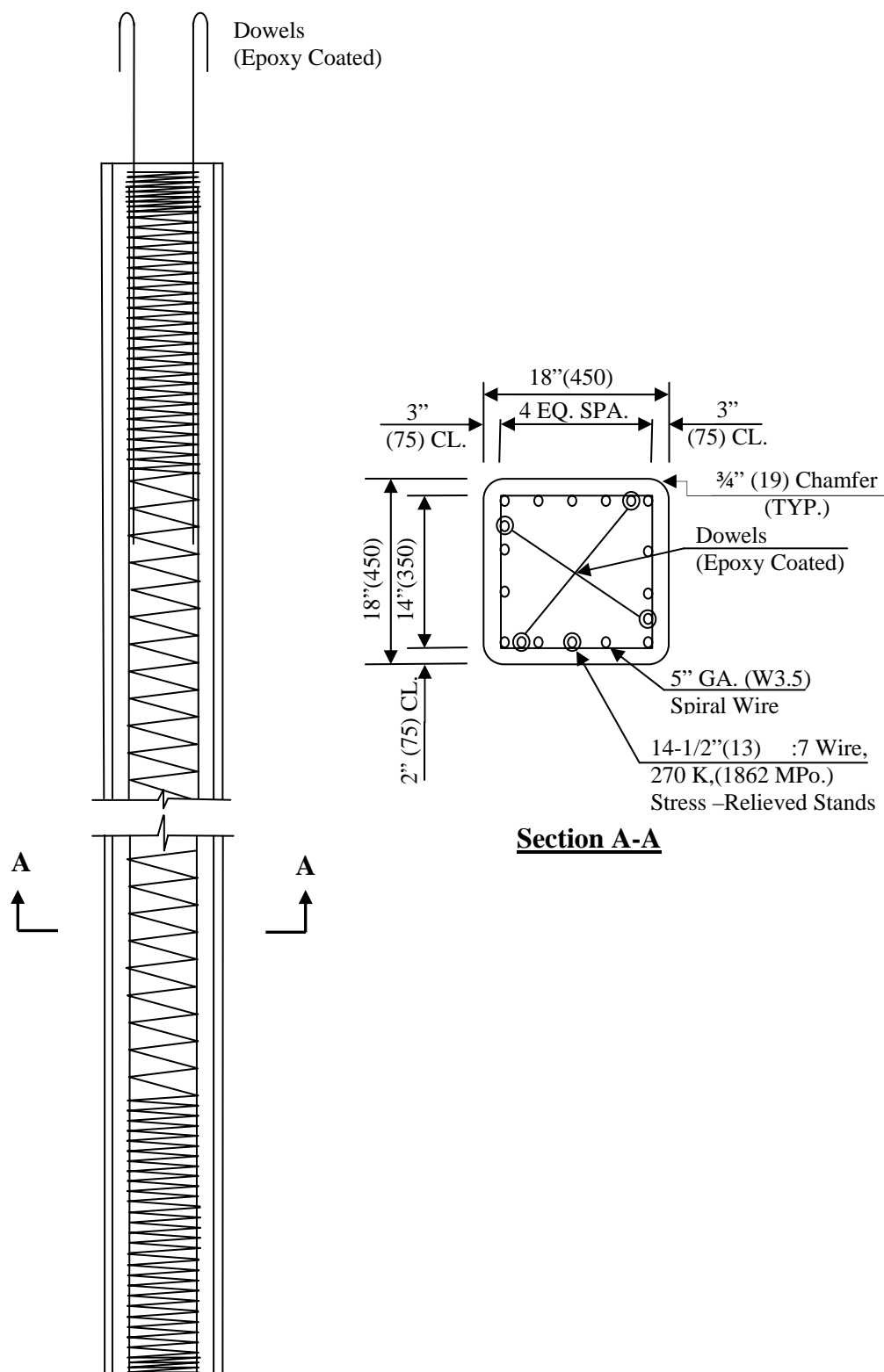


Figure 3.6 Typical Precast-Prestressed Concrete Pile Details (Delaware DOT, 2005)

3.4 STEEL PIPE PILES

Steel pipe piles filled with reinforced concrete are the most common type of foundations used to support IABs in Europe. These pipe piles are typically 700 mm (2.25 ft) in diameter but can be up to 1.2 m in diameter (4 ft). (White 2007). This type of piles is gaining popularity in the United States because of its superior bearing capacity. Steel pipe piles filled with reinforced concrete are not as flexible as H-Piles. NJDOT allows the use of hollow steel pipe piles for bridges shorter than 150 feet (46 meters) without restriction on the size of the pipe (NJDOT, 2009). To reduce the stiffness of these piles, it is a common practice in New Jersey to encase the top part of the pile below the abutment with a larger sleeve filled with sand or crushed stone. Steel pipe piles with diameters close to 600 mm (2.0 ft) have been used to support IAB's in New Jersey. NJDOT (2007) specifies ASTM 252 Grade 2 for all steel pipe piles and steel casings for drilled shafts. Typical details of steel pipe piles filled with reinforced concrete are shown in figures 3.7 and 3.8.

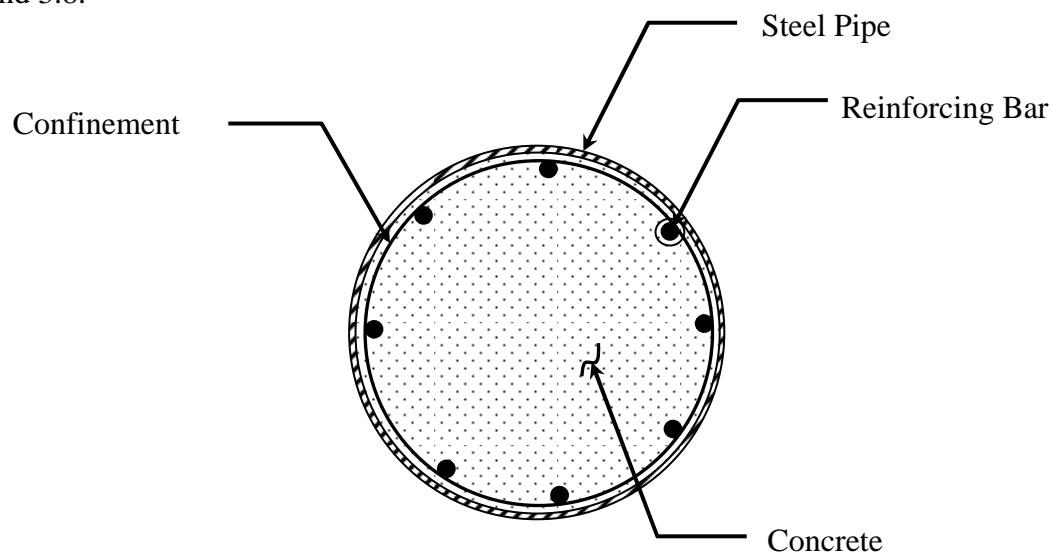


Figure 3.7 Typical Section of a Steel Pipe Pile Filled with

Figure 3.8 shows typical pile details used to support an IAB in New Jersey.

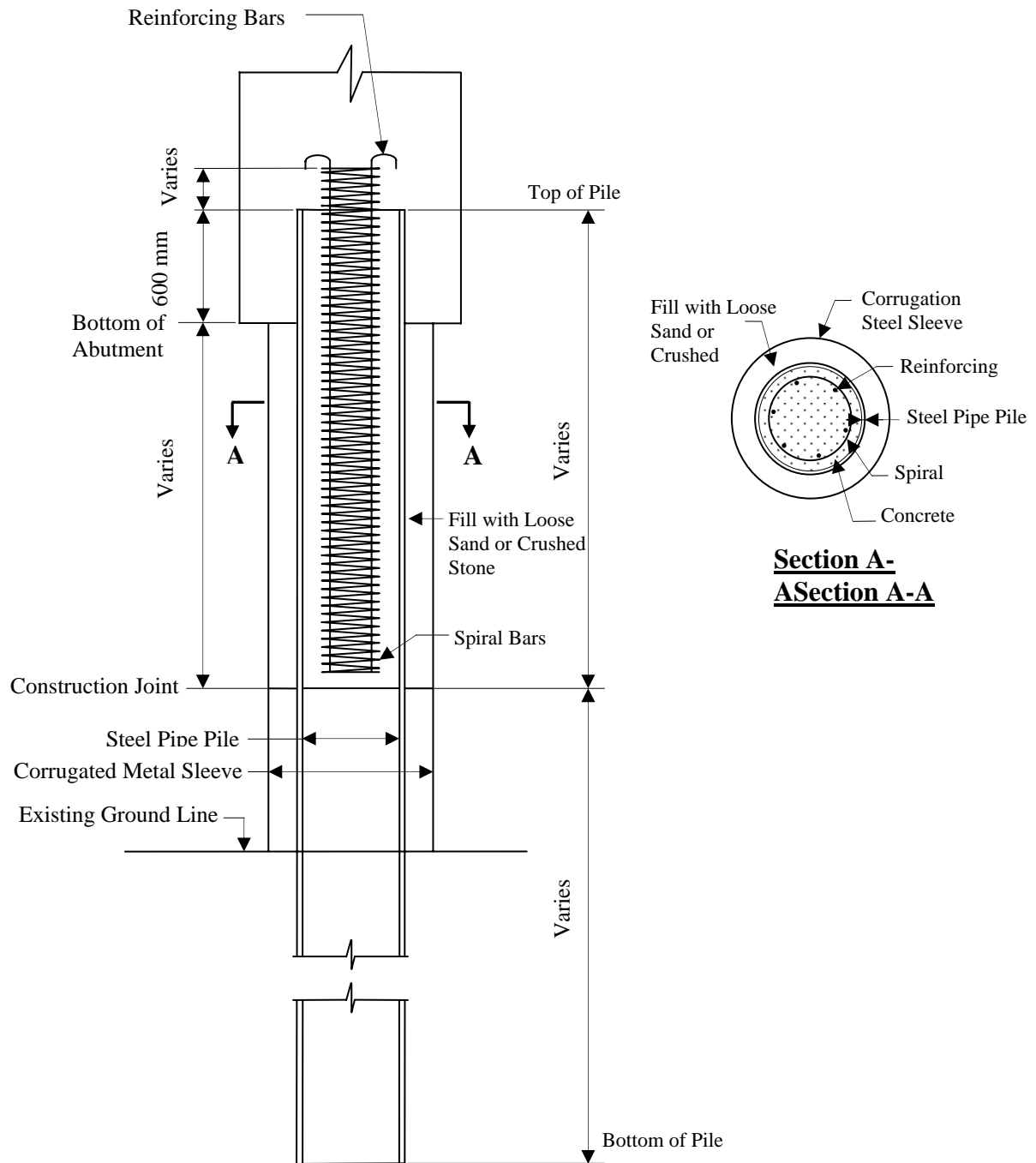


Figure 3.8 Steel Pipe Pile Filled with Concrete Details (Courtesy of NJDOT)

The effect of using steel pipe piles filled with reinforced concrete on the performance of IABs is outside the scope of this research.

The abutment is designed to carry the vertical gravity loads from the superstructure and the lateral loads from the backfill soil. When these lateral loads are significant, bridge engineers often use a laterally stiff system composed of battered (sloped) piles to support the abutment as shown in Figure 4.1. In IABs the superstructure is built monolithically with the abutment as shown in Figure 4.2.

The superstructure movement during expansion and contraction is transferred to the abutment, backfill soil, piles and foundation soil. The substructure of IABs end provides lateral restraining system that exerts lateral force in the superstructure during the expansion and contraction of the bridge.

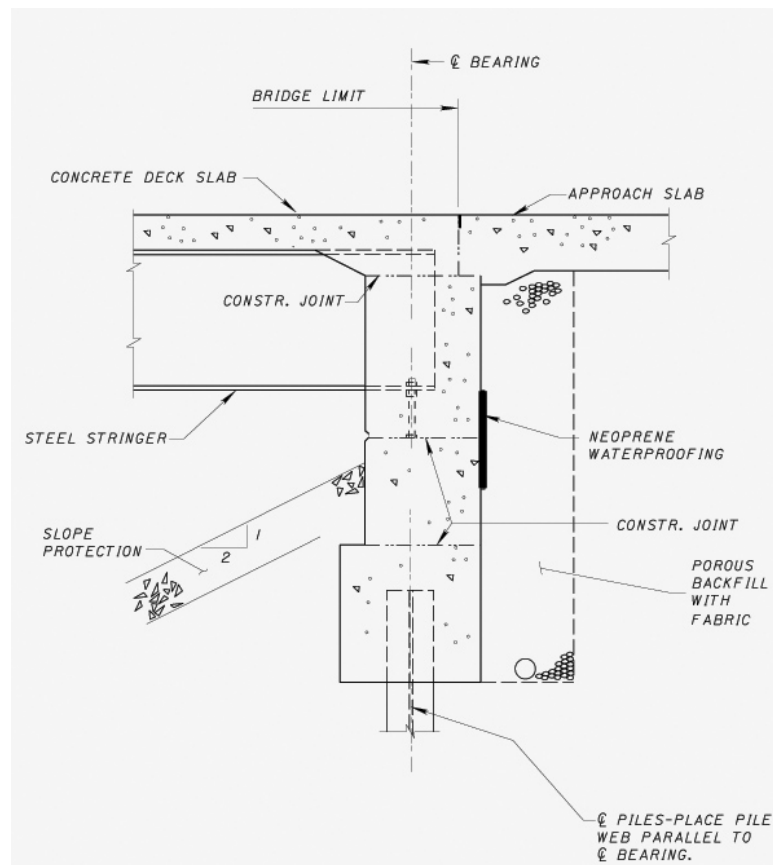


Figure 4.2 Integral Abutment Detail, Ohio DOT

Battered piles were used in early versions of IABs (Burke 2009) but were found to be very stiff and cause problems in the bridge including failure of the abutment backwall. Battered piles are no longer used in IABs. To reduce the stiffness of the substructure and subsequently allow the movement of the superstructure, IABs are usually supported by a single row of piles as shown in Figure 4.2.

The interaction between piles supporting IABs and the foundation soil and between the abutment and the backfill soil have a major impact on the displacement, rotation, and stress level in the abutment, piles, deck slab and girders. The daily and seasonal temperature changes result in imposition of cyclic horizontal displacements on the continuous bridge deck of IABs and thus on the abutments, piles and in turn on the backfill soil and foundation soils. Therefore, the interaction between these bridge components and the surrounding soil need to be carefully considered when studying the behavior of IABs under temperature variations.

The objective of this chapter is to present the theoretical background on the behavior of the foundation soil and the backfill soil under lateral loads and to present simplified analytical models used for simulating the interaction between the pile and the foundation soil and between the abutment and the backfill soil. These simplified models will be used later to represent the soil the 3D FE models. First, the general non-linear nature of soil-structure interaction is discussed. Next, the behavior of piles in both cohesive (clay) and cohesionless (sand) soils and their simplified analytical models are presented. Then, an analytical model to simulate the interaction between the abutment and backfill soil interaction is introduced. Finally, the approach slab and the wing-wall interactions with the backfill soil are discussed.

4.2 PILE-FOUNDATION SOIL INTERACTION

The interaction between the pile and the foundation soil is complex and it is nonlinear in nature. In three dimensional analyses, the pile has 3 displacements, axial displacement, lateral displacement and torsional displacement. In return the soil will exert 3 reactions on the pile, axial reaction, lateral reaction and torsional reaction as shown in Figure 4.3.

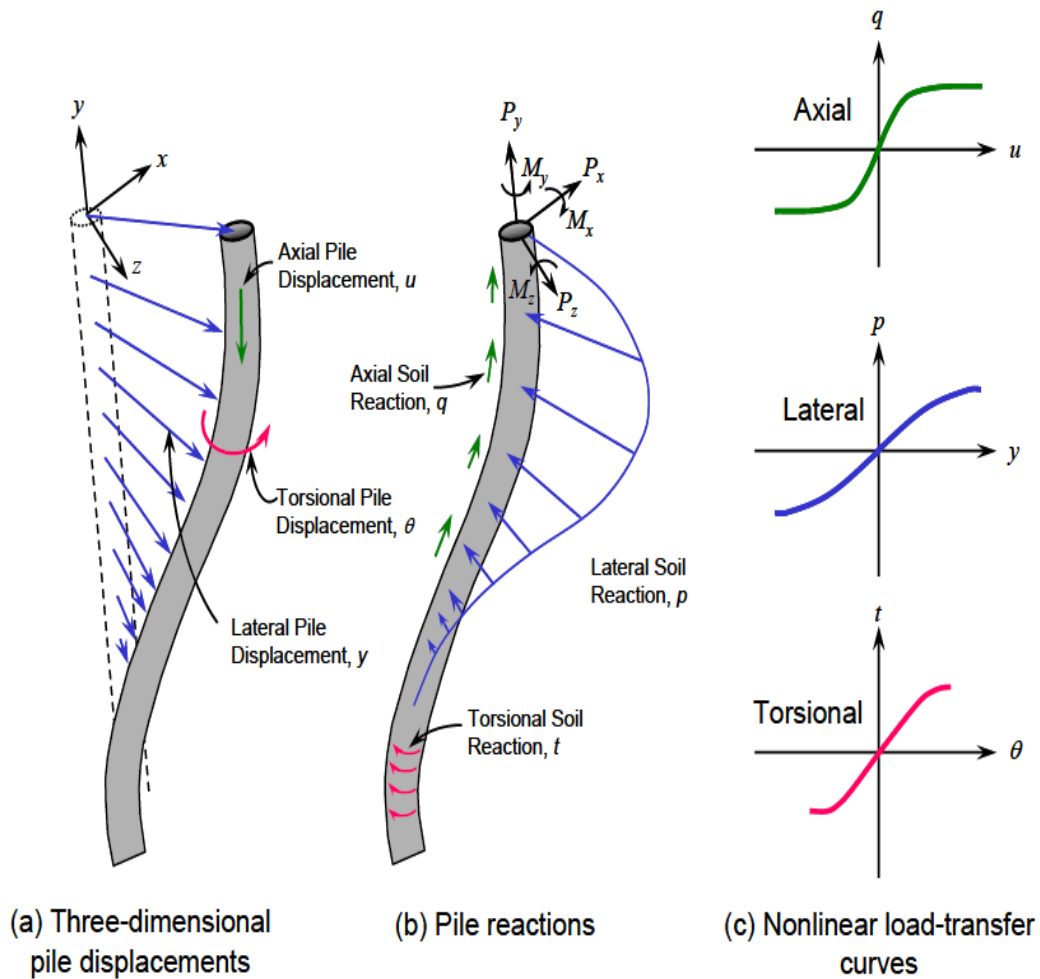


Figure 4.3 Three-Dimensional Soil Pile Interaction (Wang and Isenhower 2010)

A typical nonlinear lateral load-deflection relationship for soil is shown in Figure 4.4. As the structure gradually transfers the load to the soil, the soil initially deflects in an almost linear fashion. At higher load levels, the deformation of the soil starts to increase at a faster rate with the increase of the load and the relationship between the load and the soil deflection is nonlinear. The soil failure is assumed when the soil reaches plastic stage and that is when a very small increase in the lateral load transferred by the structure causes an additional large soil deformation. In the case of IABs, the movement of the pile is not expected to bring the soil to the heavily nonlinear stage and soil failure is not expected. The axial and torsional movement of the pile is outside the scope of this research. The research will focus on the modeling of the pile-soil and the abutment-backfill interaction in the lateral direction as it is required for the analysis of IABs. Moreover, the research will only consider single pile behavior in the modeling of pile-soil interaction.

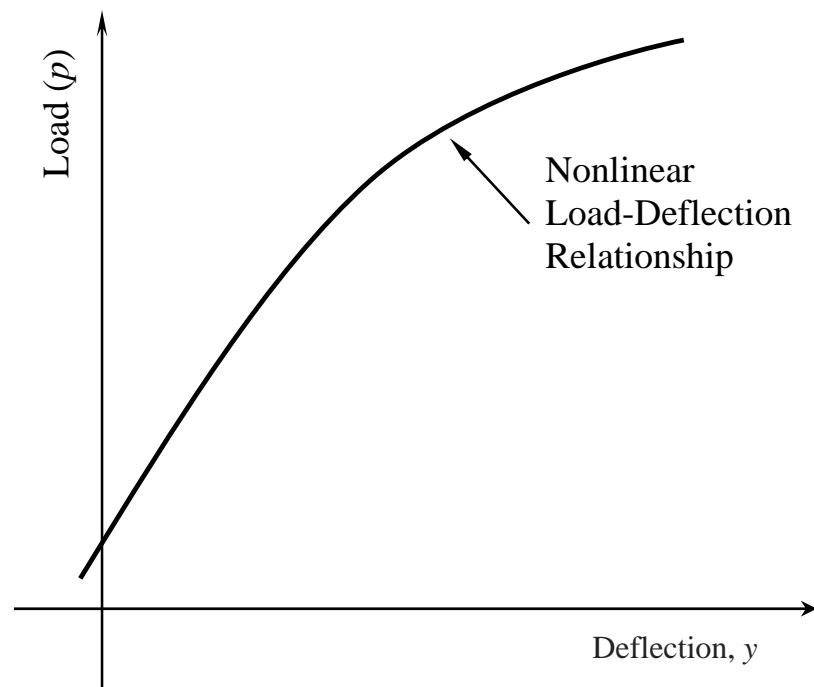


Figure 4.4 Nonlinear Load-Deflection Behavior of Soil-Structure System

4.3 MODELING OF SOIL-PILE INTERACTION FOR Laterally LOADED PILES

Generally, the soil-pile interaction for a particular point along the pile is defined by a nonlinear load (p)–deformation (y) curve or p - y curve, where p is the lateral soil resistance per unit length of pile and y is the lateral deflection of the soil at the same location. Atypical Two-Dimensional model of a single pile with p - y curves is shown in Figure 4.5

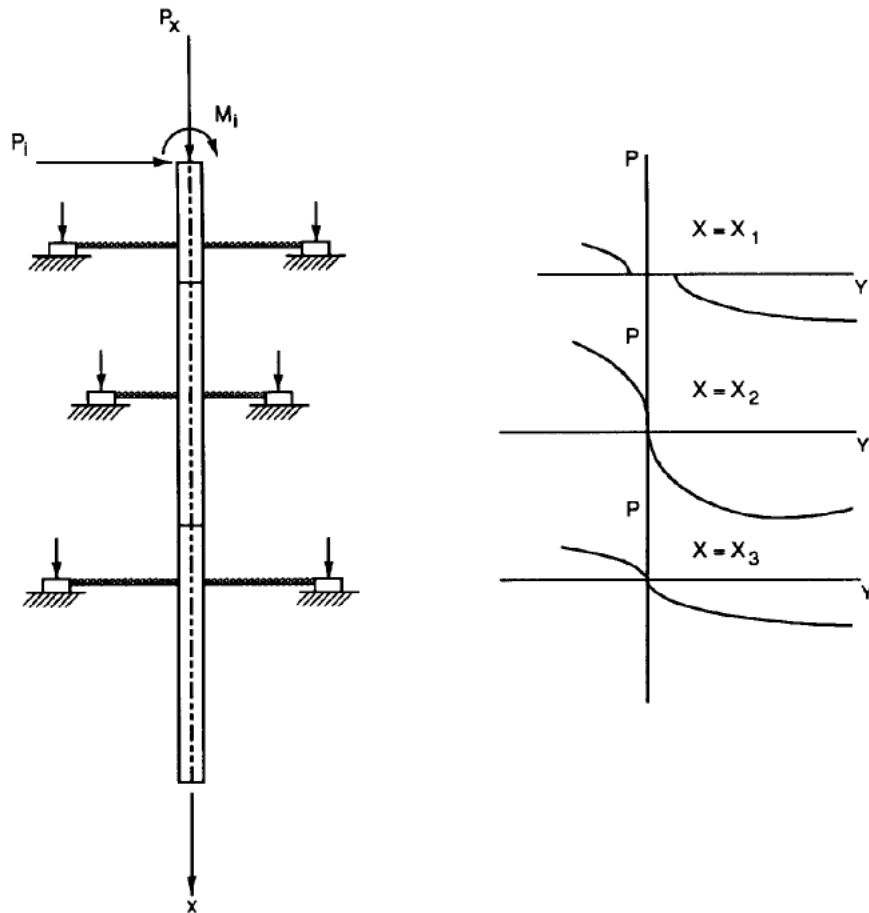


Figure 4.5 Two-Dimensional Soil Pile Interaction (Reese and Van Impe 2001)

The computation of the lateral force-displacement response of a pile involves the construction of a full set of p - y curves along the pile to model the force deformation response of the soil. A typical p - y curve is shown in Figure 4.6. In the Figure, the p - y relationship is nonlinear. For short and medium length IABs, the maximum pile deflection (soil deformation) is not expected to bring the soil behavior to the heavily nonlinear stage and the soil behavior can be approximated using linear behavior.

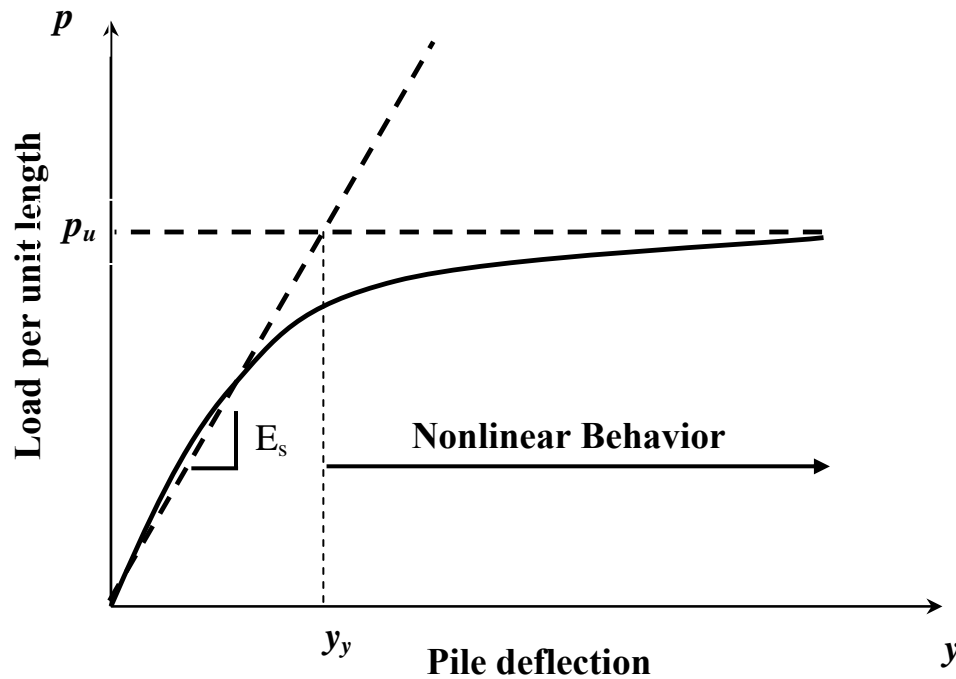


Figure 4.6 A Typical P-Y Curve and Approximate Elasto-Plastic Curve

The nonlinear load-deflection p - y curve is approximated by using the elastic part of the curve assuming that the soil has an elasto-plastic force-deformation behavior shown in dashed line in Figure 4.6. (Haliburton 1971). The elastic portion is defined with a slope equal to the initial soil modulus, E_s , and the plastic portion is defined as the ultimate soil resistance per unit length of pile, p_u .

4.4 SOIL BEHAVIOR FOR Laterally Loaded PILES IN CLAY

A typical p - y curve for soft clay (Matlock 1970) is shown with a solid line in Figure 4.7

The linear approximation is shown in the same figure is dashed line.

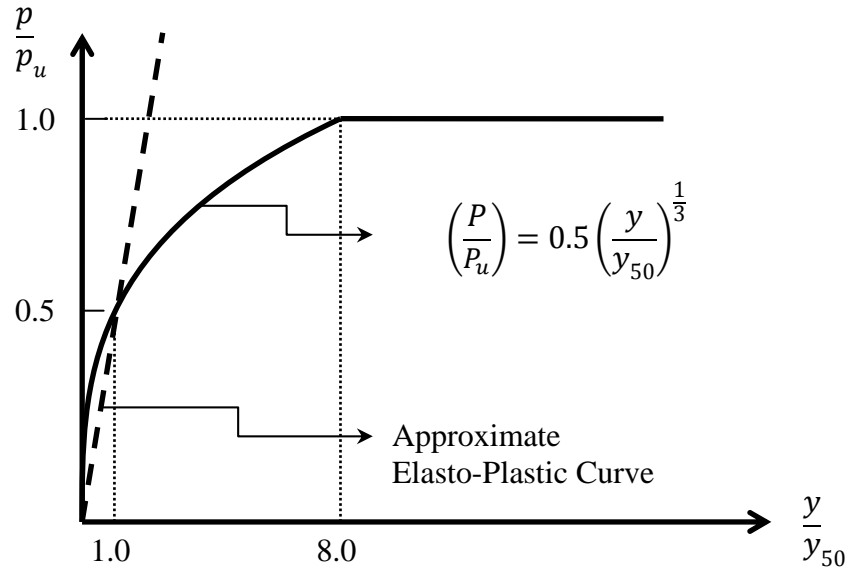


FIGURE 4.7 p - y Curve for Soft Clay with Free Water (Matlock 1970)

In the Figure the p - y relationship is nonlinear and can be expressed as follows:

$$\left(\frac{p}{p_u} \right) = 0.5 \left(\frac{y}{y_{50}} \right)^{\frac{1}{3}} \quad (4.1)$$

Where p_u = the ultimate lateral soil resistance per unit length of pile and y_{50} = 50% (one-half) of the deflection of soil at ultimate resistance and it is expressed as:

$$y_{50} = 2.5 \varepsilon_{50} b \quad (4.2)$$

Where ε_{50} is the strain corresponding to one-half the maximum principle stress difference and b is the width of pile. The value of p is assumed to be constant after soil deflection equals 8 times y_{50} .

A typical p - y curve for soft clay (Welch and Reese 1972) is shown with a solid line in Figure 4.8. The linear approximation is shown in the same figure in dashed line.

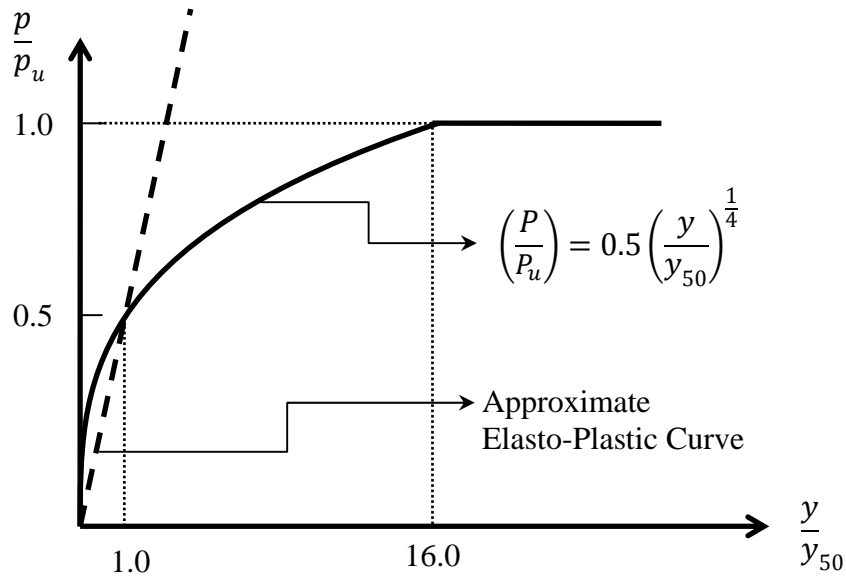


FIGURE 4.8 p - y Curve for Stiff Clay with No Free Water (Welch and Reese 1972)

In the Figure the p - y relationship is nonlinear and can be expressed as follows:

$$\left(\frac{p}{p_u} \right) = 0.5 \left(\frac{y}{y_{50}} \right)^{\frac{1}{4}} \quad (4.3)$$

Where p_u = the ultimate lateral soil resistance per unit length of pile and y_{50} = 50% (one-half) of the deflection of soil at ultimate resistance as defined in equation 4.2.

The value of p is assumed to be constant after soil deflection equals 16 times y_{50} .

4.4.1. Estimation of Ultimate Soil Resistance (p_u)

Two types of soil behavior are considered in estimating the ultimate soil resistance for laterally loaded piles in cohesive soil p_u . Near the ground surface, the pile may push up a soil wedge by lateral movement in what is called a wedge action as shown in Figure 4.9.

The figure shows the mechanism of soil behavior close to the ground surface. Because of the lack of the confinement close to the ground, the ultimate soil capacity is reduced and a wedge action failure develops before the regular nonlinear soil failure. Therefore, the ultimate soil capacity will depend on the location of soil. If the soil is closer than z_t to the ground surface then the ultimate soil capacity will be decided by the wedge action. Otherwise the ultimate soil capacity will be calculated based on confined soil behavior.

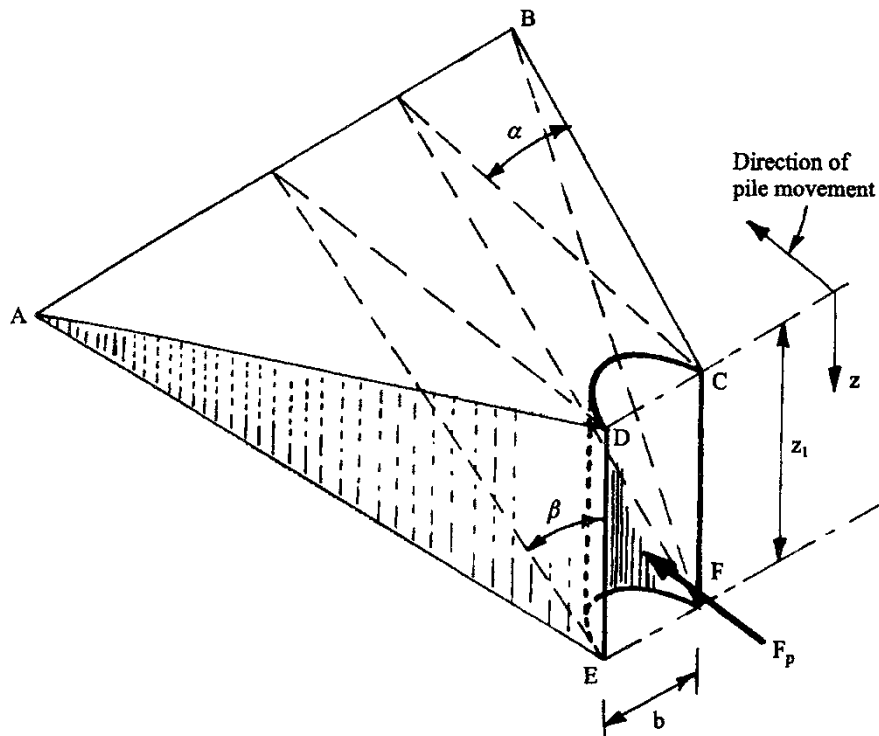


Figure 4.9 Model of Soil at Ground Surface (Reese and Van Impe 2001)

Figure 4.10 shows the change in ultimate soil capacity as a function of the soil depth.

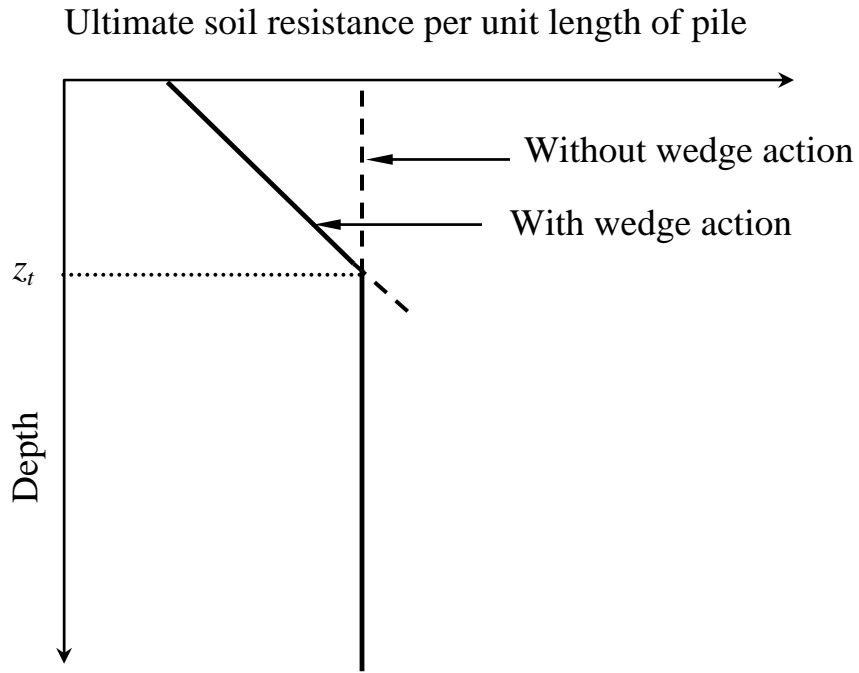


Figure 4.10 Ultimate Soil Resistances with Transition Depth in Clay

The depth of the soil under wedge action, z_t , measured from the ground surface is expressed as (Haliburton, 1971);

$$z_t = \frac{6bC_u}{(\gamma b + 0.5C_u)} \quad (4.3)$$

Where γ is the unit weight of soil and C_u is the undrained shear strength of clay.

For the top part of the soil above z_t , the ultimate soil resistance is calculated as

$$p_u = \gamma bz + 3C_u b + JC_u z \quad (4.4)$$

Where $J=0.25$ for soft clay and 0.5 for medium and stiff clay and z is the soil depth measured from the ground surface.

For the lower part of the soil below z_t , the ultimate soil resistance is calculated as

$$p_u = 9C_u b \quad (4.5)$$

The wedge action is critical for piles driven in soil where the pile top is located at or near the soil surface. In the case of IABs, the backfill soil behind the abutment and the embankment exerts a surcharge pressure on the foundation soil as shown in Figure 4.11. These surcharge pressures may prevent bulging of the soil due to the wedge action in most of the cases. Therefore, the wedge action is not considered in the calculation of p_u . Thus, equation 4.5 is used to calculate p_u at any depth.

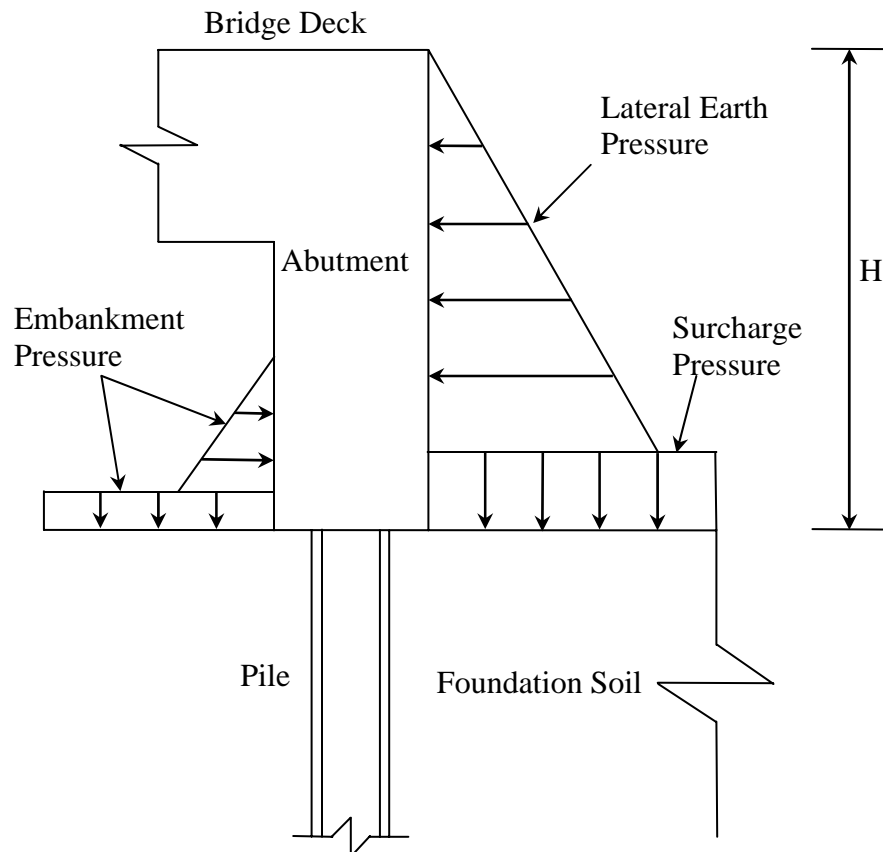


Fig.4.11 Backfill and Embankment Pressures Distribution on the Abutment and the Foundation Soil

4.4.2 Estimation of Soil Modulus (E_s)

Skempton (1951), proposed a method based on laboratory test data, correlated with field test to calculate the elastic soil modulus. Skempton found that about one-half of the ultimate soil resistance for a beam resting on soil is developed at a structure deflection equal y_{50} . Therefore the soil modulus for clay E_s can be calculated using the following expression;

$$E_s = \frac{p_u / 2}{2.5 \varepsilon_{50} b} = \frac{p_u}{5 \varepsilon_{50} b} \quad (4.5)$$

Substituting for p_u from equation 4.5:

$$E_s = \frac{9C_u b}{5 \varepsilon_{50} b} = \frac{9C_u}{5 \varepsilon_{50}} \quad (4.7)$$

Equation 4.7 shows that the soil modulus, E_s , for clay is independent of the pile width and is also independent of the depth below the ground surface. This conclusion is illustrated in Figure 4.12.

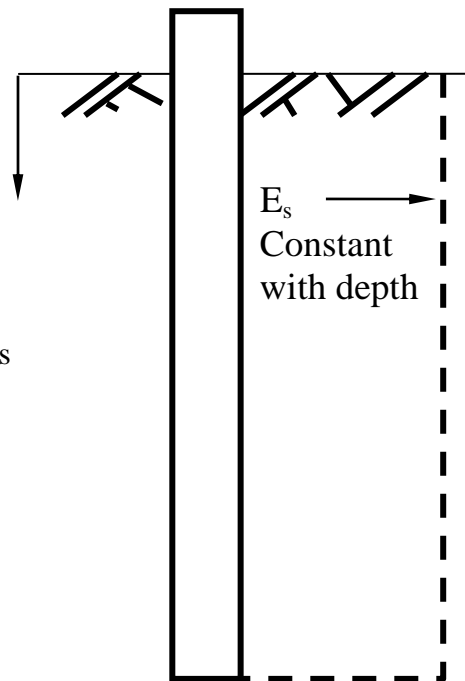


Figure 4.12 Variation of Soil Modulus with Depth for Clay

The values of C_u and ε_{50} for different types of cohesive soils used in this study are presented in table 4.1.

Table 4.1 Properties of Clay (Reese and Van Impe 2001, Bowles 1996)

Consistency of Clay	Undrained Cohesion C_u (kPa)		ε_{50}	Unit Weight γ (kN/m ³)
	Range	Average		
Soft	12-25	19	0.02	15
Medium	25-50	38	0.01	16
Stiff	50-100	75	0.0065	19
Very Stiff	100-200	150	0.005	20

Figures 4.13 through 4.16 show the nonlinear p - y curves for the four H-Piles in soft clay, medium clay, stiff clay and very stiff clay respectively. The linear (elastic) approximation is shown in the same Figure.

Figures 4.17 through 4.20 show the nonlinear p - y curves for the three Precast Prestressed Concrete Piles (PPCP) in soft clay, medium clay, stiff clay and very stiff clay respectively. The linear (elastic) approximation is shown in the same Figure.

Throughout the study the slope of the approximate linear curve will be adjusted based on the nonlinear curve and the pile displacement. The estimated maximum pile displacement for the bridges in the study is expected to be less than 0.02 meter (0.8 inch).

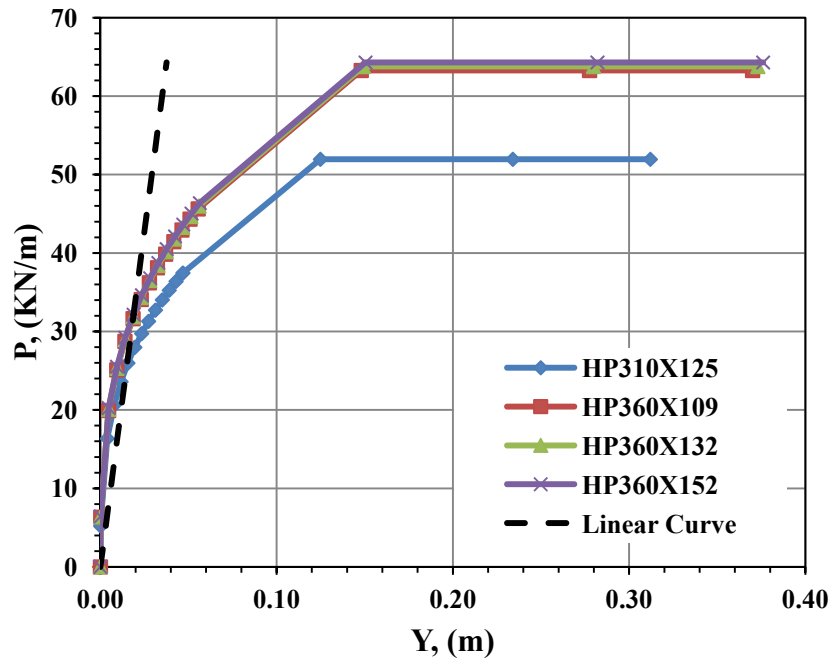


Figure 4.13 p - y Curves for H-Piles in Soft Clay

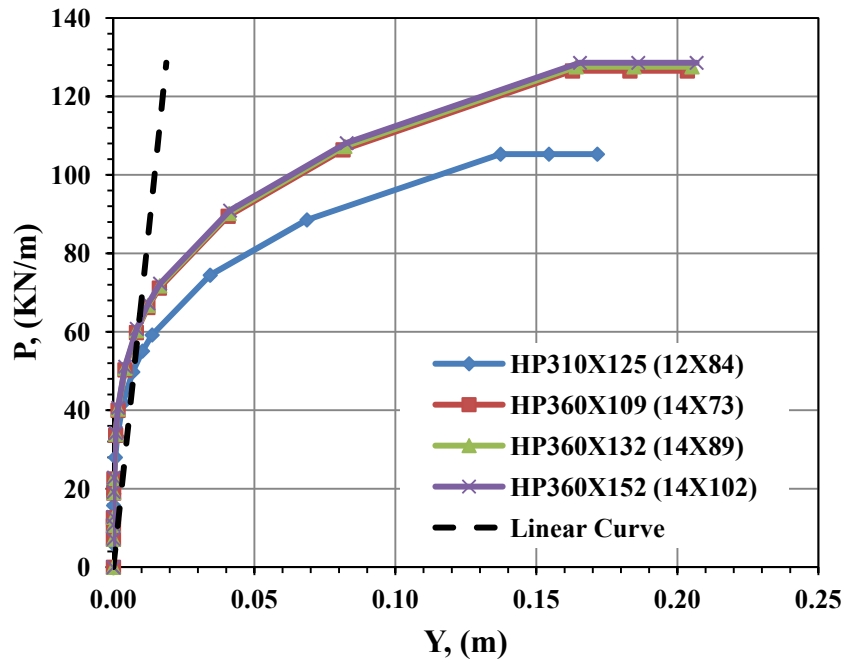


Figure 4.14 p - y Curves for H-Piles in Medium Clay

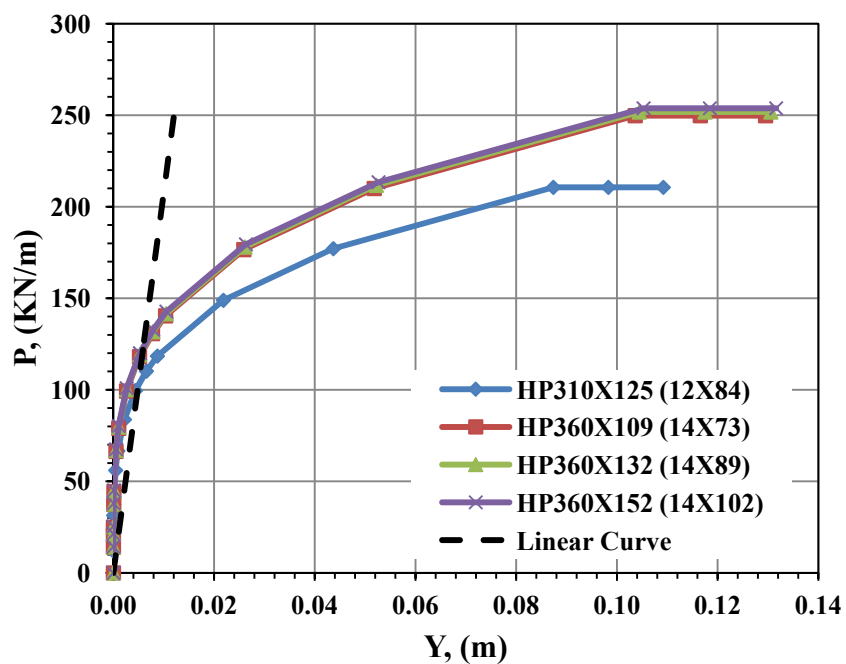


Figure 4.15 p - y Curves for H-Piles in Stiff Clay

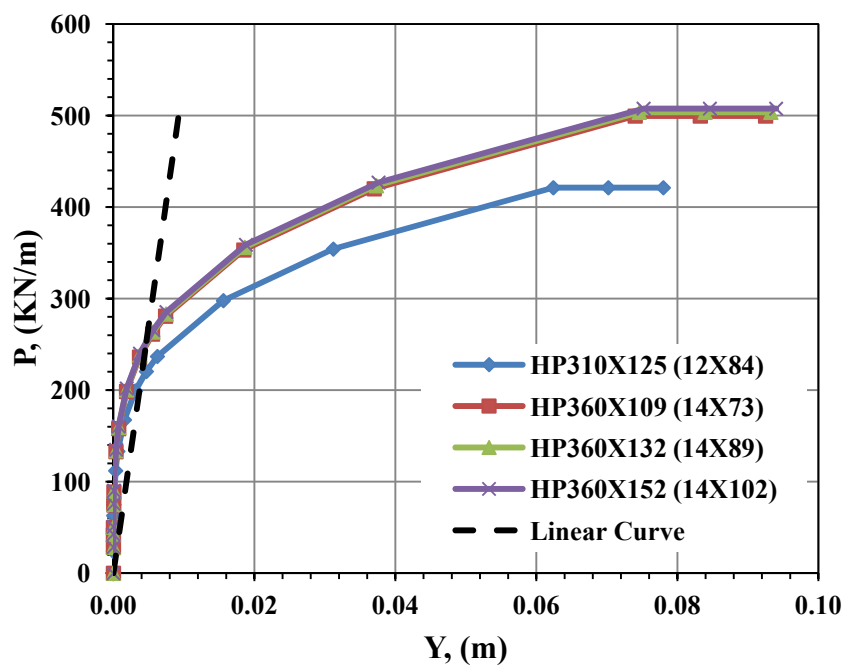


Figure 4.16 p - y Curves for H-Piles in Very Stiff Clay

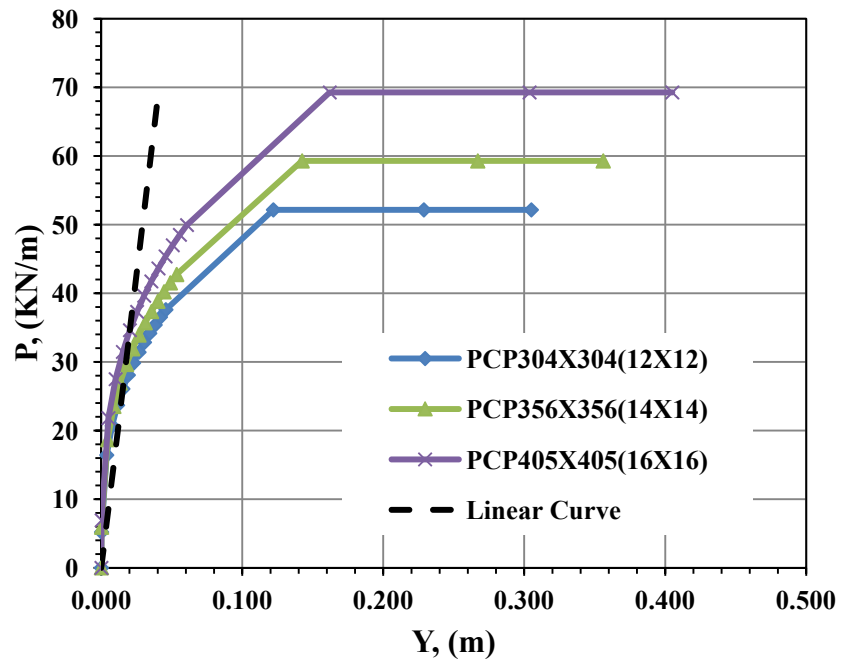


Figure 4.17 p - y Curves for PPCP in Soft clay

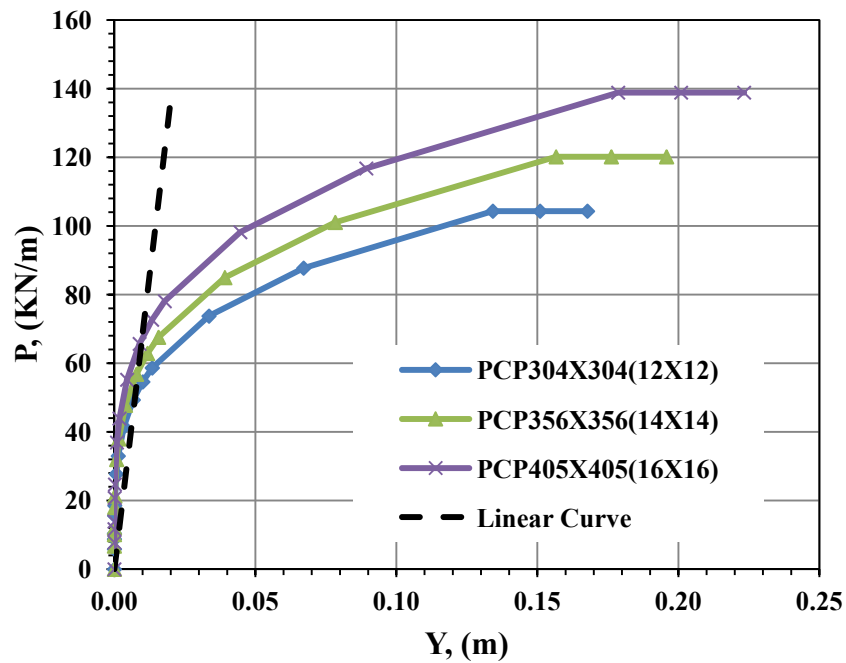


Figure 4.18 p - y Curves for PPCP in Medium Clay

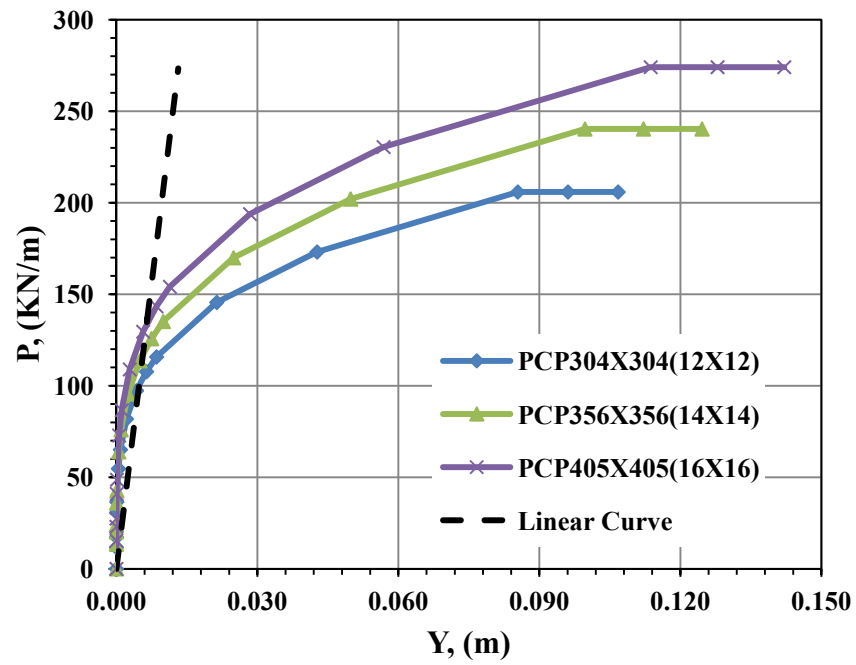


Figure 4.19 p - y Curves for PPCP in Stiff Clay

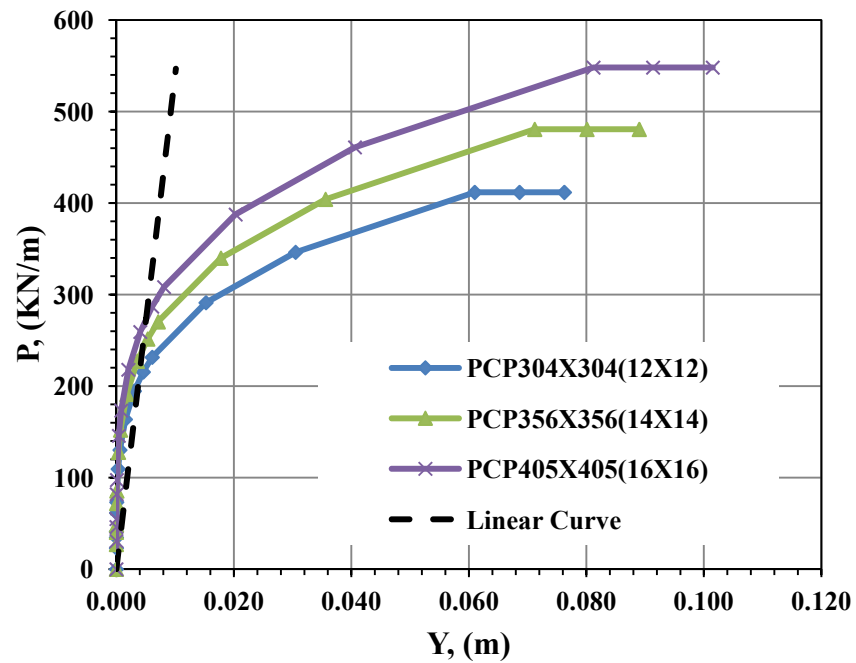


Figure 4.20 p - y Curves for PPCP in Very Stiff Clay

4.5 SOIL BEHAVIOR FOR Laterally LOADED PILES IN SAND

Constructing the p - y curve for sand is more complex than clay. Atypical p - y curve for sand is shown in Figure 4.21. Unlike the soil behavior in clay, the soil stiffness in cohesionless soils is a function of the soil depth below the ground surface. The soil modulus which represents the initial stiffness of the p - y curve is a function of the confining pressure on the soil. The confining pressure increases with the increase in soil depth and that means the initial stiffness of the soil at any location is a function of the depth of that location from the top of ground.

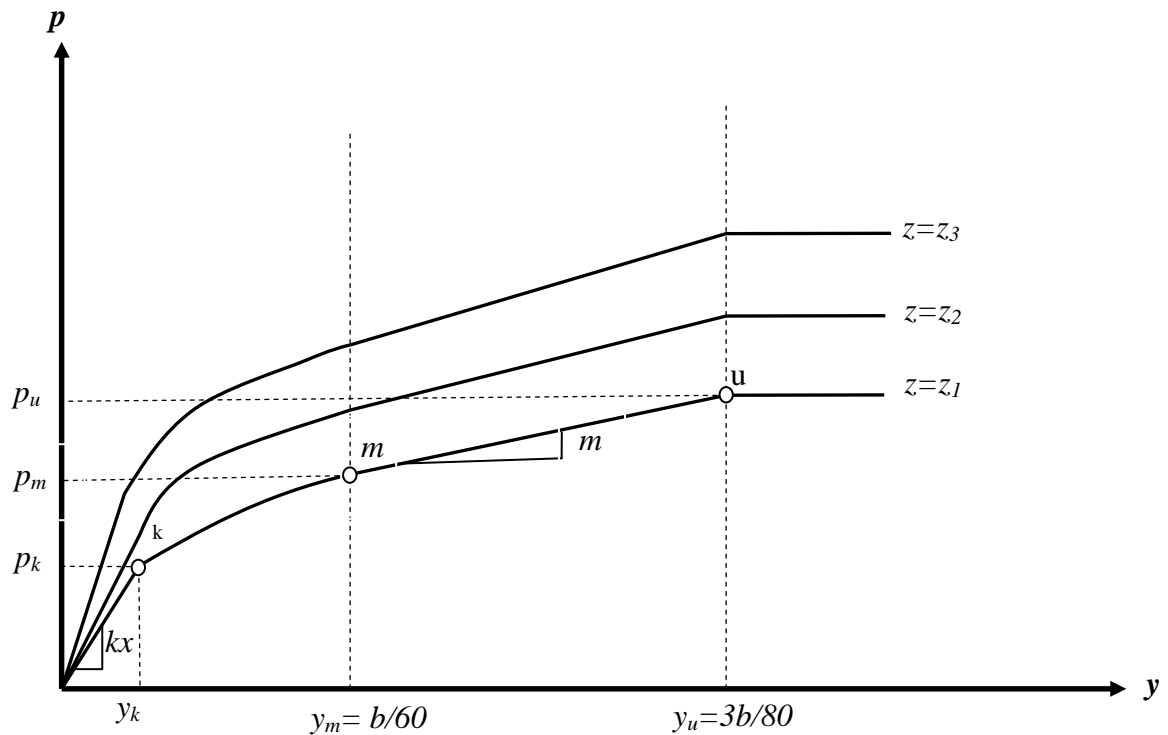


Figure 4.21 Characteristic Shape of a Set of p - y Curves for Static and Cyclic Loading in Sand (Reese and Van Impe 2001)

The Modulus, E_s , for sand is assumed to vary linearly with depth (Terzaghi, 1955) as shown in Figure 4.22 and can be expressed as,

$$E_s = kz, \quad (4.8)$$

Where k is the modulus of subgrade reaction and z is the depth of soil below the ground surface.

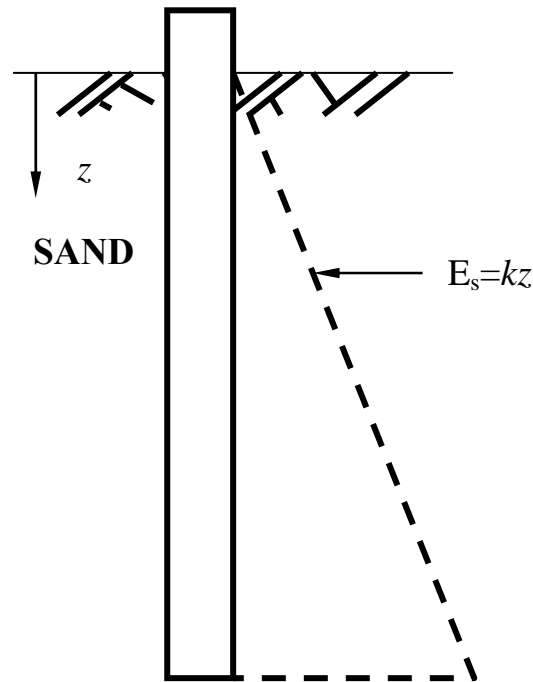


Figure 4.22 Variation of Soil Modulus with Depth in Sand

The values of the modulus of subgrade reaction k are summarized in table 4.2. The properties shown in the table are for sand above the water table.

TABLE 4.2 Properties of Sand (Reese and Van Impe 2001, Bowles 1996)

Sand	Modulus of subgrade reaction k (MN/m ³)		ϕ Internal angle of friction	Unit Weight γ (kN/m ³)
	Range	Suggested*		
Loose	3.5-10.4	6.8	30	15
Medium	13.0-40.0	24.4	35	18
Dense	51.0-102	76.0	40	20

4.5.1 Estimation of Ultimate Soil Resistance

Similar to the case of the clay, two types of soil behavior are considered in estimating the ultimate soil resistance for laterally loaded piles in sand. Near the surface, where $z < z_t$, the pile may push up a soil wedge by lateral movement resulting in wedge action. Accordingly, for soil depths smaller than z_t , the ultimate soil resistance with wedge action, p_{uw} , is expressed as (Reese et al. 1974):

$$p_{uw} = \gamma z \left[\frac{K_0 \tan \phi \tan \beta}{\tan(\beta - \phi) \cos \alpha} + \frac{\tan \beta}{\tan(\beta - \phi)} (b + z \tan \beta \tan \alpha) + \right. \\ \left. (K_0 z \tan \beta (\tan \phi \sin \beta - \tan \alpha) - K_A b) \right] \quad (4.8)$$

Where K_0 is coefficient of earth pressure at rest and it equals 0.4, K_A is coefficient of active earth pressure, α is the angle of the wedge in the horizontal direction, β is the angle of the wedge with the ground surface as shown in figure 4.9.

The terms above can be calculated as follows:

$$K_A = \tan^2(45^\circ - \frac{\phi}{2}) \quad (4.9)$$

$$\alpha = \frac{\phi}{2} \quad (4.10)$$

$$\beta = 45^\circ + \frac{\phi}{2} \quad (4.11)$$

The depth of the soil under wedge action, z_t , measured from the ground surface is expressed as (Haliburton, 1971);

$$z_t = \frac{b(\tan^5 \beta + K_0 \tan^3 \beta \tan \phi - \tan \beta)}{\tan^2 \beta \tan \alpha + K(\tan \phi - \tan \alpha)} \quad (4.12)$$

For soil depths larger than z_t , the ultimate soil resistance without wedge action, p_{unw} , is expressed as (Reese et al. 1974):

$$p_{unw} = K_A b \gamma z (\tan^8 \beta - 1) + K_0 b \gamma z \tan \phi \tan^4 \beta \quad (4.13)$$

Again the wedge action is not expected to happen in the foundation soil supporting IABs because the backfill soil behind the abutment and the embankment exerts a surcharge pressures on the foundation soil and will prevent wedge action. Therefore, the ultimate soil capacity will be calculated using equation 4.13.

4.5.2 Procedure to Construct p - y Curves in Sand

A modified Reese procedure (Reese and Van Impe 2001) was followed to construct p - y curves in sand. The modified procedure ignores the effect of wedge action and cyclic loading on the soil capacity. The following steps were followed to construct p - y curves in sand:

1. Obtain values for the angle of internal friction ϕ , the soil unit weight γ , and pile diameter b and calculate K_A , α , and β from equations 4.9 to 4.11 respectively.

2. Compute the ultimate soil resistance per unit length of pile using equation 4.13.
3. Select depth at which a p - y curve is desired.

4. Establish $y_u = \frac{3b}{80}$

Compute p_u using:

$$p_u = \bar{A}_s p_{umw}$$

By ignoring cyclic loading and the wedge action the value of A_s is assumed to be 0.88 as shown in Figure 4.23

5. Establish y_m as $b/60$. Compute p_m by the following equation:

$$p_m = B_s p_{umw}$$

By ignoring cyclic loading and the wedge action the value of B_s is assumed to be 0.5 as shown in Figure 4.24

The two straight-line portions of the p - y curve, beyond the point where y is equal to $b/60$, can now be established.

6. Establish the initial straight-line portion of the p - y curve,

$$p = (k z) y$$

Use the appropriate value of k from table 4.2.

7. Establish the parabolic section of the p - y curve,

$$p = \bar{C} y^{1/n}$$

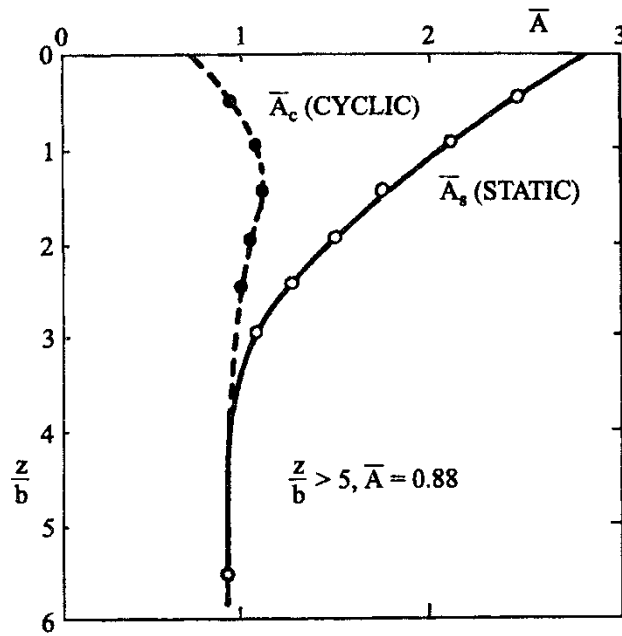


Figure 4.23 Values of Coefficients A_c and A_s (Reese and Van Impe 2001)

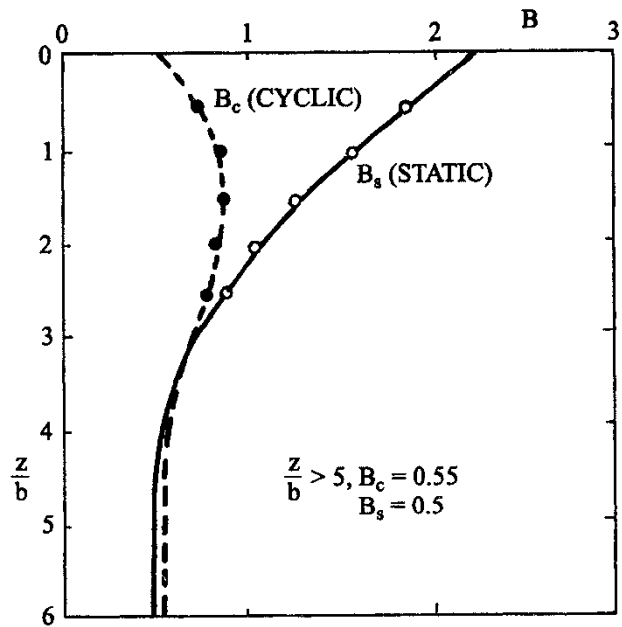


Figure 4.24 Non-dimensional Coefficient B for Soil Resistance Versus Depth (Reese and Van Impe 2001)

Fit the parabola between points k and m as follows:

- a. Get the slop of the line between points m and u by,

$$m = \frac{P_u - P_m}{y_u - y_m}$$

- b. Obtain the power of the parabolic section by,

$$n = \frac{P_m}{my_m}$$

- c. Obtain the coefficient \bar{C} as follows:

$$\bar{C} = \frac{P_m}{y_m^{1/n}}$$

- d. Determine point k as,

$$y_k = \left(\frac{\bar{C}}{kx} \right)^{\frac{n}{n-1}}$$

Figures 4.25 through 4.27 show the nonlinear p - y curves for the PPCP 356x356 in loose sand, medium dense sand and dense sand respectively. The linear (elastic) approximation is shown in the same Figure.

Figures 4.28 through 4.30 show the nonlinear p - y curves for the H-Pile 310x125 in loose sand, medium dense sand and dense sand respectively. The linear approximation is shown in the same Figure. Throughout the study the slope of the approximate linear curve will be adjusted based on the nonlinear curve and the pile displacement. The estimated maximum pile displacement for the bridges in the study is expected to be less than 0.02 meter (0.8 inch).

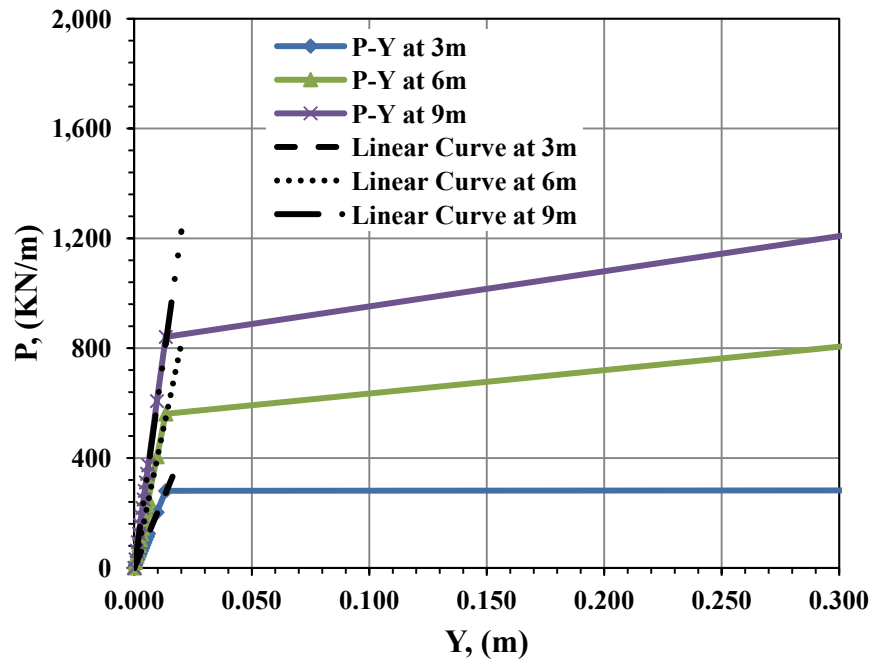


Figure 4.25 p - y Curves for PPCP356X356 in Loose Sand

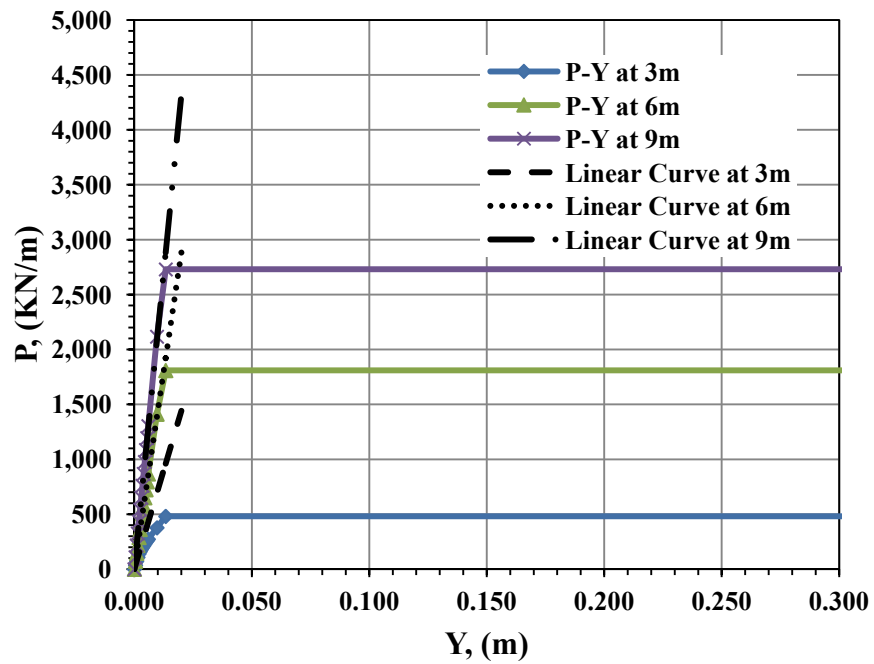


Figure 4.26 p - y Curves for PPCP356X356 in Medium Sand

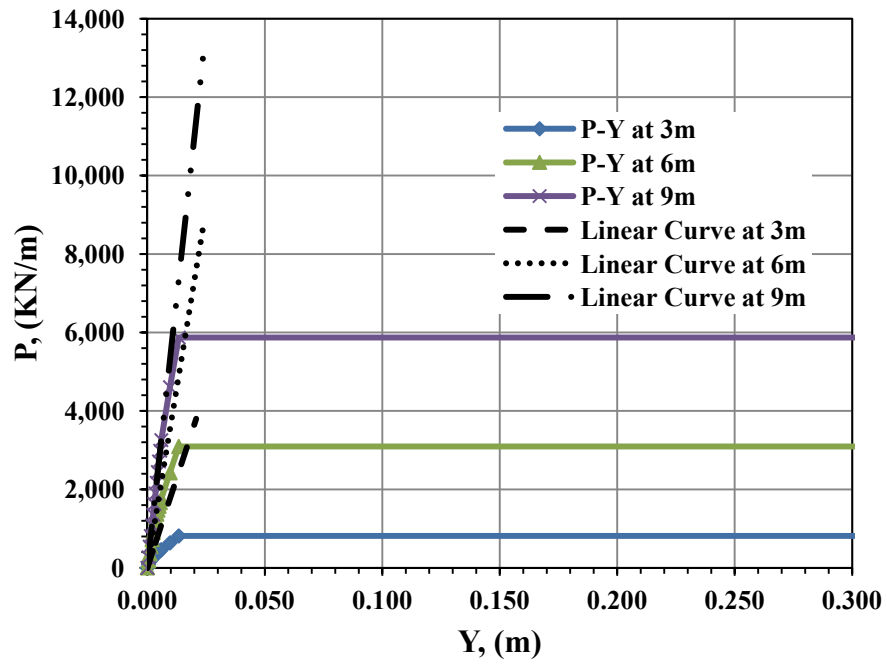


Figure 4.27 p - y Curves for PPCP356X356 in Dense Sand

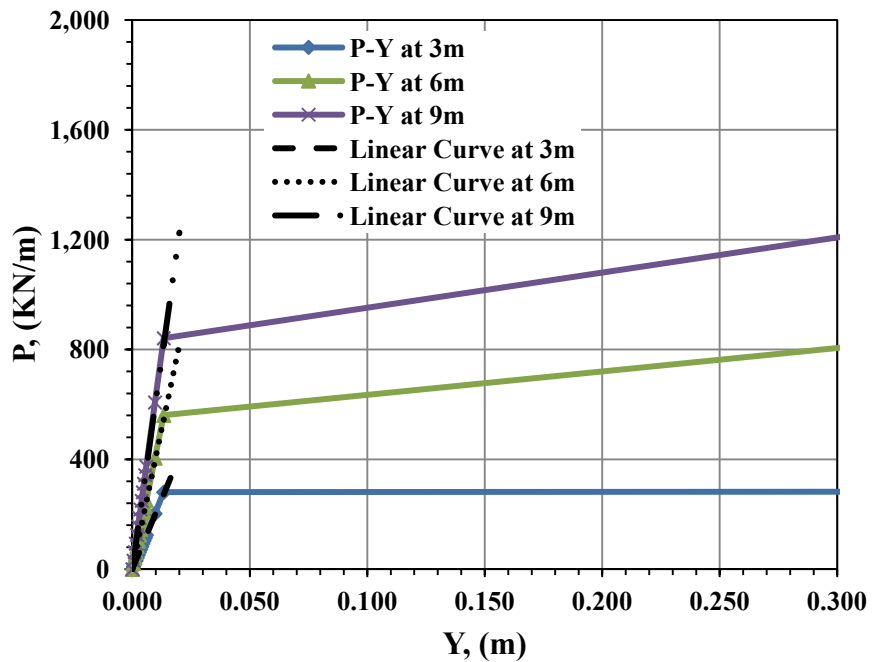


Figure 4.28 p - y Curves for HP310X125 in Loose Sand

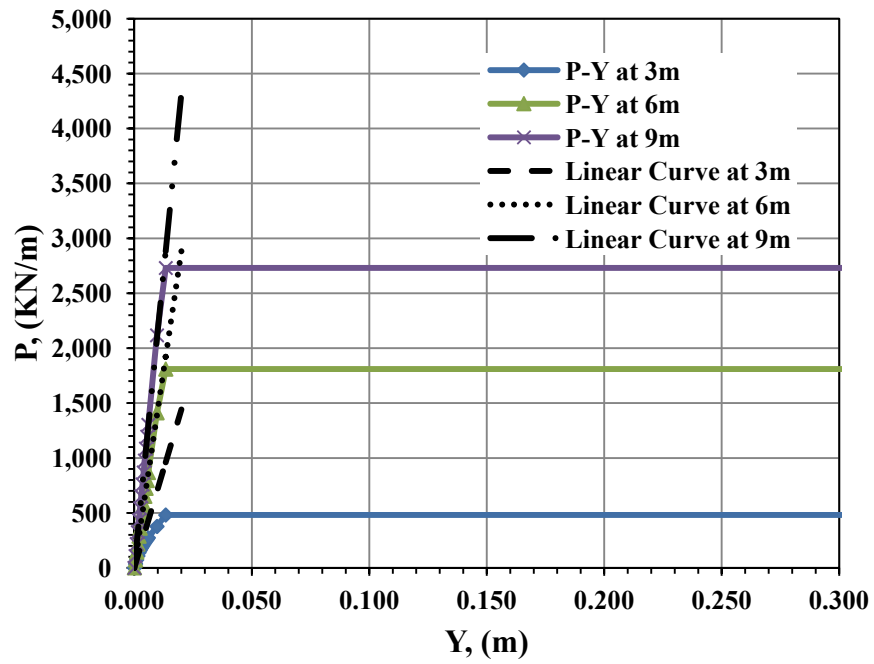


Figure 4.29 p - y Curves for HP310X125 in Medium Sand

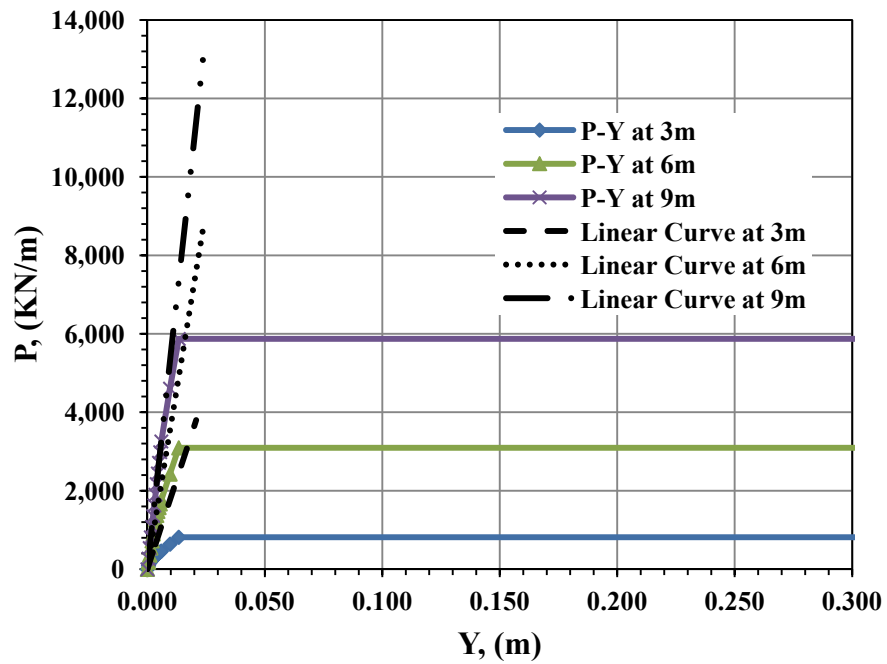


Figure 4.30 p - y Curves for HP310X125 in Dense Sand

4.6 ABUTMENT-SOIL INTERACTION

The earth pressure that is exerted on the abutment by the backfill soil depends on the extent of movement of the abutment. An integral-abutment bridge will experience elongation and contraction due to temperature variations during its service life. Thus, the earth pressure at the abutments should be considered in correlation with temperature variation. A very small displacement of the bridge away from the backfill soil can cause the development of active earth pressure conditions (Barker et al. 1991). Therefore, when the bridge contracts due to a decrease in temperature, active earth pressure will develop behind the abutment. At rest, earth pressure behind the abutment is assumed when there is no thermal movement. When the bridge elongates due to an increase in temperature, the intensity of the earth pressure behind the abutment depends on the magnitude of the bridge displacement towards the backfill soil. The actual earth pressure coefficient, K , may change between at rest, K_0 , and passive, K_p , earth pressure coefficients depending on the amount of displacement.

Past researchers have obtained the variation of earth pressure coefficient as a function of structure displacement from experimental data and finite element analyses. Clough and Duncan (1991) has developed a relationship between the earth pressure coefficient, K , and the ratio of wall movement to wall height, Δ/H , for typical backfill soils compacted to a medium dense condition. That relationship is illustrated in figure 4.31.

Examination of the figure revealed that to reach the minimum active earth pressure condition, a Δ/H ratio of no more than 0.004 is required. However, to reach the maximum passive earth pressure condition, a Δ/H ratio of about 0.04 is required. The relationship presented by Clough and Duncan (1991) is used to model the abutment-backfill soil interaction.

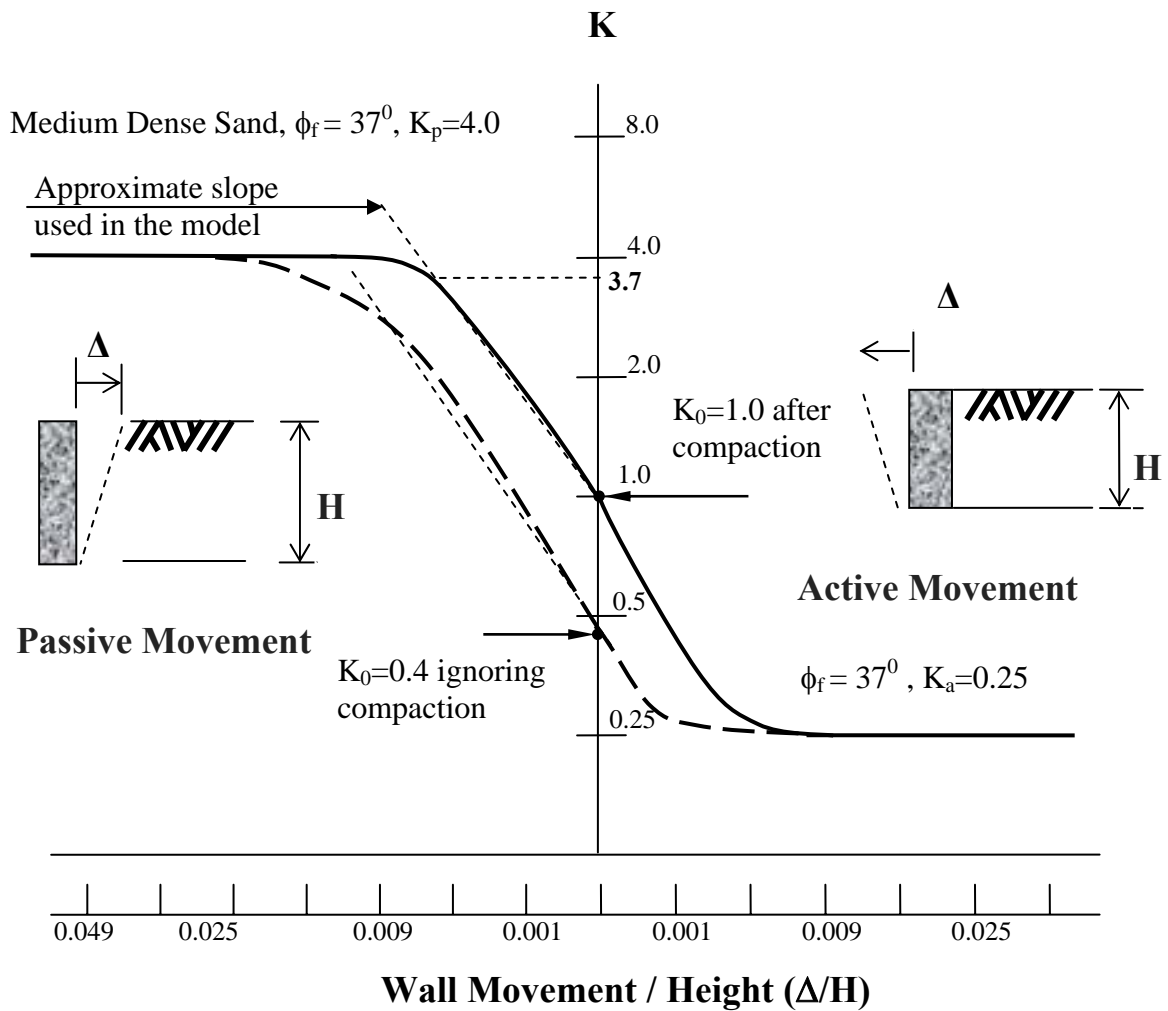


Figure 4.31 Relationship Between Wall Movement and Earth Pressure (Clough And Duncan, 1991)

Under negative temperature change (contraction), active earth pressure was applied to the abutment. The value of K was kept constant and equal to $K_a = 0.25$. Under positive temperature change (expansion), passive earth pressure was applied to the abutment as the sum of the at-rest pressure and the passive pressure beyond the at rest stage as shown in Figure 4.31. Linear springs were used to model passive pressure beyond the at rest stage. The spring constant was calculated as follows:

$$K_{spring} = \frac{(dP)}{\Delta} \quad (4.14)$$

Where dP = change in backfill pressure and Δ = top of abutment displacement and

$$dP = (K_p - K_0) \gamma z \quad (4.15)$$

Where γ = the backfill soil unit weight and z = the spring depth measure from the top of the abutment. For compacted backfill $K_0=1.0$ and for non-compacted backfill $K_0=0.4$.

Divide the numerator and denominator in equation 4.14 by the abutment height H :

$$K_{spring} = \frac{(dP)/H}{\Delta/H} \quad (4.16)$$

By approximation from Figure 4.30 for compacted backfill, $K_p = 3.7$ when $\Delta/H = 0.009$.

Substitute these values in equations 4.15 and 4.16:

$$K_{spring} = 300 \gamma z / H \quad (4.17)$$

By inspection from Figure 4.31, the same spring constant (linear curve slope) can be used for non-compacted backfill.

The interaction between the backfill and the approach slab and between the backfill and wingwall were ignored in the study.

CHAPTER 5

FINITE ELEMENT MODELING AND VALIDATION

5.1 GENERAL

Three dimensional (3D) Finite Element (FE) models for two recently constructed IABs were utilized in this research to study the effect of substructure stiffness on the behavior of IABs. To accurately capture the behavior of IABs, the entire parametric study was carried out using 3D FE Models. Using 3D modeling also captures the behavior of integral bridges in the transverse direction and gives better results than 2D models. The software LUSAS (LUSAS, 2010) was utilized throughout the study for the FE modeling. Different FE elements were used to model different elements of the bridge.

This chapter starts with the description of the various aspects of the 3D FE modeling and the 3D FE models utilized in the analysis. Next, the validation of the 3D FE model is presented. The validation is based on the field measurements from the new Scotch Road Bridge in New Jersey. Finally, a brief description of a typical two-dimensional 2D FE model is presented. The 2D models will be used later in this research for comparison purposes only.

5.2 3D FE MODELS

5.2.1 Modeling of Superstructure and Substructure

The software LUSAS (LUSAS, 2008) was utilized for the modeling of the bridges' 3D FE models. 3D thick elements were used to model all the structural elements of the superstructure and the substructure. A typical 3D FE model for the single-span bridge is shown in Figure 5.1.

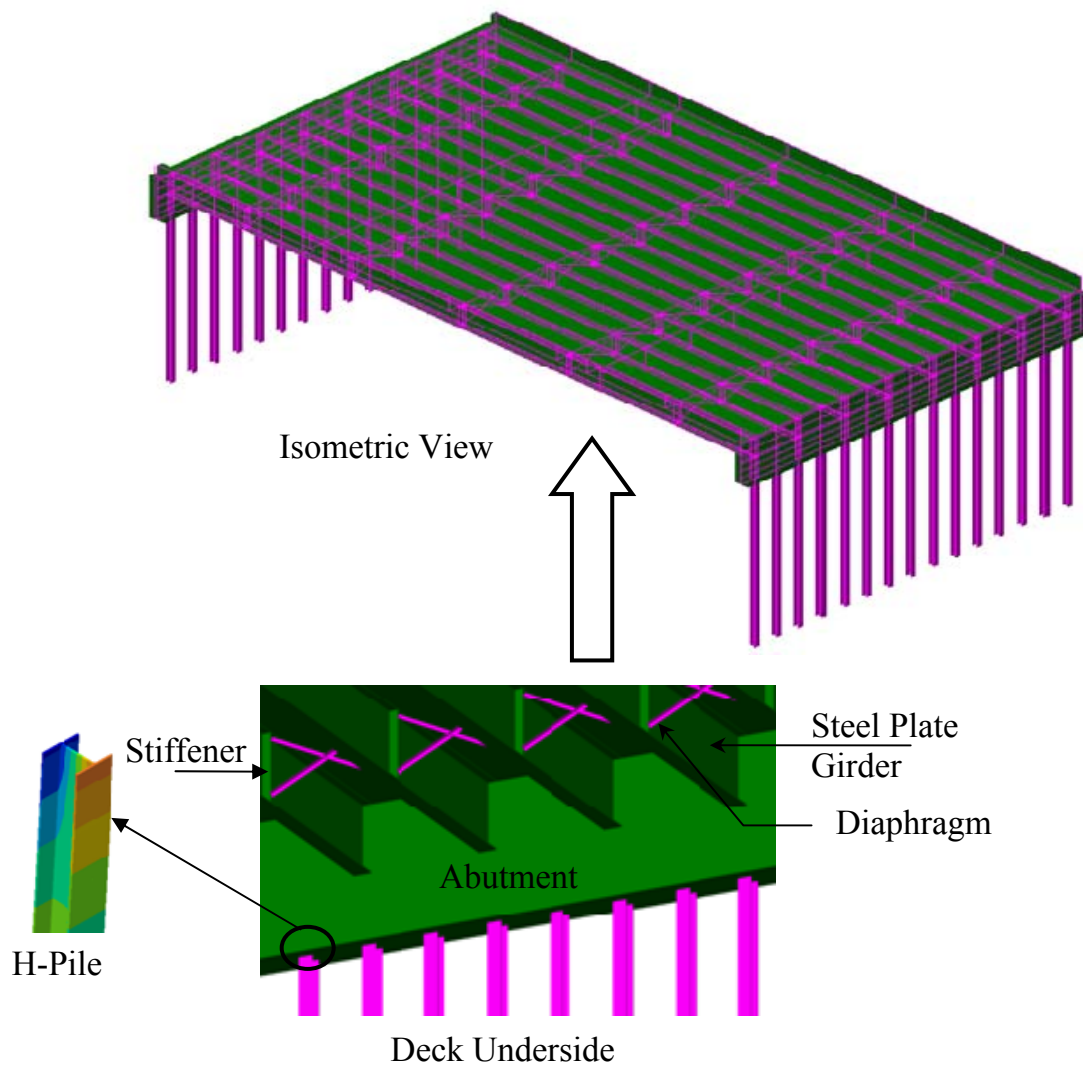
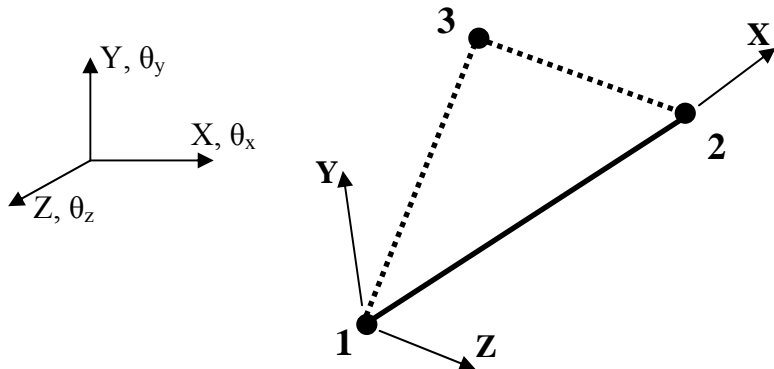


Figure 5.1 A Typical 3D FE Model for the Single-Span Bridge

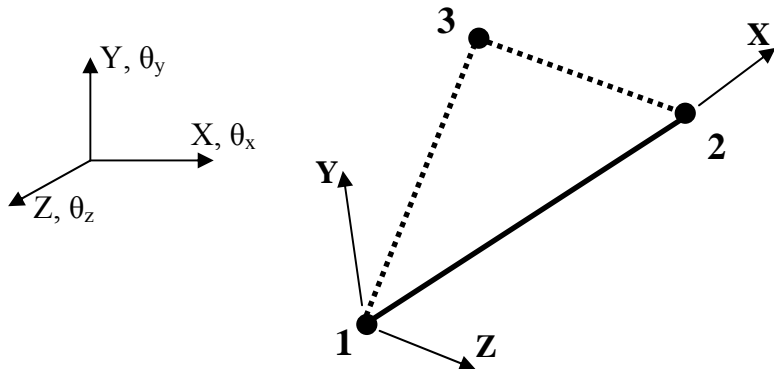
Linear 3D thick beam element known as BMS3 was utilized for the modeling of the bracing elements between the girders. A detailed description of the linear 3D thick beam element BMS3 is shown in tables 5.1.

Table 5.1 Linear 3D Thick Beam Element (LUSAS, 2008)

	
Element Name	BMS3
Element Group	Beams
Element Subgroup	Engineering Beams
Element Description	A straight beam element in 3D for which shear deformations are included. The geometric properties are constant along the length.
Number Of Nodes	3 with end release conditions. The third node is used to define the local xy-plane.
Freedom	U, V, W, θ_x , θ_y , θ_z : at end nodes.
End Releases	The element node numbers should be followed by: R restrained (default), F free defined in the order θ_y , θ_z at node 1 and then θ_y θ_z at node 2 related to local element axes
Node Coordinates	X, Y, Z: at each node.

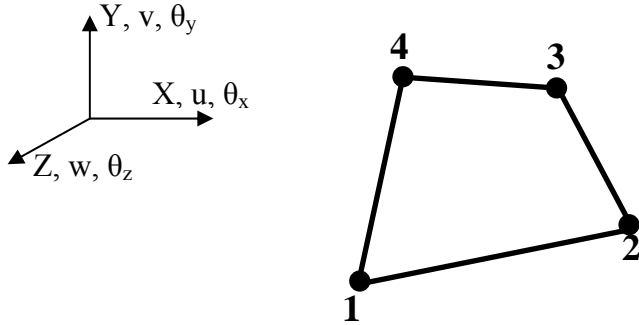
Nonlinear 3D thick beam element known as BTS3 was utilized for the modeling of the H-Piles and the concrete piles. A detailed description of the nonlinear 3D thick beam element BTS3 is shown in tables 5.2.

Table 5.2 Nonlinear 3D Thick Beam Element (LUSAS, 2008)

	
Element Name	BTS3
Element Group	Beams
Element Subgroup	Engineering Beams
Element Description	A straight beam element in 3D for which shear deformations are included. The geometric properties are constant along the length.
Number Of Nodes	3 with end release conditions. The third node is used to define the local xy-plane.
Freedom	U, V, W, θ_x , θ_y , θ_z : at end nodes.
End Releases	The element node numbers should be followed by: R restrained (default), F free defined in the order θ_y , θ_z at node 1 and then θ_y θ_z at node 2 related to local element axes.
Node Coordinates	X, Y, Z: at each node.

3D thick shell element known as QTS4 was utilized for the modeling of slab, flanges and webs of the plate girders, and abutments. A detailed description of the nonlinear 3D thick shell element QTS4 is shown in tables 5.3.

Table 5.3 3D Thick Shell Elements (LUSAS, 2008)

	
Element Name	QTS4
Element Group	Shells
Element Subgroup	Thick Shells
Element Description	A family of shell elements for the analysis of arbitrarily thick and thin curved shell geometries, including multiple branched junctions. The quadratic elements can accommodate generally curved geometry while all elements account for varying thickness. Anisotropic and composite material properties can be defined. These degenerate continuum elements are also capable of modeling warped configurations. The element formulation takes account of membrane, shear and flexural deformations. The quadrilateral elements use an assumed strain field to define transverse shear which ensures that the element does not lock when it is thin.
Number Of Nodes	4 numbered anticlockwise.
Freedom	Default: 5 degrees of freedom are associated with each node U, V, W, θ_α , θ_β . To avoid singularities, the rotations θ_α and θ_β relate to axes defined by the orientation of the normal at a node. These rotations may be transformed to relate to the global axes in some instances. Degrees of freedom relating to global axes: U, V, W, θ_x , θ_y , θ_z may be enforced using the Nodal Freedom data input, or for all shell nodes by using option 278.
Node Coordinates	X, Y, Z: at each node.
Nodal Freedom	5 or 6.

Although using thick shell elements increases the size of the model considerably, it is necessary to accurately capture the girder-abutment interaction behavior.

5.2.2 Modeling of Foundation Soil and Backfill soil

Linear spring elements are utilized to model the foundation soil supporting the piles and the backfill soil behind the abutment. The spring stiffness for the foundation soil is specified per unit length of the pile (N/m) and the spring stiffness for the backfill is specified per unit area of the abutment (N/m²). For cohesive soils (clay) supporting the piles, the spring constant is independent of the soil depth and it is calculated based on the soil modulus, E_s , described in section 4.4. For cohesionless soils (sand) supporting the piles, the spring constant is a function of the soil depth z and it was calculated based on the soil modulus, E_s , described in section 4.5.

5.3 MODEL VALIDATION

The field measurements from the new Scotch Road Bridge in New Jersey were used to validate the 3D FE model. The bridge was instrumented for research purpose by Stevens Institute of Technology (Hassiotis et al., 2006) as part of the Federal Highway Administration (FHWA) and New Jersey Department of Transportation (NJDOT) project No. FHWA-NJ-2005-025. The instrumentation of the bridge was carried out to measure among other things the stresses in the H-Piles, the bridge movement and the pressure behind the stub abutment.

5.3.1 Bridge Description

The new Scotch Road Bridge is New Jersey's first long (91 meters) Integral Abutment Bridge and it was part of the reconstruction of the Scotch Road interchange project. An aerial view of the interchange and the bridge is shown in figure 5.2. The bridge which carries vehicular traffic over Interstate I-95 was completed in 2003. The structure is a two equal span continuous bridge with a total length of 90.9 meters and a width of 31.8 meters. The bridge was designed according to AASHTO LRFD bridge design specifications. The plan and elevation of the bridge are shown in figures 5.3a and 5.3b respectively.



Figure 5.2 Aerial View Scotch Road Interchange (Photo Courtesy of NJDOT)

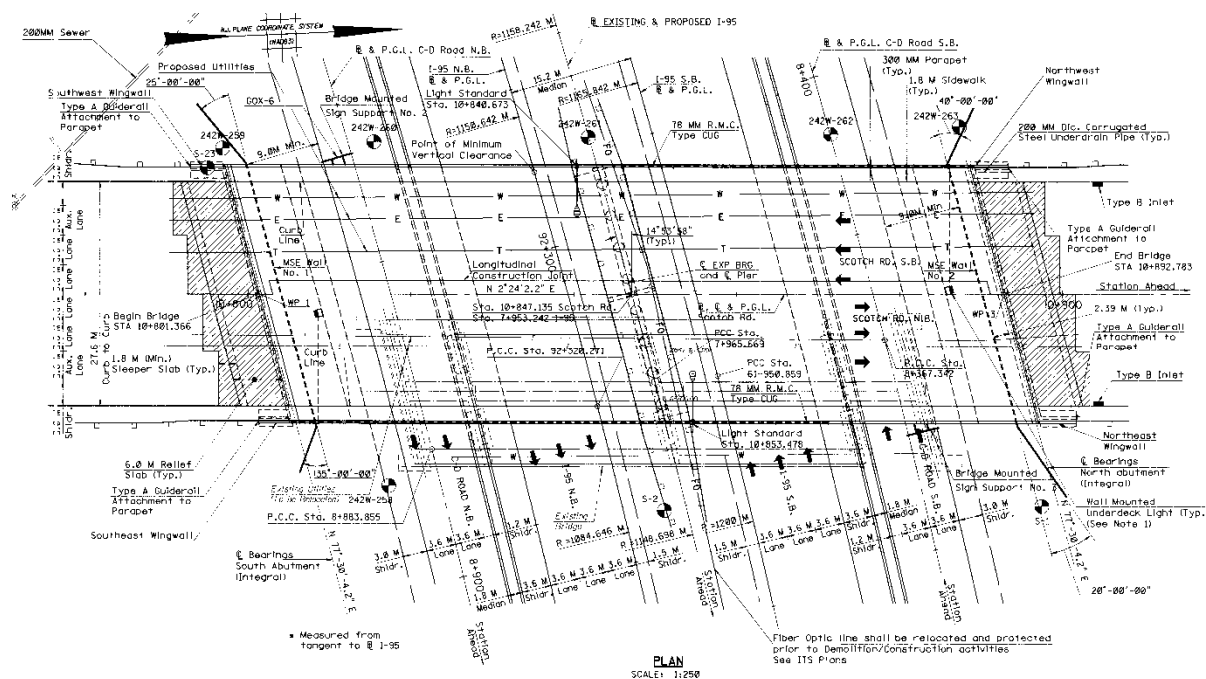


Figure 5.3a Scotch Road Bridge – Plan (Courtesy of NJDOT)

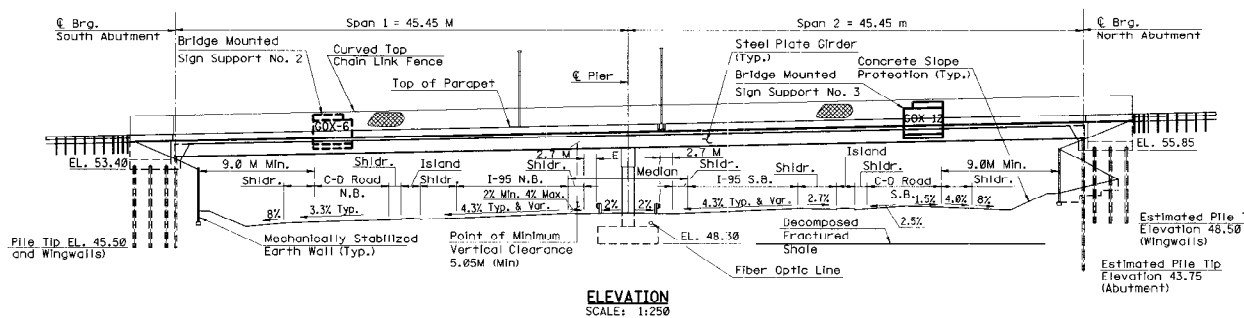


Figure 5.3b Scotch Road Bridge – Elevation (Courtesy of NJDOT)

The superstructure for the bridge consists of 10 high performance steel plate girders and a concrete deck slab that forms a skew angle of 15 degrees with the substructure. At each end, the superstructure is supported by a flexible substructure composed of a stub abutment and a single row of 19 steel H-Piles as shown in figure 5.4. The interior support of the bridge consists of two identical 4-column concrete pier bents as shown in figure 5.5. The bridge was constructed in two stages.

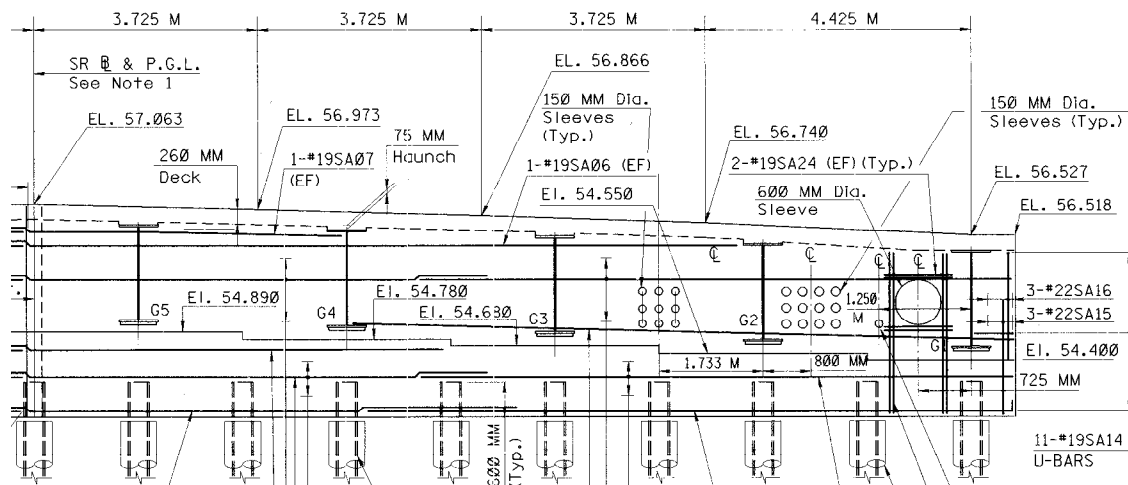


Figure 5.4 Scotch Road Bridge – Girders, Abutment and Piles (Courtesy of NJDOT)

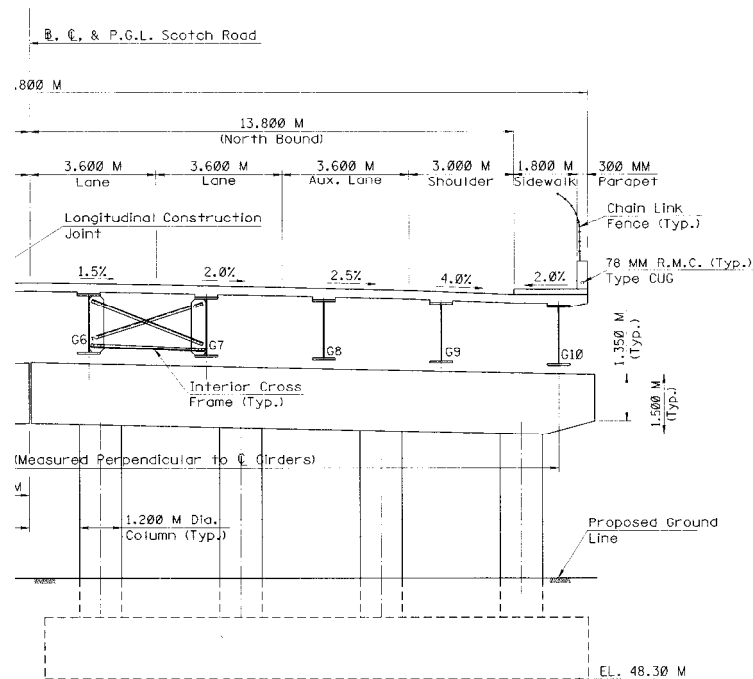


Figure 5.5 Scotch Road Bridge – Interior Pier Elevation (Courtesy of NJDOT)

To reduce the stiffness of the substructure, and to facilitate the expansion of the superstructure, the top part (4 meters) of each of the H-Piles in the new Scotch Road Bridge was enclosed by 600 mm aluminum sleeve filled with cushion sand as shown in figure 5.6. The rest of the pile was embedded inside 910 mm predrilled concrete piles supported by decomposed fracture shale.

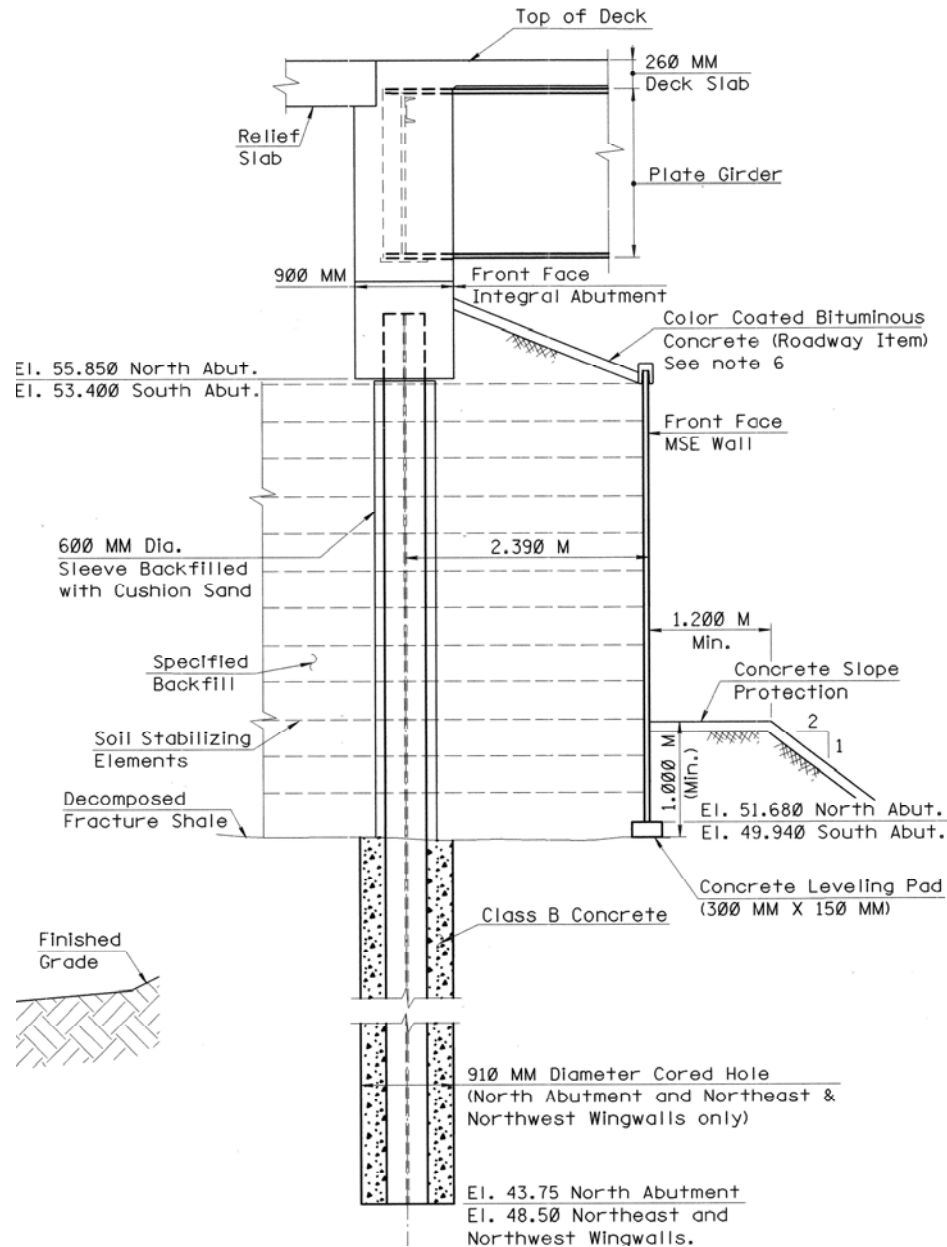


Figure 5.6 Scotch Road Bridge - Foundation Details (Courtesy of NJDOT)

The aluminum sleeve enclosures are shown in figure 5.7.



Figure 5.7 H-Piles Enclosed by Aluminum Sleeves (Courtesy of NJDOT)

NJDOT requires that the pre-bored holes be at least 2.5 meters (8 feet) below the bottom of the planned finished ground elevations for IABs with lengths of 30 meters (100 feet) or more. The hole shall be filled with cushion or uncompacted sand. The cushion or uncompacted sand shall conform, according to the provisions of the NJDOT Standard Specifications, to designation I-8 sand. (NJDOT, 2009).

Figure 5.8 summarizes the general construction staging of integral bridges and it is similar to the sequence used in the construction of Scotch Road Bridge. To reduce the rotation of the abutments and the piles, the top part of the abutment that integrates the superstructure and the substructure is cast last.

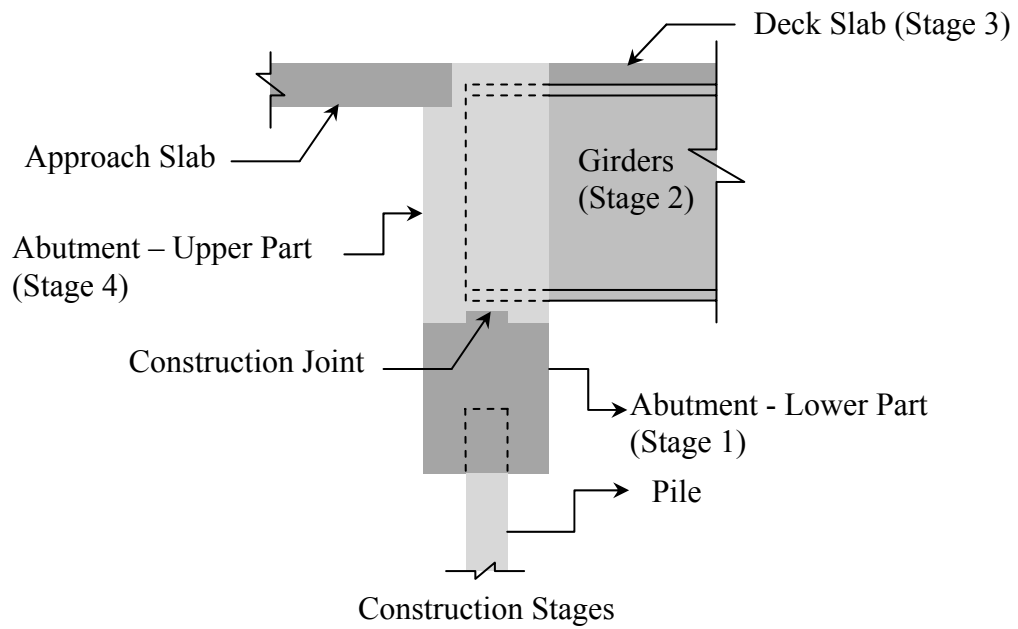


Figure 5.8 Scotch Road Bridge – Construction Stages

Figure 5.9 shows the abutment area of the bridge during construction just after the completion of stage 2.



Figure 5.9 Abutment- Girder Connection (Courtesy of ARORA and ASSOCIATES, P.C)

5.3.2 Bridge FE Model

The 3D FE LUSAS model for the new Scotch Road Bridge is shown in Figure 5.10. The steel plate girders, stiffeners, deck slab and the abutments were modeled as thick shell elements. The piles and the transverse diaphragms were modeled as thick 3D beam elements. The underside of the bridge deck is shown in figure 5.11. The backfill soil was modeled as linear spring elements with stiffness assigned per unit area (force/deformation per area) of the abutment meshed shell elements. The foundation soil is classified as decomposed fracture shale and it was modeled using the properties of weak rock with Rock-Quality Designation (RQD) equal to zero (Reese and Van Impe 2001). The soil inside the enclosure was modeled using very loose sand properties. The soil around the pile was incorporated in the 3D model using linear spring elements with stiffness assigned per unit length (force/deformation per length) of the pile meshed beam elements. Properties of compacted medium soil were used initially to model the backfill soil. The backfill soil behind the abutment was incorporated in the model using linear spring elements with stiffness assigned per unit area (force/deformation per area) of the abutment meshed shell elements. The springs for the abutment backfill and the foundation soil are shown in Figure 5.12. The skew of the bridge was ignored in the model.

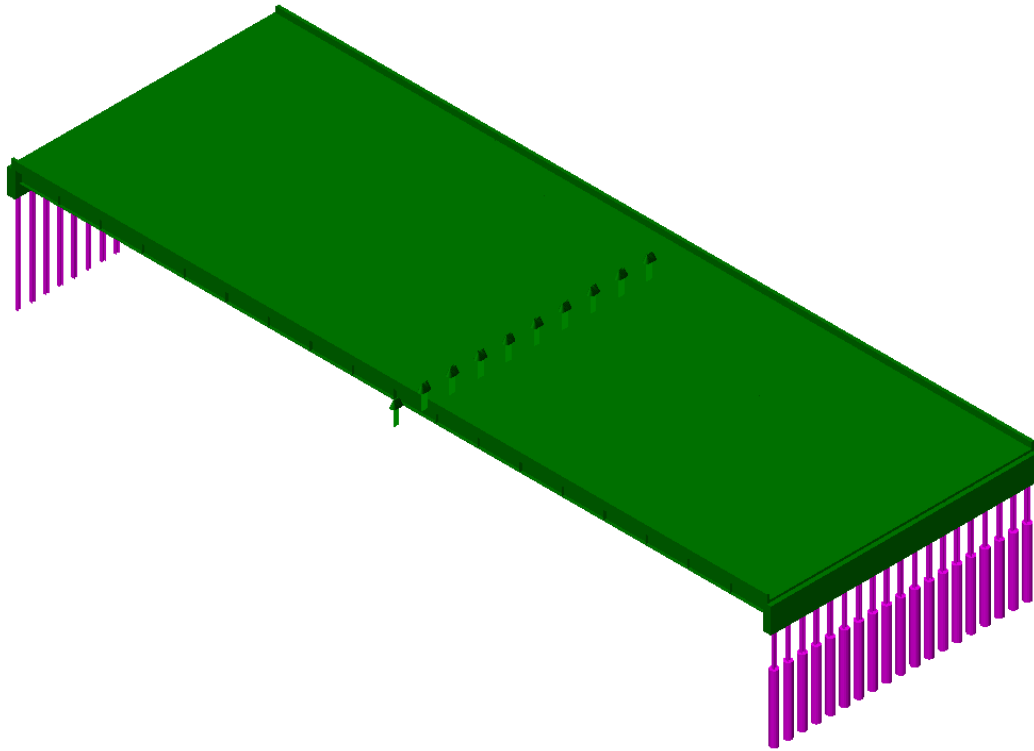


Figure 5.10 Scotch Road Bridge LUSAS 3D FE Model- Isometric View

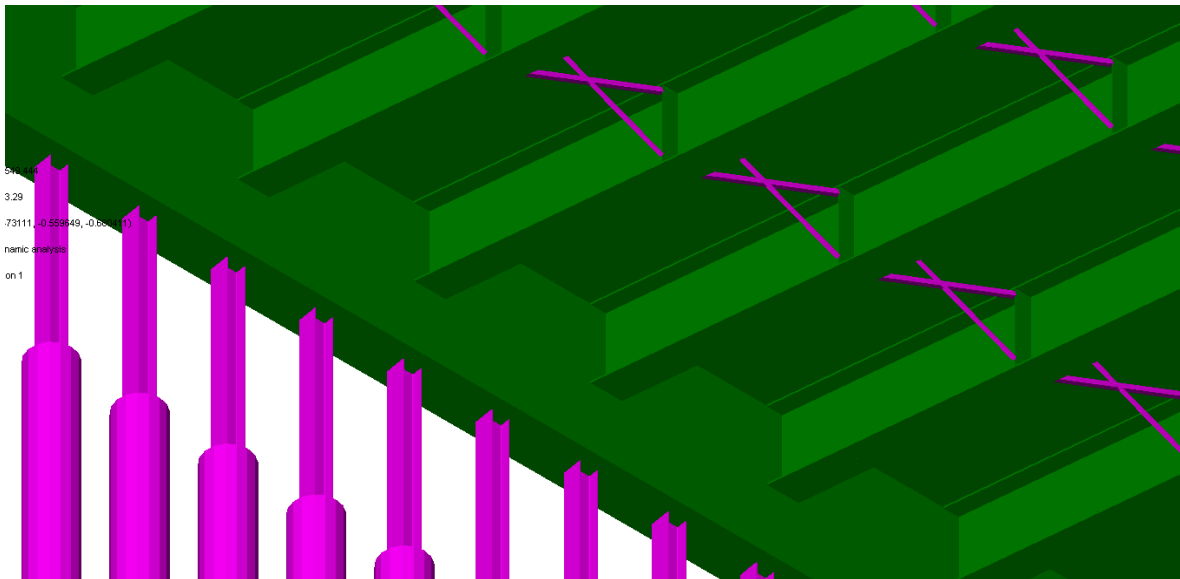


Figure 5.11 Underside of the Bridge Deck

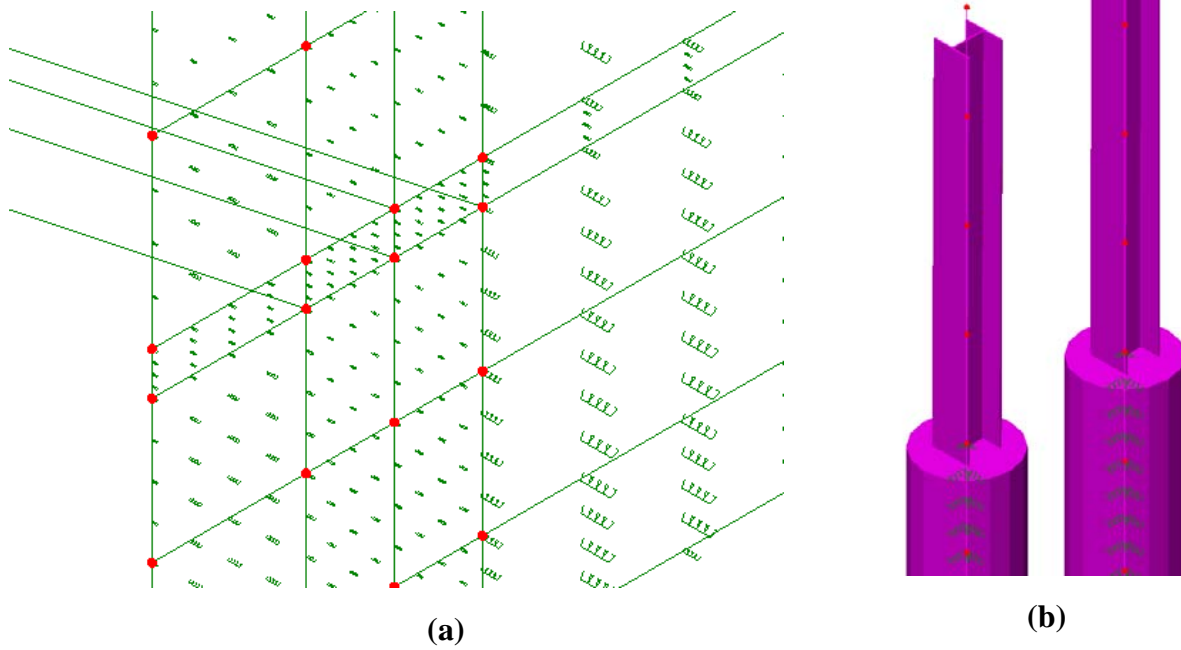


Figure 5.12 Linear Spring Models for **(a)** Abutment and **(b)** Piles

5.3.3 Validation of Results

Field data obtained from the FHWA-NJ-2005-025 project report (Hassiotis et al. 2006) was used to verify the FE model for the Scotch Road Bridge. The seasonal bridge displacement and the stress at the top of the pile were used to verify and validate the FE model. Figure 5.13 shows a plot of the displacement over more than two years at the relief slab of the bridge for the two stages of construction. The data was recorded from April 2003 until January of 2005. The temperature at the top of the girders was recorded for the same period of time. The plot of the temperature on top of girder 5 for the same period is shown in figure 5.14. The data suggests that the bridge's zero displacement happened around a superstructure temperature of 50°F (10°C). The lowest and highest displacements happened around a superstructure temperatures of 5°F (-15°C) and 95°F (35°C) respectively. These temperatures changes, + 25°C and - 25°C, were used in the 3D FE model.

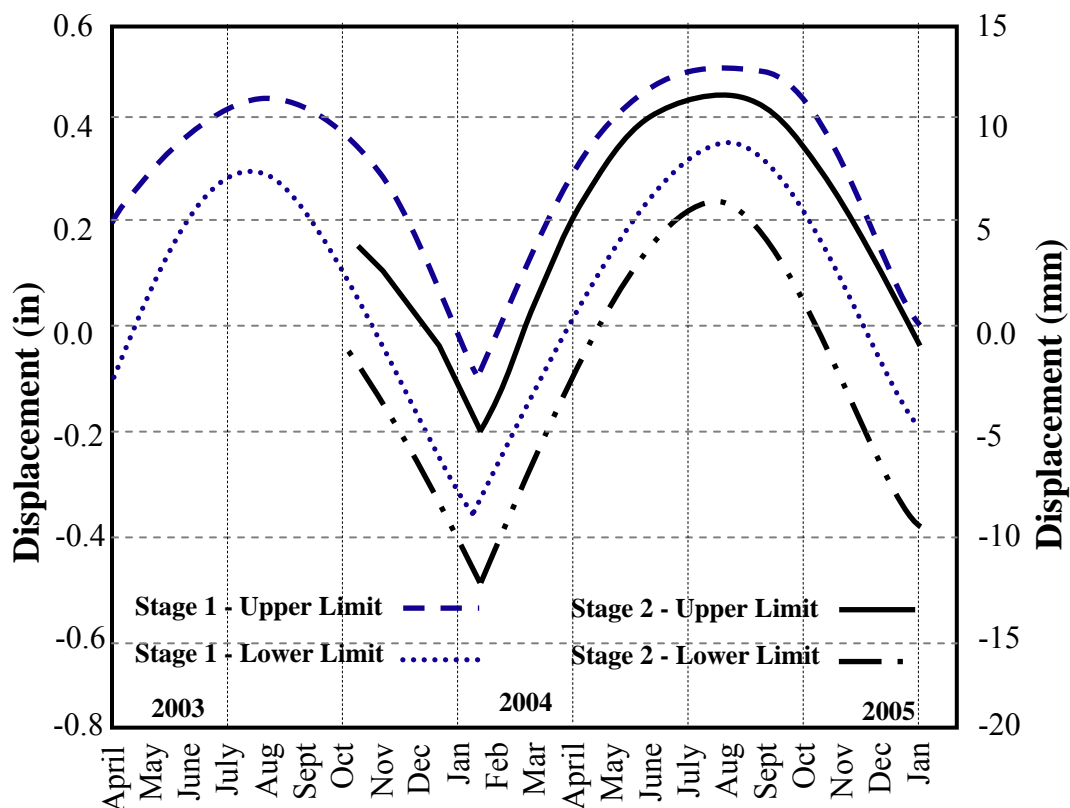


Figure 5.13 Longitudinal Bridge Displacement at the Relief Slab (Hassiotis et al. 2006)

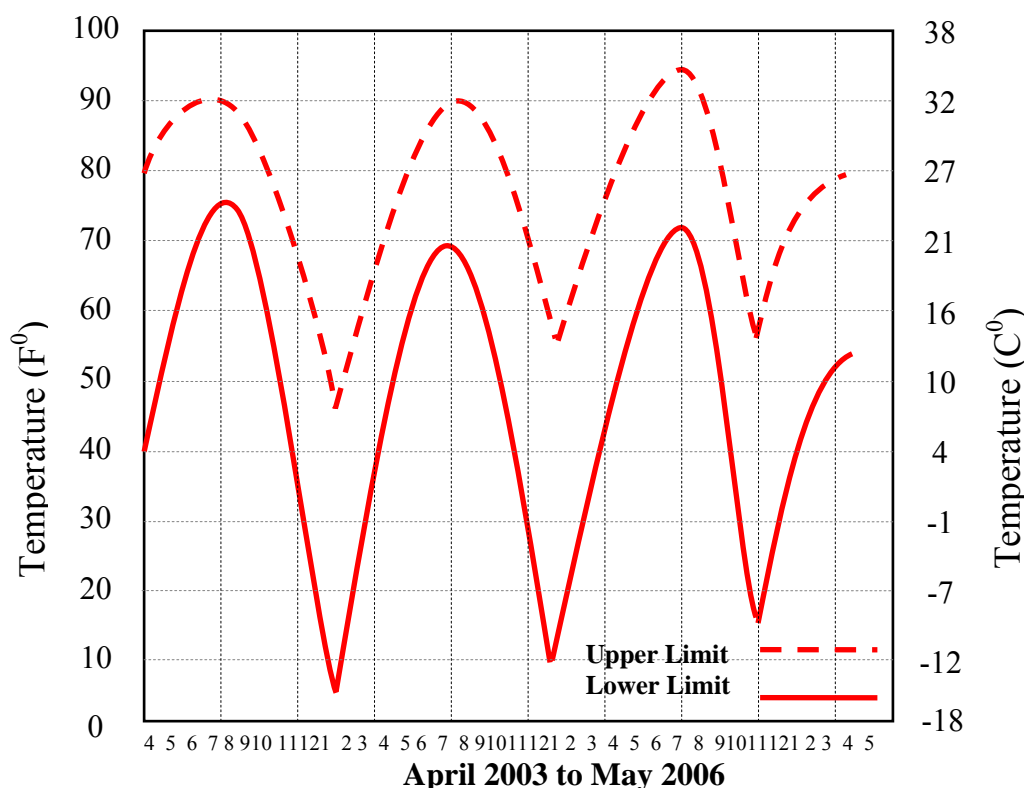


Figure 5.14 Temperature Variations at the Top of Girder 2 (Hassiotis et al. 2006)

Figure 5.15 shows the stresses at the piles just below the abutment.

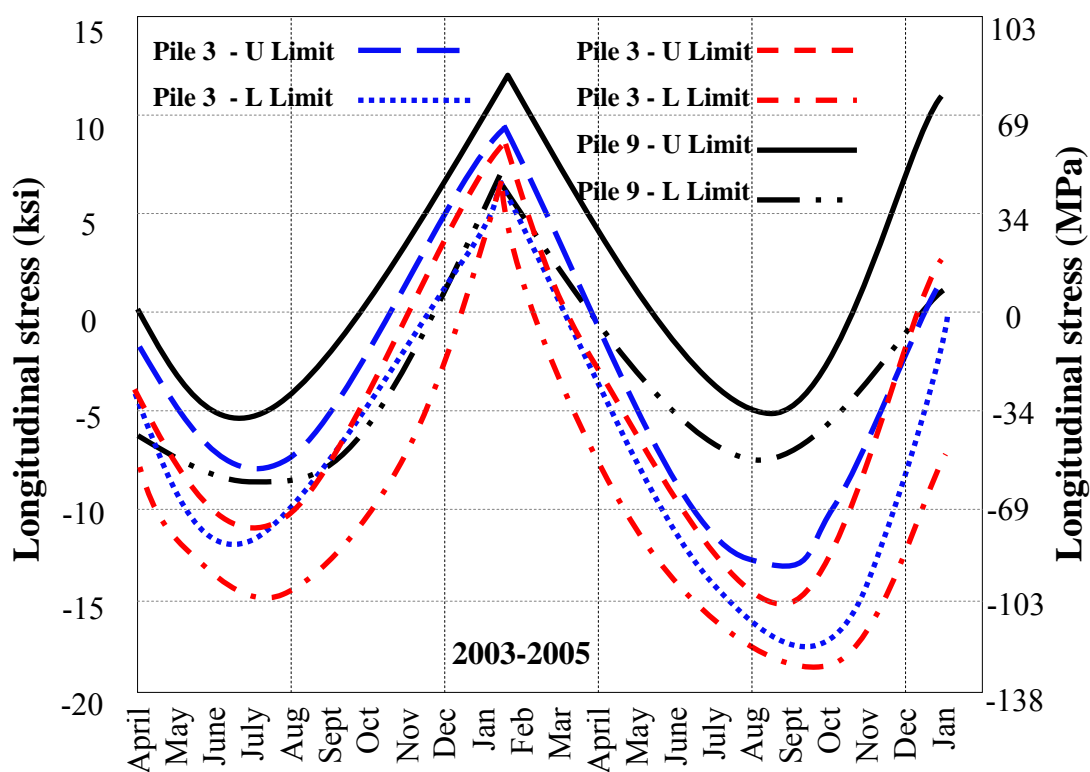


Figure 5.15 Stresses at Top of Piles 3, 6, and 9 (Hassiotis et al. 2006)

The bridge displacements from the FE model for temperature change of + 25°C and - 25°C are shown in figures 5.16 and 5.17 respectively.

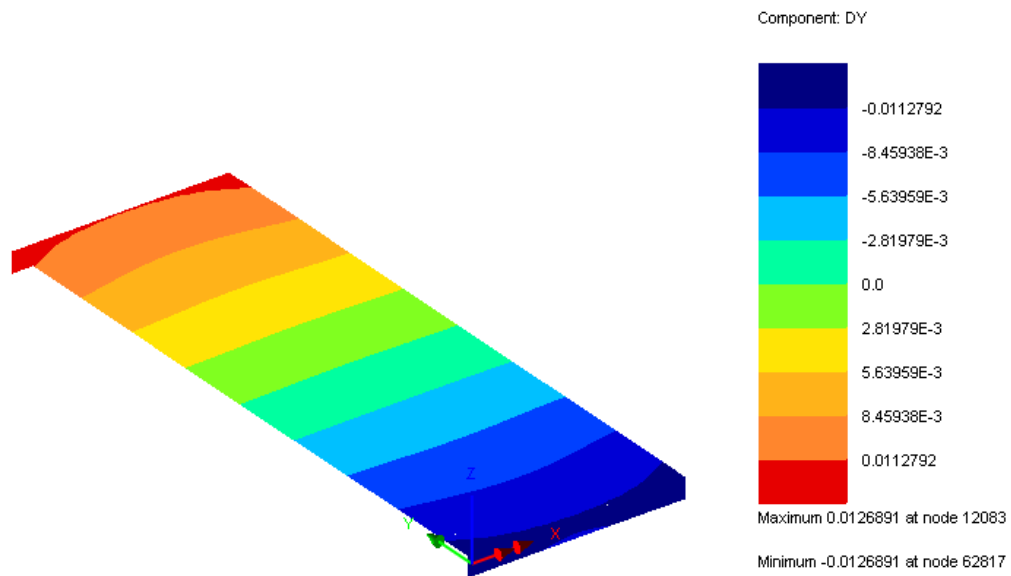


Figure 5.16 Bridge Expansion (mm) in the Longitudinal Direction, $\Delta T=25^{\circ}\text{C}$

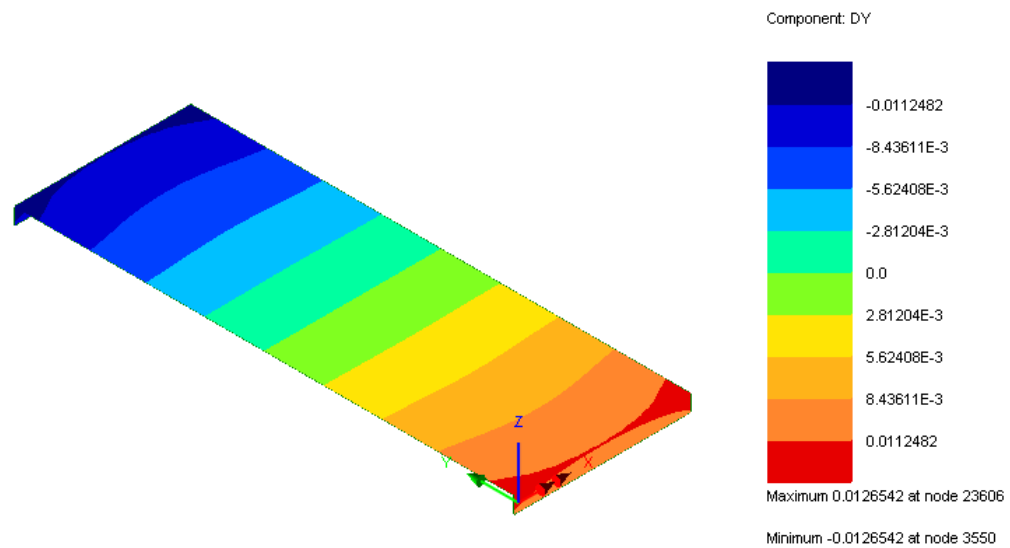


Figure 5.17 Bridge Contraction (mm) in the Longitudinal Direction, $\Delta T=-25^{\circ}\text{C}$

The stresses at the top of piles 3 and 6 at the inside face (bridge side) from the FE model for temperature change of $+25^{\circ}\text{C}$ and -25°C are shown in figures 5.18 and 5.19 respectively.

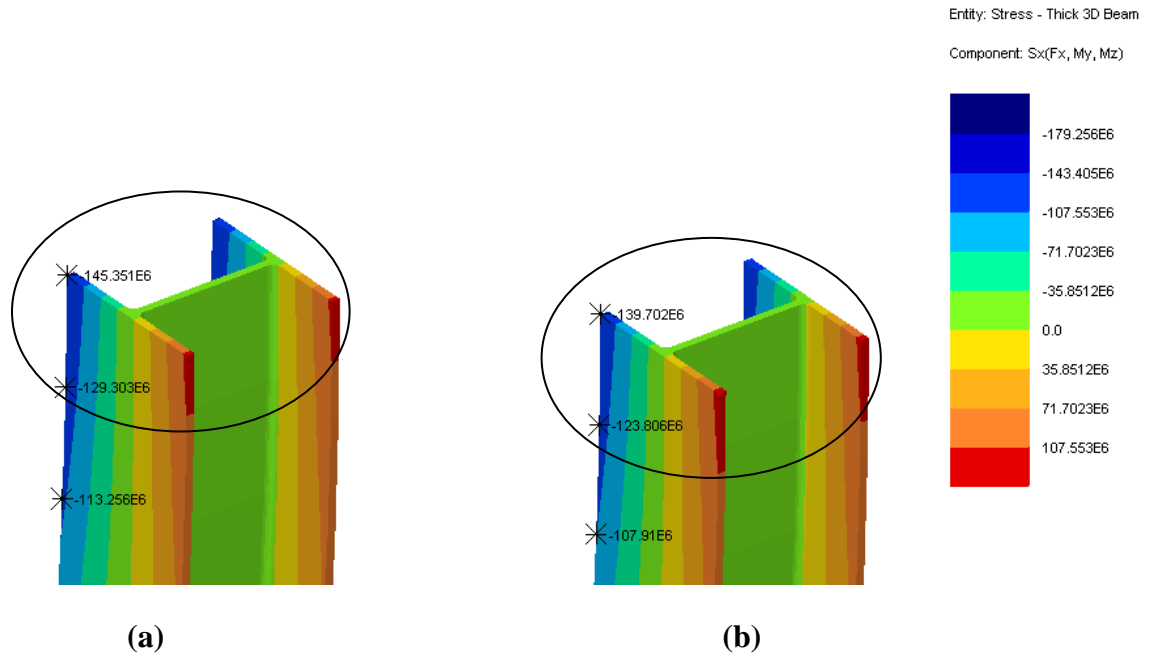


Figure 5.18 Pile Inside Face Top Stresses (N/m²), $\Delta T=25^{\circ}\text{C}$ (a) Pile 3 (b) Pile 6

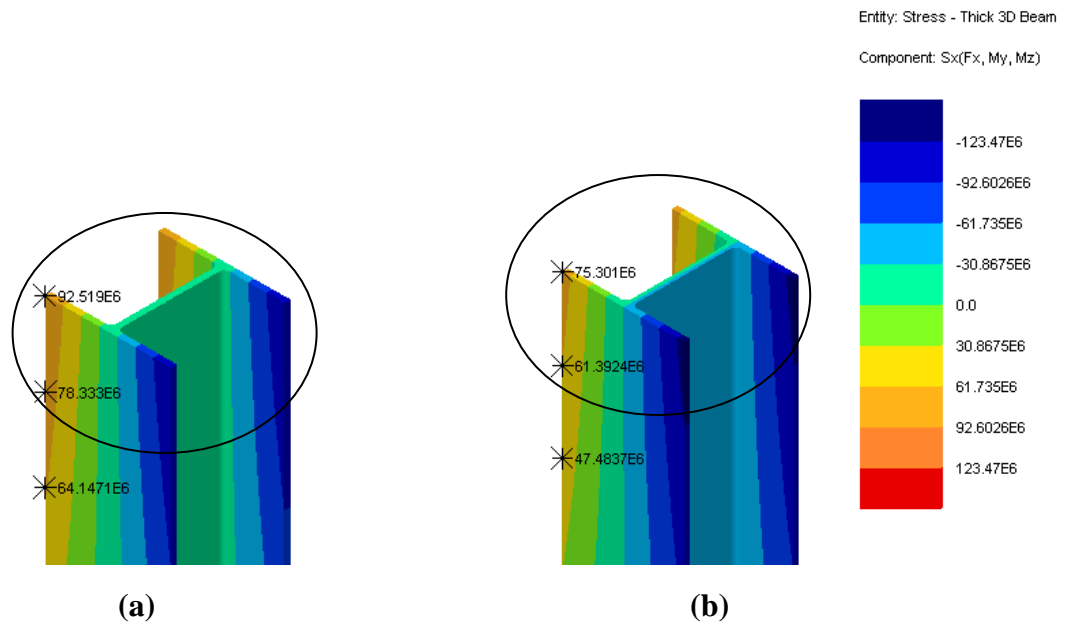


Figure 5.19 Pile Inside Face Top Stresses (N/m²) , $\Delta T=-25^{\circ}\text{C}$ (a) Pile 3 (b) Pile 6

Table 5.4 presents a comparison between the field measurements and the 3D FE model results for the bridge movement and top of pile stresses. The comparison shows reasonable agreement between the results from the field data and the FE model. The backfill soil properties were adjusted so that pressure on the abutment in the FE model matches that of the field data.

Table 5.4 Comparison between Field Data and FE Model Results

Parameter	Case	Field Data (Hassiotis et al. 2006)	FE Model
Bridge Movement Range inches (mm)	Elongation $\Delta T=30^{\circ}\text{C}$	0.40 - 0.52 (10-13)	0.44 - 0.50 (11-13)
	Contraction $\Delta T=-20^{\circ}\text{C}$	0.38 - 0.50 (10-13)	0.44 - 0.50 (11-13)
H-Pile Top Stresses Range ksi (MPa)	Elongation $\Delta T=30^{\circ}\text{C}$	13 - 18 (90-124)*	16 - 22 (110-152)
	Contraction $\Delta T=-20^{\circ}\text{C}$	8 - 12 (55-83)	11 - 16 (76-110)

* Piles 3 and 6

5.4 TWO-DIMENSIONAL 2D FE MODEL

For comparison purposes, 2D FE models were developed using 2D beam elements for all the structural elements. A typical interior girder, 2 piles, and the tributary widths of the deck and abutment were included in the 2D models. A typical 2D model for the Single-Span Bridge is shown in figure 5.20.

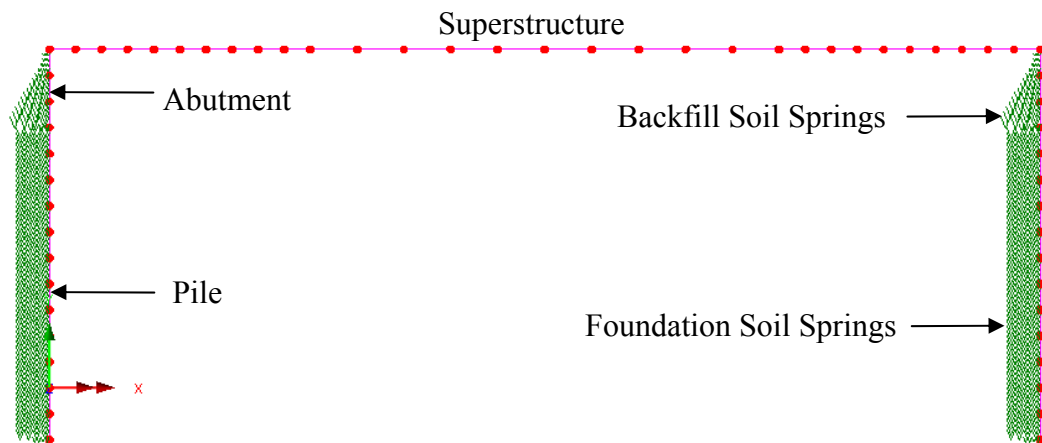


Figure 5.20 A Typical 2D FE Model for the Single-Span Bridge

CHAPTER 6

PARAMETRIC STUDY SETUP

6.1 GENERAL

A parametric study is conducted to investigate the effect of the various geotechnical and structural properties of the bridge substructure on the performance of IABs. This chapter presents the different parameters under consideration, the bridges in the study, the geotechnical properties for the different foundation soils, and the terminology used in the study.

6.2 PARAMETERS IN THE STUDY

The parametric study will investigate the effect of soil stiffness, use of pile enclosure, pile orientation, abutment stiffness, and pile type (Prestressed Concrete Piles versus Steel H-Piles) on the behavior of IABs. The effect of each of these parameters on the displacement and rotation along the abutment and the pile, the moment along the pile, the stresses in the girders and deck slab, and the backfill pressure on the abutment during bridge expansion will be investigated.

Table 6.1 below summarizes the substructure properties that were varied in the study.

Table 6.1 List of the Parameters Considered in The Study.

Parameter	Description
Abutment height	3m, 3.5m, and 4m
Foundation Soil	Soft Clay, Medium Clay, Stiff Clay, Very Stiff Clay Loose Sand, Medium Dense Sand, and Dense Sand
Backfill Soil	Compacted, Non-Compacted
Pile Type	Steel H-Piles and Prestressed Concrete (PC) Piles
Pile size	HP14, HP12, PC14, PC12
Pile Orientation	Strong Axis Orientation Weak Axis Orientation
Single Span Bridge Length	38 meters
Two Span Bridge Length	90 meters

6.3 BRIDGES IN THE STUDY

Two steel girder IABs are considered in the parametric study. The bridges depict two recently constructed IABs in the state of New Jersey. The first bridge (Short Bridge) is a 38-meter single span steel plate girder bridge. The abutment is a stub abutment supported on a single row of steel H-Piles oriented to bend around the pile's weak axis. The cross section of the bridge is shown in figures 6.1a. The second bridge (Long Bridge) is a two-equal spans steel plate girder bridge with a total length of 90 meters. The abutment is a stub abutment supported on a single row of steel H-Piles oriented to bend around the pile's weak axis. The girders are supported by roller bearings on top of the pier. The cross section of the bridge is shown in figure 6.2. The lengths of the two bridges cover a substantial range of common IABs' lengths. The two bridges were slightly modified to suite the parametric study.

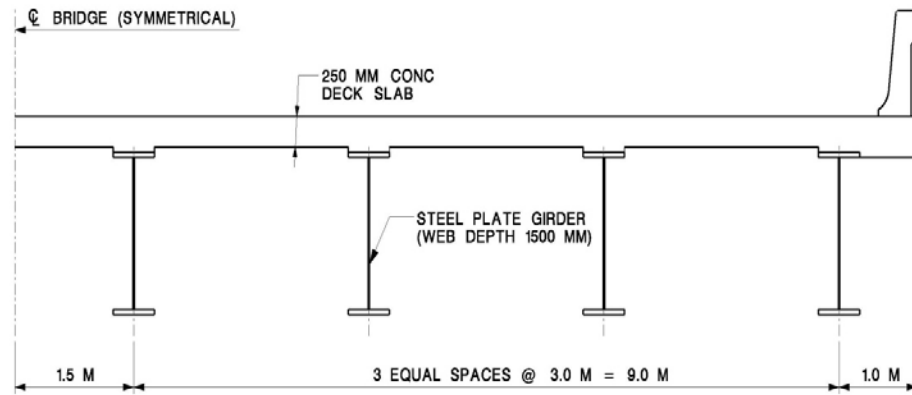


Figure 6.1 Cross Section of the Short Bridge

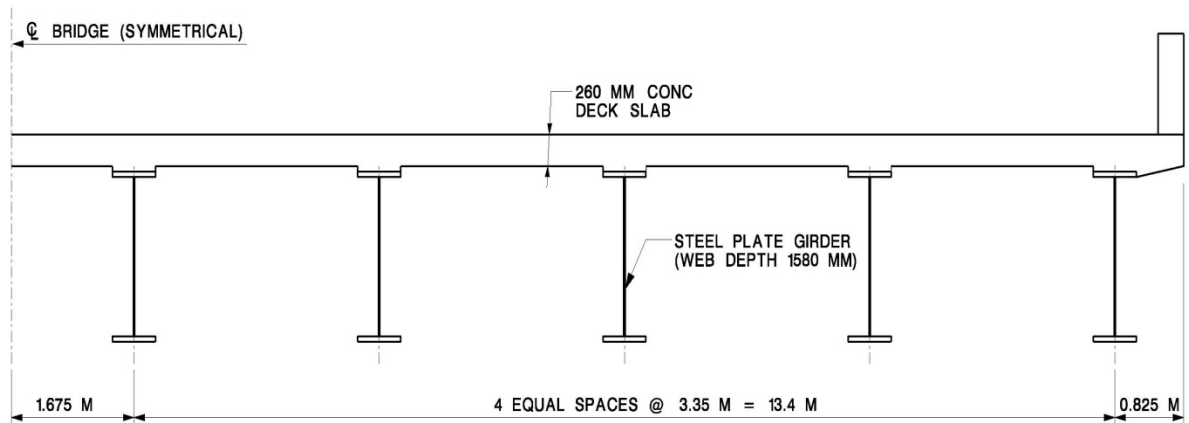


Figure 6.2 Cross Section of the Long Bridge

A typical plate girder cross section is shown. The sizes of the different plates of the steel plate girders for the two bridges are summarized in table 6.2

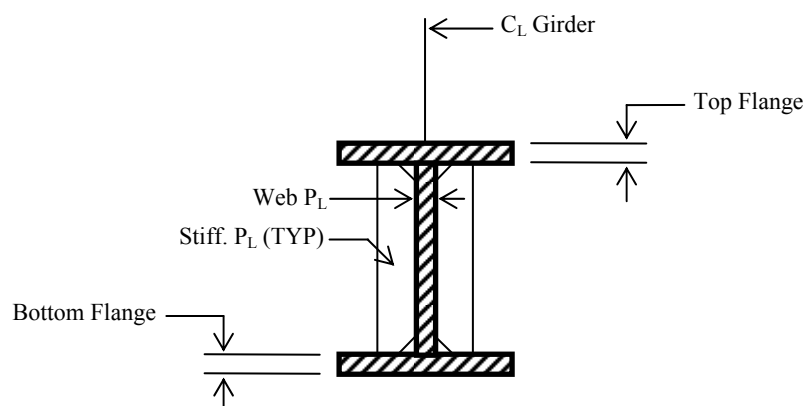


Figure 6.3 A Typical Plate Girder Cross Section

Table 6.2 Steel Plate Girders Dimensions

Bridge	Plate	At Abutment (mm)	Mid-Span (mm)	At Pier (mm)
Short Bridge	Top Flange	400x22	400x 35	N.A.
	Web	1500x16	1500x16	N.A.
	Top Flange	400x 35	400x 50	N.A.
	Stiffener	185x20	185x10	N.A.
Long Bridge	Top Flange	600x35	600x50	600x35
	Web	1580x20	1580x20	1580x20
	Top Flange	600x35	600x50	600x35
	Stiffener	185x16	185x16	280x40

6.4 SOIL MODELS

Linear spring elements were utilized to model the foundation soil supporting the piles and the backfill behind the abutment. For cohesive soils (clay) supporting the piles, the spring constant is independent of the soil depth and it was calculated based on the soil modulus, E_s , described in chapter 4. The values of the spring constant per unit length of the pile for various cohesive soils are summarized in table 6.3.

Table 6.3 Spring Constants for Cohesive Soils

Foundation Soil	C_u	ε_{50}	Δ_{50}	Δ_y	Q_u	Spring Constant
	(KN/m ²)	m/m	m	m	KN	KN/m/m
Soft clay	19	0.02	0.018	0.036	61.56	1,700
Medium clay	38	0.01	0.009	0.018	123.12	6,800
Stiff clay	75	0.0065	0.00585	0.0117	243	20,769
Very Stiff clay	150	0.005	0.0045	0.009	486	54,000

For cohesionless soils (sand) supporting the piles, the spring constant is a function of the soil depth z and it was calculated based on the soil modulus, E_s , described in chapter 4.

The values of the spring constant per unit length of the pile for various cohesionless soils are summarized in table 6.4.

Table 6.4 Spring Constants for Cohesionless Soils

Foundation Soil	Modulus of subgrade reaction k		ϕ Internal angle of friction	Unit Weight γ	Spring Constant
	Range	Suggested*			
	MN/m ³	MN/m ³	Degrees	KN/m ³	KN/m/m
Loose	3.5-10.4	6.8	30	15	6800 z
Medium	13.0-40.0	24.4	35	18	24,400 z
Dense	51.0-102	76.0	40	20	76,000 z

The stiffness of the cohesionless backfill soil behind the abutment was specified as a variable per unit area of the abutment. The spring constant was calculated based on the Clough and Duncan model for medium sand described in section 4.6. The values of the spring constant per unit area of the abutment for different abutment heights are summarized in table 6.5.

Table 6.5 Spring Constants for Backfill Soil

Abutment Height	ϕ Internal angle of friction	Unit Weight γ	Spring Constant
m	Degrees	KN/m ³	KN/m ² /m
3.0	37	20	2,000 z
3.5	37	20	1,700 z
4.0	37	20	1,500 z

Throughout the study, the slope of the approximate linear curve was adjusted based on the nonlinear curve and the pile displacement to approximate the nonlinear behavior of the soil. The adjustment is illustrated in figure 6.4.

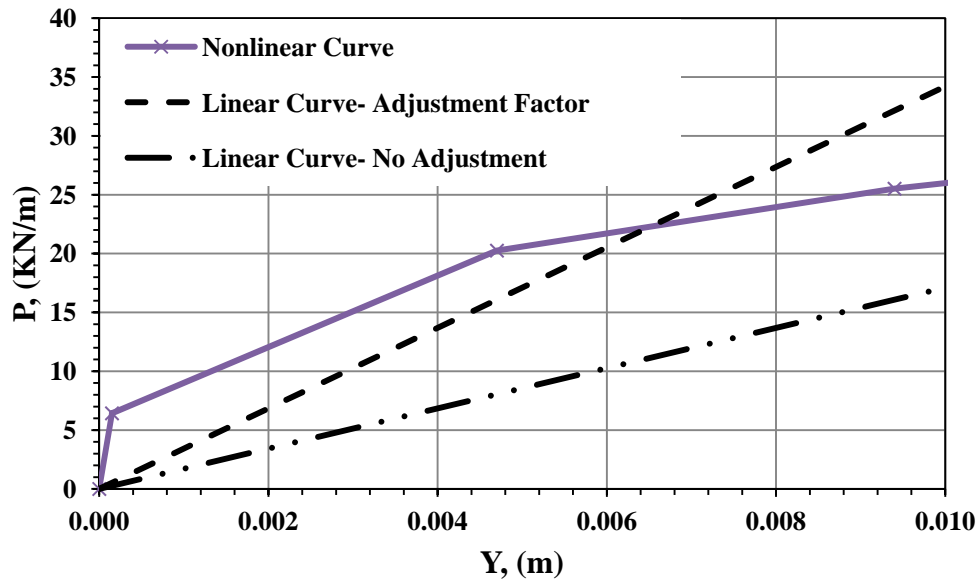


Figure 6.4 Soil Spring Adjustment Factor Illustration- 10 mm Displacement in Soft Clay

6.5 TERMINOLOGY IN THE STUDY

This section presents the terminology that will be used in presenting the results of the parametric study in the next chapter. The general approximate deflection shape of the short bridge in the longitudinal direction during bridge expansion is shown in figure 6.5. In the figure, the bridge is under positive thermal change that is causing the bridge to expand in the longitudinal and the transverse directions of the bridge. Similarly, figure 6.6 shows the general approximate deflection shape of the short bridge in the longitudinal direction during bridge contraction. In the figure, the bridge is under negative thermal change that is causing the bridge to contract in the longitudinal and the transverse directions of the bridge. The terminology shown in the figures will be used throughout the parametric study. The general approximate deflection shapes of the long bridge in the longitudinal direction during bridge contraction and expansion are shown in figures 6.7 and 6.8 respectively. Figure 6.9 shows the general deflection and moment diagrams along the pile. The terminology shown in the figure will be used through the parametric study. In general, the piles will have two inflection points in the deflection shape (displacement diagram) and the moment diagram along the pile. In the figure, the maximum absolute moment is shown at the top of the pile and the reversed moment is shown at the first inflection point. That will be the case for the majority of the moment diagrams shown in the next chapter. In few cases, the absolute value of the reversed moment will be higher than the moment at the top of the pile.

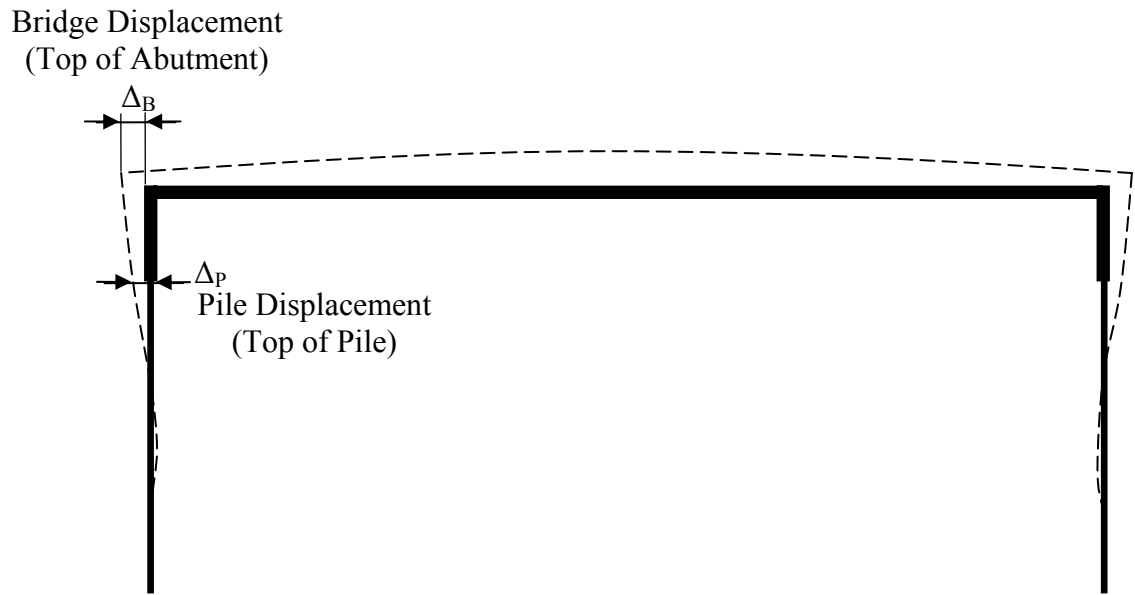


Figure 6.5: Single-Span Bridge, General Deflection Shape - Expansion

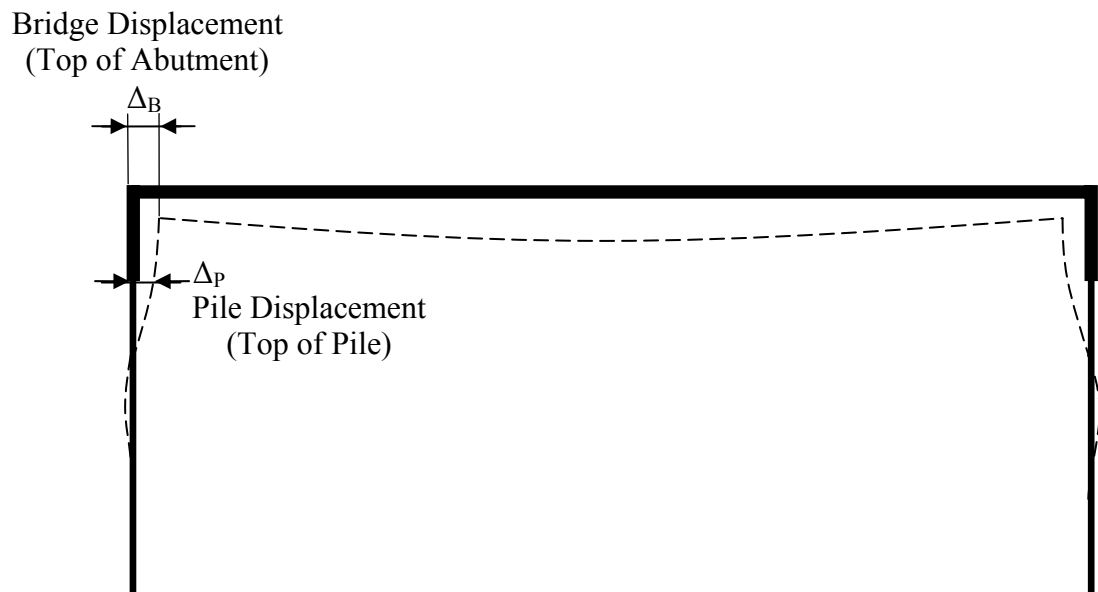


Figure 6.6 Single-Span Bridge, General Deflection Shape - Contraction

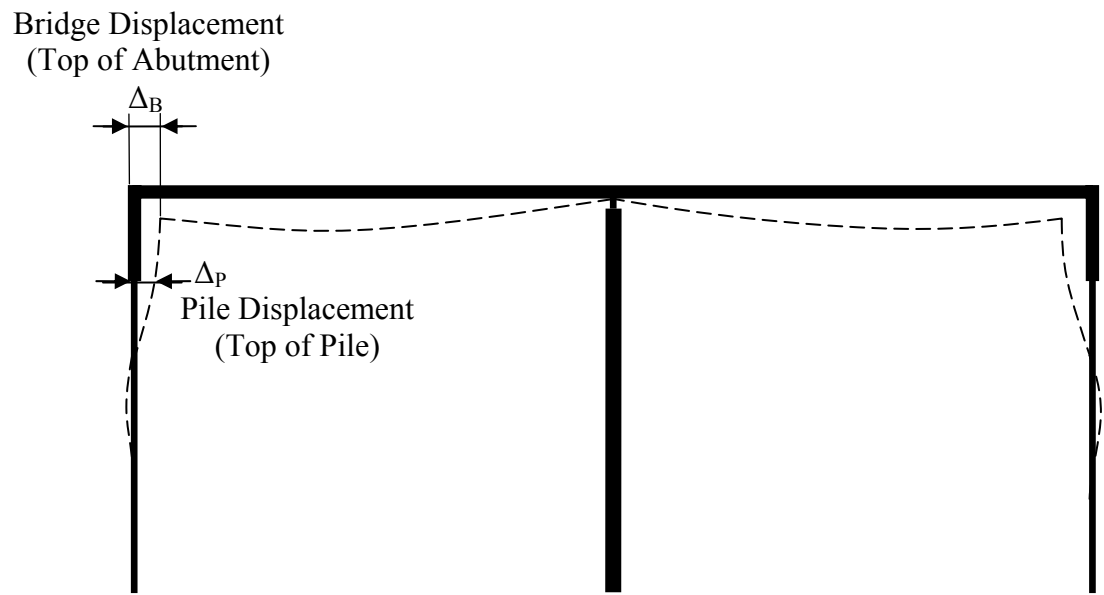


Figure 6.7: Two-Span Bridge, General Deflection Shape - Contraction

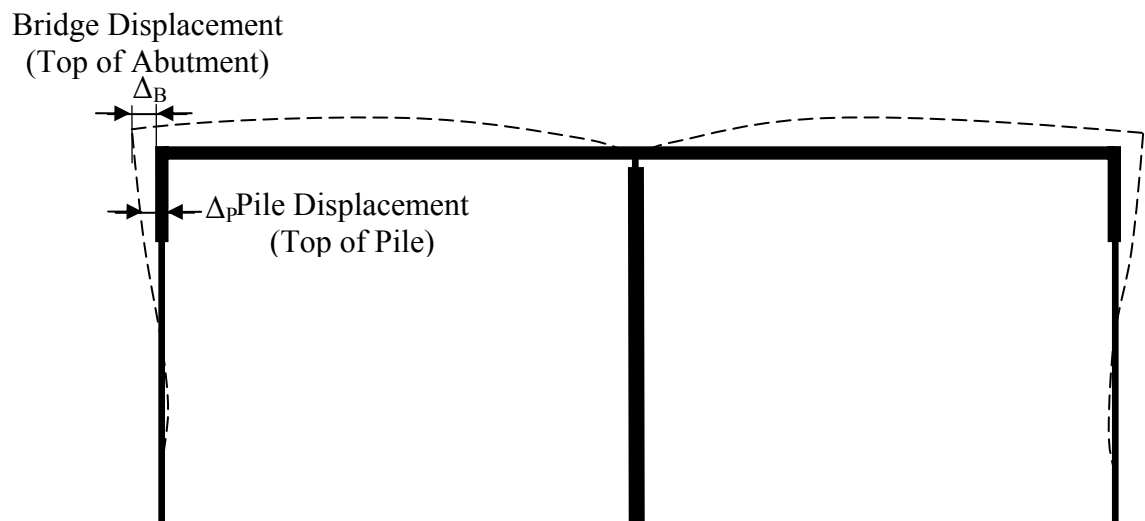


Figure 6.8: Two-Span Bridge, General Deflection Shape - Expansion

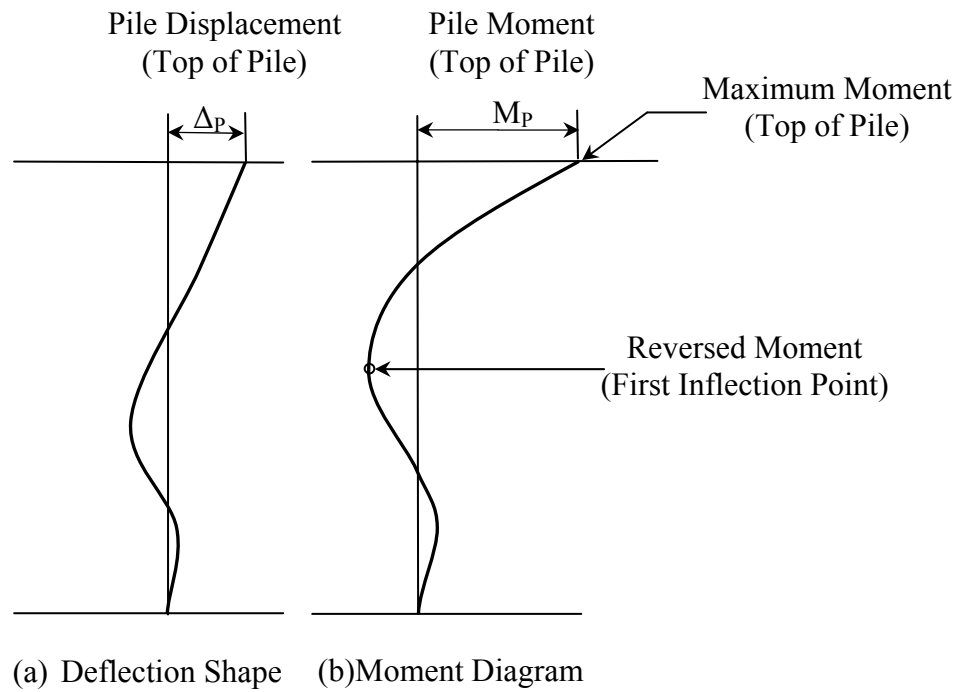


Figure 6.9 Pile's General Deflection Shape and Moment Diagram

CHAPTER 7

PARAMETRIC STUDY RESULTS

7.1 GENERAL

The parametric study results showed that the substructure stiffness has a significant effect on the performance of short and long IABs. The displacements, rotations, and consequently the stresses in the different components of the superstructure and the substructure are sensitive to the stiffness of the substructure. In general, the stiffness of the substructure has more effect when the bridge is under contraction than when it is under expansion. Among the investigated parameters, the foundation soil stiffness stands as the most important factor that affect the performance of IABs. The study also showed that the top part of the foundation soil has the most effect on the performance of the bridge especially on the behavior of the piles. The effect of the top part of the soil was obvious during the study of the effect of using an enclosure around the top portion of the pile. The study also showed that for short IABs, Prestressed Concrete Piles (PCPs) present a viable alternative to steel H-Piles especially in harsh corrosive conditions where the use of H-Piles is prohibited. For longer bridges, special considerations are needed to reduce the tensile stresses in the PCPs. The study also showed that the stiffness of the abutment and the stiffness of the pile have notable effect on the performance of IABs. The backfill pressure on the abutment was noticed to be insensitive to the abutment height range considered in the study.

This chapter presents the effects of the different parameters described in the previous chapter on the performance of IABs. These effects will be presented in the following order:

- The effect of soil stiffness
- The effect of using pile enclosure
- The effect of pile orientation
- The effect of abutment stiffness
- The effect of pile type (Prestressed Concrete Piles versus Steel H-Piles)

For every parameter, the following behaviors will be examined:

- The displacement and rotation along the abutment and the pile
- The moment along the pile
- The stresses in the girders
- The backfill pressure on the abutment during bridge expansion

The effect of every parameter on every behavior will be presented in the form of graphs and it will be followed by a discussion. All the graphs shown in this chapter present the effect due to thermal loads only. All the different effects will be examined for the short bridge supported by clay during expansion and contraction. Most of the effects will be also examined for the short bridge supported by sand during expansion and contraction, the long bridge supported by clay during expansion and contraction, and the long bridge supported by sand during expansion and contraction.

7.2 EFFECT OF SOIL STIFFNESS

The study showed that the soil stiffness has a significant effect on the performance of IABs. The displacement and rotation along the abutment and along the piles are sensitive to the stiffness of the soil. The stresses in the girders and the backfill pressure are also sensitive to the stiffness of the soil. The effect of the soil stiffness on the performance of IABs is presented in the following subsections.

7.2.1 Effect of Soil Stiffness on the Displacement and the Rotation of the Abutment and the Piles

Figure 7.1 shows the displacement at the top of the abutment and at the top of pile (bottom of the abutment) at exterior and interior locations for the short bridge supported by clay.

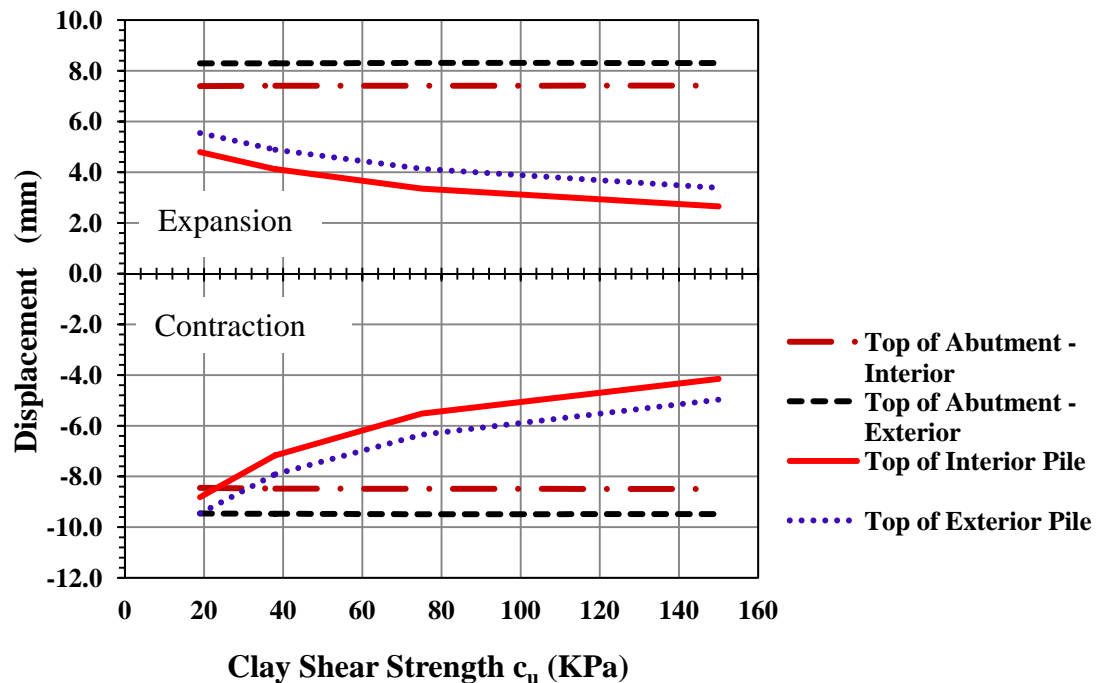


Figure 7.1 Displacement at Interior and Exterior Locations
(38-m Bridge, Clay, 3m Abutment, HP310X125 Weak Orientation)

Figure 7.1 shows that the stiffness of the clay has a minor effect on the displacement at the top of the abutment. At exterior locations the expansion at the top of the abutment is equal to 8.4 mm (0.33 in) which is the thermal expansion demand by the superstructure ($\Delta L = \alpha \Delta T L / 2$). The expansion at the interior location is less than that demanded by the superstructure. The figure reveals that the stiffness of the clay has a significant effect on the displacement at the top of the pile (bottom of the abutment) during bridge expansion and contraction. When the bridge is under contraction, the displacement at the top of the pile is almost equal to that at the top of the abutment when the piles are supported by soft clay. While the displacement at the top of the abutment does not change with the change in soil stiffness, the displacement at the top of the pile decreases significantly with the increase in soil stiffness and therefore the difference between the two displacements increases with the increase in clay stiffness. In very stiff clay, the displacement at the top of the pile is almost half the displacement at the top of the abutment. When the bridge is under expansion, the displacement at the top of the pile is about 2/3 of the displacement at the top of the abutment when the piles are supported by soft clay. The difference between the two displacements increases with the increase in clay stiffness. In very stiff clay, the displacement at the top of the pile is almost half the displacement at the top of the abutment. The displacement due to thermal loads along the abutment and the pile at the interior location can be seen in figure 7.2. The figure shows that the effect of clay stiffness on the displacement of the abutment and the pile is more significant when the bridge is under contraction.

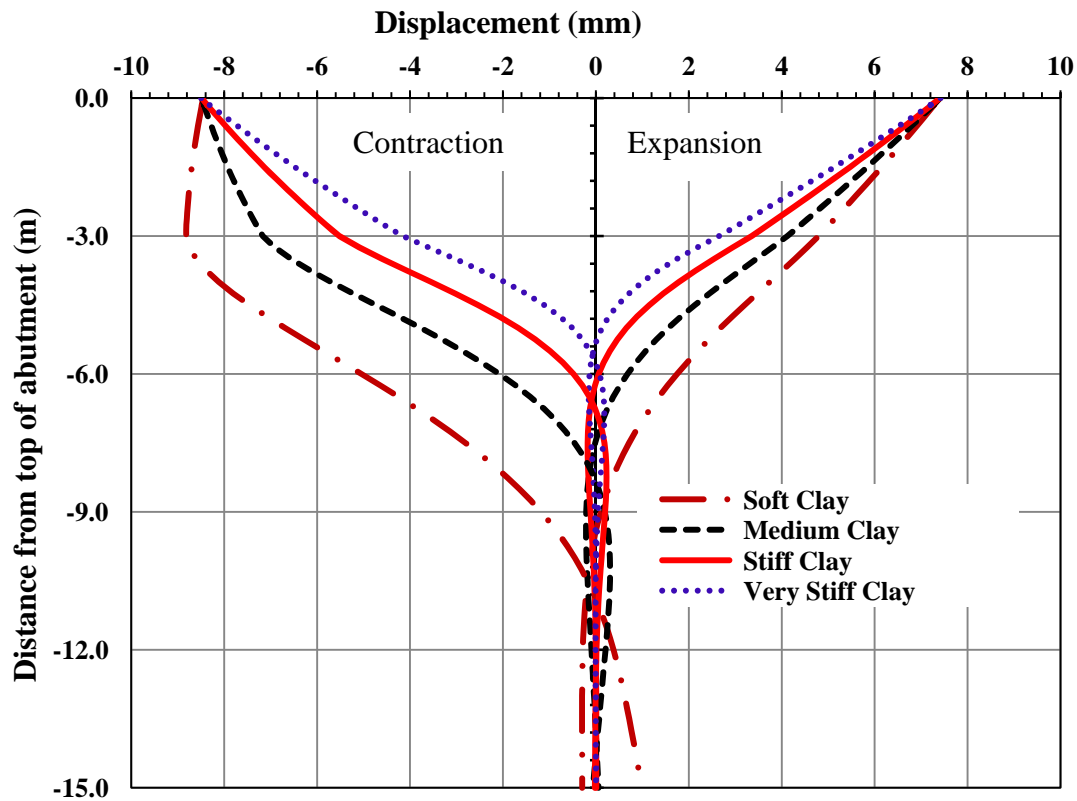


Figure 7.2 Displacement along the Abutment and the Interior Pile (38-m Bridge, Clay, 3m Abutment, HP310X125 Weak Orientation)

Figure 7.2 shows few differences in the behavior of the abutment and pile under positive (expansion) and negative (contraction) thermal changes. For similar displacement at the top of the abutment, the displacement at the top of the pile is significantly larger when the bridge is under contraction. This is due to the fact that the backfill is applying a large passive pressure on the abutment during bridge expansion. That pressure will restrict the movement of the abutment especially at the bottom of the abutment (the top of the pile). The maximum passive pressure is expected to occur at the bottom of the abutment. The second observation from figure 7.2 is the change in the displacement at the pile-abutment connection. During bridge expansion the change in abutment and pile displacement is almost constant. In the contrary, during bridge contraction there is a sudden change in the

rate of displacement change (rotation) at the pile-abutment connection zone. These observations can be seen also in figures 7.3 and 7.4.

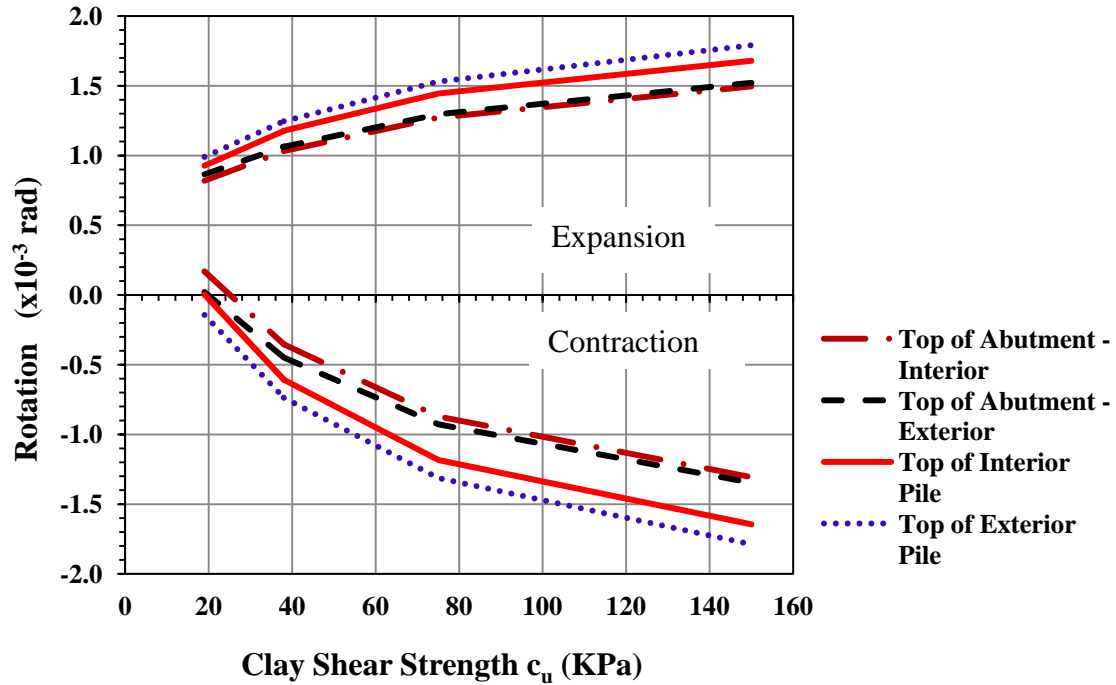


Figure 7.3 Rotation at Interior and Exterior Locations
(38-m Bridge, Clay, 3m Abutment, HP310X125 Weak Orientation)

Figure 7.3 shows the rotation (rate of displacement change) due to thermal loads at the top of the abutment and at the top of the pile for interior and exterior locations. Figure 7.4 shows the rotation due to thermal loads along the abutment and the pile at the interior location. Figure 7.4 shows that the absolute maximum rotation in the pile occurs close to the top of the pile for both the expansion and contraction cases. The distance from the top of the pile to the location of maximum rotation is inversely proportional to the stiffness of the clay. The rotation in the abutment is close to zero when the bridge is under contraction and the piles are supported by soft clay.

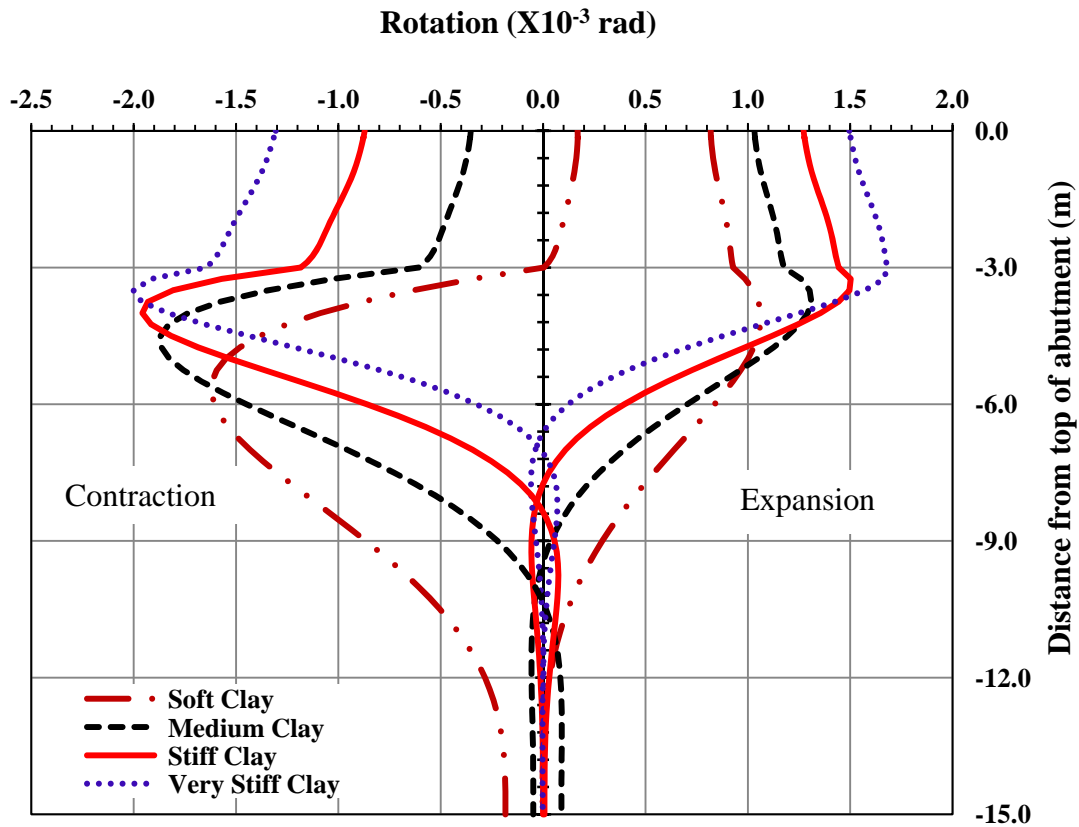


Figure 7.4 Rotation along the Abutment and the Interior Pile
(38-m Bridge, Clay, 3m Abutment, HP310X125 Weak Orientation)

Figures 7.3 and 7.4 also reveal that rigid body movement is more resembled by the abutment displacement when the bridge is under expansion. The rotation of the abutment is almost constant when the bridge is under expansion. A significant change in the rotation along the abutment is observed when the bridge is under contraction.

In general, relatively larger displacements and rotations are experienced by the piles when the bridge is under contraction and that will lead to larger moments as it will be seen in the next section.

Similar observations on the abutment behavior were observed when the bridge is supported by sand. Figure 7.5 shows the displacement due to thermal loads at the top of the abutment and the top of the pile for interior and exterior locations for the short bridge supported by sand. Figure 7.6 shows the displacement due to thermal loads along the abutment and the pile at the interior location for the short bridge supported by sand.

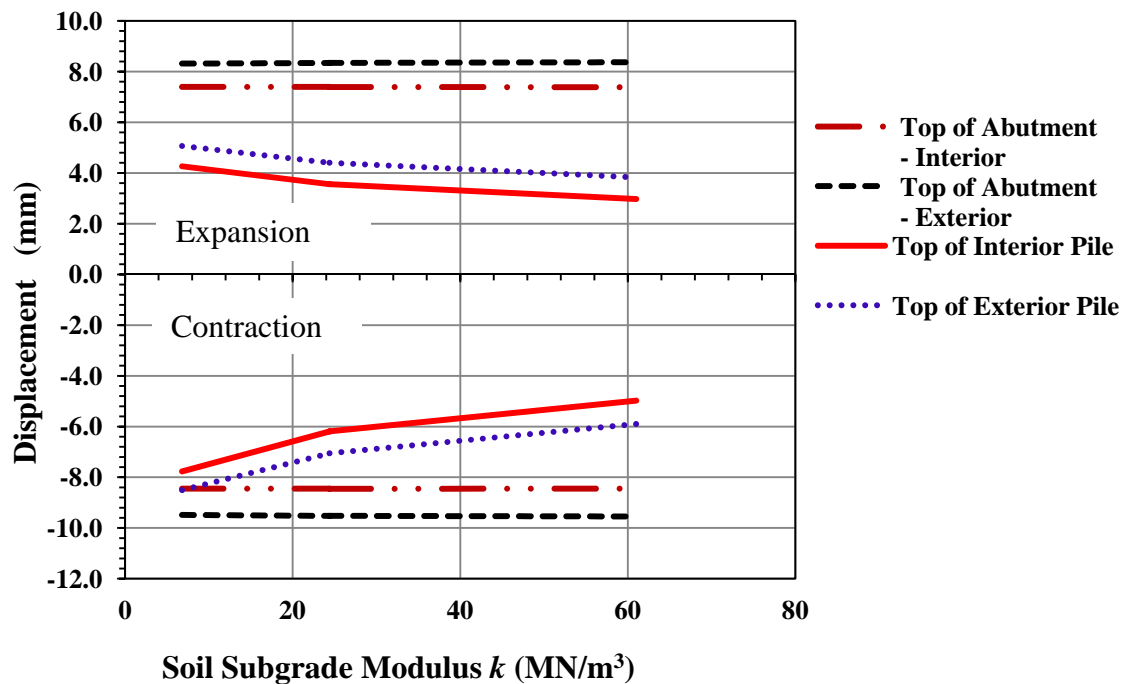


Figure 7.5 Displacement at Interior and Exterior Locations
(38-m Bridge, Sand, 3m Abutment, HP310X125 Weak Orientation)

The figures show that the displacements at the top of the abutment and at the top of the pile are very comparable in the clay and the sand cases. The similarities in the abutment behavior in the clay and sand cases can also be seen when comparing figure 7.3 with figure 7.7 which shows the rotation due to thermal loads at the top of the abutment and the top of the pile for interior and exterior locations for the short bridge in sand.

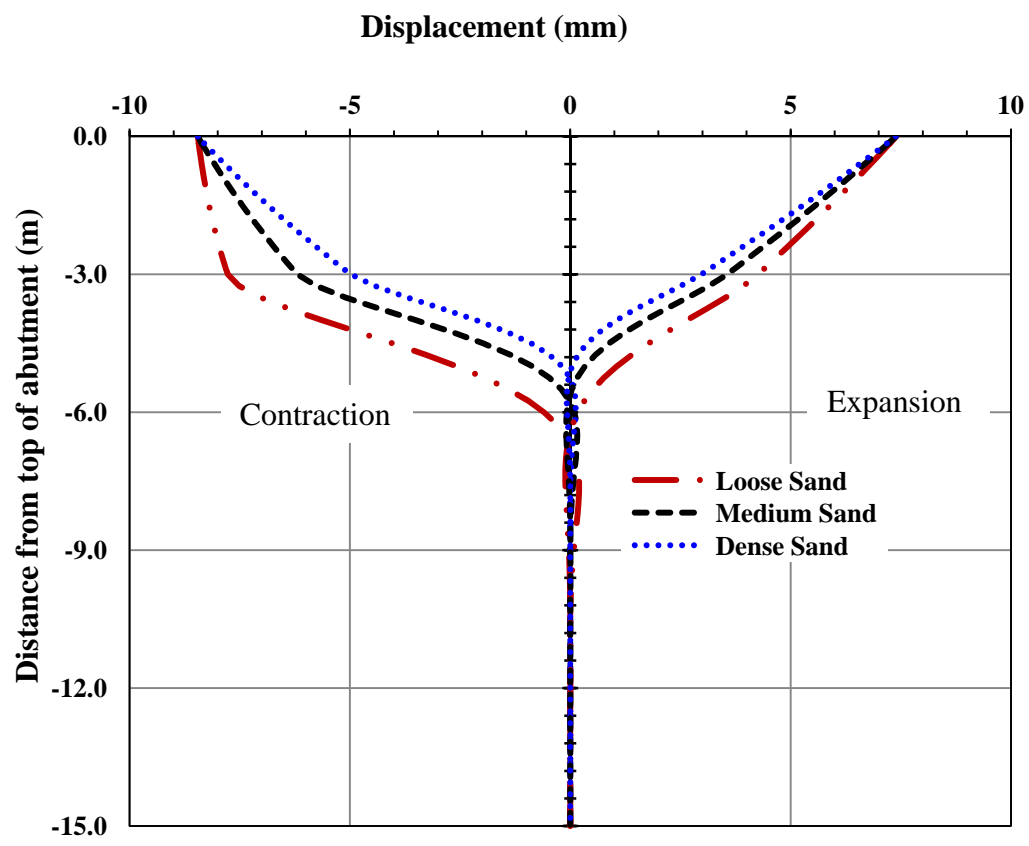


Figure 7.6 Displacement along the Abutment and the Interior Pile (38-m Bridge, Sand, 3m Abutment, HP310X125 Weak Orientation)

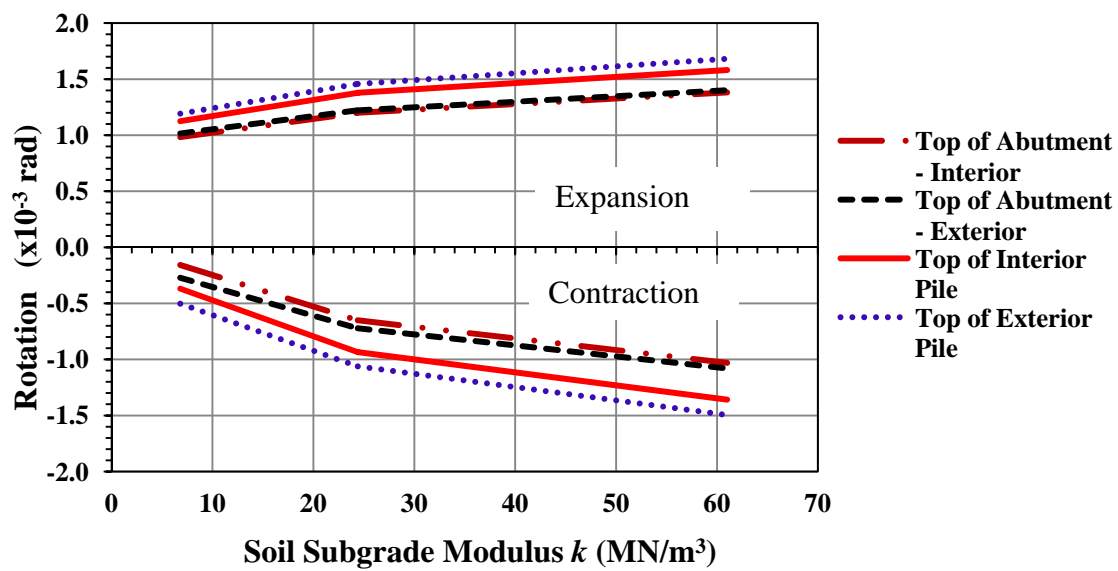


Figure 7.7 Rotation at Interior and Exterior Locations (38-m Bridge, Sand, 3m Abutment, HP310X125 Weak Orientation)

The major difference in the bridge behavior between the clay and the sand cases for the short bridge is in the displacement along the pile as shown in figure 7.6. The figure shows that the displacement along the pile decreases much faster in cohesionless soils compared to cohesive soils. This is due to the increase of soil stiffness with depth including soft sand.

That fast rate of change in the displacement is obvious when comparing figure 7.4 to figure 7.8 which shows the rotation due to thermal loads along the abutment and the pile at the interior location for the short bridge supported by sand.

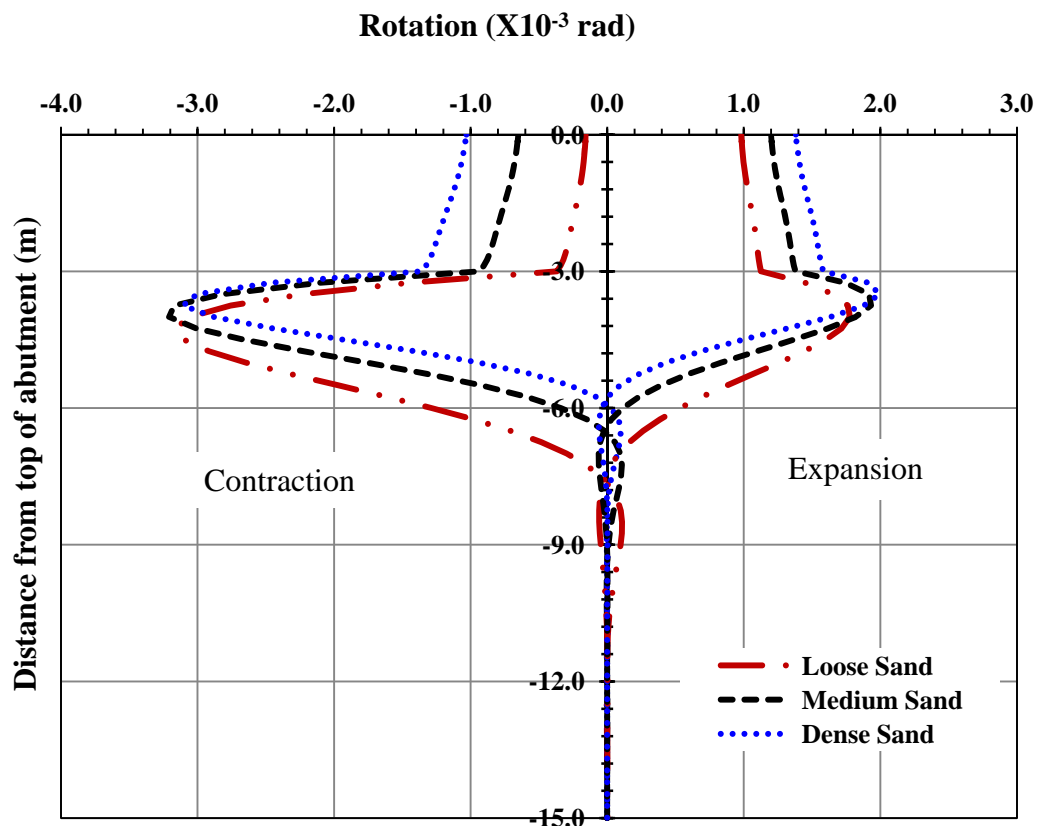


Figure 7.8 Rotation along the Abutment and the Interior Pile
(38-m Bridge, Sand, 3m Abutment, HP310X125 Weak Orientation)

The location of the absolute maximum rotation along the pile occurs at a distance close to the top of the pile. The distance from the top of the pile to the location of the absolute maximum rotation is almost the same for all types of sandy soil. This is different than the clay case where the distance from the top of the pile to the location of the absolute maximum rotation varies considerably with the variation in soil stiffness.

Similar observations were also observed on the effect of soil stiffness on the displacement and the rotation of the abutment and the piles in the long bridge. Figure 7.9 shows the displacement due to thermal loads at the top of the abutment and the top of the pile for interior and exterior locations for the long bridge supported by clay.

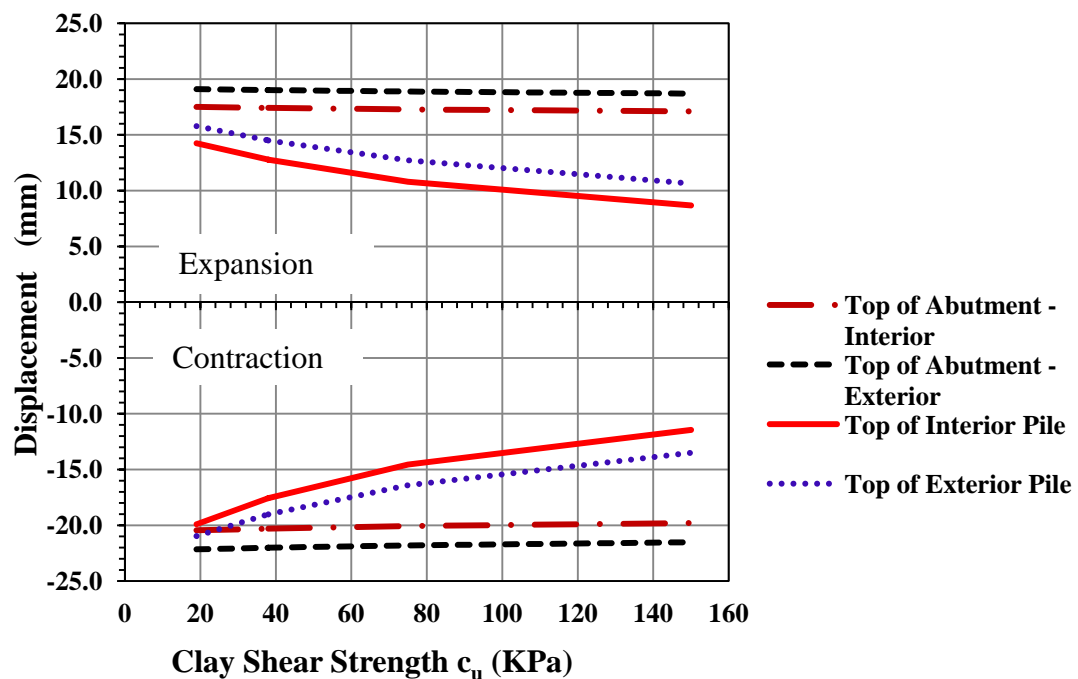


Figure 7.9 Displacement at Interior and Exterior Locations
(90-m Bridge, Clay, 3m Abutment, HP360X152 Weak Orientation)

The thermal displacement demands ($\Delta L = \alpha \Delta T L / 2$) for the 90-m bridge during expansion and contraction are 19.8 mm (0.78 in) and 22.3 mm (0.88 in) respectively. Figure 7.9 shows that the exterior displacement at the top of the abutment during bridge expansion and contraction is close to the bridge thermal displacement demand. The figure also shows that the interior displacement at the top of the abutment during bridge expansion and contraction is less than the bridge thermal displacement demand. The figure also shows that similar to the short bridge, the displacement of the abutment and the pile is more sensitive to the stiffness of the soil during bridge contraction.

The displacement due to thermal loads along the abutment and the pile at the interior location of the long bridge is shown in figure 7.10.

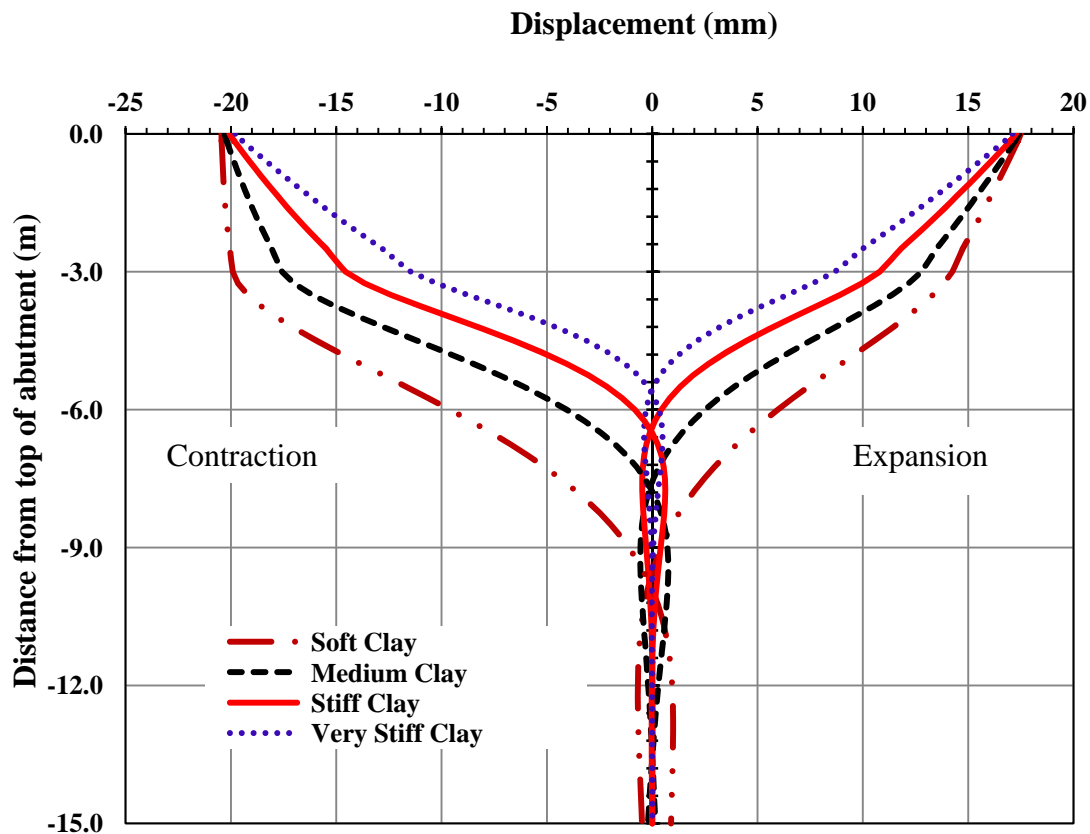


Figure 7.10 Displacement along the Abutment and the Interior Pile (90-m Bridge, Clay, 3m Abutment, HP360X152 Weak Orientation)

Figure 7.11 shows the rotation due to thermal loads at the top of the abutment and the top of the pile for interior and exterior locations and figure 7.12 shows the rotation due to thermal loads along the abutment and the pile at the interior location. Figure 7.11 shows that the rotations at the top of the abutment and at the top of the pile are almost equal. Figure 7.12 shows that the change in the rotation along the abutment is relatively small and the movement of the abutment is close to rigid body movement especially when the bridge is under expansion.

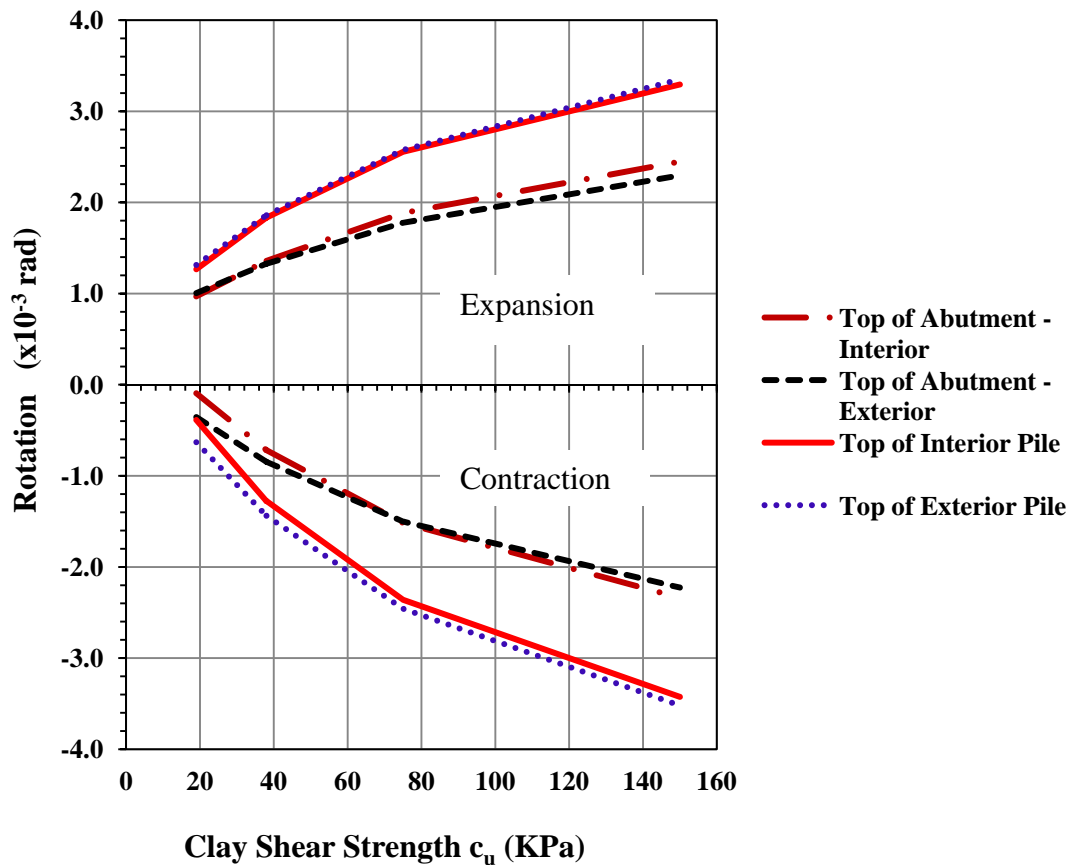


Figure 7.11 Rotation at Interior and Exterior Locations
(90-m Bridge, Clay, 3m Abutment, HP360X152 Weak Orientation)

One distinct difference between the abutment behavior in the short and in the long bridge is in the rate of change in the abutment rotation just below the superstructure. This observation is more obvious when the piles are supported by stiff and very stiff clay as shown inside the dashed rectangle in figure 7.12

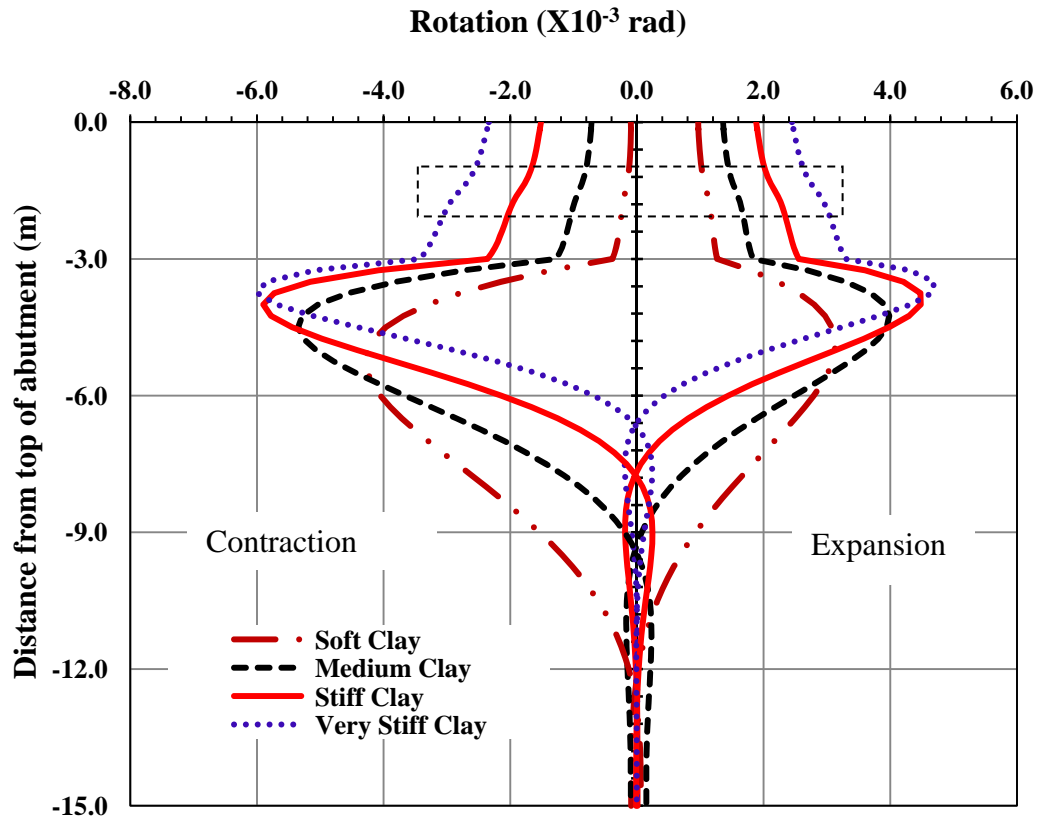


Figure 7.12 Rotation along the Abutment and the Interior Pile (90-m Bridge, Clay, 3m Abutment, HP360X152 Weak Orientation)

Similar observations were observed on the displacement and the rotation of the abutment and the piles for the long bridge built on sand as can be seen in figures 7.13 through 7.16. For additional figures showing the effect of soil stiffness on the displacement and rotation along the abutment and the piles, see figures A.1 to A.16 in appendix A.

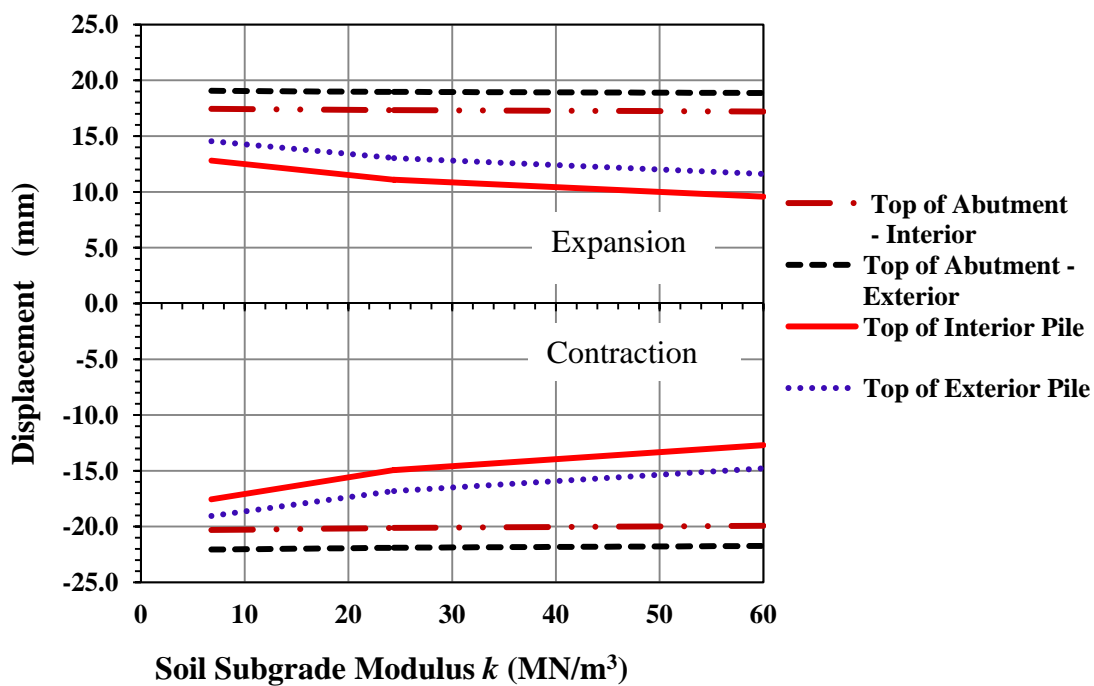


Figure 7.13 Displacement at Interior and Exterior Locations
(90-m Bridge, Sand, 3m Abutment, HP360X152 Weak Orientation)

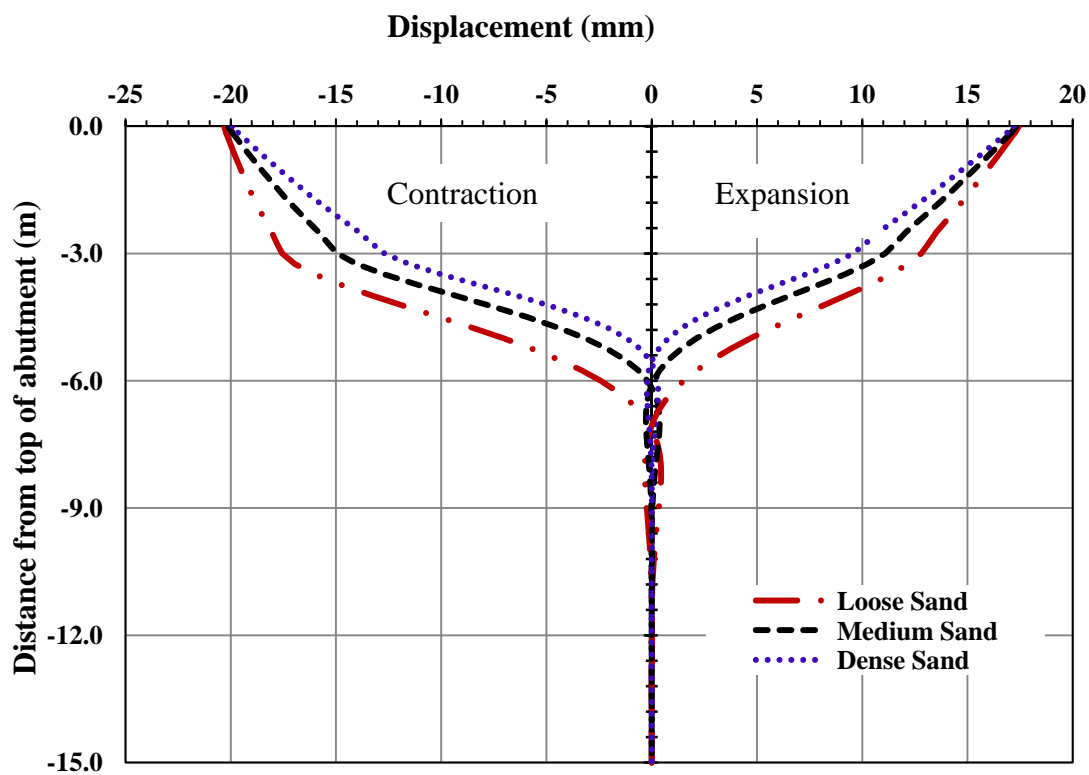


Figure 7.14 Displacement along the Abutment and the Interior Pile
(90-m Bridge, Sand, 3m Abutment, HP360X152 Weak Orientation)

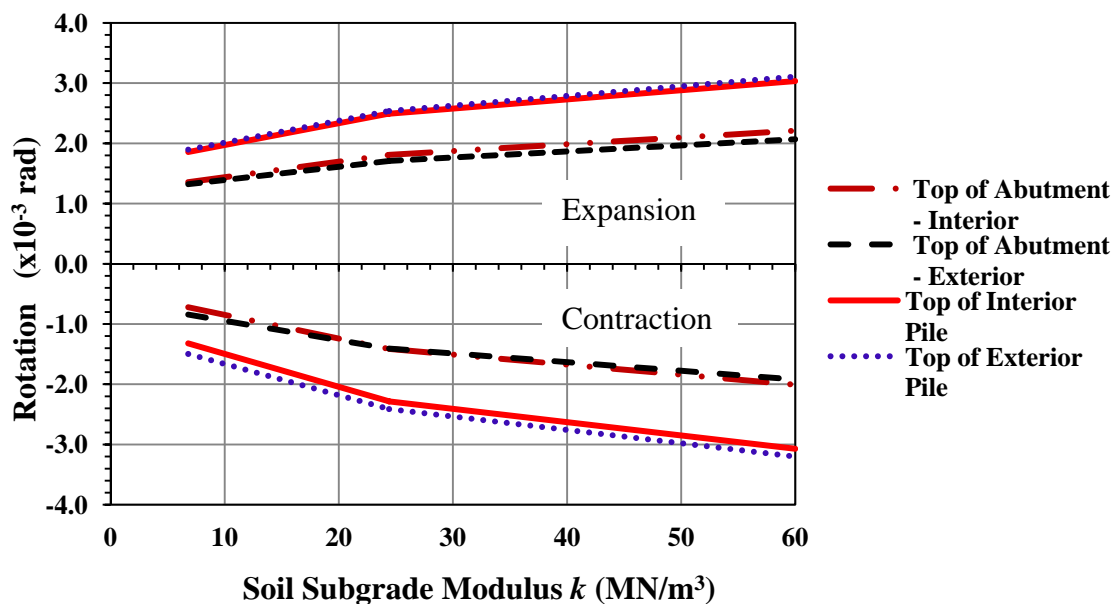


Figure 7.15 Rotation at Interior and Exterior Locations
(90-m Bridge, Sand, 3m Abutment, HP360X152 Weak Orientation)

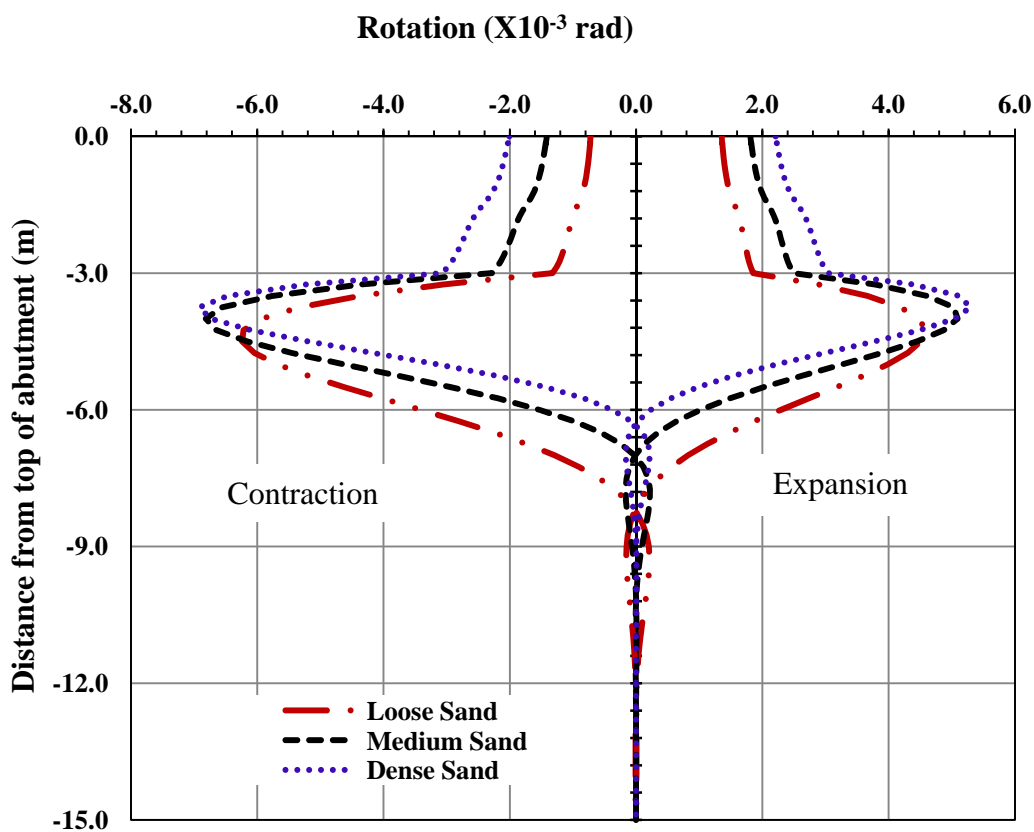


Figure 7.16 Rotation along the Abutment and the Interior pile
(90-m Bridge, Sand, 3m Abutment, HP360X1152 Weak Orientation)

7.2.2 Effect of Soil Stiffness on the Moment along the Piles

The study showed that the stiffness of the clay has a major effect on the moment along the piles and consequently the stresses due to thermal loads experienced by the piles. That effect is shown clearly in figure 7.17 which shows the moment at the top of the interior and exterior piles for the short bridge built on clay.

Figure 7.17 which shows a significant increase in the moment at the top of the pile when the shear strength of the clay increases from soft clay ($c_u = 19$ KPa) to medium clay ($c_u = 38$ KPa). This increase is more than 65% in the interior pile and more than 75% in the exterior pile. The increase in the moment at the top of the pile continues with the increase in soil stiffness but with a smaller rate for both the interior and exterior piles. The change in the moment is negligible when the stiffness of the clay increases from stiff clay ($c_u = 75$ KPa) to very stiff clay ($c_u = 150$ KPa) for both the interior and exterior piles.

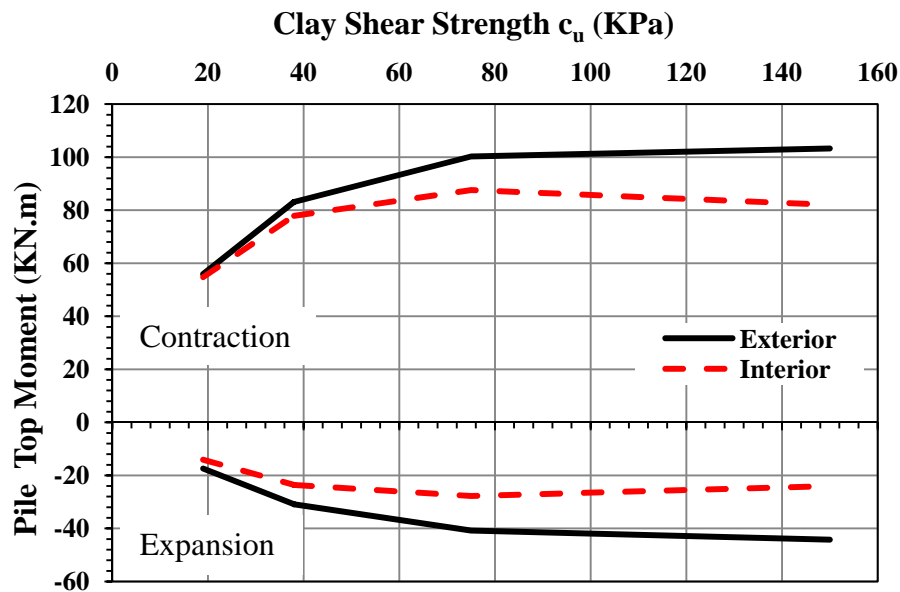


Figure 7.17 Moment at the Top of the Pile
(38-m Bridge, Clay, 3m Abutment, HP310X125 Weak Orientation)

Similar observations were noticed from the piles' behavior in the long bridge. Figure 7.18 shows the moment at the top of the interior and the exterior piles for the long bridge in clay. The figure shows that the moment at the top of the pile increases sharply when the stiffness of the clay increases from soft clay to medium clay in both the interior and the exterior piles. The moment at the top of piles continues to increase with the increase in soil stiffness but with a smaller rate. The difference in the value of the moment at the top of the interior and the exterior piles increases with the increase in soil stiffness. For the contraction case, the moments at the top of the pile for the stiff clay and very stiff clay cases are larger than the yield moment of the pile. The piles in the models were assumed to behave in a linear fashion for all cases for illustration purposes.

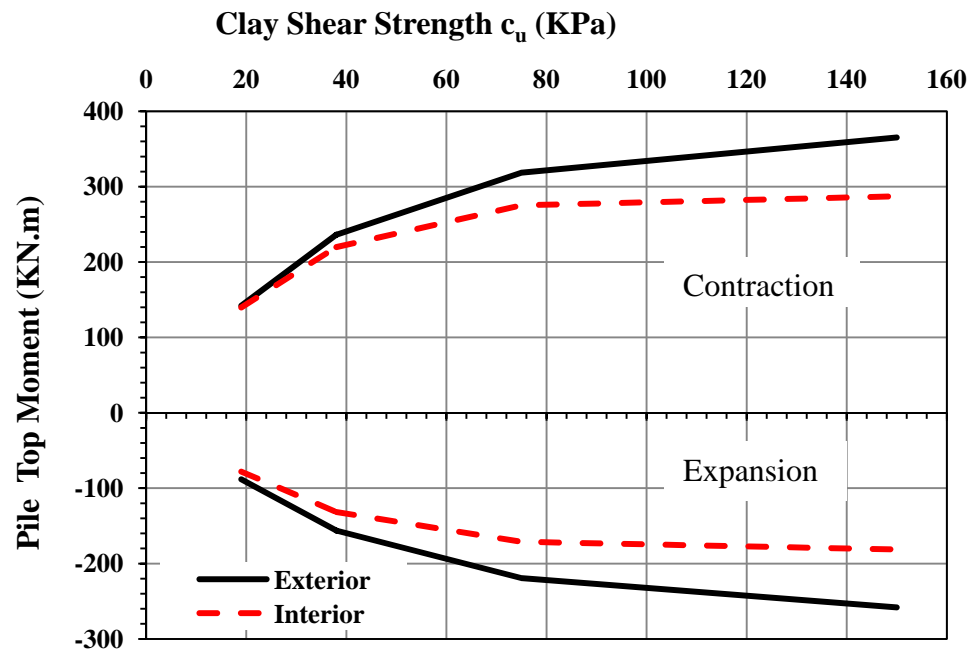


Figure 7.18 Moment at the top of the Pile
(90-m Bridge, Clay, 3m Abutment, HP360X152 Weak Orientation)

Figure 7.19 shows the moment along the interior pile for the short bridge in clay. The figure shows that the absolute maximum moment along the pile occurs at the top of the pile. According to the sign convention used in the research, the moment at the top of the pile is usually negative when the pile is under contraction and positive when the bridge is under expansion. The figure also shows that the moment at the top of the pile is considerably larger when the bridge is under contraction. The figure also shows that a second maximum (reversed) moment occur at a distance below the top of the pile. The magnitude of the reversed moment is considerably smaller than the moment at the top of the pile when the bridge is under contraction.

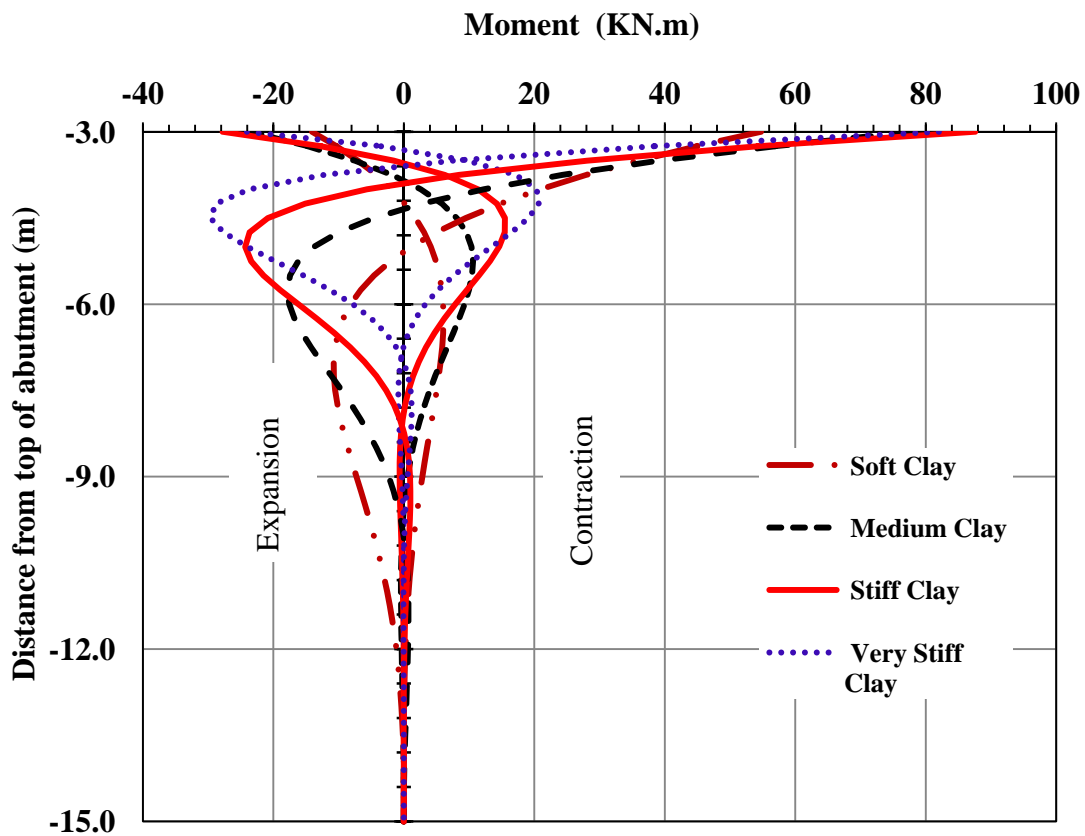


Figure 7.19 Moment Loads along the Interior Pile
(38-m Bridge, Clay, 3m Abutment, HP310X125 Weak Orientation)

The magnitude of the reversed moment is comparable to the moment at the top of the pile when the bridge is under expansion. Unlike the moment at the top of the pile, the increase in the second maximum moment continues in stiff and very stiff clays. The distance from the location of the reversed moment to the top of the pile decreases with the increase in the stiffness of the clay in both the expansion and the contraction cases.

Similar observations were observed in the long bridge. Figure 7.20 shows the moment along the interior pile for the long bridge in clay.

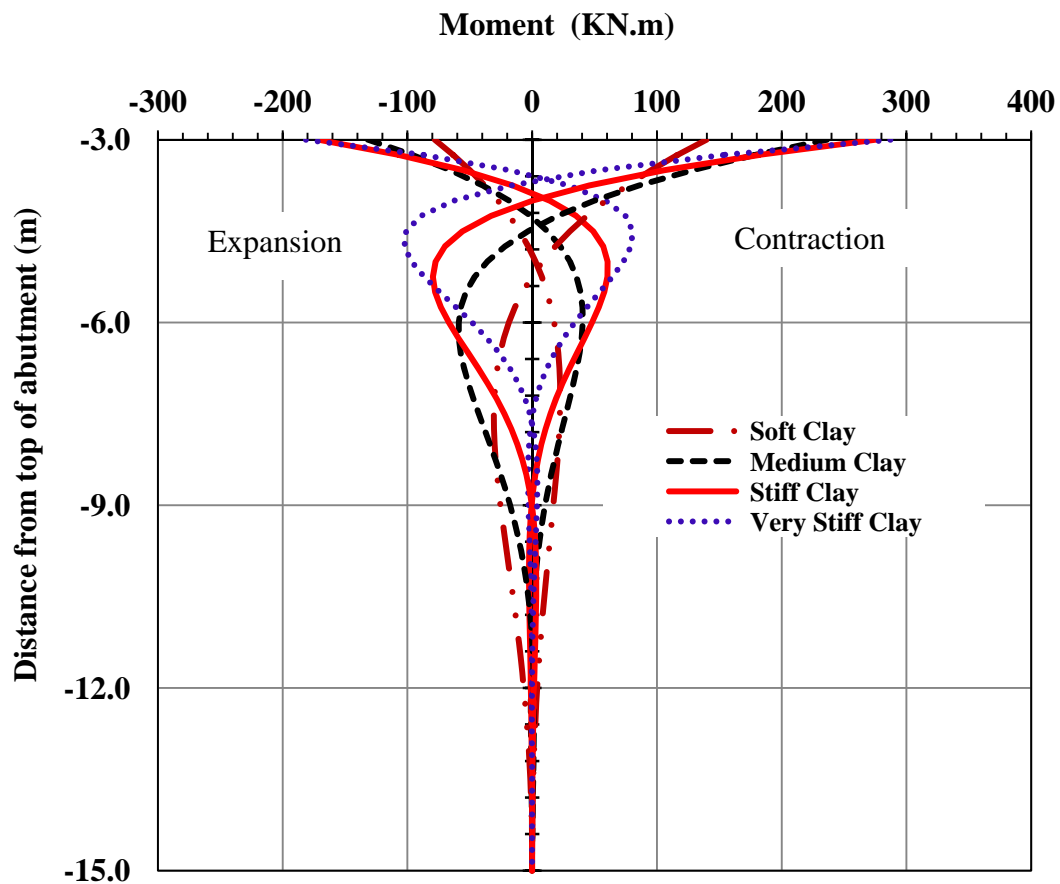


Figure 7.20 Moment along the Interior Pile
(90-m Bridge, Clay, 3m Abutment, HP360X152 Weak Orientation)

In the long bridge and during bridge expansion, the magnitude of the reversed moment is comparable to the magnitude of moment at the top of the pile in soft and medium clay and it is larger than the magnitude of the moment at the top of the pile in stiff and very stiff clays. The magnitude of the moment at the top of the pile is still considerably larger than the magnitude of the reversed moment during bridge contraction especially for soft clay where the ratio of the two moments is about 3.

The distribution of the moment along the pile in the short bridge supported by sand is similar to the clay case as shown in figures 7.21 and 7.22.

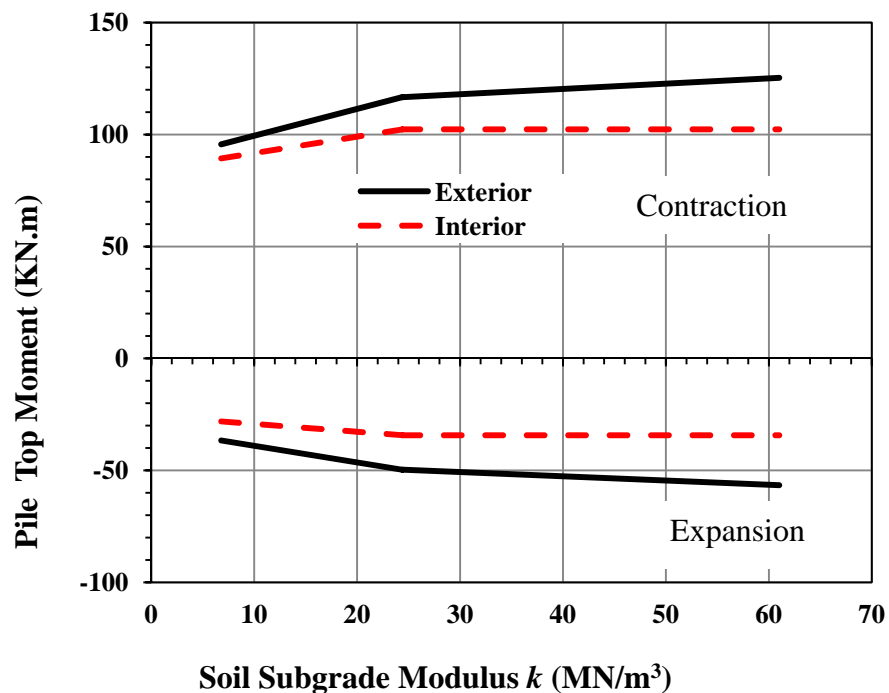


Figure 7.21 Moment at the Top of the Pile
(38-m Bridge, Sand, 3m Abutment, HP310X125 Weak Orientation)

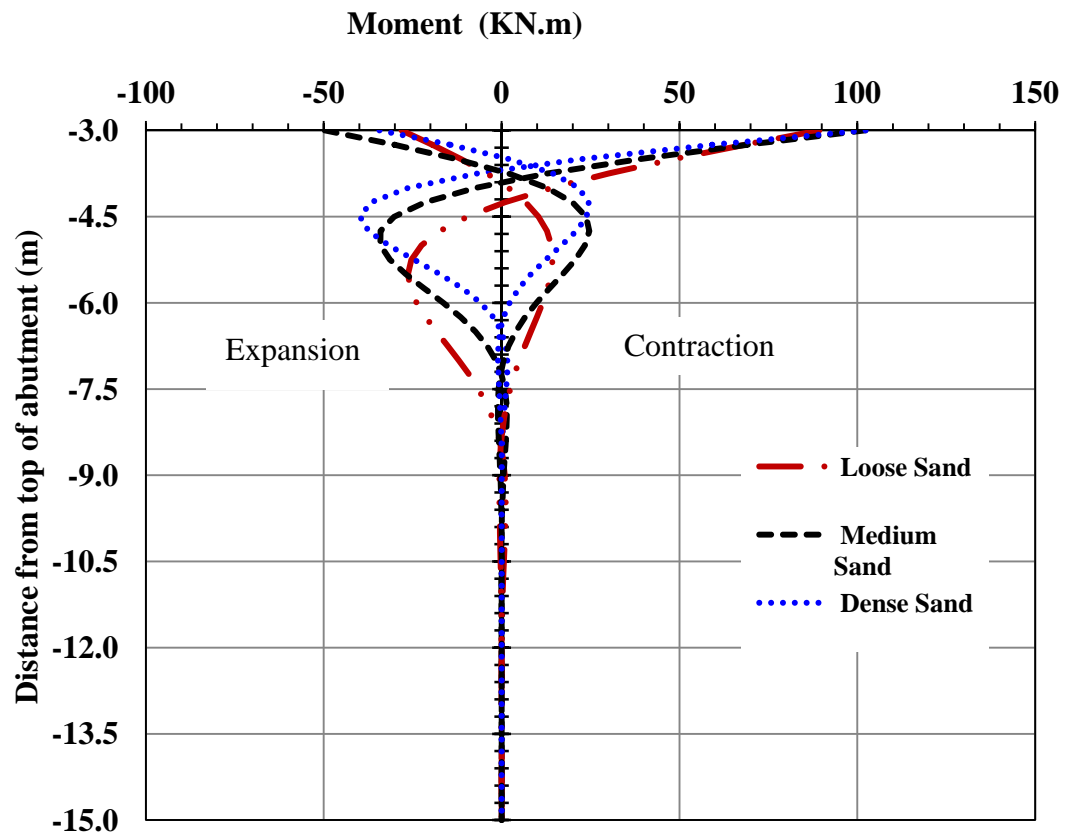


Figure 7.22 Moment along the Interior Pile
(38-m Bridge, Sand, 3m Abutment, HP310X125 Weak Orientation)

The moment distribution along the piles in the long bridge in sand is similar to the clay case as shown in figures 7.23 and 7.24. The magnitude of the moment at the top of the interior and exterior piles increases with any increase in the soil stiffness (sand subgrade modulus). For the contraction case, the moments at the top of the pile for the medium dense and dense sand cases are larger than the yield moment of the pile. The piles in the models were assumed to behave in a linear fashion for all cases for illustration purposes.

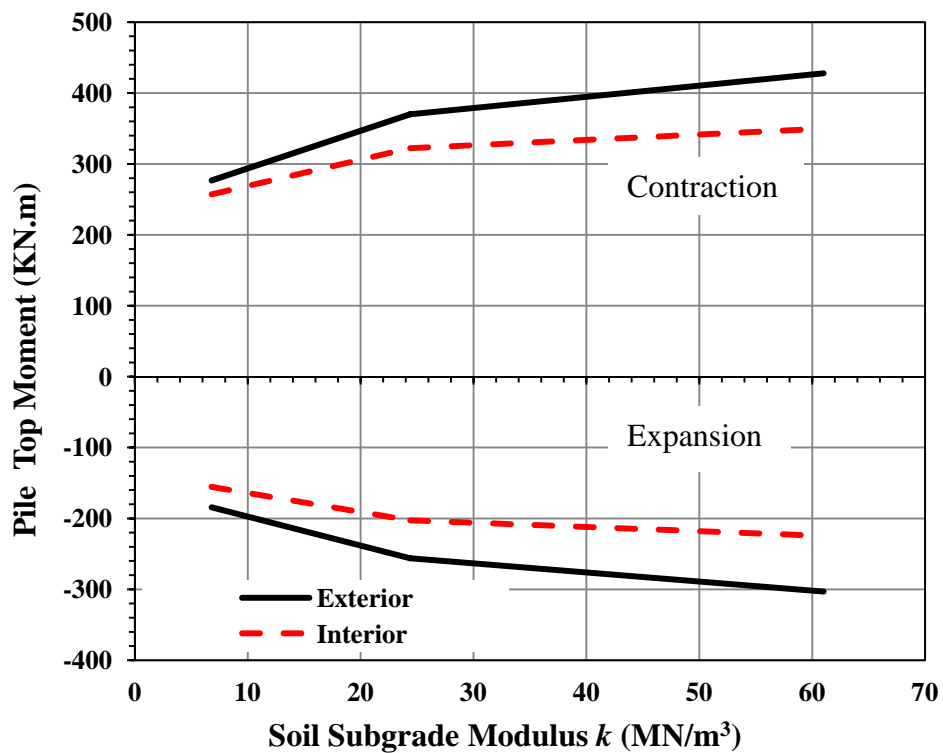


Figure 7.23 Moment at the Top of the Pile
(90-m Bridge, Clay, 3m Abutment, HP360X152 Weak Orientation)

Figure 7.24 shows that the magnitude of the reversed moment in the interior and the exterior piles continues to increase with any increase in the soil stiffness. It also shows that the magnitude of the reversed moment is higher than the magnitude of the moment at the top of pile for any soil stiffness when the bridge is under expansion. In the contraction case, the magnitude of the reversed moment is less than the magnitude of the top moment for the loose sand but it becomes larger in the dense soil.

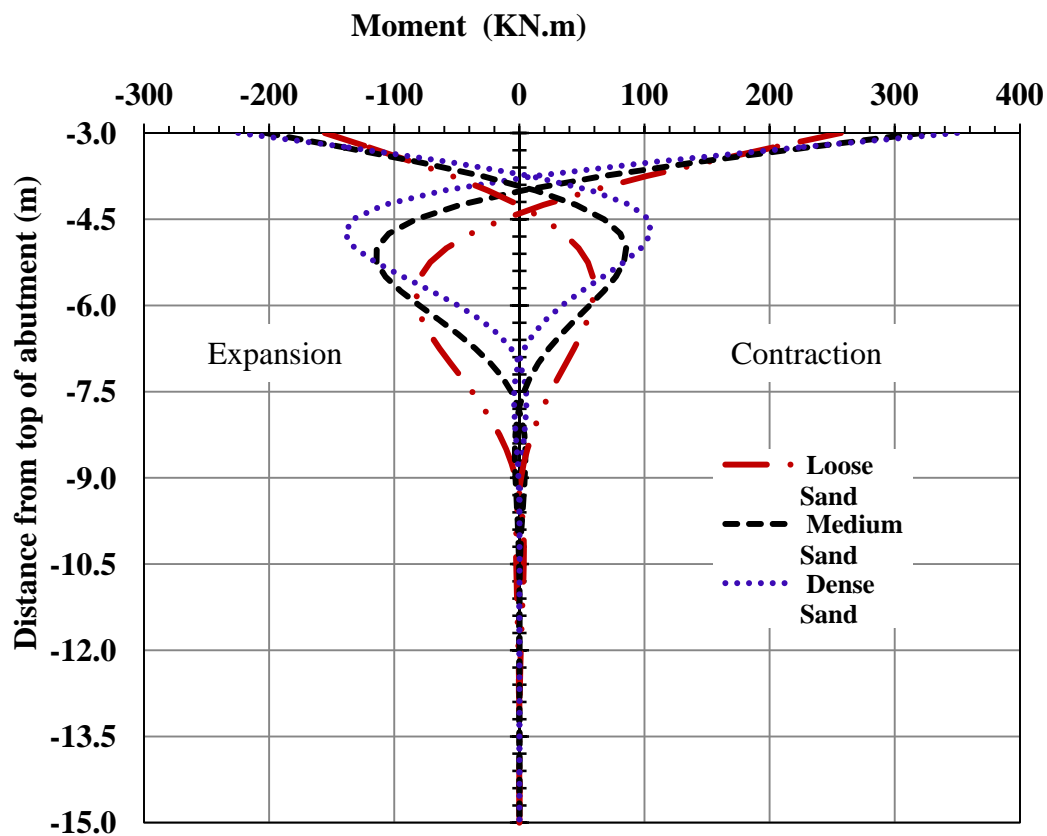


Figure 7.24 Moment along the Interior Pile
(90-m Bridge, Sand, 3m Abutment, HP360X152 Weak Orientation)

For additional figures showing the effect of soil stiffness on the moment along the piles, see figures A.17 to A.24 in appendix A.

7.2.3 Effect of Soil Stiffness on the Stresses in the Girders

The study showed that the stiffness of the soil has a major effect on the stress levels in the girders. That effect can be seen clearly in figure 7.25 which shows the relationship between the stresses in the girders and the stiffness of the clay for the short bridge in clay. The figure shows that the magnitude of the compression stresses (negative) due to thermal loads in the interior and the exterior girders during bridge expansion are much larger than the tension stresses (positive) due to thermal loads in the interior and the exterior girders during bridge contraction in soft clay. The figure also shows significant increase in the stress levels in the interior and the exterior girders with the increase in soil stiffness for both the expansion and the contraction with a slightly higher stress sensitivity to soil stiffness in the contraction case (tension stresses).

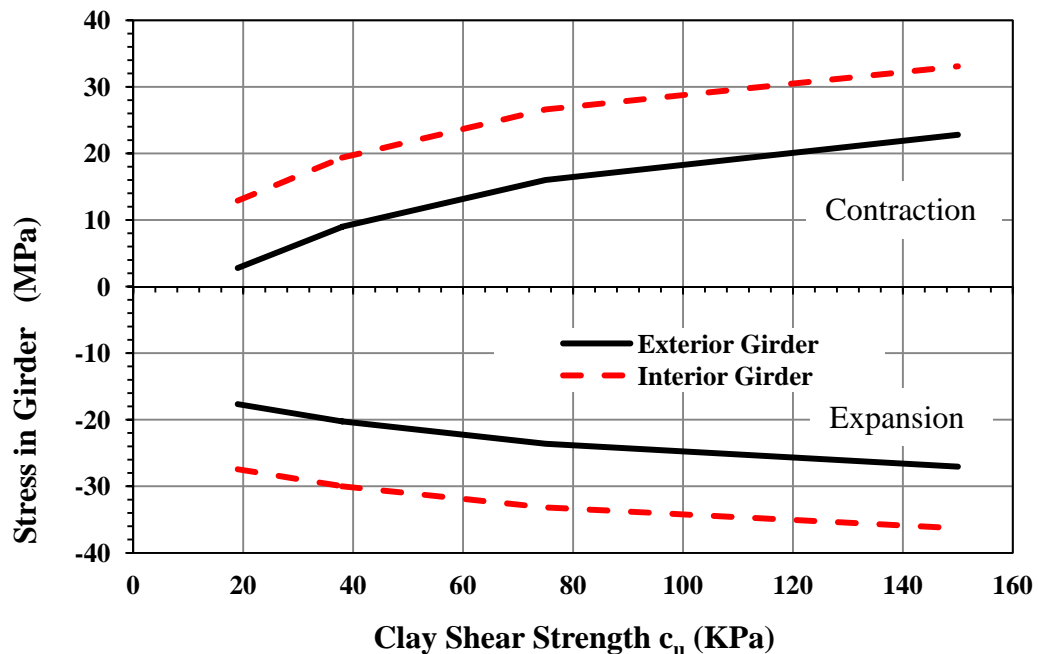


Figure 7.25 Stresses in the Girders
(38-m Bridge, Clay, 3m Abutment, HP310X125 Weak Orientation)

For example, during bridge contraction the stress in the exterior girder increases by about 300% when the soil stiffness increases from soft clay to stiff clay. This percentage increase is more than 500% in the interior girder for the same change in soil stiffness.

The figure also shows that when the wingwall is not rigidly attached to the abutment, the stresses in the interior girders are considerably larger than the stresses in the exterior girders. The magnitude of the difference in the stresses between the exterior and the interior girder is almost constant regardless of the stiffness of the soil for both the expansion and the contraction cases.

Similar observations were noticed when the short bridge is supported by sand as shown in figure 7.26.

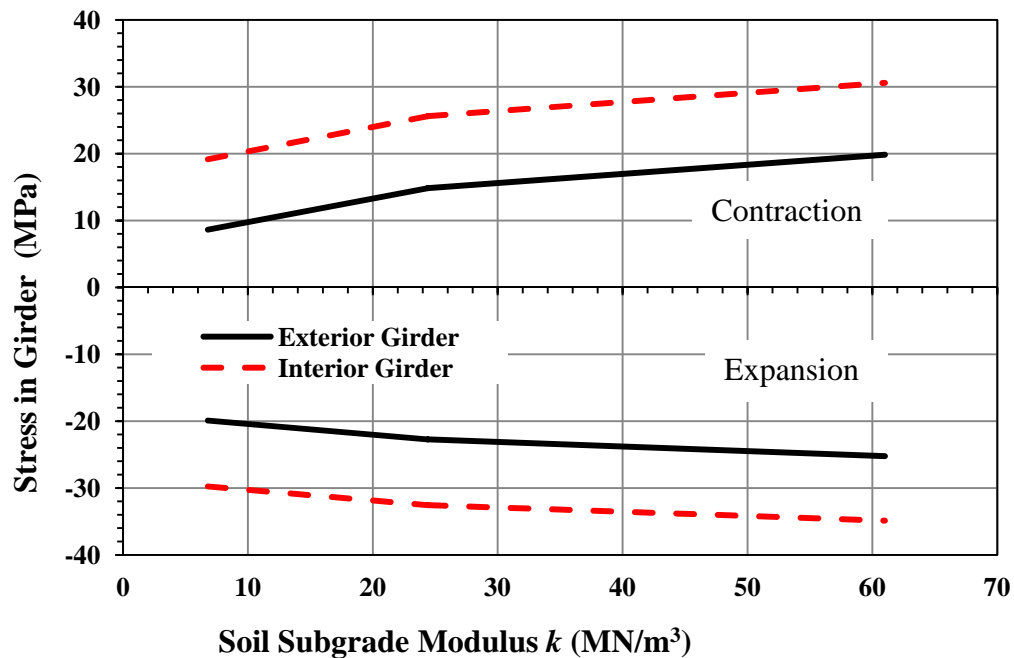


Figure 7.26 Stresses in the Girders
(38-m Bridge, Sand, 3m Abutment, HP310X125 Weak Orientation)

Similar observations with some differences were observed in the behavior of the long bridge during bridge expansion and bridge contraction as shown in figures 7.27 and 7.28 which show the clay and the sand cases respectively.

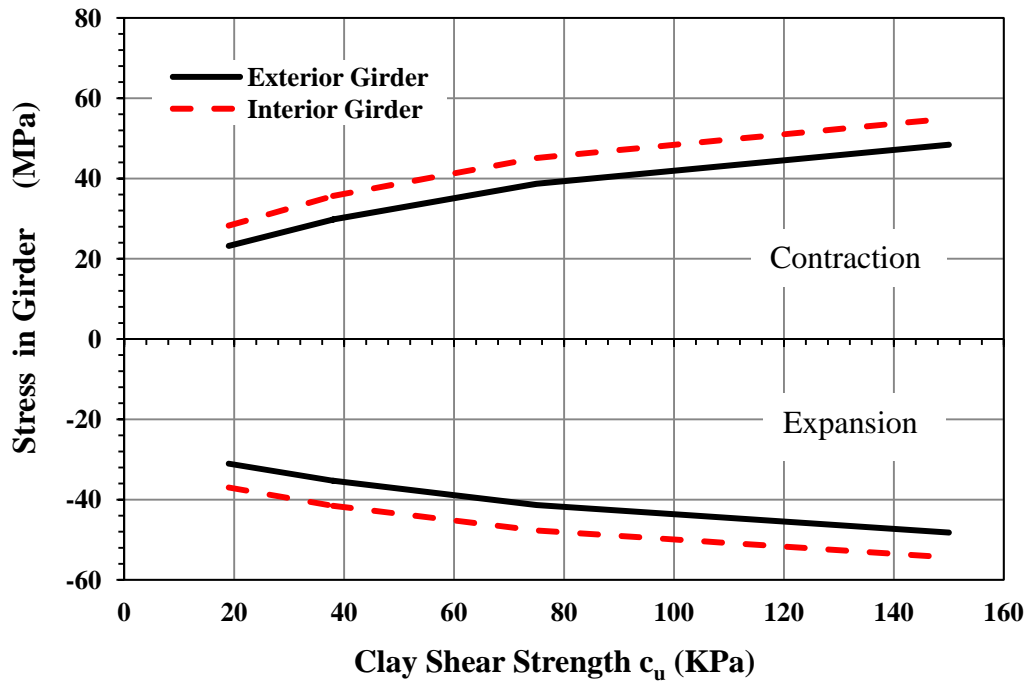


Figure 7.27 Stresses in the Girders
(90-m Bridge, Clay, 3m Abutment, HP360X152 Weak Orientation)

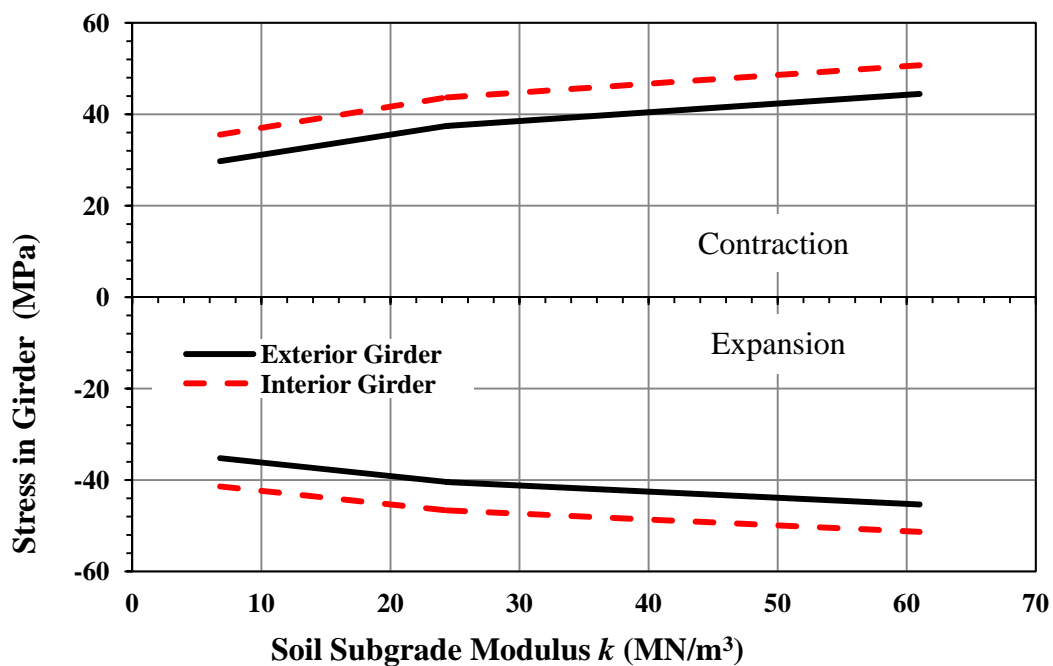


Figure 7.28 Stresses in the Girders
(90-m Bridge, Sand, 3m Abutment, HP360X152 Weak Orientation)

For additional figures showing the effect of soil stiffness on the stresses in the girders, see figures A.25 to A.28 in appendix A.

7.2.4 Effect of Soil Stiffness on the Backfill Pressure on the Abutment

The study showed that the stiffness of the soil has a modest effect on the backfill pressure on the abutment. This effect is shown in figures 7.29 and 7.30 which show the backfill pressure on the abutment for the short bridge built on clay and sand respectively during bridge expansion. The figures show that the sensitivity of backfill pressure to soil stiffness is negligible at the upper third of the abutment and maximum at the bottom of the abutment. The figures show a close to linear relationship between the increase in the backfill pressure and the depth from the top of the abutment especially for soft clay and loose sand.

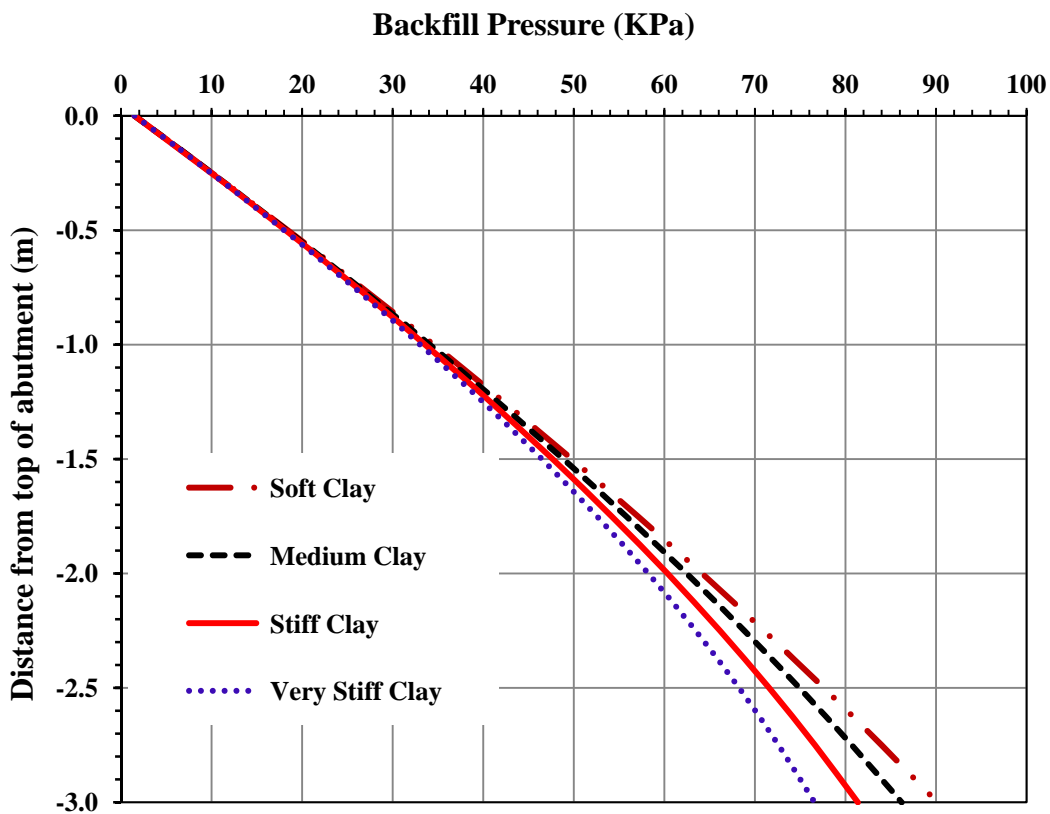


Figure 7.29 Backfill Pressure on the Abutment
(38-m Bridge, Clay, 3m Abutment, HP310X125 Weak Orientation)

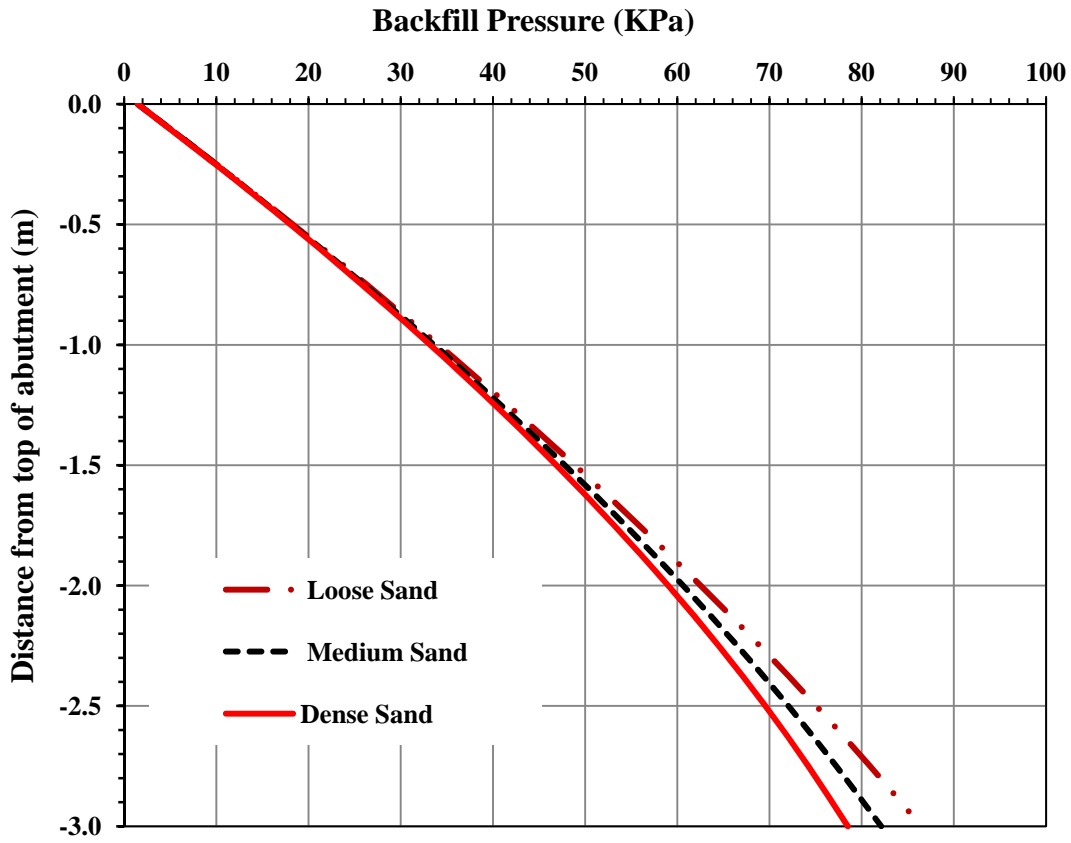


Figure 7.30 Backfill Pressure on the Abutment
(38-m Bridge, Sand, 3m Abutment, HP310X125 Weak Orientation)

The stiffness of the soil has a slightly larger effect on the backfill pressure magnitude and distribution in the long bridge as shown in figures 7.31 and 7.32 which show the backfill pressure on the abutment for the long bridge built on clay and sand respectively during bridge expansion. The figures also show that the distribution of the backfill pressure is close to triangular distribution at the upper half of the abutment. The distribution changes to a parabolic distribution close to the bottom of the abutment especially in stiff soils for both clay and sand cases. Figure 7.31 shows that the pressure at the bottom of the abutment decreased by 25% when the soil pressure increased from soft clay to stiff clay.

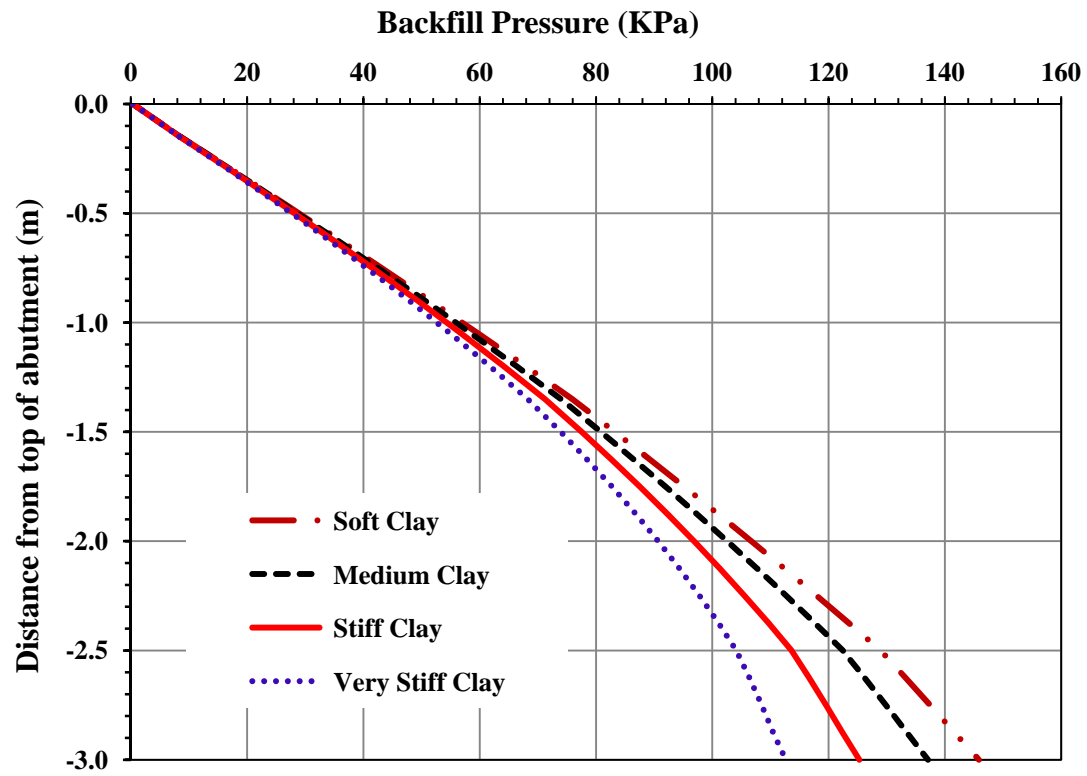


Figure 7.31 Backfill Pressure on the Abutment
(90-m Bridge, Clay, 3m Abutment, HP360X152 Weak Orientation)

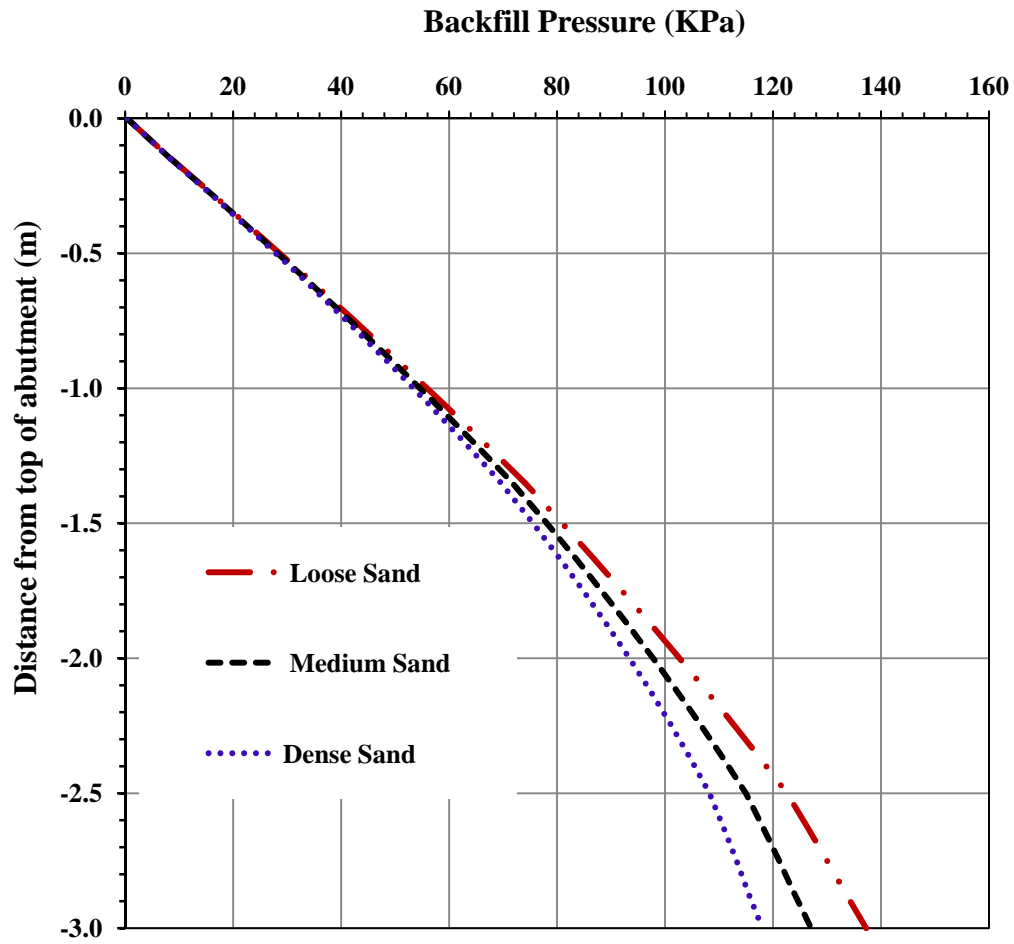


Figure 7.32 Backfill Pressure on the Abutment
(90-m Bridge, Sand, 3m Abutment, HP360X152 Weak Orientation)

7.3 EFFECT OF PILE ENCLOSURE

The study showed that using pile enclosure around the top part of the pile has a significant effect on the performance of IABs. The displacement and rotation along the abutment and along the piles are sensitive to the length of the enclosure. The stresses in the girders and the backfill pressure are also sensitive to the length of the enclosure. The effect of using pile enclosure on the performance of IABs is presented in the following subsections. 0 m, 2 m, 3 m, and 4 m long pile enclosures were considered in the study.

7.3.1 Effect of Pile Enclosure on the Displacement and the Rotation of the Abutment and the Piles

Figure 7.33 shows the displacement at the top of the abutment and at the top of the pile (bottom of the abutment) at the interior location for the short bridge supported by clay during contraction. The displacements are shown for different lengths (0 m, 2 m, 3 m, and 4 m) of pile enclosure.

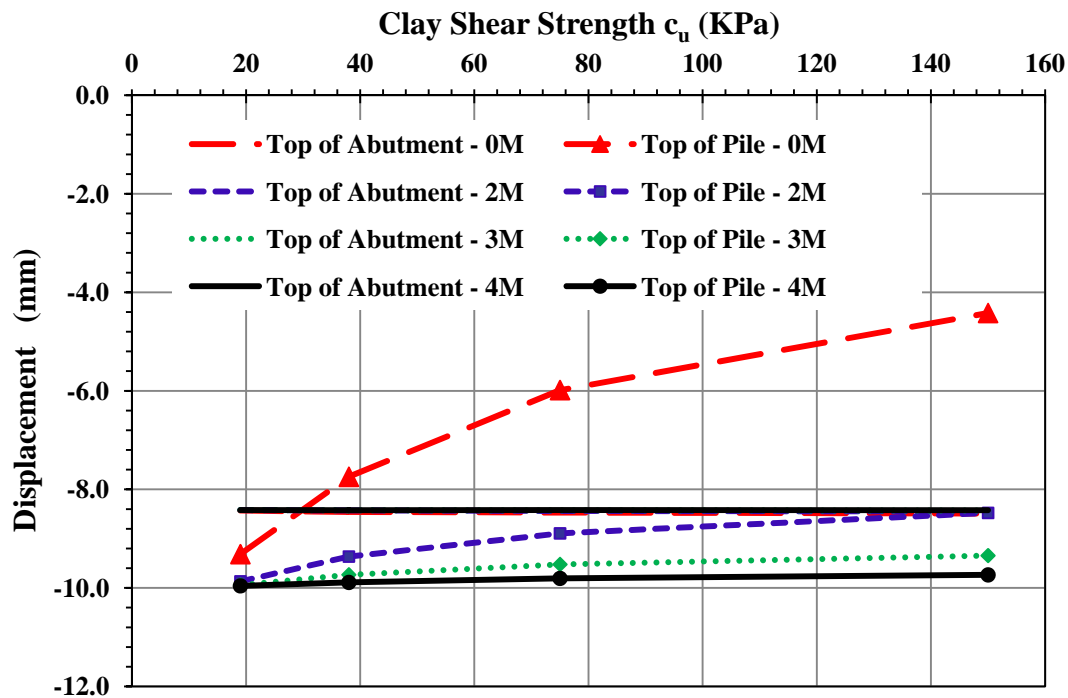


Figure 7.33 Displacement (Contraction) at the Interior Location (38-m Bridge, Clay, 3m Abutment, HP310X125 Weak Orientation with Pile Enclosure)

The figure reveals that using pile enclosure has no effect on the displacement at the top of the abutment but has a significant effect on the displacement at the top of the pile. The significance of the effect of the pile enclosure on the displacement at the top of the pile increases with the increase in soil stiffness. The figure shows that by using 2-meter pile enclosure, the displacement at the top of the pile had increased by about 6% in soft soil, 50% in stiff soil and more than 90% in very stiff soil. The displacement at the top of the pile continues to increase with longer pile enclosures. The sensitivity of the displacement at the top of the pile to soil stiffness decreases with the increase in enclosure length and it almost diminishes for a pile enclosure of 4 meters. The displacement along the abutment and the pile for 0 meter and 2 meter enclosures is show in figure 7.34.

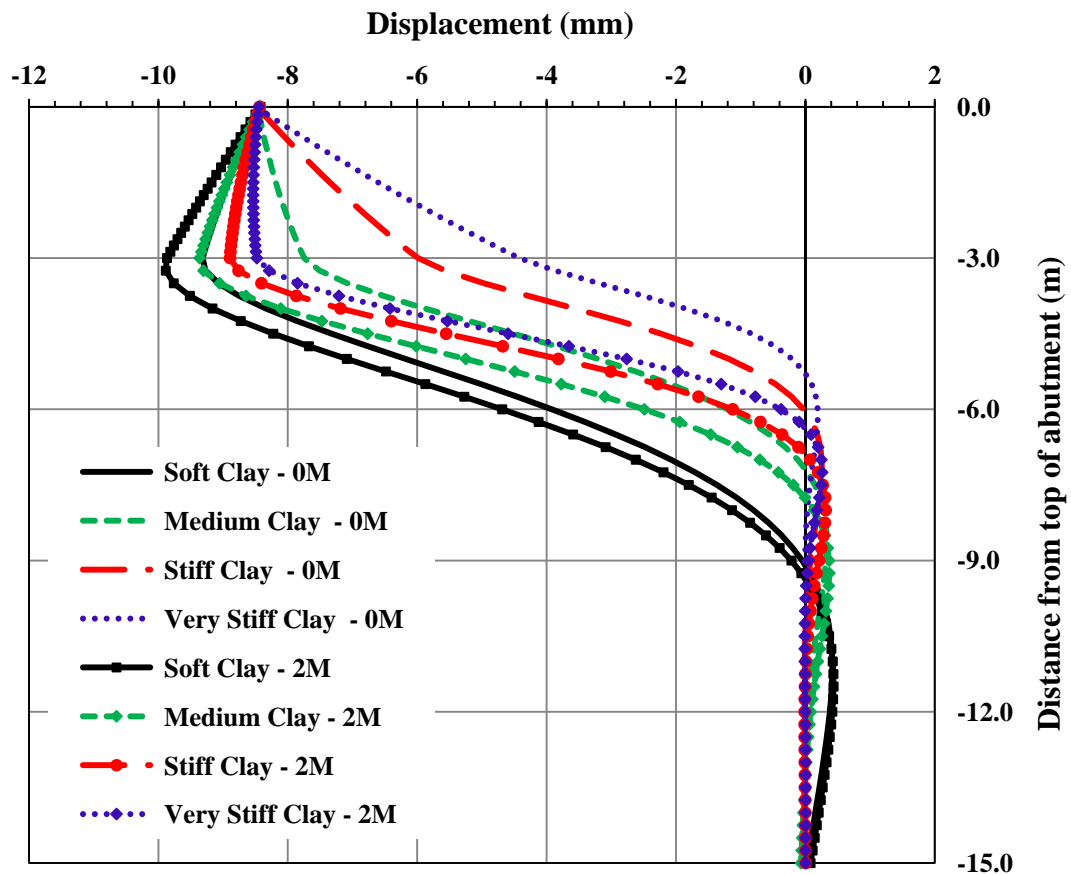


Figure 7.34 Displacement (Contraction) along the Abutment and the Interior Pile (38-m Bridge, Clay, 3m Abutment, HP310X125 Weak Orientation with Pile Enclosure)

Similar behavior was noticed during bridge expansion as shown in figure 7.35. During bridge expansion, the displacement at the top of the abutment does not change with the use of pile enclosure. The displacement at the top of the pile increases significantly with the use of 2-meter pile enclosure especially in stiff soils. Increasing the pile enclosure height to more than 2 meters has a negligible effect on the displacement at the top of the pile.

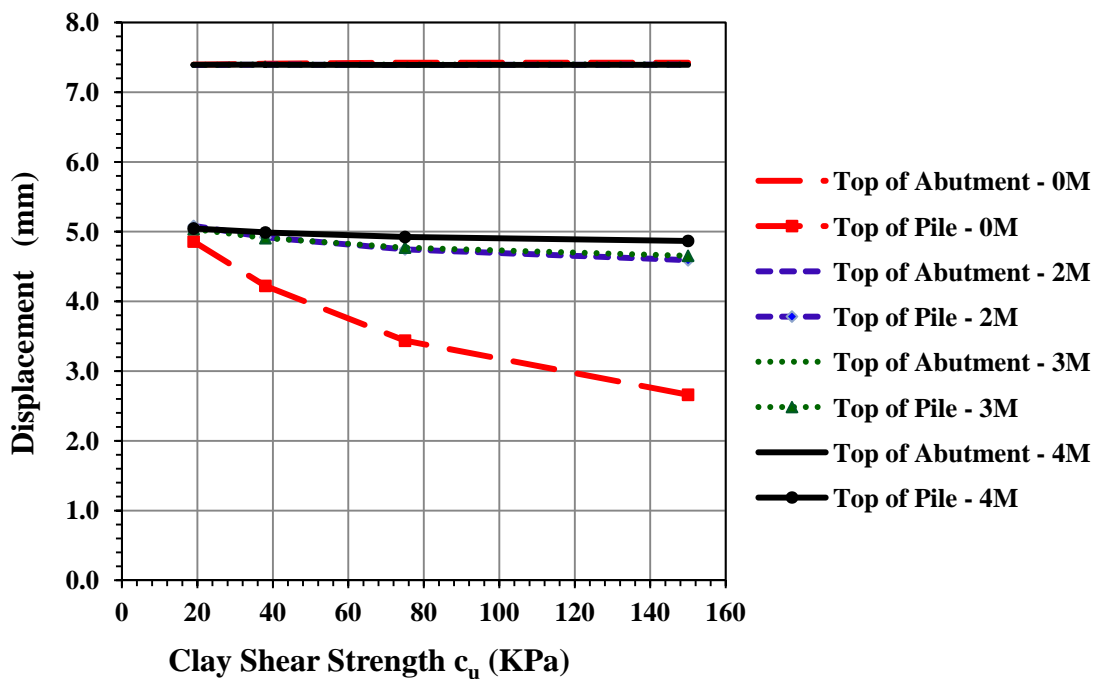


Figure 7.35 Displacement (Expansion) at the Interior Location
(38-m Bridge, Clay, 3m Abutment, HP310X125 Weak Orientation with Pile Enclosure)

Figure 7.36 shows the displacement along the abutment and the pile during bridge expansion for zero and 2-meter pile enclosures at the top of the pile. The effect of the pile enclosure is obvious in very stiff clay where the displacement at the top of the pile increases by more than 50% by using 2-meter pile enclosure. The figure also shows that the effect of the pile enclosure diminishes in the lower half of the pile.

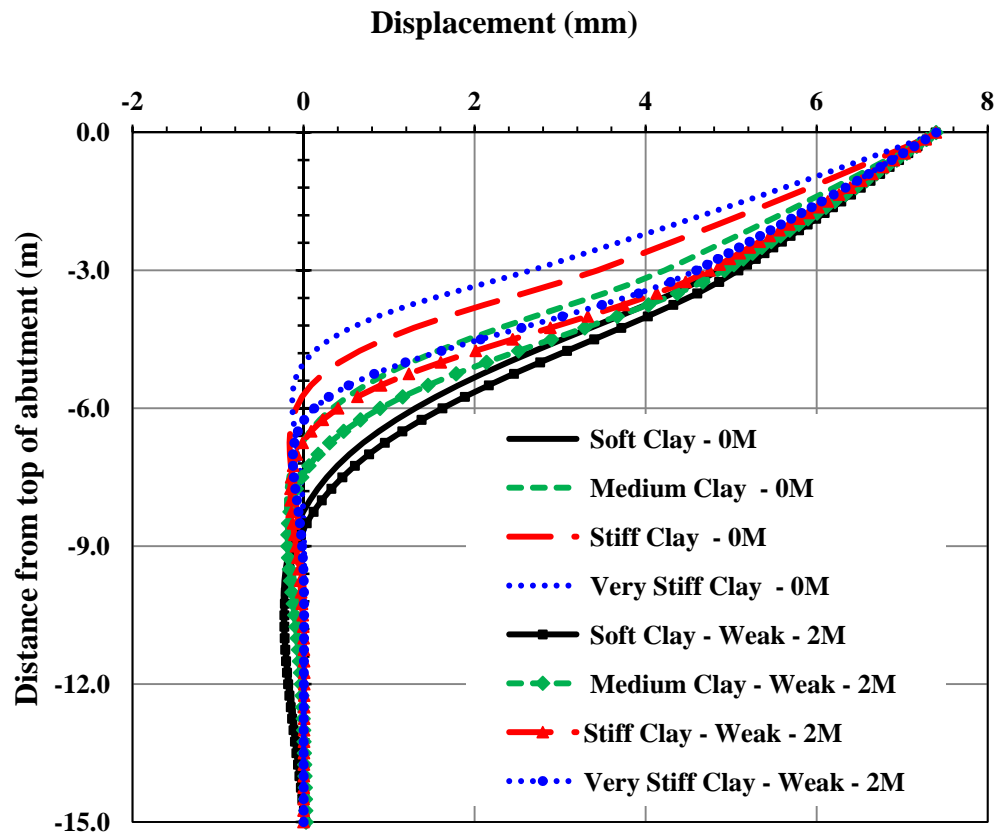


Figure 7.36 Displacement (Expansion) along the Abutment and the Interior Pile (38-m Bridge, Clay, 3m Abutment, HP310X125 Weak Orientation with Pile Enclosure)

Similar displacement behavior was also observed in the long bridge as shown in figures 7.37 and 7.38.

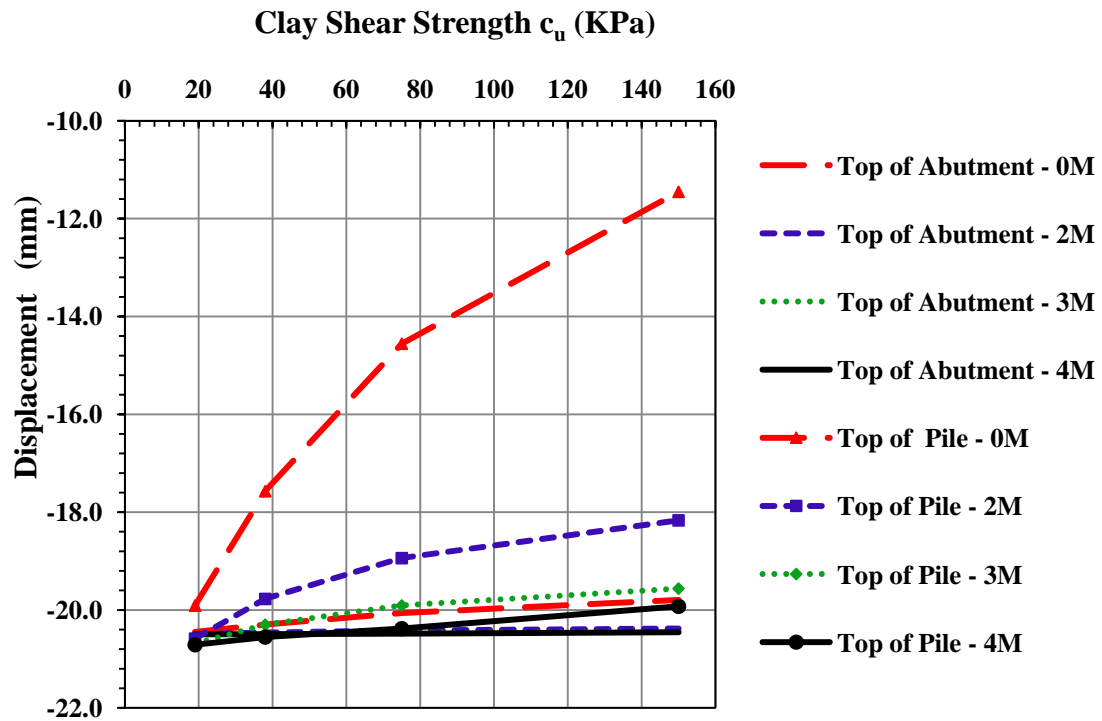


Figure 7.37 Displacement (Contraction) at the Interior Location (90-m Bridge, Clay, 3m Abutment, HP360X152 Weak Orientation with Pile Enclosure)

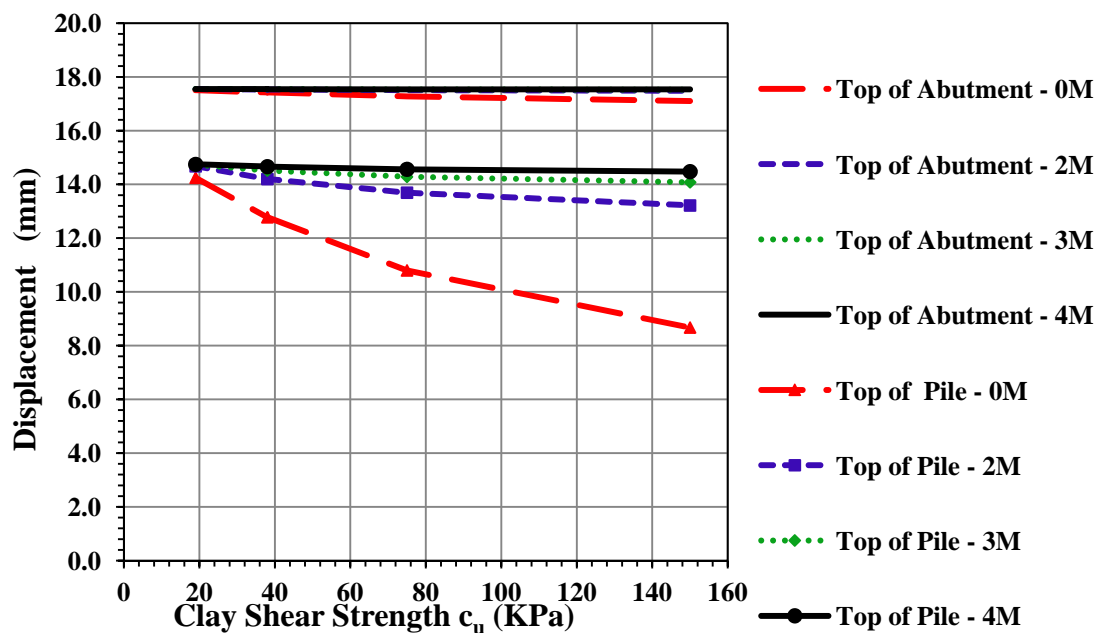


Figure 7.38 Displacement (Expansion) at the Interior Location (90-m Bridge, Clay, 3m Abutment, 360X152 Weak Orientation with Pile Enclosure)

Figure 7.39 shows the displacement along the abutment and the pile in the long bridge during bridge contraction. The figure shows the effect of using a 4-meter enclosure at the top of the pile. The figure shows that the displacements at the top and bottom of the abutment are almost equal when 4-meter pile enclosure is used which means that the abutment stays in the vertical position during thermal movement. The figure also shows that the effect of the pile enclosure continues in the lower part of the pile.

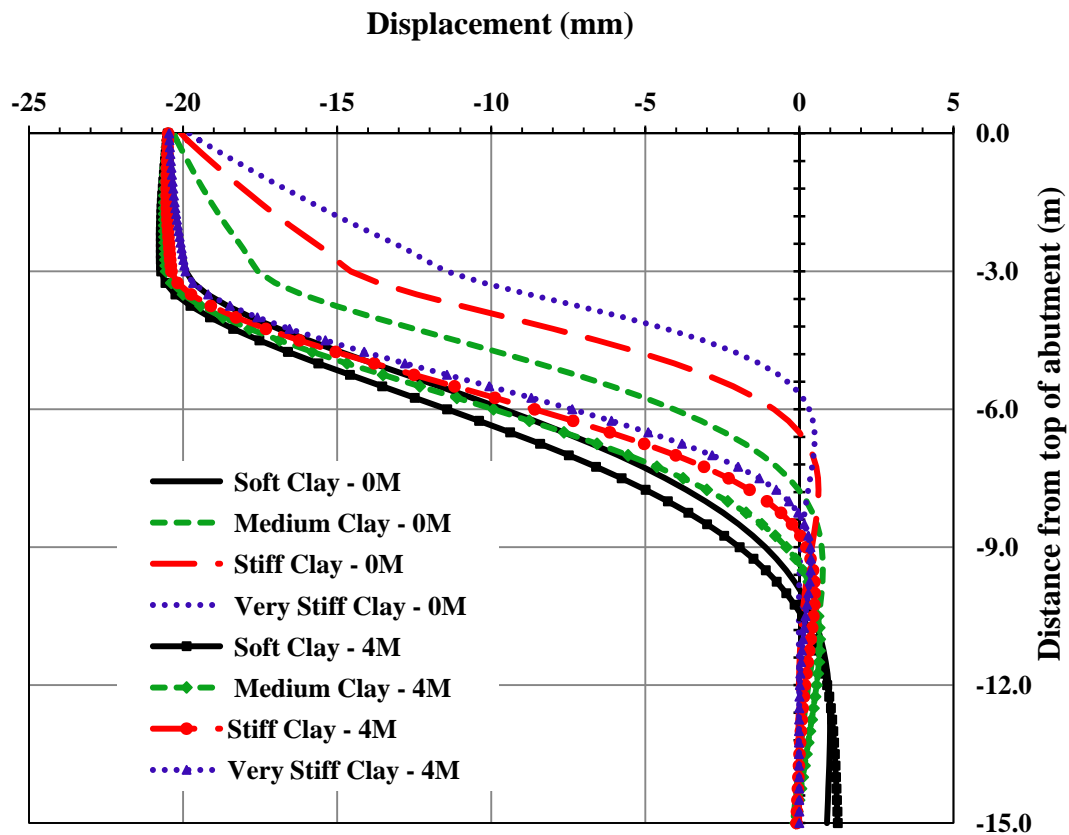


Figure 7.39 Displacement (Contraction) along the Abutment and the Interior Pile (90-m Bridge, Clay, 3m Abutment, 360X152 Weak Orientation with Pile Enclosure)

The rotation at the top of the pile decreases significantly with the use of pile enclosure as shown in figure 7.40. In stiff soil, the rotation sign (direction) at the top of the pile changes with the use of pile enclosure. A long (>2m) pile enclosure is required to cause rotation sign change in very stiff soil. The sensitivity of the rotation at the top of the pile and at the top of the abutment decreases with the increase in pile enclosure length and it almost diminishes for a pile enclosure of 4 meters.

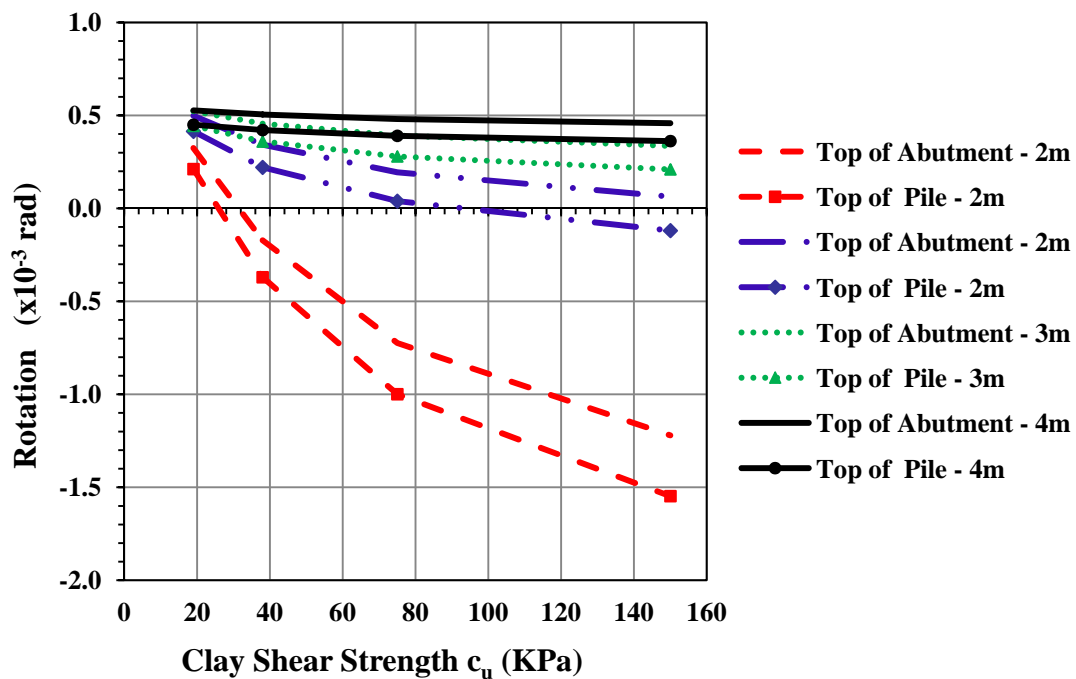


Figure 7.40 Rotation (Contraction) at the Interior Location
(38-m Bridge, Clay, 3m Abutment, HP310X125 Weak Orientation with Pile Enclosure)

The rate of change in rotation in the abutment and consequently the difference in rotation between the top and bottom of the abutment also decreases with the use of pile enclosure and that leads to abutment movement closer to rigid body movement especially in soft soil as shown in figure 7.41. The figure also shows that the rotation along the upper half of the pile decreases significantly with the use of a pile enclosure especially in stiff soils.

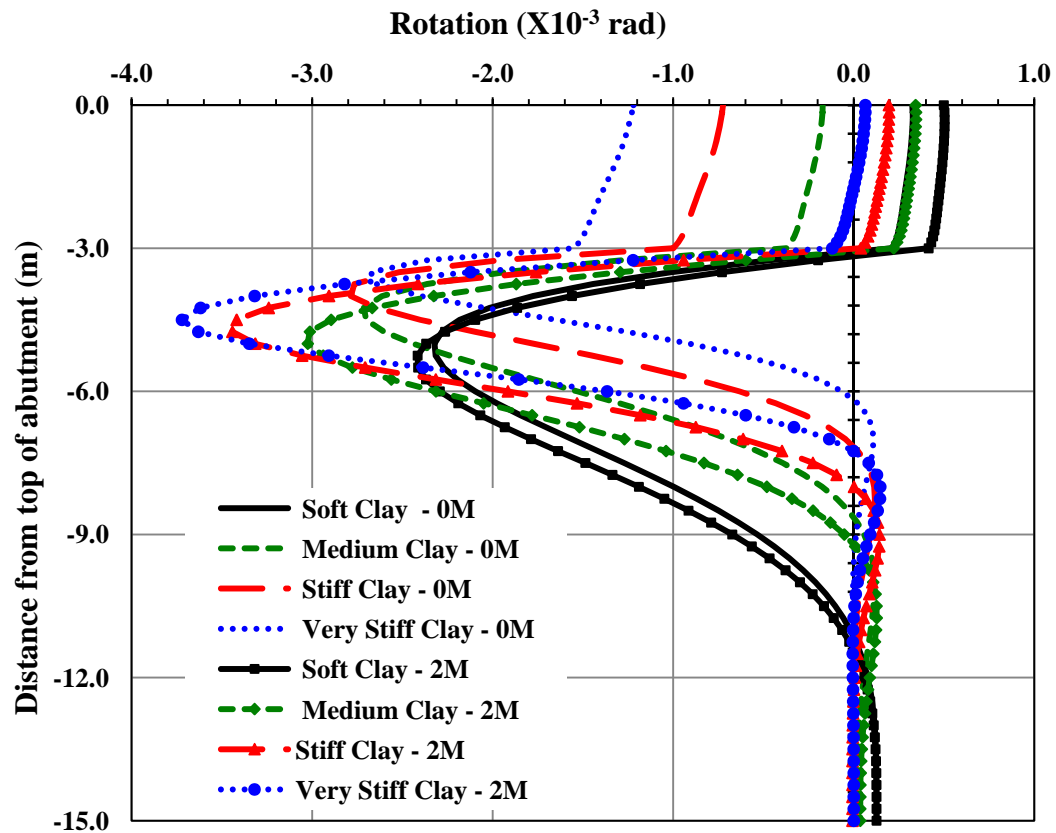


Figure 7.41 Rotation (Contraction) along the Abutment and the Interior Pile (38-m Bridge, Clay, 3m Abutment, HP310X125 Weak Orientation with Pile Enclosure)

Similar rotation behavior was also observed in the long bridge during contraction and expansion as shown in figures 7.42 and 7.43 respectively. The figures show that the sensitivity of the abutment rotation to the stiffness of the soil diminishes with the use of 4-meter pile enclosure. Figure 7.42 shows that the rotations at the top of the abutment and at the top of the pile are close to zero when 4-meter pile enclosure is used in the contraction case.

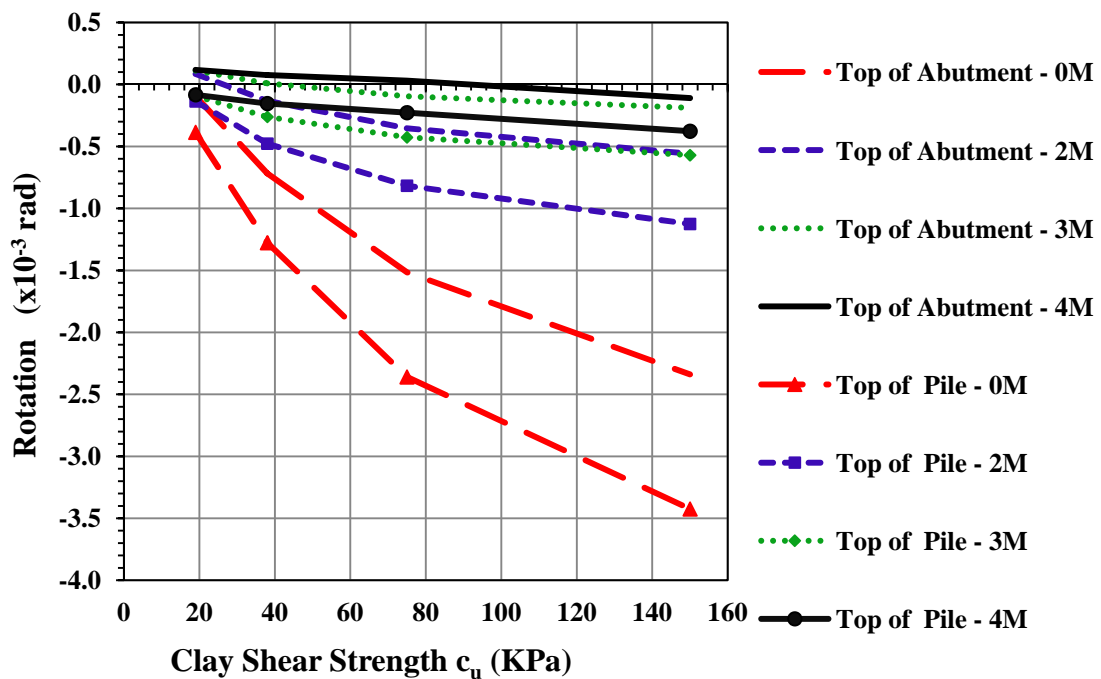


Figure 7.42 Rotation (Contraction) at the Interior Location
(90-m Bridge, Clay, 3m Abutment, HP360X152 Weak Orientation with Pile Enclosure)

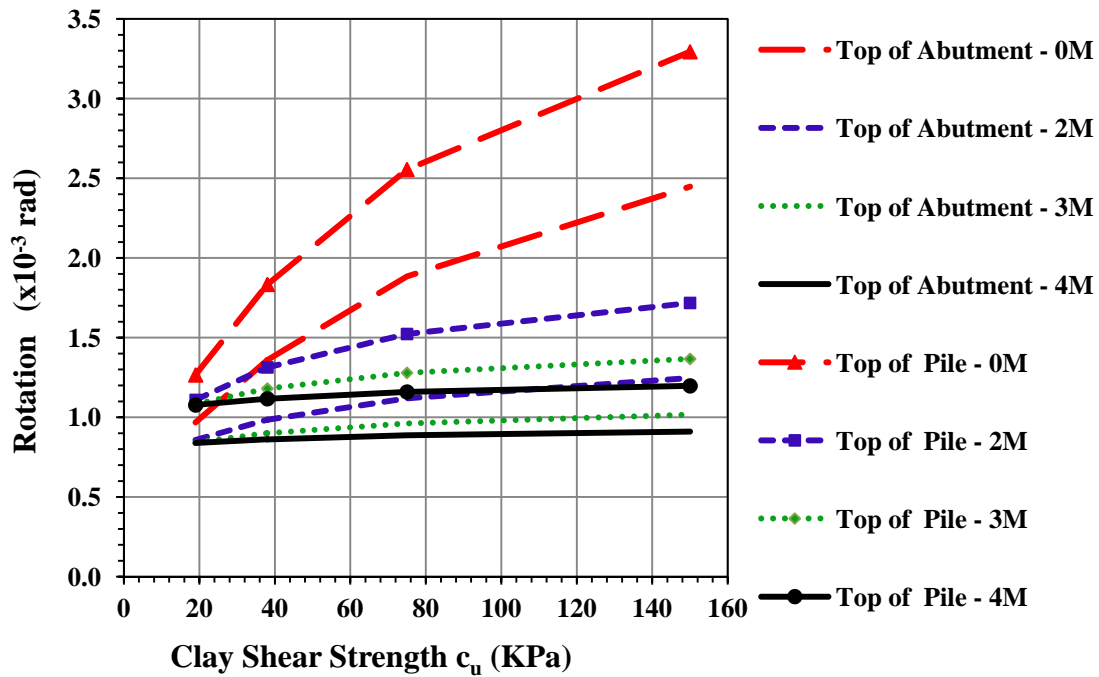


Figure 7.43 Rotation (Expansion) at the Interior Location
(90-m Bridge, Clay, 3m Abutment, HP360X152 Weak Orientation with Pile Enclosure)

For additional figures showing the effect of pile enclosure on the displacement and rotation along the abutment and the piles, see figures A.29 to A.31 in appendix A.

7.3.2 Effect of Pile Enclosure on the Moment along the Piles

The study showed that using pile enclosure has a major effect on the moment and consequently the stresses due to thermal loads experienced by the piles. That effect is shown clearly in figure 7.44 which shows the moment at the top of the exterior pile for the short bridge built on clay. The effect of using pile enclosure is more significant when the bridge is under contraction. During bridge contraction, the moment at the top of the pile dropped by 20%, 35% and 42% for 2-meter, 3-meter, and 4-meter pile enclosures respectively for medium clay and dropped by 20%, 38% and 48% for 2-meter, 3-meter, and 4-meter pile enclosures respectively for stiff clay. During the bridge expansion the

moment at the top of the pile also decreases with the use of pile enclosure. The sensitivity of the moment at the top of the pile to the stiffness of the soil nearly diminishes when 4-m pile enclosure is used for both the expansion and contraction cases.

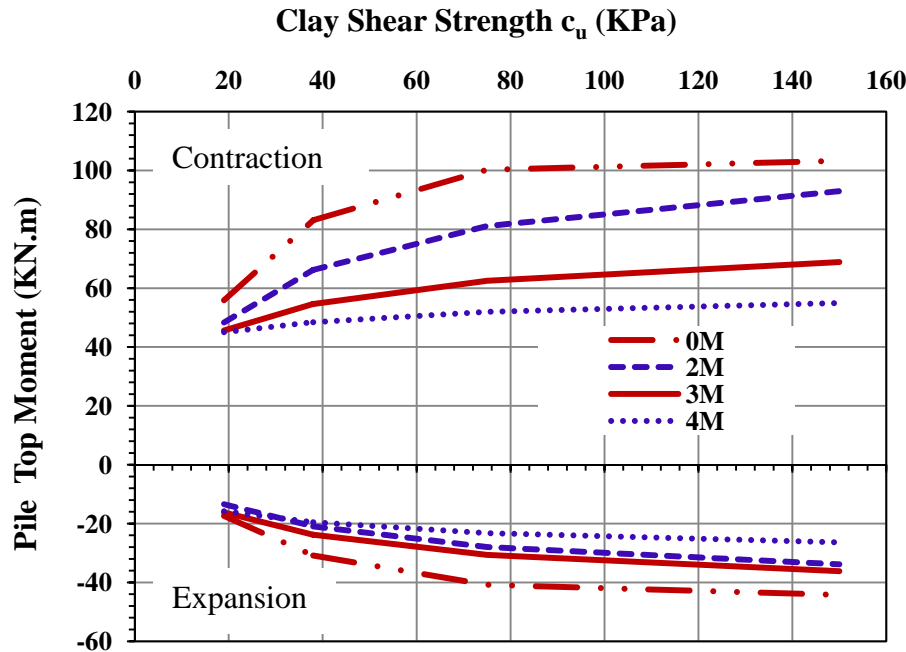


Figure 7.44 Moment at the Top of the Exterior Pile
(38-m Bridge, Clay, 3m Abutment, HP310X125 Weak Orientation with Pile Enclosure)

Figure 7.45 shows the moment along the exterior pile for the short bridge built on clay with 0-meter and 2-meter pile enclosures. The figure shows a slight drop in the reversed moment magnitude with the use of pile enclosure. The figure also shows a shift in the location of the reversed moment. The use of pile enclosure moves the location of the reversed moment deeper in the soil. In general, the effect of using pile enclosure diminishes in the lower part of the pile.

Similar moment behavior was also observed in the long bridge as shown in figures 7.46, 7.47, and figure A.32 in appendix A.

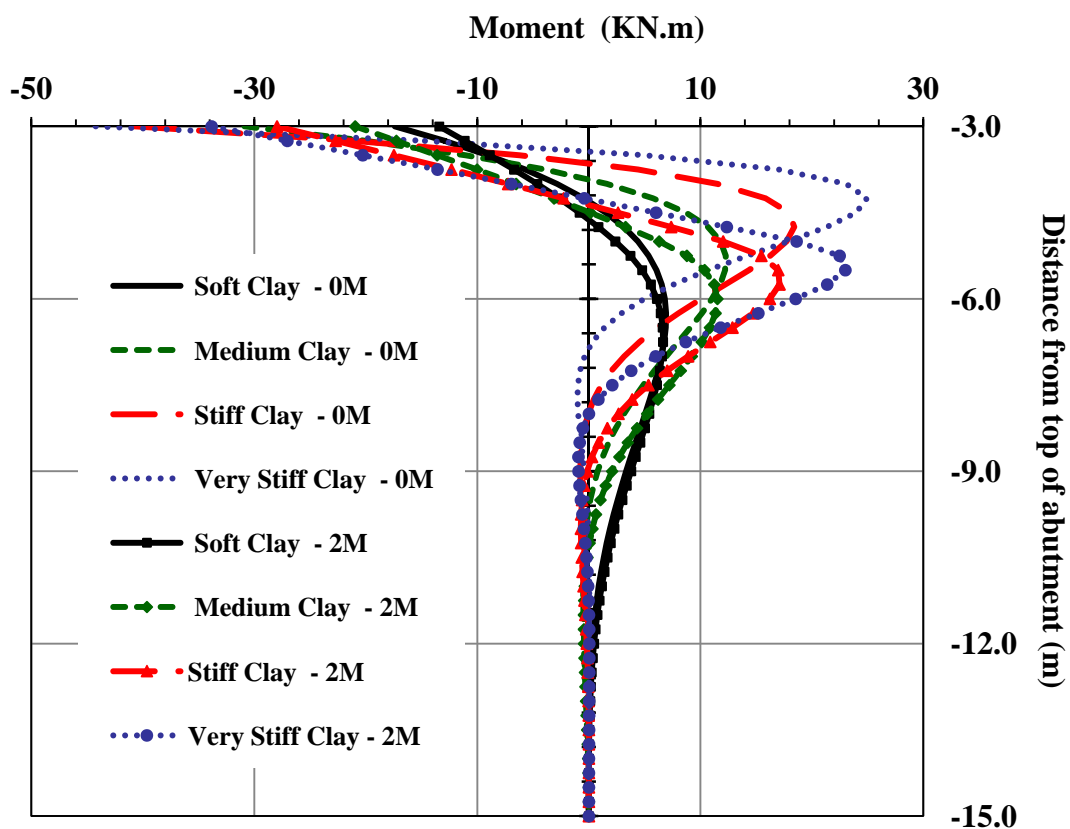


Figure 7.45 Moment (Contraction) along the Exterior Pile
(38-m Bridge, Clay, 3m Abutment, HP310X125 Weak Orientation with Pile Enclosure)

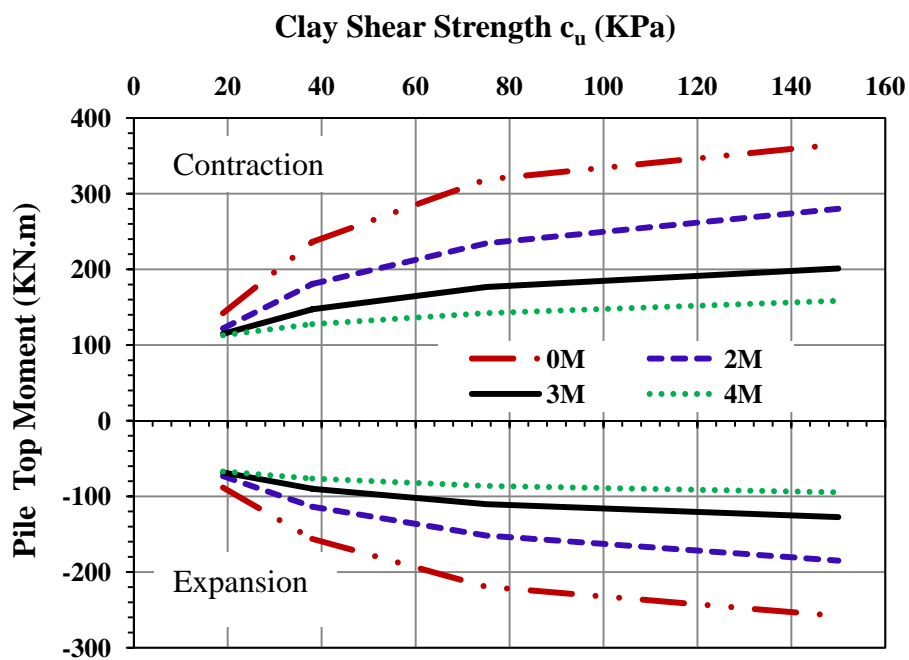


Figure 7.46 Moment at the Top of the Exterior Pile
(90-m Bridge, Clay, 3m Abutment, HP360X152 Weak Orientation with Pile Enclosure)

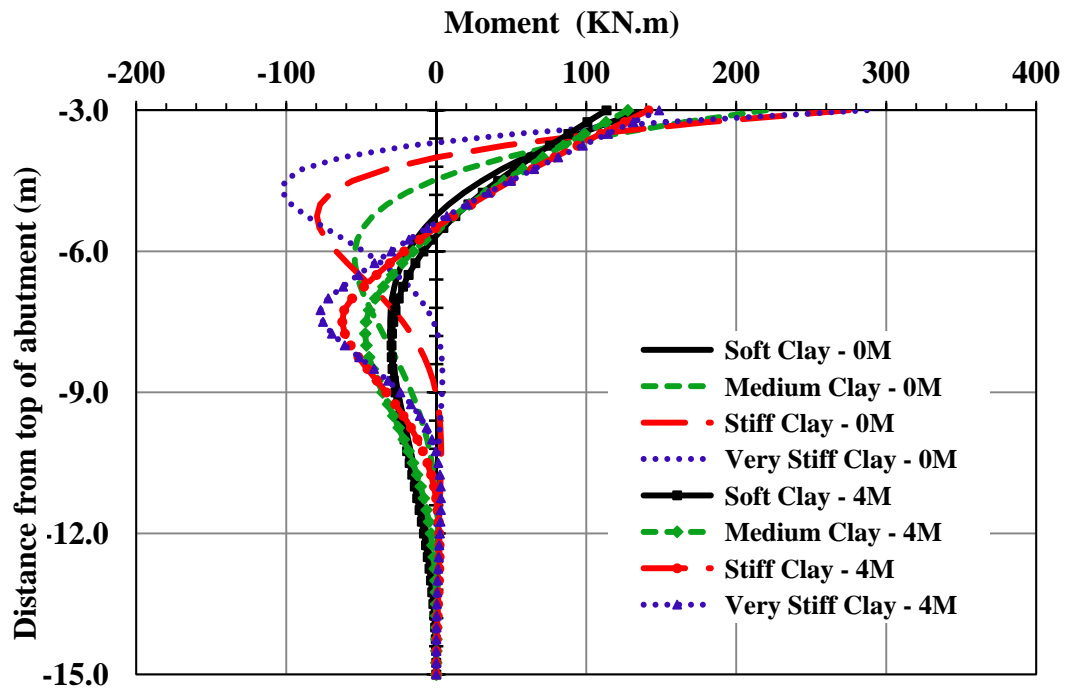


Figure 7.47 Moment (Contraction) along the Exterior Pile
(90-m Bridge, Clay, 3m Abutment, HP360X152 Weak Orientation with Pile Enclosure)

7.3.3 Effect of Pile Enclosure on the Stresses in the Girders

Using pile enclosure significantly reduces the stresses in the girders during bridge expansion and contraction as shown in figure 7.48. During the bridge contraction, the stresses in the girders can be reduced significantly by using a 2-meter pile enclosure especially in stiff soils. During bridge contraction, the stress in the girder web dropped by about 35% and 45% for medium clay and stiff clay respectively when a 2-meter pile enclosure was used. During bridge contraction, the stresses in the girders continue to decrease with the increase in pile enclosure length. During bridge expansion no further reduction in girder stresses was noticed by increasing the pile enclosure length to more than 2-meters. The sensitivity of the stresses in the girders to the stiffness of the soil nearly diminishes when 4-meter and 2-meter pile enclosures were used in the contraction and the expansion cases respectively.

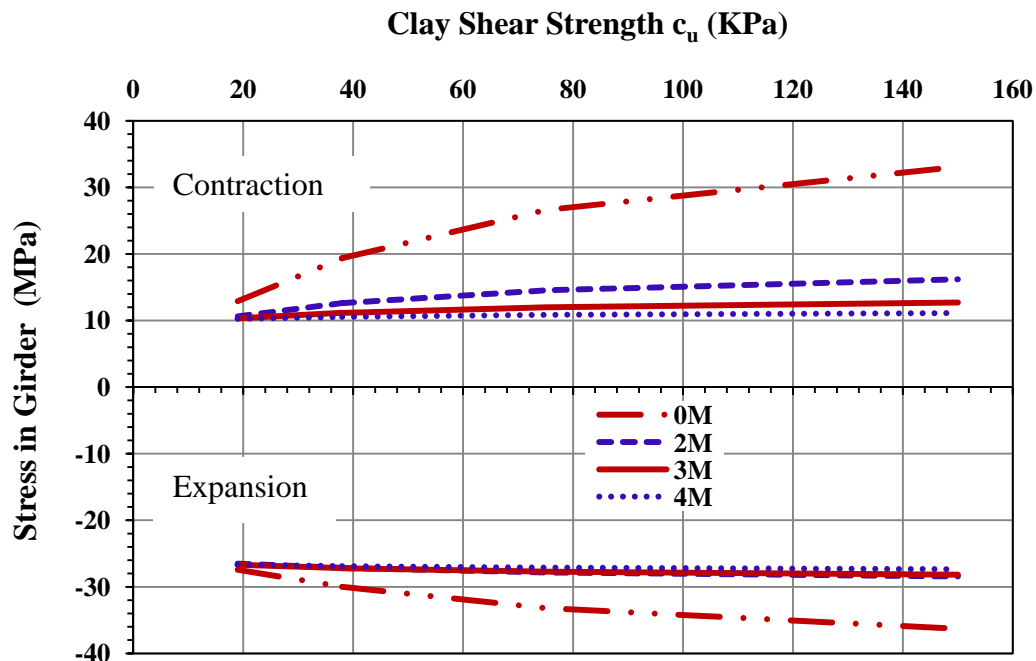


Figure 7.48 Stresses in the Interior Girder
(38-m Bridge, Clay, 3m Abutment, HP310X125 Weak Orientation with Pile Enclosure)

Similar behavior was also observed in the long bridge as shown in figure 7.49.

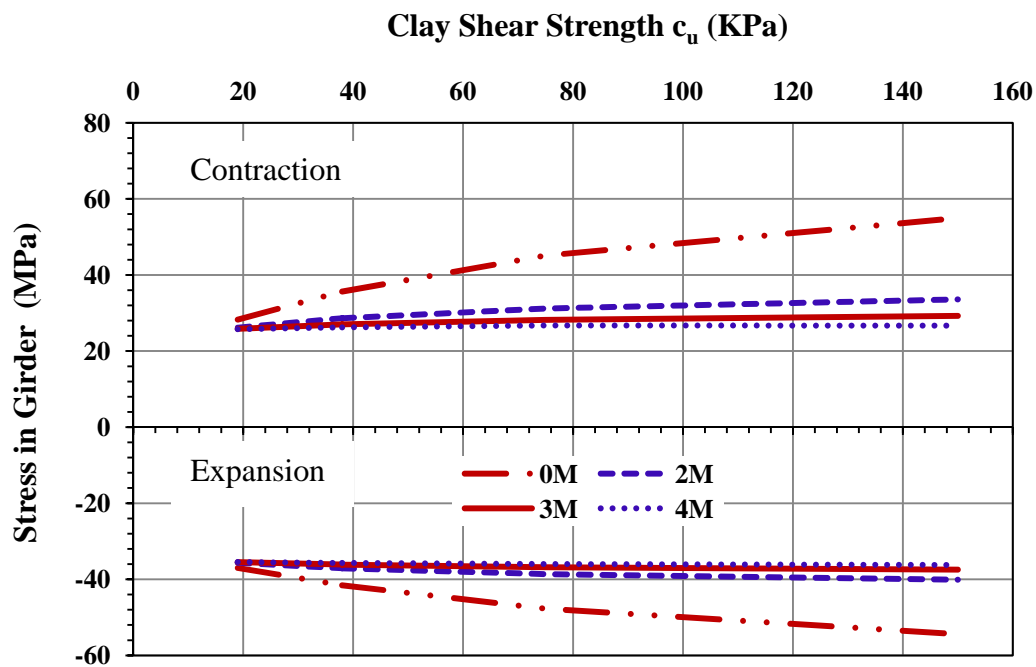


Figure 7.49 Stresses in the Interior Girder
(90-m Bridge, Clay, 3m Abutment, HP360X152 Weak Orientation with Pile Enclosure)

7.3.4 Effect of Pile Enclosure on the Backfill Pressure on the Abutment

The study showed that pile enclosure has a modest effect on the backfill pressure on the abutment. This effect is shown in figures 7.50 and 7.51 which show the backfill pressure on the abutment for the short bridge and the long bridge respectively during bridge expansion. Using a 2-meter pile enclosure increases the backfill pressure on the abutment. No increase in backfill pressure was noticed for pile enclosures longer than 2 meters.

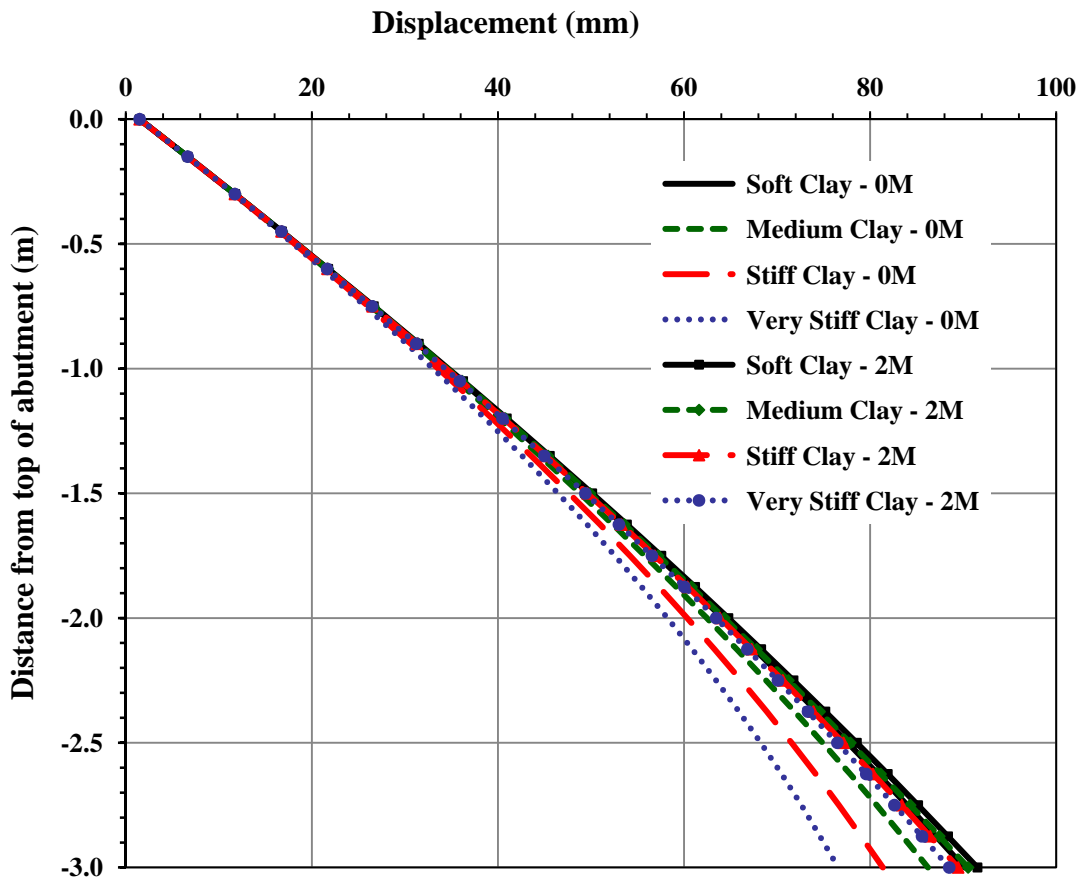


Figure 7.50 Backfill Pressure on the Abutment
(38-m Bridge, Clay, 3m Abutment, HP310X125 Weak Orientation with Pile Enclosure)

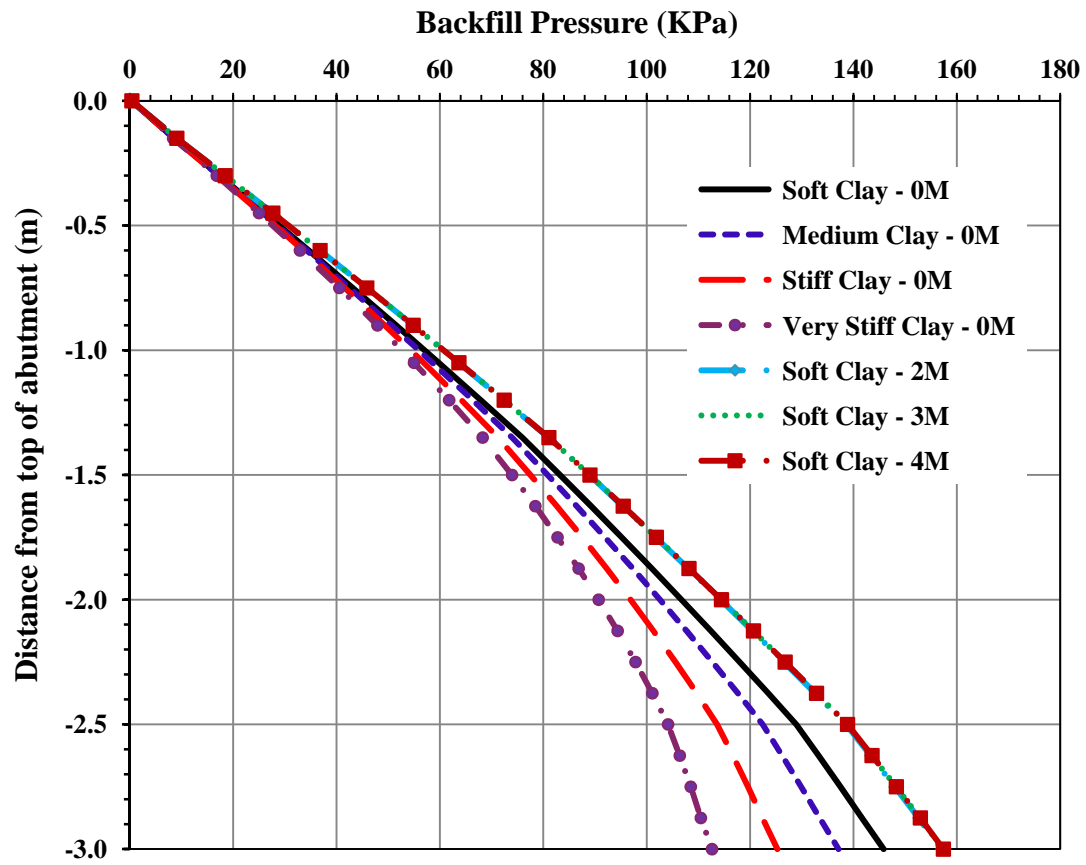


Figure 7.51 Backfill Pressure on the Abutment
(90-m Bridge, Clay, 3m Abutment, HP360X152 Weak Orientation with Pile Enclosure)

7.4 EFFECT OF PILE ORIENTATION

The study showed that pile orientation has a noticeable effect on the performance of IABs. The effect of pile orientation is more significant during bridge contraction than during bridge expansion. The effect of pile orientation on the performance of IABs is presented in the following subsections.

7.4.1 Effect of Pile Orientation on the Displacement and the Rotation of the Abutment and the Piles

The study showed that during bridge expansion, pile orientation has negligible effect on the displacement and rotation along the abutment and a small effect on the displacement and rotation along the piles as shown in figures 7.52 to 7.55. The figures also show that the effect of pile orientation on the displacement and rotation along the piles is less significant in stiff soils.

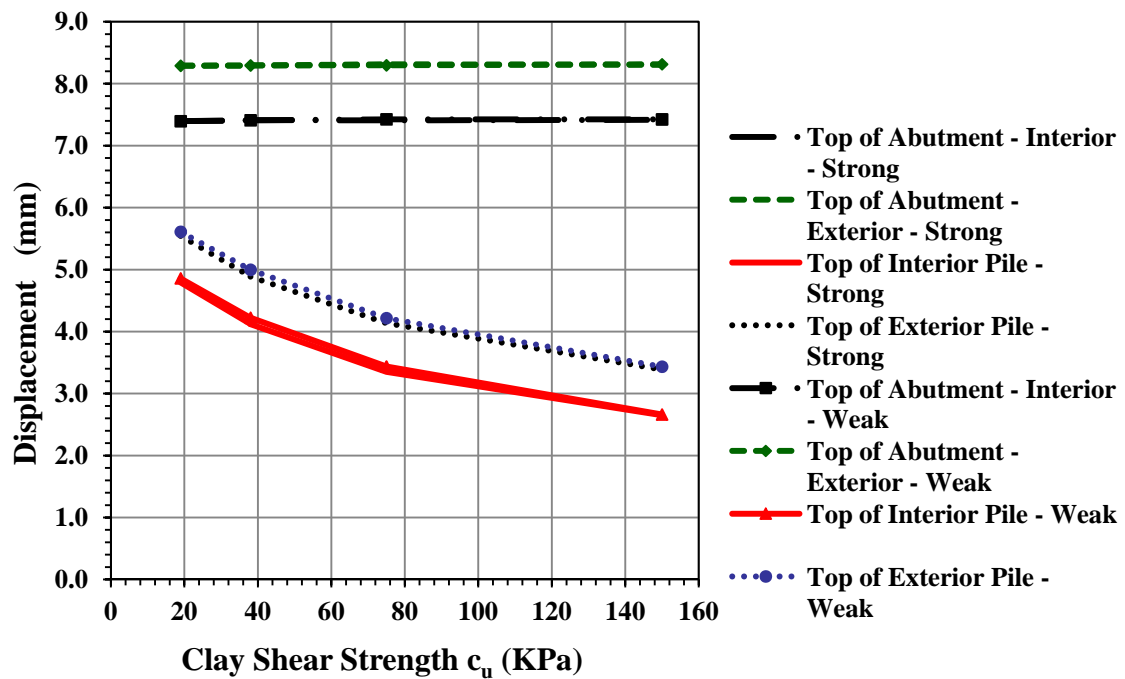


Figure 7.52 Displacement (Expansion) at Interior and Exterior Locations (38-m Bridge, Clay, 3m Abutment, HP310X125 Strong and Weak Orientation)

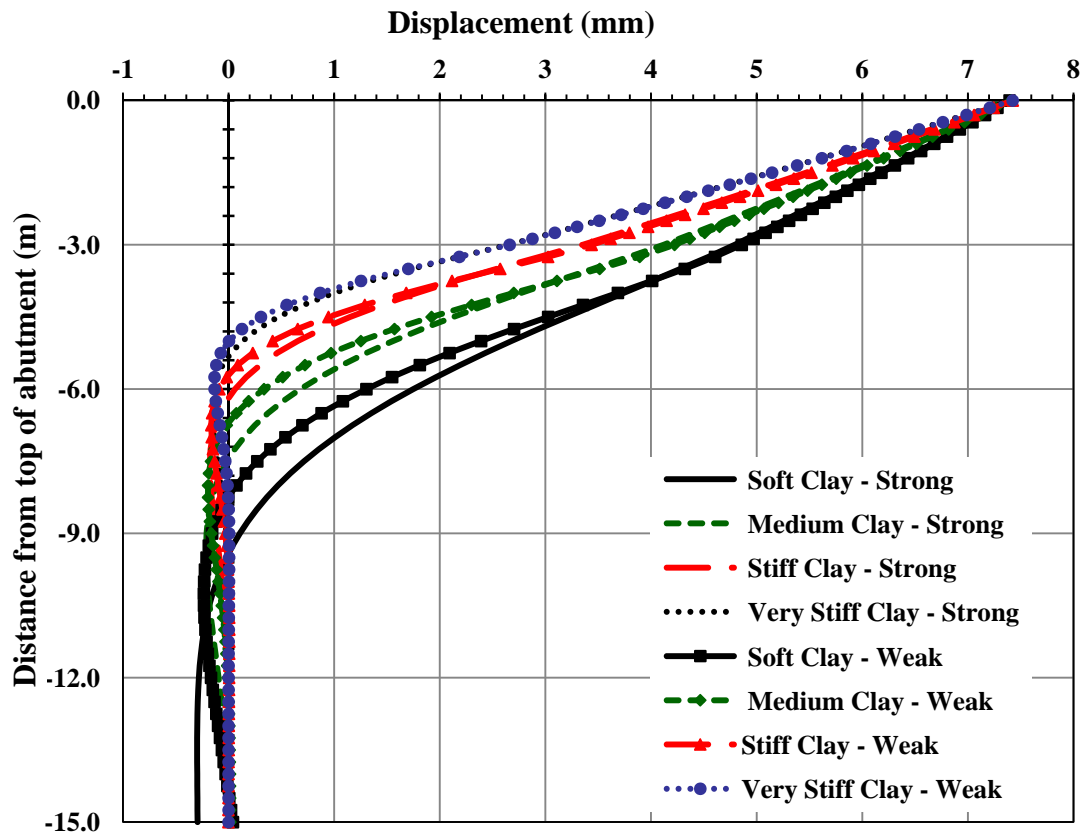


Figure 7.53 Displacement (Expansion) along the Abutment and the Interior Pile (38-m Bridge, Clay, 3m Abutment, HP310X125 Strong and Weak Orientation)

Figures 7.54 and 7.55 show that pile orientation has a negligible effect on the rotation at the top of the pile but has a noticeable effect on the rotation just below (about 1 meter) the top of the pile with sizable increase in the rotation of the piles oriented to bend around the weak axis. The figures also show that the effect of pile orientation on the rotation of the piles decreases with the increase in soil stiffness.

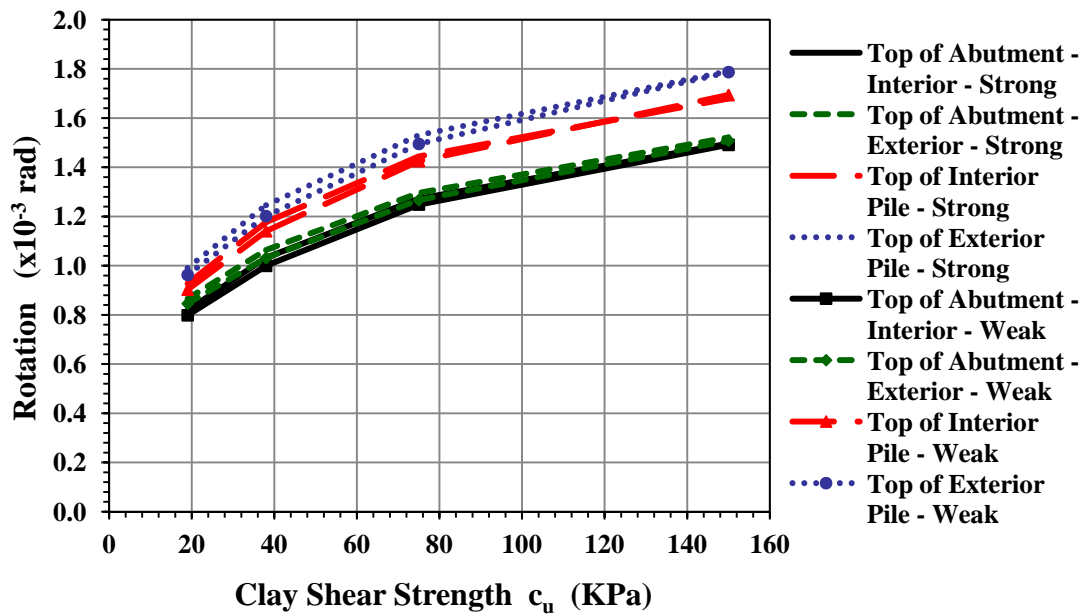


Figure 7.54 Rotation (Expansion) at Interior and Exterior Locations (38-m Bridge, Clay, 3m Abutment, HP310X125 Strong and Weak Orientation)

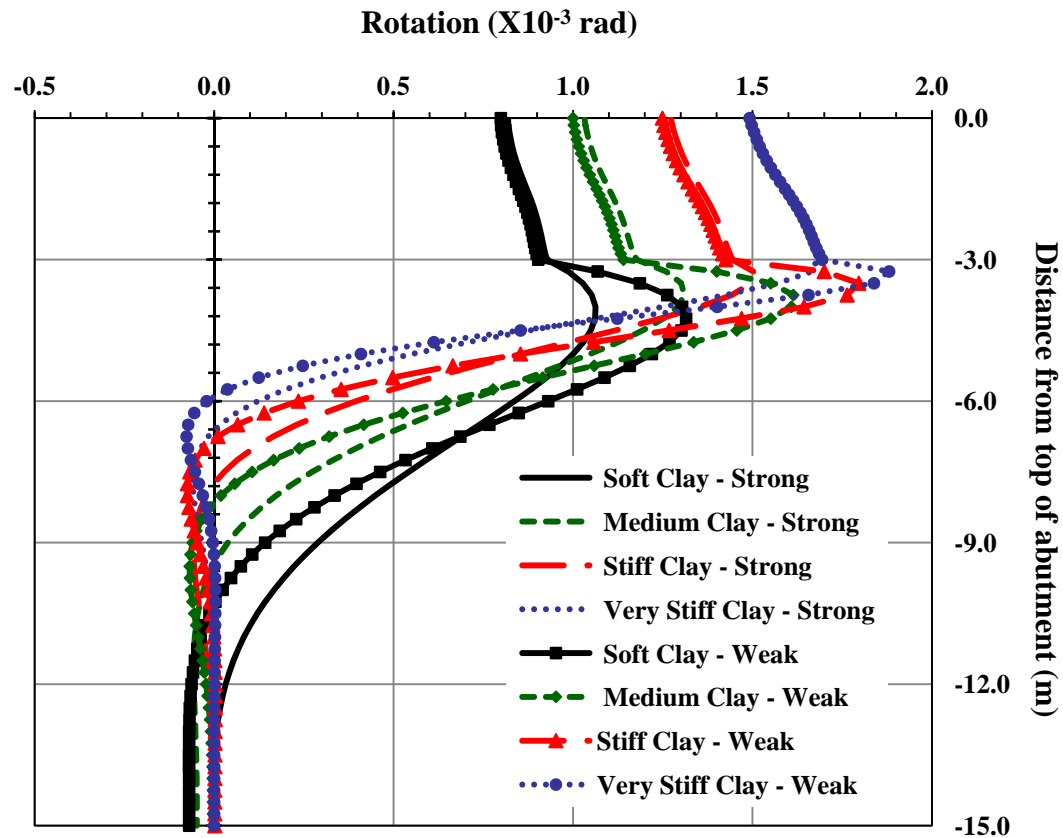


Figure 7.55 Rotation (Expansion) the Abutment and the Interior Pile (38-m Bridge, Clay, 3m Abutment, HP310X125 Strong and Weak Orientation)

The effect of pile orientation has a slightly larger effect on the displacement and rotation along the abutment and the piles during bridge contraction as shown in figures 7.56 to 7.59. The figures also show that the effect of pile orientation on the displacement and rotation along the piles slightly decreases with the increase in soil stiffness.

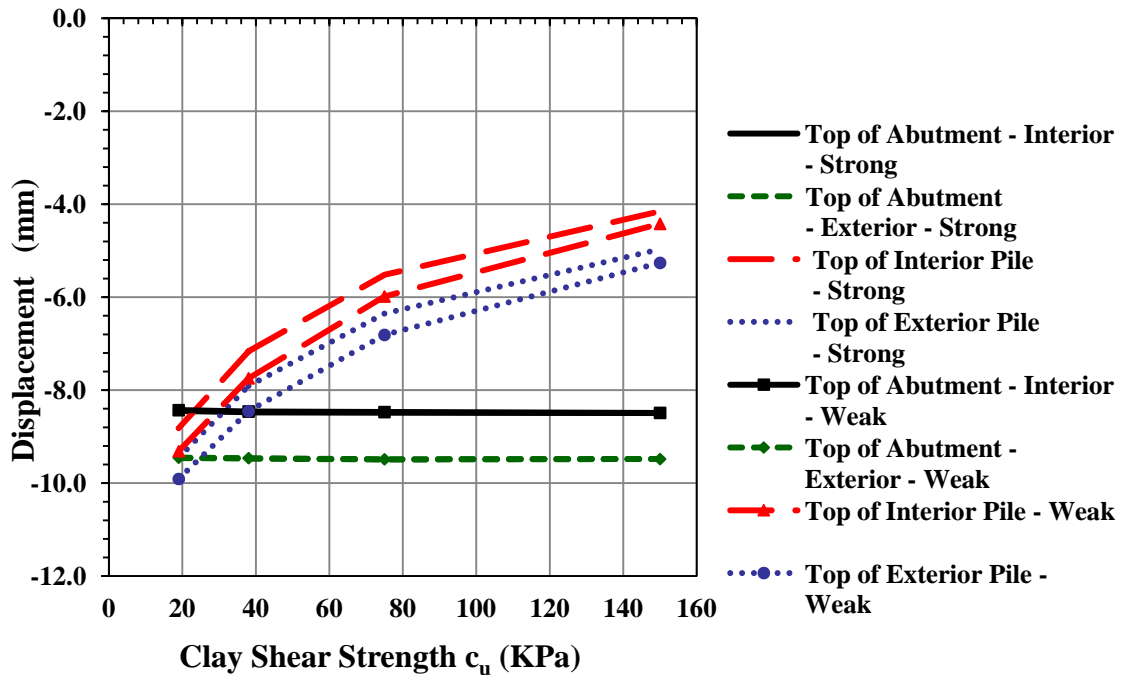


Figure 7.56 Displacement (Contraction) at Interior and Exterior Locations (38-m Bridge, Clay, 3m Abutment, HP310X125 Strong and Weak Orientation)

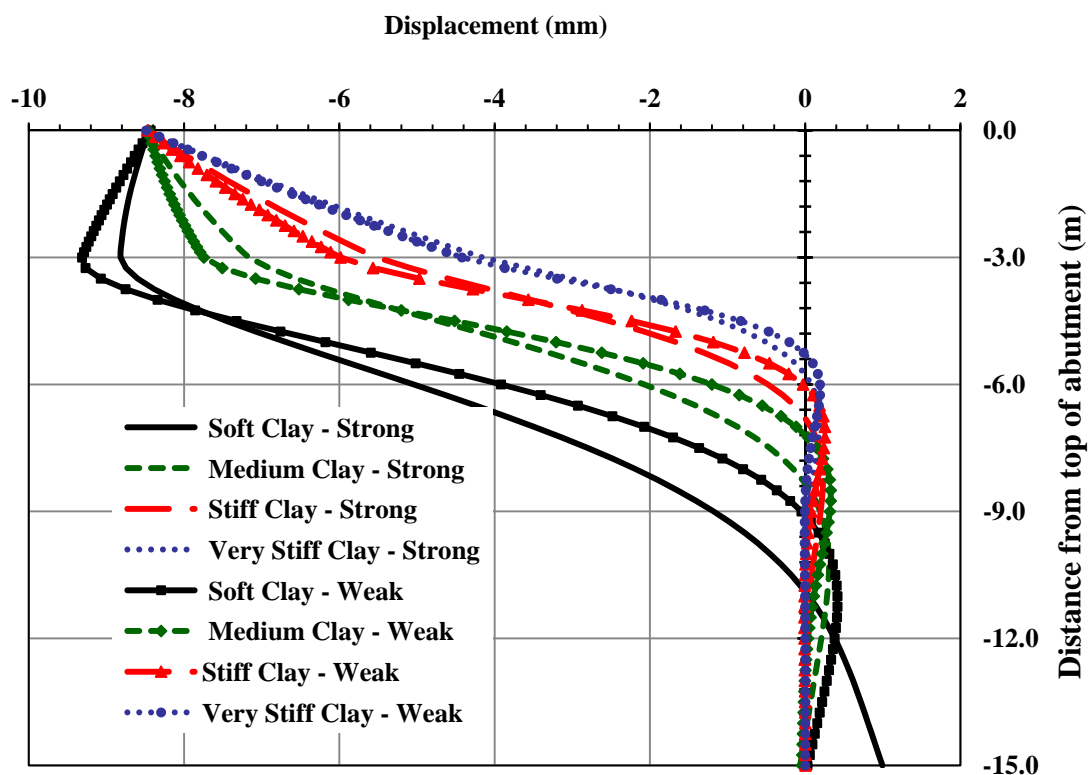


Figure 7.57 Displacement (Contraction) along the Abutment and the Interior Pile (38-m Bridge, Clay, 3m Abutment, HP310X125 Strong and Weak Orientation)

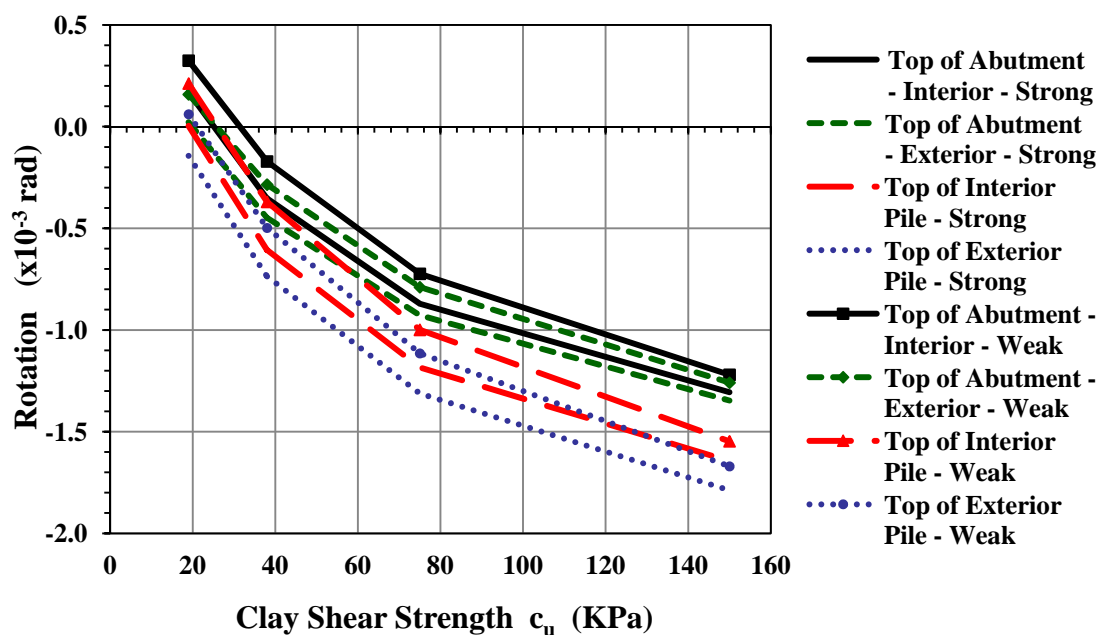


Figure 7.58 Rotation (Contraction) at Interior and Exterior Locations (38-m Bridge, Clay, 3m Abutment, HP310X125 Strong and Weak Orientation)

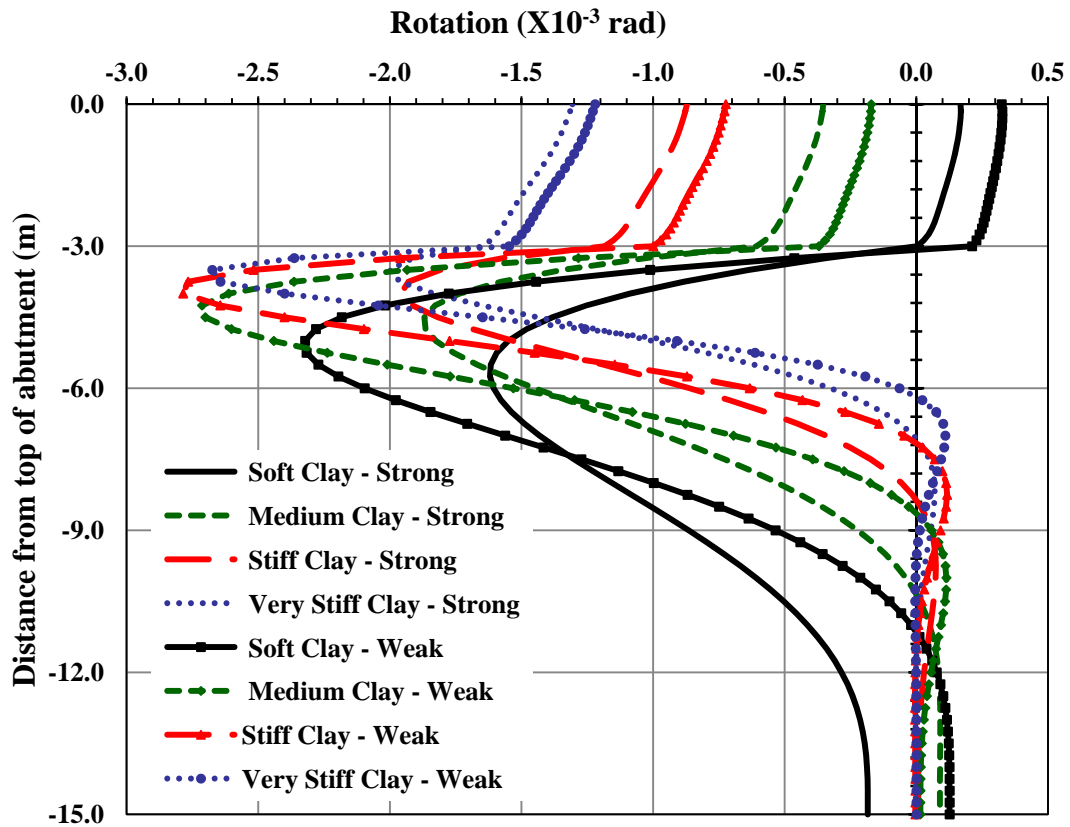


Figure 7.59 Rotation (Contraction) along the Abutment and the Interior Pile (38-m Bridge, Clay, 3m Abutment, HP310X125 Strong and Weak Orientation)

Similar observations on the effect of pile orientation on the moment along the piles were observed when the short bridge is supported by sand in both the expansion and contraction cases. Abutment and pile top displacements, abutment and pile top rotation, displacement along the abutment and the pile, and rotation along the abutment and the pile for the contraction case are shown in figures 7.60, 7.61, 7.62, and 7.63 respectively. Similar observations were also noticed for the long bridge when supported by clay and sand in both the expansion and the contraction cases. The displacement along the abutment and the pile, and the rotation along the abutment and the pile for the long bridge supported by clay during contraction are shown in figures 7.64, and 7.65 respectively.

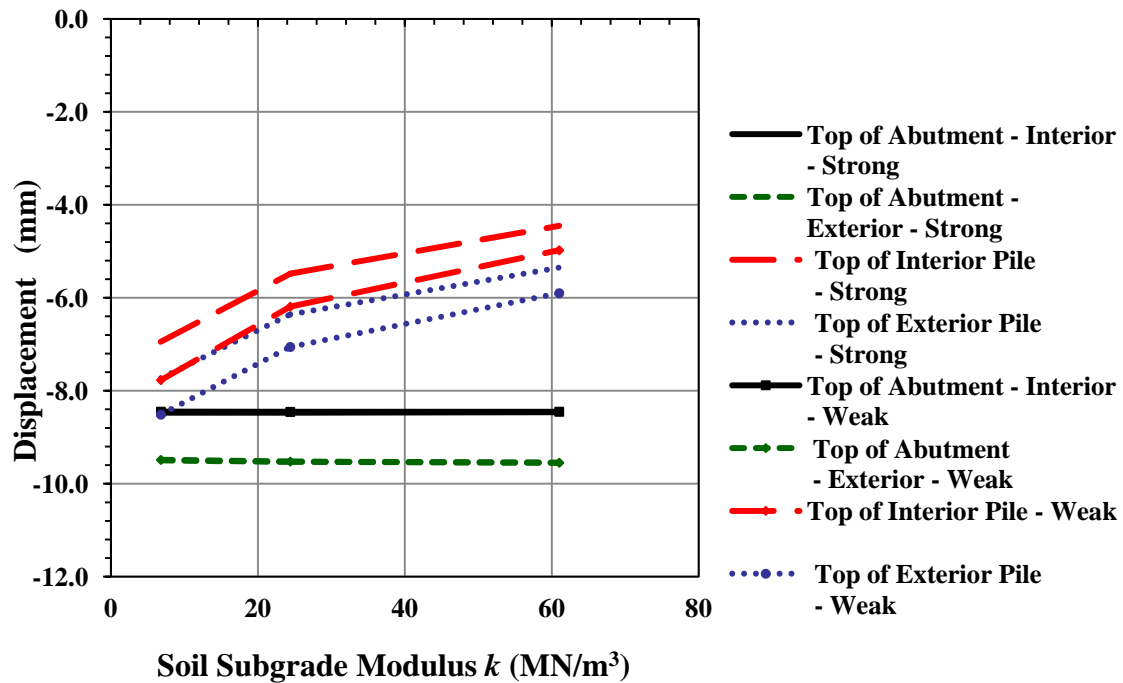


Figure 7.60 Displacement (Contraction) at Interior and Exterior Locations (38-m Bridge, Sand, 3m Abutment, HP310X125 Strong and Weak Orientation)

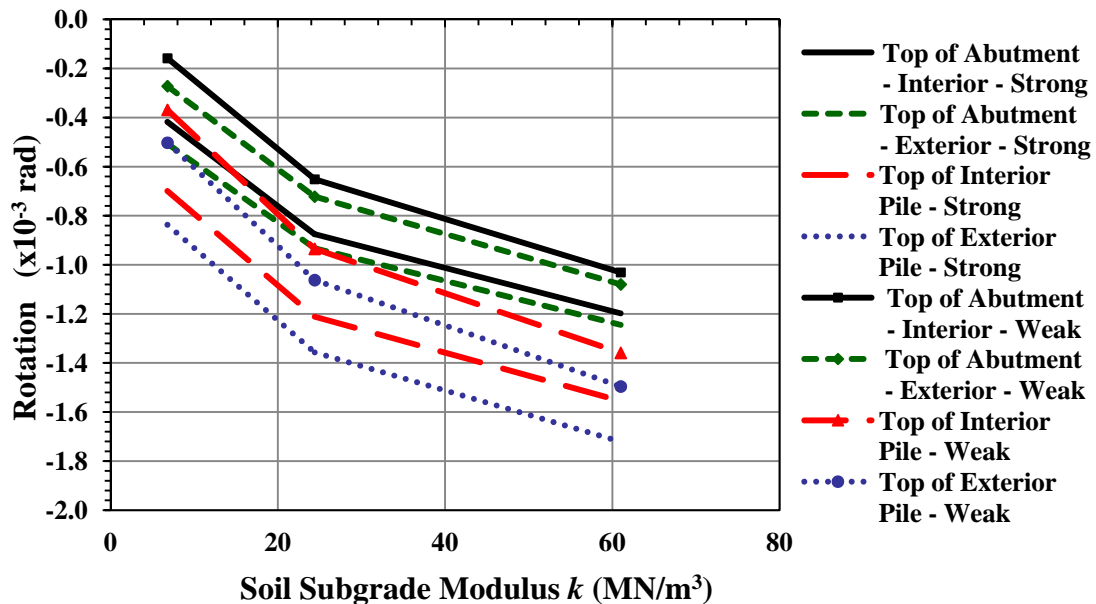


Figure 7.61 Rotation (Contraction) at Interior and Exterior Locations (38-m Bridge, Sand, 3m Abutment, HP310X125 Strong and Weak Orientation)

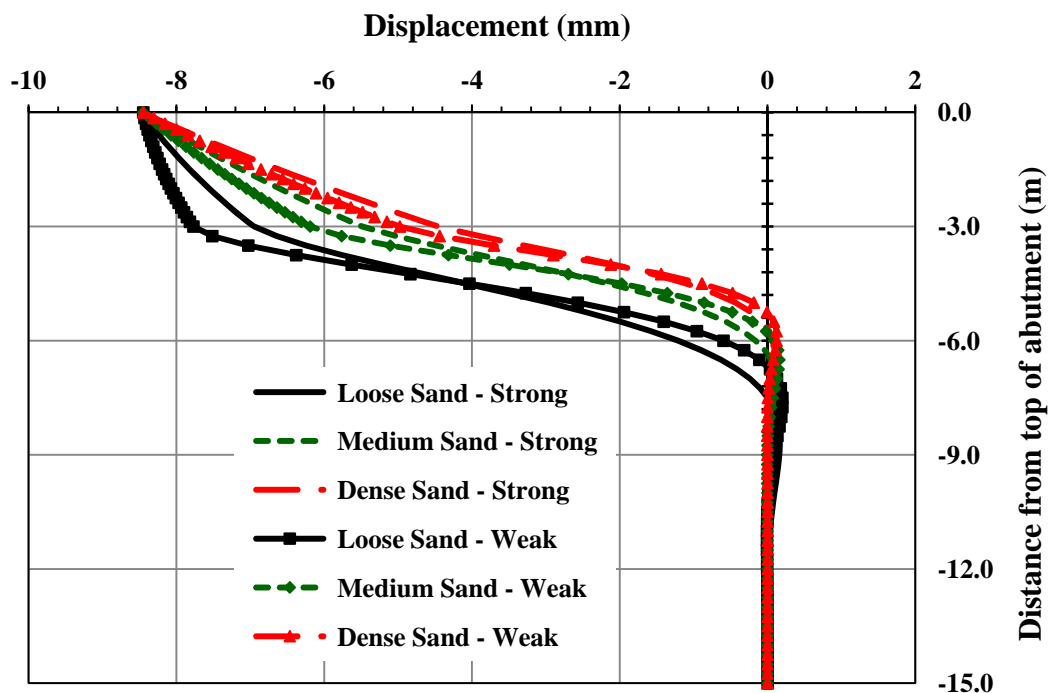


Figure 7.62 Displacement (Contraction) along the Abutment and the Pile at the Interior Location (38-m Bridge, Sand, 3m Abutment, HP310X125 Strong and Weak Orientation)

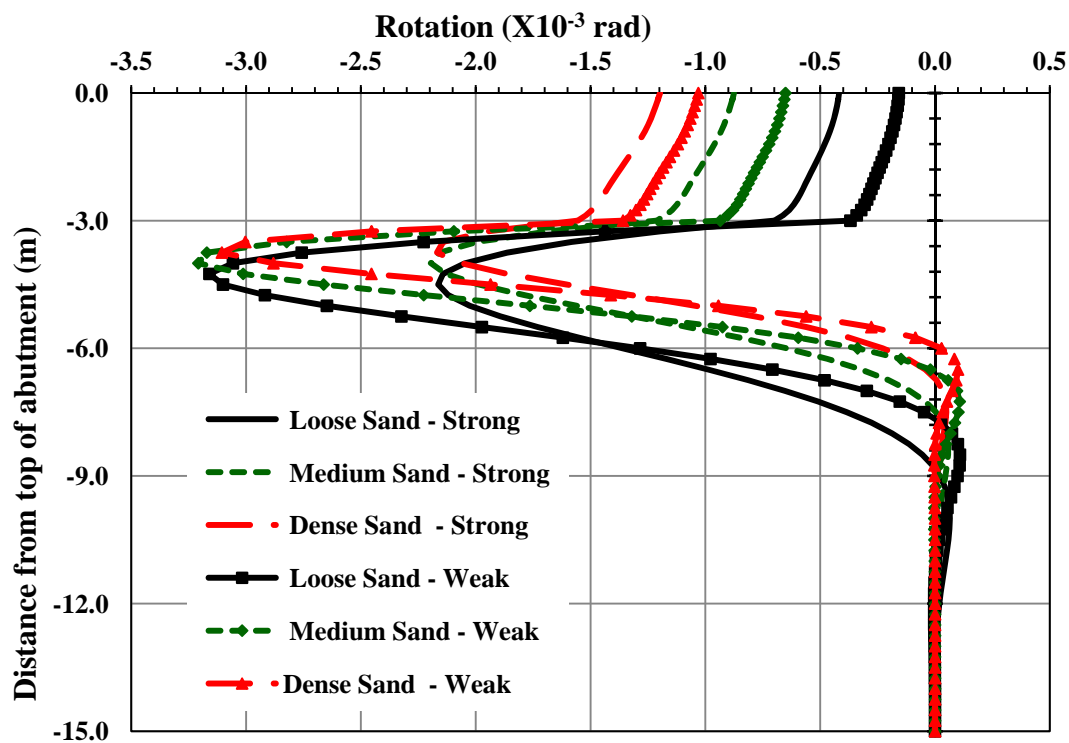


Figure 7.63 Rotation (Contraction) along the Abutment and the Interior Pile (38-m Bridge, Sand, 3m Abutment, HP310X125 Strong and Weak Orientation)

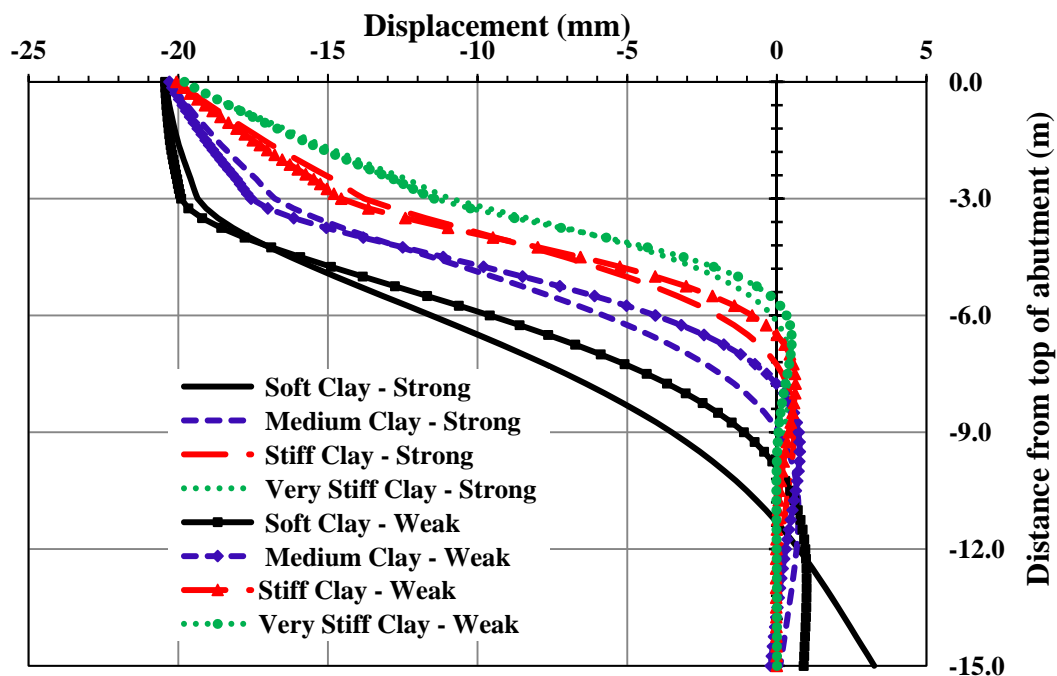


Figure 7.64 Displacement (Contraction) along the Abutment and the Interior Pile (90-m Bridge, Clay, 3m Abutment, HP360X152 Strong and Weak Orientation)

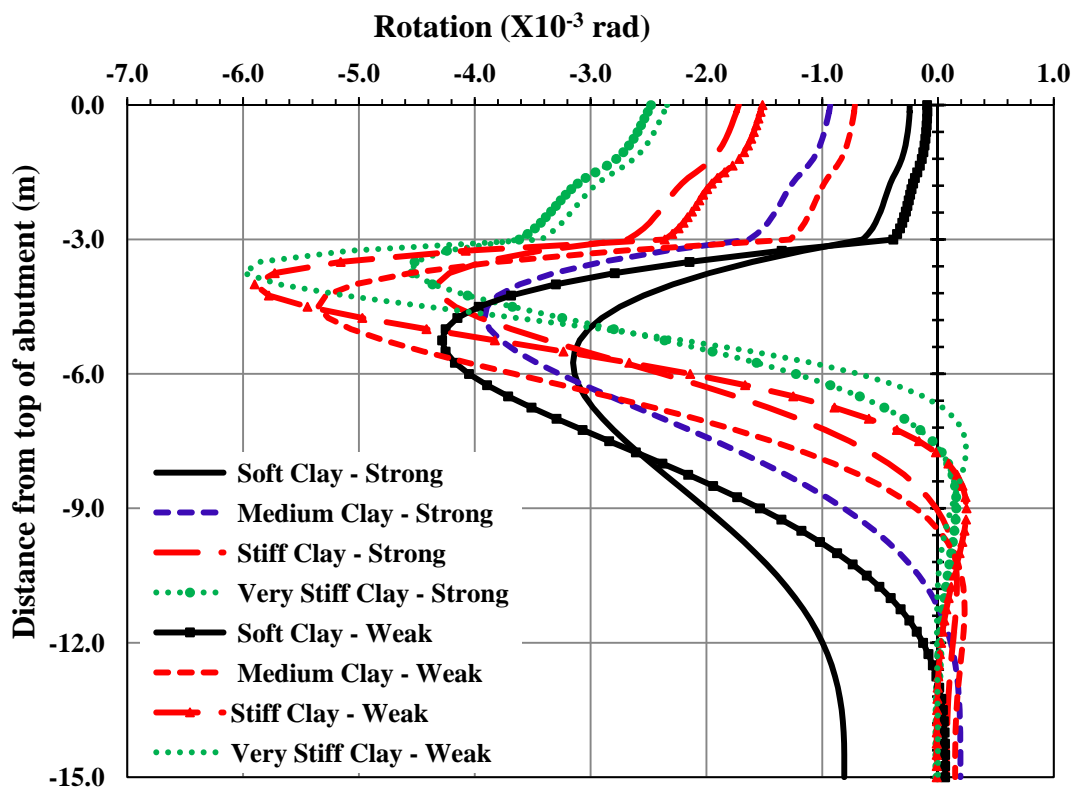


Figure 7.65 Rotation (Contraction) along the Abutment and the Interior Pile (90-m Bridge, Clay, 3m Abutment, HP360X152 Strong and Weak Orientation)

7.4.2 Effect of Pile Orientation on the Moment along the Piles

The study showed that pile orientation has a negligible effect on the pile top moment during bridge expansion but has a noticeable effect when the bridge is under contraction as shown in figure 7.66. During bridge contraction the moment at the top of the pile increases by more than 50% when the pile orientation changes from weak to strong in soft soil. The increase in pile top moments drops to 10% in very stiff soil.

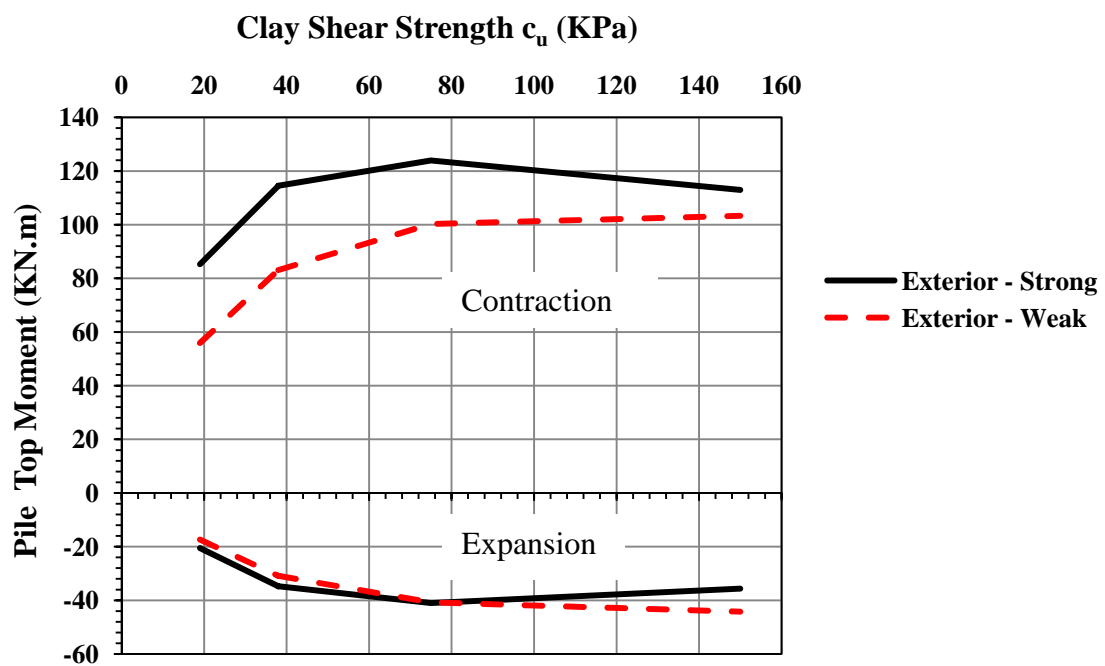


Figure 7.66 Moment at the Top of the Interior Pile
(38-m Bridge, Clay, 3m Abutment, HP310X125 Weak and Strong Orientation)

The pile orientation has a noticeable effect on the moment distribution along the pile for both the expansion and contraction cases as shown in figures 7.67 and 7.68. The figures show that during bridge expansion and contraction the reversed moment is considerably higher when the pile is oriented to bend around the strong axis for all types of soil. The increase in the reversed moment is larger during bridge expansion. The effect of pile orientation on the location of the reversed moment is negligible.

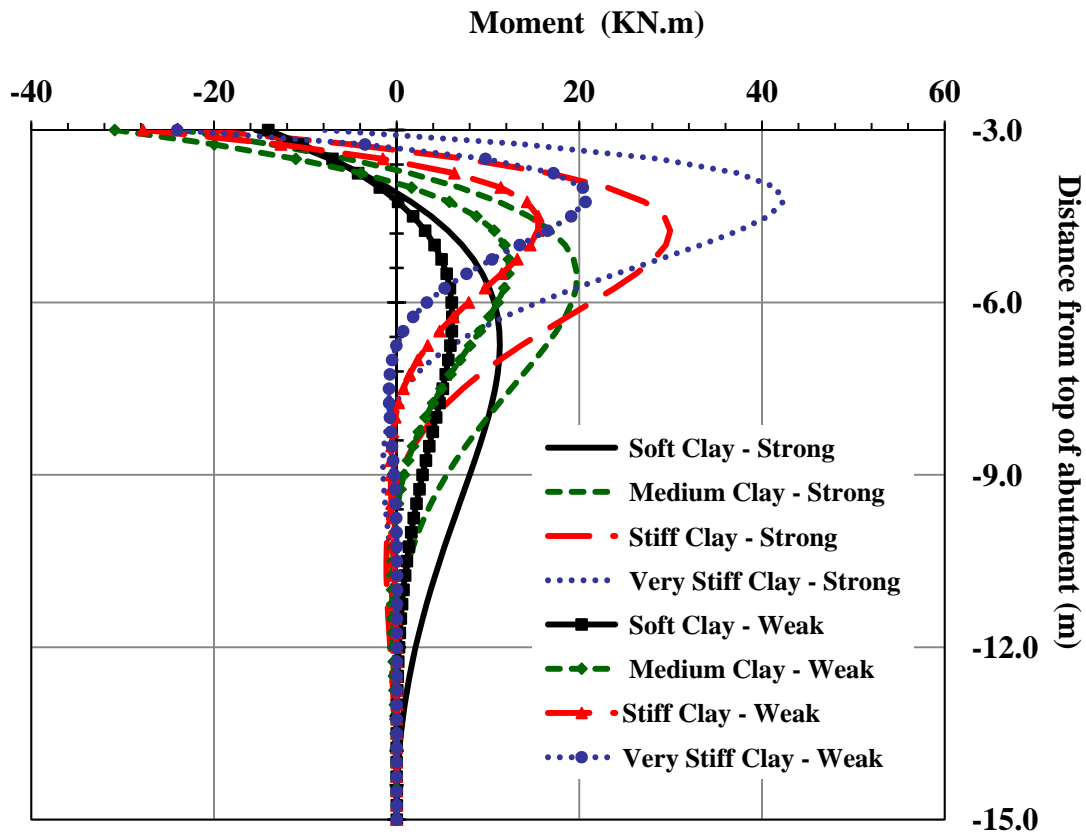


Figure 7.67 Moment (Expansion) along the Interior Pile
(38-m Bridge, Clay, 3m Abutment, HP310X125 Weak and Strong Orientation)

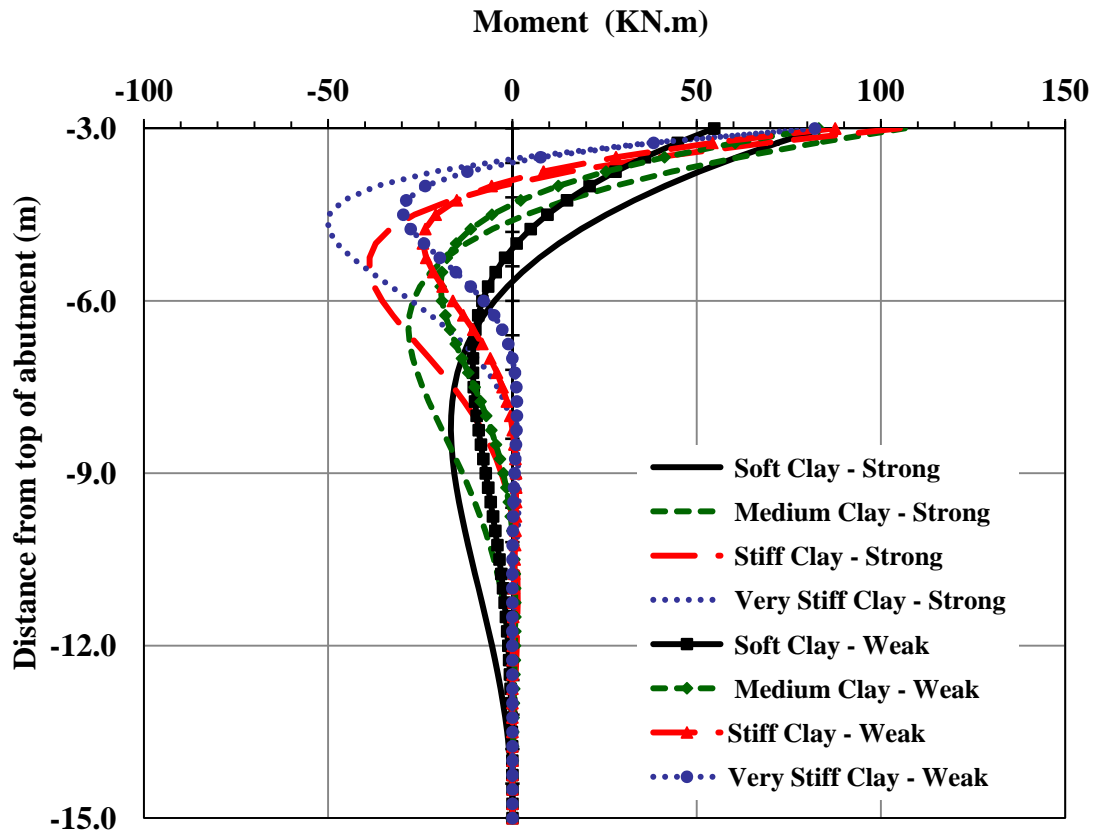


Figure 7.68 Moment (Contraction) along the Interior Pile
(38-m Bridge, Clay, 3m Abutment, HP310X125 Weak and Strong Orientation)

Similar observations on the effect of pile orientation on the moment along the piles were observed when the short bridge is supported by sand. Figures 7.69 and 7.70 show the moment distribution along the interior pile for the short bridge supported by sand for the expansion and contraction cases respectively.

Similar observations were also noticed for the long bridge when supported by clay or sand in both the expansion and contraction cases. The moment along the pile for the long bridge supported by clay during expansion and contraction are shown in figures 7.71, and 7.72 respectively.

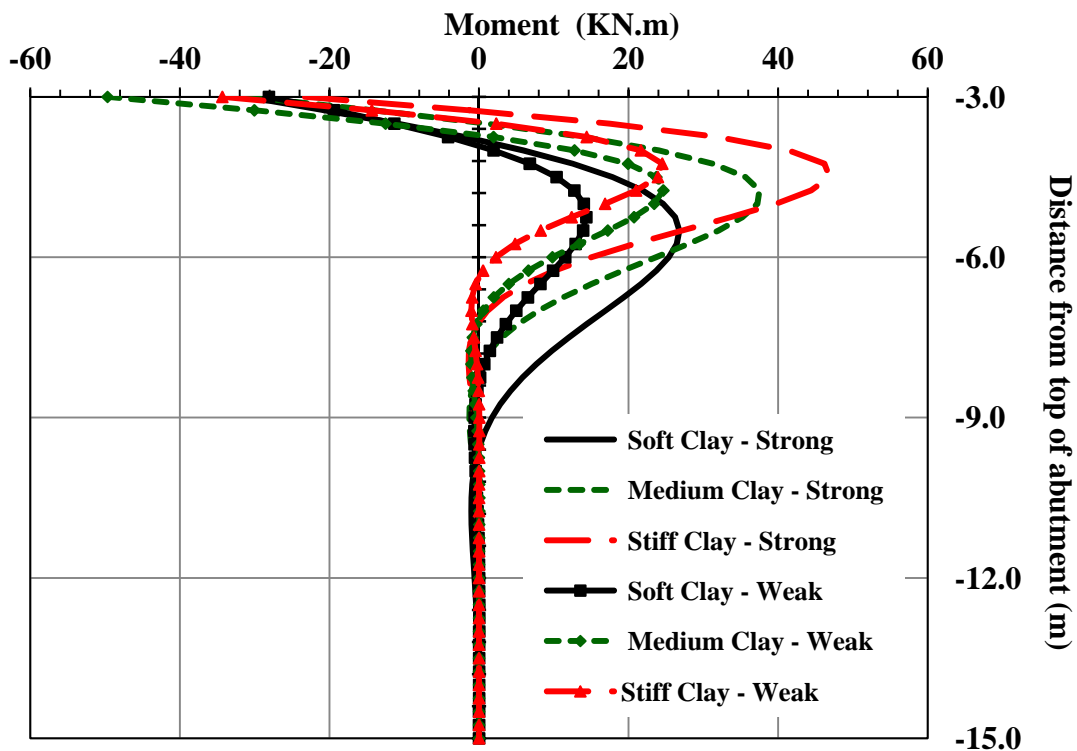


Figure 7.69 Moment (Expansion) along the Interior Pile
(38-m Bridge, Sand, 3m Abutment, HP310X125 Weak and Strong Orientation)

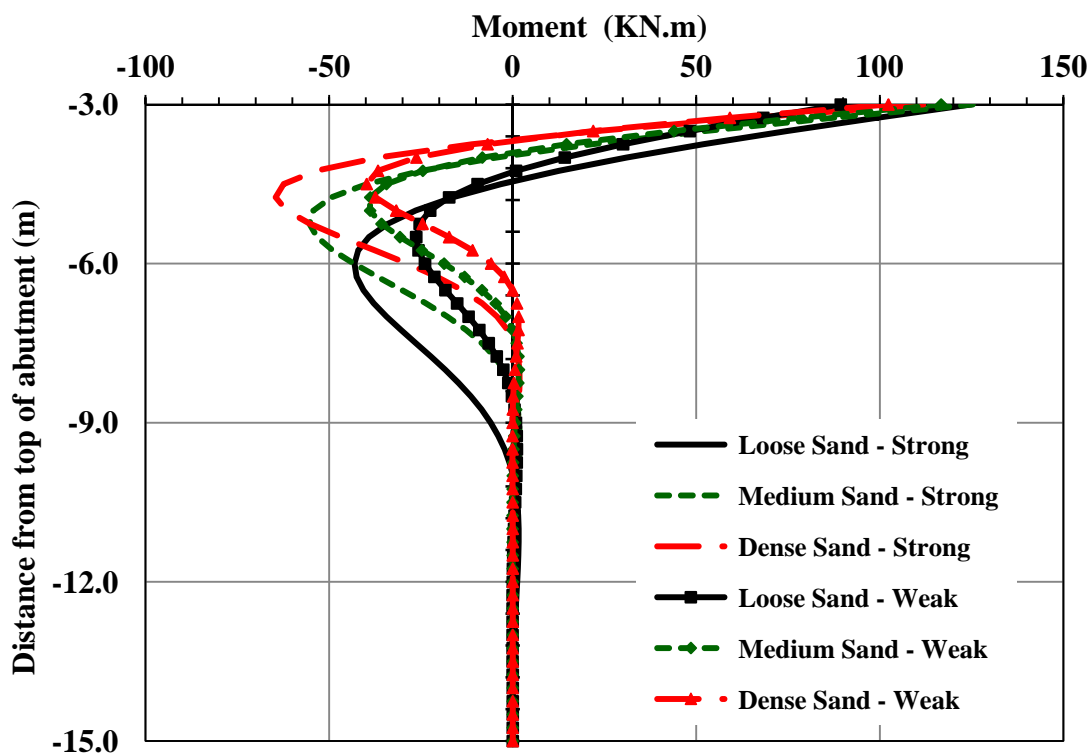


Figure 7.70 Moment (Contraction) along the Interior Pile
(38-m Bridge, Sand, 3m Abutment, HP310X125 Weak and Strong Orientation)

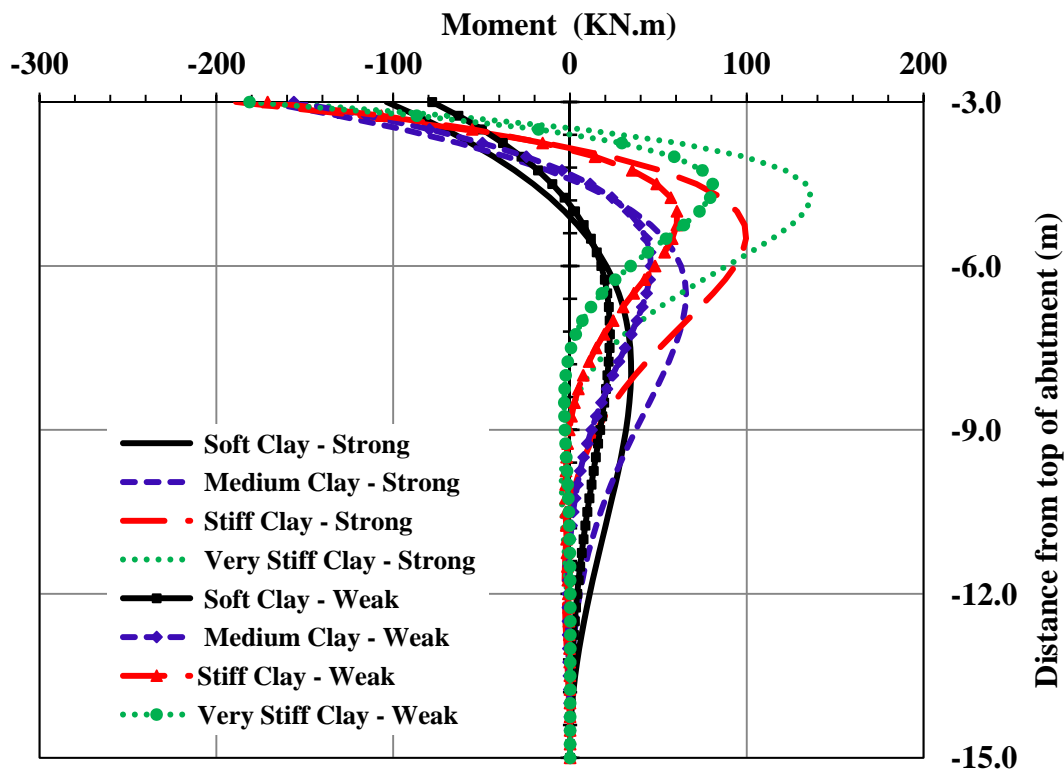


Figure 7.71 Moment (Expansion) along the Interior Pile
(90-m Bridge, Clay, 3m Abutment, HP360X152 Weak and Strong Orientation)

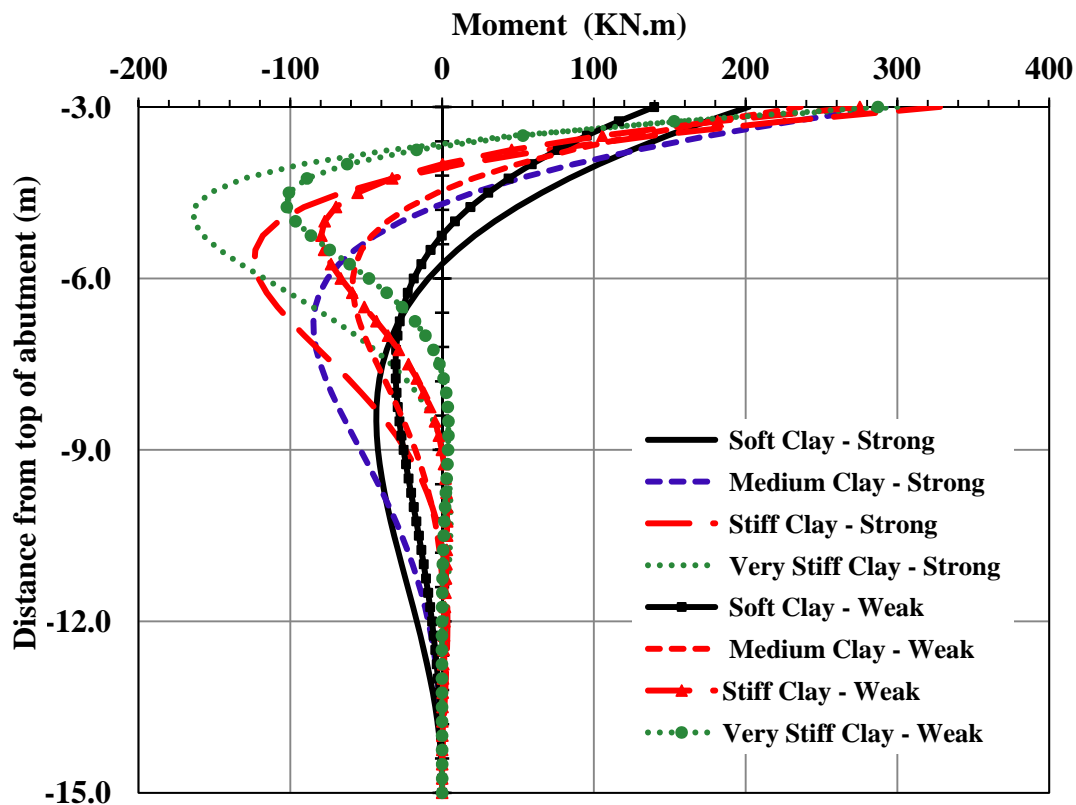


Figure 7.72 Moment (Contraction) along the Interior Pile
(90-m Bridge, Clay, 3m Abutment, HP360X152 Weak and Strong Orientation)

7.4.3 Effect of Pile Orientation on the Stresses in the Girders

The study showed that pile orientation has a negligible effect on the stresses in the girders as shown in figures 7.73 and 7.74.

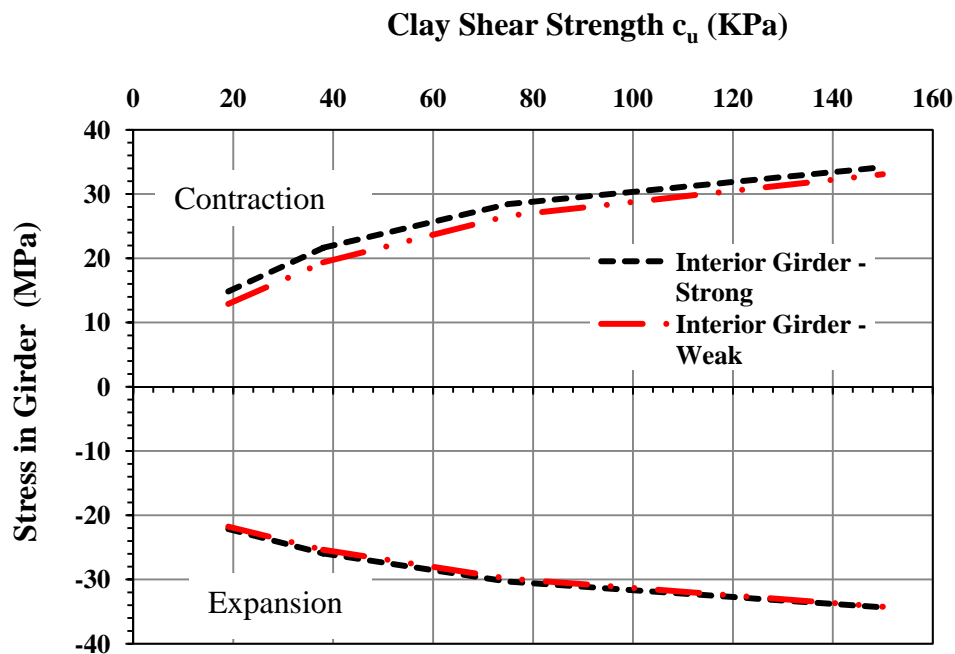


Figure 7.73 Stresses in the Interior Girder
(38-m Bridge, Clay, 3m Abutment, HP310X125 Weak and Strong Orientation)

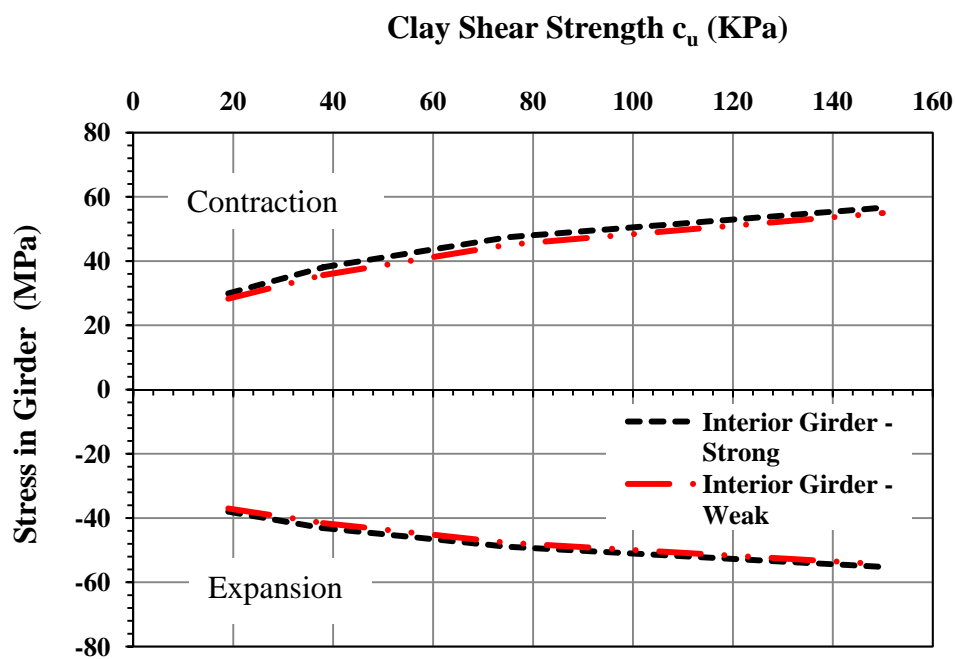


Figure 7.74 Stresses in the Interior Girder
(90-m Bridge, Clay, 3m Abutment, HP360X152 Weak and Strong Orientation)

7.4.4 Effect of Pile Orientation on the Backfill Pressure on the Abutment

The study showed that pile orientation has a negligible effect on the stresses on the girders as shown in figures 7.75 and 7.76.

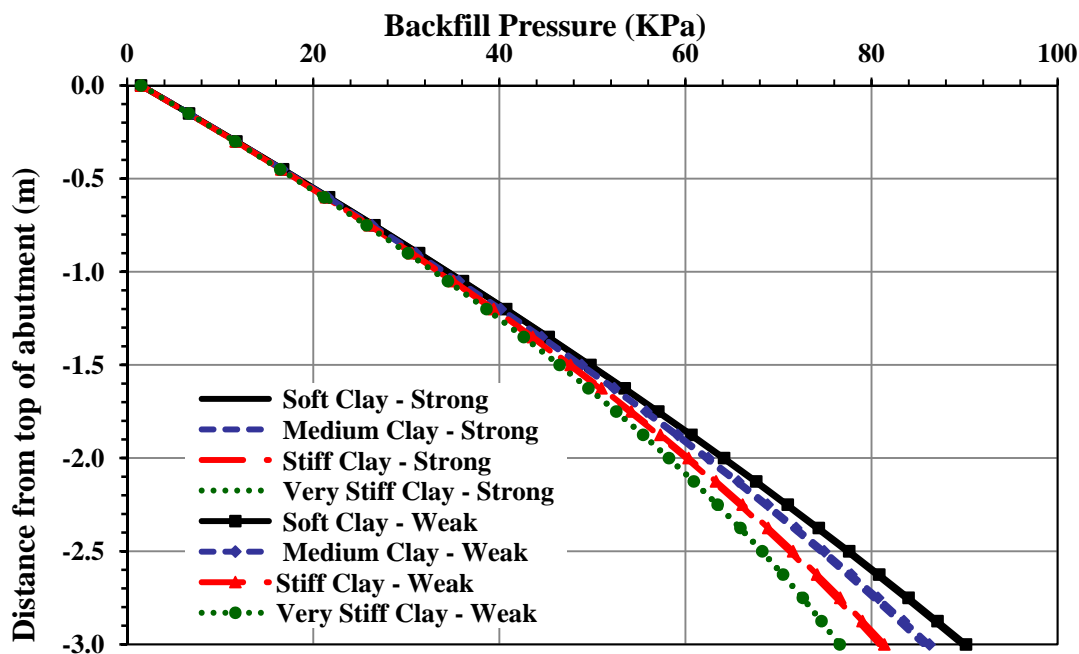


Figure 7.75 Backfill Pressure on the Abutment
(38-m Bridge, Clay, 3m Abutment, HP310X125 Weak and Strong Orientation)

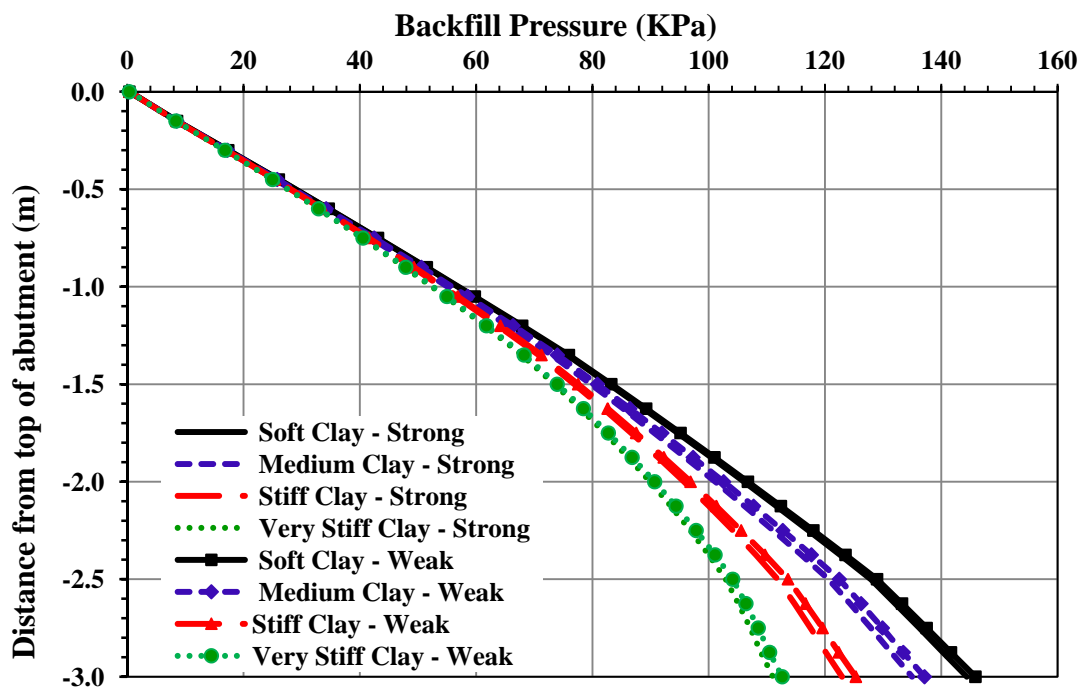


Figure 7.76 Backfill Pressure on the Abutment
(90-m Bridge, Clay, 3m Abutment, HP360X152 Weak and Strong Orientation)

7.5 EFFECT OF ABUTMENT HEIGHT

The study showed that abutment height has a significant effect on the performance of the substructure and negligible effect on the performance of the superstructure in IABs. The effect of the height of the abutment on the performance of IABs is presented in the following subsections.

7.5.1 Effect of Pile Orientation on the Displacement and the Rotation of the Abutment and the Piles

The study showed that abutment height has negligible effect on the displacement at the top of the abutment but has a significant effect on the displacement at the bottom of the abutment and the rotation at the top and bottom of the abutment. Figures 7.77 and 7.78 show the displacement at the top and bottom of the abutment during the short bridge expansion and contraction respectively.

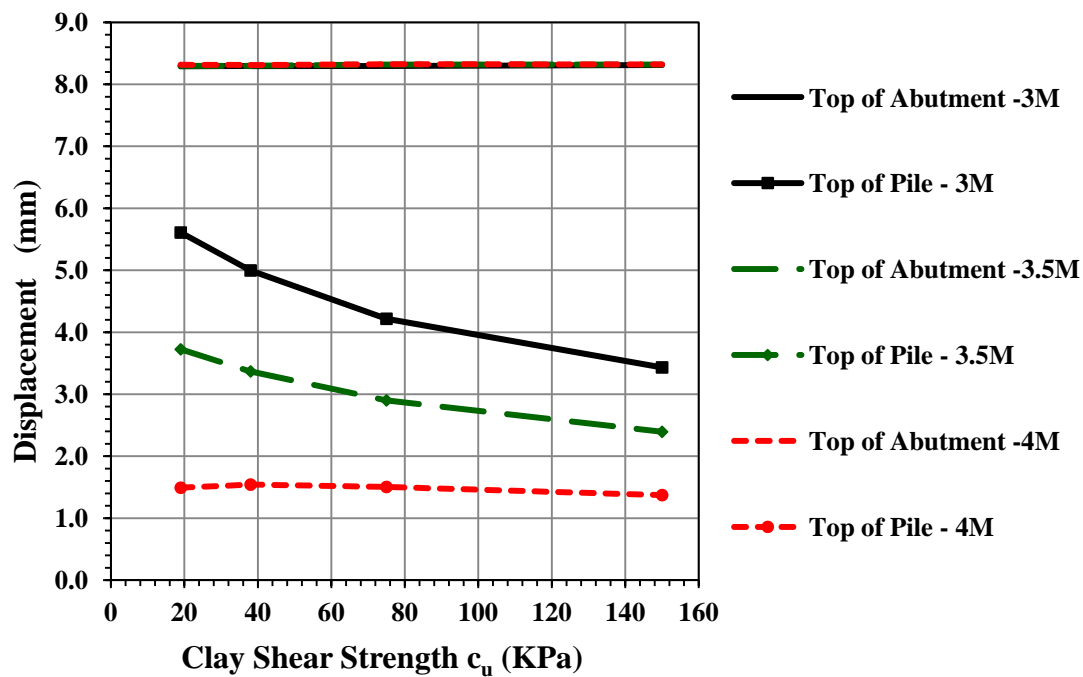


Figure 7.77 Displacement (Expansion) at Exterior Locations (38-m Bridge, Clay, Variable Abutment Height, HP310X125 Weak Orientation)

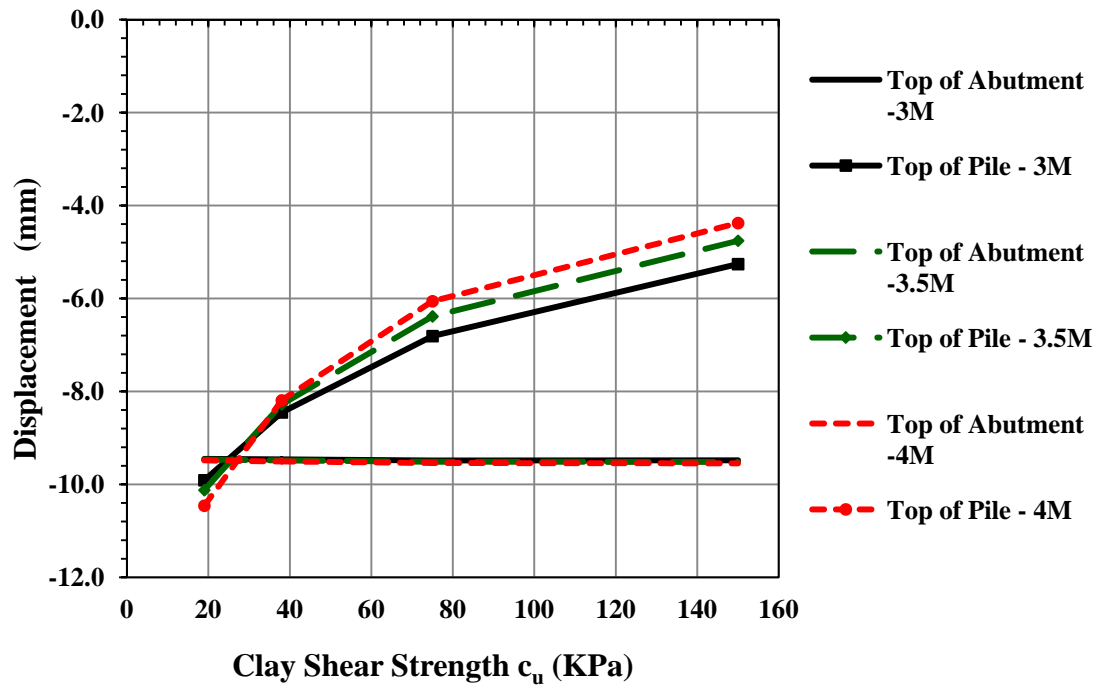


Figure 7.78 Displacement (Contraction) at the Exterior Location
(38-m Bridge, Clay, Variable Abutment Height, HP310X125 Weak Orientation)

Figure 7.77 shows that in the expansion case, the displacement at the top of the abutment is the same for different abutment heights. The displacement at the top of the pile had decreased by 30% and 85% when the abutment height increased by 0.5 meter and 1.0 meter respectively. Similar effect but in a smaller scale was noticed in the bridge contraction case. The displacement at the top of the pile decreased by 11% and 21% when the abutment height increased by 0.5 meter and 1.0 meter respectively as can be seen in figure 7.78. During bridge expansion, the effect of the soil stiffness on the abutment displacement becomes negligible when the abutment height reaches 4 meters as can be seen in figure 7.77.

Figures 7.79 and 7.80 show that the rotation at the top and bottom of the abutment during the short bridge expansion and contraction respectively. The figures show that the

abutment height has a significant effect on the abutment rotation during bridge expansion.

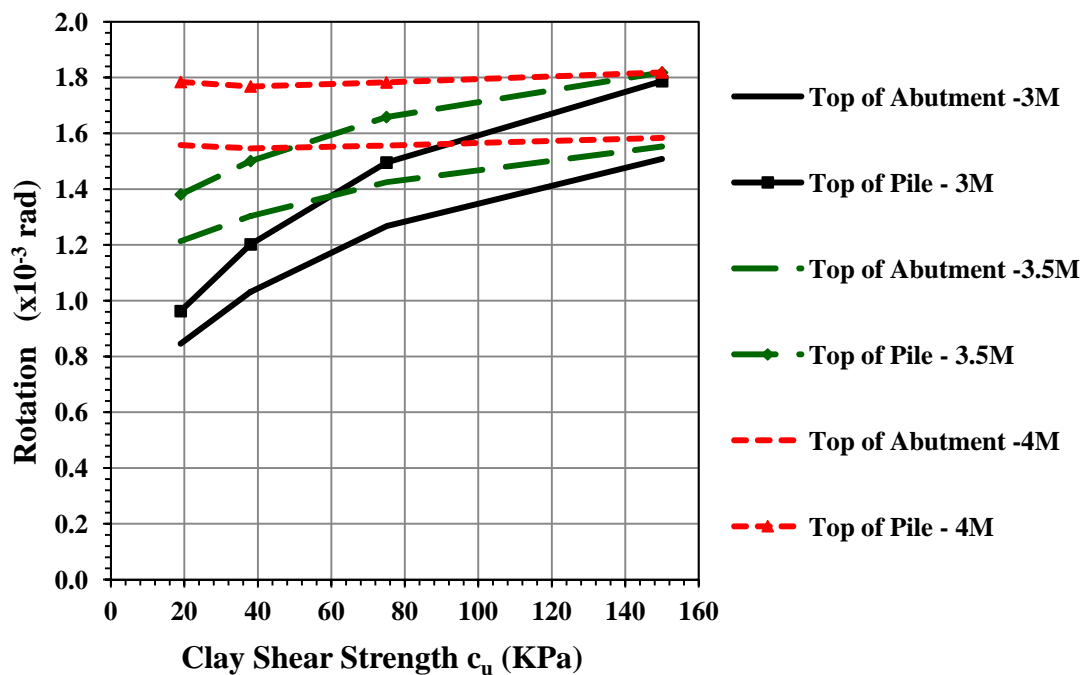


Figure 7.79 Rotation (Expansion) at the Exterior Location
(38-m Bridge, Clay, Variable Abutment Height, HP310X125 Weak Orientation)

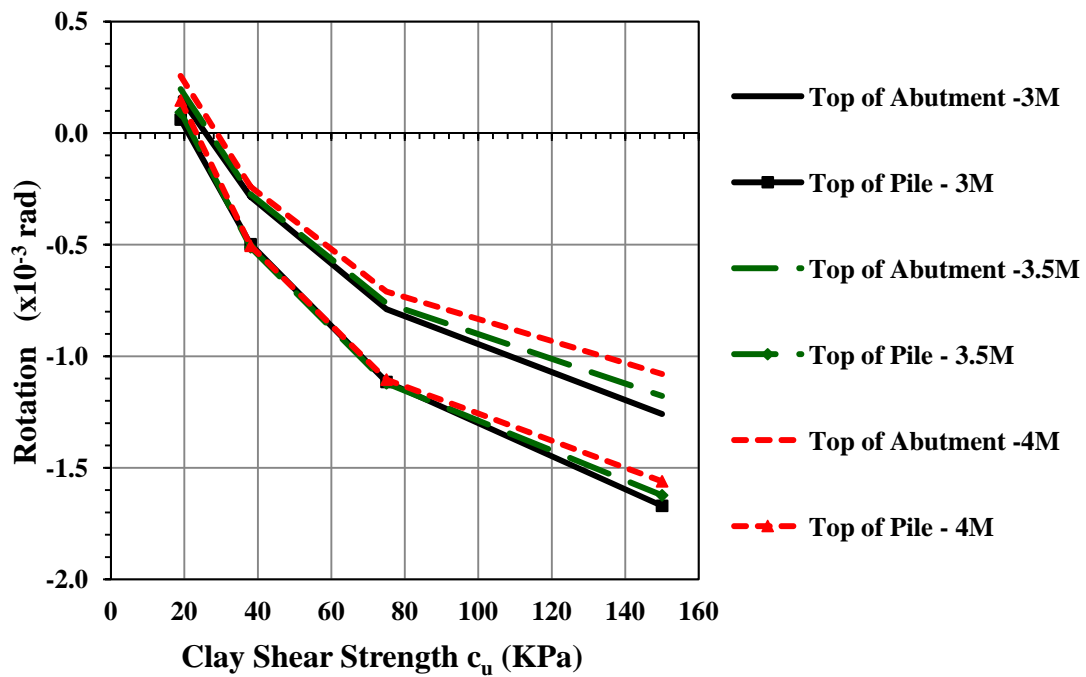


Figure 7.80 Rotation (Contraction) at the Exterior Location
(38-m Bridge, Clay, Variable Abutment Height, HP310X125 Weak Orientation)

Figures 7.81 and 7.82 show the displacement and rotation respectively along the abutment and the pile at interior locations during bridge expansion.

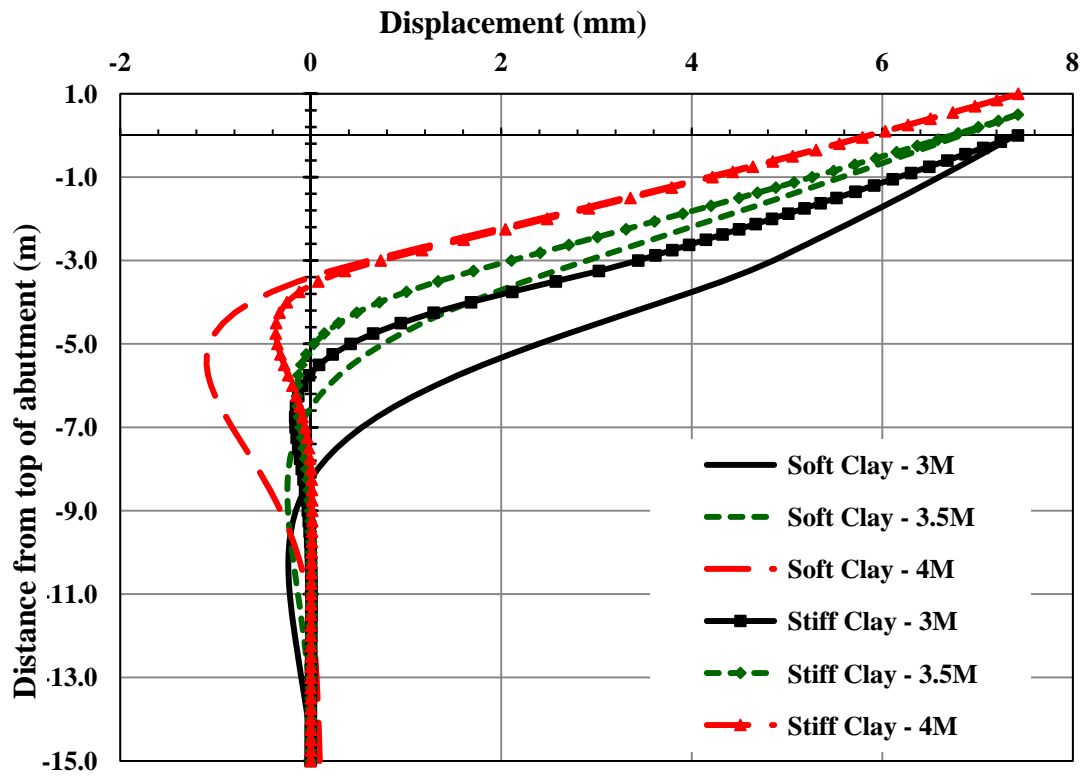


Figure 7.81 Displacement (Expansion) along the Abutment and the Interior Pile (38-m Bridge, Clay, Variable Abutment Height, HP310X125 Weak Orientation)

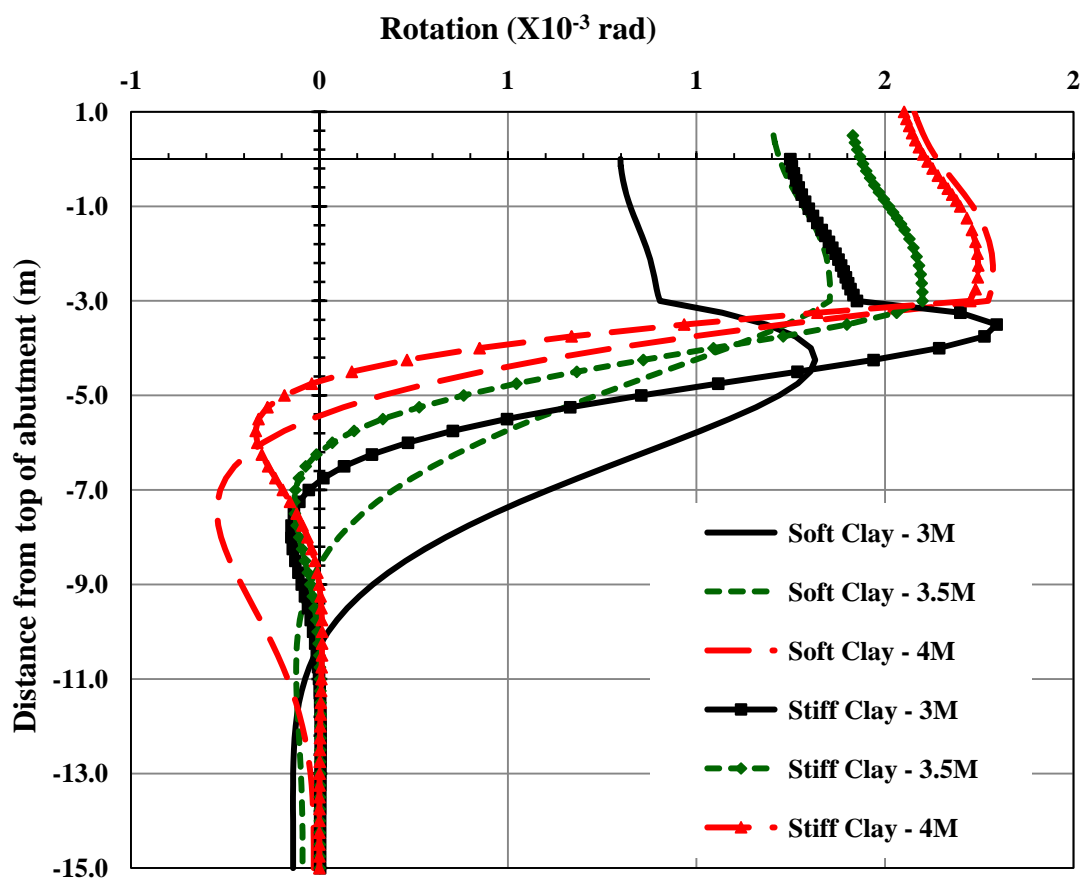


Figure 7.82 Rotation (Expansion) along the Abutment and the Interior Pile (38-m Bridge, Clay, Variable Abutment Height, HP310X125 Weak Orientation)

7.5.2 Effect of Pile Orientation on the Moment along the Piles

The study showed that abutment height has a significant effect on the moment along the pile especially during bridge expansion. The effect of the abutment height increases with the increase in soil stiffness. Figure 7.83 shows the pile top moment during bridge expansion and contraction and figure 7.84 shows the moment along the interior pile for the bridge expansion case.

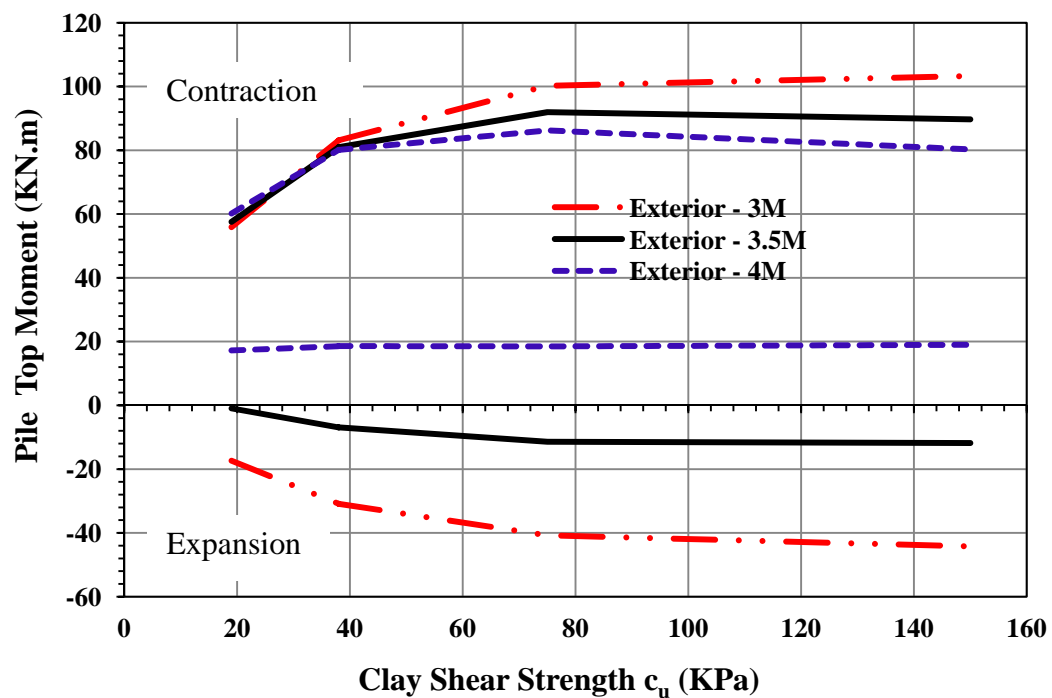


Figure 7.83 Moment at the Top of the Interior Pile
(38-m Bridge, Clay, Variable Abutment Height, HP310X125 Weak Orientation)

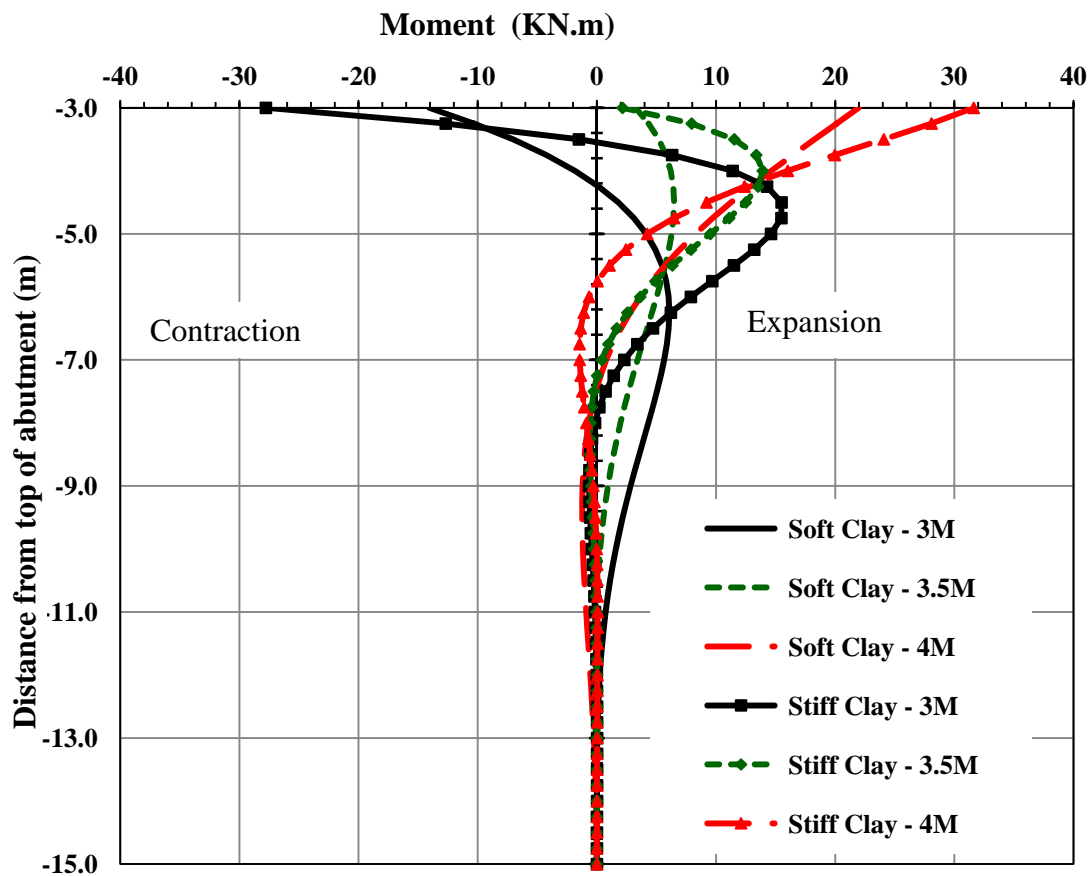


Figure 7.84 Moment (Expansion) along the Interior Pile
(38-m Bridge, Clay, Variable Abutment Height, HP310X125 Weak Orientation)

7.5.3 Effect of Pile Orientation on the Stresses in the Girders

The study showed that the abutment height has a negligible effect on the stresses in the interior and exterior girders during bridge contraction and has a noticeable effect on the stresses in the interior and exterior girders during bridge expansion as shown in figure 7.85. The effect of abutment height during bridge expansion becomes negligible in stiff soils.

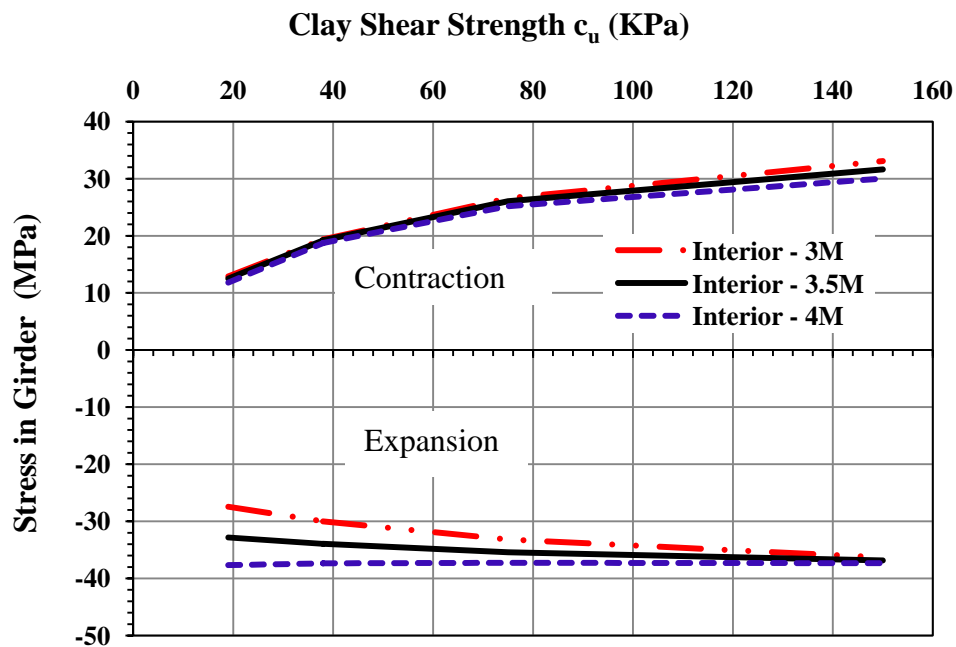


Figure 7.85 Stresses in the Girders
(38-m Bridge, Clay, Variable Abutment Height, HP310X125 Weak Orientation)

7.5.4 Effect of Pile Orientation on the Backfill Pressure on the Abutment

The study showed that the abutment height increase from 3 meters to 4 meters has a negligible effect on maximum backfill pressure experienced by the abutment as shown in figure 7.86.

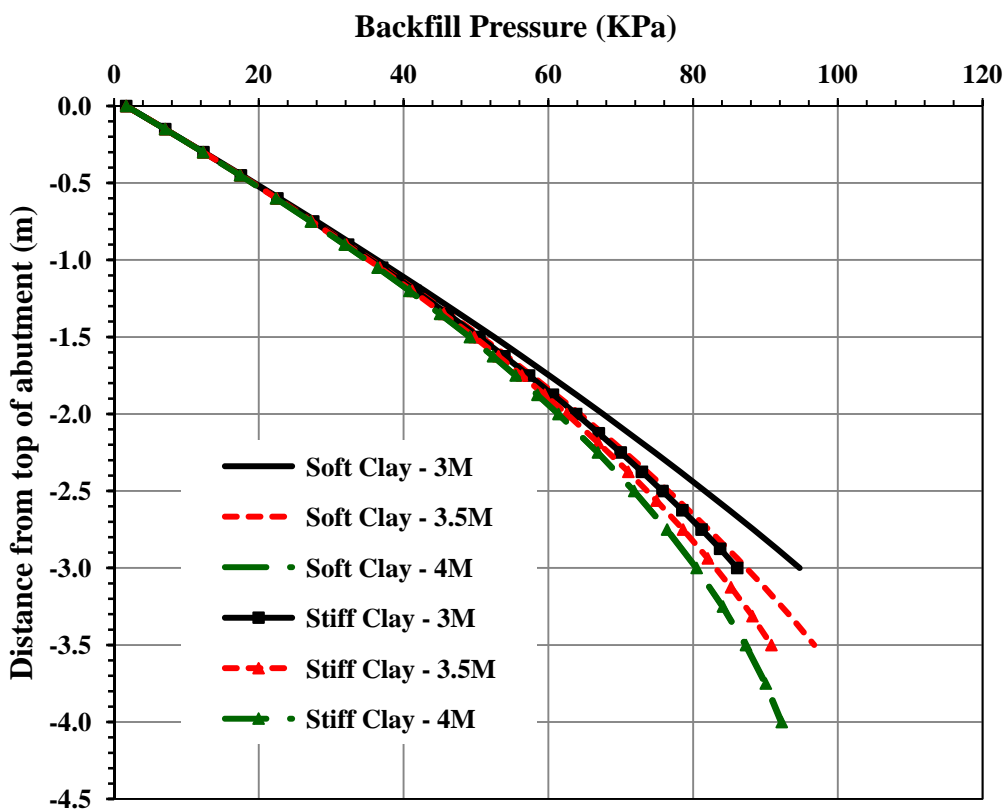


Figure 7.86 Backfill Pressure on the Abutment
(38-m Bridge, Clay, Variable Abutment Height, HP310X125 Weak Orientation)

7.6 EFFECT OF PILE TYPE (Prestressed Concrete Piles Versus Steel H-Piles)

The study showed that the behavior of short IABs supported by Steel H-Piles and Prestressed Concrete Piles (PCP) are similar and the pile type has a negligible effect on the performance of short IABs. The effect of pile type on the performance of IABs is presented in the following subsections.

7.6.1 Effect of Pile Type on the Displacement and the Rotation of the Abutment and the Piles

The study showed that pile type has negligible effect on the displacement and rotation at the top of the abutment and at the top of the piles during bridge expansion as shown in figure 7.87 which shows the displacement at the top of the abutment and the top of the pile (bottom of the abutment) during short bridge expansion. The effect is more noticeable during bridge contraction as shown in figure 7.88 which shows the displacement at the top of the abutment and at the top of the pile during short bridge contraction.

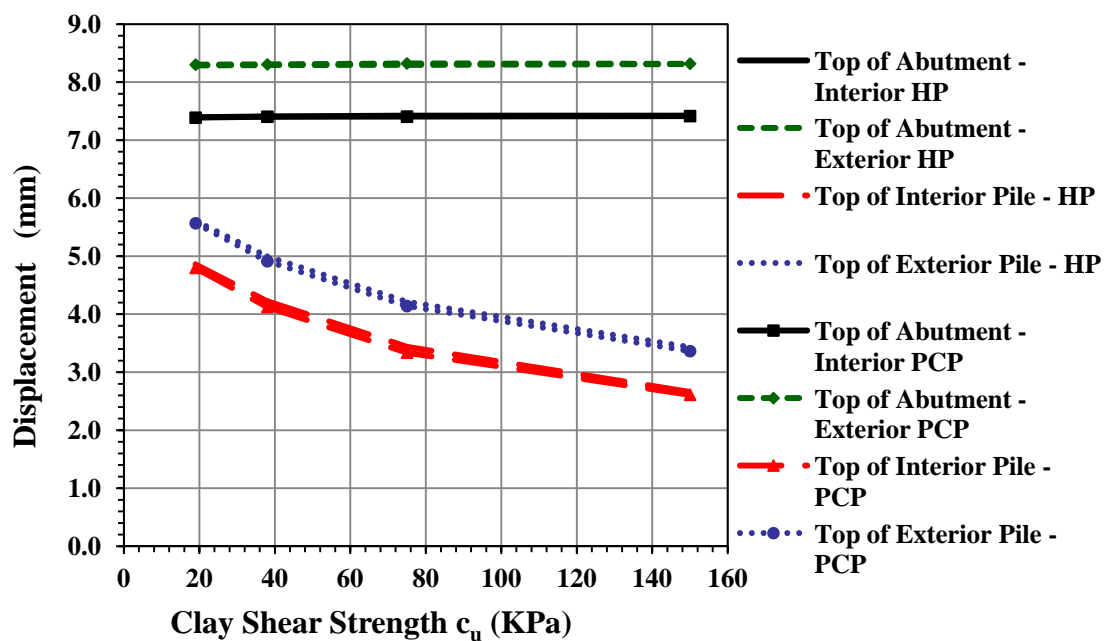


Figure 7.87 Displacement (Expansion) at Interior and Exterior Locations (38-m Bridge, Clay, 3m Abutment, PCP 356X356 versus HP310X125 Weak Orientation)

Figure 7.88 shows a slight decrease in the displacement at the top of interior and exterior pile when PC piles are used.

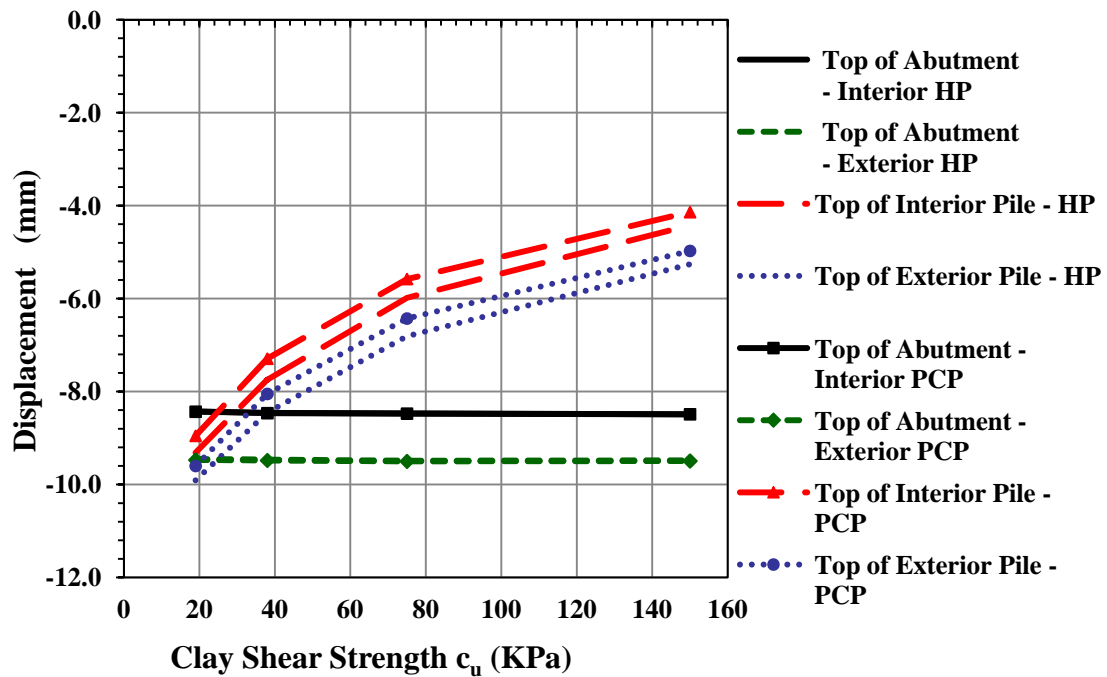


Figure 7.88 Displacement (Contraction) at Interior and Exterior Locations (38-m Bridge, Clay, 3m Abutment, PCP 356X356 versus HP310X125 Weak Orientation)

Figures 7.89 and 7.90 show the rotation at the top of the abutment and at the top of the piles during the short bridge expansion and contraction respectively. The figures show that the abutment and pile rotation is slightly higher when PCPs are used to support the bridge especially during bridge contraction.

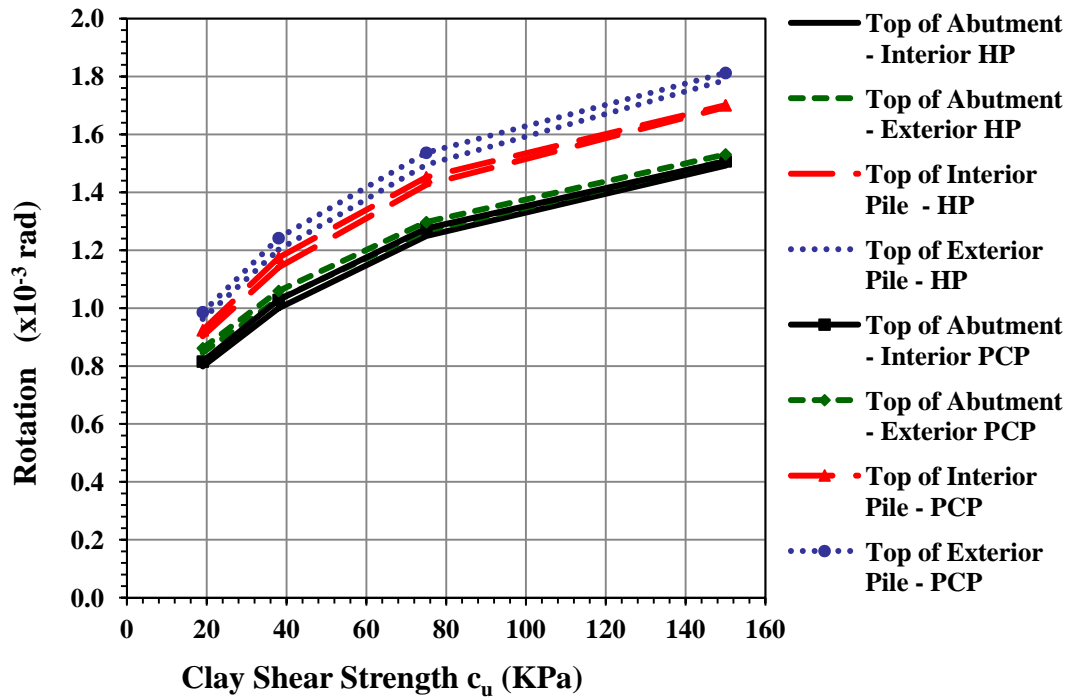


Figure 7.89 Rotation (Expansion) at Interior and Exterior Locations
(38-m Bridge, Clay, 3m Abutment, PCP 356X356 versus HP310X125 Weak Orientation)

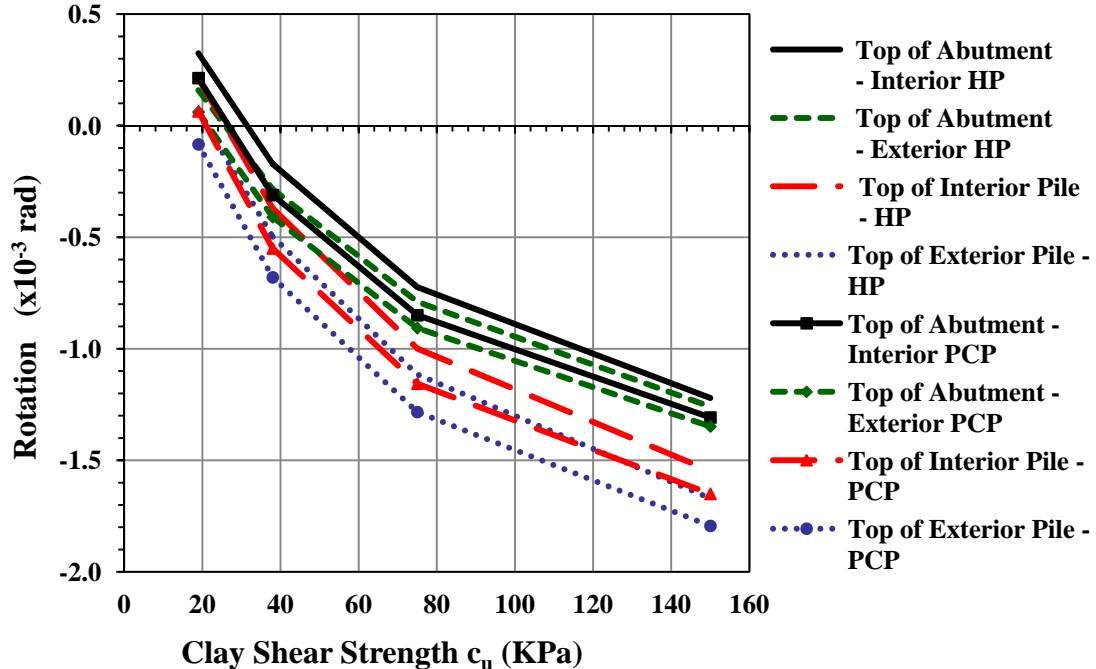


Figure 7.90 Rotation (Contraction) at Interior and Exterior Locations
(38-m Bridge, Clay, 3m Abutment, PCP 356X356 versus HP310X125 Weak Orientation)

Figures 7.91 and 7.92 show the displacement and rotation respectively along the abutment and the pile at interior locations during bridge contraction.

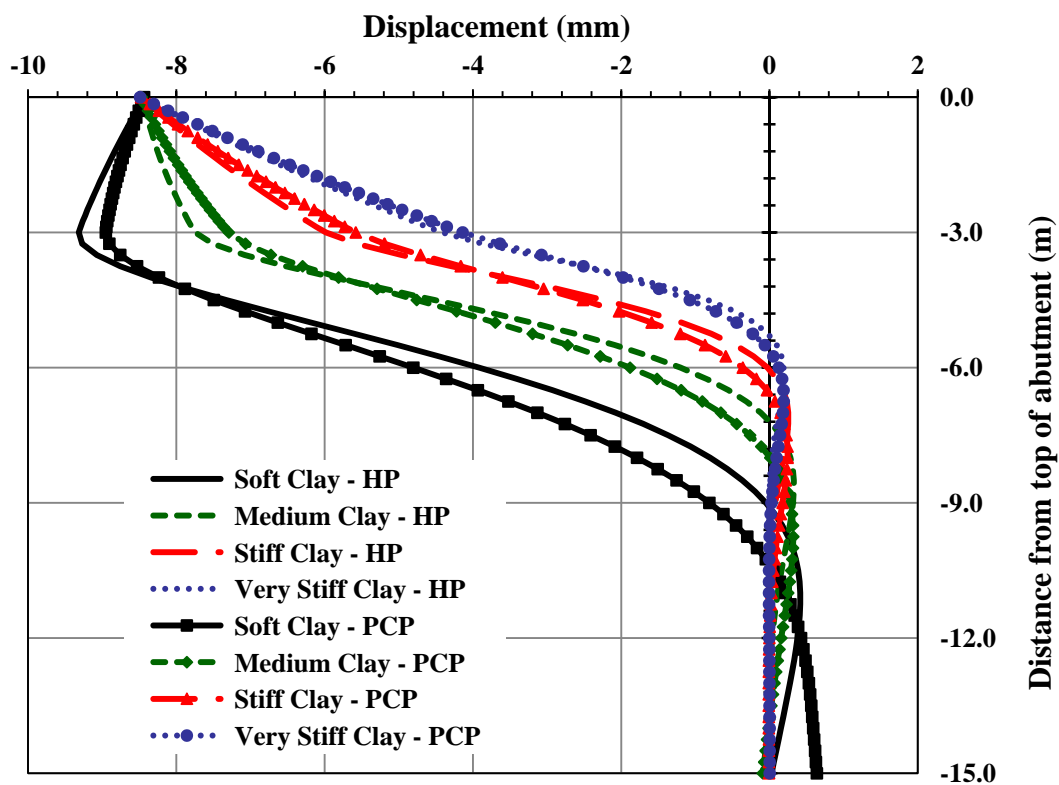


Figure 7.91 Displacement (Contraction) along the Abutment and the Interior Pile (38-m Bridge, Clay, 3m Abutment, PCP 356X356 versus HP310X125 Weak Orientation)

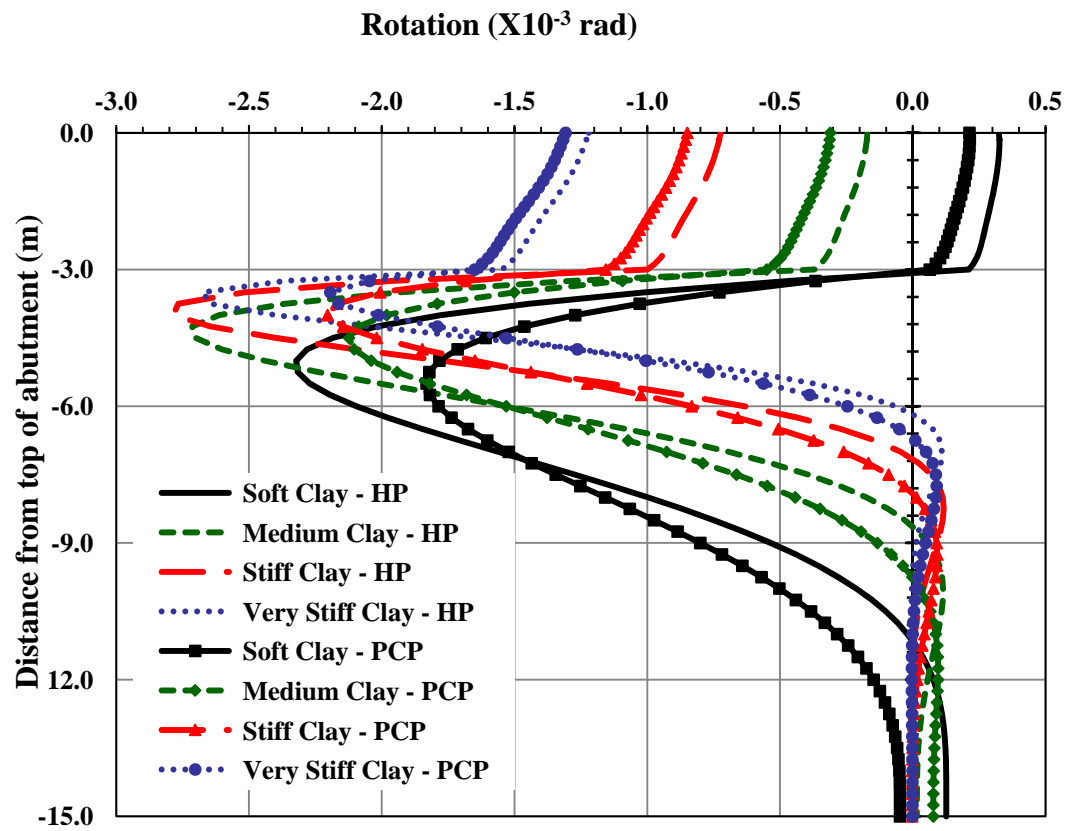


Figure 7.92 Rotation (Contraction) along the Abutment and the Interior Pile
(38-m Bridge, Clay, 3m Abutment, PCP 356X356 versus HP310X125 Weak Orientation)

7.6.2 Effect of Pile Type on the Moment along the Piles

The study showed that pile type has a noticeable effect on the moment along the pile especially during bridge contraction. Figure 7.93 shows the pile top moment during bridge expansion and contraction. Figures 7.94 and 7.95 show the moment along the interior pile during bridge expansion and contraction respectively.

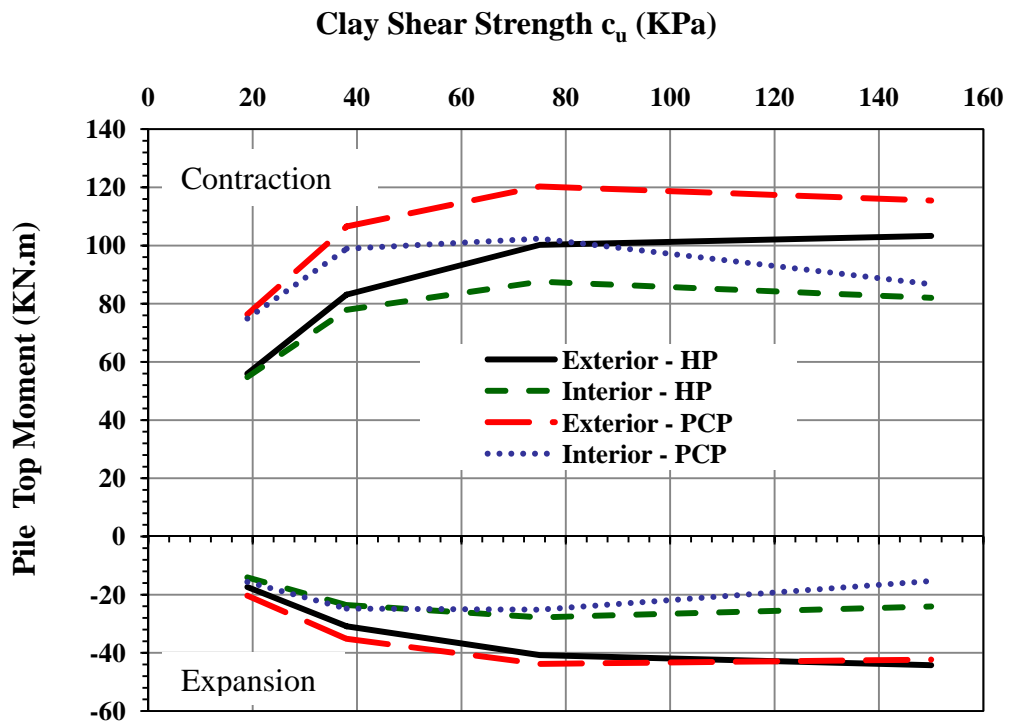


Figure 7.93 Moment at the top of the Interior Pile
(38-m Bridge, Clay, 3m Abutment, PCP 356X356 versus HP310X125 Weak Orientation)

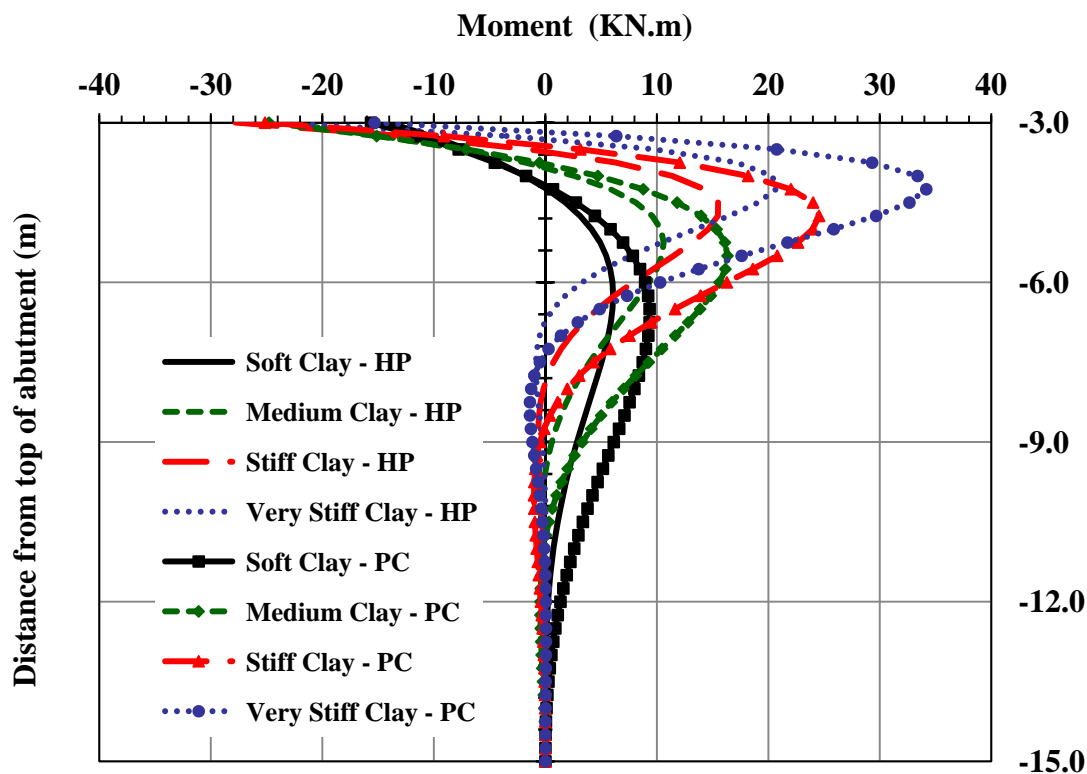


Figure 7.94 Moment (Expansion) along the Interior Pile
(38-m Bridge, Clay, 3m Abutment, PCP 356X356 versus HP310X125 Weak Orientation)

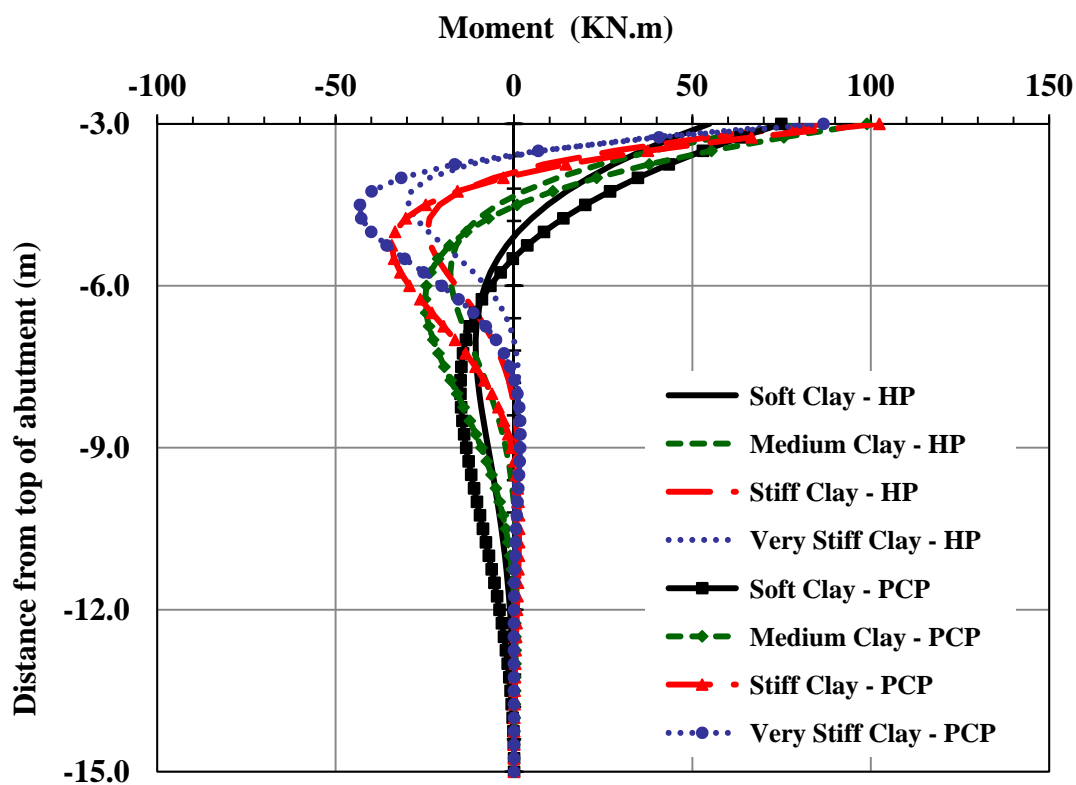


Figure 7.95 Moment (Contraction) along the Interior Pile
(38-m Bridge, Clay, 3m Abutment, PCP 356X356 versus HP310X125 Weak Orientation)

7.6.3 Effect of Pile Type on the stresses in the girders

The study showed that pile type has a negligible effect on the stresses in the interior and exterior girders as shown in figure 7.96.

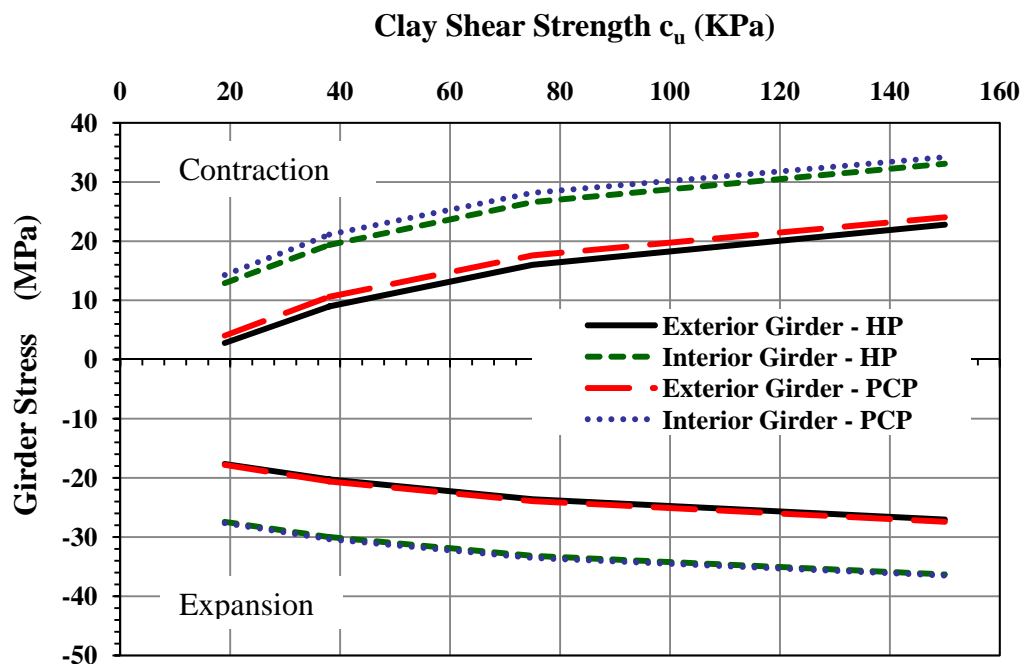


Figure 7.96 Stresses in the Girders
(38-m Bridge, Clay, 3m Abutment, PCP 356X356 versus HP310X125 Weak Orientation)

7.6.4 Effect of Pile Type on the Backfill Pressure on the Abutment

The study showed that pile type has a negligible effect on the backfill pressure on the abutment as shown in figure 7.97.

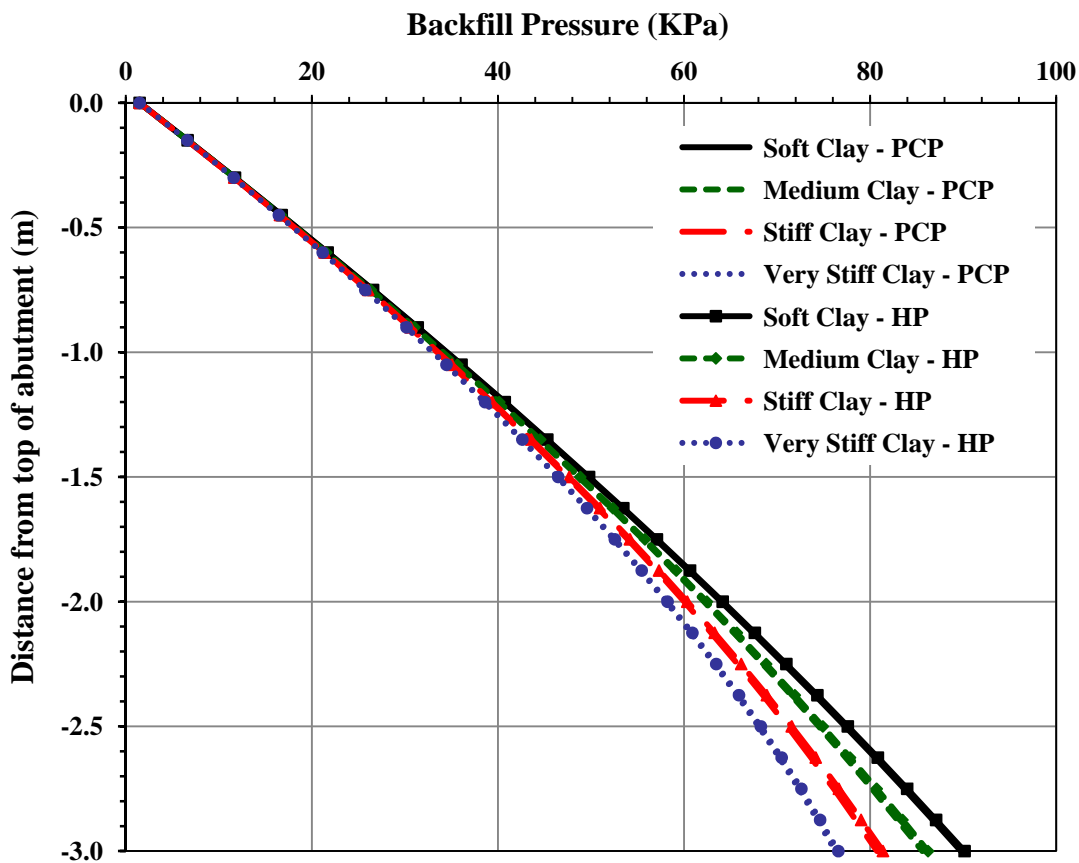


Figure 7.97 Backfill Pressure on the Abutment
(38-m Bridge, Clay, 3m Abutment, PCP 356X356 versus HP310X125 Weak Orientation)

CHAPTER 8

ANALYSIS OF INTEGRAL ABUTMENT BRIDGES

8.1 GENERAL

This chapter presents simple analytical tools to help bridge engineers in the analysis and design of IABs. First, simple equations and charts will be introduced to estimate the displacement and rotation at the top of the abutment and at the top of the pile (bottom of the abutment) at interior and exterior locations. The next section presents a comparison between the analysis results obtained from the 3D FE models to those obtained from the 2D FE models. The comparison will focus on the displacement and rotation along the abutment and the piles at interior and exterior locations. The comparison will be presented in the form of graphs and tables. Additional graphs comparing the moment along the pile from the 3D and 2D models are presented in appendix A.

After the comparison, simple equations, base on the work of Girton et al. (1989), will be presented to calculate the equivalent pile length. The equivalent pile length for all the steel H-Piles are tabulated for strong axis and weak axis orientations.

Finally, the equations that were developed by Albhaisi (2003) to calculate the ultimate displacement capacity for steel H-Piles and the relative displacement of the abutment in both cohesive and cohesionless soils when the pile reaches its ultimate displacement capacity will be presented for reference. These equations were verified in a previous research by Albhaisi (2003).

8.2 SUBSTRUCTURE DISPLACEMENT

The total displacement of the bridge, Δ_B , can be divided into two main displacements. Those are the displacement of the pile, Δ_P , and displacement of the abutment, Δ_A , which is the displacement of the top of the abutment relative to the top of the pile (bottom of the abutment). Both displacements are shown in figure 8.1. The parametric study results showed that, the movement of the abutment can be approximated by rigid body movement as shown in figure 8.1.

Thus, the total bridge displacement, Δ_B , of the bridge deck is expressed as:

$$\Delta_B = \Delta_P + \Delta_A \quad (8.1)$$

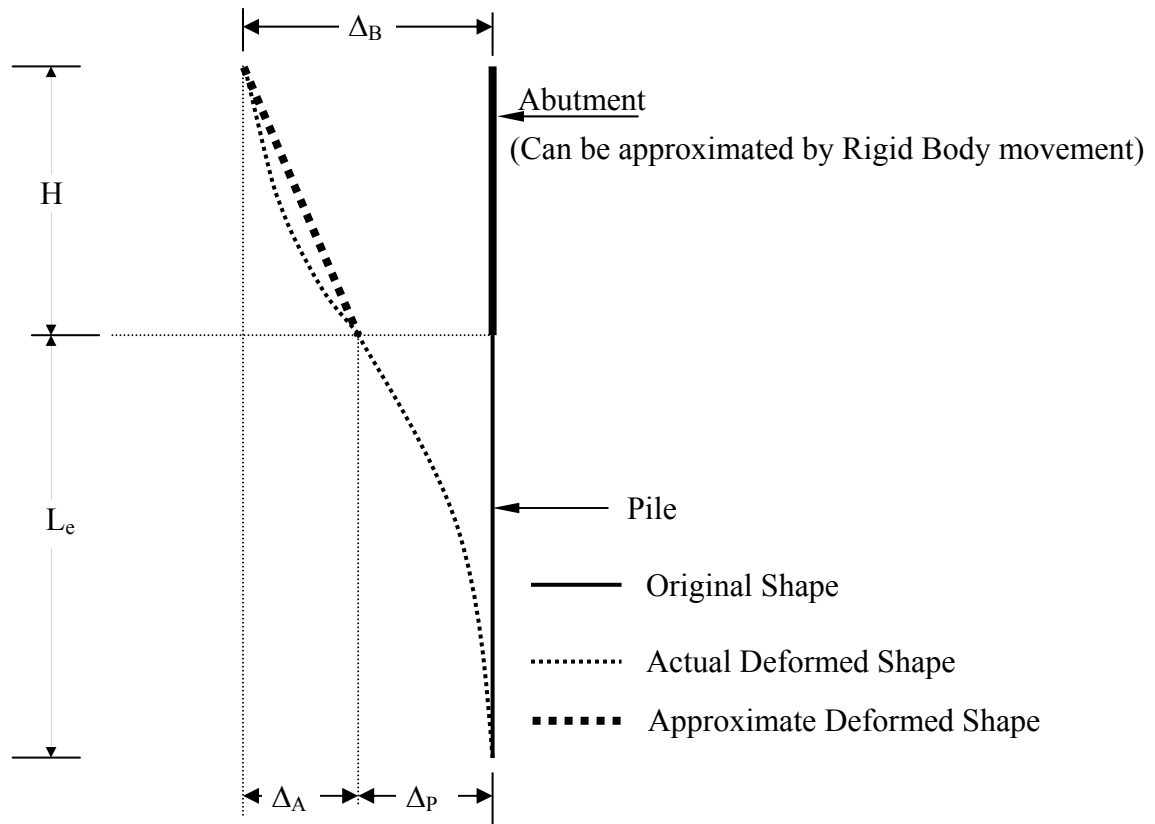


Figure.8.1 Deformed Shape of the Abutment and the Pile

It was noticed throughout the study that the total displacement of the bridge Δ_B is not sensitive to the stiffness of the substructure for both the contraction and expansion cases. It was noticed that for both the expansion and contraction cases, the bridge exterior displacement, Δ_{Bex} , is almost equal to the thermal displacement demand of the bridge and it can be expressed as:

$$\Delta_{Bex} = \alpha.L.\Delta T \quad (8.2)$$

Where, α , is the thermal expansion coefficient for structural steel (Girders).

It was also noticed that for both the expansion and contraction cases, the bridge interior displacement Δ_{Bin} is less than the thermal displacement demand of the bridge and it can be expressed as:

$$\Delta_{Bin} = m.\alpha.L.\Delta T \quad (8.3)$$

Where m is a factor ≤ 1.0

Throughout the study the interior displacement was noticed to be about 10% less than thermal displacement demand of the bridge and therefore the value of m is taken as 0.9.

Values close to 0.85 can be assumed for expansion of long bridges very stiff soils.

Equation 8.3 can be rewritten as:

$$\Delta_{Bin} = 0.9\alpha.L.\Delta T \quad (8.4)$$

On the other hand, the displacement of the pile, Δ_p , and relative displacement of the abutment, Δ_A , are sensitive to the stiffness of the substructure. The pile displacement decreases when the stiffness of the foundation soil increases. The pile displacement is almost equal to the total displacement of the bridge when the bridge is under contraction in soft clay or loose sand as can be seen in figures 7.1 and 7.5 respectively.

The summation of the ratio of the relative displacement of the abutment to the total displacement of the bridge and the ratio of the displacement of the pile to the total displacement of the bridge equals unity, or:

$$\frac{\Delta_A}{\Delta_B} + \frac{\Delta_P}{\Delta_B} = 1 \quad (8.5)$$

Figure 8.2 shows the ratio of the relative displacement of the abutment and displacement of the pile to the total displacement of the bridge in clay during bridge contraction.

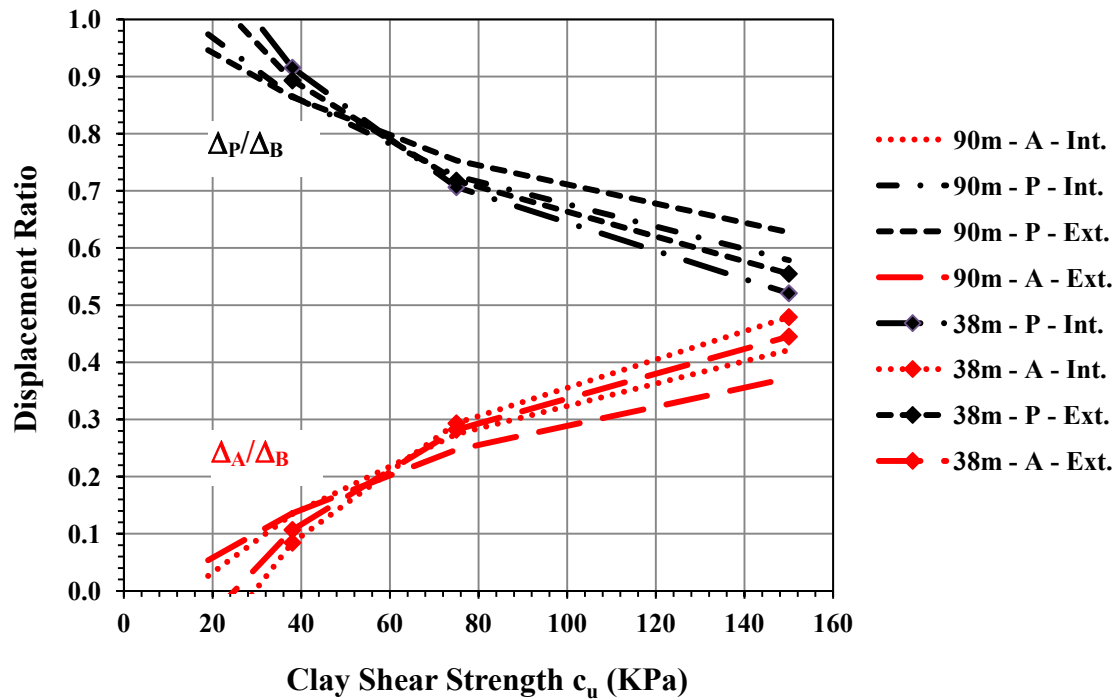


Figure 8.2 Substructure Displacement Ratios (Weak, Contraction, Clay)

Figure 8.2 can be utilized to estimate the relative displacement of the abutment and the displacement of the pile during bridge contraction for various bridge lengths. The figure shows that during bridge contraction, the stiffness of the clay is the dominant factor in determining the displacement ratios for the abutment and the pile.

In the graphs the letters A and P refers to the locations at the top of Abutment and at the top of the pile respectively.

Figure 8.3 shows the ratios of the relative displacement of the abutment and displacement of the pile to the total displacement of the bridge in clay during expansion.

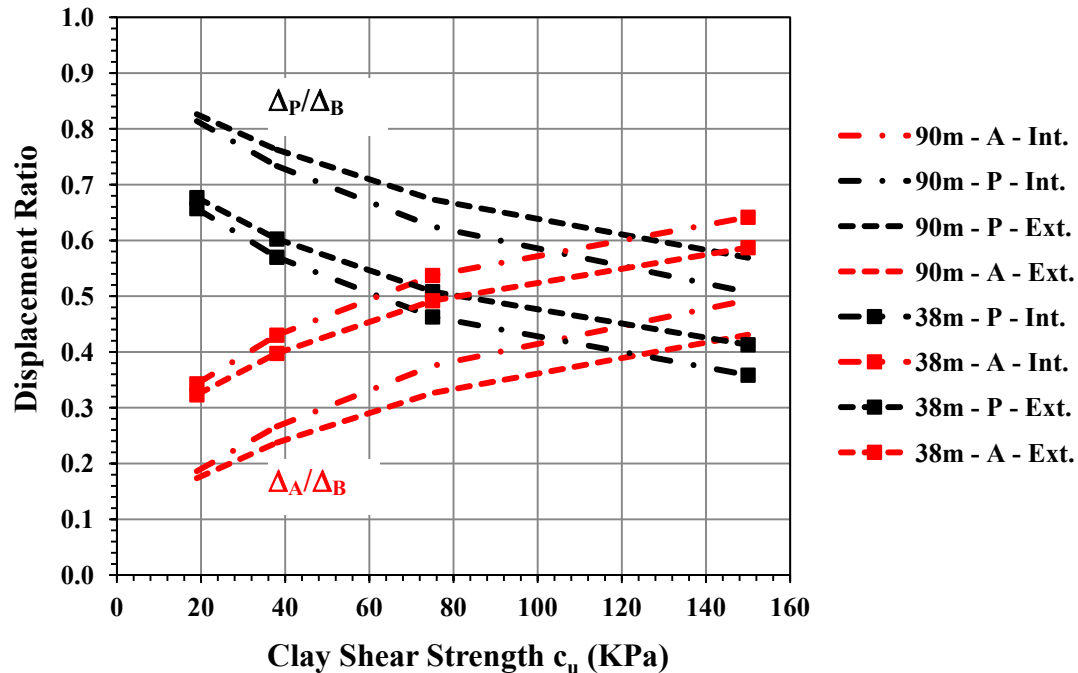


Figure 8.3 Substructure Displacement Ratios (Weak, Expansion, Clay)

Figure 8.3 can be utilized to estimate the relative displacement of the abutment and the displacement of the pile during bridge expansion for various bridge lengths. The figure shows that during bridge expansion, although the stiffness of the clay is the dominant factor in determining the displacement ratios for the abutment and the pile, other factors also contribute in determining these ratios.

Figures 8.4 and 8.5 show the ratios of the relative displacement of the abutment and displacement of the pile to the total displacement of the bridge in sand during bridge

contraction and expansion respectively. Similar observations were noticed in the sand case for both contraction and expansion.

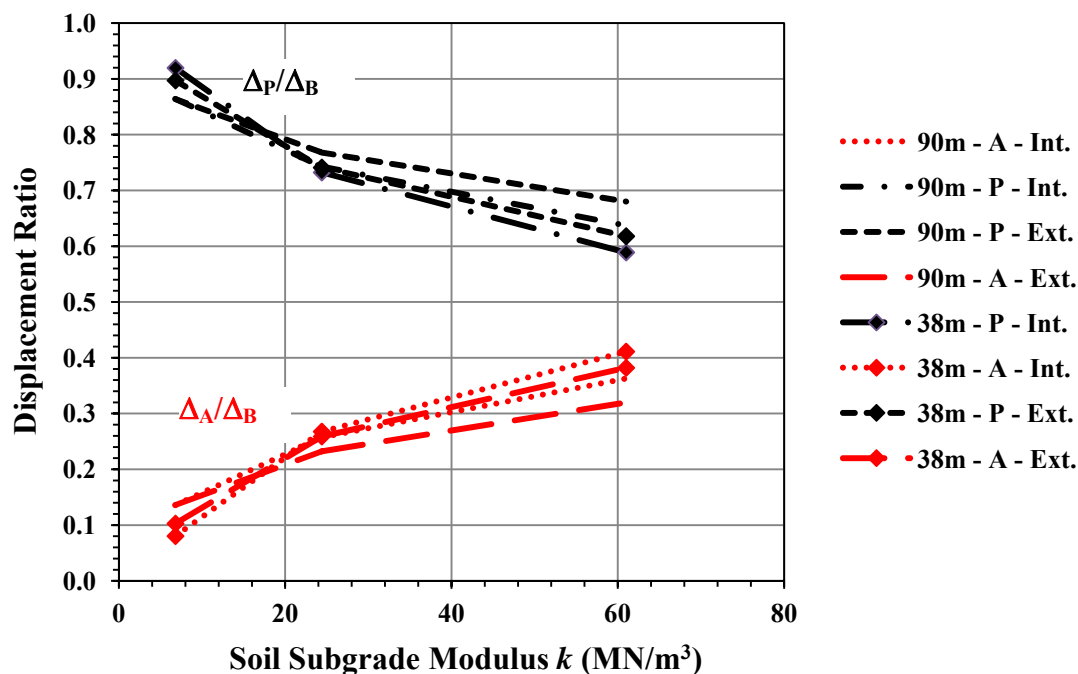


Figure 8.4 Substructure Displacement Ratios (Weak, Contraction, Sand)

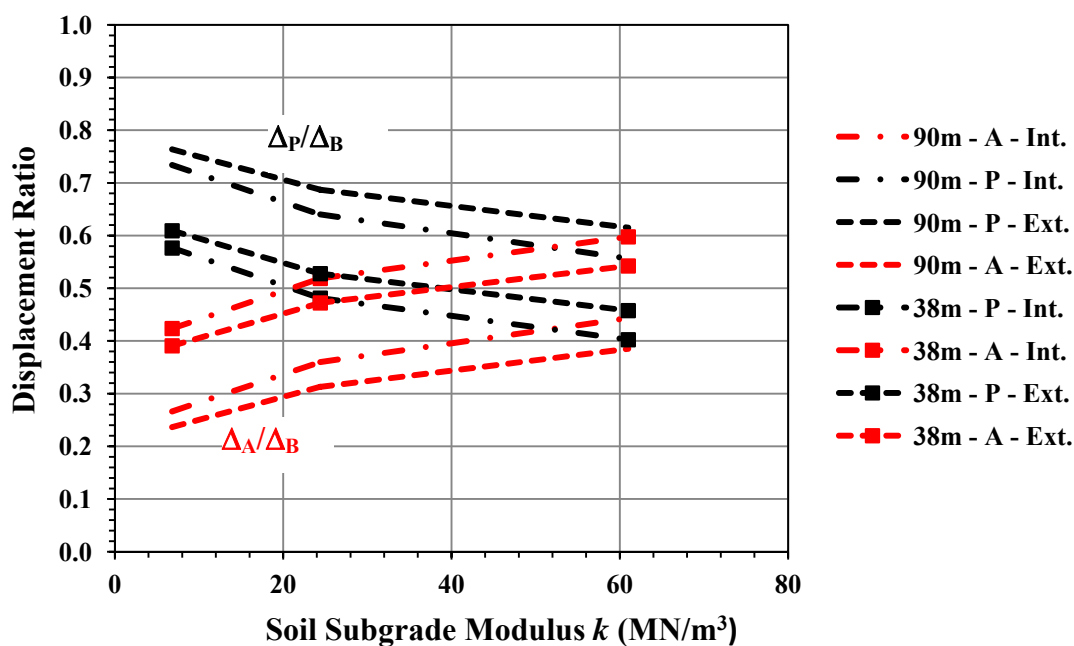


Figure 8.5 Substructure Displacement Ratios (Weak, Expansion, Sand)

Figures 8.6 through 8.9 show the substructure displacement ratio for the cases where the piles are oriented to bend around the strong axis.

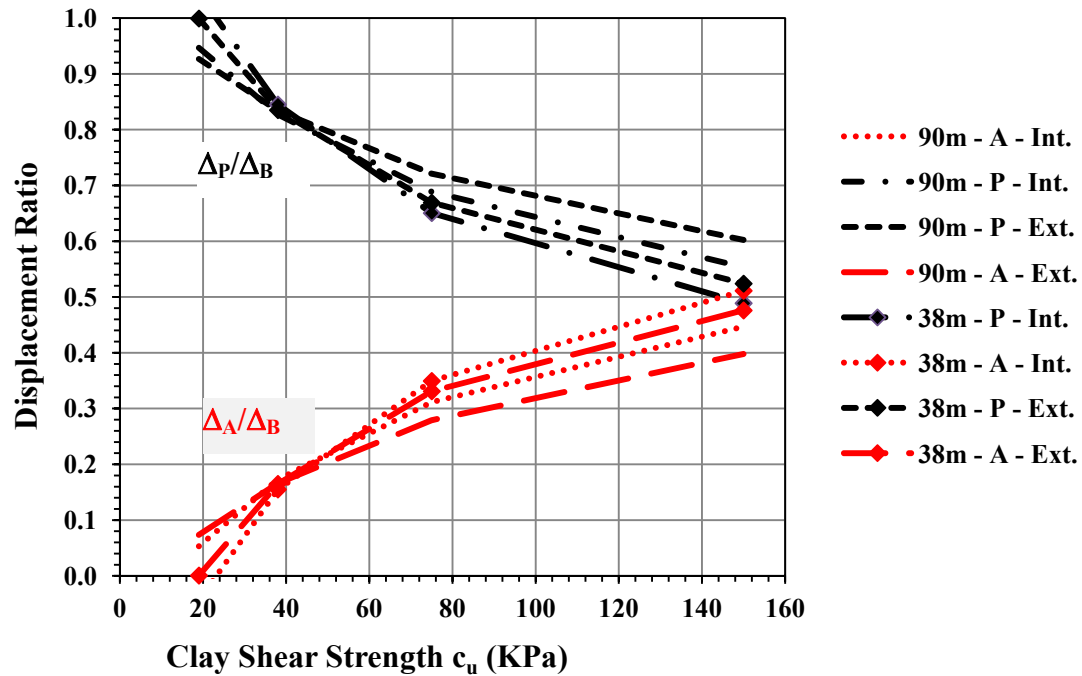


Figure 8.6 Substructure Displacement Ratios (Strong, Contraction, Clay)

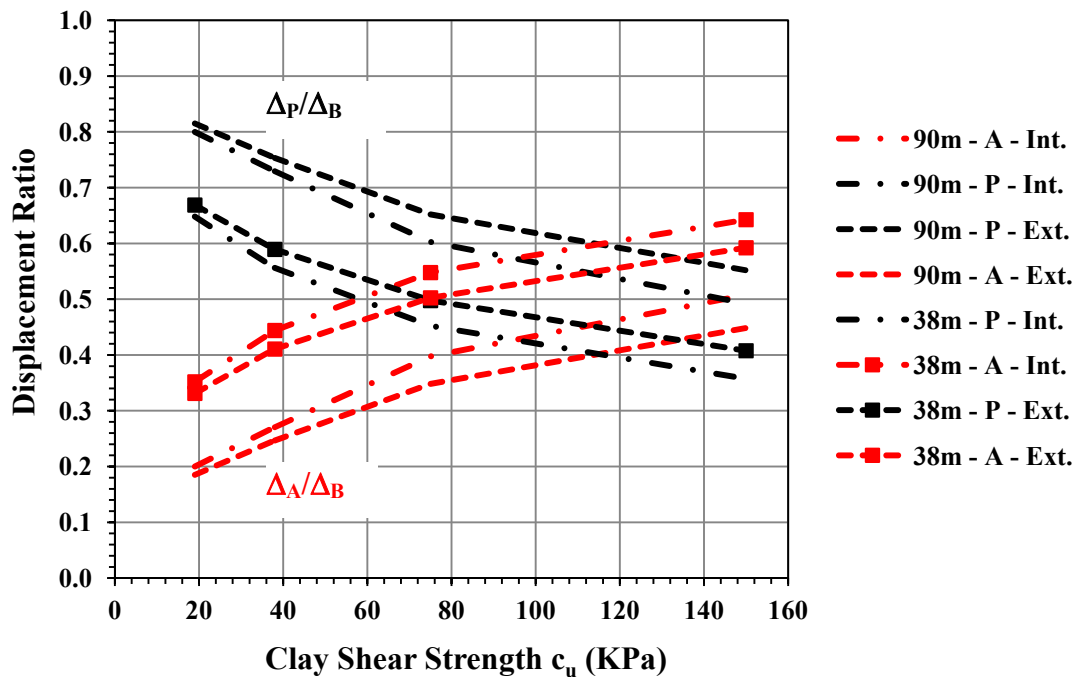


Figure 8.7 Substructure Displacement Ratios (Strong, Expansion, Clay)

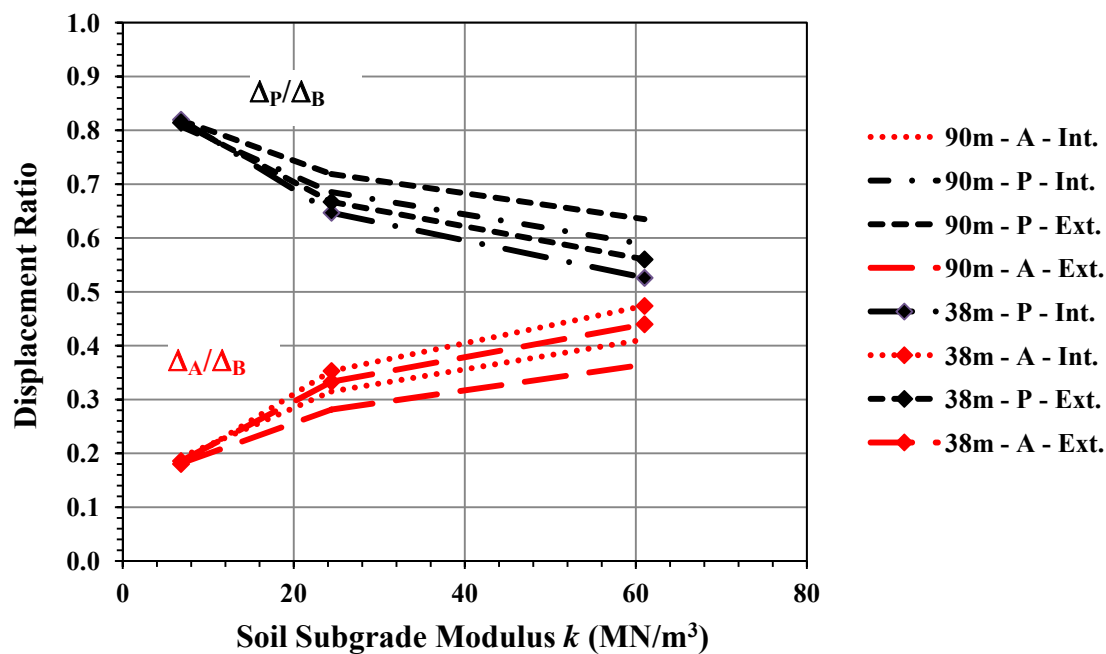


Figure 8.8 Substructure Displacement Ratios (Strong, Contraction, Sand)

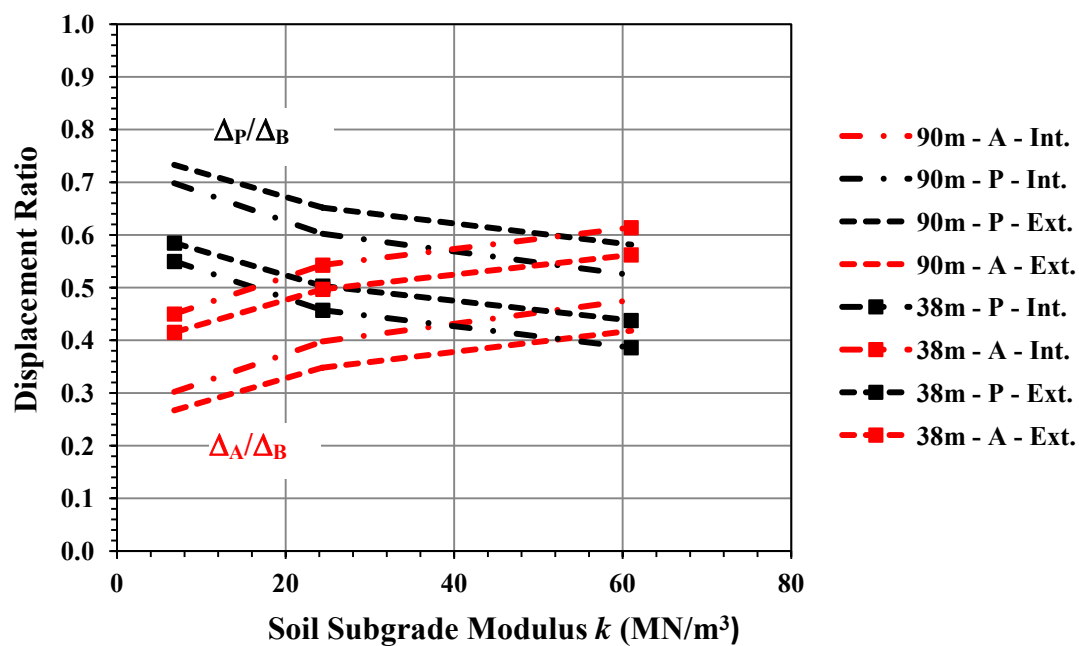


Figure 8.9 Substructure Displacement Ratios (Strong, Expansion, Sand)

8.3 SUBSTRUCTURE ROTATION

A simple presentation of the rotation along the abutment is shown in figure 8.10. The 3D FE models study showed that the abutment movement can be approximated by a rigid body movement. Based on that observation, the average rotation along the abutment θ_A can be utilized to calculate the rotation at the top of the abutment and at the top of the pile.

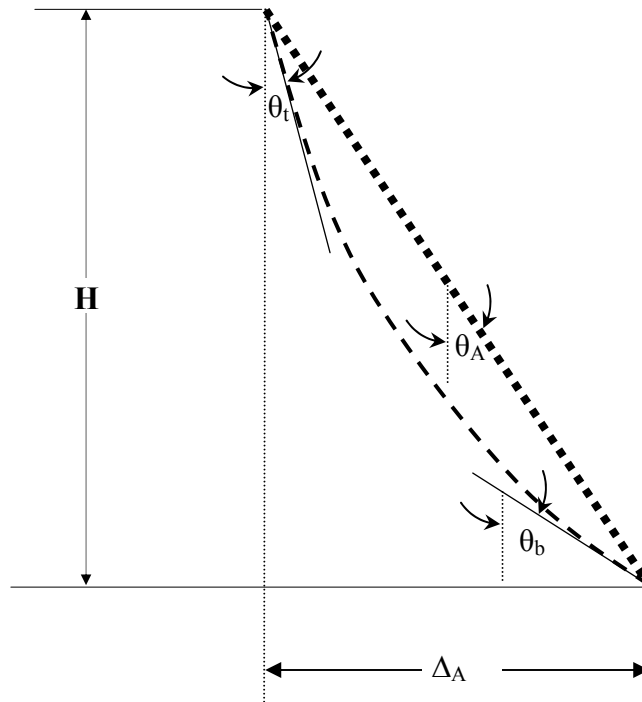


Figure 8.10 Simplified Model for the Abutment Displacement

Once the relative displacement of the abutment Δ_A is estimated, The average rotation along the abutment θ_A can be calculated as follows:

$$\theta_A = ATAN\left(\frac{\Delta_A}{H}\right) \quad (8.6)$$

The rotations at the top of the abutment, θ_t , and at the bottom of the abutment (top of the pile), θ_b , can be estimated as follows:

$$\theta_t = m_1 * \theta_A \quad (8.7)$$

$$\theta_b = m_2 * \theta_A \quad (8.7)$$

Where m_1 and m_2 are constants and can be estimated from figures 8.11 through 8.14 for bridges with steel H-Piles oriented to bend around the weak axis and from figures 8.15 through 8.18 for bridges with steel H-Piles oriented to bend around the strong axis.

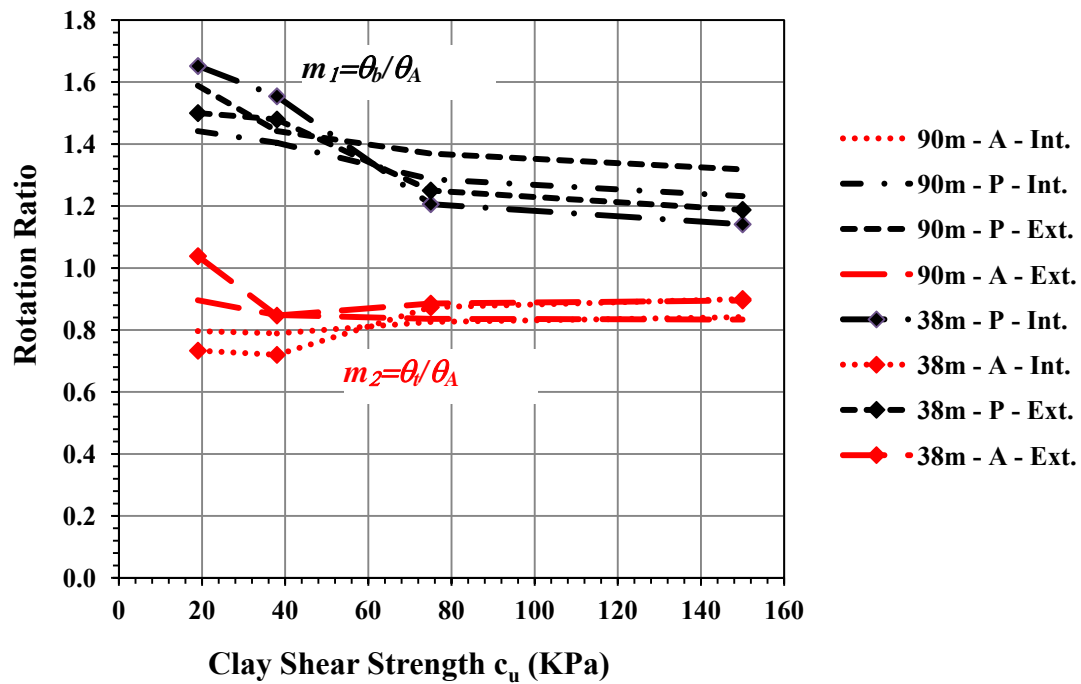


Figure 8.11 Substructure Rotation Ratios (Weak, Contraction, Clay)

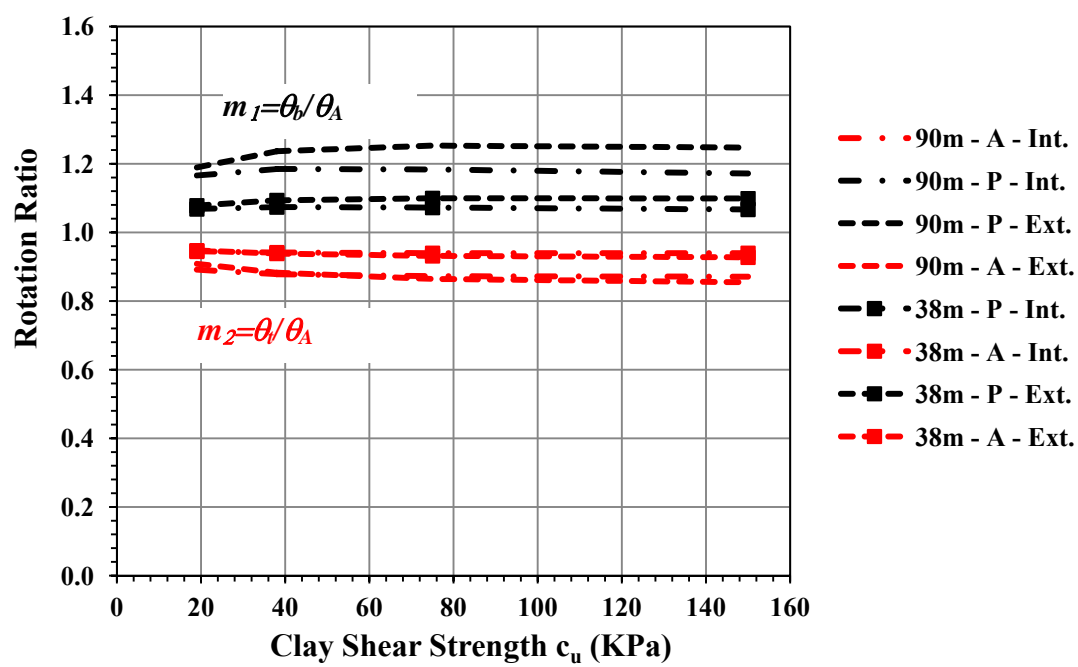


Figure 8.12 Substructure Rotation Ratios (Weak, Expansion, Clay)

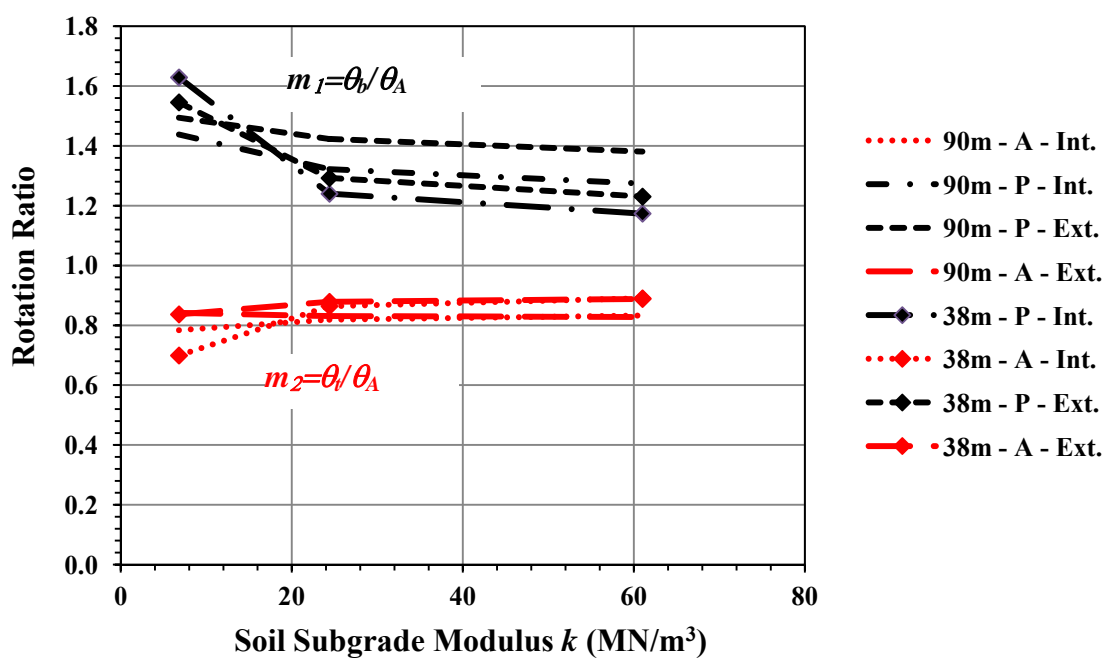


Figure 8.13 Substructure Rotation Ratios (Weak, Contraction, Sand)

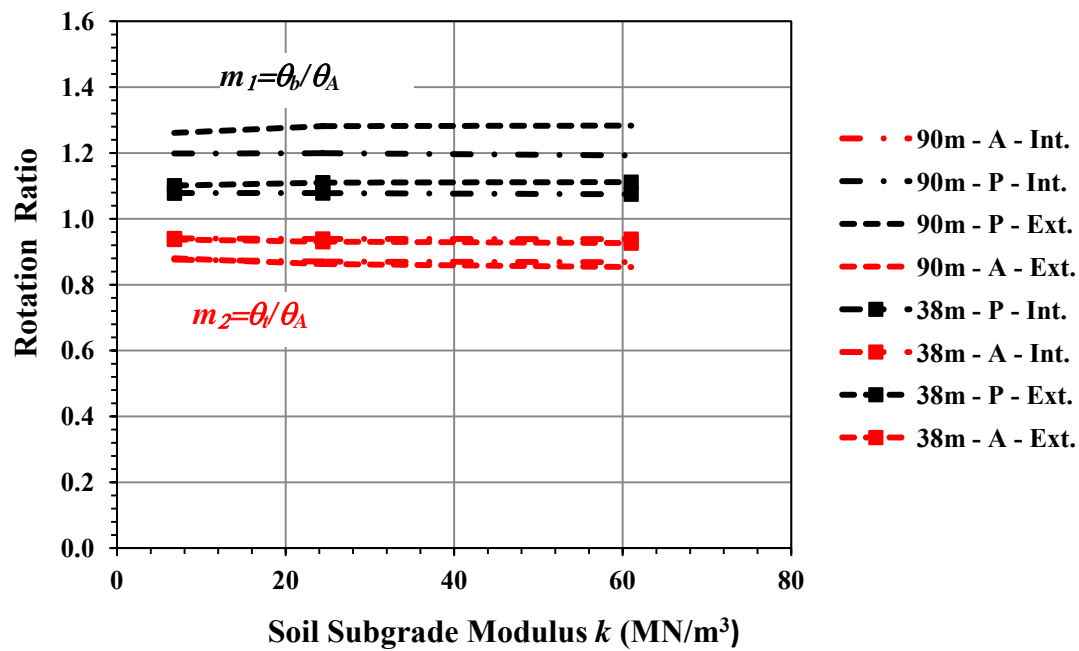


Figure 8.14 Substructure Rotation Ratios (Weak, Expansion, Sand)

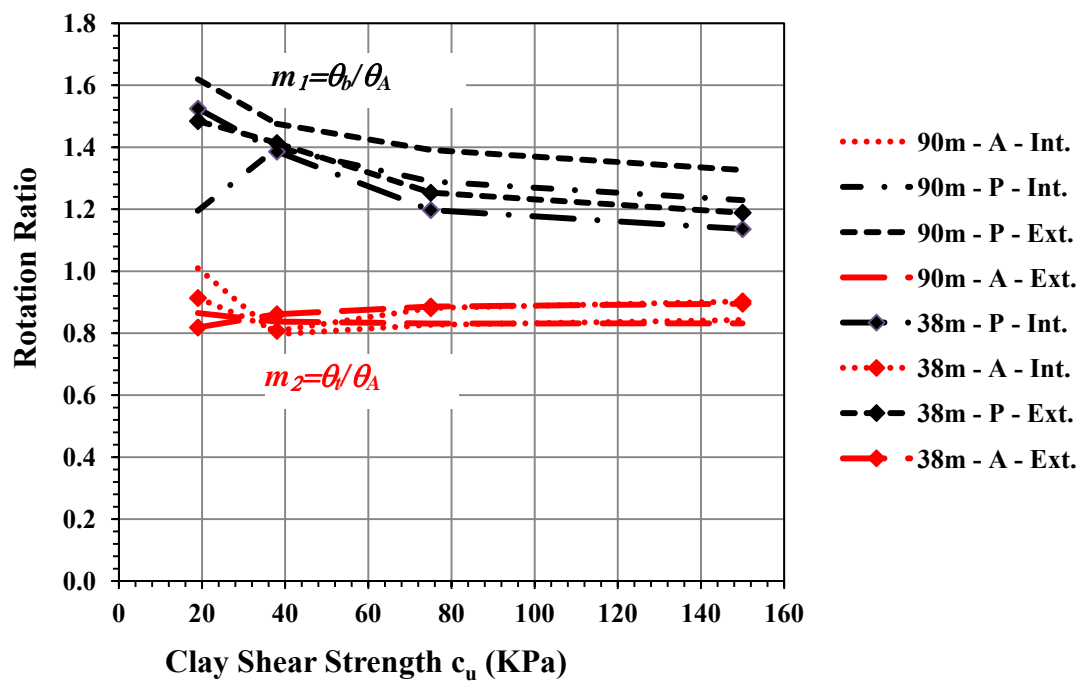


Figure 8.15 Substructure Rotation Ratios (Strong, Contraction, Clay)

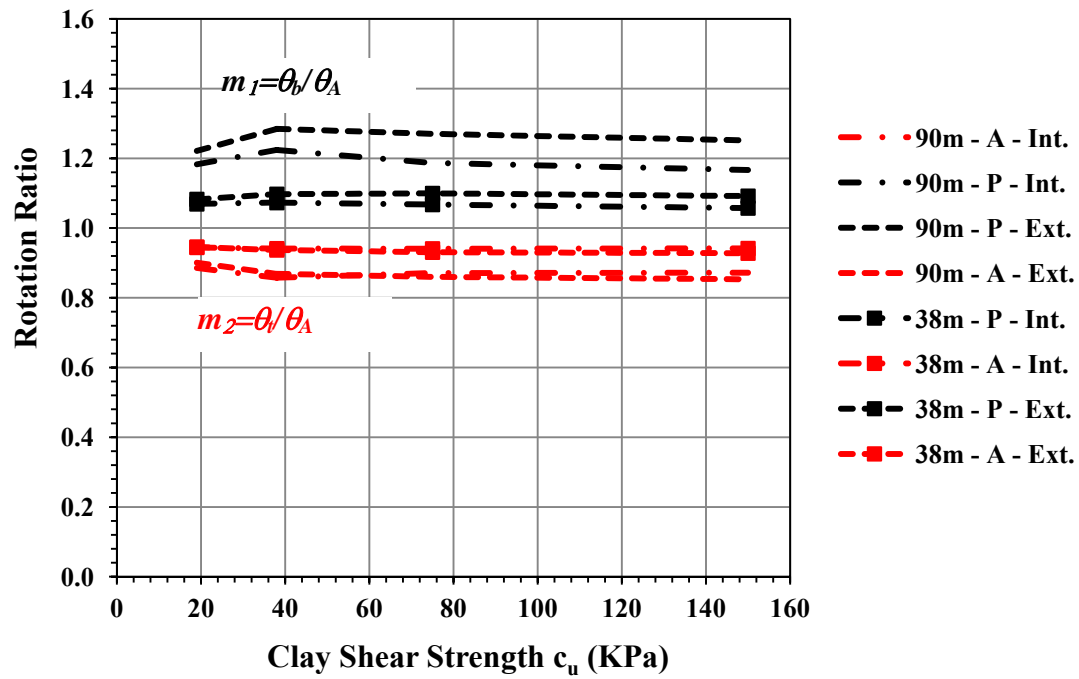


Figure 8.16 Substructure Rotation Ratios (Strong, Expansion, Clay)

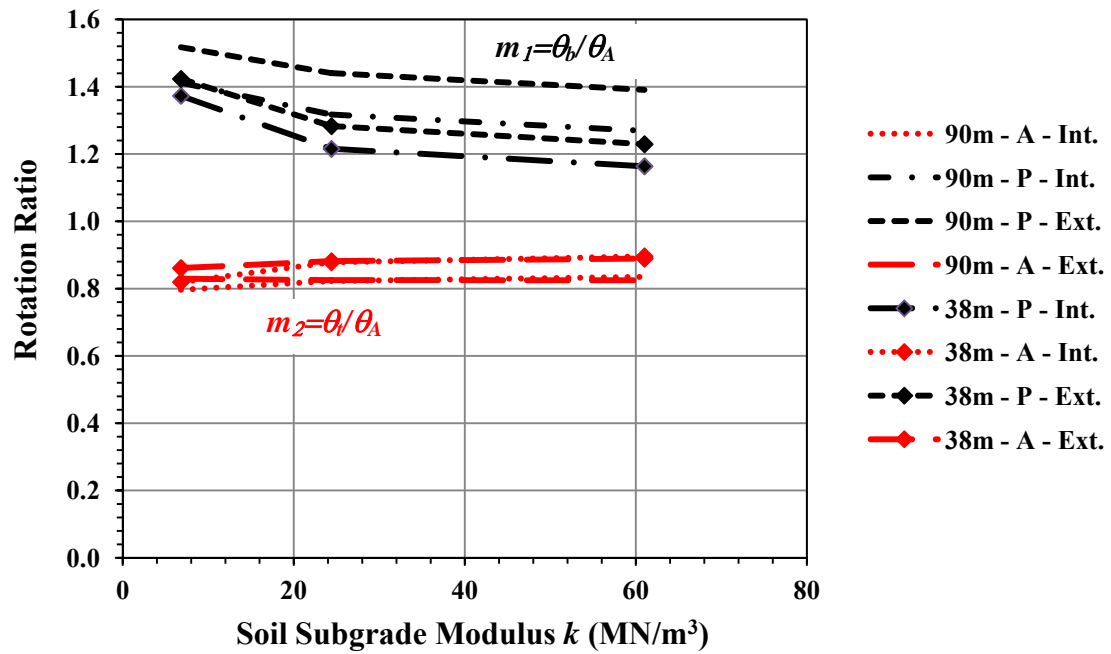


Figure 8.17 Substructure Rotation Ratios (Strong, Contraction, Sand)

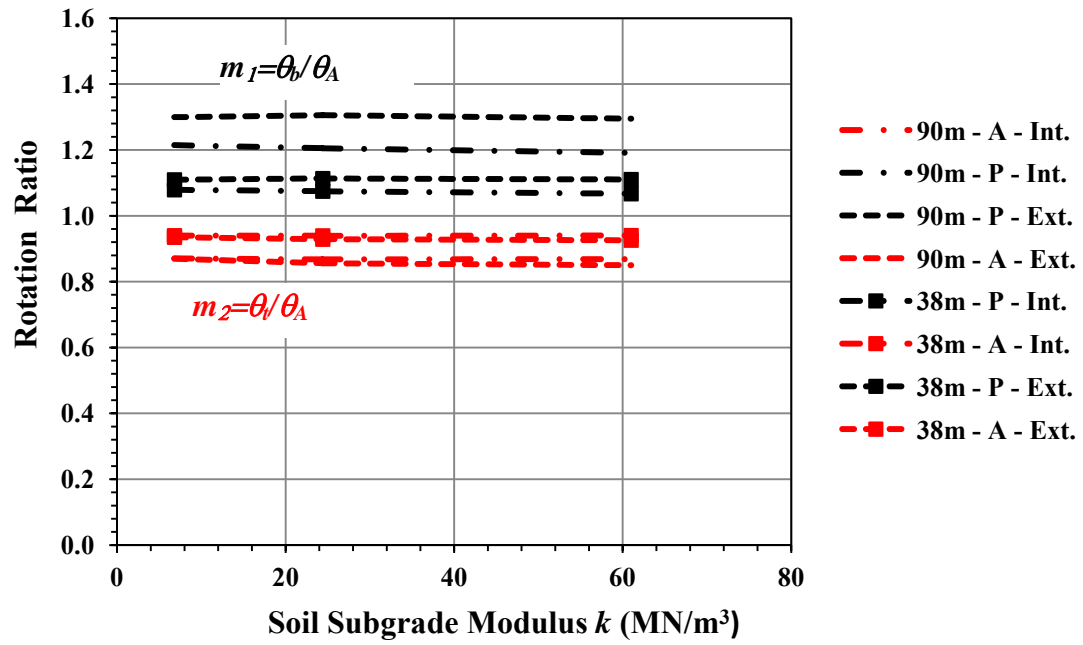


Figure 8.18 Substructure Rotation Ratios (Strong, Expansion, Sand)

8.4 2D VERSUS 3D

This section presents a comparison between the analysis results obtained from the 3D model to those obtained from the 2D model. The comparison will focus mainly on the displacements and rotations along the abutment and the pile. Figures 8.19 and 8.20 show the displacement and rotation along the abutment and the pile for the interior location in the short bridge during contraction. The ratios between the displacements and rotations at the top of the abutment and the piles for the same case are summarized in table 8.1. Figure 8.19 shows a general agreement between the results from the 2D and the 3D models. The two types of analysis give closer results for soft soils.

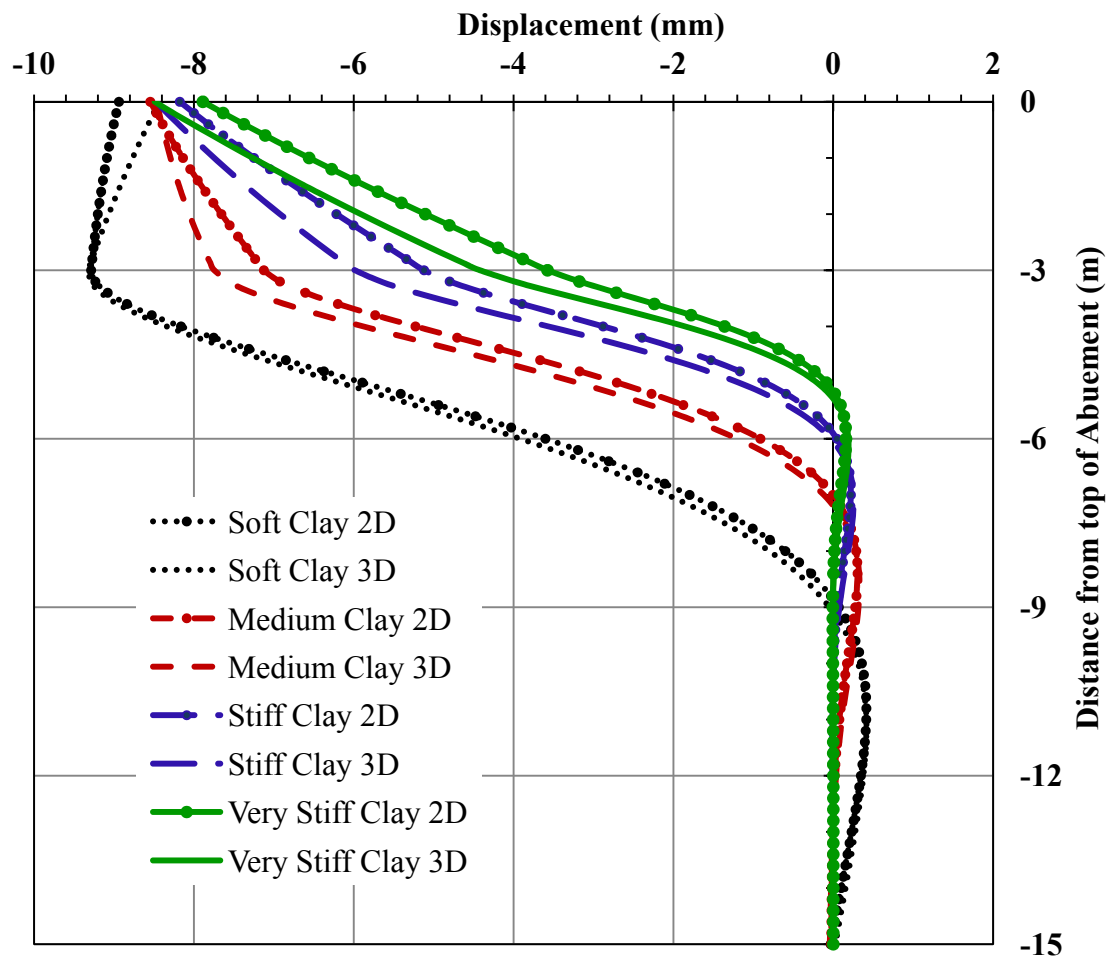


Figure 8.19 Displacement (Contraction) at Interior Location 2D Versus 3D
(38-m Bridge, Clay, 3m Abutment, HP310X125 Weak Orientation)

Figure 8.20 shows also a general agreement between the results from the 2D and the 3D models. For the rotation of the pile, the analysis results are closer in soft soils and for the rotation of the abutment, the analysis results are closer in stiff soils.

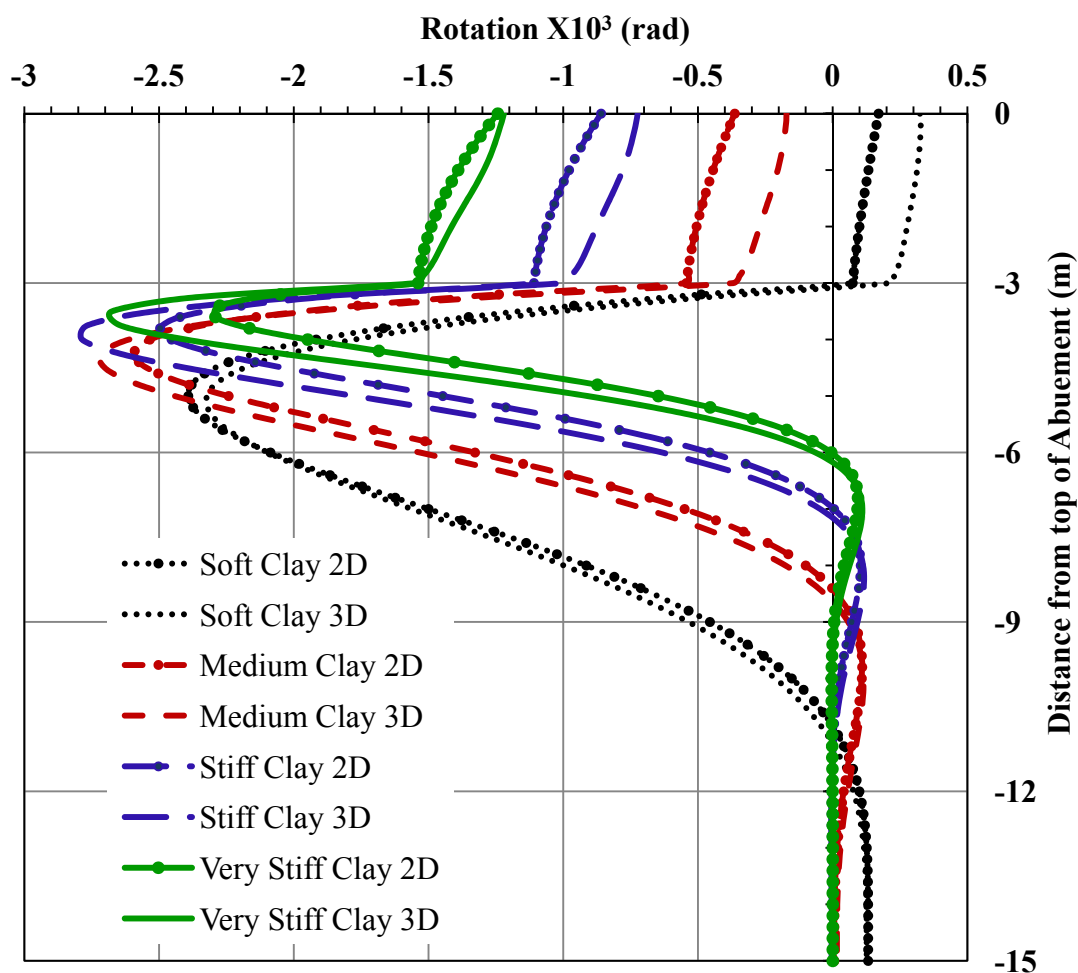


Figure 8.20 2D Versus 3D, Rotation (Contraction) at Interior Location (38-m Bridge, Clay, 3m Abutment, HP310X125 Weak Orientation)

Table 8.1 2D versus 3D (Short Bridge – Contraction - Interior Location)

Consistency of Clay	Top of Abutment(2D/3D)		Top of Pile (2D/3D)	
	Displacement	Rotation	Displacement	Rotation
Soft	1.06	1.06	1.00	0.35
Medium	1.01	1.01	0.92	1.47
Stiff	0.97	0.97	0.86	1.11
Very Stiff	0.93	0.93	0.81	0.35

Figures 8.21 and 8.22 show the displacement and rotation along the abutment and the pile for the exterior location in the short bridge during contraction. The ratios between the displacements at the top of the abutment for the same case are summarized in table 8.2. For the displacement at exterior locations, there is less agreement between the results from the 2D and the 3D models as can be seen in figure 8.21 especially in stiff soils.

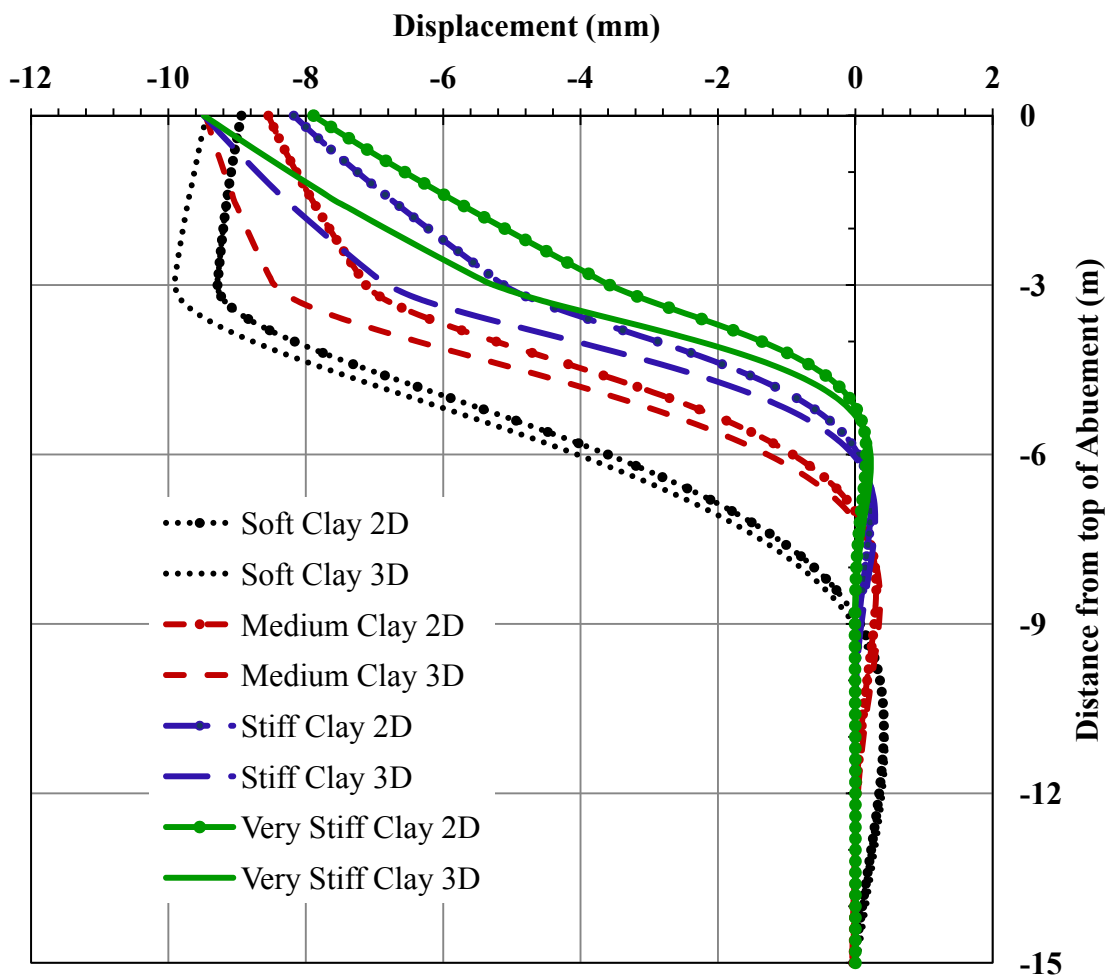


Figure 8.21 Displacement (Contraction) at Exterior Location 2D Versus 3D
(38-m Bridge, Clay, 3m Abutment, HP310X125 Weak Orientation)

For the rotation along the abutment at exterior locations, there is a good agreement between the results from the 2D and the 3D models but not for the rotation along the exterior piles in stiff soils as can be seen in figure 8.22.

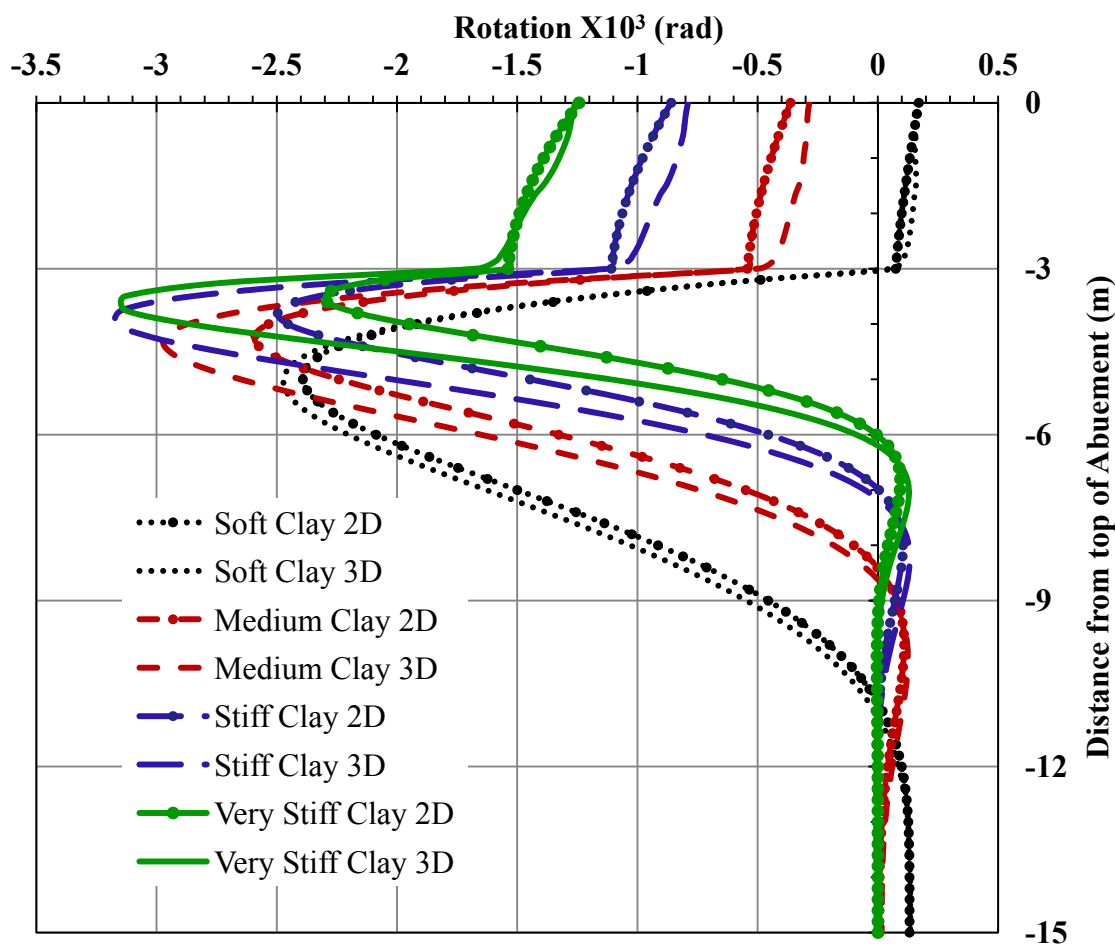


Figure 8.22 2D Versus 3D, Rotation (Contraction) at Exterior Location (38-m Bridge, Clay, 3m Abutment, HP310X125 Weak Orientation)

Table 8.2 2D versus 3D Results (Short Bridge - Contraction – Exterior Location)

Consistency of Clay	Top of Abutment(2D/3D)		Top of Pile (2D/3D)	
	Displacement	Rotation	Displacement	Rotation
Soft	0.95	1.07	0.94	1.22
Medium	0.90	1.28	0.84	1.09
Stiff	0.86	1.09	0.75	0.99
Very Stiff	0.83	0.99	0.68	0.92

Figures 8.23 and 8.24 show the displacement and rotation along the abutment and the pile for the interior location in the short bridge during expansion. The ratios between the displacements at the top of the abutment for the same case are summarized in table 8.3. In general, there is less agreement between the results from the 2D and the 3D models for the expansion cases especially in soft soils as can be seen in figures 8.23 and 8.24. These disagreements can be attributed to the different contributions of the backfill in the two types of analysis.

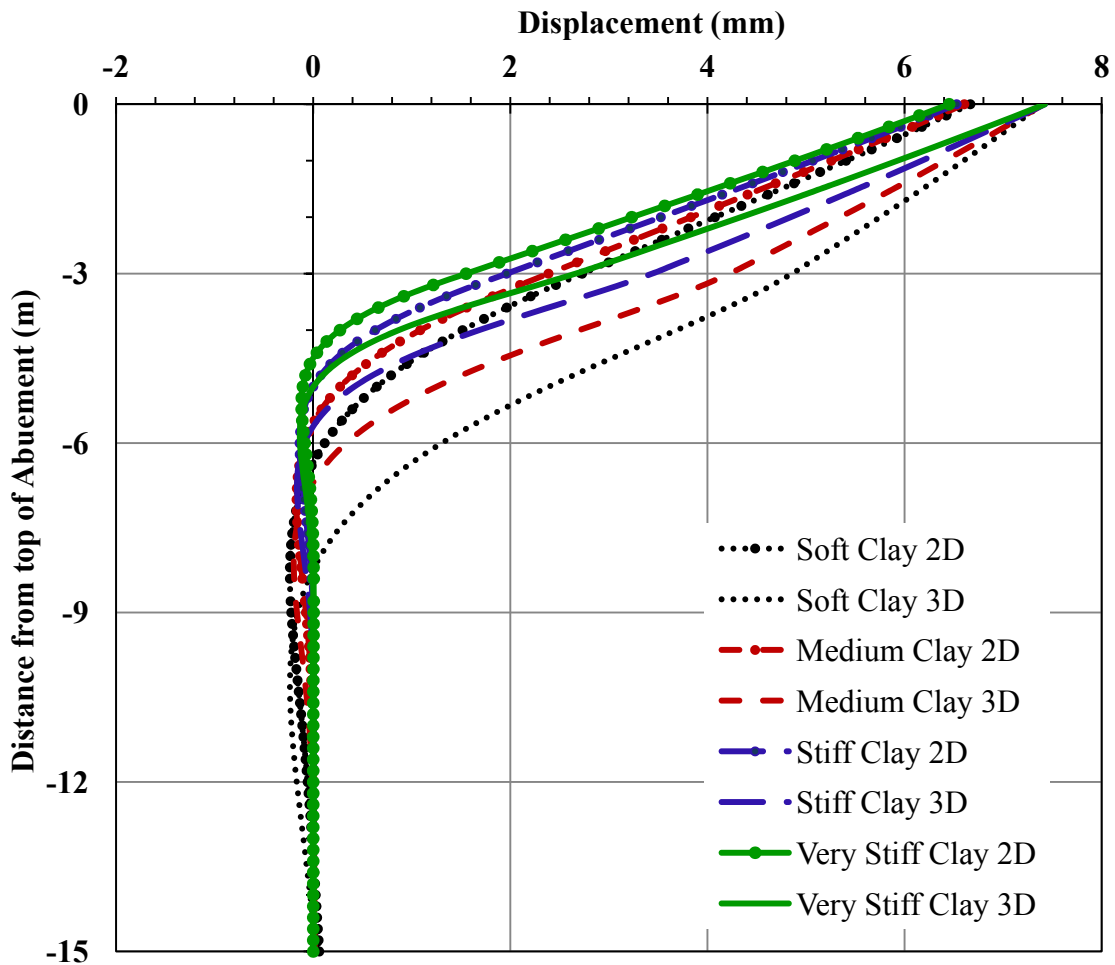


Figure 8.23 Displacement (Expansion) at Interior Location 2D Versus 3D (38-m Bridge, Clay, 3m Abutment, HP310X125 Weak Orientation)

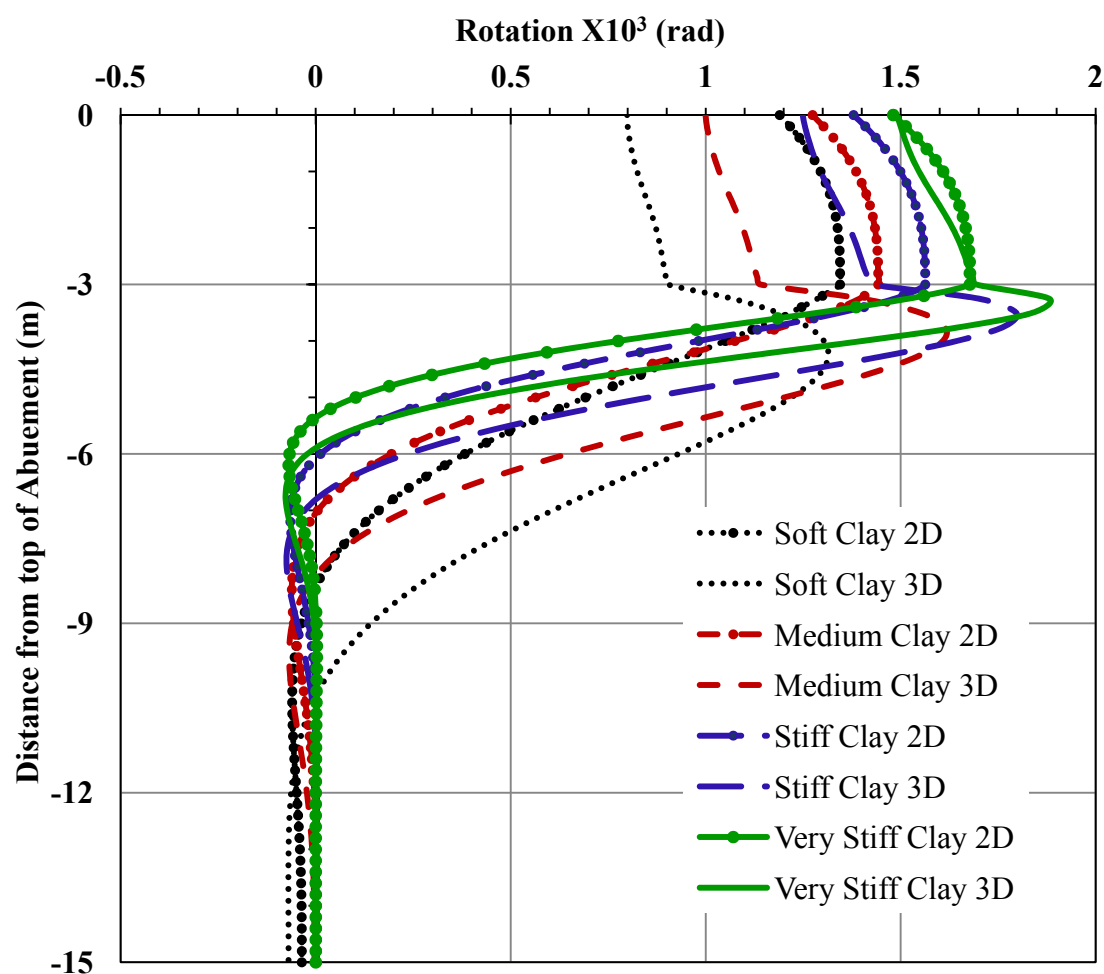


Figure 8.24 2D Versus 3D, Rotation (Expansion) at Interior Location
(38-m Bridge, Clay, 3m Abutment, HP310X125 Weak Orientation)

Table 8.3 2D versus 3D Results (Short Bridge - Expansion – Interior Location)

Consistency of Clay	Top of Abutment(2D/3D)		Top of Pile (2D/3D)	
	Displacement	Rotation	Displacement	Rotation
Soft	0.90	1.49	0.56	1.49
Medium	0.89	1.27	0.57	1.26
Stiff	0.88	1.10	0.57	1.10
Very Stiff	0.87	0.99	0.58	0.99

Figures 8.25 and 8.26 show the displacement and rotation along the abutment and the pile for the exterior location in the short bridge during expansion. The ratios between the displacements at the top of the abutment for the same case are summarized in table 8.4. Similar to the expansion at interior location case, there is a significant disagreement between the results from the 2D and the 3D models as can be seen in figures 8.25 and 8.26. These disagreements can also be attributed to the different contributions of the backfill in the two types of analysis.

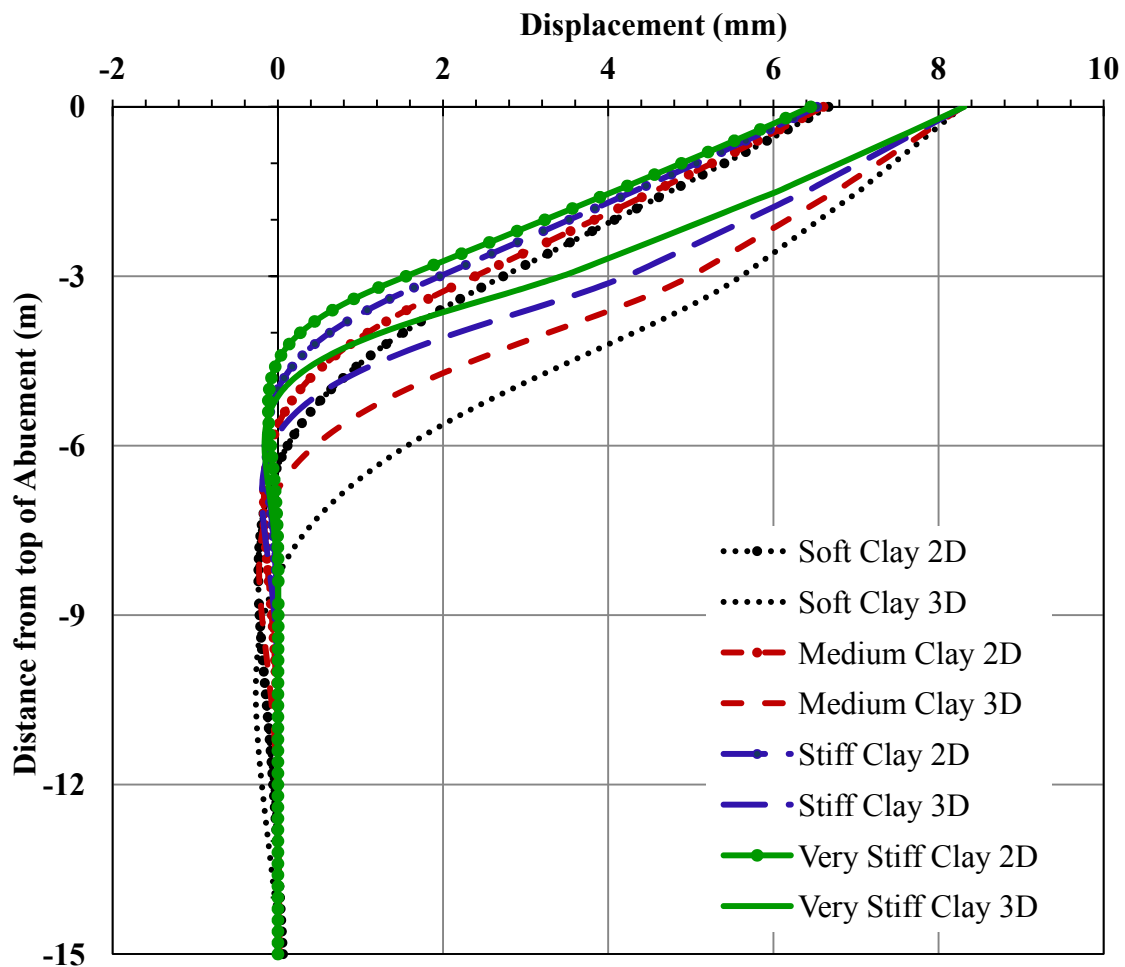


Figure 8.25 Displacement (Expansion) at Exterior Location 2D Versus 3D
(38-m Bridge, Clay, 3m Abutment, HP310X125 Weak Orientation)

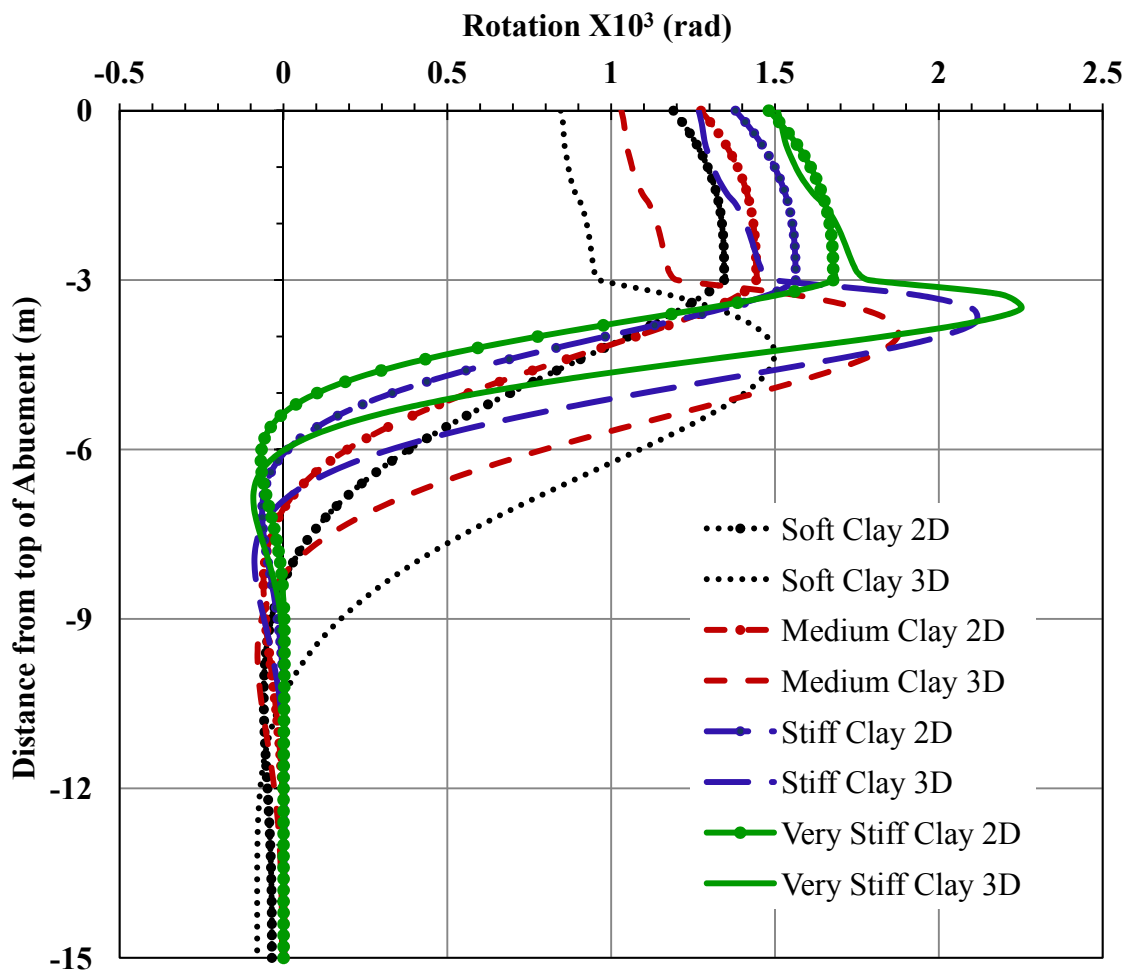


Figure 8.26 2D Versus 3D, Rotation (Expansion) at Exterior Location
(38-m Bridge, Clay, 3m Abutment, HP310X125 Weak Orientation)

Table 8.4 2D versus 3D Results (Short Bridge - Expansion – Exterior Location)

Consistency of Clay	Top of Abutment 2D/3D		Top of Pile 2D/3D	
	Displacement	Rotation	Displacement	Rotation
Soft	0.80	1.41	0.49	1.40
Medium	0.80	1.24	0.48	1.20
Stiff	0.79	1.09	0.47	1.05
Very Stiff	0.78	0.98	0.45	0.94

Figures 8.27 and 8.28 show the displacement and rotation along the abutment and the pile for the interior location in the long bridge during contraction. The ratios between the displacements at the top of the abutment for the same case are summarized in table 8.5. Figure 8.27 shows a general agreement between the results from the 2D and the 3D models. The two types of analysis give closer results for soft soils.

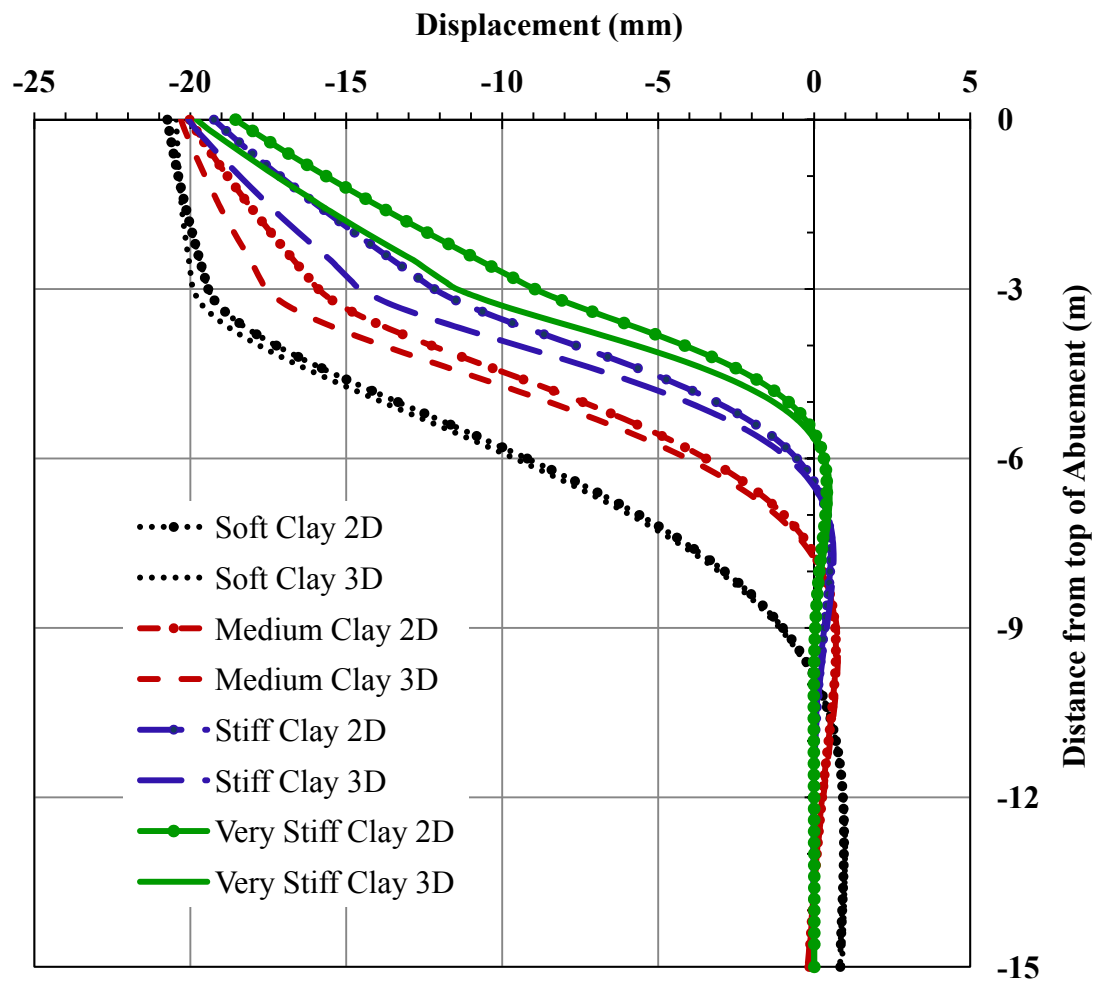


Figure 8.27 Displacement (Contraction) at Interior Location 2D Versus 3D
(90-m Bridge, Clay, 3m Abutment, HP360X152 Weak Orientation)

Figure 8.28 shows also general agreement between the results from the 2D and the 3D models. The analysis results are closer in soft soils for the rotation of the abutment and the piles at interior locations.

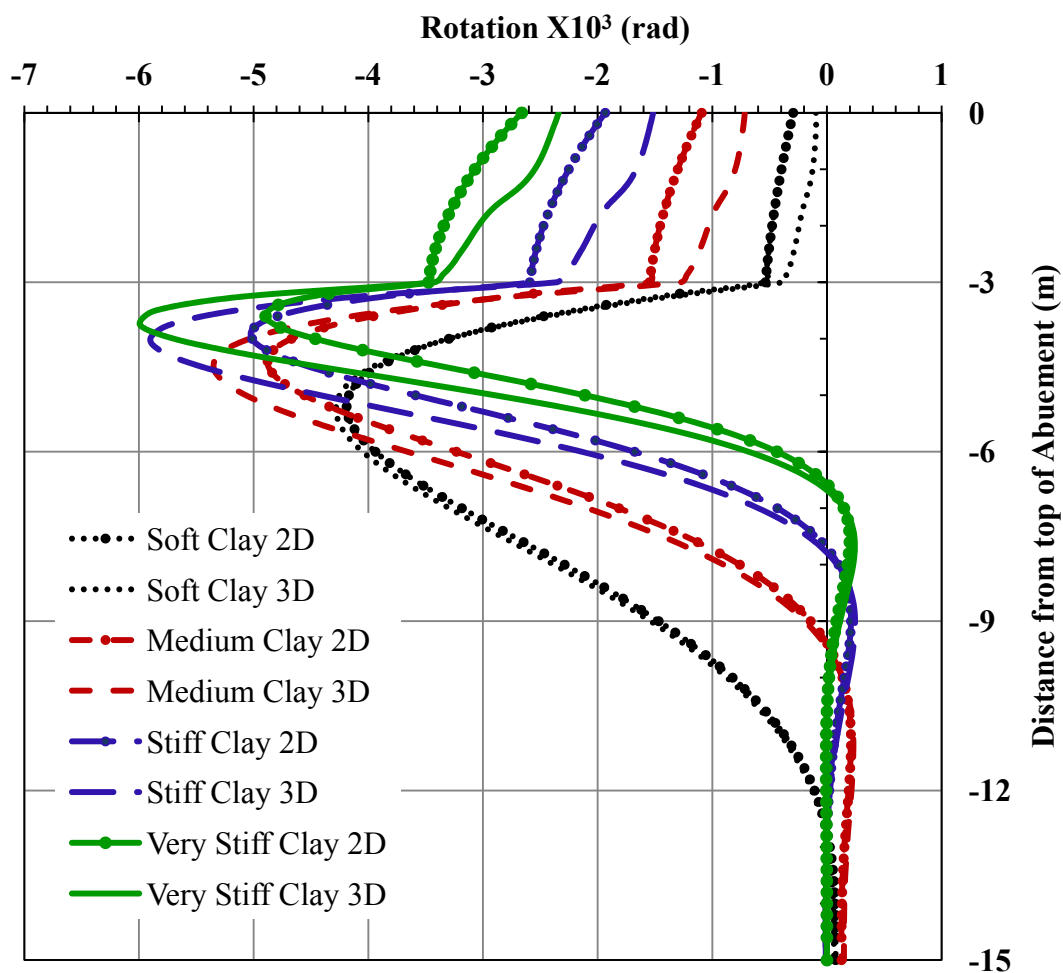


Figure 8.28 2D Versus 3D, Rotation (Contraction) at Interior Location (90-m Bridge, Clay, 3m Abutment, HP360X152 Weak Orientation)

Table 8.5 2D versus 3D (Long Bridge – Contraction - Interior Location)

Consistency of Clay	Top of Abutment(2D/3D)		Top of Pile (2D/3D)	
	Displacement	Rotation	Displacement	Rotation
Soft	1.01	3.11	0.98	1.39
Medium	0.99	1.52	0.90	1.21
Stiff	0.96	1.28	0.84	1.10
Very Stiff	0.94	1.14	0.78	0.30

Figures 8.29 and 8.30 show the displacement and rotation along the abutment and the pile for the exterior location in the long bridge during contraction. The ratios between the displacements at the top of the abutment for the same case are summarized in table 8.6.

There are significant disagreements between the results from the 2D models and the 3D models for the abutment displacement during bridge contraction at exterior locations as can be seen in figure 8.29. The significant disagreement between the two models continues through the upper part of the piles.

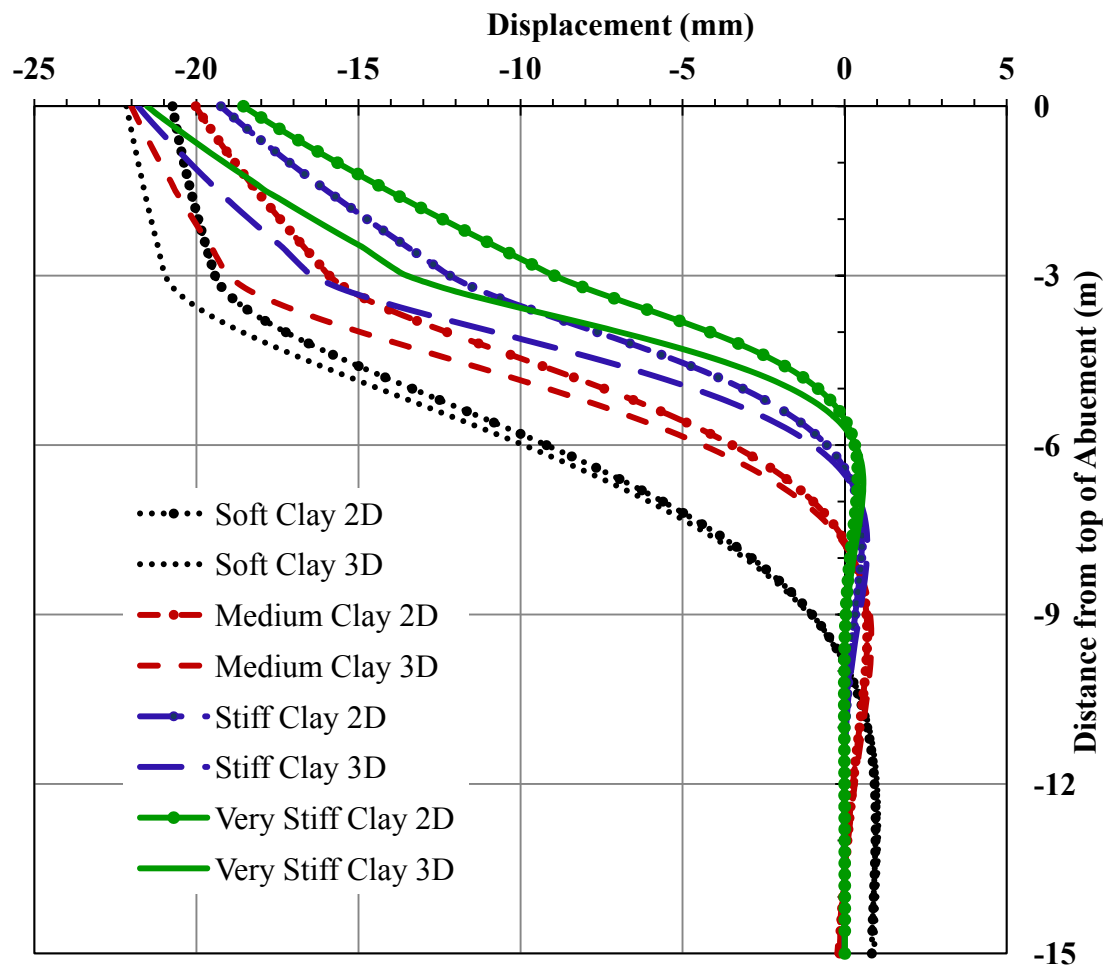


Figure 8.29 Displacement (Contraction) at Exterior Location 2D Versus 3D
(90-m Bridge, Clay, 3m Abutment, HP360X152 Weak Orientation)

There are also significant disagreements between the results from the 2D models and the 3D models for the abutment and pile rotation during bridge contraction in stiff soils as can be seen in figure 8.30.

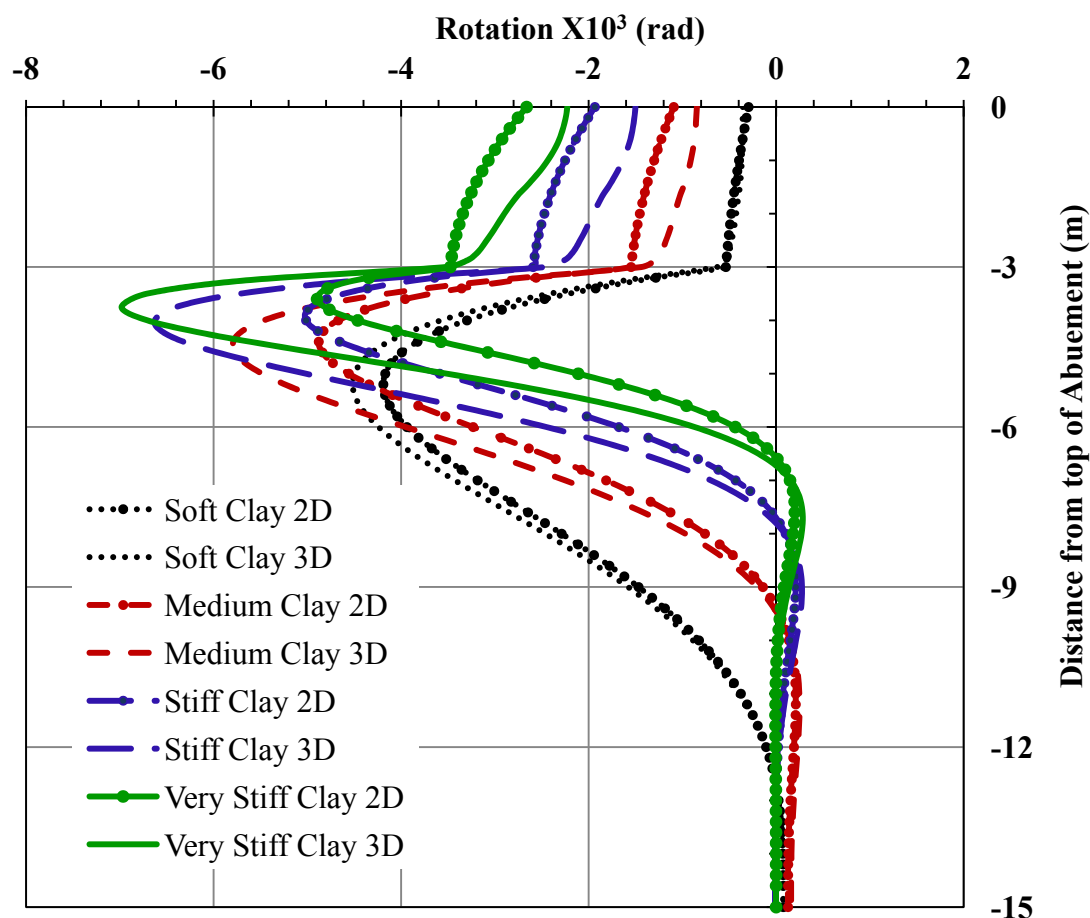


Figure 8.30 2D Versus 3D, Rotation (Contraction) at Exterior Location (90-m Bridge, Clay, 3m Abutment, HP360X152 Weak Orientation)

Table 8.6 2D versus 3D Results (Long Bridge - Contraction – Exterior Location)

Consistency of Clay	Top of Abutment(2D/3D)		Top of Pile (2D/3D)	
	Displacement	Rotation	Displacement	Rotation
Soft	0.94	0.83	0.93	0.85
Medium	0.91	1.29	0.84	1.08
Stiff	0.88	1.29	0.74	1.05
Very Stiff	0.86	1.20	0.66	0.99

Figures 8.31 and 8.32 show the displacement and rotation along the abutment and the pile for the interior location in the short bridge during expansion. The ratios between the displacements at the top of the abutment for the same case are summarized in table 8.7. In general, there is less agreement between the results from the 2D and the 3D models for the expansion cases especially in soft soils as can be seen in figures 8.31 and 8.32.

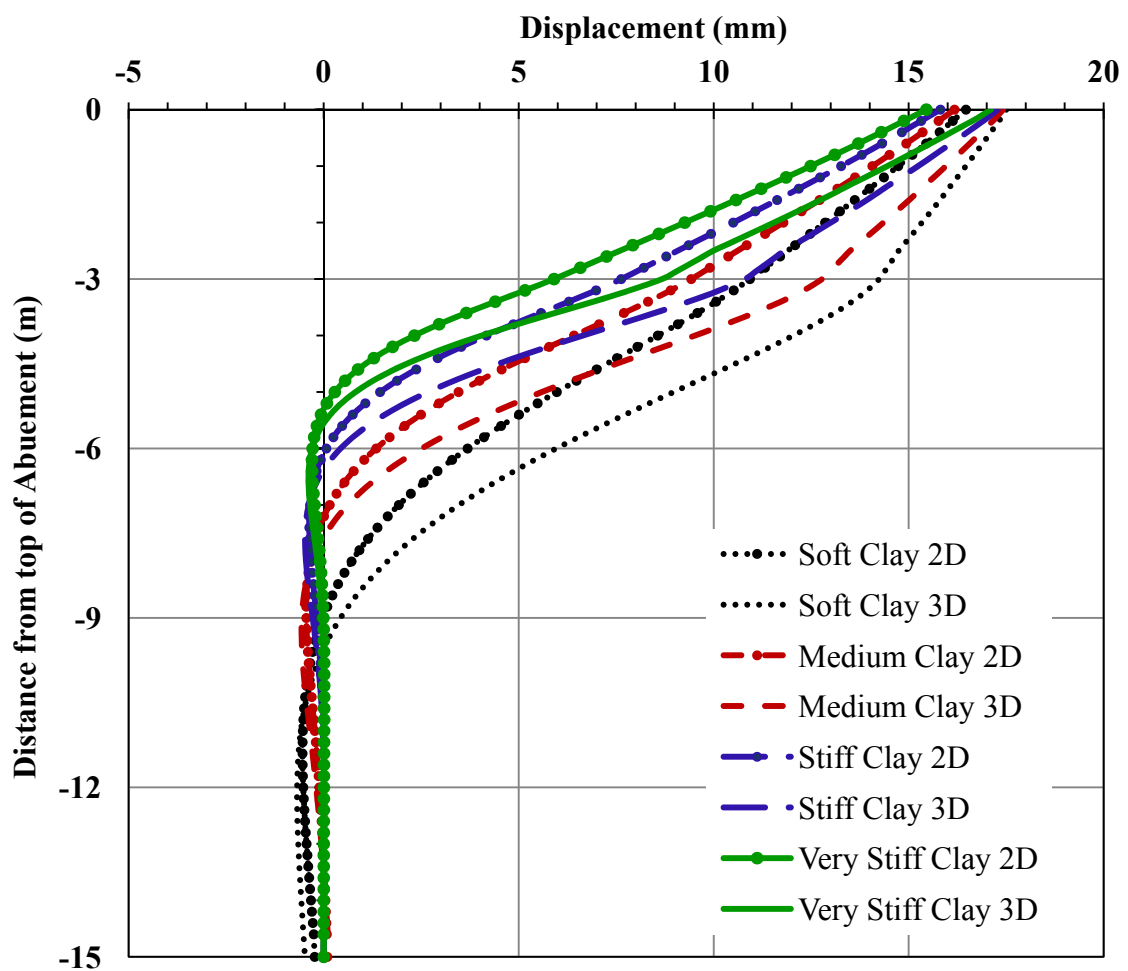


Figure 8.31 Displacement (Expansion) at Interior Location 2D Versus 3D (90-m Bridge, Clay, 3m Abutment, HP360X152 Weak Orientation)

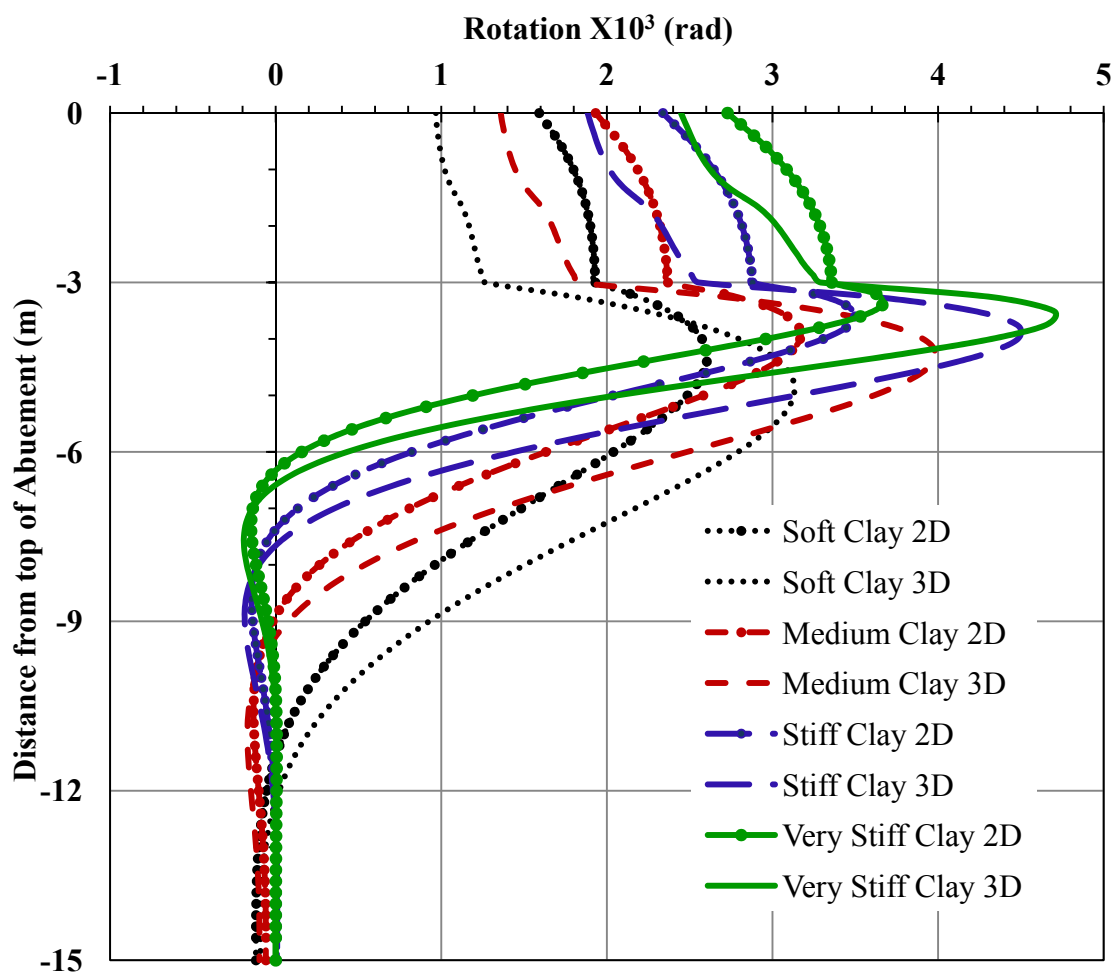


Figure 8.32 2D Versus 3D, Rotation (Expansion) at Interior Location (90-m Bridge, Clay, 3m Abutment, HP360X152 Weak Orientation)

Table 8.7 2D versus 3D Results (Long Bridge - Expansion – Interior Location)

Consistency of Clay	Top of Abutment(2D/3D)		Top of Pile (2D/3D)	
	Displacement	Rotation	Displacement	Rotation
Soft	0.94	1.64	0.77	1.52
Medium	0.93	1.42	0.74	1.29
Stiff	0.92	1.24	0.71	1.13
Very Stiff	0.90	1.11	0.68	1.02

Figures 8.33 and 8.34 show the displacement and rotation along the abutment and the pile for the exterior location in the short bridge during expansion. The ratios between the displacements at the top of the abutment for the same case are summarized in table 8.8. Similar to the expansion at interior location case, there are significant disagreements between the results from the 2D and the 3D models as can be seen in figures 8.33 and 8.34.

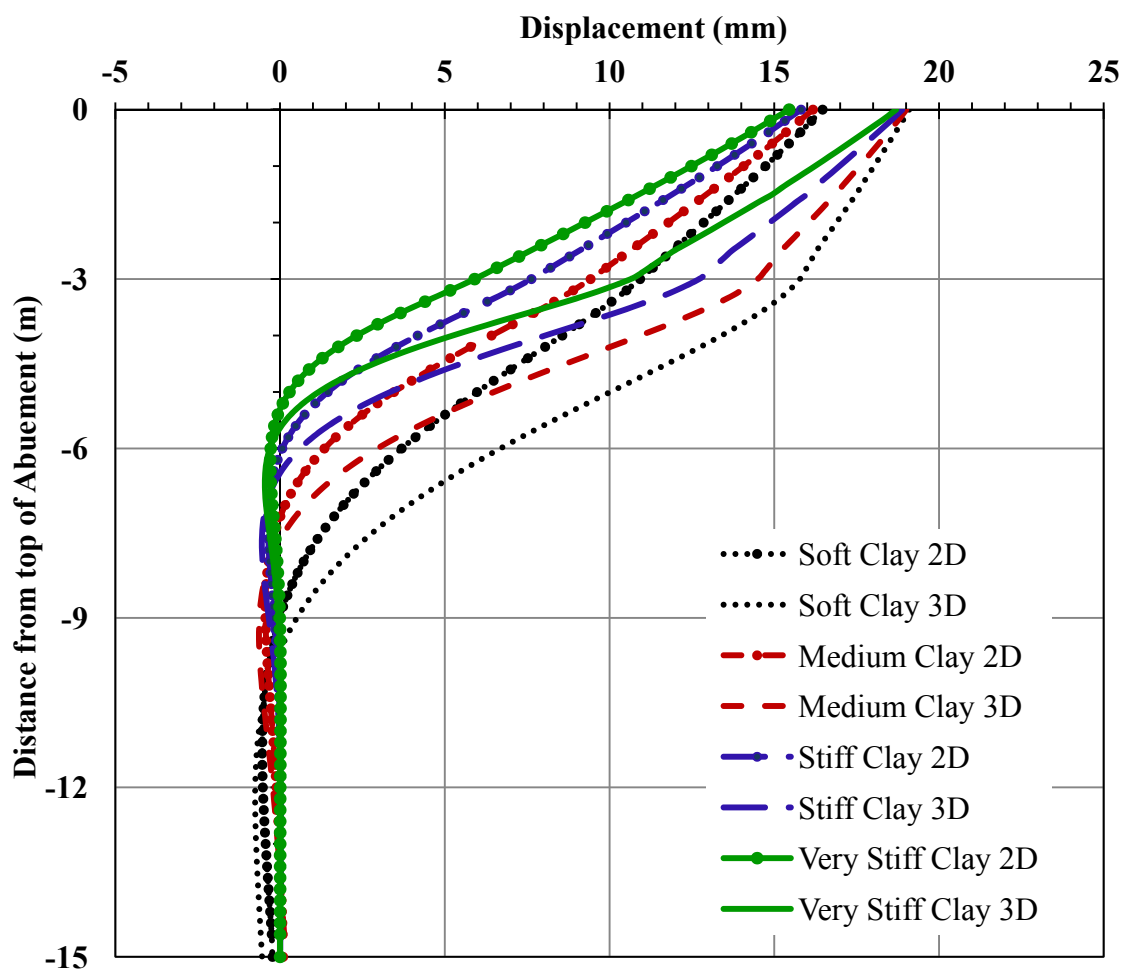


Figure 8.33 Displacement (Expansion) at Exterior Location 2D Versus 3D (90-m Bridge, Clay, 3m Abutment, HP360X152 Weak Orientation)

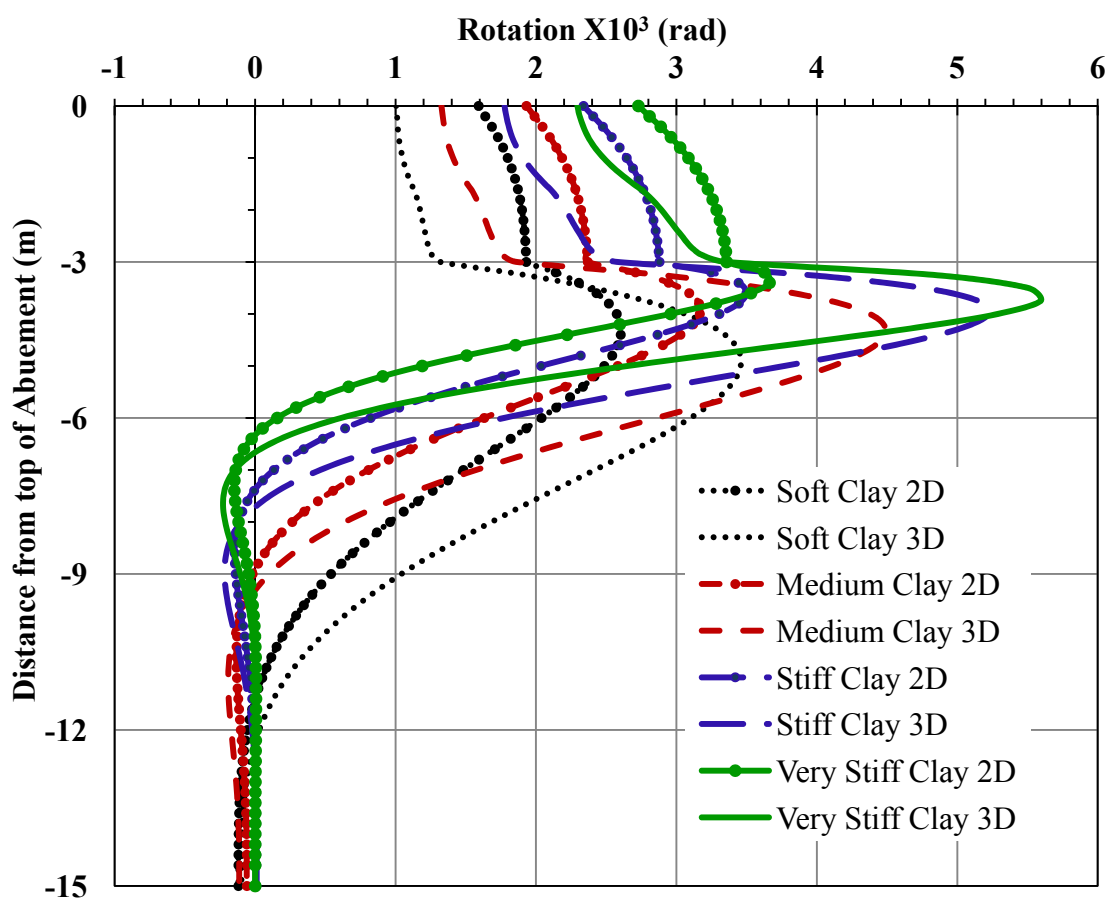


Figure 8.34 2D Versus 3D, Rotation (Expansion) at Exterior Location (90-m Bridge, Clay, 3m Abutment, HP360X152 Weak Orientation)

Table 8.8 2D versus 3D Results (Long Bridge - Expansion – Exterior Location)

Consistency of Clay	Top of Abutment(2D/3D)		Top of Pile (2D/3D)	
	Displacement	Rotation	Displacement	Rotation
Soft	0.86	1.58	0.69	1.47
Medium	0.85	1.46	0.65	1.27
Stiff	0.84	1.32	0.60	1.12
Very Stiff	0.83	1.19	0.55	1.00

Figures A.33 to A.40 in appendix A, show a comparison between the moment along the piles from the 2D models and the 3D modes results.

8.5 PILE IDEALIZATION

To simplify the analysis of bridges with deep foundations, the pile can be idealized with an equivalent cantilever length based on the structural properties of the pile and the geotechnical properties of the surrounding soil. The work by Girton et al. (1989) in pile idealization is shown in figure 8.35.

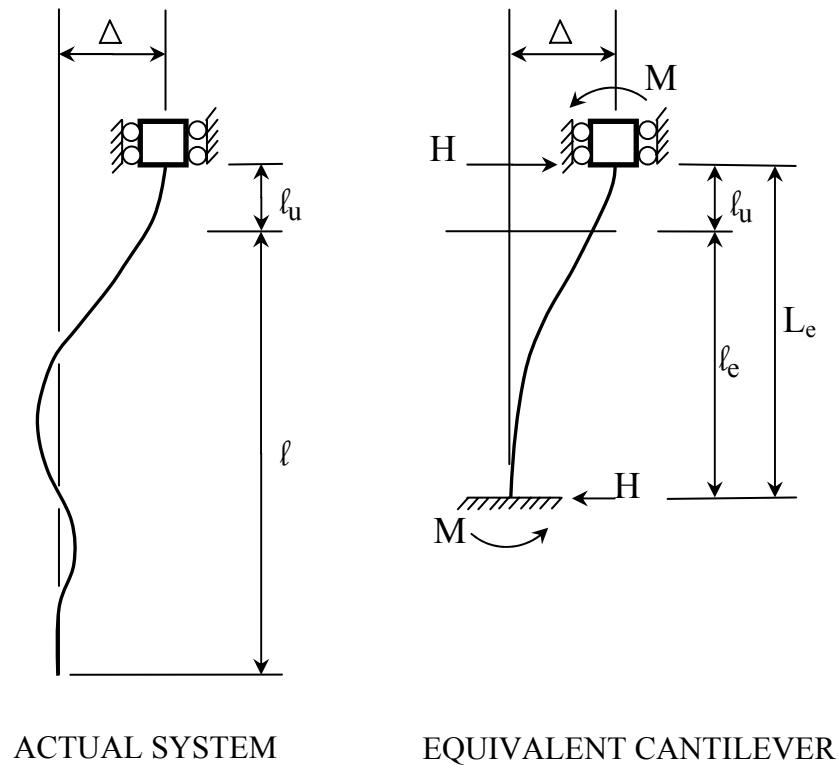


Figure 8.35 Pile Idealization as Equivalent Cantilever (Girton et al. 1989)

The pile equivalent cantilever length, L_e , is the sum of the pile unsupported length ℓ_u and the pile equivalent length ℓ_e which is defined as a function of the critical length, ℓ_c . The

critical length, l_c , is defined as the depth below at which the displacements and bending moments at the pile head have little effect (Girton et al. 1989).

l_c can be calculated as follows:

$$l_c = 4\sqrt[4]{\frac{E_p I_p}{k_h}} \quad (8.1)$$

Where E_p is the pile's modulus of elasticity, I_p is the pile's moment of inertia, and k_h is the initial soil lateral stiffness. Table 8.9 summarizes the values of k_h for clay and sand.

Table 8.9 Initial Soil Stiffness, k_h

Case	k_h
Clay	$\frac{9C_u}{2.5\varepsilon_{50}}$
Sand	kx

Where x is the distance measured from the pile's top.

That relationship between the equivalent cantilever length l_e and the critical length l_c is illustrated in figure 8.36.

For horizontal stiffness analysis and for piles completely embedded in soil, the value of l_u

= 0 and $l_e/l_c = 0.5$. Substituting in equation 8.1:

$$L_e = l_e = 0.5 * l_c = 2\sqrt[4]{\frac{E_p I_p}{k_h}} \quad (8.1a)$$

Substituting for k_h from equation 4.7 for cohesive soils:

$$L_e = 2\sqrt[4]{\frac{5\varepsilon_{50} E_p I_p}{9C_u}} = 1.73\sqrt[4]{\frac{\varepsilon_{50} E_p I_p}{9C_u}} \quad (8.1b)$$

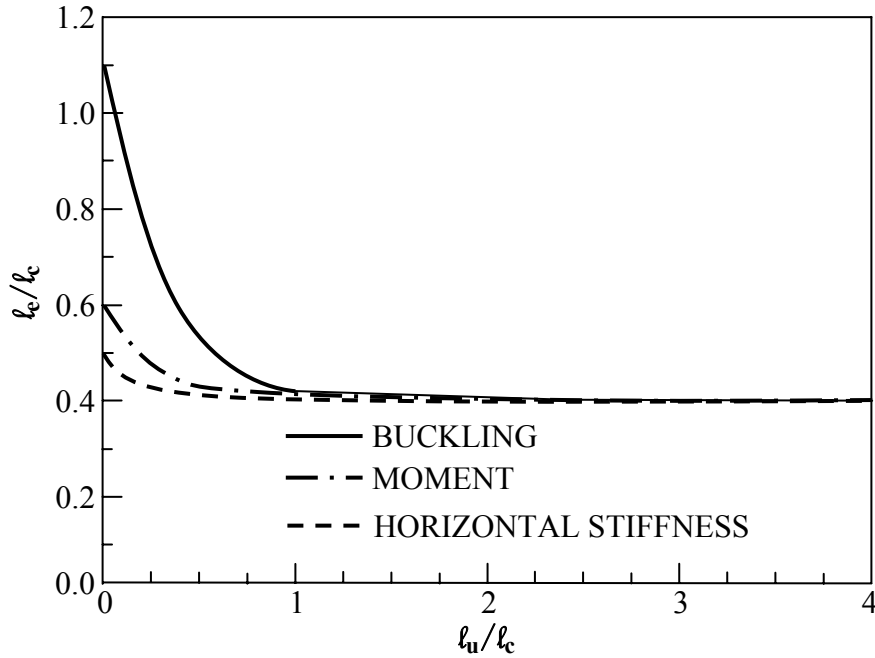


Figure 8.36 Equivalent Cantilevers for Fixed-Head Piles Embedded in Uniform Soil (Girton et al. 1989)

The effective pile length L_e for H-Piles embedded in soft clay, medium clay, stiff clay and very stiff clay are summarized in tables 8.10, 8.11, 8.12, and 8.13 respectively. The values can be adjusted based on the adjustment factors presented in table 6.6.

In general, the l_c values summarized in the tables for H-Pile 310X125 (HP12X84) and H-Pile 360X152 (HP14X102) are in good agreement with the values obtained from the 2D and 3D models. For piles with pile enclosure, the value of l_e/l_c can be assumed to be 0.4.

The results from this research show very good agreement with the results from the equations proposed by Girton et al. (1989) for the equivalent piles length.

Table 8.10 The Effective Pile Length L_e for H-Piles Embedded in Soft Clay

H-Pile	E	I_x (Strong)	I_y (Weak)	L_e/L_c	Strong Orientation		Weak Orientation	
					L_c	L_e	L_c	L_e
Metric (English)	(N/mm ²)	(mm ⁴)	(mm ⁴)		(mm)	(mm)	(mm)	(mm)
HP360X174 (HP14X117)	2.00E+05	5.08E+08	1.84E+08	0.5	11,100	5,550	8,600	4,300
HP360X152 (HP14X102)	2.00E+05	4.37E+08	1.58E+08	0.5	10,700	5,350	8,300	4,150
HP360X132 (HP14X89)	2.00E+05	3.76E+08	1.36E+08	0.5	10,300	5,150	8,000	4,000
HP360X108 (HP14X73)	2.00E+05	3.03E+08	1.09E+08	0.5	9,800	4,900	7,600	3,800
HP310X125 (HP12X84)	2.00E+05	2.71E+08	8.87E+07	0.5	9,500	4,750	7,200	3,600
HP310X110 (HP12X74)	2.00E+05	2.37E+08	7.74E+07	0.5	9,200	4,600	6,900	3,450
HP310X93 (HP12X63)	2.00E+05	1.96E+08	6.37E+07	0.5	8,800	4,400	6,600	3,300
HP310X79 (HP12X53)	2.00E+05	1.64E+08	5.29E+07	0.5	8,400	4,200	6,300	3,150
HP250X85 (HP10X57)	2.00E+05	1.22E+08	4.20E+07	0.5	7,800	3,900	6,000	3,000
HP250X62 (HP10X42)	2.00E+05	8.74E+07	2.98E+07	0.5	7,200	3,600	5,500	2,750
HP200X53 (HP8X36)	2.00E+05	4.95E+07	1.68E+07	0.5	6,200	3,100	4,700	2,350

Table 8.11 The Effective Pile Length L_e for H-Piles Embedded in Medium Clay

H-Pile	E	I_x (Strong)	I_y (Weak)	L_e/L_c	Strong Orientation		Weak Orientation	
					L_c	L_e	L_c	L_e
Metric (English)	(N/mm ²)	(mm ⁴)	(mm ⁴)		(mm)	(mm)	(mm)	(mm)
HP360X174 (HP14X117)	2.00E+05	5.08E+08	1.84E+08	0.5	7,900	3,950	6,100	3,050
HP360X152 (HP14X102)	2.00E+05	4.37E+08	1.58E+08	0.5	7,600	3,800	5,900	2,950
HP360X132 (HP14X89)	2.00E+05	3.76E+08	1.36E+08	0.5	7,300	3,650	5,600	2,800
HP360X108 (HP14X73)	2.00E+05	3.03E+08	1.09E+08	0.5	6,900	3,450	5,300	2,650
HP310X125 (HP12X84)	2.00E+05	2.71E+08	8.87E+07	0.5	6,700	3,350	5,100	2,550
HP310X110 (HP12X74)	2.00E+05	2.37E+08	7.74E+07	0.5	6,500	3,250	4,900	2,450
HP310X93 (HP12X63)	2.00E+05	1.96E+08	6.37E+07	0.5	6,200	3,100	4,700	2,350
HP310X79 (HP12X53)	2.00E+05	1.64E+08	5.29E+07	0.5	5,900	2,950	4,500	2,250
HP250X85 (HP10X57)	2.00E+05	1.22E+08	4.20E+07	0.5	5,500	2,750	4,200	2,100
HP250X62 (HP10X42)	2.00E+05	8.74E+07	2.98E+07	0.5	5,100	2,550	3,900	1,950
HP200X53 (HP8X36)	2.00E+05	4.95E+07	1.68E+07	0.5	4,400	2,200	3,300	1,650

Table 8.12 The Effective Pile Length L_e for H-Piles Embedded in Stiff Clay

H-Pile	E	I_x (Strong)	I_y (Weak)	L_e/L_c	Strong Orientation		Weak Orientation	
					L_c	L_e	L_c	L_e
Metric (English)	(N/mm ²)	(mm ⁴)	(mm ⁴)		(mm)	(mm)	(mm)	(mm)
HP360X174 (HP14X117)	2.00E+05	5.08E+08	1.84E+08	0.5	5,900	2,950	4,600	2,300
HP360X152 (HP14X102)	2.00E+05	4.37E+08	1.58E+08	0.5	5,700	2,850	4,400	2,200
HP360X132 (HP14X89)	2.00E+05	3.76E+08	1.36E+08	0.5	5,500	2,750	4,300	2,150
HP360X108 (HP14X73)	2.00E+05	3.03E+08	1.09E+08	0.5	5,200	2,600	4,000	2,000
HP310X125 (HP12X84)	2.00E+05	2.71E+08	8.87E+07	0.5	5,100	2,550	3,800	1,900
HP310X110 (HP12X74)	2.00E+05	2.37E+08	7.74E+07	0.5	4,900	2,450	3,700	1,850
HP310X93 (HP12X63)	2.00E+05	1.96E+08	6.37E+07	0.5	4,700	2,350	3,500	1,750
HP310X79 (HP12X53)	2.00E+05	1.64E+08	5.29E+07	0.5	4,500	2,250	3,400	1,700
HP250X85 (HP10X57)	2.00E+05	1.22E+08	4.20E+07	0.5	4,200	2,100	3,200	1,600
HP250X62 (HP10X42)	2.00E+05	8.74E+07	2.98E+07	0.5	3,800	1,900	2,900	1,450
HP200X53 (HP8X36)	2.00E+05	4.95E+07	1.68E+07	0.5	3,300	1,650	2,500	1,250

Table 8.12 The Effective Pile Length L_e for H-Piles Embedded in Very Stiff Clay

H-Pile	E	I_x (Strong)	I_y (Weak)	L_e/L_c	Strong Orientation		Weak Orientation	
					L_c	L_e	L_c	L_e
Metric (English)	(N/mm ²)	(mm ⁴)	(mm ⁴)		(mm)	(mm)	(mm)	(mm)
HP360X174 (HP14X117)	2.00E+05	5.08E+08	1.84E+08	0.5	4,700	2,350	3,600	1,800
HP360X152 (HP14X102)	2.00E+05	4.37E+08	1.58E+08	0.5	4,500	2,250	3,500	1,750
HP360X132 (HP14X89)	2.00E+05	3.76E+08	1.36E+08	0.5	4,300	2,150	3,400	1,700
HP360X108 (HP14X73)	2.00E+05	3.03E+08	1.09E+08	0.5	4,100	2,050	3,200	1,600
HP310X125 (HP12X84)	2.00E+05	2.71E+08	8.87E+07	0.5	4,000	2,000	3,000	1,500
HP310X110 (HP12X74)	2.00E+05	2.37E+08	7.74E+07	0.5	3,900	1,950	2,900	1,450
HP310X93 (HP12X63)	2.00E+05	1.96E+08	6.37E+07	0.5	3,700	1,850	2,800	1,400
HP310X79 (HP12X53)	2.00E+05	1.64E+08	5.29E+07	0.5	3,500	1,750	2,700	1,350
HP250X85 (HP10X57)	2.00E+05	1.22E+08	4.20E+07	0.5	3,300	1,650	2,500	1,250
HP250X62 (HP10X42)	2.00E+05	8.74E+07	2.98E+07	0.5	3,000	1,500	2,300	1,150
HP200X53 (HP8X36)	2.00E+05	4.95E+07	1.68E+07	0.5	2,600	1,300	2,000	1,000

8.6 BRIDGE'S DISPLACEMENT CAPACITY (ALBHAISI 2003)

8.6.1 H-Pile's Displacement Capacity

Albhaisi (2003) has developed equations to estimate the displacement capacity of steel H-Piles based on a study that utilized 2D pushover analyses. In the study, the pile head displacement capacity, Δ_p , consists of two parts as illustrated in figure 8.37. The first part is the displacement, Δ_{p1} , due to the bending of the pile and the second part is the rigid body displacement, Δ_{p2} , due to the rotation of the pile's top. as illustrated in figure 8.37.

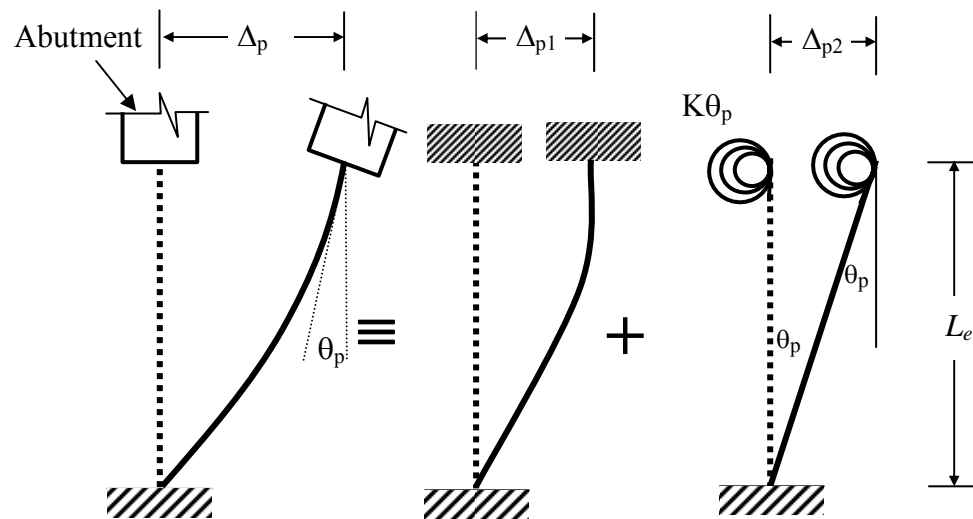


Figure 8.37 Pile's Displacement Components (Albhaisi 2003)

At ultimate failure, the maximum moment at the pile head is equal to M_u as illustrated in figure 3.4. The moment distribution along the equivalent length is assumed to be linear.

The curvature corresponding to this linear moment distribution along the equivalent length of the pile is also illustrated in figure 8.38. By approximating the MCR between the points corresponding to the yield moment, M_y , and the moment, M_u , at ultimate

failure by a linear line as shown in figure 8.38, a linear variation between the curvature, ϕ_y , at yield and curvature, ϕ_u , at ultimate failure is obtained.

The displacement, Δ_{p1} , of the pile, is then obtained by taking the moment of the area under the curvature diagram of figure 8.38 about the free end of the equivalent cantilever. Thus,

$$\begin{aligned} \Delta_{p1} = & \frac{1}{3} \phi_y \left(\frac{M_y}{M_u} L_e \right)^2 + \phi_y \left(1 - \frac{M_y}{M_u} \right) L_e \left[\frac{M_y}{M_u} L_e + \frac{1}{2} \left(1 - \frac{M_y}{M_u} \right) L_e \right] \\ & + \frac{1}{2} (\phi_u - \phi_y) \left(1 - \frac{M_y}{M_u} \right) L_e \left[\frac{M_y}{M_u} L_e + \frac{2}{3} \left(1 - \frac{M_y}{M_u} \right) L_e \right] \quad (\text{Albhaisi 2003}) \end{aligned} \quad (8.8)$$

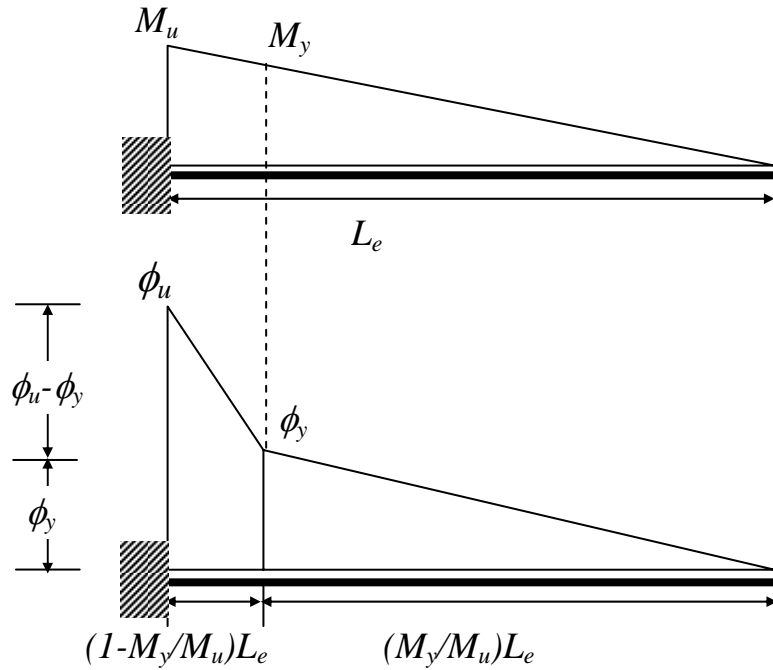


Figure 8.38 Moment Distribution along the Idealized Pile (Albhaisi2003)

Assuming that;

$$m = \frac{M_y}{M_u} \quad (8.9)$$

Substituting Eq.8.9 into Eq.8.8 and further simplifying, the pile displacement, Δ_{p1} , due to the bending action is expressed as:

$$\Delta_{p1} = \frac{\phi_y L_e^2}{6} (1 + m) + \frac{\phi_u L_e^2}{6} (2 - m - m^2) \quad (8.10)$$

To calculate the pile's rigid body displacement, Δ_{p2} , due to the rotational flexibility of the structure above the pile, the stiffness, K_θ , of the spring is assumed to be equal to the rotational stiffness of the structure above the pile. Then, Δ_{p2} can be expressed as follows:

$$\Delta_{p2} = n_p \frac{M_u}{K_\theta} L_e \quad (\text{Albhaishi 2003}) \quad (8.11)$$

Where n_p is the number of piles per girder.

To calculate the rotational stiffness, K_θ , the span adjacent to the abutment was only considered since it provides most of the restraining to the rotation at the pile's head. Furthermore, the span adjacent to the abutment was assumed to have a roller pin support at the far end as shown in figure 8.39.

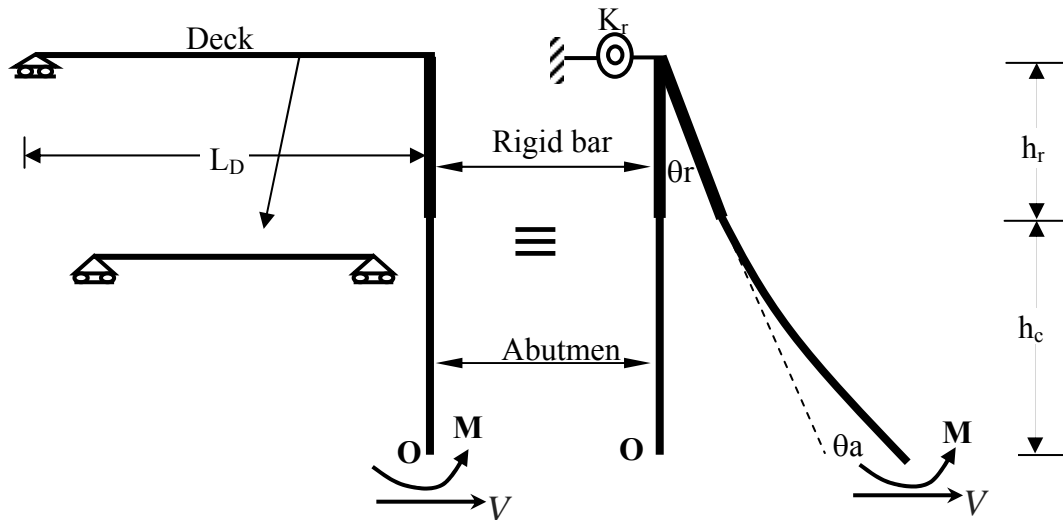


Figure 8.39 Simplified Model for the Abutment-Deck Rotation (Albhaishi, 2003)

Accordingly, the rotational stiffness of the deck adjacent to the abutment is calculated assuming a simply supported beam as illustrated in figure 8.39. Thus, the rotational stiffness of the deck, K_r , is calculated as:

$$K_r = \frac{3E_D I_D}{L_D} \quad (8.12)$$

The total rotation at the pile head (point O in figure 8.39) is equal to the rotation of the bridge deck, θ_r , and the rotation due to the bending of the abutment, θ_a .

Thus,

$$\theta = \theta_r + \theta_a \quad (8.13)$$

For a moment, M , applied at point O, the rotation, θ , is expressed as:

$$\theta = \frac{M}{K_r} + \frac{M h_c}{E_a I_a} \quad (8.14)$$

Where, E_a , and, I_a , are the modulus of elasticity and the moment of inertia for the abutment respectively.

Rearranging Eq.8.14:

$$\theta = M \left(\frac{1}{K_r} + \frac{h_c}{E_a I_a} \right) \quad (8.15)$$

If θ is set to be equal to unity, then the moment, M , becomes the rotational stiffness, K_θ , of the spring at the pile top.

$$1 = K_\theta \left(\frac{1}{K_r} + \frac{h_c}{E_a I_a} \right) \quad (8.16)$$

Solving for K_θ ,

$$K_{\theta} = \frac{1}{\left(\frac{1}{K_r} + \frac{h_c}{E_a I_a} \right)} \quad (8.17)$$

Substituting for K_r , from Eq.8.12;

$$K_{\theta} = \frac{1}{\left(\frac{L_D}{3E_D I_D} + \frac{h_c}{E_a I_a} \right)} \quad (8.18)$$

Substituting Eq. 8.18 into Eq.8.11, the rigid body displacement, Δ_{p2} , due to the rotation at the pile head is calculated as:

$$\Delta_{p2} = n_p M_f l_{ed} \left(\frac{L_D}{3E_D I_D} + \frac{h_c}{E_a I_a} \right) \quad (8.19)$$

The sum of the two components of the pile's displacement, gives the total displacement of the pile, Δ_p . Therefore;

$$\Delta_p = \Delta_{p1} + \Delta_{p2} \quad (8.20)$$

Substituting Eq. 8.10 and Eq. 8.19 for Δ_{p1} , and, Δ_{p2} , respectively,

Δ_p , is expressed as,

$$\Delta_p = \frac{\phi_y L_e^2}{6} (1+m) + \frac{\phi_u L_e^2}{6} (2-m-m^2) + n_p M_u L_e \left(\frac{L_D}{3E_D I_D} + \frac{h_c}{E_a I_a} \right) \quad (8.21)$$

8.6.2 Relative Displacement of the Abutment at Pile's Failure

Albhaisi (2003) has also developed an expression to calculate the relative displacement of the abutment when the H-Piles reach its ultimate capacity. As shown in figure 8.40, the relative displacement of the abutment is defined as the sum of the displacement, Δ_r , due to the rotation of the deck-abutment joint, and the displacement, Δ_d , due to the bending of the abutment. Accordingly;

$$\Delta_a = \Delta_r + \Delta_d \quad (8.22)$$

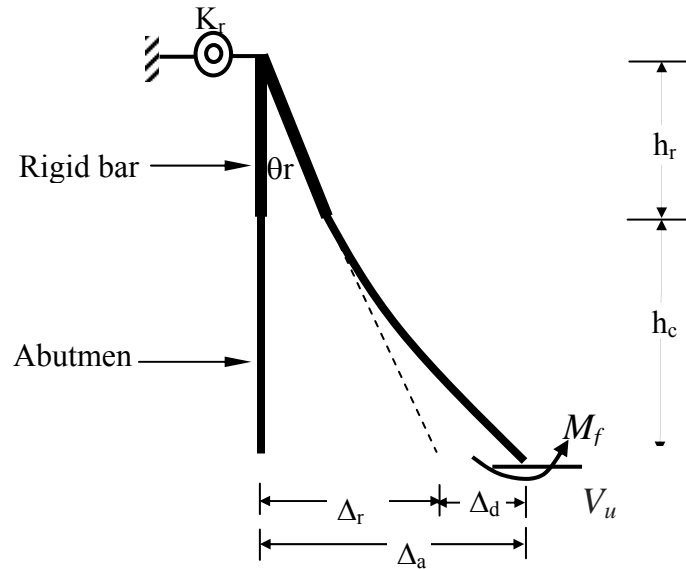


Figure 8.40 Simplified Model for the Abutment Displacement (Albhaisi 2003)

In figure 8.40, the rotational stiffness, K_r , at the top of the abutment accounts for the rotational stiffness of the deck. The abutment displacement due to the rotation of the deck-abutment joint, Δ_r , is calculated as follows:

$$\Delta_r = \theta_r (h_c + h_r) \quad (8.23)$$

Where, h_r is the distance from the centerline of the deck to the bottom of the girder, h_c is the depth of the abutment below the girder.

The total moment, M_T , at the abutment-deck joint due to the shear and bending moment transferred from the pile is defined as

$$M_T = n_p (M_u + V_u (h_c + h_r)) \quad (8.24)$$

Where, V_u , and M_u , are the shear and the moment transferred from the pile to the abutment at ultimate failure respectively. The rotation, θ_r , of the abutment-deck joint is obtained by dividing the total moment, M_T , by the rotational stiffness, K_r , of the deck. Thus,

$$\theta_r = \frac{M_T}{K_r} \quad (8.25)$$

Substituting Eq. 8.24 into Eq. 8.25 and then into Eq. 8.23; the displacement, Δ_r , is obtained as:

$$\Delta_r = n_p \frac{M_f + V_f (h_c + h_r)}{K_r} (h_c + h_r) \quad (8.26)$$

Re-arranging Eq.8.26; the displacement, Δ_r , due to the rotation of the deck-abutment joint is expressed as:

$$\Delta_r = n_p \frac{M_u (h_c + h_r)}{K_r} + n_p \frac{V_u (h_c + h_r)^2}{K_r} \quad (8.27)$$

The displacement, Δ_d , due to the bending action of the abutment, is expressed as the sum of the displacements due to the effects of V_u , and M_u respectively. Thus,

$$\Delta_d = n_p \frac{V_u h_c^3}{3E_a I_a} + n_p \frac{M_u h_c^2}{2E_a I_a} \quad (8.28)$$

The total relative displacement of the abutment is then calculated by adding Eqs. 8.27 and 8.28;

$$\Delta_a = n_p \left(\frac{V_u (h_c + h_r)^2}{K_r} + \frac{M_u (h_c + h_r)}{K_r} + \frac{V_u h_c^3}{3E_a I_a} + \frac{M_u h_c^2}{2E_a I_a} \right) \quad (8.29)$$

The shear force at the abutment-pile connection, V_u , can be expressed as a function of the moment M_u , using a theoretical equivalent shear length for the pile, l_{ev} , as shown in figure 8.41.

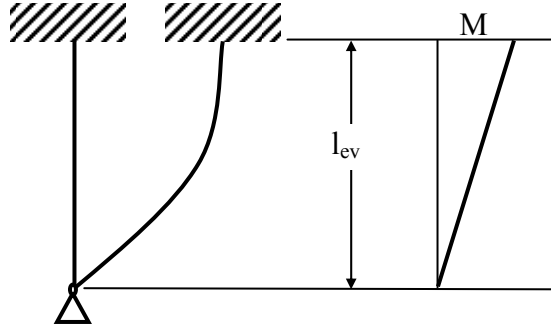


Fig.8.41 Equivalent shear length, l_{ev} (Albhaisi 2003)

Thus,

$$V_u = \frac{M_u}{l_{ev}} \quad (8.30)$$

Substituting Eq. 8.30 into Eq.8.29, the relative displacement of the abutment is expressed as:

$$\Delta_a = n_p \left(\frac{M_u (h_c + h_r)^2}{l_{ev} K_r} + \frac{M_u (h_c + h_r)}{K_r} + \frac{M_u h_c^3}{3l_{ev} E_a I_a} + \frac{M_u h_c^2}{2E_a I_a} \right) \quad (8.31)$$

l_{ev} can be expressed as a function of the critical length, l_c , as

$$l_{ev} = \delta l_c \quad (8.32)$$

Where, δ is a constant. Substituting Eq. 8.32 into Eq. 8.31;

$$\Delta_a = n_p \left(\frac{M_u (h_c + h_r)^2}{(\delta l_c) K_r} + \frac{M_u (h_c + h_r)}{K_r} + \frac{M_u h_c^3}{3(\delta l_c) E_a I_a} + \frac{M_f h_c^2}{2 E_a I_a} \right) \quad (8.33)$$

A value of 0.25 was found to be reasonable for the factor δ for clay and 0.3 for sand.

Thus,

For clay

$$l_{ev} = 0.25 l_c \quad (8.34a)$$

For Sand

$$l_{ev} = 0.3 l_c \quad (8.34b)$$

Substituting Eq. 8.34 into Eq. 8.33, the relative displacement, Δ_a , of the abutment at ultimate failure of the pile is obtained as:

For clay:

$$\Delta_a = n_p \left(\frac{M_u (h_c + h_r)^2}{0.25 l_c K_r} + \frac{M_u (h_c + h_r)}{K_r} + \frac{M_u h_c^3}{0.75 l_c E_a I_a} + \frac{M_u h_c^2}{2 E_a I_a} \right) \quad (8.35)$$

For sand:

$$\Delta_a = n_p \left(\frac{M_u (h_c + h_r)^2}{0.3 l_c K_r} + \frac{M_u (h_c + h_r)}{K_r} + \frac{M_u h_c^3}{0.9 l_c E_a I_a} + \frac{M_u h_c^2}{2 E_a I_a} \right) \quad (8.36)$$

Substituting the expression from Eq. 8.12 for the rotational stiffness, K_r , of the deck, the relative displacement, Δ_a , of the abutment at ultimate failure of the pile is expressed as:

For clay:

$$\Delta_a = n_p \left(\frac{M_u l_D (h_c + h_r)^2}{0.75 l_c E_D I_D} + \frac{M_u l_D (h_c + h_r)}{3 E_D I_D} + \frac{M_u h_c^3}{0.75 l_c E_a I_a} + \frac{M_u h_c^2}{2 E_a I_a} \right) \quad (8.37)$$

For sand:

$$\Delta_a = n_p \left(\frac{M_u l_D (h_c + h_r)^2}{0.9 l_c E_D I_D} + \frac{M_u l_D (h_c + h_r)}{3 E_D I_D} + \frac{M_u h_c^3}{0.9 l_c E_a I_a} + \frac{M_u h_c^2}{2 E_a I_a} \right) \quad (8.38)$$

CHAPTER 9

SUMMARY AND CONCLUSIONS

9.1 SUMMARY

This research investigated the effect of substructure stiffness on the performance of short and medium span length Integral Abutment Bridges (IABs) subjected to thermal load. Various parameters such as foundation soil stiffness, pile orientation, pile type, and abutment geometry on the performance of IABs, were considered.

Three-dimensional (3D) Finite Element (FE) models were developed using the FE software LUSAS to capture the behavior of IABs including the variations in displacement and rotation in the transverse direction for the various components of the superstructure as well as the substructure. Field measurements from a recently constructed two-span steel girder IAB were utilized to validate the 3D FE models. Using the validated model, a parametric study was carried out to study the effect of the above parameters on the performance of IABs under thermal loading using AASHTO-LRFD temperature ranges. The study results showed that among the investigated parameters, the foundation soil stiffness stands as the most important factor that affects the performance of IABs. In general, the bridge behavior is more sensitive to the foundation soil stiffness during bridge contraction. The results from this study showed considerable variations in displacement and rotation in the transverse direction for the various components of the superstructure and the substructure in relatively wide IABs. This research suggests that Prestressed Concrete Piles can be a viable alternative to steel H-Piles for short span bridges. It was also noticed that the stress level due to thermal loading in the various components of the bridge can be significantly reduced by enclosing the top part of the

pile in an enclosure filled with crushed stone or loose sand. Moreover, this research suggests that the pile orientation has a minimum effect on the behavior of IABs, while a slight increase in the abutment height can significantly reduce the displacement and rotation along the piles during bridge expansion. Additionally, the research suggests that 3D models are necessary to capture the behavior of IABs especially during bridge expansion. The research provided simple equations and charts to help bridge engineers calculate the displacement and rotation along the substructure.

9.2 CONCLUSIONS

The substructure stiffness has a significant effect on the performance of IABs. The effect of the substructure stiffness on the behavior of IABs is more significant when the bridge is under contraction. The detailed conclusions of this research are presented in the following sub-sections.

9.2.1 Foundation Soil

- Although the stiffness of foundation soil has a negligible effect on the displacement at the top of the abutment, it has a major effect on the displacement and rotation along the abutment and the piles, as well as the stresses in the superstructure and the substructure.
- At exterior locations, the displacement of the bridge due to thermal expansion and contraction is equal to thermal demand of the bridge when the retaining walls are not attached to the abutment. At interior locations, the displacement of the bridge due to thermal expansion and contraction is about 10% to 15% less than the thermal demand of the bridge.
- For the same displacement at the top of the abutment, the displacement at the top of the pile is significantly larger when the bridge is under contraction.

- The movement of the abutment can be approximated by rigid body movement during bridge expansion and contraction. The rate of change in rotation of the abutment during bridge expansion is considerably smaller than during bridge contraction thus exhibiting more rigid body movement.
- There are significant variations in displacements and rotations along the top of the piles in the transverse direction causing significant variation in stresses.
- The stresses in the superstructure due to thermal loads during bridge expansion and contraction are higher in interior girders. The variation in girder stress between exterior and interior girders is larger in short span bridges.
- The backfill pressure on the abutment increases notably with the increase in top of pile displacement especially in long span bridges.

9.2.2 Pile Enclosure

- Using pile enclosure is very effective in reducing the stresses at the top of the pile. It significantly increases the displacement and reduces the rotation at the top of the pile. Using two meters enclosure could reduce the stresses at the top of the pile due to thermal loads by up to 50%.
- Using pile enclosure larger than four meters in length is not necessary and can be counterproductive by decreasing the confinement of the pile.
- Using pile top enclosure is very effective in reducing the stresses in the girders in short bridges built on stiff soils especially during bridge contraction. That effect is less significant in long bridges.

9.2.3 Pile Orientation

- Pile orientation has a negligible effect on displacement and rotation of the abutment during bridge expansion. The effect of pile orientation is more noticeable in soft soils especially during bridge contraction.
- Pile orientation has a negligible effect on the stresses in the superstructure during bridge expansion in both short and long bridges. Pile orientation has a notable effect on the stresses in the superstructure during bridge contraction in short bridges especially in soft soils.

9.2.4 Abutment Height

- Abutment height has a negligible effect on the displacement at the top of the abutment, but it has a significant effect on the rotation along the abutment and on the displacement and rotation along the pile.
- The displacement at the top of the pile could be reduced by more than 50% if the abutment height increased from 3 to 4 meters.

9.2.5 H-Piles versus Prestressed Concrete Piles (PCPs)

- The behavior of bridges supported by H-Piles is comparable to those supported by PCPs. PCPs can be a viable alternative to steel H-Piles for short bridges in corrosive environments.
- PCPs should not be used for medium and long span IABs without the use of pile enclosures and/or other special considerations.

9.2.6 2D versus 3D

- 3D models are necessary to capture the behavior of IABs.
- 2D model results give good approximation to 3D model results during bridge contraction especially in soft soils; however, 2D model results could not predict the behavior of IABs during bridge expansion especially in stiff soils.

9.2.7 Additional Conclusions

- Thermal loads on superstructures of IABs could induce significant axial loads on the piles.
- The axial loads on the piles due to thermal loads on the superstructure vary significantly between interior and exterior piles in relatively wide IABs.

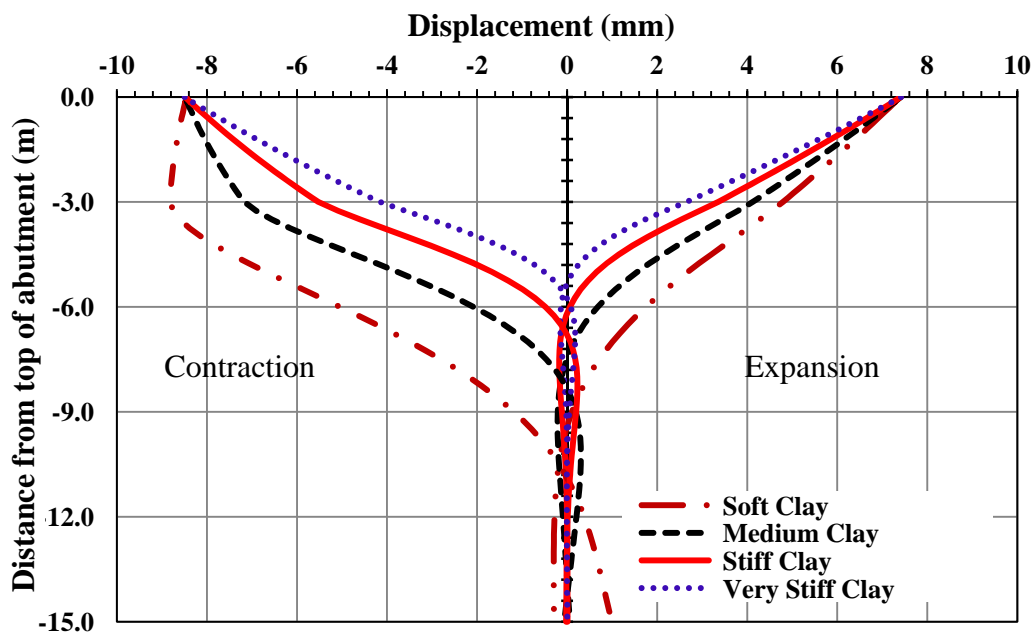
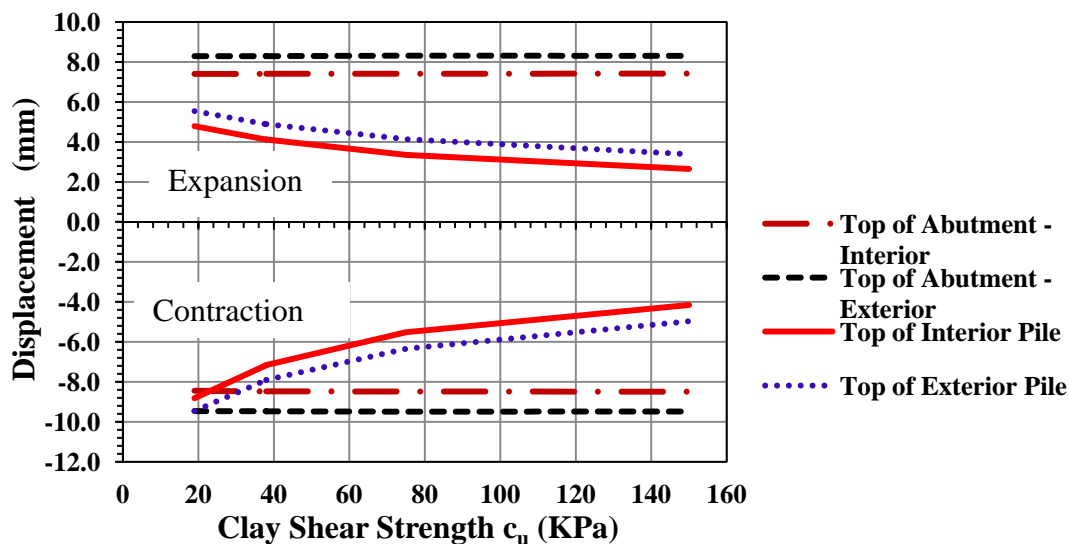
9.3 RECOMMENDATIONS FOR FUTURE RESEARCH

The use of Integral Abutment Bridges in the United States and around the world is becoming very popular. With the increasing popularity of Integral Abutment Bridges, there is a need to investigate the performance of this type of bridges under different loads and in different service conditions. The effect of substructure stiffness on the performance of square Integral Abutment Bridges under thermal loads was investigated in this research. The following are recommendations for future research on issues that were not considered in this study:

- The behavior of skewed IABs under thermal loads.
- The interaction between live load and thermal loads in IABs.
- The behavior of IABs under large lateral loads, particularly seismic loads.
- Long term field investigation of the performance of IABs.
- The effect of substructure stiffness on the performance of long IABs.
- The effective width of the abutment at the abutment-pile joint.
- Comprehensive design guidelines for IABs.

APPENDIX A

ADDITIONAL FIGURES



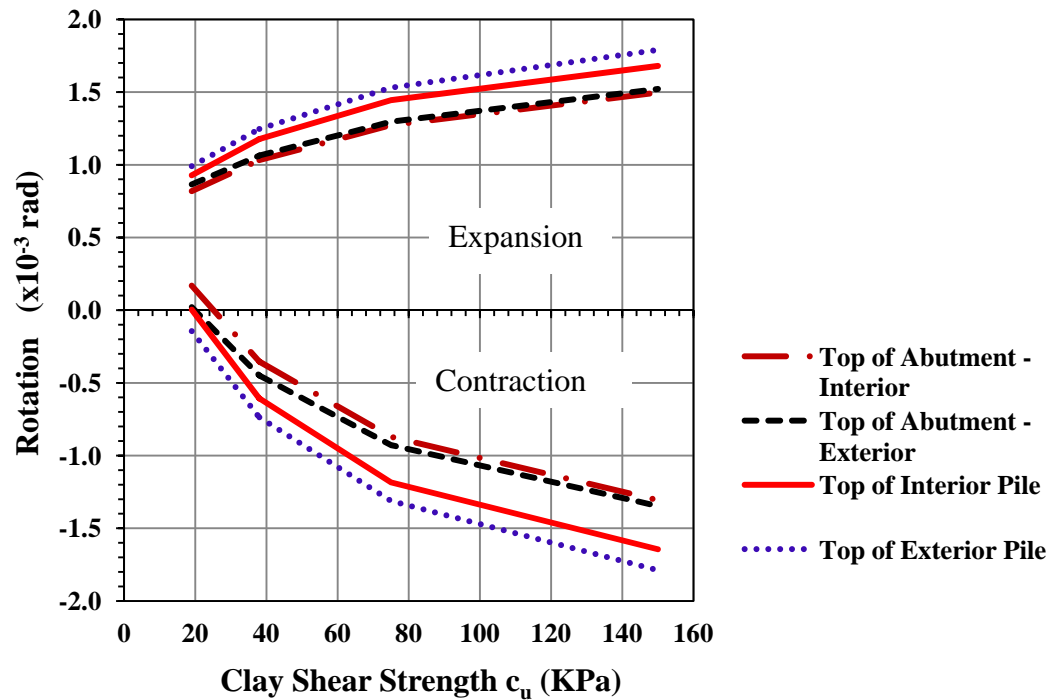


Figure A.3 Rotation at Interior and Exterior Locations
(38-m Bridge, Clay, 3m Abutment, HP310X125 Strong Orientation)

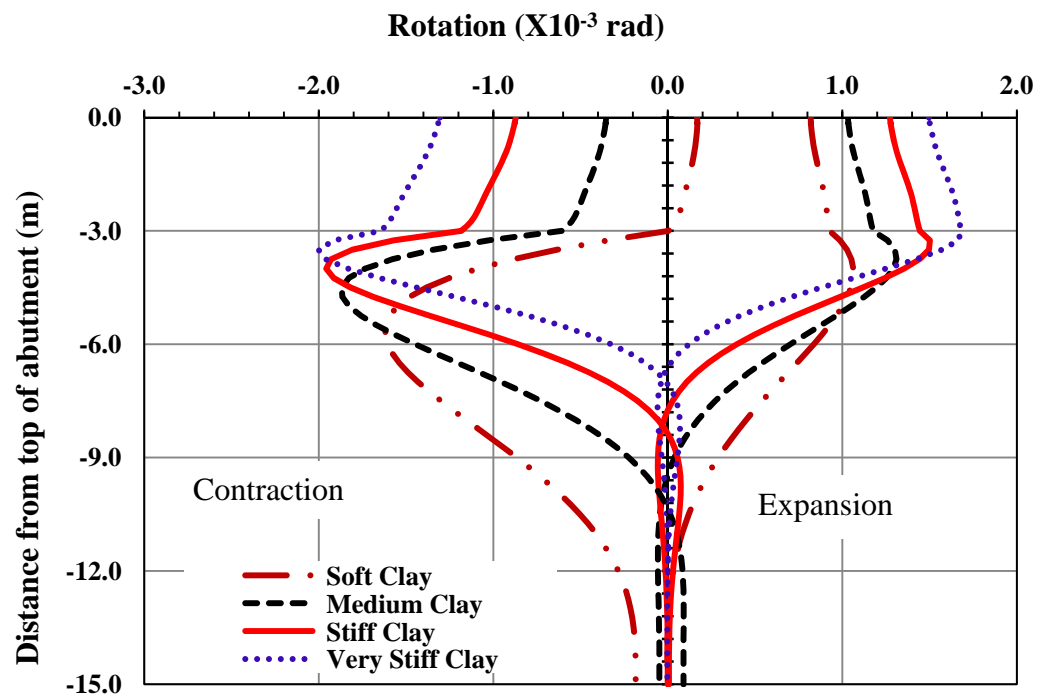


Figure A.4 Rotation along the Abutment and the Interior Pile
(38-m Bridge, Clay, 3m Abutment, HP310X125 Strong Orientation)

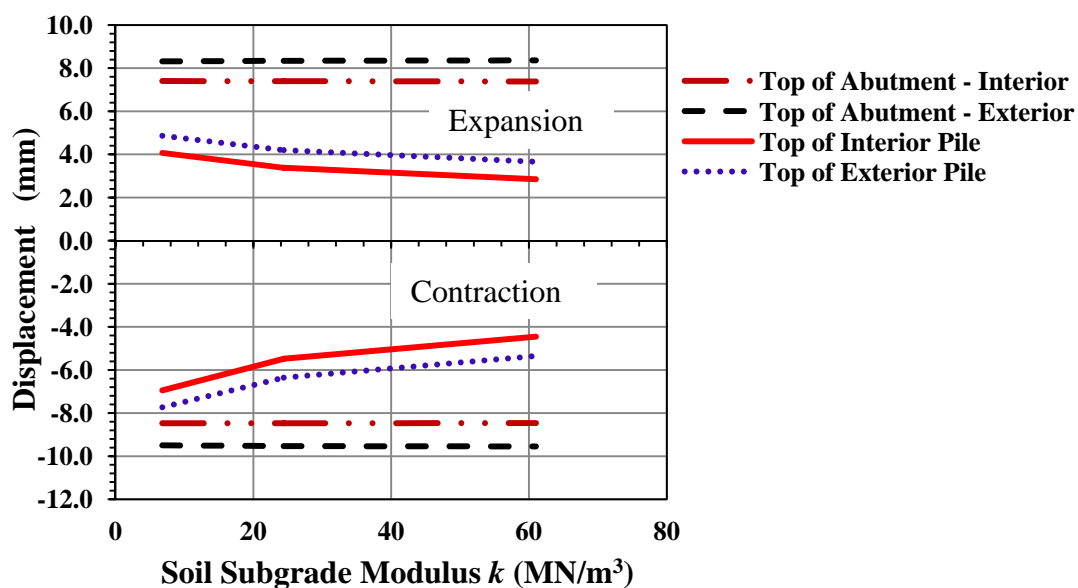


Figure A.5 Displacement at Interior and Exterior Locations
(38-m Bridge, Sand, 3m Abutment, HP310X125 Strong Orientation)

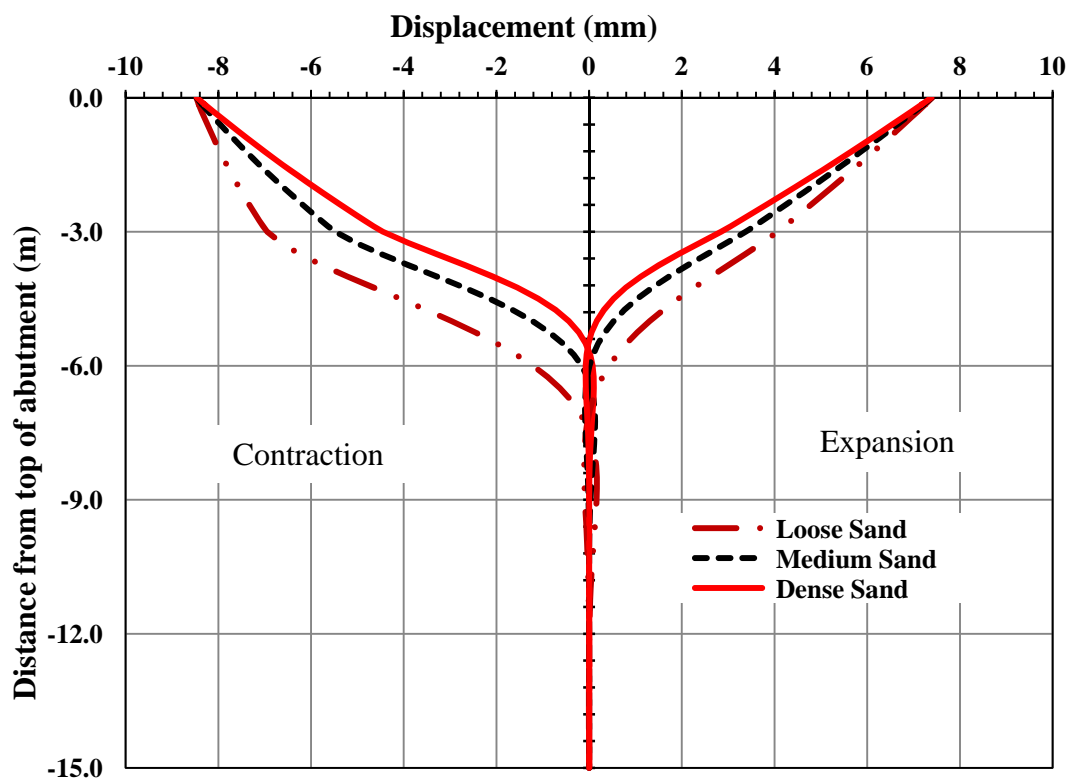


Figure A.6 Displacement along the Abutment and the Interior Pile
(38-m Bridge, Sand, 3m Abutment, HP310X125 Strong Orientation)

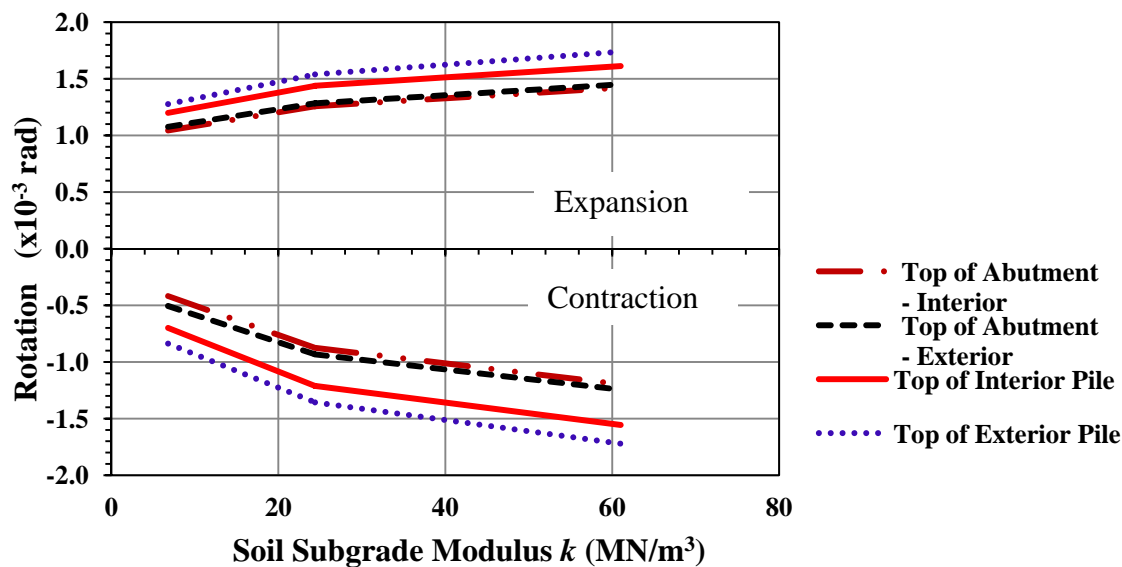


Figure A.7 Rotation at Interior and Exterior Locations
(38-m Bridge, Sand, 3m Abutment, HP310X125 Strong Orientation)

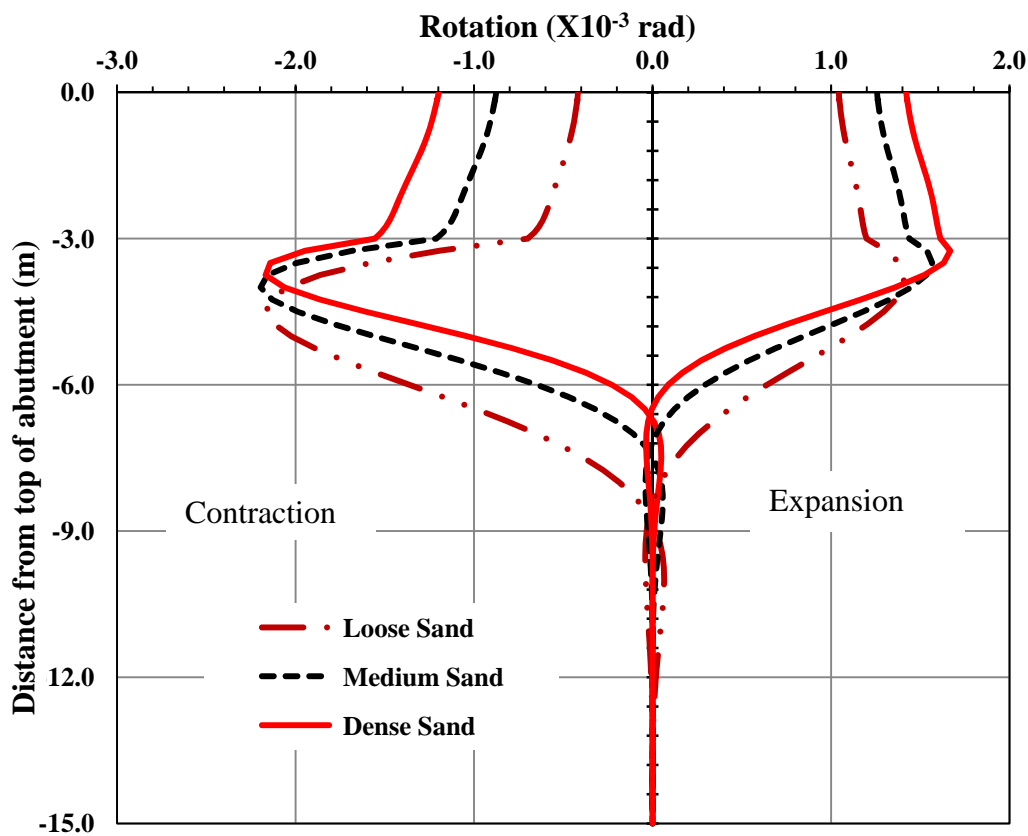


Figure A.8 Rotation along the Abutment and the Interior Pile
(38-m Bridge, Sand, 3m Abutment, HP310X125 Strong Orientation)

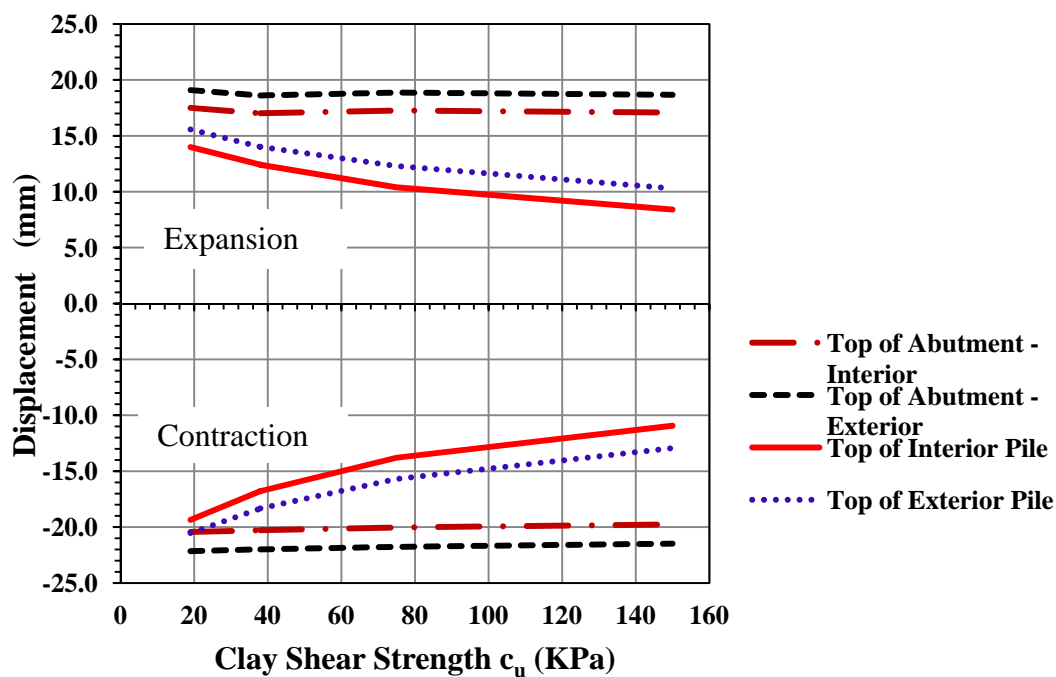


Figure A.9 Displacement at Interior and Exterior Locations
(90-m Bridge, Clay, 3m Abutment, HP360X152 Strong Orientation)

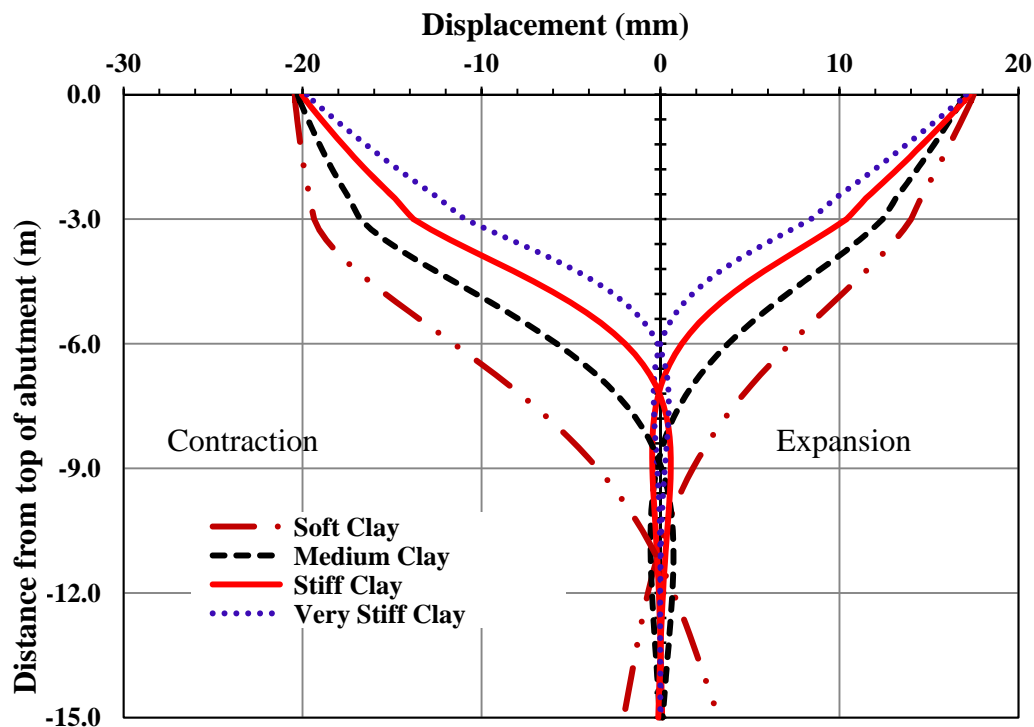


Figure A.10 Displacement along the Abutment and the Interior Pile
(90-m Bridge, Clay, 3m Abutment, HP360X152 Strong Orientation)

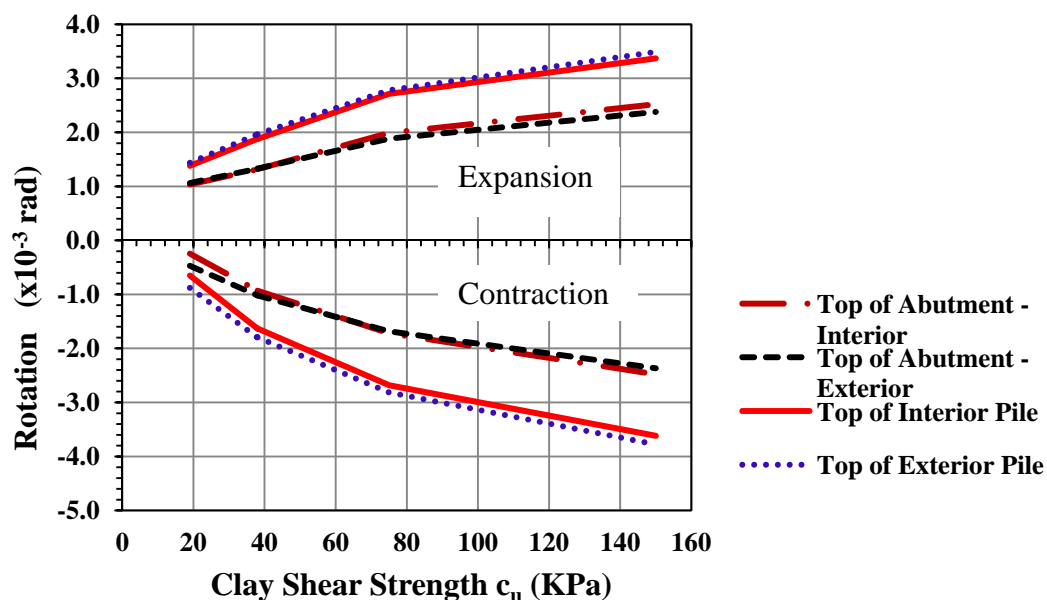


Figure A.11 Rotation at Interior and Exterior Locations
(90-m Bridge, Clay, 3m Abutment, HP360X152 Strong Orientation)

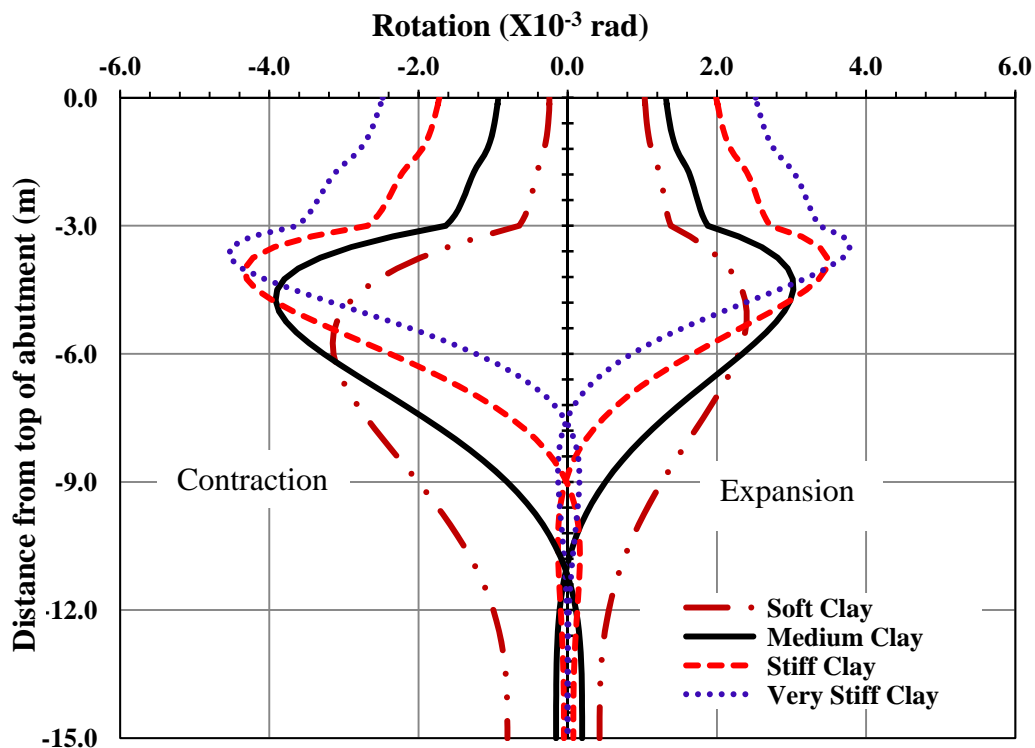


Figure A.12 Rotation along the Abutment and the Interior Pile
(90-m Bridge, Clay, 3m Abutment, HP360X152 Strong Orientation)

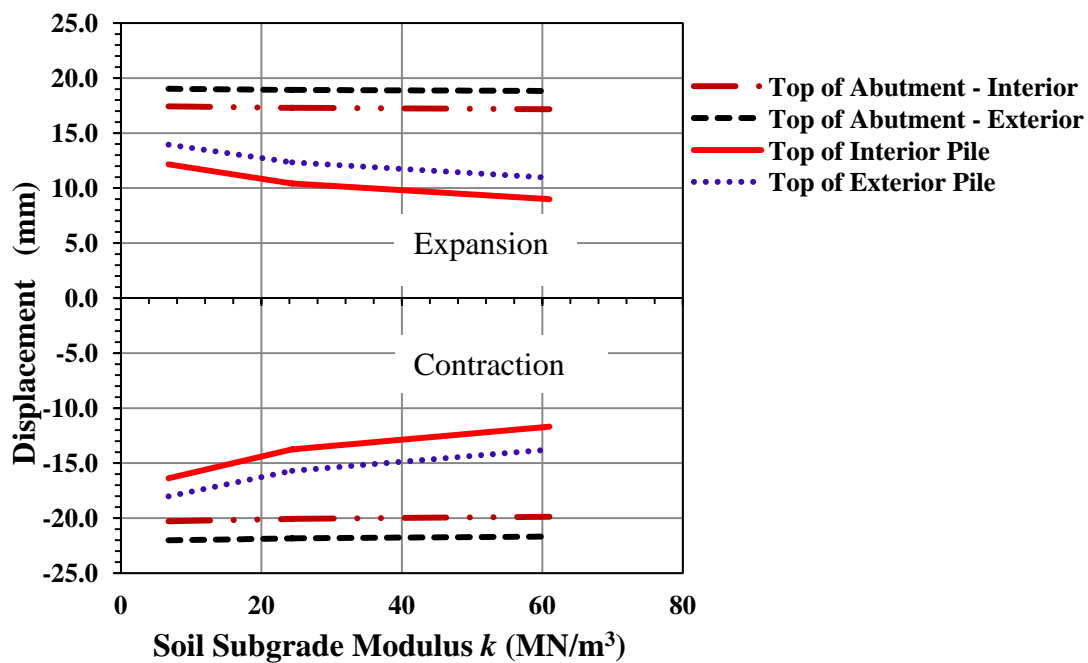


Figure A.13 Displacement at Interior and Exterior Locations
(90-m Bridge, Sand, 3m Abutment, HP360X152 Strong Orientation)

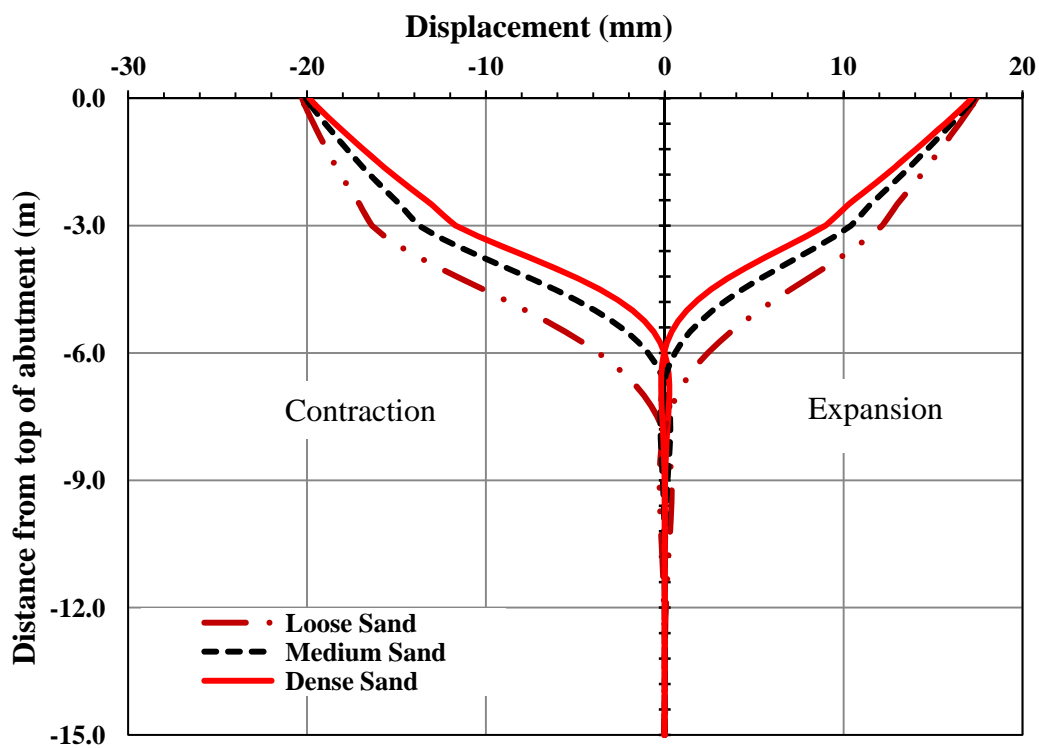


Figure A.14 Displacement along the Abutment and the Interior Pile
(90-m Bridge, Sand, 3m Abutment, HP360X152 Strong Orientation)

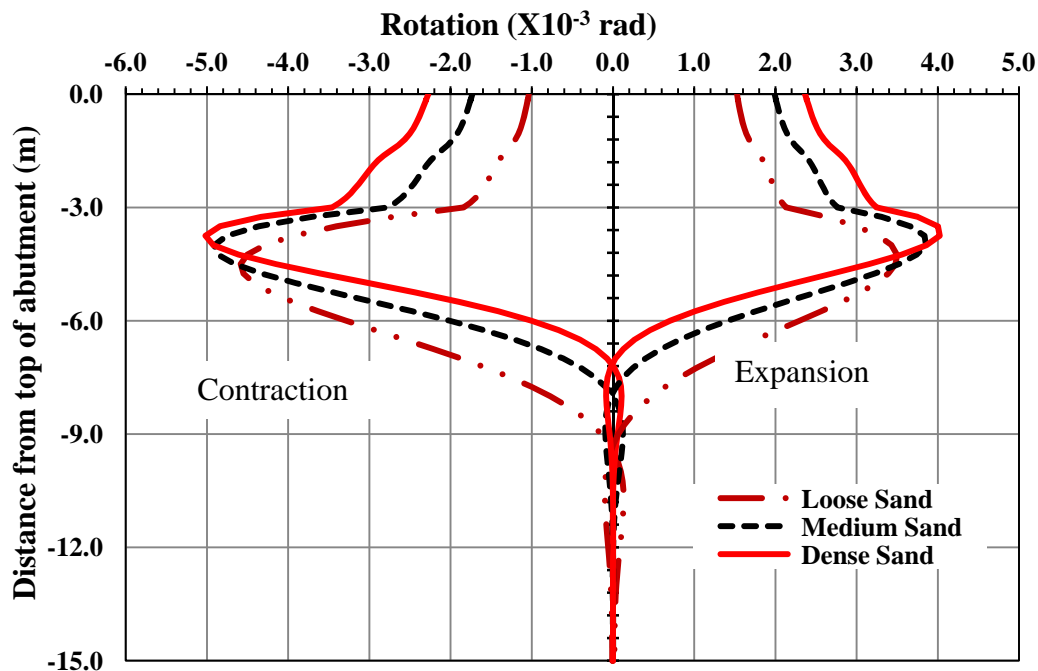


Figure A.15 Rotation at Interior and Exterior Locations
(90-m Bridge, Sand, 3m Abutment, HP360X152 Strong Orientation)

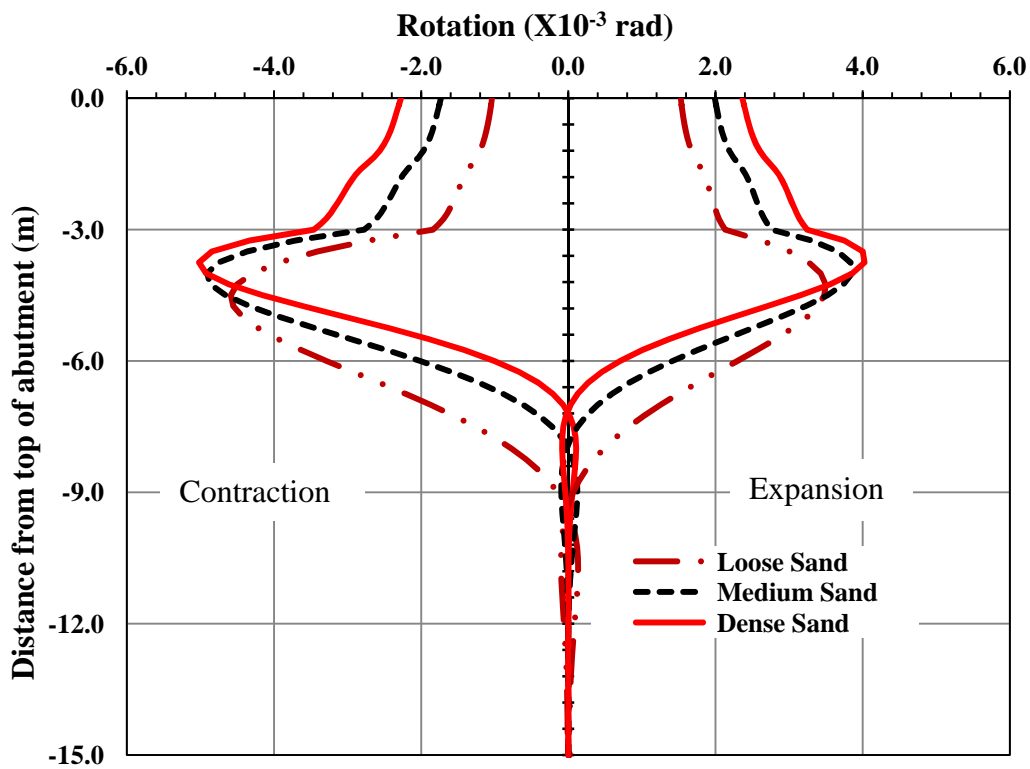


Figure A.16 Rotation along the Abutment and the Interior pile
(90-m Bridge, Sand, 3m Abutment, HP360X1152 Strong Orientation)

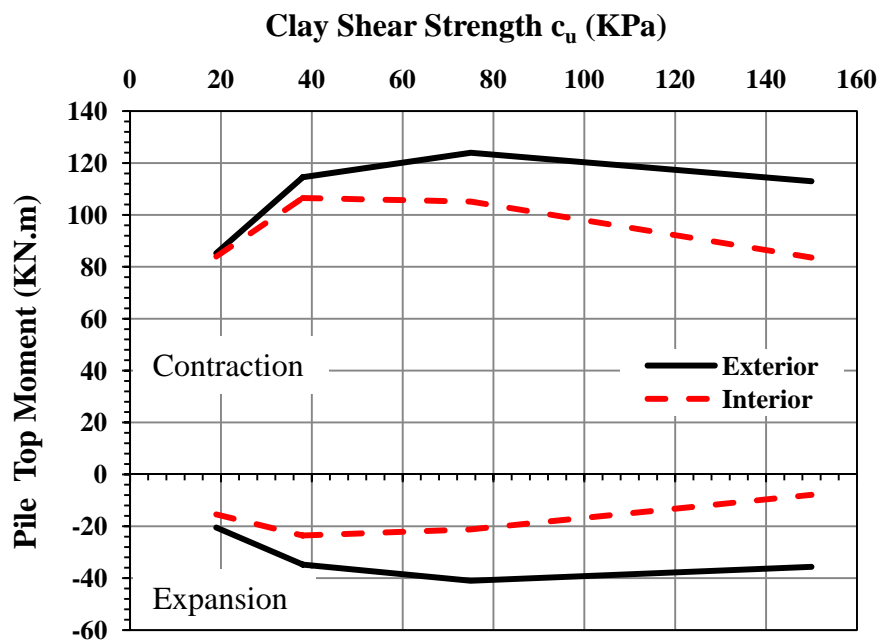


Figure A.17 Moment at the Top of the Pile
(38-m Bridge, Clay, 3m Abutment, HP310X125 Strong Orientation)

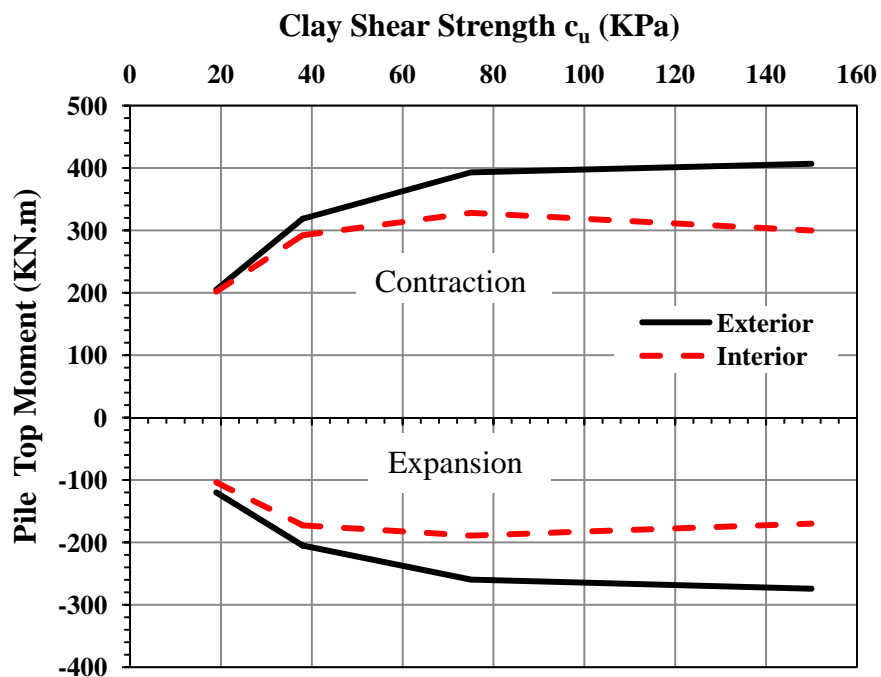


Figure A.18 Moment at the top of the Pile
(90-m Bridge, Clay, 3m Abutment, HP360X152 Strong Orientation)

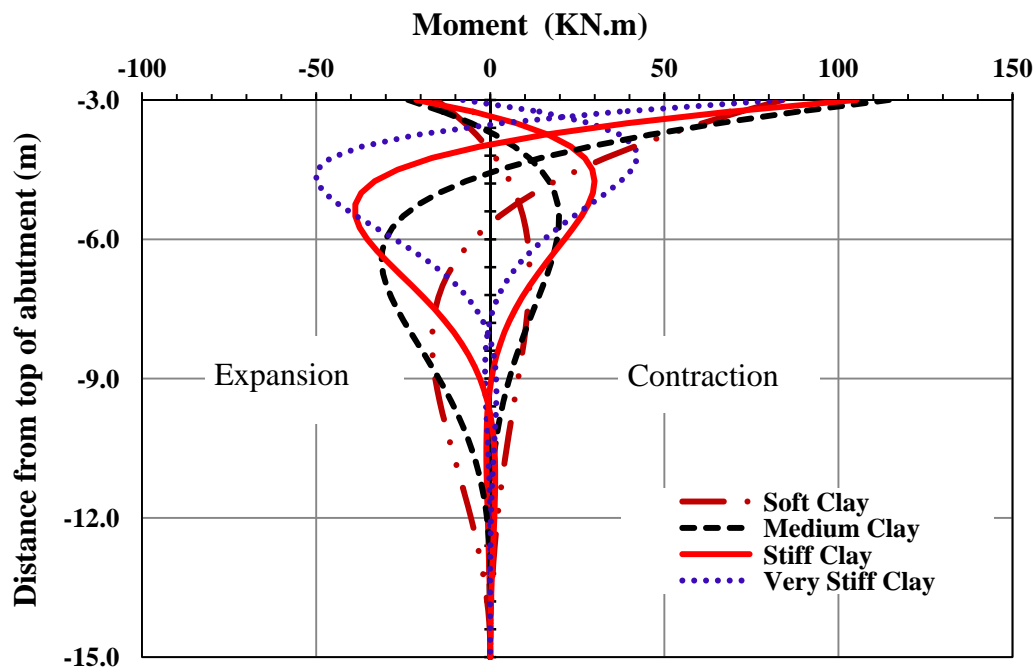


Figure A.19 Moment Loads along the Interior Pile
(38-m Bridge, Clay, 3m Abutment, HP310X125 Strong Orientation)

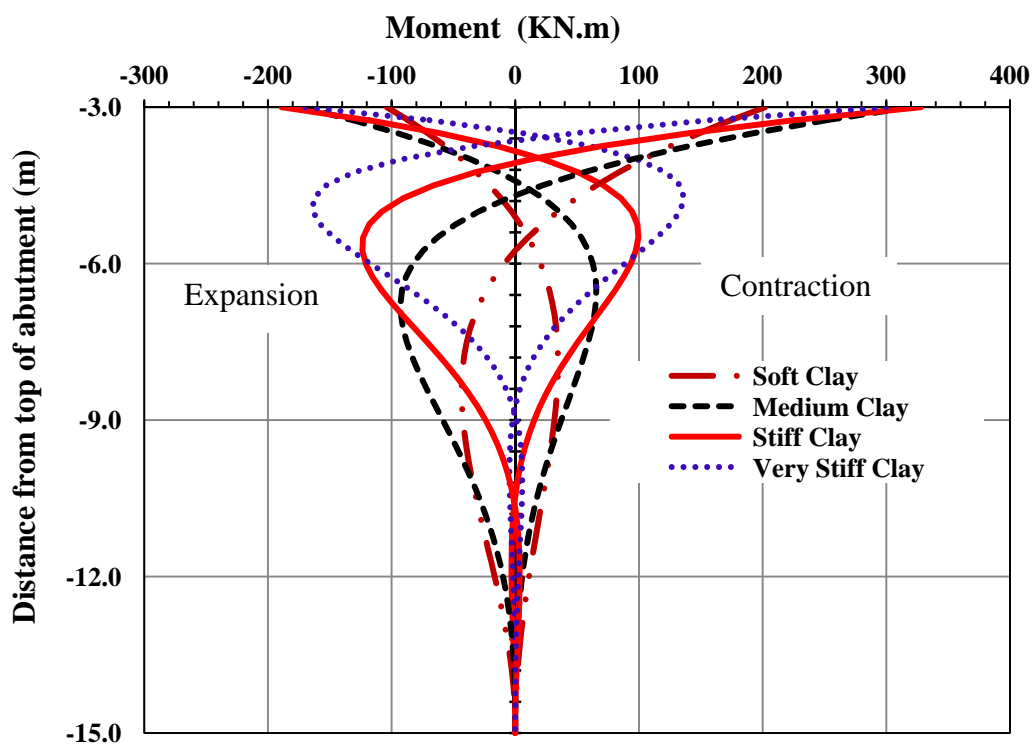


Figure A.20 Moment along the Interior Pile
(90-m Bridge, Clay, 3m Abutment, HP360X152 Strong Orientation)

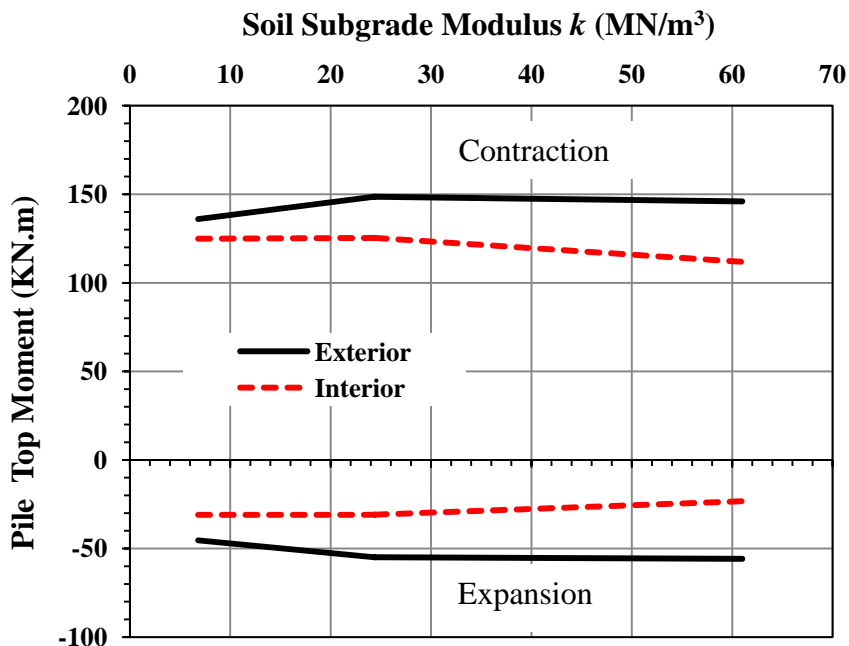


Figure A.21 Moment at the Top of the Pile
(38-m Bridge, Sand, 3m Abutment, HP310X125 Strong Orientation)

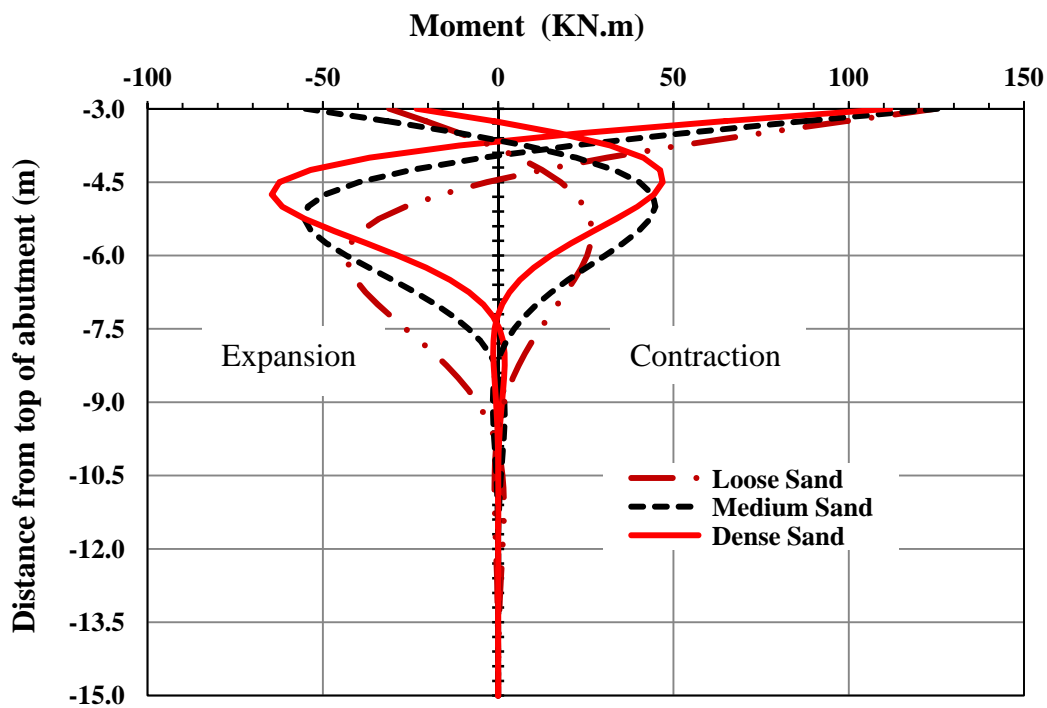


Figure A.22 Moment along the Interior Pile
(38-m Bridge, Sand, 3m Abutment, HP310X125 Strong Orientation)

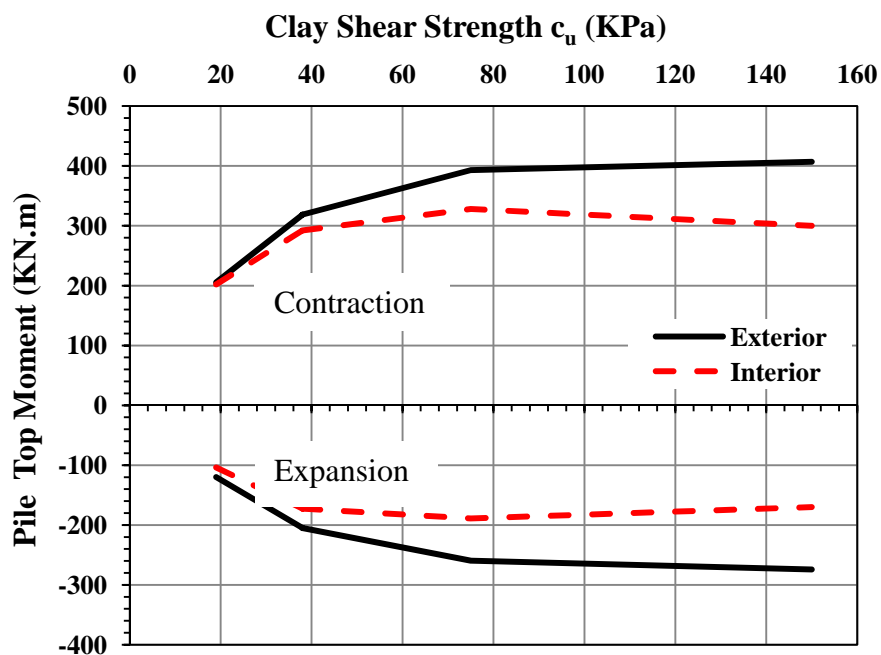


Figure A.23 Moment at the Top of the Pile
(90-m Bridge, Clay, 3m Abutment, HP360X152 Strong Orientation)

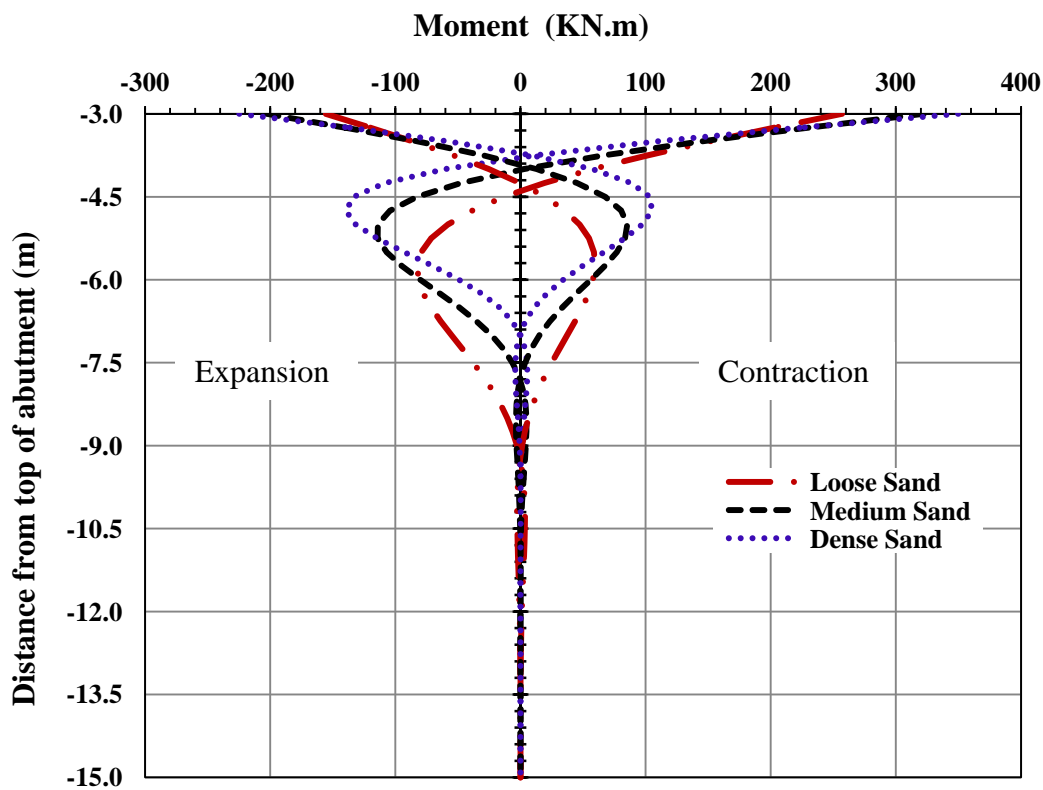


Figure A.24 Moment along the Interior Pile
(90-m Bridge, Sand, 3m Abutment, HP360X152 Strong Orientation)

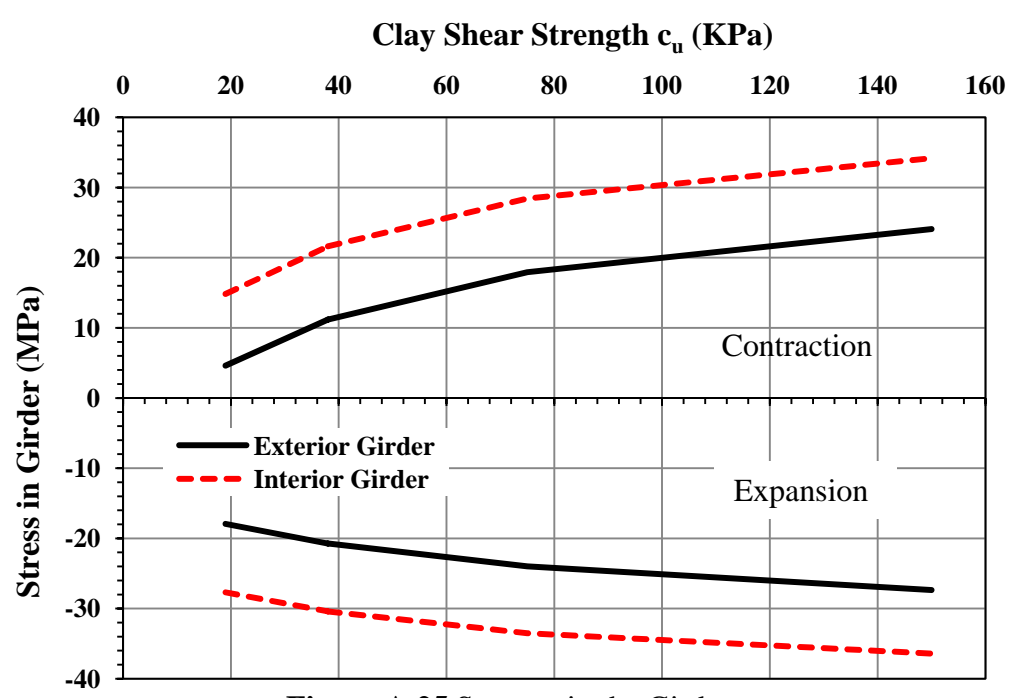


Figure A.25 Stresses in the Girders
(38-m Bridge, Clay, 3m Abutment, HP310X125 Strong Orientation)

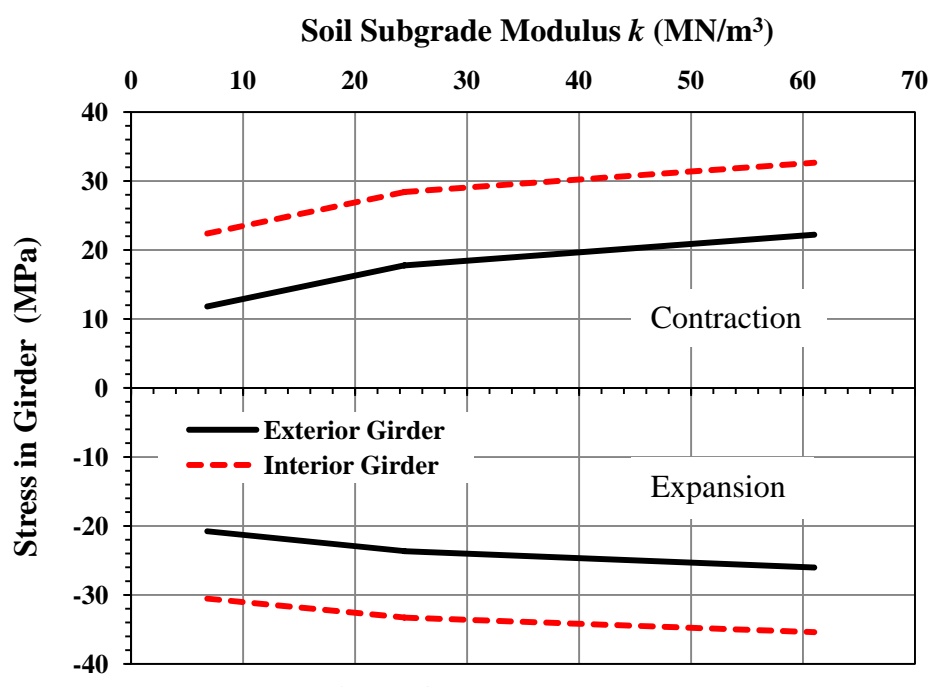


Figure A.26 Stresses in the Girders
(38-m Bridge, Sand, 3m Abutment, HP310X125 Strong Orientation)

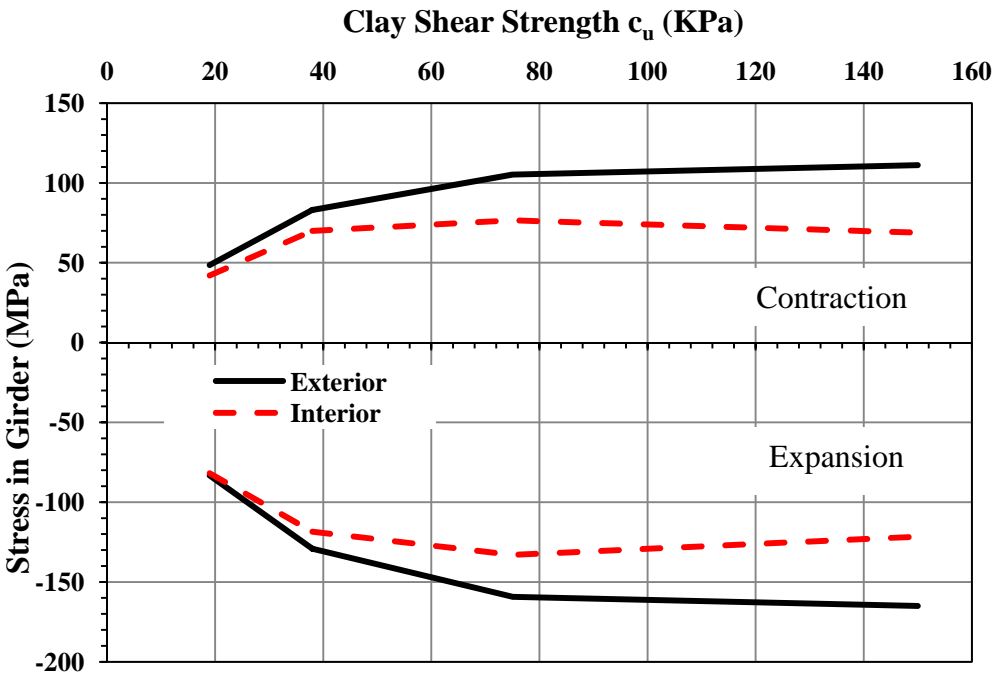


Figure A.27 Stresses in the Girders
(90-m Bridge, Clay, 3m Abutment, HP360X152 Strong Orientation)

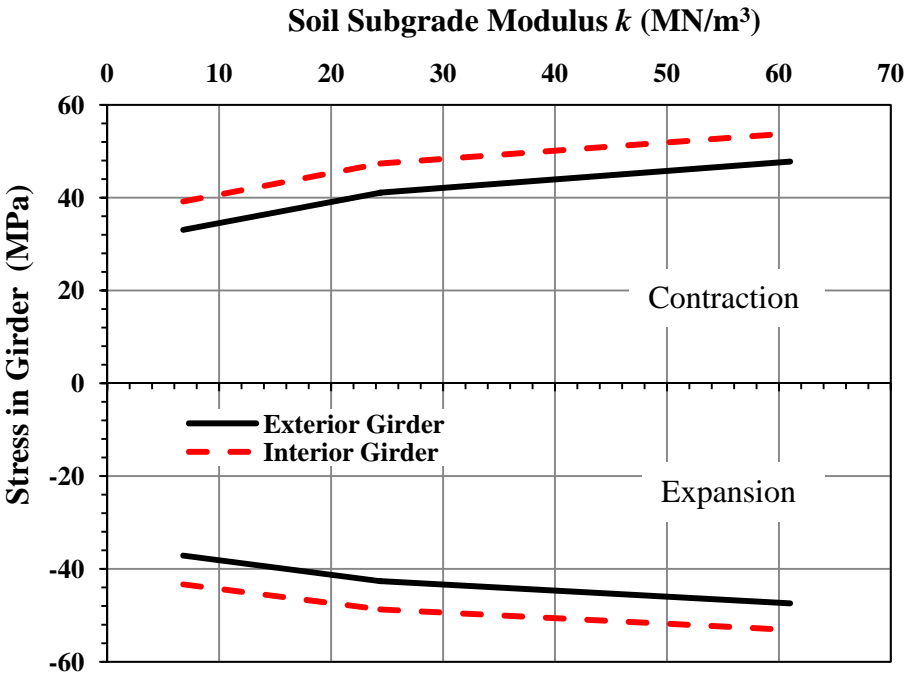


Figure A.28 Stresses in the Girders
(90-m Bridge, Sand, 3m Abutment, HP360X152 Strong Orientation)

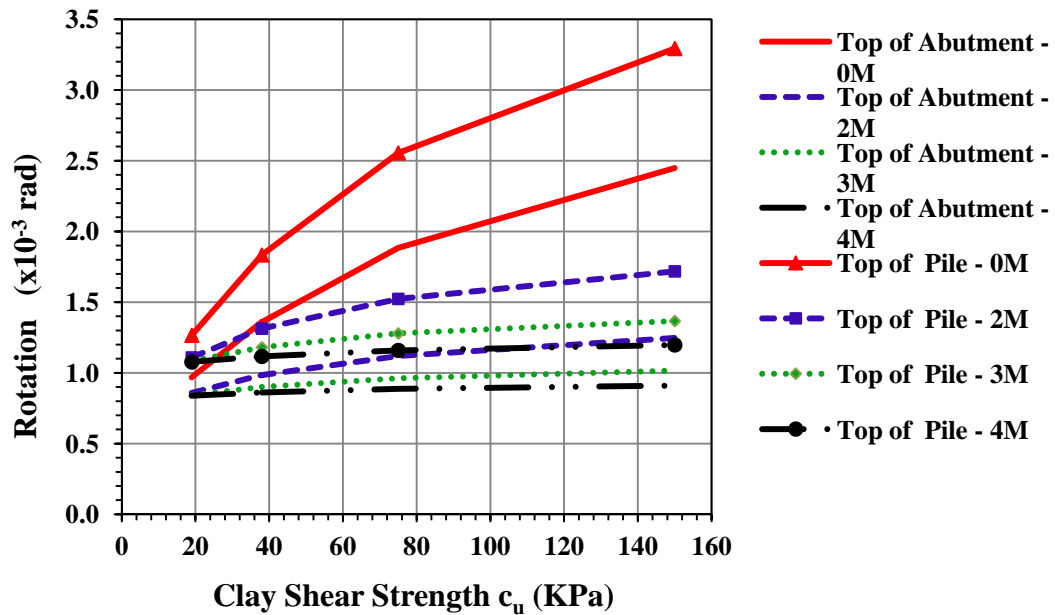


Figure A.29 Rotation (Expansion) at the Interior Location
(90-m Bridge, Clay, 3m Abutment, 360X152 Weak Orientation with Pile Enclosure)

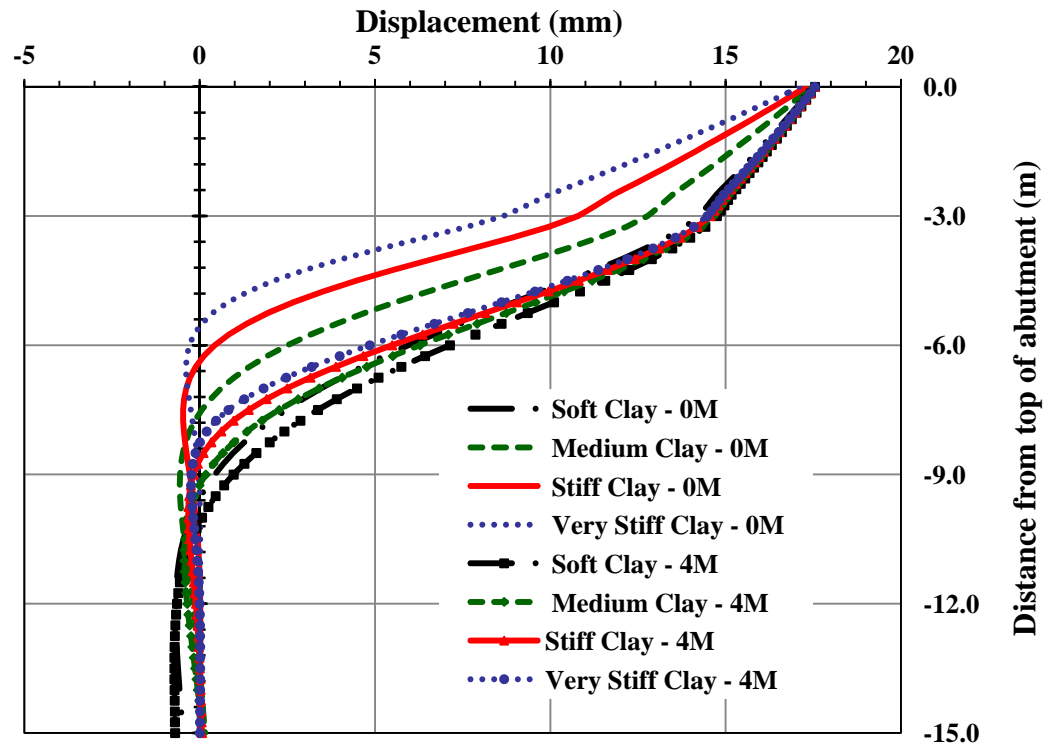


Figure A.30 Displacement (Expansion) along the Abutment and the Interior Pile
(90-m Bridge, Clay, 3m Abutment, HP310X125 Weak Orientation with Pile Enclosure)

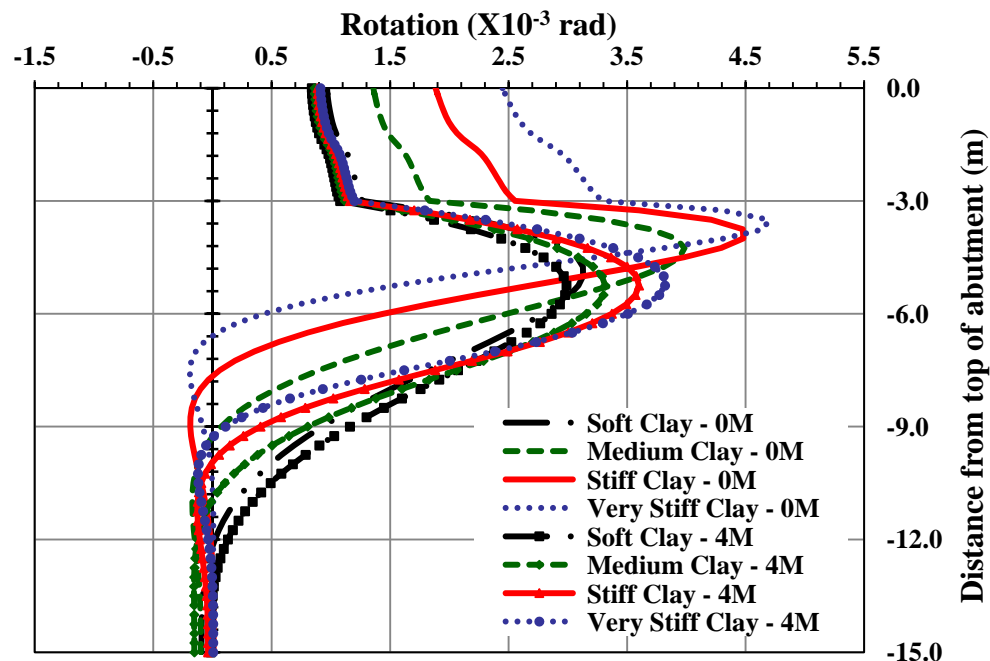


Figure A.31 Rotation (Expansion) along the Abutment and the Interior Pile (90-m Bridge, Clay, 3m Abutment, HP310X125 Weak Orientation with Pile Enclosure)

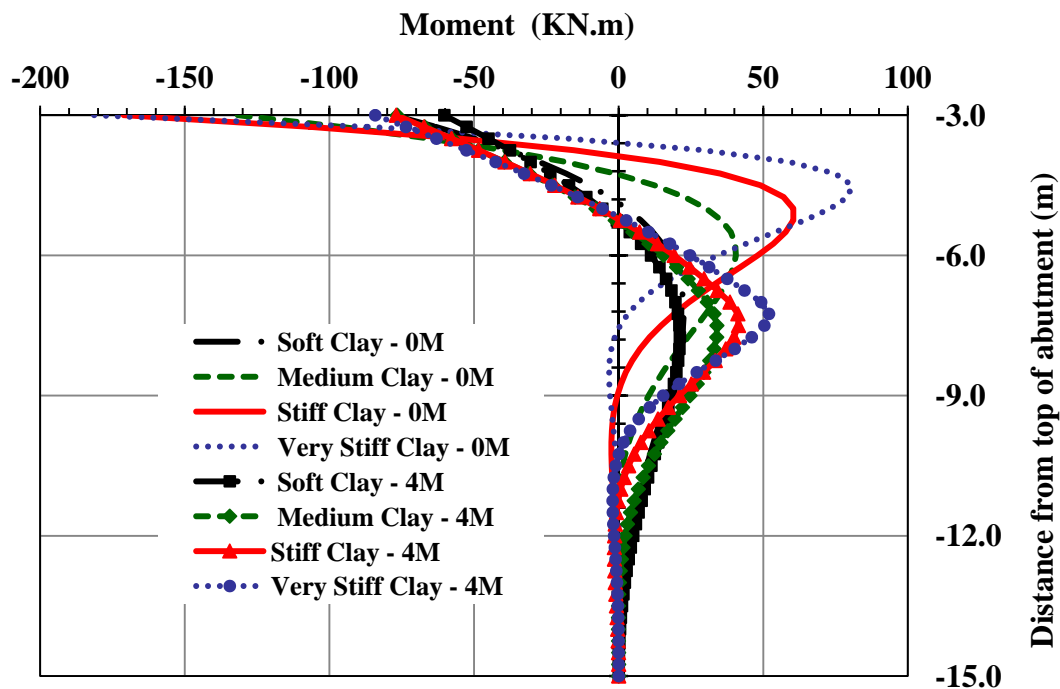


Figure A.32 Moment (Expansion) along the Exterior Pile (90-m Bridge, Clay, 3m Abutment, HP310X125 Weak Orientation with Pile Enclosure)

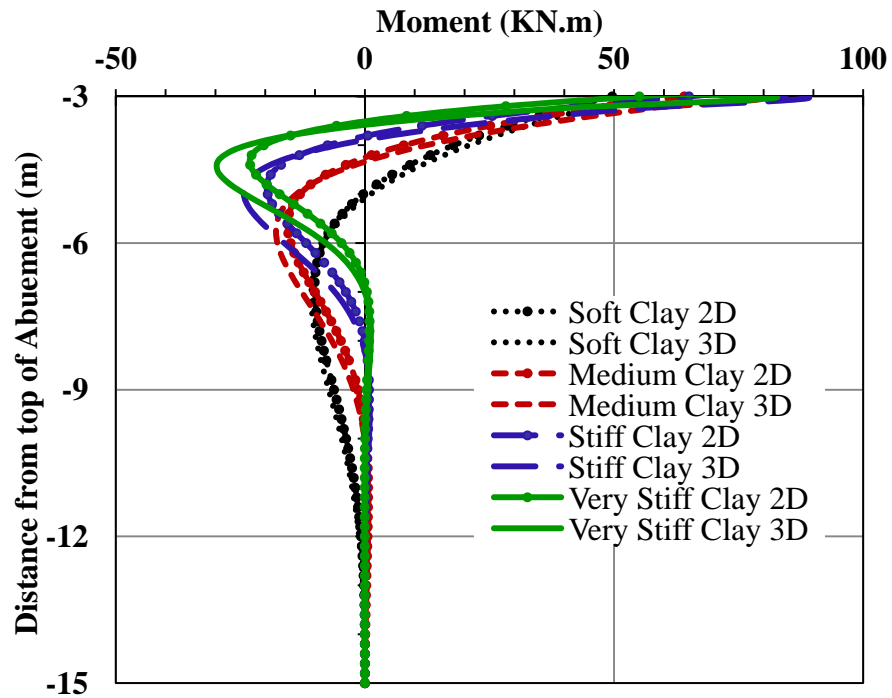


Figure A.33 Moment at Top of Interior Pile (Contraction) 2D Versus 3D
(38-m Bridge, Clay, 3m Abutment, HP310X125 Weak Orientation)

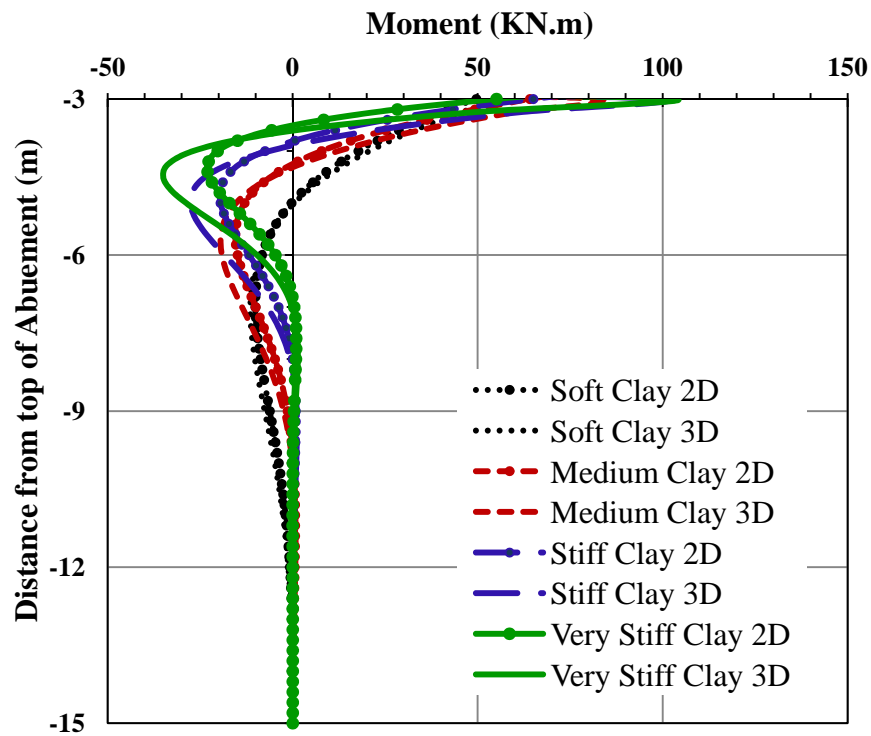


Figure A.34 Moment at Top of Exterior Pile (Contraction) 2D Versus 3D
(38-m Bridge, Clay, 3m Abutment, HP310X125 Weak Orientation)

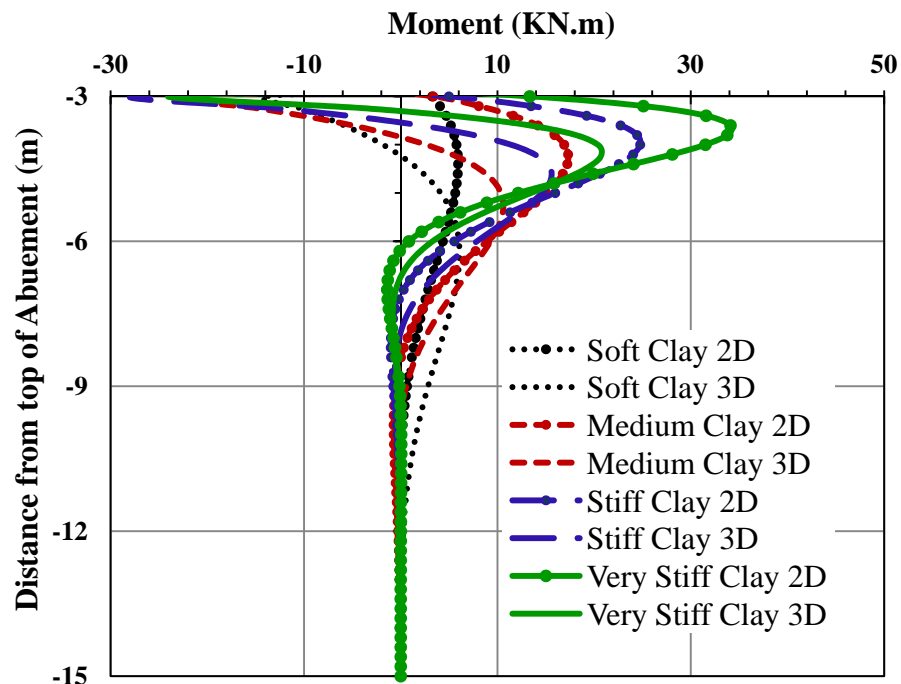


Figure A.35 Moment at Top of Interior Pile (Expansion) 2D Versus 3D
(38-m Bridge, Clay, 3m Abutment, HP310X125 Weak Orientation)

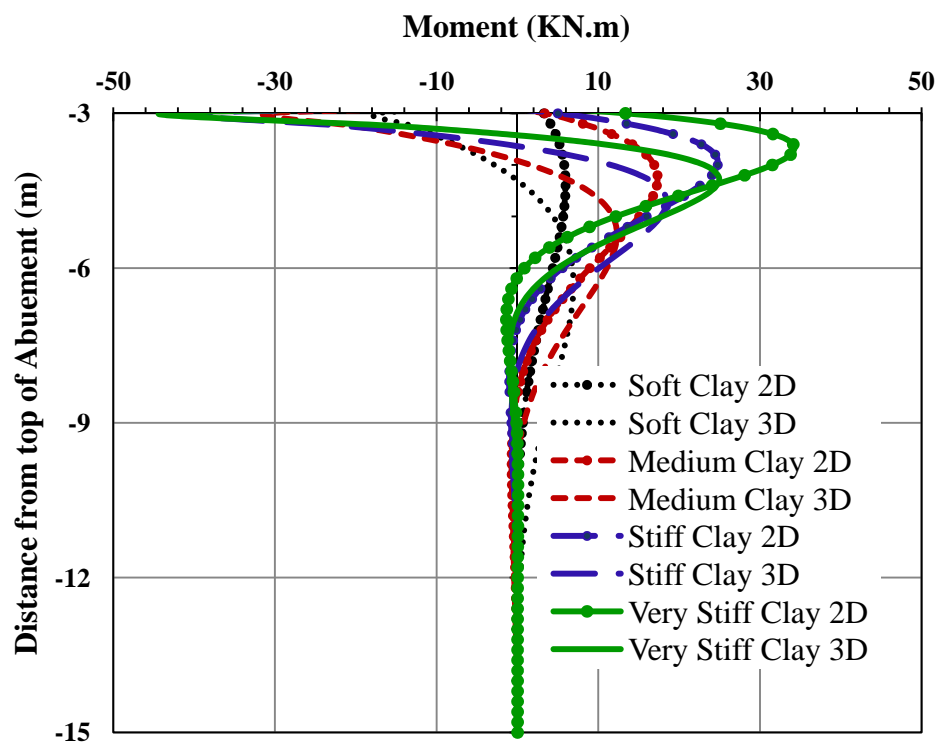


Figure A.36 Moment at Top of Exterior Pile (Expansion) 2D Versus 3D
(38-m Bridge, Clay, 3m Abutment, HP310X125 Weak Orientation)

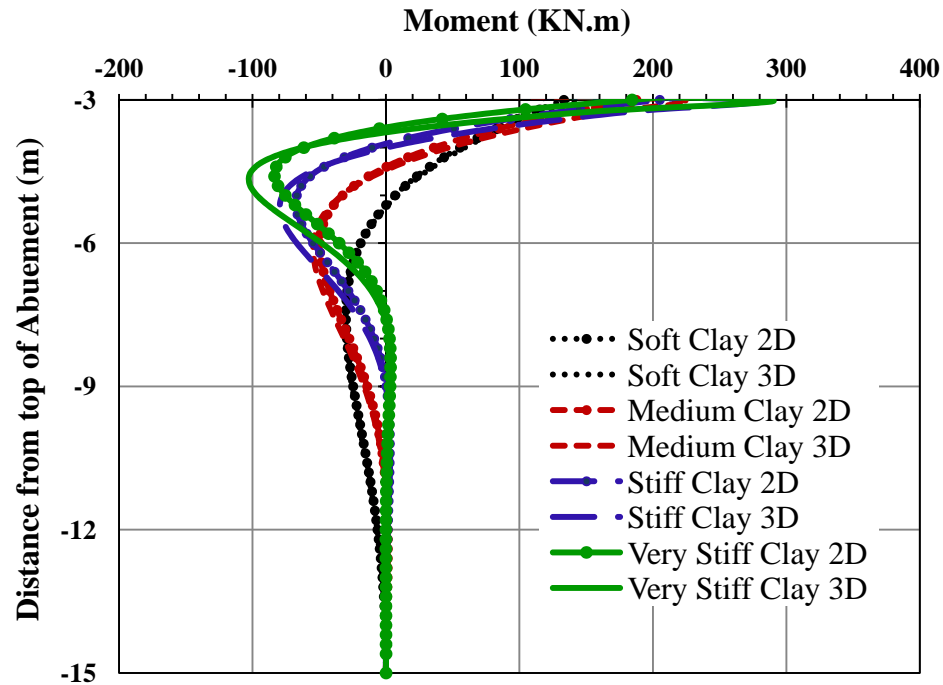


Figure A.37 Moment at Top of Interior Pile (Contraction) 2D Versus 3D
(90-m Bridge, Clay, 3m Abutment, 360X152 Weak Orientation with Pile Enclosure)

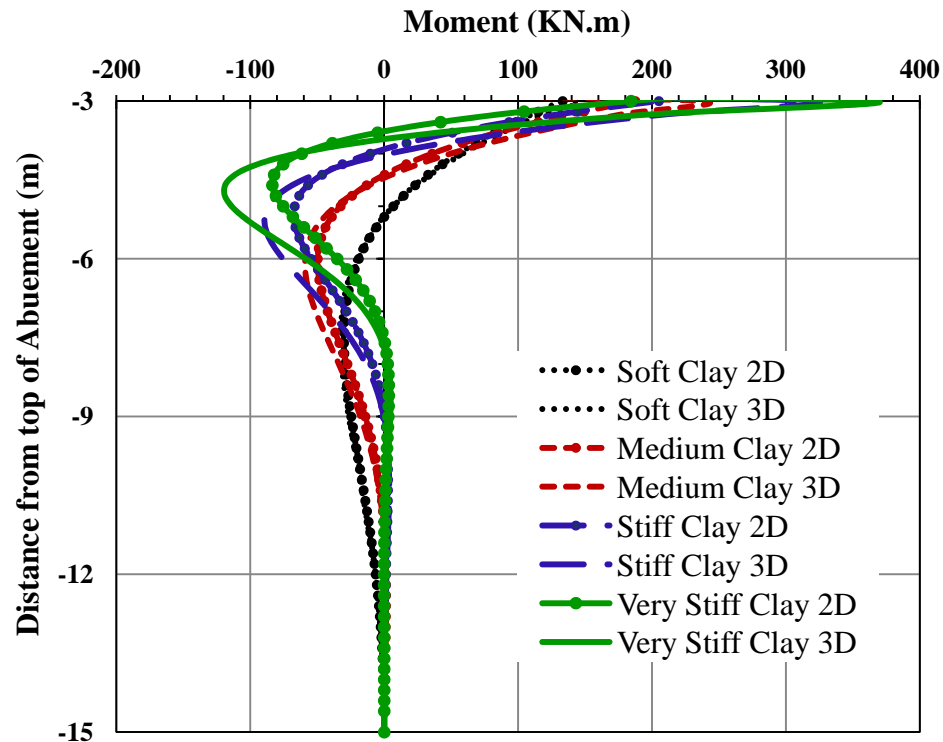


Figure A.38 Moment at Top of Exterior Pile (Contraction) 2D Versus 3D
(90-m Bridge, Clay, 3m Abutment, HP310X125 Weak Orientation with Pile Enclosure)

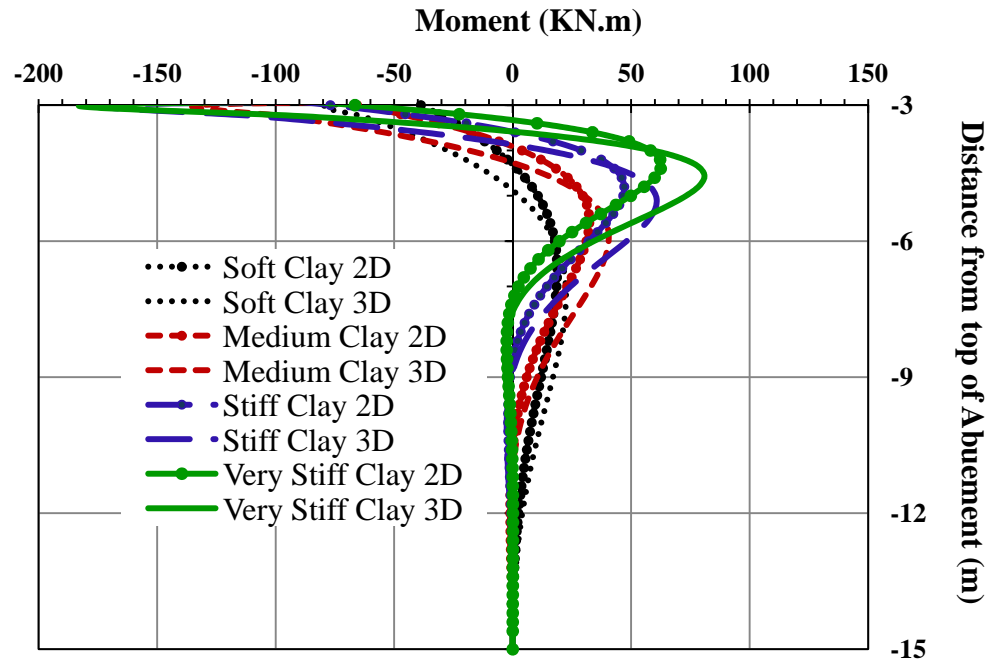


Figure A.39 Moment at Top of Interior Pile (Expansion) 2D Versus 3D
(90-m Bridge, Clay, 3m Abutment, HP310X125 Weak Orientation with Pile Enclosure)

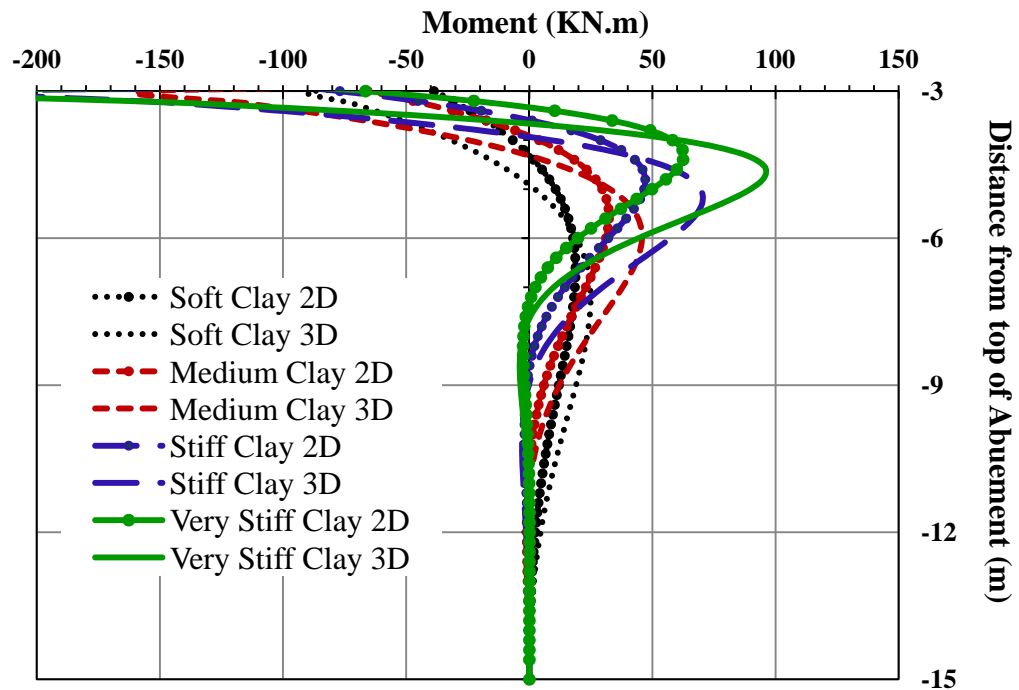


Figure A.40 Moment at Top of Exterior Pile (Expansion) 2D Versus 3D
(90-m Bridge, Clay, 3m Abutment, HP310X125 Weak Orientation with Pile Enclosure)

APPENDIX B

DISTRIBUTION OF STRESSES IN GIRDERS AND PILES

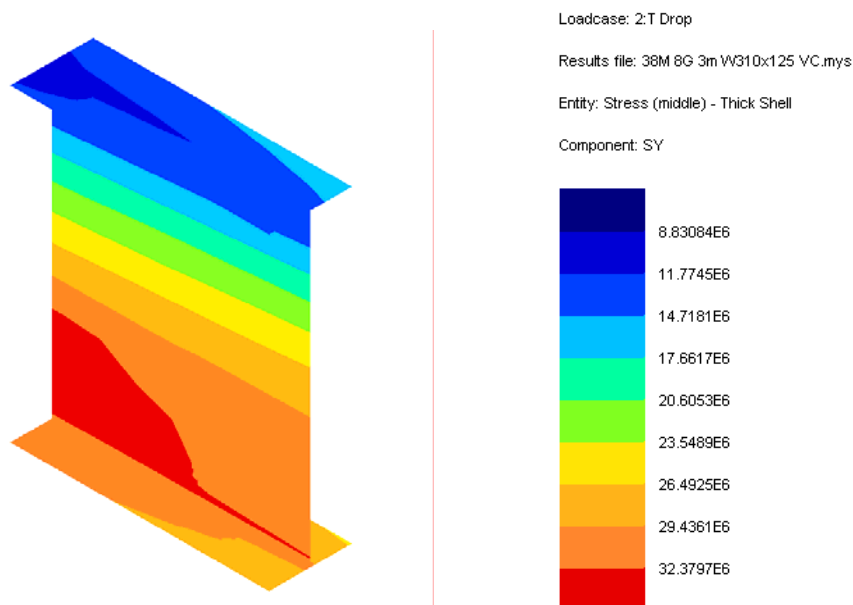


Figure B.1 Stress Distribution in the Interior Girder (Contraction, Girder's End)
(38-m Bridge, Very Stiff Clay, 3m Abutment, HP310X125 Weak Orientation)

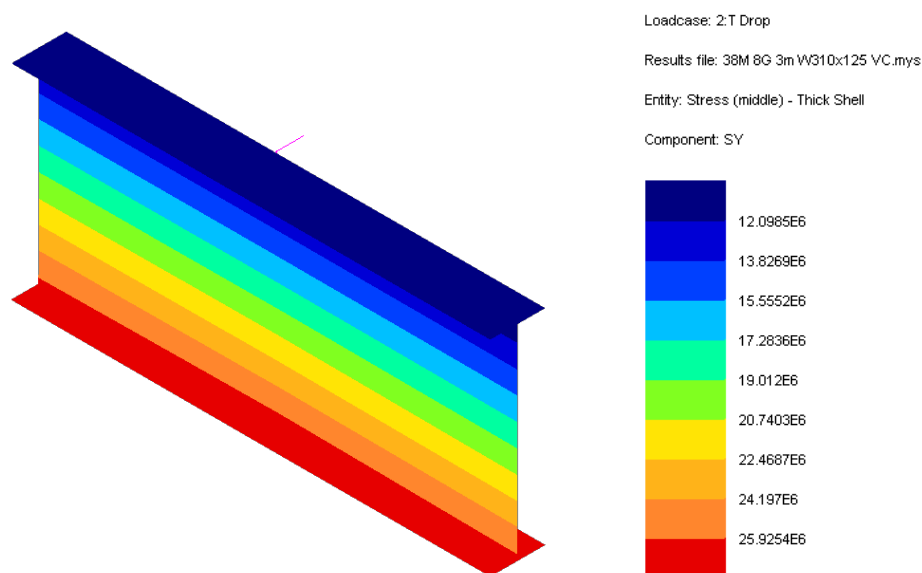


Figure B.2 Stress Distribution in the Interior Girder (Contraction, Mid-Span)
(38-m Bridge, Very Stiff Clay, 3m Abutment, HP310X125 Weak Orientation)

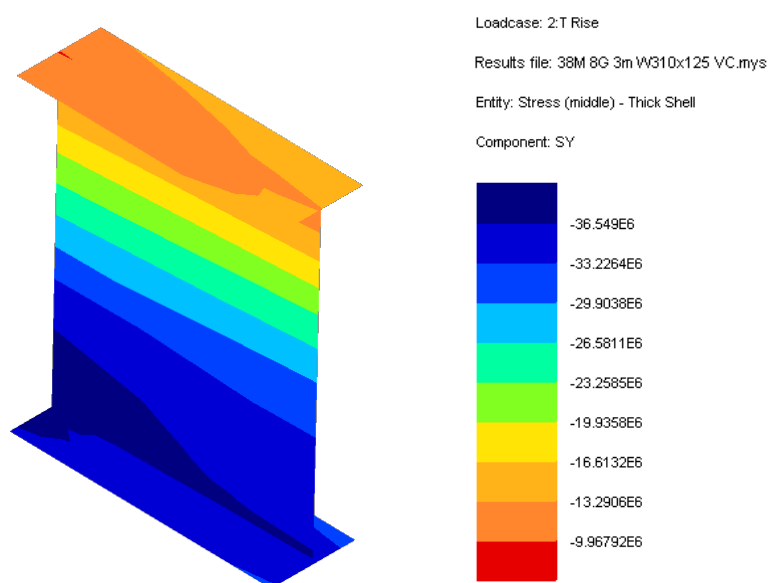


Figure B.3 Stress Distribution in the Interior Girder (Expansion, Girder's End)
(38-m Bridge, Very Stiff Clay, 3m Abutment, HP310X125 Weak Orientation)

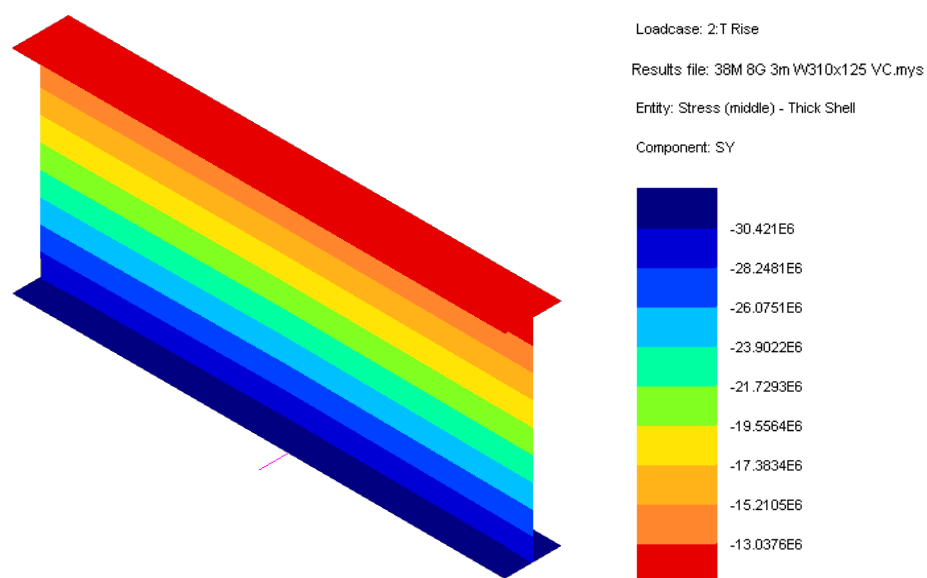


Figure B.4 Stress Distribution in the Interior Girder (Expansion, Mid-Span)
(38-m Bridge, Very Stiff Clay, 3m Abutment, HP310X125 Weak Orientation)

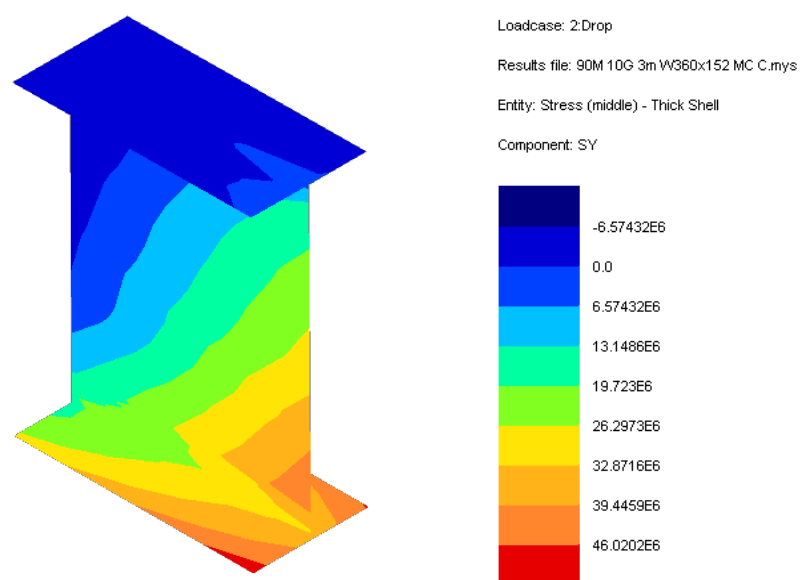


Figure B.5 Stress Distribution in the Interior Girder (Contraction, Girder's End)
(90-m Bridge, Medium Clay, 3m Abutment, HP360X152 Weak Orientation)

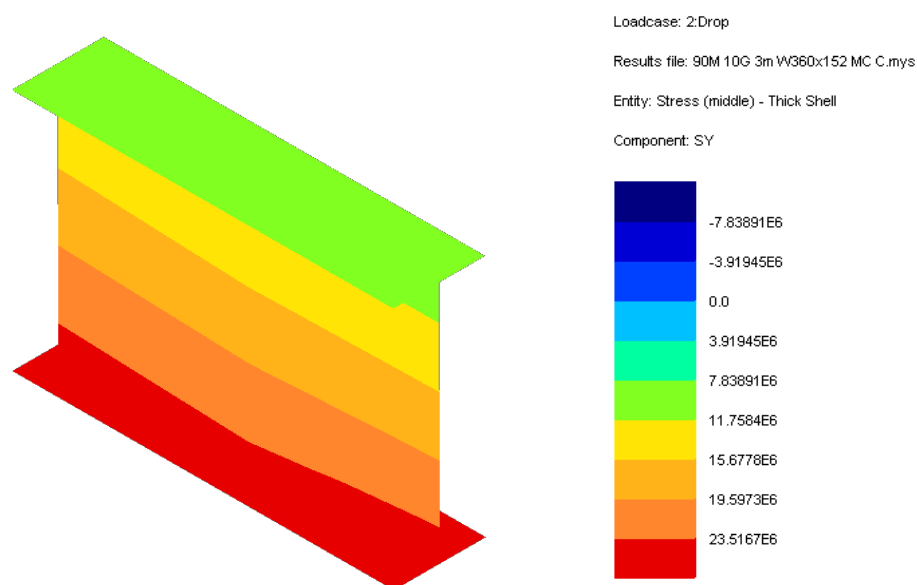


Figure B.6 Stress Distribution in the Interior Girder (Contraction, 1/4-Span from End)
(90-m Bridge, Medium Clay, 3m Abutment, HP360X152 Weak Orientation)

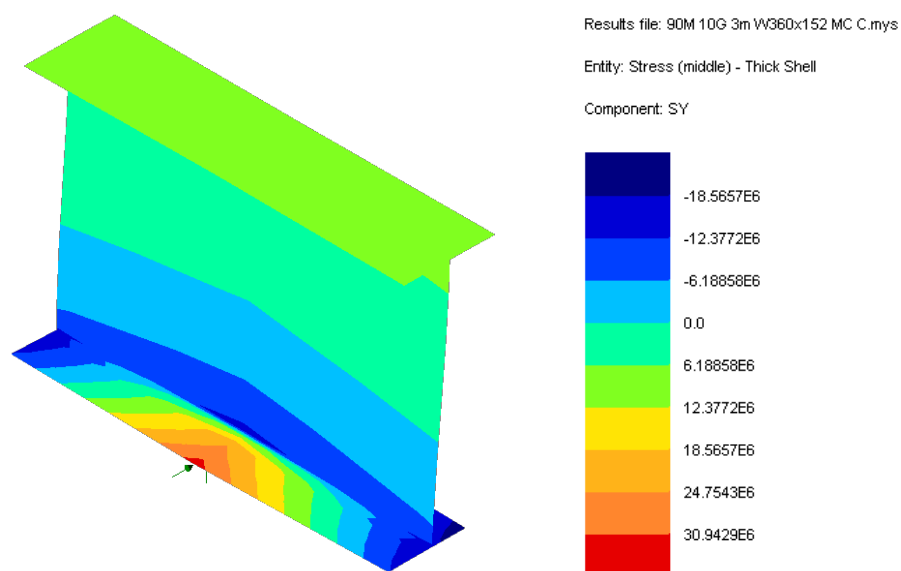


Figure B.7 Stress Distribution in the Interior Girder (Contraction, At Pier)
(90-m Bridge, Medium Clay, 3m Abutment, HP360X152 Weak Orientation)

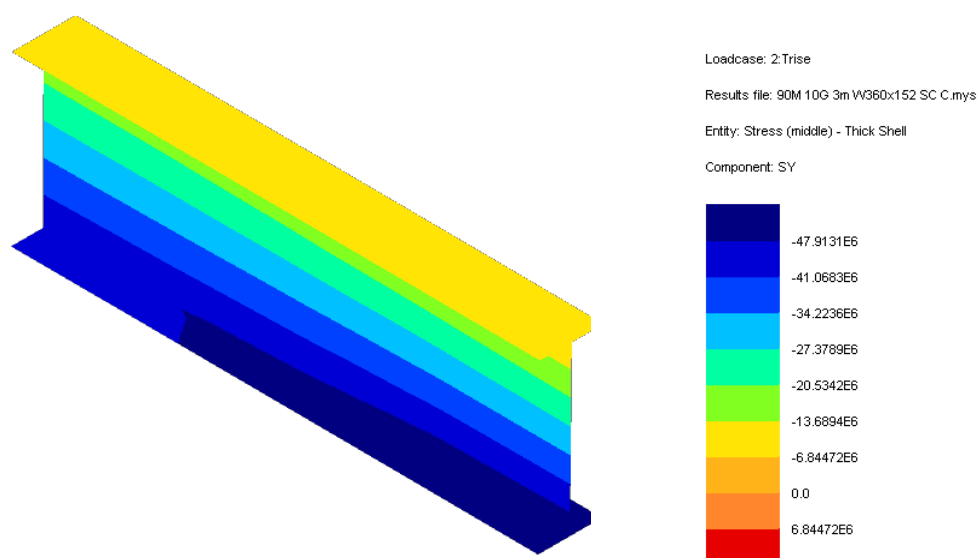


Figure B.8 Stress Distribution in the Interior Girder (Expansion, Girder's End)
(90-m Bridge, Stiff Clay, 3m Abutment, HP360X152 Weak Orientation)

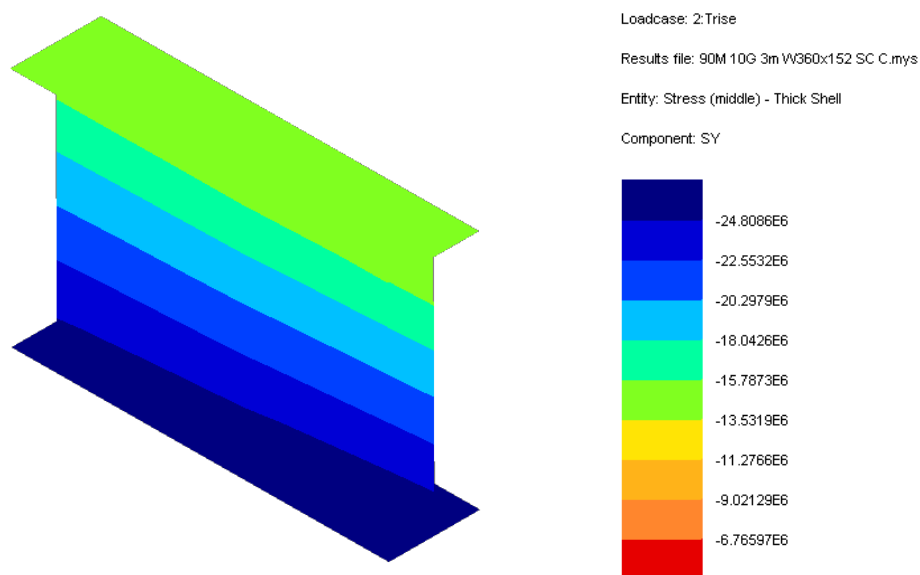


Figure B.9 Stress Distribution in the Interior Girder (Expansion, Mid-Span)
(90-m Bridge, Stiff Clay, 3m Abutment, HP360X152 Weak Orientation)

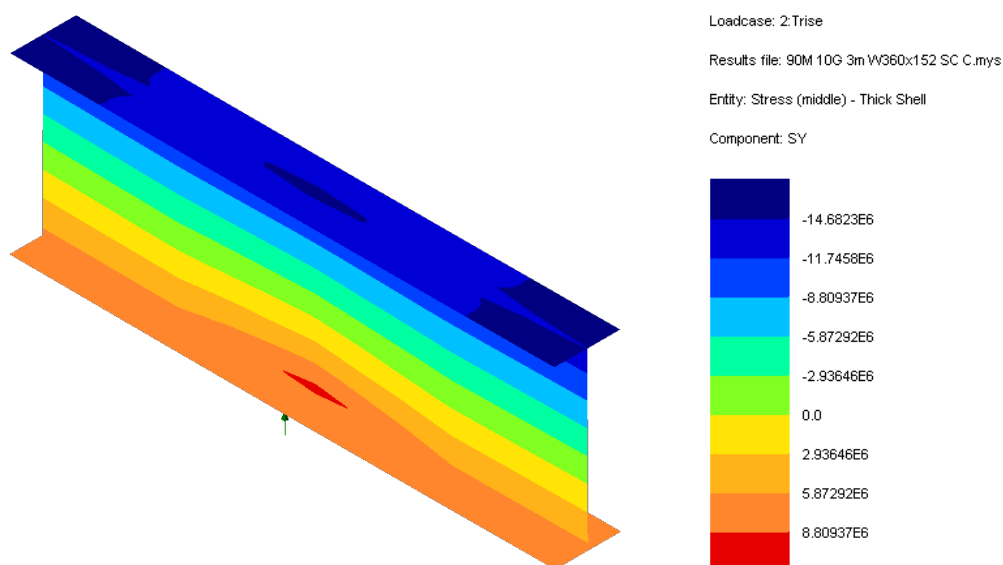


Figure B.10 Stress Distribution in the Interior Girder (Expansion, At Pier)
(90-m Bridge, Stiff Clay, 3m Abutment, HP360X152 Weak Orientation)

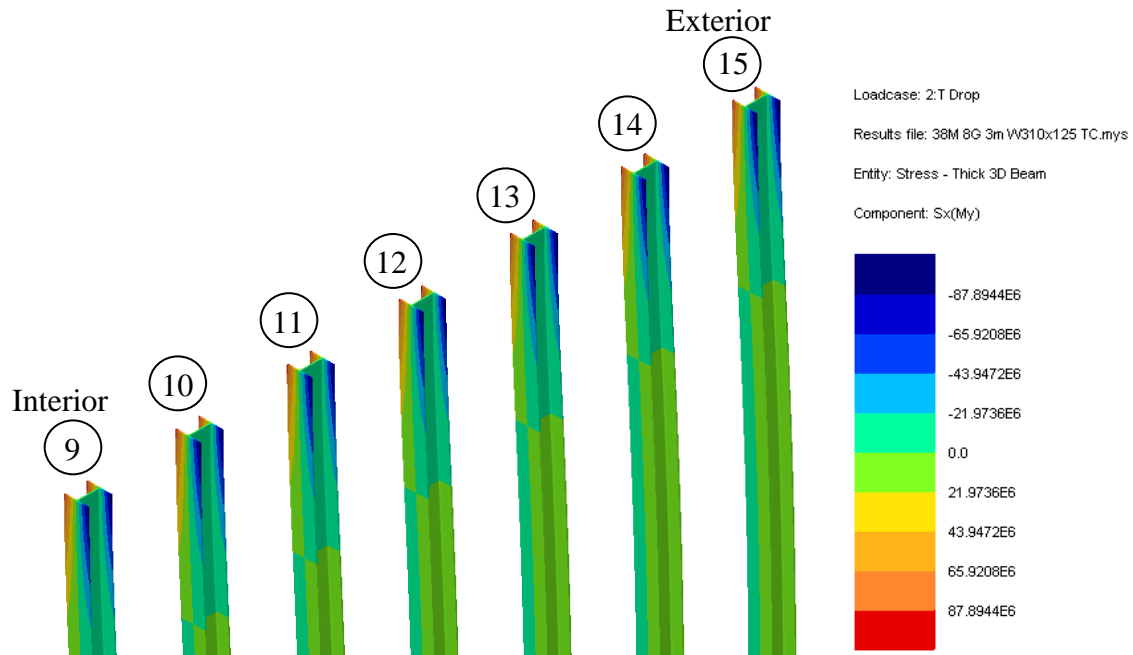


Figure B.11 Stress Distribution in the Piles (Contraction)
(38-m Bridge, Soft Clay, 3m Abutment, HP310X125 Weak Orientation)

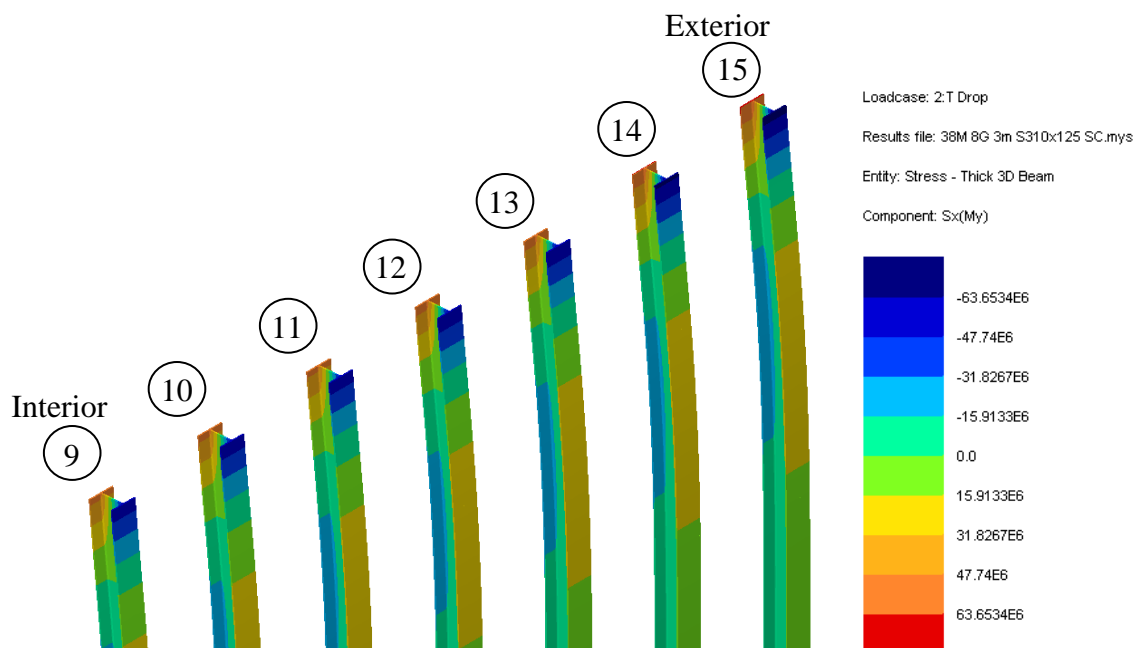


Figure B.12 Stress Distribution in the Piles (Contraction)
(38-m Bridge, Stiff Clay, 3m Abutment, HP310X125 Strong Orientation)

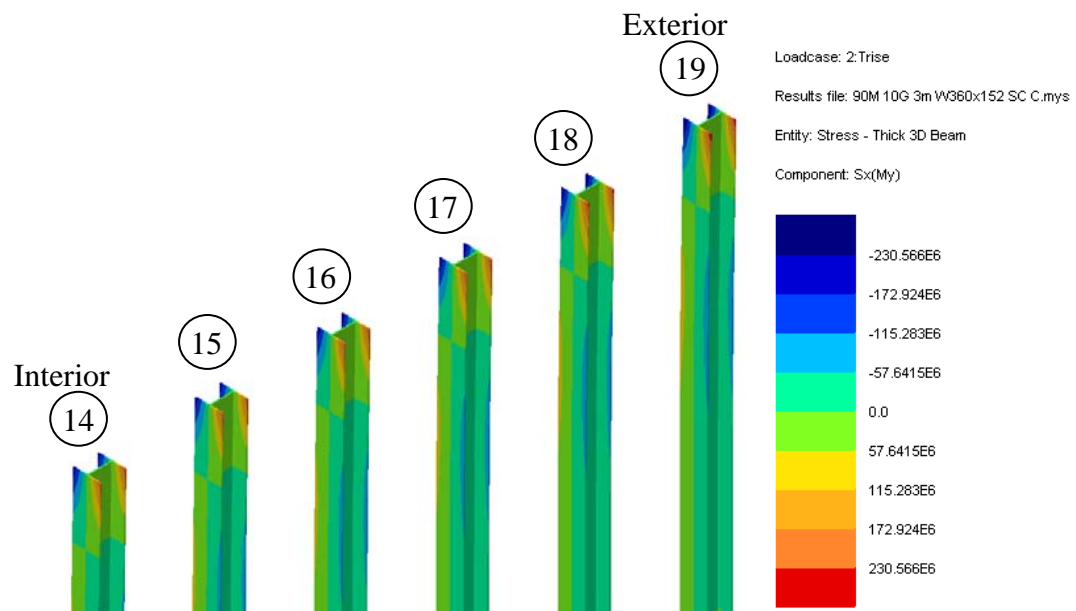


Figure B.13 Stress Distribution in the Piles (Expansion)
(90-m Bridge, Stiff Clay, 3m Abutment, HP360X152 Weak Orientation)

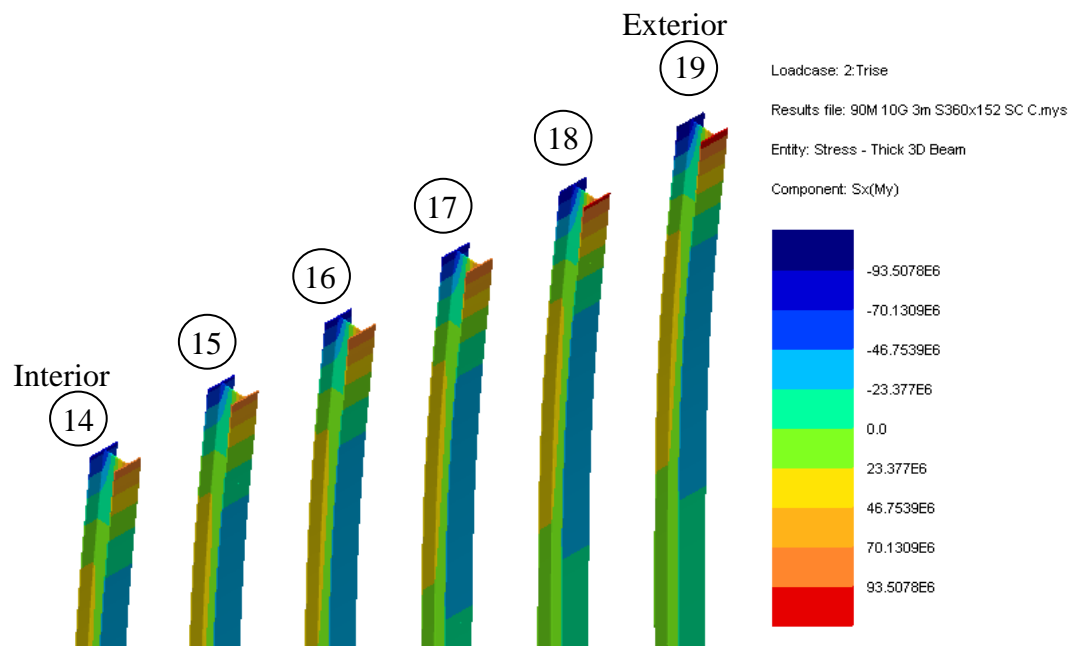


Figure B.14 Stress Distribution in the Piles (Expansion)
(90-m Bridge, Stiff Clay, 3m Abutment, HP360X152 Strong Orientation)

REFERENCES

- Abendroth, R. E., Greimann, L. F., (1989). "A Rational Design Approach for Integral-abutment Bridge Piles", *Transportation Research Record*, No 1233, p 12-23.
- Abendroth, R. E., Greimann, L. F., Ebner, P. B., (1989). "Abutment Pile Design for Jointless Bridges", *ASCE Journal of Structural Engineering*., 115 (11), p 14-29.
- Abendroth, R. E., Greimann, L. F., Ebner, P. B., (1990). "Pile behavior established from model tests", *Journal of Geotechnical Engineering*, v 116, n 4, p 571-588.
- Abendroth, R. E., Greimann, L. F., (2005). "Field Testing of Integral Abutments". Final Report, HR-399. Center for Transportation Research and Education, Iowa State University.
- Abendroth, R. E., Greimann, L. F., LaViolette, M. D., (2007). "An Integral Abutment Bridge with Precast Concrete Piles". Final Report, IHRB Project TR-438. Center for Transportation Research and Education, Iowa State University.
- Alberta Transportation., (2008). *Appendix A - Integral Abutments*. Alberta Transportation Bridge Structure. Design Criteria, Version 6.1.
- Albhaisi, S.M., (2003). "Maximum Lengths of Integral Abutment Bridges Based on the Strength of Abutments and the performance of Steel H-Piles under Cyclic Thermal Loading". Master Thesis, Department of Civil Engineering and Construction, Bradley University, Peoria, IL.
- Alampali, S., Yannotti, A.P., (1998). "In-service performance of integral bridges and jointless decks", *Transportation Research Record*, n 1624, p 1-7.
- Anagnostopoulos, C., Georgiadis, m., (1993). " Interaction of axial and lateral pile responses ", *Journal of Geotechnical Engineering*, v 119, n 4, p 793-798.
- American Association of State Highway Transportation Officials, (2010). *AASHTO LRFD Bridge Design Specifications*, Fifth Edition, Washington, D. C.
- American Association of State Highway Transportation Officials, (2002). *Standard Specifications for Highway Bridges*, 17th Edition, Washington, D. C.
- Amde, A.M., Chin, S.A., Mafis, M., (1997). "Model study of H-piles subjected to combined loading", *Geotechnical and Geological Engineering*, v 15, n 4, p 343-355.
- American Institute of Steel Construction (AISC). (2005). *Manual of Steel Construction*, 13th Edition, Chicago, IL.

American Institute of Steel Construction (AISC). (2011). *Manual of Steel Construction*, 14th Edition, Chicago, IL.

American Society for Testing and Materials (ASTM) A572/A572M-07, (2007). *Standard Specification for High-Strength Low-Alloy Columbium-Vanadium Structural Steel*, West Conshohocken, Pennsylvania.

American Society for Testing and Materials (ASTM) A36/A36M-08, (2008). *Standard Specification for Carbon Structural Steel*, West Conshohocken, Pennsylvania.

Bakeer, R.M., Mattei, N.J., Almalik, B.K., Homes, D., (2005). "Evaluation of DOTD Semi-Integral Bridge and Abutment System". Report No: FHWA/LA.05/397. Louisiana Transportation Research Center, Tulane University, New Orleans, Louisiana.

Ballio, G., Calado, L., Castiglioni, C.A., (1997). "Low cycle fatigue behavior of structural steel members and connections", *Fatigue and Fracture of Engineering Materials & Structures*, v 20, n 8, p 1129-1146.

Barker, R. M., Duncan, J. M. K., Rojiani, K. B., Ooi, P. S. K., Kim, S.G., (1991). "Manuals For The Design of Bridge Foundations", NCHRP Report 343, *Transportation Research Board*, National Research Council, Washington, D.C., USA.

Bowles, J.E., (1996). *Foundation Analysis and Design*, 5th Edition, McGraw-Hill, New York.

Breña, S.F., Bonczar, C.H., Civjan, S.A., DeJong, J.T., Crovo, D.S., (2007). "Evaluation of Seasonal and Yearly Behavior of an Integral Abutment Bridge", *Journal of Bridge Engineering*, ASCE, Vol. 12 (3), p 296-305.

British Colombia Ministry of Transportation, (2007). *Bridge Standards and Procedures Manual*, v1, Supplement to CHBDC S6-06.

Burdette, E.G., Howard, S.C., Tidwell, J.B., Wasserman, E.P., Ingram, E.E. Deatherage, J.H., Goodpasture, D.W., (2004). "Lateral Load Tests on Prestressed Concrete Piles Supporting Integral Abutments". *Precast/Prestressed Concrete Institute Journal*, September-October, p 70-77.

Burke, M. P., Jr., (1993a). "Integral Bridges: Attributes and Limitations", *Transportation Research Record*, No 1393, *Transportation Research Board*, National Research Council, Washington, D.C., USA, 1-8.

Burke, M. P., Jr., (1993b). "The Design of Concrete Integral Bridges", *Concrete International*, p 37-42.

Burke, M. P., Jr., (1999). "Cracking of concrete decks and other problems with integral-type bridges", *Transportation Research Record*, n1688, Nov, p 131-138.

Burke, M. P., Jr., (2009). "*Integral and Semi-Integral Bridges*", Wiley-Blackwell. United Kingdom. ISBN: 978-1-4051-9418-1.

Canadian Standards Association, (2006). *Canadian Highway Bridge Design Code*. CAN/CSA-S6-06, 10 th ed. Canadian Standards Association, Ontario, Canada.

Connal, J., (2004). "*Integral Abutment Bridges: Australian and US Practice*", *Fifth Austroads Bridge Conference, Hobart, Tasmania, Australia*. Transport Research Laboratory, Wokingham, Berkshire, UK.

Clough, G. M., Duncan, J. M., (1991). *Foundation Engineering Handbook*, 2cd Edition, Edited by H. Y., Fang, Van Nostrand Reinhold, New York, USA.

Connal, J., (2004). "*Integral Abutment Bridges : Australian and US Practice*". Fifth Austroads Bridge Conference, Transport Research Laboratory, Wokingham, Berkshire, UK.

Cross, H., (1932). "Analysis Of Continuous Frames By Distributing Fixed-End Moment", *Transactions of American Society of Civil Engineers*, vol. 96 , p 1-156.

Daali, M.L., Korol, R.M., (1995). "Low cycle fatigue damage assessment in steel beams", *Structural Engineering and Mechanics*, v3, n4, p 341-358.

Delaware Department of Transportation (DelDOT)., (2005). *Bridge Design Manual*. Dover, Delaware.

Dowling, N.E., (2006). *Mechanical Behavior of Materials-Engineering Methods for Deformation, Fracture and Fatigue*, 3rd Edition, Prentice Hall.

Dunker, K.F., Liu, D., (2007). "*Foundations for Integral Abutments*". Practice Periodical on Structural Design and Construction, ASCE, p 161-182.

England G. L., Tsang C. M., Bush D., (2000). "*Integral Bridges - A Fundamental Approach to the Time Temperature Loading Problem*". Thomas Telford, London. ISBN 0-7277-2845-8.

Federal Highway Administration (FHWA), (1980). "Integral, No-Joint Structures and Required Provisions of Movement", *Technical Advisory T5140.13*, U.S. FHWA-IP-87-6, U.S. Department of Transportation, Federal Highway Administration, Washington, D. C., USA.

Frosch, R.J., Kreger, M.E., Talbott, A.M., (2009). "*Earthquake Resistance of Integral Abutment Bridges*". Final Report, FHWA/IN/JTRP-2008/11. Joint Transportation Research Program, Purdue University.

Galambos, T.V., Ravindra, M.K., (1978). "Properties Of Steel For Use In LRFD", *ASCE Journal of Structural Division*, v 104, n 9, p 1459-1468.

Girton, D. D., Hawkinson, T. R., Greimann, L. F., Bergenson, K., Ndon, U., Abendorth, R. E., (1989). "*Validation of Design Recommendations for Integral-abutment Piles*", Iowa Department of Transportation, Project HR-292, Ames, Iowa, USA.

Greimann, L. F., Abendtroth, R. E., Johnson, D. E., Ebner, P. B., (1987). "*Pile Design and Tests for Integral-abutment Bridges*", Final Report, Iowa Department of Transportation, Project HR-273, Ames, Iowa, USA.

Hambly, E. C., Nicholson, B. A., (1990). "Prestressed Beam Integral Bridges", *The structural Engineer*, 68 (23), p 474-481.

Hambly, E. C., (1997). "Integral bridges". *Proc., Institute of Civil Engineers, Transport Engineering*, V123, n1, p 30–38.

Haliburton, T. A., (1971). "*Soil Structure Interaction; Numerical Analysis of Beams and Beam Columns*", Technical Publication No. 14, School of Civil Engineering, Oklahoma State University, Stillwater, Oklahoma.

Hassiotis S., S., Khodair, Y., Roman, E., Dehne, Y., (2006). "*Evaluation of Integral Abutments*". Final Report, FHWA-NJ-2005-025. New Jersey Department of Transportation.

Harvey, D.I., Kennedy, D.W., and Ruffo, G.W., (2006). "Integral Abutment Bridges-Design and Constructability", *Integral Abutment Bridges*. p 1-8.

Horvath, J.S., (2000). "*Integral-abutment bridges problems and innovative solutions using EPS geof foam and other geosynthetics*", Manhattan College Research Report No. CE/GE-00-2.

Huang, J., French, C. and Shield , C., (2004). "*Behavior of Concrete Integral Abutment Bridges*" Final Report. Minnesota Department of Transportation.

Husain, I., Bagnariol, D., (1996). "*Integral-abutment Bridges*", Ontario Ministry of Transportation, Report SO-96-01, St. Catharines, Ontario, Canada.

Indiana Department of Transportation (INDOT), Indianapolis.

Itani, A.M., Pekcan, G., (2011). "*Seismic Performance of Steel Plate Girder Bridges with Integral Abutments*", Report No. FHWA-HIF-11-043. FHWA Office of Bridge Technology, Washington DC.

Kamel, M. R., Benak, J. V., Tadros, M. K., and Jamshidi, M., (1995). "Application of Precast, Prestressed Concrete Piles in Integral Abutment Bridges"; *Fourth International*

Bridge Engineering Conference; Vol. 2, Nebraska DOT, the Precast Concrete Associations of Nebraska, and the Center for Infrastructure Research Univ. of Nebraska, p 146-157.

Kato, B., (1989). " Rotation capacity of H-section members as determined by local buckling", *Journal of Constructional Steel Research*, v 13, n 2-3, p 95-109.

Kemp, A.R., (1986) . " Factors Affecting The Rotation Capacity Of Plastically Designed Members", *Structural Engineer, Part B: R&D Quarterly*, v 64B, n 2, p 28-35.

Kemp, A.R., (1996). "Inelastic local and lateral buckling in design codes", *ASCE Journal of Structural Engineering*, v122, n4, Apr, p 374-382.

Koh, S.K., Stephens, R.I., (1991). "Mean stress effects on low cycle fatigue for a high strength steel", *Fatigue and Fracture of Engineering Materials & Structures*, v 14, n 4, p 413-428.

Khan, M.A., (2004). "*Modeling and Seismic Analysis of Integral Abutments*". American Society of Civil Engineering.

Knickerbocker, D.J., Basu, P.K., Holloran, M.A., and Wasserman, E.P., (2003). "Recent Experience with High-Performance Concrete Jointless Bridges in Tennessee," *Journal of the Transportation Research Board*, No. 845, 2003, p 104-114.

Kuhlmann, U., (1989). "Definition of flange slenderness limits on the basis of rotation capacity values", *Journal of Constructional Steel Research*, v 14, n 1, p 21-40.

Kunin, J., Alampalli, S., (1999). "*Integral Abutment Bridges: Current Practice in United States and Canada*", Special Report No. 132. Transportation Research and Development Bureau. NYSDOT, Albany, NY.

Kunin, J., Alampalli, S., (2000). "*Integral Abutment Bridges: Current Practice in United States and Canada*" *Journal of Performance of Constructed Facilities*, p 104-111.

Laman , J.A., Pugasap, K., Kim, W., (2006). "*Field Monitoring of Integral Abutment Bridges*". Final Report, FHWA-PA-2006-006-510401-01. The Pennsylvania Department of Transportation.

Lay, M.G., Galambos, T.V., (1967). "Inelastic Beams Under Moment Gradient", *ASCE Journal of Structural Devision*. VOL. 93, No. ST1, p 381-399.

Lehane, B.M., Keogh, D.L., and O'Brien, E.J., (1999). "*Simplified elastic model for restraining effects of backfill soil on integral bridges*". Department of Civil, Structural and Environmental Engineering, Trinity College, Dublin , Ireland. *Computers and Structures* 73, p 303-313.

Loveall, C. L., (1985). "Jointless Bridge Decks", *Civil Engineering (New York)*, v 55, n 11, Nov, p 64-67.

Lucky, A.F., Adams, P.F., (1969). "Rotation Capacity Of Beams Under Moment Gradient", *ASCE Journal of Structural Division*.VOL. 95, No. ST6, p 1173-1189.

Lutenegger, T. A., Thomson, Jr., C. Riccardi, (1998.). "*Passive Earth Pressures in Integral Abutment Bridges*", Report No. UMTC-97-16, University of Massachusetts, Transportation Center, Amherst, Massachusetts.

LUSAS V14, (2010). Finite Element Analysis Software. Finite Element Analysis Ltd. United Kingdom.

Mander, J.B., Panthaki, F.D., Kasalanti, A., (1994). "Low-cycle fatigue behavior of reinforcing steel", *Journal of Materials in Civil Engineering*, v6, n4, Nov, p 453-468.

Maruri, R.F., Petro, S.H., (2005). "Integral Abutments and Jointless Bridges (IAJB) 2004 Survey Summary", *Proceeding of the FHWA Conference on Integral Abutment and Jointless Bridges*, Baltimore, March 16-18.

Maine Department of Transportation (MaineDOT). (2003). *Bridge Design Guide* . Augusta, Maine.

Massachusetts Department of Transportation (MassDOT). (2009). *LRFD Bridge Manual*. Boston, Massachusetts.

Matlock, H., (1970). "Correlation for Design of Laterally Loaded Piles in Soft Clay" *Proceedings of the II Annual Offshore Technology Conference*, Houston, Texas, (OTC 1204). p 577-594.

Minnesota Department of Transportation (MnDOT)., (2011). *LRFD Bridge Design Manual*. Oakdale, Minnesota.

Mourad, S., Tabsh, S.W., (1999). "Deck Slab Stresses In Integral Abutment Bridges". *Journal of Bridge Engineering*, Vol. 4, No. 2, p 125-130.

Najm, H., Albhaisi, S., Nassif, H., Khoshkbari, P., Gucunski, N., (2005). "Seismic Analysis of Retaining Walls, Buried Structures, Embankments, and Integral Abutments". *Center for Advanced Infrastructure & Transportation (CAIT)*. Report number FHWA-NJ-2005-002. Rutgers, The State University of new Jersey. Piscataway, New jersey.

Naval Facilities Engineering Command. (1971). Foundations and Earth Structures, Department of the Navy, *Design Manual NAVFAC_DM7_02* , Alexandria, Virginia.

New Jersey Department of Transportation (NJDOT)., (2009). *Design Manual for Bridges and Structures*, Fifth Edition. Trenton , New Jersey.

New York State Department of Transportation (NYSDOT)., (2008). *Bridge Manual*. Albany, New York.

Olson, S.M., Long, J.H., Hansen, J.R., Renekis, D., LaFave, J.M., (2009). “*Modification of IDOT Integral Abutment Design Limitations and Details*”, Report No. FHWA-ICT-09-054, Illinois Department of Transportation, Springfield, IL.

Oesterle, R.G., Hamid, R.L., (2005). “Effective Temperature and Longitudinal Movement in Integral Abutment Bridges”, *Proceeding of the FHWA Conference on Integral Abutment and Jointless Bridges, (IAJB2005)*, Baltimore, March 16-18.

Ooi, P. S. K., Lin, X., Hamada, H.S., (2010). “Field Behavior of an Integral Abutment Bridge Supported on Drilled Shafts”, *Journal of Bridge Engineering*, ASCE, Vol. 15, No. 1, p 4-18.

Oregon Department of Transportation (ORDOT) , (2004). *Bridge Design & Drafting Manual*. Salem, Oregon.

Paraschos, A., Amde, M.A., (2011). “*A survey on the status of use, problems, and costs associated with Integral Abutment Bridges*”, Better Roads Magazine, February.

Popov, E.P., Bertero, V.V., (1973). "Cyclic Loading Of Steel Beams And Connections", *ASCE Journal of Structural Devision*. V. 99, No.ST6, p 1189-1204.

Reese, L. C., Cox, W. R., Koop, F. D., (1974). “Analysis of Laterally Loaded Piles in Sand”, *Proceedings*, 6th Annual Offshore Technology Conference, Houston, TX, p 473-485.

Rees, L.C., Van Impe, W.F., (2001). *Single Piles and Pile Group under Lateral Loading*. A.A. Balkema, Rotterdam.

Roeder, C.W., (2003). “Proposed Design Method for Thermal Bridge Movements”, *Journal of Bridge Engineering*, American Society of Civil Engineers, v16, n4, p 44-48.

Shama, A.A., Mander, J.B., Blabac B.B., Chen, S.S., (2001). “Experimental Investigation and Retrofit of Steel Pile Foundations and Pile Bents Under Cyclic Lateral Loadings”, Technical Report: MCEER-01-0006, Multidisciplinary Center for Earthquake Engineering and Research, State University of New York at Buffalo, Buffalo, NY.

Sanford, T.C., Elgaaly, M., (1993). "Skew effects on backfill pressures at frame bridge abutments", *Transportation Research Record*, n 1415, p 1-11.

Skempton, A.W., (1951). “The bearing capacity of clays”, *Proceedings, Building Research Congress*, Division 1, London, England.

Stanford, T.C., Davids, W.G., Hartt, S., (2006). "Construction-Induced Stresses in H-Piles Supporting an Integral Abutment Bridge", *Transportation Research Record: Journal of the Transportation Research Board*, No. 1975, Transportation Research Board of the National Academies, Washington, D.C., p 39–48.

Thippeswamy, H.K., Gangarao, H.V.S., (1995). "Analysis of in-service jointless bridges", *Transportation Research Record*, n1476, p 162-170.

Thippeswamy, H. K., GangaRao, H. V. S., Franco, J. M., (2002). "Performance evaluation of jointless bridges", *Journal of Bridge Engineering*, ASCE, Vol. 7(5), p 267-289.

Ting, S.F., (1998). "*Streamlined Analysis and Design of Integral Abutment Bridges*", Report No. UMTC-97-13, University of Massachusetts, Transportation Center, Amherst, Massachusetts.

Tomlinson, M., Woodward, J., (2008). *Piles Design and Construction Practice*, 5th Edition. Publisher: Taylor & Francis.

Van Lund, J.A., Breto, B.B., (1999). "Jointless bridges and bridge deck joints in Washington State", *Transportation Research Record*, n1688, p 116-123.

Vermont, Agency of Transportation (VTrans)., (2008). Integral Abutment Bridge Design Guidelines, 2nd Edition. (2008). *VTrans, Integral Abutment Committee*. VTrans, Structures Section . Montpelier, Vermont.

Wang, S.T., Isenhower, W.M., (2010). "*User's Manual for LPile, Version 6, A Program for the Analysis of Piles and Drilled Shafts Under Lateral Loads*", Ensoft, Inc., p 68-74.

Wasserman, E.P., (2009). "A Brief History of Concrete Bridge Construction in Tennessee", *ASPIRE, the Concrete bridge Magazine*, p 46-48.

Welch, R.C., Reese, L.C., (1972). "*Laterally loaded behavior of drilled shafts*", Research Report 3-5-65-89. Center for Highway Research. University of Texas, Austin.

White, H., (2007). "Integral Abutment Bridges: Comparison of Current Practice between European Countries and The United States of America", Final Report, FHWA/NY/SR-07/152. *Transportation Research and Development Bureau*, NYSDOT.

White, H., Pétursson, H., Collin, P., (2010). "Integral Abutment Bridges: The European Way", *Practice Periodical on Structural Design and Construction*, ASCE, p 201-208.

Wolde-Tinsae, A. M., Klinger, J. E., White, E.J., (1988a). "Performance of Jointless Bridges", *ASCE Journal of Performance of Constructed Facilities*, 2 (2), p 111-128.

Wolde-Tinsae, A. M., Greimann, L., Yang, P., (1988b). "End-Bearing Piles in Jointless Bridges", *ASCE Journal of Structural Engineering*, v 114, n 8, p 1870-1884.

Yura, J.A., Galambos, T.V., Ravindra, M.K., (1978). "The Bending Resistance Of Steel Beams", *ASCE Journal of Structural Division*, v 104, n 9, p 1355-1370.

Yohchia, C., (1997). "Important considerations, guidelines, and practical details of integral bridges", *Journal of Engineering Technology*, v14, n1, p 16-19.

Zenner, H., Simburger, A., Liu, j., (2000). "On The Fatigue Limit of Ductile Metals Under Complex Multiaxial Loading", *International Journal of Fatigue*, v22, n2. Publisher: Elsevier, p 137-145.

CURRICULUM VITA

SUHAIL ALBHAISI, Ph.D., P.E.

EDUCATION

- | | |
|----------|---|
| May 2012 | Ph.D., Civil Engineering (4.0 GPA)
Rutgers, The State University of New Jersey, New Brunswick, NJ |
| May 2003 | M.S., Civil Engineering (4.0 GPA)
Bradley University, Peoria, IL |
| May 1998 | B.S., Civil Engineering (High Distinction)
Birzeit University, West Bank, Palestine |

PUBLICATIONS

Suhail Albhaisi, Hani H. Nassif, Eui-Seung Hwang, "Effect of Substructure Stiffness on the Performance of Steel Integral Abutment Bridges". *Transportation Research Record*, accepted for publication.

Murad Dicleli, **Suhail Albhaisi**, Mohammed Mansour, "Static Soil-Structure Interaction Effects in Seismic Isolated Bridges," ASCE Practice Periodical on Structural Design and Construction, Vol. 10, No. 1, pp-22-33, 2005.

Murad Dicleli, **Suhail Albhaisi**, "Analytical Formulation of Maximum Length Limits for Integral Bridges Built on Cohesive Soils," Canadian Journal of Civil Engineering, Volume 32, Number 4, pp 726-738, August 2005.

Murad Dicleli, **Suhail Albhaisi**, "Static Soil-Structure Interaction Effects in Seismic Isolated Bridges," ASCE Practice Periodical on Structural Design and Construction, Vol. 10, No. 1, pp-22-33, 2005.

Murad Dicleli, **Suhail Albhaisi**, "Estimation of Length Limits for Integral Bridges Built on Clay," ASCE Journal of Bridge Engineering, Vol. 9, No. 6, pp. 572-581, 2004.

Murad Dicleli, **Suhail Albhaisi**, "Effect of Cyclic Thermal Loading on the Performance of Steel H-Piles in Integral Bridges with Stub-Abutments," Journal of Constructional Steel Research, Elsevier Science, Vol. 60, No. 2, pp 161-182, 2004.

Murad Dicleli, **Suhail Albhaisi**, "Performance of Abutment-Backfill System under Thermal Variations in Integral Bridges Built on Clay," Engineering Structures, Elsevier Science, Vol. 26, No. 7, pp 949-962, 2004.

Murad Dicleli, **Suhail Albhaisi**, "Maximum Length of Integral Abutment Bridges Supported on Steel H-Piles Driven in Sand," Engineering Structures, Elsevier Science, Vol. 25, No.12, 1491-1504, 2003.

CONSULTING EXPERIENCE

Jacobs Engineering Group, Iselin New Jersey (2005-Current)

Senior Structural Engineer (2011-Current)

Construction, Contract 1, Wittpenn Bridge, Lift Bridge Substructure

Senior Structural Engineer (2010- Current)

Final Design, Contract 4, Wittpenn Bridge, Approach Ramps

Structural Engineer - (2008-2010)

Final Design, Contract 3, Wittpenn Bridge, Lift Bridge Superstructure

Structural Engineer and Deputy Project Manager (2008-2010)

Major Rehabilitation of the Existing Wittpenn Bridge, (Construction completed)

Structural Engineer (2008-2009)

Final Design, Contract 2, Wittpenn Bridge, Mainline Approach Spans

Structural Engineer (2007-2009)

Final Design, Contract 1, Wittpenn Bridge, Lift Bridge Substructure

Structural Engineer (2005-2007)

Preliminary Design, Wittpenn Bridge

Structural Engineer (2005-2010)

NJDOT, Replacement of Route 36 Highlands Bridge over the Shrewsbury River, NJ
(Construction completed)

TEACHING EXPERIENCE

Part Time Lecturer (2007-Current) Rutgers University, New Jersey

Classes taught: Bridge Design I, Mechanics of Solids.

Teaching Assistant (1998-2000) Birzeit University, West Bank, Palestine

Classes taught: Soil Mechancis Lab, Conrete Technology Lab, Survying Lab I, II.

Teaching Assistant for : Mechanics of Materials, Adavnced Structural Analysis.

RESEARCH EXPERIENCE

Graduate Research Assistant (2003-2005) Rutgers University, New Jersey

Ph.D. Dissertation: "Effect of Substructure Stiffness on The Performance of Integral Abutment Bridges under Thermal Loads".

Graduate Research Assistant (2000-2003) Bradley University, Illinois

M.S. Thesis: "Maximum Lengths of Integral Bridges Based on the Strength of Steel H-Piles Under Cyclic Thermal Loading".